April 2000

Chem. Pharm. Bull. **48**(4) 447—453 (2000)

447

Catalytic Mechanism of Class A β-Lactamase. I. The Role of Glu166 and Ser130 in the Deacylation Reaction

Masayuki HATA,* Yasuyuki FUJII, Miho ISHII, Tyuji HOSHINO, and Minoru TSUDA

Laboratory of Physical Chemistry, Faculty of Pharmaceutical Sciences, Chiba University, Chiba 263-8522, Japan.

The tetrahedral intermediate formation process, which is the first step in the deacylation reaction by class A β-lactamase, was investigated by the *ab initio* molecular orbital method. In this study, benzyl penicillin was used as the substrate. From the results of our molecular dynamics study of the structure of β-lactam antibiotics–β-lactamase complex, the substrate, Ser70, Lys73, Ser130, Glu166 and a water molecule for the deacylation reaction were considered for construction of a model for calculation. The calculation results indicated that Glu166 plays a role in holding a water molecule, which is necessary for the deacylation reaction, and that the hydrogen bond network among Lys73Nζ, Ser130Oγ, and the carboxyl group of the β-lactam antibiotics was formed by the uptake of β-lactam antibiotics by β-lactamase. The activation energy for this reaction was 33.3 kcal/mol, and it is very likely that the reaction occurred at body temperature. Subsequent calculation results obtained by using the model excluding Ser130 and the carboxyl group of the substrate indicated that the activation energy for this reaction was 40.8 kcal/mol, which is 7.5 kcal/mol higher than that of the previous reaction. It was found that the hydrogen bond network plays an important role in decreasing the activation energy for the tetrahedral intermediate formation reaction. Lys73Nζ, which is located at the edge of the hydrogen bond network, played a role in forming a hydrogen bond with Glu166Oε in order to help the deacylation reaction. The role of amino acid residues around the active site of class A β-lactamase was also discussed.

Key words β-lactamase; tetrahedral intermediate; *ab initio* molecular orbital method; hydrogen bond network; Lys73; deacylation reaction

β-Lactamases are produced by pathogenic bacteria and contribute to a resistance to β-lactam antibiotics by deteriorating the pharmacological effect of catalyzing the hydrolysis of the β-lactam ring.[1] β-Lactam antibiotics react with β-lactamase in the same way as penicillin-binding protein (PBP); *i.e.*, an acylation reaction is initiated by the opening reaction of the β-lactam ring. In the case of β-lactamase, however, the deacylation reaction occurs after the acylation reaction and its activity is recovered, which differs from PBP. We investigated the deacylation reaction in order to elucidate the catalytic mechanism of class A β-lactamase by quantum chemical calculations.

Since the report by Knox *et al.* suggested that the E166A mutant of β-lactamase from *Bacillus licheniformis* induces the accumulation of an acyl-enzyme intermediate,[2] the catalytic residue involved in the deacylation reaction has been presumed to be only Glu166. However, it is difficult to conclude that the deacylation reaction occurs only due to Glu166 because the distance between Ser70Oγ and Glu166Oε is too far to interact (*ca.* 3.74 Å) according to the results of our molecular dynamics (MD) study on the structure of β-lactam antibiotics–β-lactamase complex (Fig. 1). It is thought that not only Glu166 but also Lys73 is involved in the deacylation reaction because Lys73Nζ is located between Ser70 and Glu166 and interacts with Ser70Oγ and Glu166Oε, nearly forming hydrogen bonds (2.77 and 3.21 Å, respectively). Furthermore, it is thought that a hydrogen bond network among Lys73Nζ, Ser130Oγ and the carboxyl group of the substrate (β-lactam antibiotics) should be taken into account. Ishiguro *et al.* also discussed the importance of the hydrogen bond network based on the results of their molecular mechanics calculations.[3] In the present study, we investigated the tetrahedral intermediate formation process, which is the first step of the deacylation reaction by β-lactamase and is caused by

the interaction between a water molecule and β-lactam antibiotics (benzyl penicillin)–β-lactamase complex, by means of the *ab initio* molecular orbital (MO) method, and we clarified the activation energy using the structure and potential energy changes for the reaction and the function of the hydrogen bond network binding by Glu166Oε–Lys73Nζ–Ser70Oγ–Ser130Oγ–the carboxyl group of benzyl penicillin.
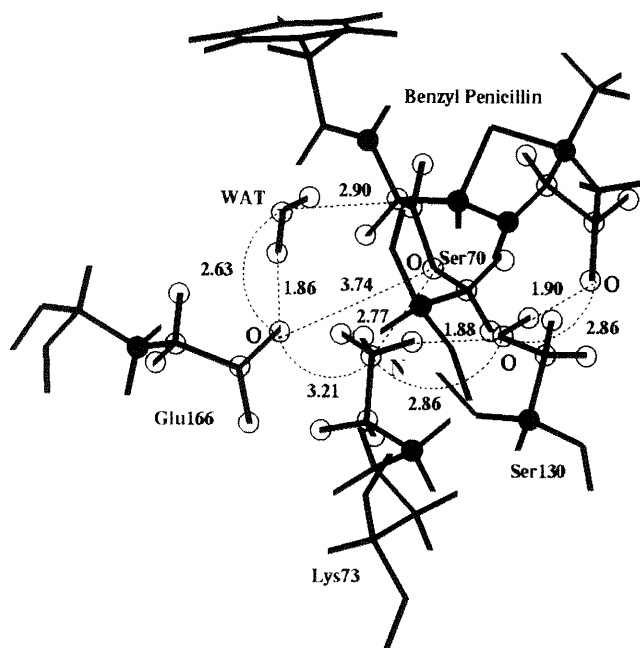

Fig. 1. Active Site of Benzyl Penicillin-Bound Acyl-Enzyme Intermediate Obtained by MD Calculation

Important residues for the deacylation reaction by β-lactamase are extracted and are shown in this figure. Numerals are distance between each atom in Å. WAT is a water molecule for the deacylation reaction by class A β-lactamase.

* To whom correspondence should be addressed.

Method

Construction of the Model for Calculations In order to obtain a model compound for quantum chemical calculations, the MD simulation was performed using the full structure of clavulanic acid-bound β-lactamase from *Staphylococcus aureus* PC1[4] registered in the Protein Data Bank (PDB).[5][7] Energy minimization and MD calculation were performed with the program package AMBER, Version 4.1.[8] The united-atom force field[9] was applied except for a substrate (clavulanic acid and benzyl penicillin), Ser70, Lys73, Ser130, Asn132, Glu166, Lys234 and Gln237, for which the all-atom force field[10] was used. The solvent was the TIP3P water model,[11] and a rectangular parallelepiped of about 4000 water molecules was generated by the Monte Carlo method.[8] The size is 67.4×54.7×47.4 Å. The center of the mass corresponded to that of the solute. To simplify this calculation, the SHAKE procedure[12] was used. The calculations of the non-bonded term were accelerated with a hardware accelerator, called MD-engine.[13] The MD simulation was performed starting from the energy minimized structure. The temperature was gradually increased by heating up to 310 K for the first 20 ps, then it was kept at 310 K for the next 100 ps. The trajectory at that temperature (310 K for 100 ps) was considered to be the most probable structure under physiologic conditions, and the average structure in the 100 ps MD simulation was obtained.

Since the β-lactam ring and the adjacent five-membered ring of clavulanic acid are cleaved in this data, the inhibitor was regenerated by closing the two rings, and a balanced structure was obtained by means of MD calculation for 100 ps at 310 K. A benzyl penicillin–β-lactamase complex as an acyl-enzyme intermediate was obtained by superimposing the β-lactam ring of benzyl penicillin on that of clavulanic acid in the above-mentioned complex. The complex was fully stabilized under an aqueous condition by MD calculation for 100 ps at 310 K, and the change in the distance of the hydrogen bond (below 3 Å) is not more than 0.1 Å.[14] The active site of the complex is shown in Fig. 1. The model for calculation was constructed by extracting the atoms represented by open and closed circles of benzyl penicillin, Ser70, Lys73, Glu166 and a water molecule (WAT) from the active site of the structure, all of which were considered to be involved in the reaction, and by replacing the atoms represented by closed circles with hydrogen atoms. In actual class A β-lactamase, the movement of residues is restricted by other residues around them. Movement of the carbonyl oxygen of benzyl penicillin binding with the enzyme is also restricted by the oxy-anion hole formed by two main-chain nitrogen atoms of Ser70 and Gln237.[15] To illustrate this fact in the constructed model, some of the atoms of the model were fixed to their initial positions in performing quantum chemical calculations. The fixed atoms are shown by asterisks in Figs. 4(a) and 7(A).

Quantum Chemical Calculation The Schrödinger equations of the model reaction system were solved by the *ab initio* MO method at the Hartree–Fock (HF) level using the 6-31G** basis set. The transition-state (TS) structure in the tetrahedral intermediate formation process of the deacylation reaction by class A β-lactamase was determined by geometry optimization using the energy gradient method, and it was confirmed by normal vibrational analysis that only one normal vibrational mode with imaginary frequency existed. The steepest path on the potential energy hypersurface from the TS structure in the forward and reverse directions of this normal vibrational mode was solved because the direction of the normal vibrational mode matches that of the reaction coordinate. The minimum structures on the potential energy hypersurface, which are located at the last point of the steepest path, are the initial and final states of the reaction, which were obtained theoretically. The computational program used was Gaussian 94.[16]

Results

The potential energy change following the steepest reaction path of the tetrahedral intermediate formation reaction in the deacylation reaction by class A β-lactamase and the structures that appeared on the reaction path are shown in Figs. 2 to 4, respectively.

TS Structure Starting from the model reaction system shown in Fig. 1, TS structure (c) was determined by geometry optimization. It was confirmed by normal vibrational analysis that only one normal vibrational mode with imaginary frequency existed. This is shown by arrows in Fig. 3. In the largest vibration, OH⁻ from H₂O approached the carbonyl carbon of β-lactam antibiotics binding with Ser70Oγ
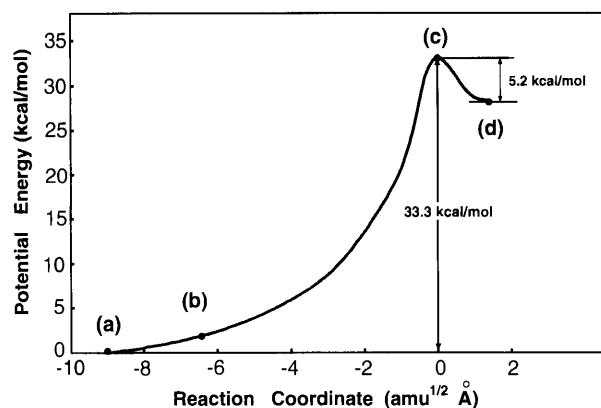

Fig. 2. The Lowest Potential Energy Change Following the Tetrahedral Intermediate Formation Reaction in the Deacylation Step by Class A β-Lactamase

Horizontal and vertical axes represent the reaction coordinates along the steepest path (amu$^{1/2}$ Å) and the potential energy change (kcal/mol), respectively.
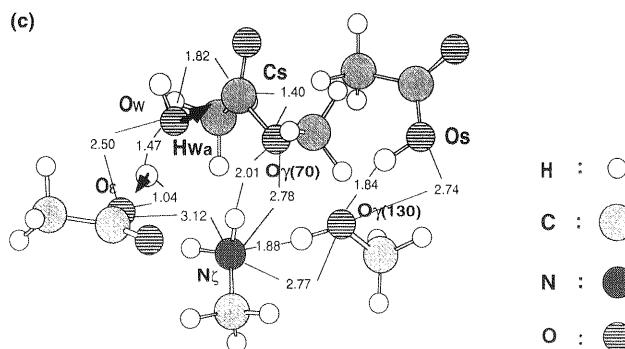

Fig. 3. TS Structure (c) of the Tetrahedral Intermediate Formation Reaction in the Deacylation Step by Class A β-Lactamase

Arrows represent the only normal vibrational mode with an imaginary frequency obtained by normal vibrational analysis.

(Cs), and the proton from H₂O approached Glu166 in the second largest vibration.

ES Complex Structure A minimum structure (a) on the potential energy hypersurface was obtained by calculating the steepest descent path along the reverse direction to the only normal vibrational mode with the imaginary frequency of the TS structure (c). Structure (a), which was obtained theoretically, was almost the same as that shown in Fig. 1, which was obtained experimentally, except for the positions of protons in the hydrogen bond network Lys73Nζ–Ser130Oγ–the carboxyl group of the substrate. In structure (a), a water molecule involved in the deacylation reaction formed a hydrogen bond with Glu166Oε (2.72 Å) and interacted with the carbonyl carbon atom of the substrate binding with Ser70Oγ (3.03 Å); i.e., Glu166Oε holds a water molecule in an ES complex. Glu166Oε interacted with Lys73Nζ (3.18 Å), and Lys73Nζ formed hydrogen bonds with Ser70Oγ (2.77 Å) and Ser130Oγ (2.81 Å). Ser130Oγ formed a hydrogen bond with the carboxyl oxygen of the substrate (2.73 Å). These results indicated that a hydrogen bond network was constructed in the ES complex.

Tetrahedral Intermediate Structure Structure (d) was obtained by calculating the steepest descent path along the only normal vibrational mode with the imaginary frequency of the TS structure (c). This structure (d) is the tetrahedral intermediate for the deacylation reaction by class A β-lacta-
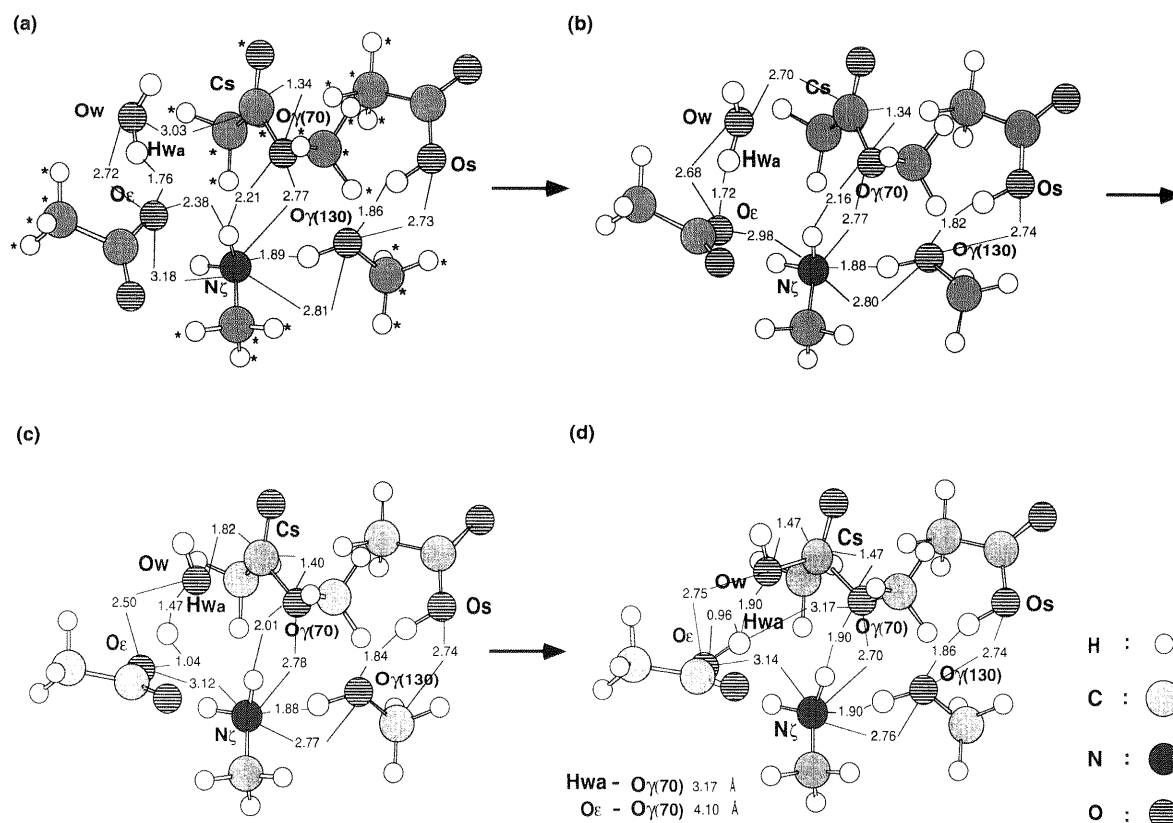
Fig. 4. Structural Changes Following the Tetrahedral Intermediate Formation Reaction in the Deacylation Step by Class A β-Lactamase

(a)—(d) correspond to that shown in Fig. 2

mase. The oxygen atom of the water molecule held by Glu166Oε in the ES complex (a) formed a covalent bond with the carbonyl carbon of the β-lactam ring bound with Ser70Oγ (1.47 Å) and a hydrogen bond with Glu166Oε (2.75 Å). The hydrogen bond chain Lys73Nζ–Ser130Oγ–the carboxyl oxygen atom of the substrate, was always maintained in the tetrahedral intermediate formation process.

Water Molecule-Holding Mechanism in the Deacylation Reaction by β-Lactamase In Fig. 4(a), proton migrations from Lys73Nζ to Ser130Oγ and from Ser130Oγ to the carboxyl oxygen of β-lactam antibiotics occurred. This change will be described in Discussion. When the water molecule held by Glu166Oε approached the carbonyl carbon of the β-lactam ring bound with Ser70Oγ, the structure shown in Fig. 3(b) appeared due to rotation of the water molecule and the carboxyl group of Glu166. The distance between the oxygen atom of the water molecule and the carbonyl carbon of the β-lactam ring was 2.70 Å. It should be noted that a hydrogen bond is formed between Glu166Oε and Lys73Nζ in structure (b). This hydrogen bond plays a role in stabilizing the water molecule which is held by Glu166 and is used for the deacylation reaction. When the water molecule approaches the carbonyl carbon of the β-lactam ring bound with Ser70Oγ, it begins to decompose into a proton and OH$^-$. Hwa, a proton in the water molecule, migrates to Glu166Oε, while OH$^-$ approaches the carbonyl carbon of the substrate, thereby leading to the formation of a TS structure (c). The distance between the proton Hwa and Glu166Oε is 1.04 Å, which is almost equal to the bond length of the O–H bond, and the distance between Ow of OH$^-$ and the carbonyl carbon Cs of the β-lactam ring of the substrate is

1.82 Å. The distance between Cs and Ser70Oγ increases gradually from 1.34 Å in structure (a) and becomes 1.40 Å in structure (c). It was clearly indicated in the vibrational mode shown in structure (c) (Fig. 3), that the proton from the water molecule which was involved in the deacylation reaction by class A β-lactamase connects with Glu166Oε, and OH$^-$ connects with the acyl carbon of the β-lactam ring of the substrate. Figure 2 shows that, starting from the ES complex structure (a), the reaction intermediate (d) was formed *via* structure (b) and the TS structure (c); *i.e.*, (a) was connected with (d) by the steepest path. It was found from the potential energy change shown in Fig. 2, that the activation energy for the tetrahedral intermediate formation reaction was 33.3 kcal/mol. It is very likely that this reaction occurs at body temperature. The role of Glu166 is to hold a water molecule for the deacylation reaction by class A β-lactamase in the reaction system. It is considered that an acyl intermediate accumulates in the Glu166Ala mutant of β-lactamase,[2] because the mutant loses this function.

Discussion

Reaction mechanism There have been many studies on mechanism of substrate inactivation by β-lactamase. Strynadka *et al.* reported from the result of their X-ray crystallographic analysis of RTEM-1 β-lactamase, that Lys73Nζ is neutral because the pK_a of Lys73 decreases due to a positive environment that is produced by residues around Lys73, that Lys73 only takes part in the acylation of the OH group of Ser70, and that only Glu166 takes part in the deacylation reaction of β-lactamase.[17] On the other hand, Damblon *et al.* showed from their NMR experiments that only Glu166, not

Lys73, takes part in the acylation reaction of Ser70Oγ and the deacylation reaction, because the pK_a of Lys73 is about 10 where protonated Lys73Nζ is stable.[18] Knox et al. reported that only Glu166 takes part in the deacylation reaction of β-lactamase on the basis of their experimental results which showed an accumulation of acyl intermediate in the Glu166Ala mutant of β-lactamase from Bacillus licheniformis.[2] Using the ab initio MO method, we investigated the tetrahedral intermediate formation reaction, which is the first step of the deacylation reaction of the substrate-bound class A β-lactamase, in the β-lactam antibiotics inactivation mechanism by β-lactamase, and found that Glu166 plays a role in holding the water molecule used for hydrolysis. As the above-mentioned scholars report, if only Glu166 takes part in

the deacylation reaction, then Hwa from the water molecule, which connects with Glu166, must migrate to Ser70Oγ (Fig. 4(d)). However, it is reasonable to assume that the proton migration occurs via a Glu166Oε–Lys73Nζ–Ser70Oγ hydrogen bond network rather than from Glu166, because the distance between Glu166Oε and Ser70Oγ is too far for proton migration to occur (4.10 Å, Fig. 4(d)). It should be considered that not only Glu166Oε but also Lys73Nζ take part in the deacylation reaction. Lys73Nζ, however, is neutral in structure (d) and it is necessary for proton migration from Lys73Nζ to Ser70Oγ to provide a proton from Glu166Oε or Ser130Oγ. It is thought that the proton might be provided from Ser130Oγ because a lone pair of Lys73Nζ is oriented toward Ser130Oγ. The mechanism is now being investigated.

Importance of the Carboxyl Group of the β-Lactam Antibiotics-Ser130-Lys73 Hydrogen Bond Network In
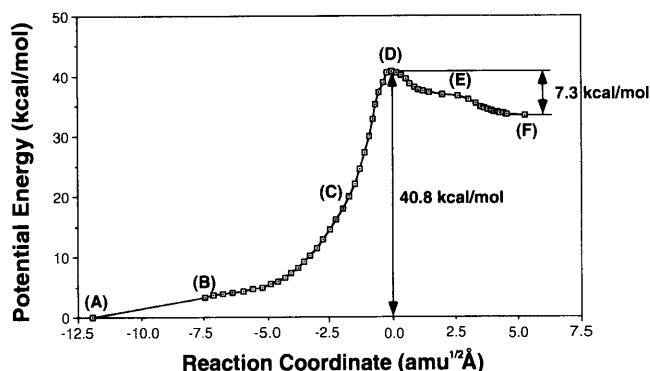

Fig. 5. The Lowest Potential Energy Change Following the Tetrahedral Intermediate Formation Reaction in the Deacylation Step by Class A β-Lactamase, Obtained by Using the Model Excluding Ser130 and a Carboxyl Group of the Substrate from that Shown in Fig. 4

Horizontal and vertical axes represent the reaction coordinate along the steepest path (amu$^{1/2}$ Å) and the potential energy change (kcal/mol), respectively.
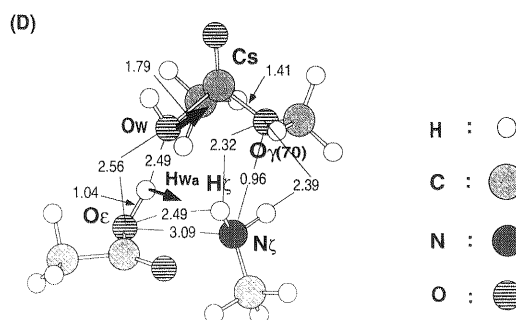

Fig. 6. TS Structure (D) of the Tetrahedral Intermediate Formation Reaction in the Deacylation Step by Class A β-Lactamase, Obtained by Using the Model Excluding Ser130 and a Carboxyl Group of Substrate from That Shown in Fig. 4

Arrows represent the only normal vibrational mode with an imaginary frequency obtained by normal vibrational analysis.
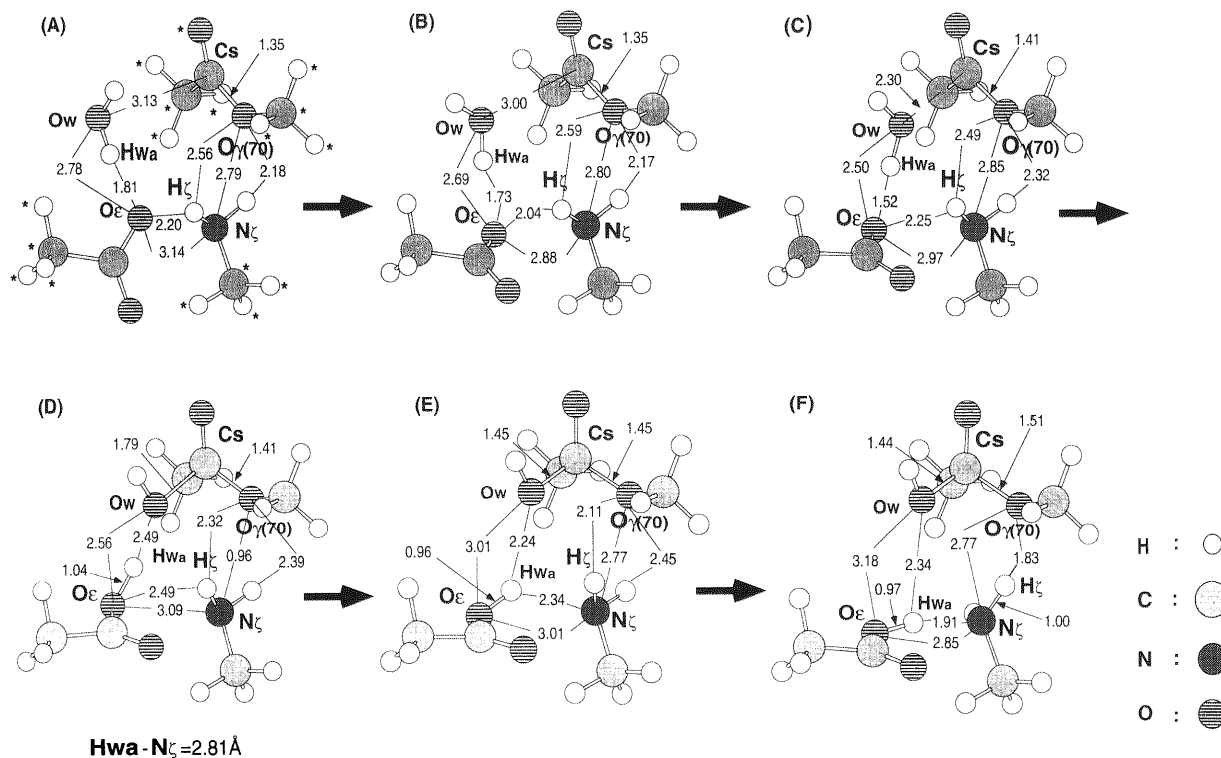

Hwa-Nζ =2.81Å

Fig. 7. Structural Changes Following the Tetrahedral Intermediate Formation Reaction in the Deacylation Step by Class A β-Lactamase, Obtained by Using the Model Excluding Ser130 and a Carboxyl Group of Substrate from That Shown in Fig. 4

(A)—(F) correspond to that shown in Fig. 5.

the previous section, it was stated that a hydrogen bond network is produced between Lys73, Ser130 and the carboxyl group of the β-lactam antibiotics, and that the proton relay between the hydrogen bond network is involved in the activity of class A β-lactamase. When the substrate, benzyl penicillin, is caught by β-lactamase, its carboxyl group is incorporated in the hydrogen bond network. The protonated Lys73Nζ is neutralized and is activated by the proton relay via Ser130Oγ. The mechanism in which the hydrogen bond network works effectively is shown in Fig. 4. The mechanism shown in this figure is reasonable because the potential energy of the structure, which assumes that the tetrahedral intermediate is produced without proton relay from Lys73Nζ to the carboxyl group of the substrate via Ser130Oγ, is 23.5 kcal/mol higher than that of structure (d).

Ser130 and the carboxyl group of the substrate were excluded from the model reaction system to estimate the effect of the Lys73–Ser130–substrate hydrogen bond network. The potential energy change and the structural changes obtained by quantum chemical calculations are shown in Figs. 5 to 7, respectively. A hydrogen atom of protonated Lys73Nζ, which forms a hydrogen bond with Ser130Oγ, was removed from this model structure because Ser130 was not included in the model structure. In Fig. 7, structural changes from an initial structure (A) to a TS structure (D) did not differ greatly from that in Fig. 4. However, it is observed in the only normal vibrational mode with an imaginary frequency of the TS structure (D) that proton Hwa from the water molecule involved in the deacylation reaction is oriented toward Lys73Nζ (Fig. 6). Moreover, after passing the TS structure (D), a point of inflection appeared in the potential energy change shown in Fig. 5, which did not appear in that shown in Fig. 4. The structure is shown in Fig. 7(E). Structure (E) is a point of inflection that appeared as a result of stabilization in which the proton Hwa from the water molecule changes its moving direction naturally in order to break the hydrogen bond with
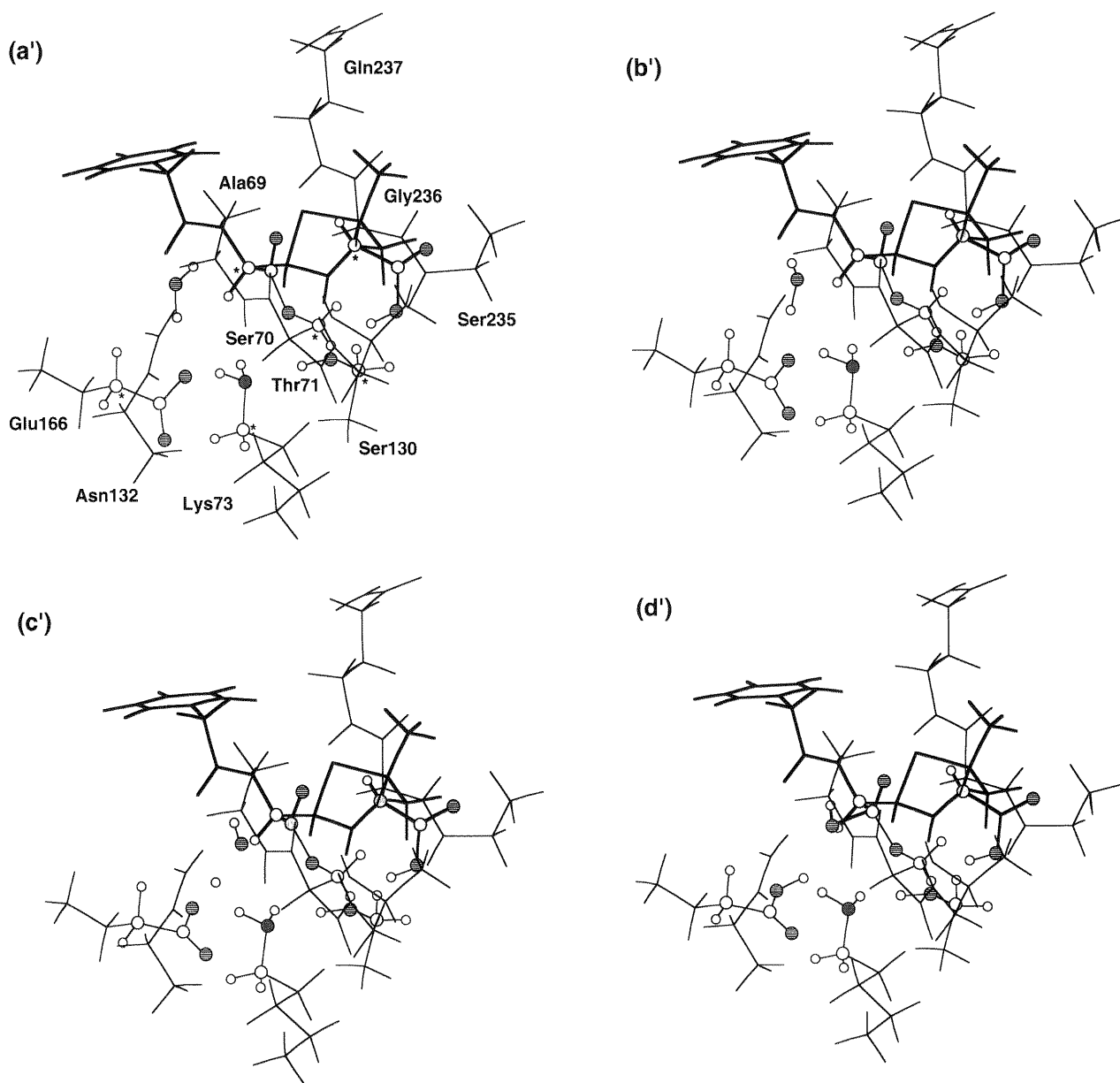

Fig. 8.   Structures of Expanded Models

Atoms which are also used for the elucidation of a tetrahedral intermediate formation reaction mechanism (Results) are shown by circles. In Results, atoms marked by asterisks in these figures were always fixed. Residue shown by a thick line is benzyl penicillin.

the Ow oxygen atom of the water molecule and to form a hydrogen bond with Lys73Nζ. From structure (E), the exchange of the hydrogen bond occurred and a stable tetrahedral intermediate (F) was produced; *i.e.*, in the tetrahedral intermediate structure (F), Hζ, which connects with Lys73Nζ, forms a hydrogen bond only with Ser70Oγ (1.83 Å), whereas in the TS structure (D), it interacts with Glu166Oε and Ser70Oγ, whose distances are 2.49 and 2.32 Å, respectively. It is thought that an exclusion of Ser130 and the carboxyl group of the β-lactam antibiotics causes these structural changes. Due to this exclusion, the activation energy of this reaction is 40.8 kcal/mol, which is 7.5 kcal/mol higher than that obtained in Results. For this reason, it is concluded that the hydrogen bond network consisting of Lys73, Ser130 and the carboxyl group of the β-lactam antibiotics plays an important role in remarkably decreasing the activation energy of the tetrahedral intermediate formation reaction, which is the first step of the deacylation reaction, by a proton relay among this network.

Role of Amino Acid Residues around the Active Site of Class A β-Lactamase It is considered that amino acid residues and solvent molecules, which are located around the active site, also affect enzymatic reaction mechanisms and the potential energy change. Though it is quantitatively difficult to take all these factors into computation, we constructed a larger model than that shown in Fig. 4, based on the structure shown in Fig. 1. The model is called expanded model. The expanded model includes four active site residues (Ser70, Lys73, Ser130, Glu166), six residues near the active-site (Ala69, Thr71, Asn132, Ser235, Gly236, Gln237) and the full structure of the benzyl penicilloyl moiety. The water molecule which is involved in the expanded model as a solvent molecule is only WAT, as shown in Fig. 1, because the nearest water molecule from WAT did not interact with the active site, including WAT.

From this structure, the positions of the atoms included in both the expanded model and the model reaction system in Fig. 4 were changed into those of structure (a) to (d) in Fig. 4. (Because atoms marked by asterisks in Fig. 4(a) were fixed through investigation on the deacylation reaction mechanism of class A β-lactamase, the positions of each atom are equal to those shown by asterisks in Fig. 8.) The structures are shown in Fig. 8.

An expanded model for an acyl-enzyme intermediate was also constructed. First, an acyl-enzyme intermediate (structure (Int.)) was optimized by the same method as described in Method. The geometry was almost the same as that shown in Fig. 1. Second, the optimized data was put through the same process, converting (a') to (d'). The structure (structure (Int.')) is shown in Fig. 9. For these expanded models, only potential energy calculations were performed at the HF level using a 6-31G** basis set because of computational limits.

The result is shown in Fig. 10. It should be noted that structure (Int') is more stable than structure (a'), although the potential energy of structure (Int.) is 6.4 kcal/mol higher than that of structure (a). This result suggests that the amino acid residues around the active site of class A β-lactamase might play an important role in the stabilization of protonated Lys73 and the carboxyl group of the substrate in acyl-enzyme intermediate. It is predicted that structure (Int') links to structure (a') by a proton relay from Lys73Nζ to the carboxyl
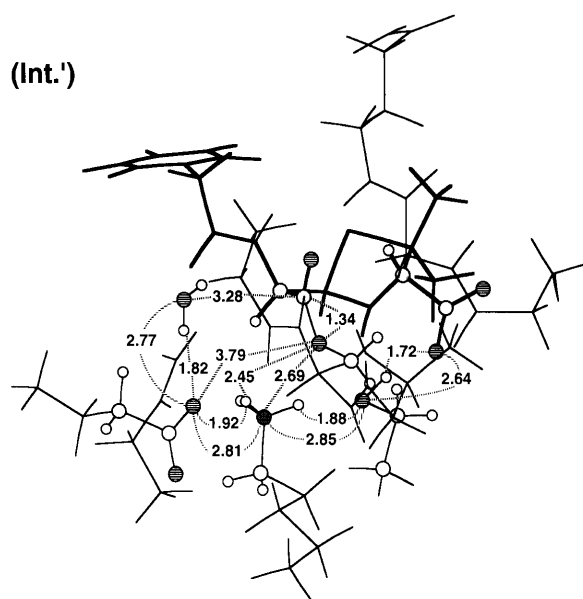

(Int.')

Fig. 9. Structure of Expanded Model (Int'.)

Atoms shown by circles are used for geometry optimization on the structure (Int.) (see text). Residue shown by a thick line is benzyl penicillin. Numerals are inter-atomic distances (Å) obtained by geometry optimization.
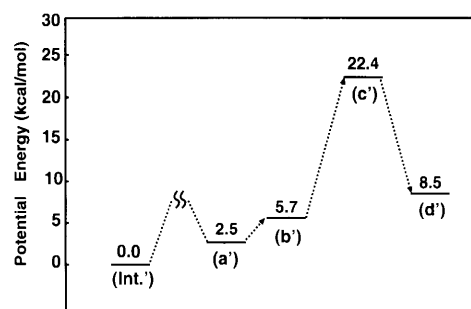

Fig. 10. Potential Energy Diagram on Structures (Int'.) and (a') to (d'), Which Were Obtained by Potential Energy Calculations at the HF/6-31G** Level

group of the substrate *via* Ser130Oγ, on the potential energy hypersurface. The mechanism is now being investigated.

The activation energy for tetrahedral intermediate formation process is 19.9 kcal/mol ((a')→(c')). The value is smaller than that shown in Fig. 2 (33.3 kcal/mol). Furthermore, the stabilization energy from the TS structure (c') to the tetrahedral intermediate (d') is 13.9 kcal/mol. The value is larger than that shown in Fig. 2 (5.2 kcal/mol, (c)→(d)). It is thought that the amino acid residues around the active-site of class A β-lactamase might also play roles in decreasing the activation energy for tetrahedral intermediate formation reaction and in stabilizing the tetrahedral intermediate.

Conclusions

The conclusions obtained in this investigation are as follows. 1. Glu166 plays a role in holding a water molecule, which is necessary for the deacylation reaction by class A β-lactamase. For this reason, an acyl intermediate accumulates in the Glu166Ala mutant. 2. The hydrogen bond network consisting of Lys73Nζ, Ser130Oγ and the carboxyl group of the β-lactam antibiotics is formed by the uptake of β-lactam antibiotics by β-lactamase, and plays an important role in de-

creasing the activation energy for the tetrahedral intermediate formation reaction, which is the first step of the deacylation reaction, by the proton relay among this network. 3. Lys73Nζ, which is located at the edge of the hydrogen network, forms a hydrogen bond with Glu166Oε in order to help the deacylation reaction by the water molecule held by Glu166. 4. Amino acid residues around the active site of class A β-lactamase might play the roles of stabilizing protonated Lys73 and the carboxyl group of the substrate in the acyl-enzyme intermediate, in stabilizing the tetrahedral intermediate, and in decreasing the activation energy for tetrahedral intermediate formation reaction.

References and Notes
1) Abraham E. P., Chain E. B., *Nature* (London), **146**, 837 (1940).
2) Knox J. R., Moews P. C., Escobar W. A., Fink A. L., *Protein Engineering*, **6**, 11—18 (1993).
3) Ishiguro M., Imajo S., *J. Med. Chem.*, **39**, 2207—2218 (1996).
4) Chen C. C. H., Herzberg O., *J. Mol. Biol.*, **224**, 1103—1113 (1992).
5) Bernstein F. C., Koetzle T. F., Williams G. J. B., Meyer E. F., Jr., Brice M. D., Rodgers J. R., Kennard O., Shimanouchi T., Tasumi M., *J. Mol. Biol.*, **112**, 535—542 (1977).
6) Abola E. E., Bernstein F. C., Bryant S. H., Koetzle T. F., Weng J., Protein Data Bank, in Crystallographic Databases - Information Content, Software Systems, Scientific Applications, Allen F. H., Bergerhoff G., Sievers R., eds., Data Commission of the International Union of Crystallography: Bonn/Cambridge/Chester, 1987; pp. 107—132.
7) Abola E. E., Manning N. O., Prilusky J., Stampf D. R., Sussman J. L., *J. Res. Natl. Inst. Stand. Technol.*, **101**, 231—241 (1996).
8) Pearlman D. A., Case D. A., Caldwell J. W., Ross W. S., Cheatham T. E. III, Ferguson D. M., Seibel G. L., Singh U. C., Weiner P. K., Kollman P. A., AMBER 4.1, University of California, San Francisco, 1995.
9) Weiner S. J., Kollman P. A., Case D. A., Singh U. C., Ghio C., Alagona G., Profeta S., Jr., Weiner P., *J. Am. Chem. Soc.*, **106**, 765—784 (1984).
10) Weiner S. J., Kollman P. A., Nguyen D. T., Case D. A., *J. Comput. Chem.*, **7**, 230—252 (1986).
11) Jorgensen W. L., Chandrasekhar J., Madura J. D., *J. Chem. Phys.*, **79**, 926—935 (1983).
12) Ryckaert J. P., Ciccotti G., Berendsen H. J. C., *J. Comput. Phys.*, **23**, 327—341 (1977).
13) Toyoda S., Miyagawa H., Kitamura K., Amisaki T., Hashimoto E., Ikeda H., Kusumi A., Miyakawa N., *J. Comput. Chem.*, **20**, 185—199 (1999).
14) Futatsugi, *et al.* performed a 100 ps MD calculation with a time step of 1 femto second (fs) by using an MD-engine.[13] When the average distances of one hundred continuous sets of coordinates were plotted, the fluctuation of the hydrogen bond distance (below 3 Å) was not more than 0.1 Å in 1 ps. This result is to be submitted for publication in *Nature*.
15) Herzberg O., *J. Mol. Biol.*, **217**, 701—719 (1991).
16) Frisch M. J., Trucks G. W., Schlegel H. B., Gill P. M. W., Johnson B. G., Robb M. A., Cheeseman J. R., Keith T., Petersson G. A., Montgomery J. A., Raghavachari K., Al-Laham M. A., Zakrzewski V. G., Ortiz J. V., Foresman J. B., Cioslowski J., Stefanov B. B., Nanayakkara A., Challacombe M., Peng C. Y., Ayala P. Y., Chen W., Wong M. W., Andres J. L., Replogle E. S., Gomperts R., Martin R. L., Fox D. J., Binkley J. S., Defrees D. J., Baker J., Stewart J. P., Head-Gordon M., Gonzalez C., Pople J. A., Gaussian 94, RevisionE2, Gaussian Inc., Pittsburgh, PA, 1995.
17) Strynadka N. C. J., Adachi H., Jensen S. E., Johns K., Sielecki A., Betzel C., Sutoh K., James M. N. G., *Nature* (London), **359**, 700—705 (1992).
18) Damblon C., Raquet X., Lian L.-Y., Lamotte-Brasseur J., Fonze E., Charaier P., Roberts G. C. K., Frére J.-M., *Proc. Natl. Acad. Sci. U.S.A.*, **93**, 1747—1752 (1996).

454

Chem. Pharm. Bull. **48**(4) 454—457 (2000)

Vol. 48, No. 4

Enzymatic Reactivity and Anti-tumor Activity of 1-(β-D-Arabinofuranosyl)-2-thiocytosine Derivatives

Takeo Kawaguchi,*,[a] Tomohisa Ichikawa,[a] Tetsuya Hasegawa,[a] Mineo Saneyoshi,[b]
Toshiyuki Wakayama,[c] Hisatoyo Kato,[c] Ayako Yukita,[c] and Toshiyuki Nagata[c]

*Department of Pharmaceutical Sciences, Josai University,[a] 1-1 Keyakidai, Sakado, Saitama 320–0295, Japan, Department
of Biological Sciences, Teikyo University of Science and Technology,[b] 2525 Yatsuzawa, Uenohara, Yamanashi 409–0133,
Japan, and Tsukuba Research Laboratory, Toagosei Co., Ltd.,[c] 2 Ohkubo, Tsukuba, Ibaraki 300–2611, Japan.
Received July 19, 1999; accepted December 18, 1999*

Sixteen derivatives of 1-(β-D-arabinofuranosyl)-2-thiocytosine (araSC), including five 5′-esters, three 3′-esters, five N^4-amides and three 5′-phosphodiesters, were synthesized and their reactivity to mouse tissue homogenates, including plasma, liver and intestine, and antitumor activity in mice bearing P388 cells were measured. The ester derivatives had a potent effect on the enzyme systems while the amide and phosphodiester derivatives were less active. The reactivity of ester derivatives was highly dependent on their chemical structure. The reactivity of amides and phosphodiester derivatives on mouse plasma and intestinal homogenate was also dependent on the chemical structure, although their action on intestinal enzymes was very similar. Two of eight ester derivatives showed considerable antitumor activity *in vivo*, although they also showed serious toxicity indicated by a weight loss in the mice. Four out of five amides and two out of three phosphodiesters showed antitumor activity, and two were highly effective (>200% in T/C, the ratio of the mean survival time of the treated group to that of the control group) with only a very slight weight loss.

Key words 1-(β-D-arabinofuranosyl)-2-thiocytosine; enzymatic regeneration; P388; tissue homogenate; prodrug

1-(β-D-Arabinofuranosyl)-2-thiocytosine (araSC) is a sulfur-substituted derivative of arabinosylcytosine (araC).[1] Our previous studies demonstrated that it exhibited potent cytotoxicity and unique cytokinetics.[2] The cytotoxic effect of araSC against several tumor cell lines *in vitro* is comparable or slightly less than that of araC, although the antitumor activity *in vivo* is dependent on many factors and can be modified by changes in retention, enzymatic and chemical stability, physicochemical properties, *etc.* To improve its activity as an antitumor agent, and obtain information to help in further possible modifications, sixteen derivatives of araSC were synthesized. Each carried a different chemical moiety with an ester, amide or phosphodiester linkage. These derivatives can behave as prodrugs, regenerating the parent compound, araSC, following enzymatic and/or chemical hydrolysis in the body. The effects of these compounds were examined in mice bearing P388 leukemia cells, and the relationship between the activity and enzymatic reactivity to tissue homogenates will be discussed.

Materials and Methods

Chemicals AraC was purchased from Yamasa Co. (Choshi, Japan). AraSC was prepared from uridine by the method reported by Ruyle and Shen.[1] AraSC derivatives (Table 1) were synthesized from araSC hydrochloride, purified and identified by the following methods.

General Procedure for Obtaining 5′-O-Acyl Derivatives (1—5) AraSC (3.0 mmol) was dissolved in 10 ml *N*,*N*-dimethylacetamide, and the appropriate acyl chloride (3.3 mmol) was added dropwise. After stirring at room temperature for 2 d, water (0.5 ml) was added to the solution which was then concentrated under reduced pressure. The residue was partitioned between ethyl acetate and aq. NaHCO₃ and the organic layer was separated, washed twice with NaCl-saturated water, dried with Na₂SO₄, and concentrated *in vacuo*. The residue was purified by silica gel column chromatography to afford 5′-O-acyl araSC. This material was dissolved in methanol, and aq. HCl was added. Excess HCl and solvent were removed under reduced pressure. The residue was recrystallized from ethyl acetate–hexane.

1-(5′-O-Octanoyl-β-D-arabinofuranosyl)-2-thiocytosine (**1**): Yield: 77%, ¹H-NMR (DMSO-d_6+D₂O) δ: 0.85 (3H, t, *J*=6.8 Hz, CH₃), 1.25 (8H, br s, CH₂×4), 1.54 (2H, br t, COCH₂CH₂), 2.33 (2H, t, *J*=7.8 Hz, COCH₂), 3.96

(1H, s, 3′-H), 4.08 (1H, m, 4′-H), 4.21 (1H, dd, *J*=4.9, 11.72 Hz, 5′-H), 4.25 (1H, d, 2′-H), 4.38 (1H, dd, *J*=4.9, 11.7 Hz, 5′-H), 6.47 (1H, d, *J*=7.8 Hz, 5-H), 6.73 (1H, d, *J*=3.4 Hz, 1′-H), 7.89 (1H, d, *J*=7.8 Hz, 6-H). FAB-MS *m/z*: 386 (55, MH⁺), 259 (3, M⁺−base), 128 (100, base+2H⁺).

1-(5′-O-Lauroyl-β-D-arabinofuranosyl)-2-thiocytosine (**2**): Yield: 71%, mp 111—113 °C. ¹H-NMR (DMSO-d_6) δ: 0.85 (3H, t, *J*=6.8 Hz, CH₃), 1.23 (16H, br s, CH₂×8), 1.53 (2H, m, COCH₂CH₂), 2.33 (2H, t, *J*=7.3 Hz, COCH₂), 3.95 (1H, m, 3′-H), 4.07 (1H, ddd, *J*=2.0, 4.4, 7.8 Hz, 4′-H), 4.21 (1H, dd, *J*=4.4, 11.7Hz, 5′-H), 4.25 (1H, m, 2′-H), 4.37 (1H, dd, *J*=7.8, 11.7 Hz, 5′-H), 6.42 (1H, d, *J*=7.8 Hz, 5-H), 6.74 (1H, d, *J*=2.9 Hz, 1′-H), 7.88 (1H, d, *J*=7.8 Hz, 6-H). FAB-MS *m/z*: 442 (32, MH⁺), 315 (2, M⁺−base), 183 (3, C₁₁H₂₃CO⁺), 128 (100, base+2H⁺). *Anal.* Calcd for C₂₁H₃₅N₃O₅SHCl: C, 52.76; H,7.59; N,8.79. Found: C, 52.51; H, 7.49; N, 8.79.

1-(5′-O-Myristoyl-β-D-arabinofuranosyl)-2-thiocytosine (**3**): Yield: 95%, mp 124—125 °C. ¹H-NMR (DMSO-d_6) δ: 0.86 (3H, t, *J*=6.8 Hz, CH₃), 1.23 (20H, br s, CH₂×10), 1.54 (2H, m, COCH₂CH₂), 2.33 (2H, t, *J*=7.3 Hz, COCH₂), 3.95 (1H, m, 3′-H), 4.07 (1H, ddd, *J*=1.5, 4.4, 7.8 Hz, 4′-H), 4.21 (1H, dd, *J*=4.4, 11.7 Hz, 5′-H), 4.25 (1H, dd, *J*=1.5, 2.9 Hz, 2′-H), 4.37 (1H, dd, *J*=7.8, 11.7 Hz, 5′-H), 6.40 (1H, d, *J*=7.8 Hz, 5-H), 6.75 (1H, d, *J*=2.9 Hz, 1′-H), 7.87 (1H, d, *J*=7.8 Hz, 6-H). FAB-MS *m/z*: 470 (5, MH⁺), 343 (1, M⁺−base), 211 (5, C₁₃H₂₇CO⁺), 128 (40, base+2H⁺), 112 (100, cytosine). *Anal.* Calcd for C₂₃H₃₉N₃O₅SHCl: C, 54.58; H, 7.97; N, 8.30. Found: C, 54.22; H, 7.95; N, 8.25.
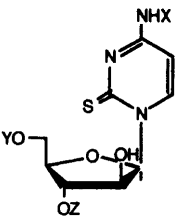
1-(5′-O-Palmitoyl-β-D-arabinofuranosyl)-2-thiocytosine (**4**): Yield: 90%, mp 88—89 °C. ¹H-NMR (CDCl₃) δ: 0.88 (3H, t, *J*=6.8 Hz, CH₃), 1.25 (24H, br s, CH₂×12), 1.61 (2H, br t, COCH₂CH₂), 2.35 (2H, m, COCH₂), 4.16 (2H, br s, 3′-H and 4′-H), 4.33 (1H, m, 5′-H), 4.46 (1H, m, 5′-H), 4.73 (1H, br s, 2′-H), 6.12 (1H, d, *J*=7.3 Hz, 5-H), 6.91 (1H, s, 1′-H), 7.74 (1H, d, *J*=7.3 Hz, 6-H). FAB-MS *m/z*: 498 (17, MH⁺), 371 (2, M⁺−base), 239 (2 C₁₅H₃₁CO⁺), 128 (100, base+2H⁺). *Anal.* Calcd for C₂₅H₄₃N₃O₅S: C, 60.33; H, 8.71; N, 8.44. Found: C, 60.75; H, 9.24; N, 8.15.

1-(5′-O-Stearoyl-β-D-arabinofuranosyl)-2-thiocytosine (**5**): Yield: 53%, mp 120—122 °C. ¹H-NMR (DMSO-d_6) δ: 0.86 (3H, t, *J*=6.8 Hz, CH₃), 1.23 (28H, br s, CH₂×14), 1.53 (2H, m, COCH₂CH₂), 2.33 (2H, t, *J*=7.3 Hz, COCH₂), 3.96 (1H, br s, 3′-H), 4.08 (1H, ddd, *J*=2.0, 4.4, 8.3 Hz, 4′-H), 4.21 (1H, dd, *J*=4.4, 11.7 Hz, 5′-H), 4.25 (1H, dd, *J*=3.4 Hz, 2′-H), 4.38 (1H, dd, *J*=8.3, 11.7 Hz, 5′-H), 6.47 (1H, d, *J*=7.8 Hz, 5-H), 6.72 (1H, d, *J*=3.4 Hz, 1′-H), 7.89 (1H, d, *J*=7.8 Hz, 6-H). FAB-MS *m/z*: 526 (13, MH⁺), 128 (100, base+2H⁺). *Anal.* Calcd for C₂₇H₄₇N₃O₅SHCl: C,57.68; H,8.60; N, 7.47. Found: C, 57.32; H, 8.60; N, 7.48.

General Procedure for Obtaining 3′-O-Ester Derivatives (6—8) O²,2′-Anhydro-1-(3′-O-acyl-β-D-arabinofuranosyl)cytosine hydrochloride

Table 1. Chemical Structures of AraSC and Its Derivatives

Comp. No.	X	Y	Z	mp (°C)
AraSC	H	H	H	125—126
1	H	CO(CH$_2$)$_6$CH$_3$	H	Syrup
2	H	CO(CH$_2$)$_{10}$CH$_3$	H	111—113
3	H	CO(CH$_2$)$_{12}$CH$_3$	H	124—125
4	H	CO(CH$_2$)$_{14}$CH$_3$	H	88—89
5	H	CO(CH$_2$)$_{16}$CH$_3$	H	120—122
6	H·HCl	H	CO(CH$_2$)$_6$CH$_3$	180—181
7	H·HCl	H	CO(CH$_2$)$_{12}$CH$_3$	179—180
8	H·HCl	H	CO(CH$_2$)$_{16}$CH$_3$	176—177
9	CO(CH$_2$)$_7$CH$_3$	H	H	101—102
10	CO(CH$_2$)$_{12}$CH$_3$	H	H	105—107
11	CO(CH$_2$)$_{14}$CH$_3$	H	H	102—104
12	CO(CH$_2$)$_{16}$CH$_3$	H	H	115—116
13	CO(CH$_2$)$_{18}$CH$_3$	H	H	92—93
14	H	PO(ONa)O(CH$_2$)$_7$CH$_3$	H	195—197 (dec.)
15	H	PO(ONa)O(CH$_2$)$_{13}$CH$_3$	H	200 (dec.)
16	H	PO(ONa)O(CH$_2$)$_{17}$CH$_3$	H	214—216 (dec.)

was obtained by the reaction of 2-acyloxyisobutyryl chloride and cytidine.[3] O^2,2'-Anhydro-1-(3'-O-acyl-β-D-arabinofuranosyl)cytosine hydrochloride (10 mmol), NH$_4$HCO$_3$ (40 mmol) and NaSH (40 mmol) were added to anhydrous N,N-dimethylformamide (20 ml), and stirred for 15 h at room temperature. The reaction mixture was poured into water and extracted with ethyl acetate. The organic layer was washed twice with NaCl-saturated water, and dried with Na$_2$SO$_4$. After removal of the solvent under reduced pressure, the residue was dissolved in methanol and aq. HCl was added dropwise. The deposited crystals were filtered and dried to obtain 1-(3'-O-acyl-β-D-arabino-furanosyl)-2-thiocytosine hydrochloride.

· 1-(3'-O-Octanoyl-β-D-arabinofuranosyl)-2-thiocytosine Hydrogen Chloride (6): Yield: 45%, mp 180—181 °C. ^{1}H-NMR (DMSO-d_6+D$_2$O) δ: 0.86 (3H, t, J=6.8Hz, CH$_3$), 1.27 (8H, br s, CH$_2$×4), 1.56 (2H, br t, J=6.8 Hz, COCH$_2$CH$_2$), 2.38 (2H, t, J=7.3 Hz, COCH$_2$), 3.68 (2H, m, 5'-H), 4.07 (1H, m, 4'-H), 4.38 (1H, dd, J=1.0, 3.4 Hz, 2'-H), 4.97 (1H, s, 3'-H), 6.37 (1H, d, J=7.8Hz, 5-H), 6.67 (1H, d, J=3.4Hz, 1'-H), 8.00 (1H, d, J=7.8 Hz, 6-H). FAB-MS m/z: 386 (50, MH$^+$), 259 (3, M$^+$−base), 128 (100, base+2H$^+$). *Anal.* Calcd for C$_{17}$H$_{27}$N$_3$O$_5$SHCl: C, 48.39; H, 6.69; N, 9.96. Found: C, 47.99; H, 6.86; N, 9.82.

1-(3'-O-Myristoyl-β-D-arabinofuranosyl)-2-thiocytosine Hydrogen Chloride (7): Yield: 69%, mp 179—180 °C. ^{1}H-NMR (DMSO-d_6+D$_2$O) δ: 0.86 (3H, t, J=6.8Hz, CH$_3$), 1.24 (20H, br, s, CH$_2$×10), 1.54 (2H, m, COCH$_2$CH$_2$), 2.37 (2H, t, J=7.3 Hz, COCH$_2$), 3.66 (1H, dd, J=5.9, 11.7Hz, 5'-H), 3.71 (1H, dd, J=6.4, 11.7 Hz, 5'-H), 4.06 (1H, m, 4'-H), 4.38 (1H, d, J=3.4 Hz, 2'-H), 4.97 (1H, s, 3'-H), 6.46 (1H, d, J=7.8 Hz, 5-H), 6.63 (1H, d, J=3.4 Hz, 1'-H), 8.03 (1H, d, J=7.8 Hz, 6-H). FAB-MS m/z: 470 (15, MH$^+$), 343 (3, M$^+$−base), 211 (3, C$_{13}$H$_{27}$CO$^+$), 128 (100, base+2H$^+$). *Anal.* Calcd for C$_{23}$H$_{39}$N$_3$O$_5$SHCl: C, 54.58; H, 7.97; N, 8.30. Found: C, 54.81; H, 8.14; N, 8.44.

1-(3'-O-Stearoyl-β-D-arabinofuranosyl)-2-thiocytosine hydrogen chloride (8): Yield: 50%, mp 176—177 °C. ^{1}H-NMR (DMSO-d_6+D$_2$O) δ: 0.86 (3H, t, J=6.8 Hz, CH$_3$), 1.24 (28H, br s, CH$_2$×14), 1.55 (2H, br t, J=6.8 Hz, COCH$_2$CH$_2$), 2.37 (2H, t, J=7.3 Hz, COCH$_2$), 3.66 (1H, dd, J=5.9, 11.7Hz, 5'-H), 3.70 (1H, dd, J=6.8, 11.7 Hz, 5'-H), 4.06 (1H, m, 4'-H), 4.38 (1H, d, J=3.4 Hz, 2'-H), 4.97 (1H, s, 3'-H), 6.46 (1H, d, J=7.8 Hz, 5-H), 6.63 (1H, d, J=3.4 Hz, 1'-H), 8.03 (1H, d, J=7.8 Hz, 6-H). FAB-MS m/z: 526 (10, MH$^+$), 399 (2, M$^+$−base), 128 (100, base+2H$^+$). *Anal.* Calcd for C$_{27}$H$_{47}$N$_3$O$_5$SHCl: C, 57.68; H, 8.60; N, 7.47. Found: C, 57.34; H, 8.52; N, 7.59.

General Procedure for Obtaining N^4-acyl Derivatives. (9—13) To a solution of araSC (5.0 mmol) in 25 ml pyridine was added trimethylchlorosi-

lane (25.0 mmol) dropwise. The mixture was stirred for 30 min at room temperature, and the appropriate acyl chloride (5.5 mmol) was added to the solution, followed by stirring for 1 h. The reaction mixture was cooled in an ice bath, and water was added. The mixture was concentrated under reduced pressure, diluted with chloroform, washed twice with water, dried with MgSO$_4$, and concentrated *in vacuo*. The residue was diluted with chloroform (30 ml) and 3.5 ml trifluoroacetic acid was added, followed by stirring for 30 min. The mixture was concentrated under reduced pressure, diluted with chloroform, washed twice with water, and dried with MgSO$_4$. The chloroform layer was concentrated *in vacuo* and the residue was crystallized from methanol to afford N^4-acyl-araSC.

N^4-Nonanoyl-1-(β-D-arabinofuranosyl)-2-thiocytosine (9): Yield: 53%, mp 101—102 °C. ^{1}H-NMR (DMSO-d_6+CDCl$_3$) δ: 0.88 (3H, t, J=6.4Hz, CH$_3$), 1.28 (10H, m, CH$_2$×5), 1.67 (2H, m, COCH$_2$CH$_2$), 2.43 (2H, t, J=6.8 Hz, COCH$_2$), 3.87 (2H, m, 5'-H), 4.20 (2H, m, 3'-H and 4'-H), 4.63 (1H, m, 2'-H), 5.37 (3H, br s, OH), 6.95 (1H, d, J=4.0Hz, 1'-H), 7.70 (1H, d, J=7.6 Hz, 5-H), 8.42 (1H, d, J=7.6Hz, 6-H), 10.50 (1H, br s, NH). FAB-MS m/z: 400 (35, MH$^+$), 268 (100, N-(COC$_8$H$_{17}$)-base+2H$^+$), 128 (80, base+2H$^+$). *Anal.* Calcd for C$_{18}$H$_{29}$N$_3$O$_5$S: C, 54.12; H, 7.32; N, 10.52. Found: C, 54.51; H, 7.54; N, 10.54.

N^4-Myristoyl-1-(β-D-arabinofuranosyl)-2-thiocytosine (10): Yield: 82%, mp 105—107 °C. ^{1}H-NMR (DMSO-d_6) δ: 0.85(3H, t, J=6.4 Hz, CH$_3$), 1.24 (20H, m, CH$_2$×10), 1.55 (2H, m, COCH$_2$CH$_2$), 2.41 (2H, t, J=6.8 Hz, COCH$_2$), 3.64 (2H, m, 5'-H), 3.93 (2H, m, 3'-H and 4'-H), 4.36 (1H, m, 2'-H), 5.09 (1H, br s, 5'-OH), 5.52 (2H, m, 2'-OH and 3'-OH), 6.87 (1H, d, J=3.6 Hz, 1'-H), 7.59 (1H, d, J=7.2 Hz, 5-H), 8.24 (1H, d, J=7.2 Hz, 6-H), 11.27 (1H, br s, NH). FAB-MS m/z: 470 (35, MH$^+$), 338 (100, N-(COC13H$_{27}$)-base+2H$^+$), 128 (80, base+2H$^+$). *Anal.* Calcd for C$_{23}$H$_{39}$N$_3$O$_5$S: C, 58.82; H, 8.37; N, 8.95. Found: C, 58.46; H, 8.56; N, 8.80.

N^4-Palmitoyl-1-(β-D-arabinofuranosyl)-2-thiocytosine (11): Yield: 82%, mp 102—104 °C. ^{1}H-NMR (DMSO-d_6) δ: 0.85 (3H, t, J=6.8 Hz, CH$_3$), 1.24 (24H, m, CH$_2$×12), 1.54 (2H, m, COCH$_2$CH$_2$), 2.40 (2H, t, J=7.2 Hz, COCH$_2$), 3.64 (2H, m, 5'-H), 3.93 (2H, m, 3'-H and 4'-H), 4.36 (1H, m, 2'-H), 5.09 (1H, t, J=5.6 Hz, 5'-OH), 5.51 (2H, m, 2'-OH and 3'-OH), 6.87 (1H, d, J=3.6 Hz, 1'-H), 7.59 (1H, d, J=7.2 Hz, 5-H), 8.24 (1H, d, J=7.2 Hz, 6-H), 11.26 (1H, br s, NH). FAB-MS m/z: 498 (21, MH$^+$), 366 (80, N-(COC$_{15}$H$_{31}$)-base+2H$^+$), 128 (100, base+2H$^+$). *Anal.* Calcd for C$_{25}$H$_{43}$N$_3$O$_5$S: C, 60.33; H, 8.71; N, 8.44. Found: C, 59.98; H, 8.89; N, 8.34.

N^4-Stearoyl-1-(β-D-arabinofuranosyl)-2-thiocytosine (12): Yield: 81%, mp 115—116 °C. ^{1}H-NMR (DMSO-d_6) δ: 0.85 (3H, t, J=6.8 Hz, CH$_3$), 1.24 (28H, m, CH$_2$×14), 1.54 (2H, m, COCH$_2$CH$_2$), 2.41 (2H, t, J=7.2 Hz,

COCH₂), 3.64 (2H, m, 5'-H), 3.93 (2H, m, 3'-H and 4'-H), 4.36 (1H, m, 2'-H), 5.09 (1H, br s, 5'-OH), 5.52 (2H, m, 2'-OH and 3'-OH), 6.87 (1H, d, $J=3.6$ Hz, 1'-H), 7.59 (1H, d, $J=8.0$ Hz, 5-H), 8.24 (1H, d, $J=8.0$ Hz, 6-H), 11.27 (1H, br s, NH). FAB-MS m/z: 526 (15, MH⁺), 394 (60, N-(COC₁₇H₃₅)-base+2H⁺), 128 (100, base+2H⁺). Anal. Calcd for C₂₇H₄₇N₃O₅S: C, 61.68; H, 9.01; N, 7.99. Found: C, 61.98; H, 9.05; N, 7.81.

N^4-Eicosanoyl-1-(β-D-arabinofuranosyl)-2-thiocytosine (13): Yield: 70%, mp 92—93 °C. ¹H-NMR (DMSO-d_6+CDCl₃) δ: 0.88 (3H, t, $J=6.4$ Hz, CH₃), 1.20 (32H, m, CH₂×16), 1.63 (2H, m, COCH₂CH₂), 2.44 (2H, t, $J=7.6$ Hz, COCH₂), 3.81 (2H, m, 5'-H), 4.12 (1H, m, 4'-H), 4.18 (1H, m, 3'-H), 4.47 (1H, m, 2'-H), 5.31 (3H, m, OH), 6.99 (1H, d, $J=3.6$ Hz, 1'-H), 7.71 (1H, d, $J=7.6$ Hz, 5-H), 8.42 (1H, d, $J=7.6$ Hz, 6-H), 10.85 (1H, br s, NH). FAB-MS m/z: 554 (10, MH⁺), 422 (40, N-(COC₁₉H₃₉)-base+2H⁺), 128 (100, base+2H+). Anal. Calcd for C₂₉H₅₁N₃O₅S: C, 62.90; H, 9.28; N, 7.59. Found: C, 63.25; H, 9.34; N, 7.49.

General Procedure for Obtaining 5'-O-(O-alkylphosphate) Derivatives (14—16) A solution of araSC (5.0 mmol) and trimethylphosphate (20 ml) was cooled to −10 °C, and phosphoryl chloride (7.5 ml) was added dropwise. After stirring for 2 h at room temperature, the appropriate alcohol (20 mmol) dissolved in 40 ml tetrahydrofuran (THF) was added, followed by stirring at room temperature for 18 h. The reaction mixture was poured into ice-water (200 ml) containing NaHCO₃ (1.89 g). After extraction with diethyl ether, the aqueous layer was adjusted to pH 1—2, and extracted with CHCl₃. The CHCl₃ layer was concentrated under reduced pressure, and the residue was recrystallized from CHCl₃–EtOH to afford 5'-O-(O-alkylphosphate) derivatives. This material was suspended in 20 ml water, and adjusted to pH 7 by addition of 1 N NaOH. After addition of MeOH (100 ml) to the mixture, the solution was cooled to 4—5 °C. The insoluble materials were filtered off, and the filtrate was concentrated under reduced pressure. The residue was crystallized from H₂O–EtOH to afford 5'-O-(O-alkylphosphate) sodium salt.

1-(5'-O-(O-Octylphosphate)-β-D-arabino-furanosyl)-2-thiocytosine Sodium Salt (14): Yield: 25%, mp 195—197 °C (decomp.). ¹H-NMR (D₂O) δ: 0.72 (3H, t, $J=6.8$ Hz, CH₃), 1.11 (10H, m, CH₂×5), 1.50 (2H, m, P(O)OCH₂CH₂), 3.77 (2H, m, 3'-H and 4'-H), 4.02—4.10 (4H, m, 5'-H and P(O)OCH₂), 4.55 (1H, m, 2'-H), 6.27 (1H, d, $J=8.0$ Hz, 5-H), 6.96 (1H, d, $J=5.6$ Hz, 1'-H), 7.92 (1H, d, $J=8.0$ Hz, 6-H). FAB-MS m/z: 496 (10, MNa⁺), 474 (10, MH⁺), 347 (12, M⁺−base), 128 (100, base+2H⁺). Anal. Calcd for C₁₇H₂₉N₃O₇PSNa: C, 43.13; H, 6.17; N, 8.88. Found: C, 42.84; H, 6.30; N, 8.61.

1-(5'-O-(O-Myristylphosphate)-β-D-arabinofuranosyl)-2-thiocytosine Sodium Salt (15): Yield: 54%, mp 200 °C (decomp.). ¹H-NMR (D₂O) δ: 0.65 (3H, t, $J=6.8$ Hz, CH₃), 1.03 (22H, m, CH₂×11), 1.49 (2H, m, P(O)OCH₂CH₂), 3.77 (2H, m, 3'-H and 4'-H), 3.95—4.20 (4H, m, 5'-H and P(O)OCH₂), 4.59 (1H, m, 2'-H), 6.33 (1H, d, $J=7.6$ Hz, 5-H), 6.87 (1H, d, $J=5.6$ Hz, 1'-H), 8.00 (1H, d, $J=7.6$ Hz, 6-H). FAB-MS m/z: 580 (10, MNa⁺), 558 (10, MH⁺), 431 (15, M⁺−base), 128 (100, base+2H⁺). Anal. Calcd for C₂₃H₄₁N₃O₇PSNa: C, 49.54; H, 7.41; N, 7.54. Found: C, 49.22; H, 7.32; N, 7.36.

1-(5'-O-(O-Stearoylphosphate)-β-D-arabinofuranosyl)-2-thiocytosine Sodium Salt (16): Yield: 39%, mp 214—216 °C (decomp.). ¹H-NMR (D₂O) δ: 0.66 (3H, t, $J=6.8$ Hz, CH₃), 1.04 (30H, m, CH₂×15), 1.51 (2H, m, P(O)OCH₂CH₂), 3.79 (2H, m, 3'-H and 4'-H), 3.95—4.25 (4H, m, 5'-H and P(O)OCH₂), 4.59 (1H, m, 2'-H), 6.33 (1H, d, $J=7.6$ Hz, 5-H), 6.87 (1H, d, $J=5.6$ Hz, 1'-H), 8.00 (1H, d, $J=7.6$ Hz, 6-H). FAB-MS m/z: 636 (10, MNa⁺), 614 (10, MH⁺), 487 (15, M⁺−base), 128 (100, base+2H⁺). Anal. Calcd for C₂₇H₄₉N₃O₇PSNa: C, 52.84; H,8.05; N, 6.85. Found: C, 52.65; H, 8.21; N, 6.74.

HPLC Analysis For quantitative analysis of araSC and its derivatives, the following mixtures were used as the mobile phase on a C18 reversed-phase (LiChrospher RP-18(e), 5 μm) 250×4 mm column at a flow rate of 1.0 ml/min: mixtures of water, methanol and acetic acid for the 3' or 5' esters; mixtures of water and methanol for the N^4-acyl derivatives; mixtures of 0.05 M phosphate buffer (pH 7.0) and acetonitrile for the acylphosphates; and a mixture of 0.02 M phosphate buffer (pH 7.0) and methanol for araSC. The wavelength of the spectrophotometer was set at 280 nm with an attenuation of 0.01 AUFS.

Measurement of Enzymatic Hydrolysis Rates Male ddY mice (25—28 g) were obtained from Tokyo Laboratory Animals (Saitama, Japan) and sacrificed to obtain blood, liver and intestine. The blood was centrifuged at 1000×g for 15 min, and the resulting plasma was stored at −40 °C until use. The tissues were homogenized with pH 7.0 isotonic phosphate buffer (0.1 M) containing 0.19 M sucrose at 0 °C to give a concentration of 4.0% (w/v). Aliquots of 1 ml of the homogenates were transferred to small glass tubes
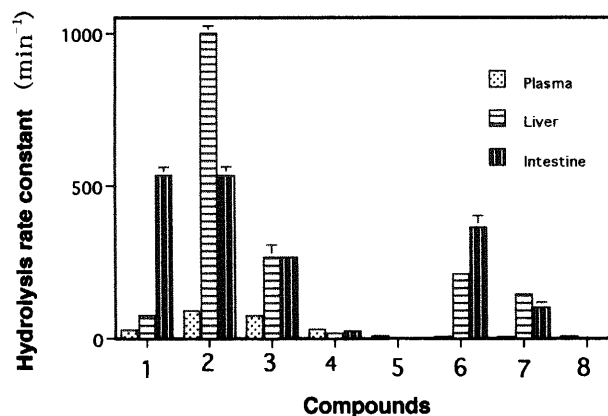

Fig. 1. Enzymatic Hydrolysis Rate of Ester Derivatives (1—8)

and stored at −80 °C until use. No reduction in the enzyme activity of the stored samples, evaluated by monitoring the hydrolysis of 2, 10 and 15, was observed during the experimental period (~12 weeks).

The enzymatic hydrolysis rates were determined in the presence of one of the enzyme systems diluted with an isotonic phosphate buffer (pH 7.0) containing 0.19 M sucrose and the experiments were perfomed at 37 °C. Hydrolysis was initiated by adding the stock solution to the test solution at an initial concentration of 4×10⁻⁵ M, the lowest concentration suitable for quantitative analysis of the derivatives. To confirm complete dissolution of the compound, another measurement was performed at a concentration of 8×10⁻⁵ M for all compounds. Changes in the concentration of both the derivatives and parent compound, araSC, were followed by HPLC analysis of samples taken periodically from the reaction mixture. The effect on enzymatic hydrolysis was evaluated as pseudo-first-order rate constants for 1.0% (w/v) plasma or homogenates.

Measurement of Chemical Hydrolysis Rates The chemical hydrolysis rates of the araSC derivatives were measured in an isotonic phosphate buffer (pH 7.0) containing 0.19 M sucrose at 37 °C. The reactivity was evaluated as described above.

Evaluation of Antitumor Activity Male CDF1 mice were purchased from Tokyo Laboratory Animals (Saitama, Japan). Mice (20—23 g) in groups of five were inoculated intraperitoneally with 1×10⁶ P388 leukemia cells. The compound suspension was given intraperitoneally on days 1, 2, 3, 4 and 5 starting 24 h after inoculation. The antitumor activities were recorded as T/C (%), the ratio of the mean survival time of the treated group (T) to that of the control group (C). To evaluate side-effects, the body weight of animals in each group was measured at the start of the experiment and on day 5.

Results and Discussion

The enzymatic reactivity of the carboxyester derivatives (1—8) is shown in Fig. 1. These derivatives regenerate parent compound, araSC, quantitatively. Higher reactivity was observed with the C6—C10 esters, and this decreased with increasing alkyl chain length in both the 3'- and 5'-esters. The reactivity to plasma enzyme system was weaker in the 3'-than in the 5'-esters. This was similar to our previous observations on 5-fluoro-2'-deoxyuridine derivatives.[4] The enzymatic reactivities of the N^4-amides and 5'-phosphodiesters are quite different from those of the carboxyesters (Fig. 2). Reactivities of these derivatives are much weaker than those of carboxyester derivatives (note the units of the vertical axis). Reactivity to intestinal homogenate was almost equivalent, although those to plasma and liver were depended on the chemical structure. Derivatives with the shortest alkyl chain, 9 and 14, showed higher reactivity, and this reactivity decreased with increasing alkyl chain length. Similar observations have been reported for the enzymatic regeneration of araC from its N4-amide prodrug, enocitabine,[5,6] and the 5'-phosphodiester prodrug, cytarabine ocfosfate.[7,8]
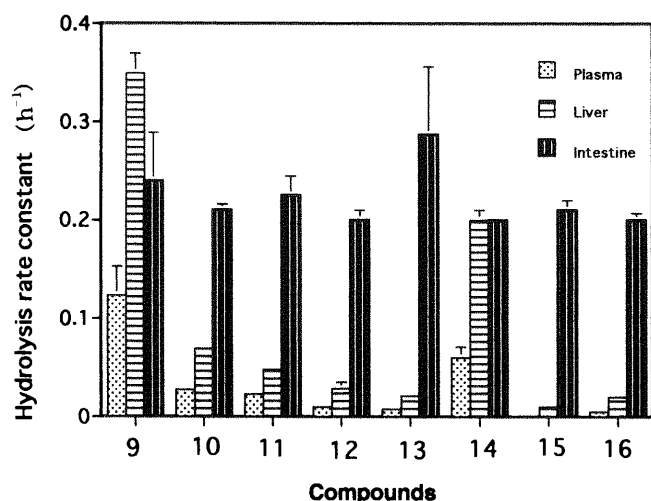
Fig. 2. Enzymatic Hydrolysis Rate of N^4-Amide and 5'-Phosphodiester Derivatives (9—16)

Table 2. Antitumor Activity of Compounds 1—8

Compounds	T/C (dose[a], mg/kg/day)				Weight change[b]			
	75	100	150	300	75	100	150	300
1	—	104	—	44	—	−0.4	—	0/5[c]
2	—	100	—	50	—	−0.3	—	0/5[c]
3	—	63	—	220	—	−2.7	—	−5.0
4	—	115	—	130	—	−0.5	—	−1.5
5	134	—	155	173	+2.1	—	+1.9	−0.3
6	98	—	78	39	−0.1	—	−0.7	−3.2
7	—	113	—	124	—	+1.6	—	−0.4
8	136	—	148	138	+1.1	—	+2.3	+2.8
AraSC	—	95	—	103	—	+2.8	—	+2.5

a) Suspension was given intraperitoneally on days 1, 2, 3, 4 and 5 starting at 24 h after inoculation. b) Body weight was measured at the start and on day 5. Changes are indicated as an average. c) None of the 5 mice survived to day 5.

The antitumor activity of the carboxyester derivatives were shown in Table 2. Only compounds 3 and 5 showed activity over 150% in T/C. Compound 3 showed activity over 200% in T/C at the highest dose, although its toxicity, indicated by weight loss, was serious (5.0 g/mouse). There was no clear relationship between the antitumor activity and enzymatic reactivity of these ester derivatives. Physicochemical properties other than biological reactivity may be more important factors for their activation to parent drug.

With the exception of compound 9, the N4-amide derivatives showed an antitumor effect (>150% in T/C) (Table 3). Compounds 10 and 11 showed high activity (>200% in T/C), although both resulted in marked weight loss (>5.0 g/mouse) at a dose of 300 mg/kg/d. Compound 9 showed no antitumor activity but toxic. This compound also showed relatively high reactivity to plasma and liver, as did in com-

Table 3. Antitumor Activity of Compounds 9—16

Compounds	T/C (dose[a], mg/kg/day)			Weight change[b]		
	75	150	300	75	150	300
9	98	94	69	+0.8	−0.6	−1.7
10	143	165	222	−2.3	−3.6	−5.5
11	143	166	223	−1.1	−4.0	−5.9
12	153	179	196	+3.0	+1.7	+2.3
13	135	150	178	+1.6	+2.2	+0.2
14	111	109	113	+5.5	+3.5	+3.8
15	105	150	189	+5.0	+1.8	−0.3
16	118	142	210	+6.1	+2.9	−0.1

a) Suspension was given intraperitoneally on days 1, 2, 3, 4 and 5 starting at 24 h after inoculation. b) Body weight was measured at the start and on day 5. Changes are indicated as an average.

pound 14 which also showed little antitumor activity. Of the 5'-phosphodiesters, compounds 15 and 16 showed high activity (>200% in T/C) with very little weight loss (less than 0.5 g/mouse). All compounds had a greater reactivity to intestinal homogenate than to plasma and liver homogenate (except 9 to liver), although this high reactivity to the intestine may not reflect their activity because of the administration route used in this experiment (Table 3).

The antitumor activity of antimetabolites is highly dependent on their release or administration rate in the body. To obtain an appropriate rate of administration, rate of enzymatic regeneration of the parent compound is manipulated by chemical modification(s). Of the derivatives studied here, compounds 15 and 16 showed promising characteristics. Both compounds showed very low reactivity to plasma and liver enzyme systems and, therefore, their regeneration of araSC is slow and prolonged release of araSC is expected. Since intraperitoneal administration was employed in this study, the intestinal enzyme system may not play a major role in the activation process. Further investigation using other administration routes (e.g. oral) should provide more information.

REFERENCES

1) Ruyle W. V., Shen T. Y., J. Med. Chem., 10, 331—334 (1967).
2) Kawaguchi T., Ichikawa T., Hasegawa T., Saneyoshi M., Yukita A., Asano M., Wakayama T., Kato H., Nagata T., Biol. Pharm. Bull., 22, 100—102 (1999).
3) Hamamura E. K., Prystasz M., Verheyden J. P. H., Moffatt J. G., J. Med. Chem., 19, 654—662 (1976).
4) Kawaguchi T., Fukushima S., Hayashi Y., Nakano M., Pharm Res., 5, 741—744 (1988).
5) Tsuruo T., Iida H., Hori K., Tsukagoshi S., Sakurai Y., Cancer Res., 41, 4484—4488 (1981).
6) Oh-ishi J., Kataoka T., Tsukagoshi S., Sakurai Y., Shibukawa M., Kobayashi H., Cancer Res., 41, 2501—2506 (1981).
7) Saneyoshi M., Morozumi M., Komada K., Machida H., Kuninaka A., Yoshino H., Chem Pharm. Bull., 28, 2915—2923 (1980).
8) Komada K., Morozumi M., Saito K., Jpn. J. Cancer Res., 80, 679—685 (1989).

A Comparison of Cellactose with Two *ad hoc* Processed Lactose–Cellulose Blends as Direct Compression Excipients

Marta Casalderrey, Consuelo Souto, Angel Concheiro, José L. Gómez-Amoza, and Ramón Martínez-Pacheco*

Departamento de Farmacia y Tecnologia Farmacéutica. Facultad de Farmacia, Universidad de Santiago de Compostela, 15706, Santiago de Compostela, Spain. Received July 21, 1999; accepted December 9, 1999

Three processed lactose–cellulose blends of similar composition, particle size and true density were compared as direct compression excipients: one was prepared by dry granulation, one by extrusion–spheronization, and the commercial product Cellactose. Differences among their flow properties depended solely on their different sphericities. Unlike those of the other blends, Cellactose particles exhibited numerous macropores. The mean yield pressures of all three blends were similar to those of direct compression lactoses. Cellactose tablets prepared at a punch pressure that largely eliminated macropores (pores >1 µm) had better mechanical properties but much poorer disintegration than tablets of the other blends prepared at the same punch pressure. However, the tensile strength and disintegration time of Cellactose tablets both fell rapidly as macropore volume was increased by reducing punch pressure, while the enthalpy of wetting/dissolution rose. The strength and water-resistance of well-compacted Cellactose tablets is attributed to the spatial distribution of lactose and cellulose in Cellactose particles, rather than to β-lactose content or extra-particular structural features.

Key words   coprocessed excipients; Cellactose; direct compression

Since the 1980s, considerable attention has been paid to direct compression excipients prepared by co-processing two or more components by means of powder engineering techniques such as coating or controlled agglomeration.[1] For direct compression tabletting, processed blends of this kind have been shown to be superior to both traditional single-component excipients[2—7] and simple mixtures of single-component excipients.[8,9] It is therefore striking that practically nothing has been published concerning the influence of particle structure and morphology on the behaviour of processed blends. As a step towards filling this gap, in this work we compared the properties of Cellactose, a typical processed blend for direct compression, with those of two granulates of similar composition and particle size, one prepared by dry granulation and the other by extrusion–spheronization.

Materials and Methods

Materials Cellactose (a processed 3 : 1 (w/w) mixture of lactose monohydrate and powdered cellulose), from Meggle, was supplied by Fher S.A. (lot 919). α-Lactose monohydrate Ph. Eur., was from Merck (lot 2444543). Avicel PH 101, from FMC Corp., was supplied by C. Barcia S.A. (lot 5648). Magnesium stearate B.P., was supplied by C. Barcia S.A. (lot 548).

Preparation of Excipients Cellactose was used as supplied. Fig.1 shows its particle size distribution, as determined by sifting a sample taken with a Quantachrome rotary microriffler through 500, 400, 315, 200, 105, 75 and 45 µm meshes in a Retsch Vibro sifter.

The dry-granulated blend (hereinafter excipient B) was prepared by blending a 3 : 1 mixture of α-lactose monohydrate and Avicel PH 101 in a Turbula T2C mixer for 15 min at 30 rpm, compacting the blend in 300 mg tablets in a sensorized Bonals B/MT eccentric tabletting machine[10] using 9 mm flat punches and a pressure of 90 MPa, fragmenting the tablets in an Erweka AR400 apparatus, separating the resulting granules in size fractions as described above for Cellactose, and blending suitable amounts of the various fractions in a Turbula T2C mixer for 15 min at 30 rpm so as to reproduce the particle size distribution of Cellactose.

The third blend (hereinafter excipient C) was prepared by blending a 3 : 1 mixture of α-lactose monohydrate and Avicel PH 101 in a Turbula T2C mixer as described above for excipient B, mixing 100 g samples of the blend with 25 ml of distilled water in a Heidolph RZR 50 planetary mixer for 10 min at 300 rpm, extruding the wet mass through 500 µm meshes in a Caleva Model 10 extruder, spheronizing the extruded pellets in a Caleva Model

120 for 10 min at 3000 rpm, drying the resulting granules under a current of hot air (40 °C) for 24 h, and separating and recombining particle size fractions as described for excipient B so as to reproduce the particle size distribution of Cellactose.

Characterization of the Blends α-Lactose and β-Lactose Contents: Powder X-Ray Diffraction. The excipient was pressed into a sample holder and the surface was smoothed with a glass slide. Room temperature X-ray diffractograms were recorded between 5 and 50°2θ in a Phillips PW1710 powder diffractometer using monochromatic CuK$_\alpha$ radiation and a scan rate of 1.2°2θ/min.

Gas Chromatography (GC). α-Lactose and β-lactose were determined by GC as per Dwivedi and Mitchell,[11] as follows. A sample of excipient was derivatized in 19.5 : 22.0 : 58.5 (v/v) dimethylsulphoxide/N-trimethylsilylimidazole/pyridine. Aliquots of this solution were injected into a Perkin Elmer 3700 GC apparatus equipped with the column described by Dwivedi and Mitchell.[11] The carrier gas was nitrogen (flow rate 20 ml/min), and the injector and column temperatures were 260 and 205 °C, respectively. The proportions of α- and β-lactose were calculated from the areas of the corresponding peaks (t_R=6—7 and 10—11 min, respectively). Final results (%) are the means of triplicate determinations.

Differential Scanning Calorimetry (DSC). DSC thermograms of 2—3 mg samples of excipient hermetically sealed in aluminium pans were recorded at a heating rate of 10 °C/min in a Shimadzu DSC-50 instrument. Dehydration enthalpy was estimated from the area of the endothermic peaks near 150 °C, and the enthalpy of the melting of lactose from that of the peak in the 215—235 °C region.
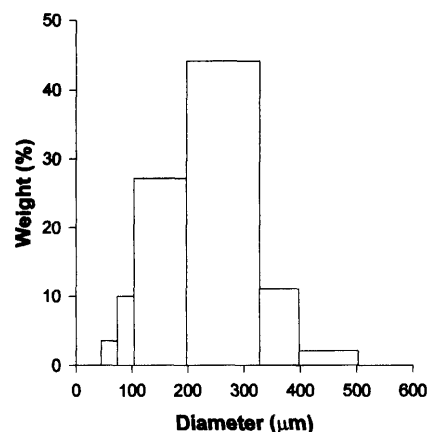

Fig. 1.   Particle Size Distribution of Cellactose

* To whom correspondence should be addressed.

Hydration Water Content: Using a Shimadzu TGA-50 apparatus, hydration water was determined thermogravimetrically as the weight lost by 2.5 mg samples over the range of 130—160 °C when heated at a rate of 10 °C/min. All determinations were performed in duplicate.

Sorbed Water Content: Samples initially weighing approximately 3 g were kept at 70 °C on a Shimadzu Libror EB-250 thermobalance until their weight remained constant. Sorbed water content was expressed as a percentage of initial total weight.

Enthalpy of Wetting/Dissolution: Enthalpies of wetting/dissolution at 25 °C were determined by immersion calorimetry using 0.1—0.2 g samples and a Tronac Mod. 458 calorimeter with a 50 ml reaction vessel containing 50 ml of distilled water.[12] All determinations were performed in duplicate.

True Density: True densities were determined in triplicate in a Quantachrome model PY2 helium pycnometer.

Particle Morphology: Photomicrographs of excipient particles (250X) were obtained by scanning electron microscopy (SEM) using a Jeol JSM T-220A microscope. Particle circularity[13] was determined using an Olympus SZ-60 stereomicroscope equipped with a PC Image VGA24 v.2.1. image analysis system (Foster Findlay Ass.).

Micropore Structure: Mercury Intrusion Porosimetry. Samples were placed in a 3 ml powder sample holder, and intruded mercury volume was determined over the pressure interval 0.6—25000 psi in a Micromeritics 9305 pore sizer. The pore volume distribution and corresponding total porosity were calculated from these data following the manufacturer's instructions.[14] All determinations were performed in triplicate.

Nitrogen Adsorption. Excipient samples were degassed by heating at 70 °C and 10^{-3} mm Hg for 24 h. Nitrogen adsorption was determined in triplicate in a Micromeritics ASAP 2000 instrument at 77 K and at relative pressures of 0.01—0.98. Specific surfaces were estimated by means of the BET model.[15] Pore size distributions were determined from the nitrogen adsorption isotherms by the BJH method.[15]

Flow Properties: Bulk Density. Bulk density was determined over 20 min in a Hosokawa PT-E Powder Tester operating at 50 taps/min. Compressibility was calculated from the initial and final bulk densities.[16]

Shear Strength. Shear strength was determined using an IPT RO-200 automatic apparatus equipped with a rotational split-level shear cell.[17] Duplicate samples of each excipient were subjected to three consolidation loads to obtain three yield loci with final normal stresses of 50, 150 and 250 g/cm². Flow factor was calculated as the reciprocal of the slope of the line obtained by regressing the unconfined yield stresses on the corresponding major consolidation stresses.[17,18]

Compression Properties: 99.5 : 0.5 (w/w) mixtures of excipient and magnesium stearate were prepared over 5 min in a Turbula T2C mixer operated at 30 rpm, and samples were tabletted in a Bonals B/MT excentric tabletting machine equipped with 9 mm flat punches and a compression data acquisition system.[10] Mean yield pressures (Py) were estimated from Heckel plots of the upper punch force-displacement data for three punch cycles.[19]

Preparation of Tablets Using the same mixtures and tabletting machine as described above and a punch pressure of 160 MPa, 250 mg tablets of each blend were prepared at a rate of 8 tablets/min. In addition, 250 mg

Cellactose tablets were prepared under the same conditions using punch pressures of 5, 50 and 100 MPa.

Characterization of Tablets Tensile Strength: The crushing strengths of six tablets of each formulation were determined using an Erweka TB2A apparatus; mean tensile strengths were then calculated from these results and the dimensions of each tablet,[20] which were measured using a Mitsutoyo digital micrometer (measuring range, 0—25 mm; precision, ±0.001 mm).

Friability: Friability was determined by measuring the weight lost in 15 min by 10 tablets in an Erweka TAP apparatus operated at 20 rpm.

Disintegration Time: Tablet disintegration time in distilled water was determined in a Turu-Grau apparatus conforming to the specifications of USP23 (1995). Results are the means of values for six tablets.

Specific Surface Area and Microporous Structure: The specific surface areas of the tablets, and their pore size distributions, were determined by the same means used for the untabletted excipients (section 2.3.7). The pore size distributions were used to obtain the total volume of pores >1 μm in diameter.

Results and Discussion

The X-ray diffractograms of all the excipients (Fig. 2) showed the expected peak for α-lactose at 12.6°2θ, but not the characteristic β-lactose peak at 10.5°2θ.[21,22] However, gas chromatography showed β-lactose contents ranging from
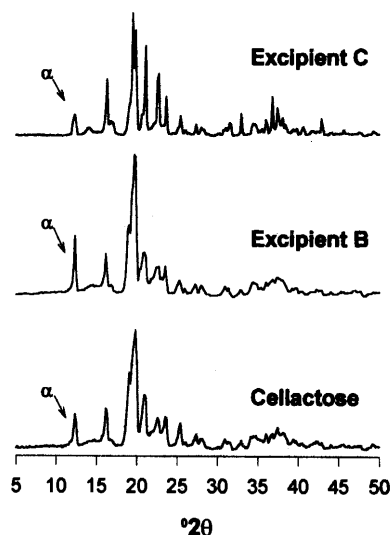
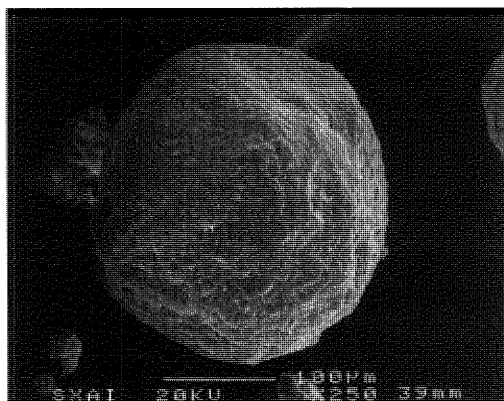Fig. 2. X-Ray Diffractograms of Cellactose and Two ad hoc Processed Cellulose/Lactose Blends

The peak for α-lactose is marked 'α'.

Table 1. Properties of Cellactose and Two ad hoc Processed Cellulose/Lactose Blends

Parameter	Excipient		
	Cellactose	B	C
Dehydration temperature, °C	152	151	151
Dehydration enthalpy, $-J \cdot g^{-1}$	107.5 (1.54)	114.9 (1.80)	109.3 (1.25)
Lactose melting temperature, °C	219	219	217
Lactose melting enthalpy, $-J \cdot g^{-1}$	79.3 (1.1)	95.5 (1.6)	91.5 (1.3)
β-Lactose content, %	8.35 (0.91)	1.11 (0.05)	2.91 (0.67)
True density, $g \cdot cm^{-3}$	1.5278 (0.0075)	1.5273 (0.0039)	1.5316 (0.0017)
Hydration water, %	3.02 (0.03)	3.39 (0.26)	3.23 (0.01)
Sorbed water, %	1.55 (0.04)	1.56 (0.04)	1.32 (0.19)
Wetting/dissolution enthalpy, $-J \cdot g^{-1}$	33.60 (0.90)	35.31 (1.26)	33.47 (2.61)
Circularity	0.754	0.735	0.817
Specific surface area, $m^2 \cdot g^{-1}$	1.14 (0.00)	1.19 (0.01)	0.49 (0.01)
Compressibility, %	23.54 (0.11)	36.83 (0.13)	14.64 (0.77)
Flow factor	11.07	6.07	27.24
Mean yield pressure, MPa	125.79 (1.10)	138.55 (4.56)	189.48 (7.66)

Mean values, with standard deviations in parentheses.

Excipient C

Excipient B
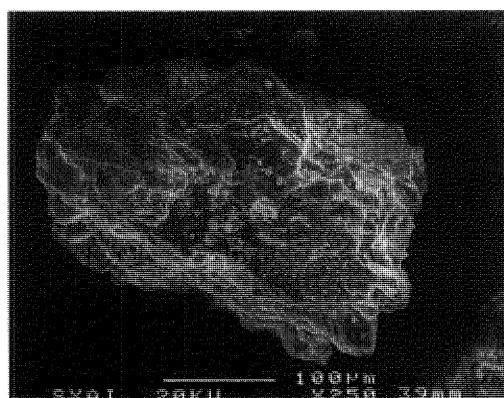
Cellactose

Fig. 3. Photomicrographs of Particles of Cellactose and Two *ad hoc* Processed Cellulose/Lactose Blends

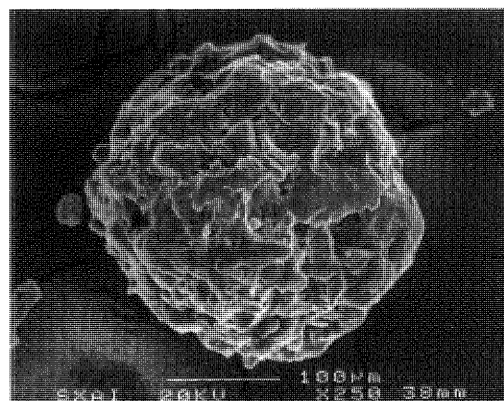1.1% for excipient B to 8.4% for Cellactose (Table 1). Because of the close correlation ($r = -0.9934$) between β-lactose content and the enthalpy of the melting of lactose as determined from the area of the lactose melting peak in DSC thermograms, the enthalpy of the melting of lactose was significantly lower for Cellactose than for excipients B and C (Table 1). The DSC peak for α-lactose dehydration appeared, as expected, near 145 °C.

Its greater β-lactose content may also be held responsible for the hydration water content of Cellactose being slightly lower than that of the other excipients (Table 1), β-lactose being anhydrous. All three excipients had very similar sorbed water contents and very similar enthalpies of wetting/dissolution (Table 1).
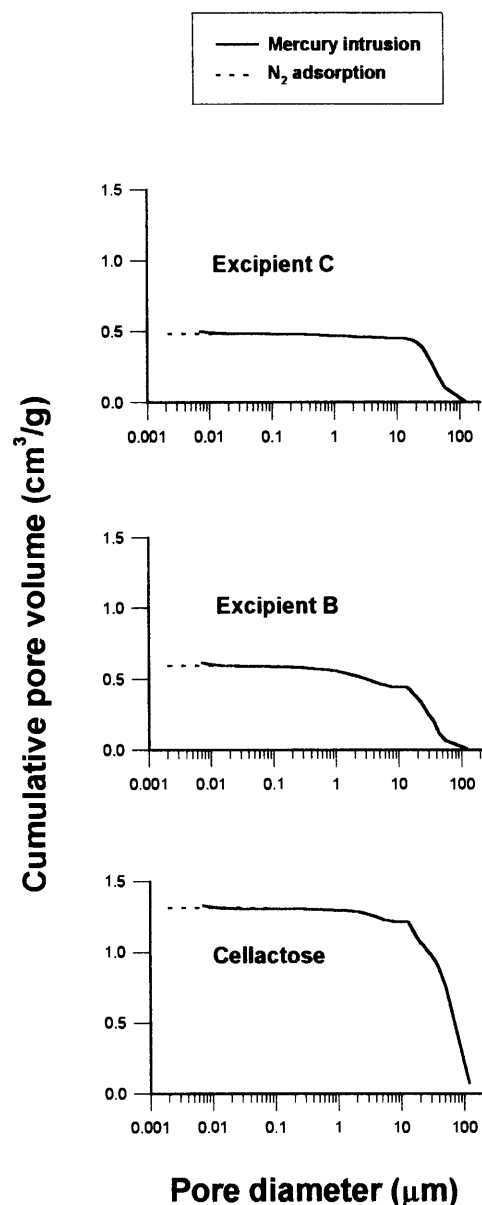
Fig. 4. Cumulative Pore Size Distributions of Particles of Cellactose and Two *ad hoc* Processed Cellulose/Lactose Blends

SEM photomicrographs show Cellactose particles to be highly spherical and to possess pores of considerable size (Fig. 3). The circularity of the spheronized blend was rather higher than that of Cellactose, and that of the dry-granulated excipient rather lower (Table 1); unlike Cellactose, neither B nor C exhibited large pores at the particle surface (Fig. 3). In consonance with the latter observation, the total pore volume of Cellactose particles, as determined by mercury intrusion and nitrogen adsorption porosimetry, was more than double that of the other excipients as the result of the much greater abundance of large pores in Cellactose particles (Fig. 4). In both Cellactose and the dry-granulated blend, the pore volume due to pores $<1\,\mu m$ in diameter was significantly greater than in the extruded/spheronized blend (Fig. 4), a circumstance that explains parallel differences in specific surface area (Table 1).

The values of compressibility and flow factor reflect the free-flowing nature of Cellactose and, in particular, the extruded/spheronized blend, while the dry-granulated blend had

Table 2. Properties of Tablets Prepared by Direct Compression from Cellactose and Two ad hoc Processed Cellulose/Lactose Blends

Parameter	Excipient					
	Cellactose				B	C
	5 MPa	50 MPa	100 MPa	160 MPa		
Tensile strength, MPa	0.10 (0.02)	0.93 (0.30)	2.05 (0.07)	3.09 (0.05)	1.28 (0.07)	0.39 (0.03)
Friability, %	1.90 (0.09)	1.92 (0.07)	2.05 (0.09)	0	0.33	0.67
Specific surface area, $m^2 \cdot g^{-1}$	0.15 (0.03)	0.11(0.05)	0.02 (0.06)	2.19 (0.08)	1.89 (0.06)	1.83 (0.06)
Disintegration time, s	7 (1)	51 (2)	97 (3)	836 (34)	13 (1)	19 (1)
Wetting/dissolution enthalpy, $-J \cdot g^{-1}$	33.06 (0.23)	30.86 (0.51)	28.77 (0.39)	27.14 (0.76)	35.29 (1.99)	34.45 (0.10)

Mean values, with standard deviations in parentheses.

deficient flow.[17,23] As these findings and Fig. 3 suggest, and as might be expected in view of the similar particle size, true densities and sorbed water content of the three excipients, flow factor was in fact determined by circularity, as is reflected by the perfect correlation between the two ($r=$ 1.0000).

The mean yield pressures of all three excipients (Table 1) were similar to those of direct compression lactoses,[24,25] and suggest that particle fragmentation makes a major contribution to their densification under pressure. We note that the value obtained for Cellactose is very similar to that reported by Garr and Rubinstein.[6]

The enthalpy of wetting/dissolution, which was quite similar for all three untabletted blends (Table 1), was significantly reduced by tabletting at 160 MPa in the case of Cellactose but not in the cases of blends B and C (Table 2). This was tentatively attributed to the elimination of macropores by compression at 160 MPa (Fig. 5), which was marked for Cellactose (which before compression had a very large macropore volume) but relatively insignificant for B and C (which before compression had small macropore volumes). Likewise, in spite of similarities among the mean yield pressures of the untabletted excipients (especially between Cellactose and B), Cellactose tablets produced using a punch pressure of 160 MPa (hereinafter "Cellactose-160 tablets") were both stronger and less friable than the tablets of B and C, which were produced under the same conditions (Table 2). In this case the difference was especially marked for the spheronized blend, possibly because the large circularity and small specific surface area of its particles (Table 1) make for better coating with the lubricant, and hence for weaker interparticle bonding. Cellactose-160 tablets also had a much longer disintegration time than B or C tablets, 836 s vs. 13 or 19 s (Table 2).

To investigate further the influence of macropore volume on the wetting/humectation enthalpy and other properties of Cellactose tablets, we characterized tablets in which the volume of pores $>1 \mu m$ was varied from 0.02 to 0.15 cm$^3 \cdot g^{-1}$ by varying the punch pressure used in the tabletting process (5, 50 or 100 MPa). Figure 6 shows the cumulative pore volume distributions of these tablets. The results of characterization (Table 2) clearly show that for Cellactose tablets tensile strength falls and wetting/humectation enthalpy rises with increasing macropore volume (Fig. 7), while disintegration time falls roughly exponentially. The properties of the more porous Cellactose tablets were quite similar to those of tablets of B and C. The fact that these latter fail to comply
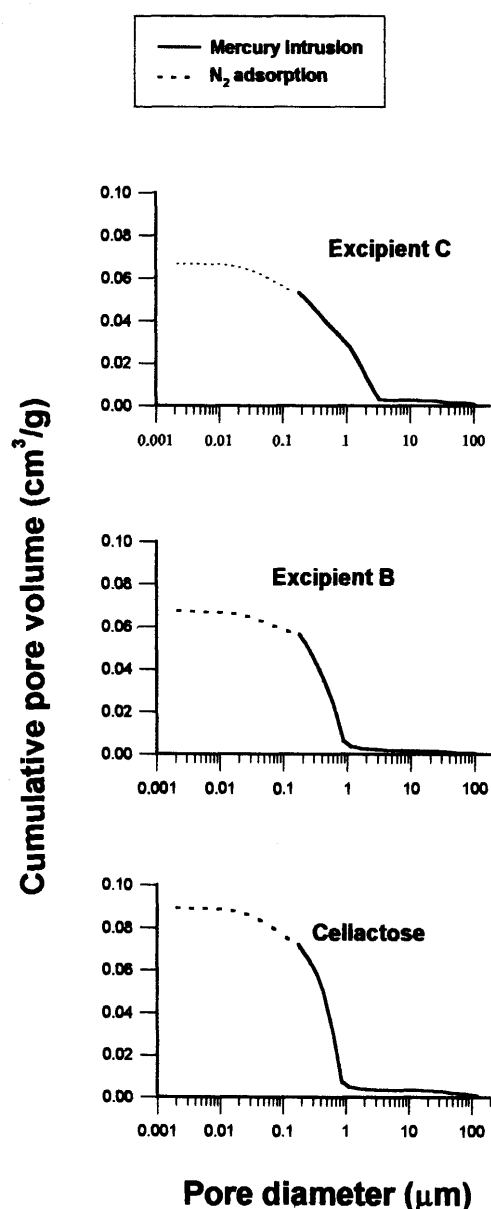

Fig. 5. Cumulative Pore Size Distributions of Tablets Obtained by Direct Compression of Cellactose and Two ad hoc Processed Cellulose/Lactose Blends at a Punch Pressure of 160 MPa

with the correlations observed for Cellactose tablets is of course expected, since the structures of B and C particles differ from Cellactose in many respects, regardless of macropore volume.
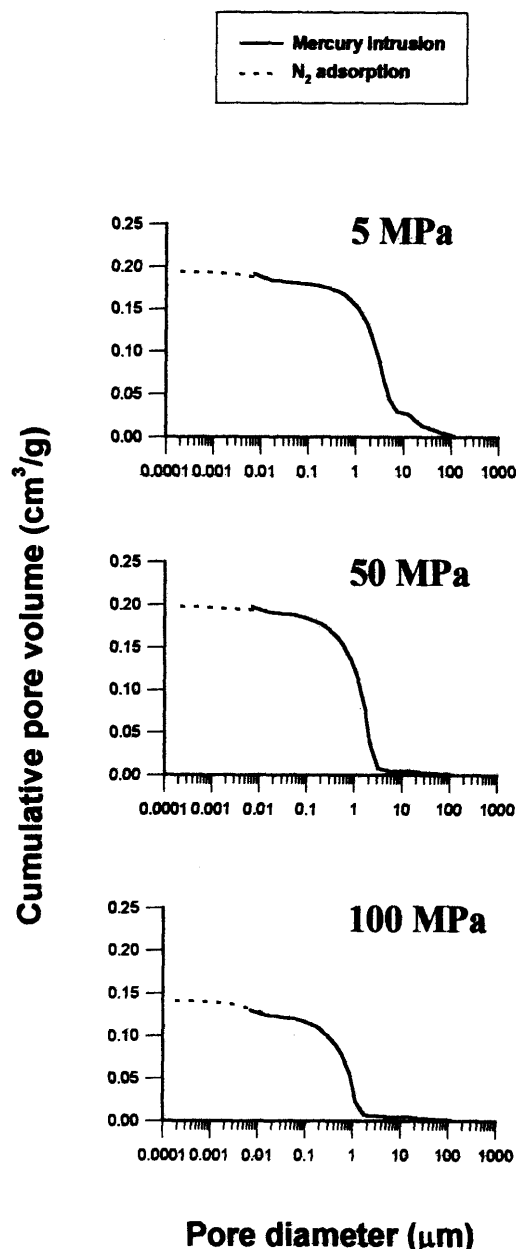
Fig. 6. Cumulative Pore Size Distributions of Cellactose Tablets Obtained by Direct Compression with Punch Pressures of 5, 50 and 100 MPa

Fig. 7. Dependence of the Enthalpy of Wetting/Dissolution (I) and Tensile Strength (II) of Cellactose Tablets on the Volume of Pores >1 μm in Diameter

Data for tablets of blends B and C are shown for comparison and were not included in the regression analysis.

The above findings suggest that, in the absence of marked macroporosity, the remaining structural characteristics of Cellactose tablets markedly impede the weakening and disintegrating action of water. The extremely poor disintegration of Cellactose-160 tablets in comparison with B and C tablets cannot be attributed simply to their greater β-lactose content, since β-lactose content by itself has little effect on disintegration time.[26] Rather, it seems likely that, as hypothesized by Schmidt and Rubensdörfer,[4] the poor disintegration of well-compacted Cellactose tablets is due to the very feature that is also thought to be responsible for their excellent mechanical properties, namely, the fact that Cellactose particles consist basically of a cellulose core coated in lactose. With this structure, the disintegrating action of the cellulose must await the prior dissolution of the lactose, and even then it is hindered by the viscosity of lactose solutions, which slows the access of water to the cellulose.[27] By contrast, the spatial distribution of lactose and cellulose in particles of blends B

and C must be much more random, allowing easier access of water to cellulose.

In conclusion, when compressed at the same punch pressure, Cellactose afforded tablets with better mechanical properties but much poorer disintegration than those of the *ad hoc* cellactose/lactose blends of similar composition prepared in this study. However, the tensile strength and disintegration time of Cellactose tablets both fell rapidly as the volume of pores >1 μm rose, while the enthalpy of wetting/dissolution rose. The strength and water-resistance of well-compacted Cellactose tablets is attributed to the spatial distribution of lactose and cellulose in Cellactose particles, rather than to β-lactose content or extra-particular structural features.

References
1) York P., *Drug Dev. Ind. Pharm.*, **18**, 677—721 (1992).
2) Muñoz-Ruiz A., Monedero-Perales M. C., Velasco-Antequera M. V., Payán-Villar T., Muñoz-Muñoz N., Jiménez-Castellanos M. R., *Int. J. Pharm.*, **95**, 201—207 (1993).
3) Velasco-Antequera M. V., Muñoz-Ruiz A., Monedero-Perales M. C., Muñoz-Muñoz N., Jiménez-Castellanos M. R., *Int. J. Pharm.*, **103**, 155—161 (1994).
4) Schmidt P. C., Rubensdörfer C. F. W., *Drug Dev. Ind. Pharm.*, **20**, 2899—2925 (1994).
5) Schmidt P. C., Rubensdörfer C. F. W., *Drug Dev. Ind. Pharm.*, **20**, 2927—2952 (1994).
6) Garr J. S. M., Rubinstein M. H., *Pharm. Technol. Int.*, **3**, 24—27 (1991).
7) Baykara T., Duman G., Özsener K. S., Ordu S., Özates B., *Drug Dev.*

Ind. Pharm., **17**, 2359—2371 (1991).

8) Reimerdes D., Reimerdes E. H., *Pharm. Manufact. Int.*, **1990**, 159—162.

9) Belda P. M., Mielck J. B., *Eur. J. Pharm. Biopharm.*, **42**, 325—330 (1996).

10) Martínez-Pacheco R., Gómez-Amoza J. L., Vila-Jato J. L., *Cien. Ind. Farm.*, **4**, 207—211 (1985).

11) Dwivedi S. K., Mitchell A. G., *J. Pharm. Sci.*, **78**, 1055—1056 (1989).

12) Lindenbaum S., McGraw S. E., *Pharm. Manuf.*, **2**, 27—30 (1985).

13) Exner H. E., Linck E., *Powder Metall. Int.*, **9**, 131—133 (1977).

14) "Instruction Micromeritics Manual Pore Size 9305," Micromeritics, Norcross, 1984.

15) Stanley-Wood N. G., "Enlargement and Compaction of Particulate Solids," ed. by Stanley-Wood N.G., Butterworths, London, 1983.

16) Thomson F. M., "Handbook of Powder Science and Technology," ed. by Fayed, M. E., Otten L., Van Nostrand Reinhold, New York, 1984.

17) Svarosky L., "Powder Testing Guide: Methods of Measuring the Physical Properties of Bulk Powders," Elsevier, Essex, 1987.

18) Brown R. L., Richards J .C., "Principles of Powder Mechanics," Pergamon Press, Ltd., Oxford, 1970.

19) Humbert-Droz P., Mordier D., Doelker E., *Pharm. Acta Helv.*, **57**, 136—143 (1982).

20) Fell J. T., Newton J. M., *J. Pharm. Sci.*, **60**, 1866—1869 (1971).

21) Di Martino P., Martelli S., Guyot-Hermann A. M., Guyot J. C., Drache M., Conflant P., *S.T.P. Pharma. Sci.*, **3**, 436—441 (1993).

22) Sebhatu T., Angberg M., Ahlneck C., *Int. J. Pharm.*, **104**, 135—144 (1994).

23) Carr R., "Chemical Engineering," McGraw-Hill Inc., New York, 1965, 166—167.

24) Roberts R. J., Rowe R. C., *J. Pharm. Pharmacol.*, **37**, 377—384 (1985).

25) Cal S., Rodríguez-Puente B., Souto C., Concheiro A., Gómez-Amoza J .L., Martínez-Pacheco R., *Int. J. Pharm.*, **136**, 13—21 (1996).

26) Cal S., Iglesias G., Souto C., Concheiro A., Gómez-Amoza J. L., Martínez-Pacheco R., *Int. J. Pharm.*, **129**, 253—261 (1996).

27) Lerk C. F., Bolhuis G. K., de Boer A. H., *Pharm. Weekbl.*, **109**, 945—955 (1974).

Studies on Thermal Aggregation of Bovine Serum Albumin as a Drug Carrier

Chikako Honda,* Hiroko Kamizono, Tomomi Samejima, and Kazutoyo Endo

Showa College of Pharmaceutical Sciences, 3-3165, Higashi-Tamagawagakuen, Machida-shi, Tokyo, 194-8543, Japan.

The irreversible thermal aggregation rate and process of bovine serum albumin (BSA) were investigated by means of light scattering technique as a function of temperature. The increasing rate of particle radius was affected by the aggregation temperature, concentration and the presence of fatty acid. The particle radius was larger and the aggregation rate was faster for fatty acid free BSA at higher temperature and concentration. Two thermal aggregation processes were observed at relatively low temperature and concentration, both for fatty acid containing (C-BSA) and fatty acid free BSA (F-BSA). The first process proceeds by an inter-monomer aggregation mechanism, and the second process by inter-aggregates aggregation. The first process is represented by a power law as $R_{happ} \propto t^z$, which is diffusion limited cluster aggregation (DLCA).

Key words bovine serum albumin; dynamic light scattering; thermal aggregation; aggregation mechanics; diffusion limited cluster aggregation

It has long been known that the irreversible thermal aggregation of globular proteins takes place in aqueous solution.[1—3] Serum albumin has been recognized as an important drug delivery carrier in the drug delivery systems, and the aggregated serum albumin has been used as ^{99m}Tc-macroaggregated albumin(^{99m}Tc-MAA) for diagnostic agents.[4] The sample must contain more than 90% mass of MAA with a particle size between 10 and 90 μm, and no MAA with particle size above 150 μm and below 5 μm for suitable use as diagnostic agents.[5] The MAA has been prepared by thermal aggregation of serum albumin. The thermal aggregation rate depends on the experimental conditions, such as albumin concentration, temperature, pH, ionic strength, fatty acids, *etc.* Recently, Sontum and Christiansen[6] discussed the denaturation kinetics and denaturation rate from the measurement of hydrodynamic radius by means of quasi elastic light scattering at a relatively incipient stage of aggregation up to 15 min as the function of pH and temperature for higher concentration (5%).

The relationship between translational diffusion coefficient, D, measured by means of dynamic light scattering and the number of particles, s, in the aggregated cluster is represented by the power law as $D \propto s^{-\gamma}$ from the simulation of three dimensional cluster–cluster aggregates.[7—9] Bovine serum albumin (BSA) is ellipsoidal protein with the major axis being 14 nm and the minor axis 4 nm.[10] It is possible to investigate the thermal aggregation mechanism or aggregation rate from the evolution of D with the elapse of time since unfolding by the thermal denaturation[11] has less influence on the D.[12]

To our knowledge, only a few detailed experimental data on the aggregation kinetics or mechanism have been reported for ellipsoidal protein as yet. The details of thermal aggregation mechanism may be important and useful for practical applications like the preparation of MAA.

In general, the thermal aggregation rate is too fast to be easily followed experimentally at high temperature and at high concentration. In the present study, we measured the D of aggregated BSA with the elapse of time at relatively low temperature in order to clarify the aggregation process and discuss the thermal aggregation mechanism.

Experimental

Materials Fatty acid containing BSA (C-BSA) (Sigma, cat. No. A-4378, crystallized and lyophilized) was used without further purification; and it contains mercapt, non-mercapt albumin and fatty acid.[13,14] C-BSA solutions for characterization were made up from 0.2 to 1.2% (w/v) in the 20 mM phosphate buffer solution at pH 7.5. The C-BSA solutions used contain not only monomer but also some amount of dimer and trimer[15] whose proportion depended on the lot. no. although the main component was the monomeric C-BSA. The dependence of diffusion coefficient on the concentration, c, at dilute solution is expressed by $D=D_0(1+k_Dc+\cdots)$, where D_0 is the diffusion coefficient at infinite dilution and k_D is the first order coefficient for concentration dependence of D. The diffusion coefficients of C-BSA linearly depend on the concentration. The hydrodynamic radius, R_h, of C-BSA, 4.15 nm, calculated with Stokes–Einstein equation from the D_0 is slightly larger than that of monomer (3.5 nm).[15] The results indicate that the C-BSA solutions contain some dimer and/or trimer other than monomer. In the following, the percentage of C-BSA monomer was estimated, assuming that the sample contained only the monomer and dimer of C-BSA, and neither trimers nor tetramers. The contribution of fatty acid contained in the sample can be neglected because the molecular mass is much smaller than that of BSA. The present sample is found to contains 61% monomeric C-BSA and 39% dimeric one.

Solutions of the C-BSA and fatty acid free BSA (F-BSA) for thermal aggregation were made up to 1% (w/v) in a buffer solution of sodium acetate (pH 5.5; 0.5 M).

Buffer Solution The 0.5 M acetate buffer (pH 5.5) was used during the thermal aggregation. The pH value of 5.5 is close to the isoelectric point of BSA, so that at this pH, the electrostatic effect between BSAs is very weak. Even though there is an electrostatic effect, this effect is shielded by small salt ions in the buffer solution.

Defatting C-BSA was defatted according to the procedure described by Chen.[16] Charcoal (Darco) was mixed into the 1% C-BSA solution and pH was lowered to 3.0 by addition of 0.2 M HCl. The solution was kept in an ice bath and stirred for 1 h. The charcoal was then removed by centrifugation at 2000 g for 20 min and filtered through a membrane-filter (pore size 0.22 μm). The solution was brought to pH 5.5 by adding 0.2 M NaOH.

Aggregation of BSA C-BSA was dissolved in the 0.5 M buffer solution to give a 1% solution. These C-BSA and F-BSA solutions were kept at various temperatures (from 56 to 80 °C) with constant stirring in an oil bath, and the temperature was controlled to within ±0.2 °C. A 5 ml solution was taken out every 2 min and immediately quenched in an ice bath at 0 °C to terminate the thermal reaction.

Particle Radius Measurement C-BSA and relatively small particles of C-BSA and F-BSA aggregates from 1 nm to 1000 nm in size were measured using a dynamic laser light scattering photometer (ALV-5000) with a semiconductor laser (500 mW maximum output) operated at 532 nm as a light source at 25 °C. Diffusion coefficient measurements were performed mainly at the angle of 90° with respect to the incident laser light except at low concentration or for small particles, since measured diffusion coefficients did

* To whom correspondence should be addressed.

not differ between 30 ° to 90°. Measurements were performed at 30° for low BSA concentrations or for small particles. Autocorrelation function $g^{(2)}(\tau)$ of the scattered light intensity was measured and $g^{(2)}(\tau)$ was transformed to the correlation function $g^{(1)}(\tau)$ of the electric field of scattered light. The $g^{(1)}(\tau)$ was analyzed by using the non-linear least square fitting to the cumulant expansion.[17] The diffusion coefficient, D, was obtained from the average decay rate $\bar{\Gamma}$ by the relation $\bar{\Gamma}=Dq^2$, where q is the length of the scattering vector. In general, random aggregation of spherical particles might be expected to produce more or less spherical particles.[18] In the present study, the theory was applied as an approximation, assuming that ellipsoidal molecules of BSA also form globular aggregates. Then, the hydrodynamic radius, R_h, was calculated with the Stokes–Einstein equation. Since the extrapolation to zero concentration for thermal aggregated samples could not be made, we evaluated R_h without the extrapolation, here referred to as the apparent hydrodynamic radius (R_{happ}). In the case of $qR_h \gg 1$, it is necessary to consider the rotational diffusion of the particles to determine the R_h exactly from the translational diffusion coefficient. The influence of rotational diffusion to the translational diffusion is less significant in this experiment since the size increment of aggregates is rapid and prominent.

Aggregated particles with radius larger than 1000 nm were measured by means of a Coulter LS-130 with 750 nm incident laser beam. Diffraction pattern analysis over 3 μm particles was based on the Fraunhofer diffraction pattern. Scattering light pattern analysis, based on the Mie scattering, was applied to the particle radius ranging from 0.4 to about 3 μm. The particle radius ranging from 0.1 to 0.4 μm could not be distinguished by the Mie scattering patterns. Then, the intensity difference between horizontally and vertically polarized light components was measured with 450, 600 and 900 nm incident light, and the polarized light pattern was analyzed as a function of scattering angle. The particle radii ranging from 800 to 1000 nm observed with the dynamic light scattering method were consistent with those of diffraction pattern analysis with the Coulter LS-130, though the measurements were based on different principles. The resolution of the equipment, defined as the standard deviation of the observed peak value divided by the value of a profile, was estimated to be 16%, using standard particles of polystyrene latex that has 0.31 ± 0.05 μm in diameter.

Results and Discussion

Effect of Fatty Acid on Thermal Aggregation Figures 1 and 2 show the particle radii of F-BSA and C-BSA with the elapsed time at 62 °C. The remarkable difference in the particle radius of the aggregates was found at the initial heating. The radius (9 μm) of F-BSA is about 1500 times greater than that (6 nm) of C-BSA *ca.* 2 min after the initiation of heating. The particle radius of F-BSA aggregates increased monotonically and gradually from 9 to 28 μm with time from 2 up to 50 min, whereas that of C-BSA increased from 6 to 100 nm with time from 2 up to 30 min at a faster rate than F-BSA. Then, the particle radius of C-BSA increased abruptly from about 100 nm (30 min after heating) to 2000 nm at 50 min. This behavior suggests that the presence of fatty acid prevents the thermal aggregation, and reflects that BSA molecules binding to at least 6 molecules of fatty acid resist thermal denaturation.[19,20]

Temperature Effect on Thermal Aggregation Figure 1 shows the particle radii of aggregates for C-BSA with elapsed time at 62 °C to 80 °C. The higher the temperature, the larger the particle radius formed. The thermal aggregation rate was too fast to follow the radius increasing process at the higher temperature of 80 °C. Two cluster forming processes became apparent at relatively low temperature (62 °C and 63 °C). At higher temperature the two processes took place simultaneously, and it was therefore difficult to observe them individually. Figure 2 shows the particle radii of aggregates for F-BSA with elapsed time at various temperatures. The behavior is similar to C-BSA at low temperature (58 °C and 59 °C). However, the second process is observed at 67 °C for C-BSA, whereas it is observed at 61 °C
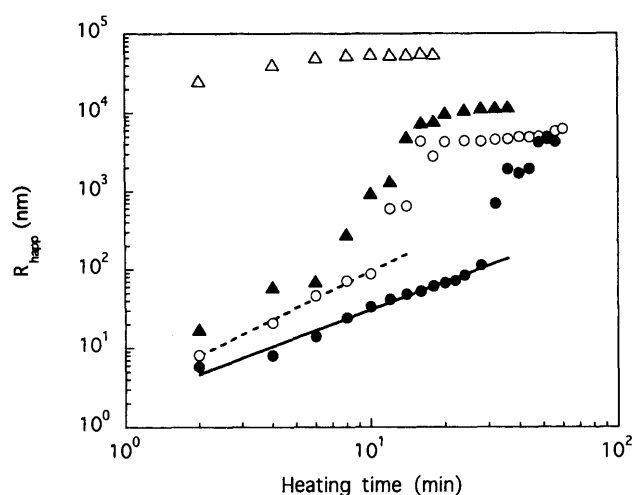
Fig. 1. Time Evolution of Particle Radii, R_{happ}, for Aggregates of C-BSA at Various Temperatures

C-BSA concentration is 1% at pH 5.5. 62 °C ($\bullet$); 63 °C ($\bigcirc$); 67 °C ($\blacktriangle$); 80 °C ($\triangle$). Lines give $R_{happ} \propto t^{1.17}$ (—) and $R_{happ} \propto t^{1.53}$ (- - -), respectively.
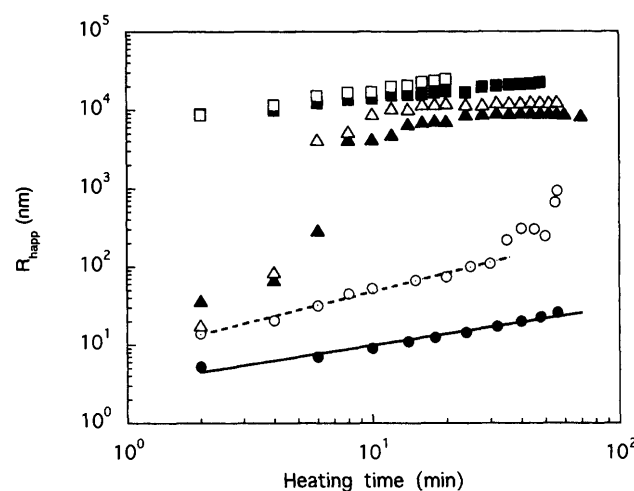
Fig. 2. Time Evolution of Particle Radii, R_{happ}, for Aggregates of F-BSA at Various Temperatures

F-BSA concentration is 1% at pH 5.5. 56 °C ($\bullet$); 58 °C ($\bigcirc$); 59 °C ($\blacktriangle$); 61 °C ($\triangle$); 62 °C ($\blacksquare$); 67 °C ($\square$). Lines give $R_{happ} \propto t^{0.49}$ (—) and $R_{happ} \propto t^{0.78}$ (- - -), respectively.

for F-BSA, indicating that the second process occurs at a temperature at least 6 °C lower for F-BSA than for C-BSA. The first process shows that R_{happ} gradually increases up to about 100 nm, after which the aggregate size increases abruptly. The gelation is assumed to be a particular kind of limited aggregation process, since concentrated BSA solution gelates at high temperature. Richardson and Ross-Murphy considered that gelation progresses in four processes,[21] *i.e.*, 1) unfolding of native protein, 2) monomer aggregation, 3) reaction of inter aggregates, and 4) intra-aggregates reaction. The first process proceeds with a first-order reaction, the second and third with second-order reaction, and the fourth with first-order one. The overall reaction order thus lies between the first and second order. In this experiment, the 1% BSA concentration was too low to gelate, and the partial unfolding of BSA helixes with the thermal denaturation was unaffected to the translational diffusion, because translational diffusion was observed as the hydrodynamic motion of aggregates. It is therefore considered that the BSA aggregation progresses *via* only the second and third

Table 1. Temperature Dependence of z on t^z (t=Elapsed Time of Heating) Obtained by DLCA Theory ($R_{happ} \propto t^z$) in the Early Stage for Aggregation Process of BSA

F-BSA		C-BSA	
Temperature (°C)	z	Temperature (°C)	z
56	0.49	62	1.17
58	0.78	63	1.53

processes described by Richardson and Ross-Murphy.[21] Namely in the first process, monomer BSA molecules aggregate so that the particle size increases to about 100 nm and almost all the monomer molecules are consumed to aggregate. In the second process, the reaction of inter aggregates takes place and the particle size increases rapidly. There after the particle size reaches a plateau where particles no longer aggregate, because the concentration of the remaining monomeric BSA is too low to aggregate further. The particle size at this plateau region depends on the temperature (for example, ca. 1 μm at 61 °C for F-BSA in Fig. 2).

The computer simulation of aggregation processes has been studied theoretically[7—9,22—25] and applied experimentally to gold sol systems and to β-lactoglogulin.[12,26—29] The theory predicts that clusters grow linearly in time for diffusion limited cluster aggregation (DLCA) or exponentially for reaction limited cluster aggregation (RLCA). A study by Gimel et al.[12] on the thermal aggregation process of globular protein, β-lactoglogulin, indicates that the process obeys a power law and an exponential cut-off time course for cluster-cluster type aggregation.

The thermal aggregation of ellipsoidal protein involves a similar process to fractal growth, and the relationship between the particle size and the time of heating is represented by the power law as $R_{happ} \propto t^z$ (DLCA) or by the exponential form as $R_{happ} \propto e^{\alpha t}$ (RLCA). The DLCA theory assumes that particles of similar size aggregate on the lattice. BSA solutions can be assumed uniform, although the solution contains some oligomers. Thermal aggregation takes place irreversibly and randomly by the diffusion of BSA particles. Consequently, DLCA can be applied to the BSA thermal aggregation systems. As shown by straight and dotted lines in Figs. 1 and 2, the early stage of thermal aggregation is consistent with the DLCA theory, and at this stage, intermonomer molecules aggregate. If the particles are nearly

equal in size, evolution of the particle radius is represented by the DLCA theory. The exponent, z, on heating time, t, of the early stage of aggregation is shown in Table 1. The z depends on the temperature, i.e., the higher the temperature, the larger the z is observed both for C- and F-BSA.

References

1) Levy M., Warner R. C., J. Phys. Chem., **58**, 106—109 (1954).
2) Warner R. C., Levy M., J. Am. Chem. Soc., **80**, 5735—5744 (1958).
3) Oakes J., J. Chem. Soc., Faraday 1., **72**, 228—273 (1976).
4) Fukuoka M., Kobayashi T., Satoh T., Tanaka A., Kubodera A., Nucl. Med. Biol., **20**, 643—648 (1993).
5) Asahara A., J. Transportn. Med., **30**, 277—287 (1976).
6) Sontum P. C., Christiansen C., J. Pharm. Biomed. Anal., **16**, 295—302 (1997).
7) Meakin P., Chen Z.-Y., Deutch J. M., J. Chem. Phys., **82**, 3786—3789 (1985).
8) Meakin P., Phys. Rev. A, **27**, 604—607 (1983).
9) Weitz D. A., Huang J. S., Lin M. Y., Sung J., Phys. Rev. Lett., **54**, 1416—1419 (1985).
10) Peters T., Jr., "The Plasma Proteins," ed. by Putnam F. W., Academic Press, 1975, pp. 133—181.
11) Lin V. J. C., Koenig J. L., Biopolymers, **15**, 203—218 (1976).
12) Gimel J.-C., Durand D., Nicolai T., Macromolecules, **27**, 583—589 (1994).
13) Sogami M., Era S., Nagaoka S., Kuwata K., Kida K., Miura K., Inoue H., Suzuki E., Hayano S., Sawada S., Int. J. Peptide Protein Res., **25**, 398—402 (1985).
14) Sogami M., Era S., Nagaoka S., Kuwata K., Kida K., Shigemi J., Miura K., Suzuki E., Muto Y., Tomita E., Hayano S., Sawada S., Noguchi K., Miyata S., J. Chromatogr., **332**, 19—27 (1985).
15) Honda C., Kambe Y., Nippon Kagaku Kaishi, **1988**, 194—200.
16) Chen R. F., J. Biol. Chem., **242**, 173—181 (1967).
17) Koppel D. E., J. Chem. Phys., **57**, 4814—4820 (1972).
18) Tombs M. P., Farad. Discuss. Chem. Soc., **1974**, 158—164.
19) Aoki K., Maezawa S., Ito T., Hiramatsu K., Yukagaku, **30**, 15—20 (1981).
20) Aoki K., Hayakawa N., Noda K., Terada H., Hiramatsu K., Colloid Polym. Sci., **261**, 359—364 (1983).
21) Richardson R. K., Ross-Murphy S. B., Int. J. Biol. Macromol., **3**, 315—322 (1981).
22) Witten T. A., Jr., Sander L. M., Phys. Rev. Lett., **47**, 1400—1403 (1981).
23) Brown M. D., Ball R. C., J. Phys. A, **18**, L517—L521 (1985).
24) Martin J. E., Ackerson B. J., Phys. Rev. A, **31**, 1180—1182 (1982).
25) Vicsek T., Family F., Phys. Rev. Lett., **52**, 1669—1672 (1984).
26) Matsushita M., Sumida K., Sawada Y., J. Phys. Soc. Jpn., **54**, 2786—2789 (1985).
27) Olivier B. J., Sorensen C. M., Phys. Rev. A, **41**, 2093—2100 (1990).
28) Lin M. Y., Klein R., Lindsay H. M., Weitz D. A., Ball R. C., Meakin P., J. Colloid Interface Sci., **137**, 263—280 (1990).
29) Asnaghi D., Carpineti M., Giglio M., Sozzi M., Phys. Rev. A, **45**, 1018—1023 (1992).

April 2000

Chem. Pharm. Bull. 48(4) 467—476 (2000)

467

Quantitative Analysis of the Kinetic Constant of the Reaction of *N,N'*-Propylenedinicotinamide with the Hydroxyl Radical Using Dimethyl Sulfoxide and Deduction of Its Structure in Chloroform

Toshio AKIMOTO*

Chemistry Research Lab., Fuji Gotemba Research Labs., Chugai Pharmaceutical Co., Ltd., 135, Komakado, 1 Chome, Gotenba-shi, Shizuoka 412-8513, Japan. Received August 11, 1999; accepted December 28, 1999

N,N'-Propylenedinicotinamide (Nicaraven) is presently being developed for the treatment of cerebral stroke including subarachnoid hemorrhage. This drug is promising because some data suggest it to have an ability to scavenge the hydroxyl radical under physiological conditions *in vivo*, while it also has a high permeability through the blood brain barrier.

Using the kinetic constant of the reaction between the hydroxyl radical and dimethyl sulfoxide, the formula derived by Babbs and Griffin (*Free Rad. Biol. Med.*, 6 1989) was applied to obtain the kinetic constant of Nicaraven with the hydroxyl radical using a dimethyl sulfoxide–xanthine oxidase–hypoxanthine–Fe system, and this yielded the kinetic constant $3.4 \times 10^9 \, \text{M}^{-1}\text{s}^{-1}$ ($1 \, \text{M} = 1 \, \text{mol} \, \text{dm}^{-3}$) for Nicaraven. Structurally related compounds were also investigated. The amide group of Nicaraven was thus found to play an important part in the reaction with the hydroxyl radical.

Methanesulfinic acid, which was obtained from the reaction between dimethyl sulfoxide and the hydroxyl radical, was found to be stable under this adopted experimental condition and therefore was used to quantify the kinetic constant of Nicaraven.

The structure of Nicaraven has also been investigated in CDCl₃ using IR spectra, computer calculations and ¹H-NMR analysis, and Nicaraven was thus shown to have an intramolecular hydrogen bond which forms a 7-membered ring that resembles a part of the 1H-1,4-benzodiazepines. This structure may play an important role in the penetration through the blood brain barrier.

Key words   hydroxyl radical; dimethyl sulfoxide; blood brain barrier; xanthine oxidase; methanesulfinic acid; benzodiazepine

Oxygen radicals are produced in the brain during cellular respiration and their production accelerates dramatically during brain insult.[1] The most reactive radical, namely, the hydroxyl radical (·OH) is able to oxidize proteins,[2] lipids[3] and nucleic acids.[2] It is therefore believed to be a very important property for potential drug therapy of brain insult to scavenge ·OH.

N,N'-propylenedinicotinamide (Nicaraven, Fig. 1) is presently being developed for the treatment of cerebral stroke including subarachnoid hemorrhage.[4,5] Nicaraven has been given to patients by intravenous drip, with four grams of the drug administered over an 8-h period, once per day for a period of 10 d in clinical trials. This drug is promising because data suggest it has an ability to scavenge ·OH under physiological conditions *in vivo*.[6,7] For example, Gidö and Wieloch demonstrated that the production of 3,4-dihydroxybenzoic acid (3,4-DHBA) from 4-hydroxybenzoic acid given to rats remarkably decreased soon after ischemia when the Nicaraven concentration was increased to 1 mg/ml/min after intravenous infusion.[6] Nicaraven also has high permeability through the blood brain barrier (BBB).[8]

Babbs and Griffin first reported a Scatchard plot analysis to determine the total ·OH production.[9] We used their slightly modified method to obtain the kinetic constant and this method proved to be very convenient, since no large apparatus was required such as is the case with electron spin resonance or gamma radiolysis. They also reported methanesulfinic acid (MSA) to be produced from a reaction of dimethyl sulfoxide (DMSO) and ·OH, and stated that MSA can be measured after diazotization.

We herein describe a method in which, after measuring the quantity of diazotized MSA and using the kinetic constant of

the reaction of DMSO with ·OH that had been obtained by gamma radiolysis, the kinetic constant of the reaction between a compound and ·OH could be obtained.

Although the MSA yielded from the reaction with DMSO cannot be regarded as a product derived with ·OH alone and other active oxygen species must also be taken into account according to the finding of Yamazaki and Piette,[10,11] the total yield of MSA was determined in this study and thereafter was used for the analysis.

Brain drugs need to penetrate the BBB and it is commonly believed that compounds with a high water solubility cannot do so.[12] Nicaraven, however, has a very high water solubility of 821 mg/ml, but nevertheless shows a good BBB penetration. Interestingly, this compound also dissolves in chloroform at 203 mg/ml. A structural analysis of Nicaraven in CDCl₃, which is a rather hydrophobic environment, was made using the IR absorption spectrum of N–H stretching vibration and a ¹H-NMR spectral analysis, while a semi-empirical quantum mechanical calculation was also performed.

The finding of a quantitative kinetic study with ·OH and the structure in CDCl₃ of Nicaraven are reported in this paper.
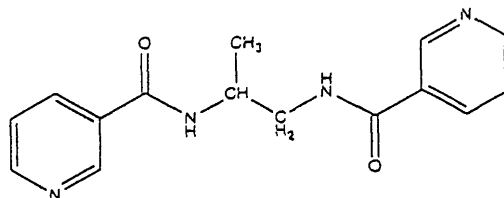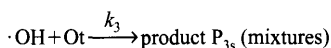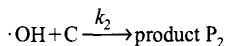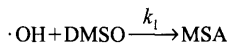

Fig. 1.   Chemical Structure of Nicaraven

Theoretical Background for Obtaining a Kinetic Constant

The mathematical formula for the Scatchard plot analysis proposed by Babbs and Griffin[9] has been modified as follows. In this formula, k_1, k_2 and k_3 are the kinetic constants when C is the test compound, e.g. Nicaraven, while Ot represents the other mixtures such as xanthine oxidase, etc.

$$\cdot OH + DMSO \xrightarrow{k_1} MSA$$

$$\cdot OH + C \xrightarrow{k_2} product\ P_2$$

$$\cdot OH + Ot \xrightarrow{k_3} product\ P_{3s}\ (mixtures)$$

The MSA produced by the attack of $\cdot OH$ is described by the equation below: The square brackets express the concentration.

$$[CH_3SOOH] = \alpha[\cdot OH]\frac{[DMSO]}{[DMSO] + \frac{k_2[C]}{k_1} + \frac{k_3[Ot]}{k_1}} \quad (1)$$

In this Eq. 1, α represents the coefficient of the MSA yield from DMSO and the diminishing factor of [MSA] by $\cdot OH$ attack.[13] When the DMSO concentration is high enough to capture all the produced $\cdot OH$, then $[\cdot OH]$ becomes $[CH_3SOOH]_{max}$ and α becomes nearly 1.0. Babbs and Griffin developed the mathematical formula noted below based on this hypothesis[9]:

When K is defined as

$$K = \frac{k_2[C]}{k_1} + \frac{k_3[Ot]}{k_1} \quad (2)$$

then

$$\frac{[CH_3SOOH]}{[DMSO]} = \frac{[CH_3SOOH]_{max}}{K} - \frac{[CH_3SOOH]}{K} \quad (3)$$

From the above Eq. 3, $1/K$ defined as Eq. 2 can be obtained from the slope of the straight line of $[CH_3SOOH]/[DMSO]$ and $[CH_3SOOH]$ which are plotted as the y-axis and x-axis, respectively. Using k_1, which represents the kinetic constant of the reaction between DMSO and $\cdot OH$ as $7 \times 10^9\,M^{-1}s^{-1}$,[14] and $k_3[Ot]/k_1 = 0$, if negligible, then, Eq. 2 can be reduced to $K = k_2[C]/k_1$.

To obtain the condition of $\alpha = 1$ and $[CH_3SOOH]_{max} = [\cdot OH]$ and if the effect of $k_3[Ot]/k_1$ can be regarded as negligible, then experiments in which [DMSO] and [MSA] have been changed in the absence of a test compound such as Nicaraven would have to be carried out (see Results). To successfully obtain a straight line in Scatchard plots, the appropriate range of the combination of [DMSO] and [C] must be determined. If [DMSO] is too high, then α in Eq. 1 would be greater than 1.0. This is because when the [DMSO] concentration is too high, the radical chain reaction between DMSO and the radical yielded from DMSO would cause an increased generation of MSA. If [DMSO] is too low, then α would become less than 1.0. This is because when [DMSO] is too low, the MSA generated from it is damaged by an $\cdot OH$ attack, and the effect of [Ot] also cannot be ruled out.

Experimental

Compounds Examined The compounds measured were Nicaraven, mannitol, N-methylnicotinamide (NM-NA), pyridine and N-methylac-

etamide (NMAA). The reason these compounds were utilized first was to get information about which moiety of the Nicaraven molecule plays a key role in the reaction with $\cdot OH$. A second reason was to determine the precision of this analytical method by comparing the results with those already published elsewhere.

Materials and Experimental Procedures Materials: The diazo compound reacted with MSA was Fast Blue BB salt (azoic diazo component 20) which was purchased from Tokyo Kasei Co., Ltd. DMSO of ultra-pure grade was obtained from Wako Pure Chemicals Co., Ltd. The MSA sodium salt was from Lancaster Co., Ltd. Butter milk xanthine oxidase (E.C.1.2.3.2) 25 U/ml 60% ammonium sulfate suspension was also from Wako. All other chemicals used in this experiment were of reagent grade.

The Stock Solutions: Hypoxanthine was dissolved in $1.0\,M$ ($1\,M = 1\,mol\,dm^{-3}$) NaOH to $40\,mM$ and diluted to $133\,\mu M$ in phosphate buffered saline (PBS, $100\,mM$ NaCl, $50\,mM$ phosphate buffer, pH7.4). Fe–EDTA was dissolved to $1.5\,mM$ in PBS. DMSO was diluted in PBS to various concentrations ranging from $30\,mM$ to $450\,mM$ (7 points). Xanthine oxidase was diluted 30 times in PBS. The concentration of the compounds examined was $150\,mM$, respectively.

Experimental Procedures: The following experimental procedures for the kinetic analysis were similar to those carried out by Babbs and Griffin.[9]

The reaction was started by adding 0.2 ml xanthine oxidase (final concentration $56\,mU/ml$) into the mixture of 0.1 ml DMSO ($1.0\,mM$ to $15\,mM$ in final), 0.1 ml of one of the compound solutions, 0.2 ml Fe–EDTA and 2.4 ml hypoxanthine solution. The blank for the optical density measurement had the same composition as the sample solution except 0.1 ml PBS was added instead of 0.1 ml DMSO solution. The final concentration of hypoxanthine was $106\,\mu M$, and the concentration of a test compound was $5.0\,mM$. The reaction was carried out under 20 min standing conditions after slight vortexing. Regarding Nicaraven, the final concentration of $10\,mM$ was also investigated.

Thereafter, the solution was treated in a similar way to that by Babbs and Griffin.[9]

Damage of MSA by $\cdot OH$ To examine the behavior of the MSA exposed to $\cdot OH$ under these experimental conditions, authentic MSA was added instead of DMSO from the beginning and the optical density was measured. The authentic MSA was also measured after the chemical treatment described above in the absence of xanthine oxidase for comparison purposes.

DMSO Concentration to Protect Yielded MSA From the above experiment, the MSA generated under experimental conditions was destroyed by the $\cdot OH$ attack if the DMSO concentration was too low to react with all of the $\cdot OH$. To further elucidate this problem, certain concentrations of MSA were added to the experiment beforehand and the decay rate of MSA was observed by changing the DMSO concentrations. The concentrations of MSA added beforehand were 0, 11, 22, 38.5 and $55\,\mu M$ in the final concentration. The DMSO concentrations were 0.47, 0.93, 4.67 and $9.33\,mM$ in the final concentration.

Protection of Yielded MSA by the Combination of DMSO and a Compound Furthermore, the same problem (MSA damage by $\cdot OH$) could occur when a test compound such as Nicaraven is added. To obtain information on this effect, a DMSO concentration of 0.47 mM and a Nicaraven concentration of 3.3 mM, a DMSO concentration of 0.47 and 0.94 mM and mannitol 3.3 mM were tested using MSA at the same concentrations as those noted above, which was added before the xanthine oxidase was added.

Scatchard Plot Analysis After a careful examination of the above results (see Results), a Scatchard plot analysis was carried out using the 5.0 mM test compound and DMSO solution with a concentration of 1.0, 1.67, 2.5, 3.3, 6.67, 10.0 and 15.0 mM.

Reactive Site of Nicaraven with $\cdot OH$ The Fenton reaction using Fe^{III} was applied[15] to determine which moiety of Nicaraven reacts with $\cdot OH$. The PBS used had the same composition as that used throughout this work. The final concentration of Nicaraven was 10 mM, while that of Fe–EDTA is 2.0 mM, and the concentrations of H_2O_2 were 0, 8.8 and 13.2 mM. The 100 ml mixed solution was left standing for 4 to 5 d. After freeze-drying this mixture, the IR and ^{1}H-NMR spectra were measured. Preparation of DMSO-d_6 solution of freeze-dried sample to measure the ^{1}H-NMR spectrum required filtration. The NMR apparatus used was a JNM-EX270 of JEOL.

From the samples obtained in the same manner as described in the preparation above (freeze-dried sample), extraction was carried out using 120 ml of dichloromethane, after which the insoluble part was dissolved in water and adjusted to pH 10.0 by sodium hydrogencarbonate, and then freeze-dried. Thereafter the extraction was done using 120 ml of dichloromethane. After obtaining an insoluble part by filtration, the extraction was carried out

using 100 ml ethanol. These three solutions for the extraction were evaporated to dryness at 40 °C. TLC ($CHCl_3$:methanol=5:1 and $CHCl_3$:methanol=5:1 plus one drop of acetic acid), and then the measurement of ^{1}H-NMR in DMSO-d_6 and IR in the KBr disk were carried out.

Structural Study of Nicaraven A structural study of IR absorption measurement was carried out using a Horiba 730 FT-IR spectrometer. The concentrations of Nicaraven were 30, 10, 3 and 0.5 mM in $CDCl_3$ and that of NM-NA was 10 mM in $CDCl_3$. The solution cell had a KBr window with spacing of 0.5 mm.

Molecular dynamics calculation was carried out using the Discover version 2.9.7 software package of Molecular Simulation, Inc. U.S.A., and every 2.5 psec, the structure was selected for simulated annealing from 900K to 300K for one psec. Successive 4 psec dynamics calculations were made at 300K, after which a total of 10 structures were geometry-optimized using molecular mechanics. One of the structures, which had two closed pyridine rings in a stack, even though a complete stacking of the two pyridine rings of this molecule is not possible, was geometry-optimized using the semi-empirical quantum mechanical program package MOPAC, version 6.0.[16] PM3 Hamiltonian was applied in this study. The hardware used was IRIS Indigo2 and Power Challenge from Silicon Graphics.

To confirm the structure obtained by both IR absorption observations and a PM3 calculation study, a ^{1}H-NMR study was carried out on Nicaraven concentrations of 2 and 20 mM in $CDCl_3$. The signals of the two methylene protons of Nicaraven appeared at different resonant positions. Based on the calculated structures by PM3, the Karplus equations were applied to support the correctness of the calculated structures. The Karplus equations used were for the peptide analysis and are expressed as follows.

$$^3J_{HNC_\alpha H}=9.4 \cos^2\theta-1.1 \cos\theta+0.4^{17)}$$

$$^3J_{HC_\alpha C_\beta H}=9.4 \cos^2\theta-1.4 \cos\theta+1.6^{18)}$$

To assign a coupling constant to each proton pair, the homo-decoupling measurements to two amide protons and to methyl protons were applied using a Varian Mercury 300. When measuring the 2 mM solution, a Bruker DRX750 was used.

Results

Determining the Total [·OH] Production By putting MSA instead of DMSO directly into the experimental reaction, the linearity of absorbance to the [MSA] exposed to ·OH was confirmed, and the linearity was good. However, the slope of absorbance/[MSA] under experimental conditions was only 1/3 that of the MSA measured in the absence of xanthine oxidase (data not shown).[13]

Figure 2 shows the absorbance at 425 nm when the known

concentrations of MSA were added before the xanthine oxidase was added to the solution. In this case, no test compound to investigate the kinetics was added. The slope of the upper two straight lines was saturated because that with DMSO 4.67 mM was steeper than that with 9.33 mM and the two y-intersections of the straight lines were equal within the range of experimental error. Furthermore, the slopes of these two lines closely coincided with the slope of the line which was drawn when the given concentration of MSA was mixed with PBS (MSA alone in Fig. 2). By averaging 2 straight lines of the y-intersections, the equation can be expressed as

$$y=0.122+2.36\times10^{-3}x$$

Here, y is the absorbance and x is MSA added with the unit of μM. This DMSO concentration region can be interpreted as follows: The added MSA was well protected from decay, because all the hydroxyl radicals were consumed by the large concentration of DMSO. The y-axis intersection is expected to be $[\cdot OH]=[CH_3SOOH]_{max}$ and $\alpha \doteqdot 1$ in the Eq. 1. The slope of this linear equation must be proportional to the added MSA concentrations. Using the above equation, the total $[\cdot OH]=[CH_3SOOH]_{max}$ was determined as 53 μM when 106 μM hypoxanthine was added. Fifty-three μM MSA corresponded to the absorbance 0.122, and thus $x=437y$ could be obtained. Here, x is MSA μM and y is the absorbance obtained.

The slopes at DMSO 0.93 mM and 0.47 mM were less than those of DMSO 4.67 and 9.3 mM. This means the MSA yielded from DMSO concentration 0.93 or 0.47 mM is partly destroyed by ·OH. At these concentrations of DMSO, MSA is not stable and the effect of [Ot] cannot be disregarded.

Appropriate Combination of Concentrations of DMSO and Test Compound The upper three lines of Fig. 3 show the behavior of the straight line when Nicaraven or mannitol 3.3 mM is added to the reaction tube, with DMSO at concentrations of 0.47 mM or 0.94 mM and MSA at certain known concentrations. If [Nicaraven] or [mannitol] and [DMSO] are high enough to capture all the ·OH yielded in the reaction, then the slopes of these lines should be equal to that of MSA

$y = -1.5693e-3 + 2.3581e-3x$ $R^2 = 0.997$
$y = 0.12629 + 2.2194e-3x$ $R^2 = 0.991$
$y = 0.11787 + 2.6604e-3x$ $R^2 = 0.994$
$y = 9.3358e-2 + 1.8317e-3x$ $R^2 = 0.996$
$y = 9.3358e-2 + 1.8317e-3x$ $R^2 = 0.996$
$y = 8.6923e-2 + 1.6971e-3x$ $R^2 = 0.997$

■ MSA alone
● DMSO(9.33 mM)
■ DMSO(4.67 mM)
● DMSO(0.93 mM)
■ DMSO(0.47 mM)
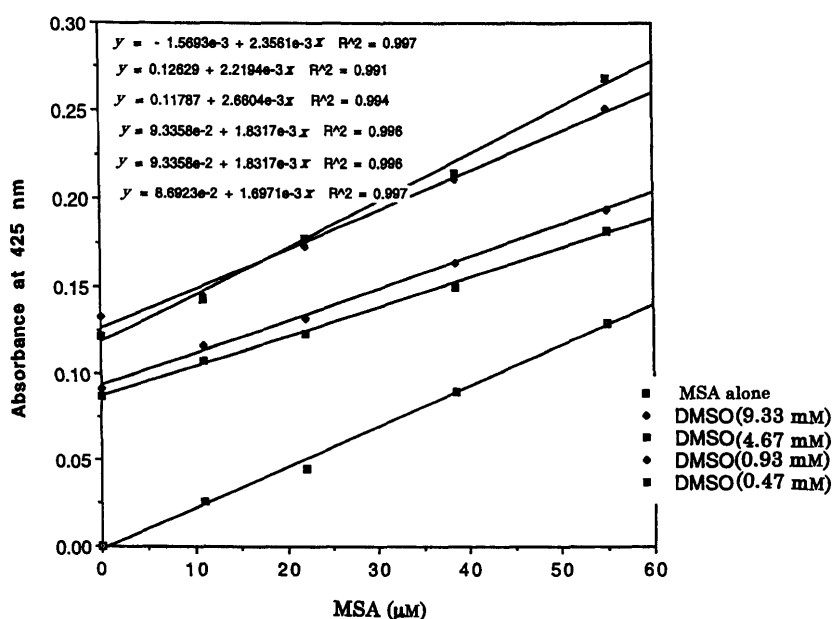
Fig. 2. The Effect of MSA Added beforehand to the Experimental Condition

$y = -1.5693e-3 + 2.3561e-3x$ $R^2 = 0.997$

$y = 2.4747e-2 + 2.2195e-3x$ $R^2 = 0.997$

$y = 3.9929e-2 + 1.8510e-3x$ $R^2 = 0.984$

$y = 8.7012e-2 + 2.0645e-3x$ $R^2 = 0.997$

■ MSA alone
◆ DMSO 0.47 mM Nicaraven 3.3 mM
■ DMSO 0.47 mM mannitol 3.3 mM
◆ DMSO 0.94 mM mannitol 3.3 mM
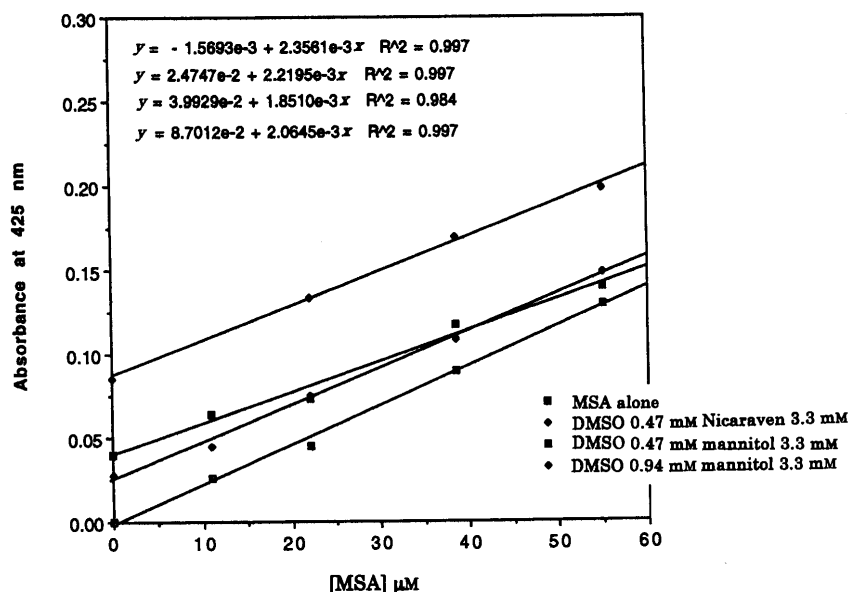
Fig. 3.   MSA Linearity at Different DMSO Concentrations When a Compound is Added
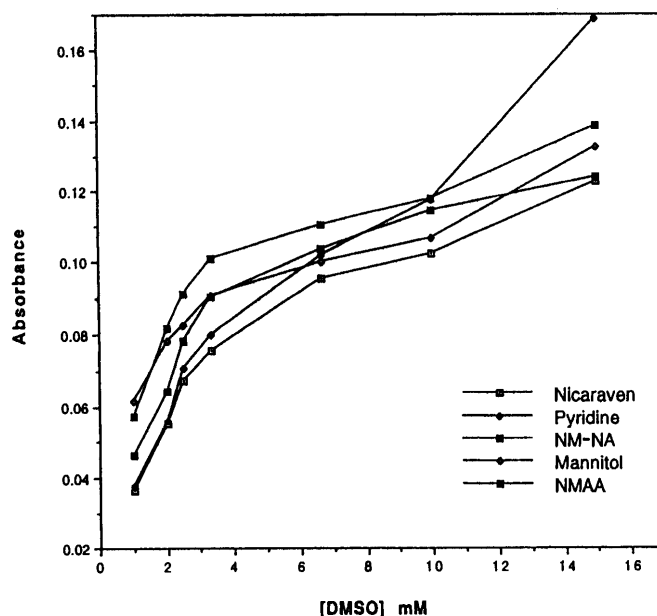
Fig. 4.   The Absorbance Change When [DMSO] is Changed

alone in Fig. 3. From this point of view, the concentrations of 0.47 mM DMSO with 3.3 mM Nicaraven, and 0.94 mM DMSO with 3.3 mM mannitol would seem to be almost applicable to the Scatchard plots. However, the concentration of DMSO 0.47 mM with mannitol 3.3 mM is clearly unusable for the plot. From these results, the experimental conditions with a higher concentration of the test compound (5 mM) and higher concentrations of DMSO (more than 1.0 mM) have been employed to obtain the kinetic constant of each compound.

Scatchard Plot Analysis   The absorbance vs. [DMSO] with each compound at a concentration of 5 mM is shown in Fig. 4.

The Scatchard plot of each compound was applied. As derived before, [MSA] $\mu M = 437 \times$ absorbance; the value of $[CH_3SOOH]_{max}$, 53 μM was also used. This value was added to obtain the Scatchard plot for each compound, namely, [MSA] $= 53 \mu M$ and [MSA]/[DMSO] $= 0.0$ was employed to

fit the straight line to each compound. If the measured [MSA] was greater than 53 μM, the point was omitted from the Scatchard plot. In this experiment, only DMSO 15 mM data had to be omitted. These data not only gave more than 53 μM of MSA, but also deviated from the straight line of the Scatchard plot (data not shown). This fact indicates that DMSO and the radical yielded from DMSO by ·OH attack thus yield extra MSA when more than 15 mM DMSO is used. The Scatchard plots of Nicaraven are shown in Fig. 5, and those of the other compounds in Fig. 6. By using each slope $(-1/K)$ and $K = k_2[C]/k_1$, k_2 value of each compound was calculated. The results are shown in Table 1.

The kinetic constant of 10 mM of Nicaraven is also exhibited in Table 1.

When sterilized water was added which contained none of the detectable metallic ions used for making PBS and no Fe–EDTA, that is, when no metals were involved in this ex-

$y = 10.419 - 0.20635x$ R^2 = 0.997

$y = 21.513 - 0.41340x$ R^2 = 0.980

■ Nicaraven 10 mM
◆ Nicaraven 5 mM

Fig. 5. Scatchard Plots of Nicaraven

$y = 23.118 - 0.38432x$ R^2 = 0.919

$y = 31.531 - 0.55163x$ R^2 = 0.943

$y = 52.662 - 1.0248x$ R^2 = 0.980

$y = 48.180 - 0.84789x$ R^2 = 0.949
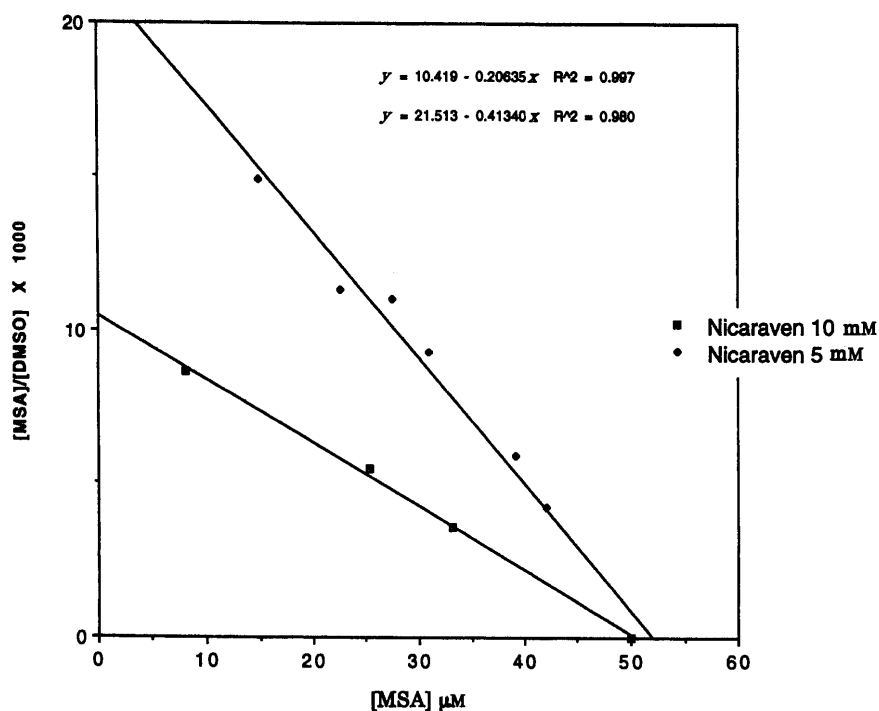
■ Pyridine
◆ NM-NA
■ Mannitol
◆ NMAA
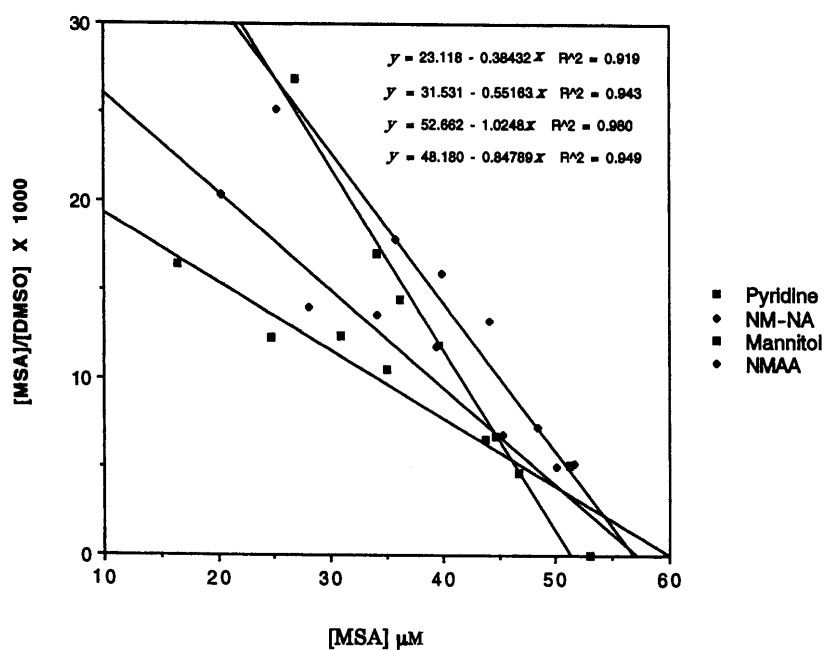
Fig. 6. Scatchard Plots of the Other 4 Compounds

Table 1. Kinetic Constants Obtained from Scatchard Plots

	Slope $\times 10^9$ M^{-1}s^{-1}	$\times 10^3$ M	Literature value for k_2 $\times 10^9$ M^{-1}s^{-1}
Nicaraven	3.4	−0.415	
Pyridine	3.6	−0.384	4.5[19]
Mannitol	1.4	−1.025	1.0—1.8[20]
NM-NA	2.5	−0.552	
NMAA	1.7	−0.848	1.6[21]
Nicaraven (10 mM)	3.4	−0.208	

The slope is the coefficient of the Scatchard plots ($-1/K$). The drug concentration is always 5.0 mM, except for the Nicaraven on the last line in which the drug concentration is 10 mM.

periment, no meaningful amount of MSA was detected.

The Reactive Site of Nicaraven with ·OH Solvent extraction was carried out to learn which moiety of Nicaraven is attacked by ·OH (see Materials and Method). The extracted weight after drying by a vacuum pump is shown in Table 2.

Nicaraven has two possible sites where the hydroxyl radical attacks; pyridine moiety[22,23] and amide moiety.[24—26] Pyridine is known to be changed to pyridinol by an ·OH attack.[22,23] Generally speaking, the phenolic proton shows signals of a higher field than 9.5 ppm on the ^{1}H-NMR spectrum, while when the amide moiety is attacked by ·OH, nicotinic acid or nicotinamide is yielded; because amino acid[24,25] or

Table 2. Weight (mg) of Each Extract when 284 mg of Nicaraven Is Used

	H_2O_2 concentration (mM)		
	0.0	8.8	13.2
CH_2Cl_2 extract (1)	280.0	209.0	186.7
CH_2Cl_2 extract (2)	11.0	28.6	25.4
Ethanol extract	81.7	71.7	81.1

See Experimental for the extraction scheme.

Table 3. The Ratio of the Strength of Absorptions Due to Stretching Vibrations of Hydrogen Bonded N–H at 3340 cm^{-1}/Free N–H at 3450 cm^{-1}

Nicaraven conc. (mM)	Absorbance ratio A_{3340}/A_{3450}
30	1.47
10	1.04
3	0.78
0.5	0.73
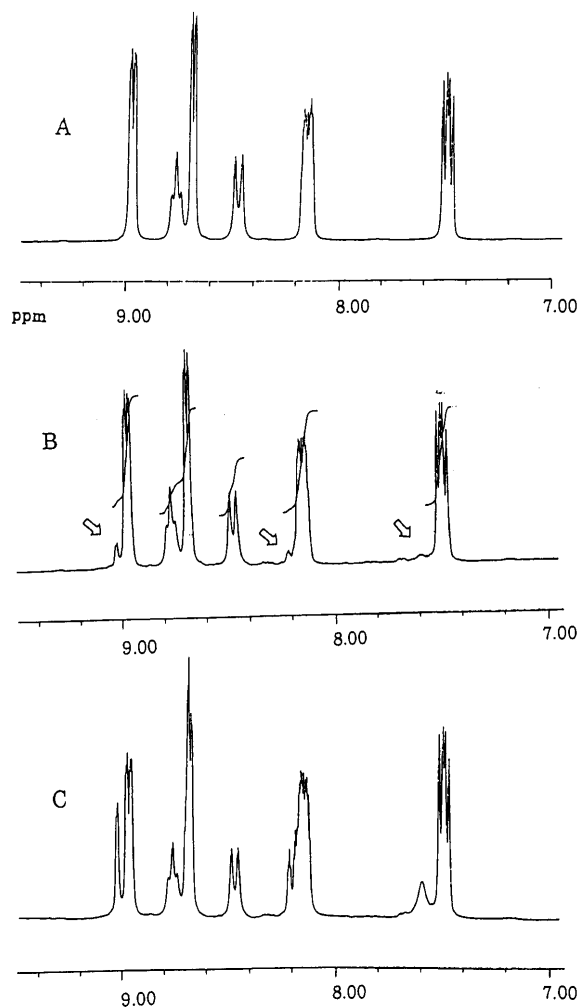
Fig. 7. ^{1}H-NMR Spectra for the Identification of Nicotinamide

A: Nicaraven, B: dichlorometane extract 2. Nicotinamide signals are shown with arrows. C: small amount of nicotinamide is added to B.

amino acid amide[26] has been hypothesized to result from protein degradation by an ·OH attack.

The search for nicotinic acid and nicotinamide was carried out by ^{1}H-NMR measurements by adding small amounts of these compounds to each extract, and non-addition and post-addition samples were compared. Nicotinamide was found from two dichloromethane extracts as shown in Fig. 7. In a pre-search of these compounds, nicotinamide was identified on TLC (data not shown).

The nicotinamide molar content found in this ^{1}H-NMR measurement was roughly 1/7 that of Nicaraven from the integration of the spectrum of dichloromethane extracts 1 and 2, because the signal strength ratio of pyridine proton of nicotinamide to Nicaraven is about 1/15 when 13.2 mM of H_2O_2 to 10 mM of Nicaraven was used. In contrast, no nico-

tinic acid was found in either ^{1}H-NMR or TLC.

No phenolic proton could be found on the ^{1}H-NMR spectra of three extracts and the freeze dried sample before the extraction was applied.

The ethanol extract showed a rather broad ^{1}H-NMR spectra (data not shown) even after the re-extraction by 2-propanol to avoid extracting inorganic compounds (data not shown). In this case, the residual 2-propanol showed sharp spectra.

It can thus be concluded that the amide groups of Nicaraven play an important role in reacting with ·OH. Other reports mention that the polymerization and precipitation of proteins occur after an ·OH attack under oxygen free conditions.[27,28]

Structure Determination of Nicaraven in $CDCl_3$ The structure in $CDCl_3$ was obtained after measuring the N–H stretching vibration and calculating the semi-empirical quantum mechanics. Below the 3 mM concentration levels of Nicaraven, the ratio of the strengths of the stretching vibrations of the hydrogen bonded N–H (3340 cm^{-1}) to free N–H (3450 cm^{-1}) is almost constant, as shown in Table 3. This means that at concentrations below 3 mM, the Nicaraven molecule has no intermolecular hydrogen bond and the dominant structure of Nicaraven has an intramolecular hydrogen bond. The 3 mM IR spectrum is shown in the upper part of Fig. 8. The spectrum of 10 mM NM-NA in the lower part of Fig. 8 is seen to have almost no intermolecular hydrogen bond.

Three of the ten structures had an intramolecular hydrogen bond after simulated annealing and the successive geometric optimization using molecular mechanics (data not shown). Although there are four possible structures having an intramolecular hydrogen bond, only two structures are possible which have a methine proton and one of the methylene protons is in the trans position (from ^{1}H-NMR measurement, see below); therefore, we do not have to consider two structures whose methyl groups are axial to a 7-membered ring formed by an intramolecular hydrogen bond. These two possible structures are shown in Fig. 9. PM3 calculation showed the upper structure of Fig. 9 to be more stable by 2.0 kcal/mol. The most stable conformation by PM3 calculation is called model I and the less-stable structure is called model II in Fig. 9.

The two different NMR signals of two methylene protons were observed for a $CDCl_3$ solution of Nicaraven as shown in the upper part of Fig. 10, which supports the IR measurements in that the main molecular structure has an intramolecular hydrogen bond. The spectrum in a more polar solvent such as DMSO-d_6 however, does not show intra-molecular hydrogen bonding as in the lower part of Fig. 10. Based on the observed coupling constants obtained in $CDCl_3$, the dihedral angles were calculated for models I and II using the
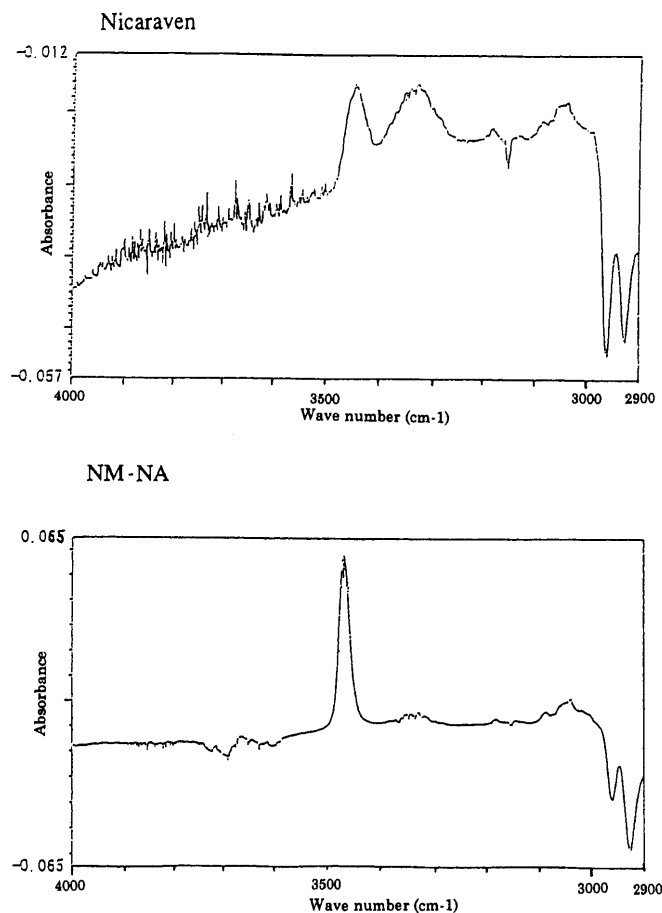
Nicaraven

NM-NA

Fig. 8. IR-Spectrum of N–H Stretching Vibration of 3 mM Nicaraven in the Upper Part of the Figure and of 10 mM NM-NA in the Lower Part

Fig. 10. ¹H-NMR Spectra

Upper: 20 mM Nicaraven in CDCl₃. Lower: 20 mM Nicaraven in DMSO-d₆.

Fig. 9. Two Optimized Structures of Nicaraven by PM3
Each proton is named as shown.

Karplus equations given before. These results are given in Table 4. It was found that the structure of model II can be disregarded due to the disagreement of the observed and calculated HNCH angles. Although the HₐNCHʙ angle does not agree with the observed value for model I, the other dihedral angles are closely similar to the observed values. The Karplus equations used in this calculation have been established from rigid molecules and for peptides. In this case, as only one hydrogen bond was seen to contribute to the cyclic structures, some disagreement between the observed and calculated dihedral angles may be permissible because the dynamic motion of the Nicaraven molecule could occur in CDCl₃. From the ¹H-NMR measurement, the model I structure could be hypothesized to be a main structure in chloroform, and this structure of Nicaraven was maintained even under concentrations as high as 20 mM.

The methylene signals at various concentrations of Nicaraven measured by JNM-EX270 are shown in Fig. 11. Signals at lower and upper fields are assigned to HB and HC, respectively. By decreasing the concentration of Nicaraven, the center of the HB proton shifts slightly down-field while that of the HC proton shifts slightly up-field and the spectra become complex at low concentrations. For this reason, we used DRX750 to obtain coupling constants at 2 mM. Although slight chemical shifts were observed when Nicaraven concentrations were changed, the main features of the spectra

Table 4. Coupling Constants Observed in this Experiment

	J_{OBS} (20 mM)	Angle (20 mM) from Karplus equation	J_{OBS} (2 mM)	Angle (2 mM) from Karplus equation	Angle of model I	Angle of model II
H_ANCH_B	6.6—6.9	±138—142	6.7	±142	−102.14	123.28
H_ANCH_C	4.6—4.7	±42—44	4.8	±44	142.30	8.41
		±128—130		±132		
H_BCCH_D	9.8—9.9	0	9.9	0	166.49	173.79
		±150—160		±150		
H_CCCH_D	3.6	±55	3.2	±60	−76.79	−69.85
H_DCNH_E	6.9	±142	5.0	±130	133.66	−114.67

The concentrations of Nicaraven are 20 and 2 mM. Based on the coupling constants, the dihedral angles were calculated using the equations noted in Experimental. The dihedral angles of model I and model II are shown in the Table. J_{OBS} 20 mM of H_DCNH_E was obtained from methine proton signals by the HOMO spin decoupling to methyl protons and H_E proton signals. J_{OBS} of 2 mM was obtained from H_E proton signals.
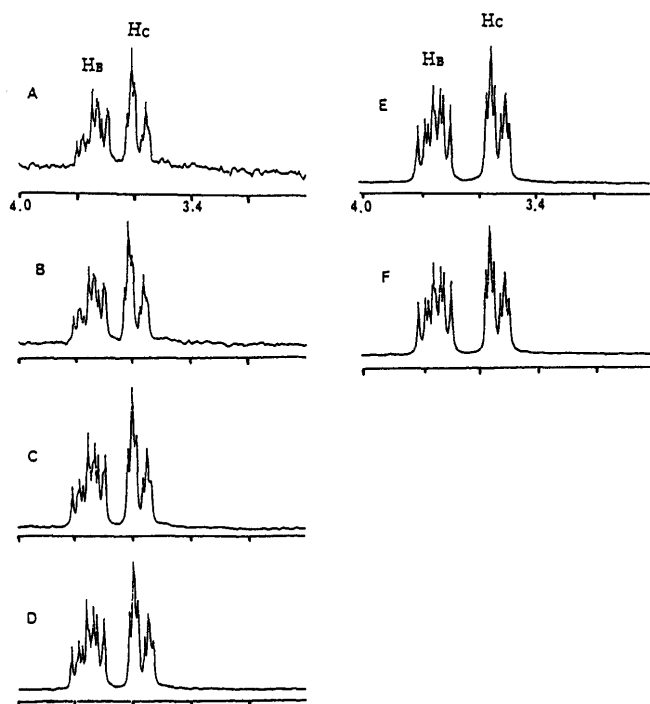
Fig. 11. The Methylene Signals of Nicaraven in $CDCl_3$ with the Change of Its Concentrations

A: 1 mM, B: 2 mM, C: 3 mM, D: 5 mM, E: 10 mM, F: 20 mM.

were very similar and no sudden conformational change was observed.

Discussion

Experimental Accuracy and Scavenging ·OH by Nicaraven The k_2 values of this experiment are in good agreement with those of the literature cited as shown in Table 1. Although a relatively high concentration of the compound was needed in this experiment, we were able to relatively easily obtain the value of k_2 by the method described in this paper.

The kinetic constant of the reaction obtained in this experiment between Nicaraven and ·OH seems relatively small when Nicaraven is regarded as a direct scavenger of ·OH. However, we do not have enough environmental information on brain in disease, nor do we have sufficient local information about the Nicaraven molecule. We must take into account the complex formation ability of Nicaraven to an isolated iron atom, although the ability of the complex formation of Nicaraven with iron is substantially weaker than that

of EDTA with iron (data not shown). This fact might support the possibility that Nicaraven molecules tend to be located near iron atoms. In particular, a pyridine nitrogen atom can bind with an iron atom and the Nicaraven molecule can react rapidly with ·OH as soon as it is produced from an iron atom owing to the short distance between an iron ion and a Nicaraven molecule. Thus, the relatively high concentration of Nicaraven around an iron ion might be expected in the natural body. It may thus be concluded that the kinetic constant is a very important factor, but we also have to consider local distance and local concentration information whenever we deal with problems including reactions with ·OH.

Furthermore, Yamazaki and Piette found that the efficacy of ·OH generation varied with the nature of the iron chelators used.[11] Nicaraven–iron complex may decrease the total ·OH production.

It is noteworthy that the studies on oxygen free radicals and iron in biology and medicine have been reviewed by Halliwell and Gutteridge.[29]

Further investigations on the complex formation of Nicaraven with iron and on the efficacy of ·OH generation of the complex are therefore necessary.

Deoxyribose Method and This Method Halliwell et al. reported a simple "test-tube" assay to determine the rate constants using deoxyribose for reactions with hydroxyl radicals.[30] Their method does not require any complex pipette operations and may be more reliable than this method.

Their method can be briefly summarized as follows:

2-Deoxy-D-ribose (DR) is degraded on exposure to ·OH produced by Fenton systems. If the resulting complex mixture of products is heated under acidic conditions, malonaldehyde (MDA) is formed and can be detected by its ability to react with thiobarbituric acid (TBA) to form a pink chromogen, namely:

·OH+DR→fragments→MDA

2TBA+MDA→chromogen
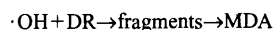
Any other molecule S added to the reaction mixture that is capable of reacting with ·OH should compete with DR for ·OH to an extent dependent on its rate constant for reaction with ·OH and its concentration relative to DR .

the rate of reaction of DR with the hydroxyl radical=k_{DR}[·OH][DR]

the rate of reaction of S with the hydroxyl radical=k_S[·OH][S]

As a result, Halliwell et al. finally derived

$$\frac{1}{A} = \frac{1}{A_0}\left(1 + \frac{k_S[S]}{k_{DR}[DR]}\right)$$

where A is the absorbance in the presence of a scavenger S at concentration [S] and A_0 is the absorbance in the absence of a scavenger. Hence, a plot of $1/A$ against [S] should give a straight line of slope $k_s/k_{DR}[DR]A_0$ with an intercept on the y-axis of $1/A_0$, and the rate constant for the reaction of S with the hydroxyl radical can be obtained from the slope of the line. They used k_{DR} as $3.1 \times 10^9 \, M^{-1}s^{-1}$ obtained by gamma radiolysis and [DR] of more than 2.8 mM.

Halliwell *et al.* stressed the linearity of the straight line plot of the compound concentration, and the inverse of absorbance as x and y-axes, respectively, guarantees the usefulness of their method. Indeed, many compounds have been tested in this way with consistently good results.[30] However, their report does not touch upon the damage of the products yielded from DR by ·OH attack. Actually, it was shown by Parij *et al.*[31] that nonlinear competition plots were observed in several nonsteroidal anti-inflammatory drugs when the amount of [DR] used was 2.8 mM, and linear plots were observed when the amount of [DR] was 15 mM.

The method established by Halliwell *et al.* can analyze the change in the kinetic constant due to a change in the concentration of a compound, namely, the concentration dependency of a kinetic constant, can be analyzed. However, we have to consider that this kind of dependency could occur only when molecular interaction or molecular conformation changes happen at low concentrations of a compound in an aqueous solution. Such changes are considered to be rare. For this reason, an analysis at a fixed concentration of [S] while changing [DR] or [DMSO] could be worth future study.

Reactive Site of Nicaraven with the Hydroxyl Radical From the Fenton reaction samples, it was found that the amide group plays an important role in reactions with ·OH. Furthermore, Hu *et al.* determined the k_2 of nicotinic acid to be $0.68 \times 10^9 \, M^{-1}s^{-1}$.[32] In addition, the cumyloxyl radical $(C_6H_5C(CH_3)_2O\cdot)$ was found by laser flash photolysis to attack the amide moiety of N-isopropylnicotinamide.[33] These facts suggest the pyridine ring of nicotinic acid derivative is not easily attacked by ·OH.

MSA Stability in This System Scaduto reported that the determination of MSA formation from DMSO underestimates the product of ·OH, because MSA is further oxidized by ·OH to methanesulfonate.[13] However, more than 5 mM of DMSO protects 100 μM MSA completely in this experiment, when the total [·OH] is around 50 μM. This means that DMSO could be a good indicator of ·OH in *in vivo* experiments, although there are some difficulties in obtaining total [·OH] as mentioned before. Actually there are several valuable *in vivo* reports.[34—36]

Nicaraven Penetration through BBB The permeability of Nicaraven into the brain is fairly good.[7] The structures of brain drugs have been summarized,[37] and both the bulkiness and the ring structures of these drugs appear to be quite important factors. Nitrogen atoms are also included more often in the structures than oxygen atoms. A chain structure is quite rare for a brain drug. Seelig *et al.* measured the surface area of the brain drugs and found that it is smaller than that of BBB non-penetrable drugs when they are of similar molecular weight.[38]

Nicaraven
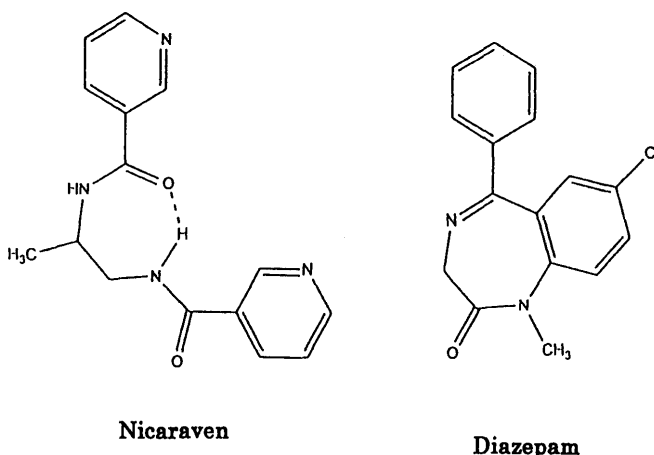
Diazepam

Fig. 12 Schematic View of Nicaraven and One of the Benzodiazepins, Diazepam

The PM3 calculation as well as the measurement of the IR and ^{1}H-NMR spectra are very interesting because the structure can be seen to partly resemble benzodiazepines, as shown in Fig. 12. The methyl in the propylene group of Nicaraven stabilizes the 7-membered ring by the 1—4 atom repulsive interaction. This could mean that Nicaraven assumes a similar, benzodiazepine-like structure when penetrating the BBB.

The benzodiazepine transporter in the brain is not known at present. There might be no specific transporter for benzodiazepines, although there are reports on the benzodiazepine inhibition of nucleoside transport in human erythrocytes[39] and on the benzodiazepine inhibition of triiodothyronine accumulation in human neuroblasts.[40] However, the concentrations of benzodiazepines in the brain are more than twice that in the total blood.[41] This fact suggests the importance of having a benzodiazepine-like structure which is able to penetrate the BBB.

References
1) Wilson J. X., *Can. J. Physiol. Pharmcol.*, **75**, 1149—1163 (1997).
2) Floyd R. A., Carney J. M., *Ann. Neurol.*, **32**, Suppl: S22—7 (1992).
3) Hall E. D., *Neurosurg. Clin. N. Am.*, **8**, 195—206 (1997).
4) Asano T., Takakura K., Sano K., Kikuchi H., Nagai H., Saito I., Tamura A., Ochiai, C., Sasaki T., *J. Neurosurg.*, **84** 792—803 (1996).
5) Germano A., Imperatore C., D'Avella D., Costa G., Tomasello F., *J. Neurosurg.*, **88**, 1075—1081 (1998).
6) Gidö G., Wieloch T., in preparation.
7) Bernnett J. P., Smith T. S., Naito S., in preparation.
8) Kamiyama H., Aso Y., in preparation.
9) Babbs C. F., Griffin D. W., *Free Rad. Biol. Med.*, **6**, 493—503 (1989).
10) Yamazaki I., Piette L. H., *J. Am. Chem. Soc.*, **113**, 7588—7593 (1991).
11) Yamazaki I., Piette L. H., *J. Biol. Chem.*, **265**, 13589—13594 (1990).
12) Koller W.C., *Neurology*, **36**, 1147 (1986).
13) Scaduto R. C., *Free Rad. Biol. Med.*, **18**, 271—277 (1995).
14) Cederbaum A. I., Dicker E., Rubin E., Cohen G., *Biochem. Biophys. Res. Commun.*, **78**, 1254—1262 (1977).
15) Gutteridge J. M. C., Wilkins S., *Biochim. Biophys. Acta*, **759**, 38—41 (1983).

16) Stewart J. J. P., *J. Comput. Aided Mol. Des.*, **4**, 1—105 (1990).

17) Bystrov V. B., *Progress in NMR Spectroscopy*, **10**, 44—81 (1976).

18) Kopple K. D., Wiley G. R., Tauke R., *Biopolymers*, **12**, 627—636 (1973).

19) Cohem H., Meyerstein D., *J. Chem. Soc. Dalton*, **1976**, 1976—1979.

20) Goldstein S., Czapski G., *Int. J. Rad. Biol.*, **46**, 725—729 (1984).

21) Hayon E., Ibata T., Lichtin N. N., Simic N., *J. Am. Chem. Soc.*, **92**, 3898—3903 (1970).

22) Steeken S., *J. Phys. Chem.*, **82**, 372—374 (1978).

23) Selvarajan N., Raghavan N. V., *J. Phys. Chem.*, **84**, 2548—2551 (1980).

24) Rana T. M., Meares C. F., *J. Am. Chem. Soc.*, **112**, 2457—2458 (1990).

25) Rana T. M., Meares C. F., *Proc. Nat. Acad. Sci. U.S.A.*, **88**, 10578—10582 (1991).

26) Puchara M., Schuessler H., *Int. J. Peptide Protein Res.*, **46**, 326—332 (1995).

27) Davis K. J. A., Lin S. W., Pacific R. E., *J. Biol. Chem.*, **262**, 9914—9920 (1987).

28) Walff S. P., Dean R. T., *Biochem. J.*, **234**, 399—403 (1986).

29) Halliwell B., Gutteridge J. M. C., *Arch. Biochem. and Biophys.*, **246**, 501—514 (1986).

30) Halliwell B., Gutteridge J. M. C., Aruoma O. I., *Anal. Biochem.*, **165**, 215—219 (1987).

31) Parij N., Nagy A. N., Neve J., *Free Rad. Res.*, **23**, 571—579 (1995).

32) Hu M. L., Chen Y. K., Lin Y. F., *Chem-Biol. Interact.*, **97**, 63—73 (1995).

33) Sugita M., Yatsuhashi M., Shimada T., Inoue H., *Res. Chem. Intermed.*, to be submitted.

34) Das D., Bandyopadhyay D., Bhattacharjee M., Banerjee R., *Free Rad. Biol. & Med.*, **23**, 8—18 (1997).

35) Tsai L., Lee K., Liu T., *Free Rad. Biol. & Med.*, **24**, 732—737 (1998).

36) Jahnke L. S., *Anal. Biochem.*, **269**, 273—277 (1999).

37) Fukai S., "New Drugs Today," 6th ed., Yakujijihou-sha, Japan, **1995**, pp.1—77.

38) Seelig A., Gottschilich R., Devant R. M., *Proc. Natl. Acad. Sci. U.S.A.*, **91**, 68—72 (1994).

39) Hammond J. R., Jarvis S. M., Paterson A. R. P., Clanachan A. S., *Biochem. Pharmacology*, **32**, 1229—1235 (1983).

40) Kragie L., Doyle D., *Endocrinology*, **130**, 1211—1216 (1992).

41) Dubey R. K., McAllister C. B., Inoue M., Wilkinson G. R., *J. Clin. Invest.*, **84**, 1155—1159 (1989).

Effect of the Linking Position of a Side Chain in Bis(quinolylmethyl)ethylenediamine as a DNA Binding Agent

Yuji Mikata,* Yoko Onchi, Maki Kishigami, and Shigenobu Yano

Department of Chemistry, Faculty of Science, Nara Women's University, Nara 630–8506, Japan.
Received August 27, 1999; accepted December 3, 1999

Two bisquinoline derivatives, *N,N'*-bis(2-quinolylmethyl)ethylenediamine (2-BQME) and *N,N'*-bis(8-quinolylmethyl)ethylenediamine (8-BQME) have been synthesized, and their ability to bind to duplex DNA was studied. 8-BQME bound to DNA more strongly than 2-BQME, judging from the extent of increase in the melting temperature of duplex DNA, the UV-vis spectral change, and ethidium displacement assay. These compounds exhibited apparent AT-specificity suggesting minor groove binding in addition to intercalation.

Key words　bisquinoline; ethylenediamine; DNA

Since potent DNA-binding agents are among the most promising candidates for chemotherapeutic drugs, a lot of natural and unnatural ligands for DNA have been extensively studied. Intercalators and groove binders have gathered the greatest attention in this area. When compared with mono-intercalators, bisintercalators have several advantages including: i) increased binding affinity, ii) enhanced specificity for DNA due to bisintercalation, and iii) improved sequence selectivity.[1,2] Among a large number of the DNA bisintercalators studied to date, bisquinolines have potential as antibiotics, antimalarial,[3—5] and antitumor agents. In addition, these compounds are useful for studying the role of chromophores in natural compounds.[6] The quinoline ring is considered to have a low potential for both intercalating and groove binding ability.[7] However, due to its small ring size, it is expected to be capable of penetrating into cell membranes and dispersing into solid tumor tissues.[8]

As a linker of bisquinoline derivatives, an ethylenediamine moiety has several advantageous features such as donation to the phosphate backbone of DNA in a protonated structure, enhancement of water solubility, ability for DNA hydrolysis, and metal chelation ability that introduces DNA modification or scission functionality.[9] Thus, a systematic study aimed at the DNA binding ability of bisquinolines with an ethylenediamine linker seems to be important; however, such a study has not been reported to date to the best of our knowledge. In the present study, we report the synthesis and evaluation of two very simple bisquinoline derivatives, *N,N'*-bis(2-quinolylmethyl)ethylenediamine (2-BQME) and *N,N'*-bis(8-quinolylmethyl)ethylenediamine (8-BQME) as DNA binding

agents by DNA-melting, spectroscopic titration, and ethidium displacement assay.

2- and 8-BQME were synthesized from the corresponding methylquinoline *via* bromination of the methyl groups, followed by dimerization using ethylenediamine. As reference compounds, 8-(aminomethyl)quinoline (8-AMQ), *N*-(8-quinolylmethyl)ethylenediamine (8-QME) and *N,N'*-dimethylethylenediamine (DMEN) were used in this study. All compounds were isolated as hydrochloride salts.

Figures 1a and 1b show the UV-melting curves of calf thymus DNA, demonstrating the enhanced thermal stability of the duplex in the presence of 2- and 8-BQME, respectively. Increasing the concentrations of both ligands leads to stabilization of the duplex. The thermal denaturation temperatures (T_m) are summarized in Table 1.

Although 8-AMQ did not show any obvious duplex stabilization, 8-BQME exhibited a significant effect. Comparing the 8-AMQ and 8-QME, the extra aliphatic nitrogen atom increased DNA affinity. The addition of an extra 8-quinolyl ring into DMEN and 8-QME also had an important effect. One quinoline ring corresponds to a 2 degree increase in T_m where the [drug]/[base pair of DNA] ratio (r) is 0.5. It should be noted that the addition of a 2-quinolyl group to DMEN has absolutely no effect on its binding affinity to DNA, since the ΔT_m values of 2-BQME and DMEN are almost identical in all cases. It is concluded that the 2-quinolyl substituent has a markedly smaller effect on DNA binding than the 8-quinolyl moiety.

These quinoline compounds exhibited their absorption maxima at 313—315 nm, and with the addition to calf thymus DNA, these absorption bands slightly decreased (Fig. 2). However, distinct isosbestic points were not observed and the spectral change in the long-wavelength region arising from the quinoline ring transition was too small to determine the association constants of these quinoline derivatives. The extent of spectral change in quinoline derivatives was parallel with the DNA-stabilizing ability obtained from UV-melting experiments (8-BQME>8-QME>2-BQME).

From the result of a duplex denaturation experiment and

2-BQME　　　　　　　　　　8-BQME

8-AMQ　　　　8-QME　　　　DMEN
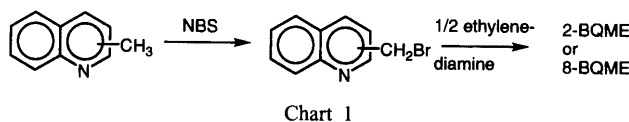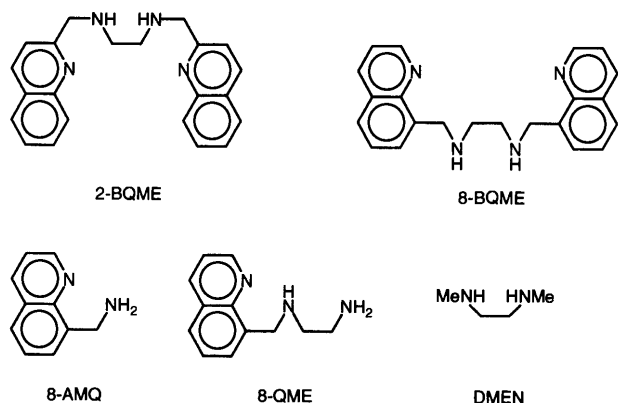
Chart 1

DNA-titration analysis, the quinoline ring moiety should interact with DNA. These quinolines were also found to drive out DNA-bound ethidium bromide. Although ethidium bromide is not fluorescent in free solution, it becomes fluorescent when intercalated into DNA. The C_{50} values (the micromolar drug concentrations necessary to reduce the fluorescence of initially DNA-bound ethidium by 50%) against calf thymus DNA, (poly[AT])$_2$, and (poly[GC])$_2$ obtained by this assay was listed in Table 2. The extent of fluorescence quenching due to a non-displacement mechanism were estimated to be small in the experiment where excess DNA was employed. Apparent AT-specificity in both compounds was observed. A higher GC/AT ratio of the C_{50} value in 8-BQME comes from the weak interaction with (poly[GC])$_2$, suggesting a minor-groove interaction of this compound with the

DNA duplex. In contrast, 2-BQME displaces ethidium in a similar manner, regardless of whether ethidium binds to calf thymus DNA or (poly[GC])$_2$. This fact suggests that electrostatic interaction governs the interaction of 2-BQME with DNA.

In conclusion, two bisquinolines with an ethylenediamine linker have been synthesized, and an 8-linked derivative was found to bind to DNA more strongly than the 2-linked derivative. AT-specific interaction of these compounds with DNA suggests the interaction mode of these compounds is primarily groove binding.

Experimental

Melting points were determined on a micro hot-stage Yanaco MP-S3. ^{1}H-NMR were measured on a Varian Gemini 2000 spectrometer at 300 MHz. The mass spectrum was measured on a JEOL SX102 mass spectrometer. Measurement of absorbance spectra and the DNA denaturation experiment were run on a Shimadzu UV-3100PC with temperature controller SPR-8. Fluorescence measurements were performed on a Jasco FP-750 with an ETC-272T temperature controller.

8-(Bromomethyl)quinoline[10] 8-Methylquinoline (9.9 g, 69 mmol) was dissolved in CCl$_4$ (70 ml) and refluxed in the presence of N-bromosuccinimide (NBS) (12.4 g, 69 mmol) and 2,2'-azobisisobutyronitrile (AIBN)

Fig. 1. UV Melting Profiles at 260 nm of Calf Thymus DNA Duplex in the Presence of Bisquinoline Derivatives

a) 2-BQME, b) 8-BQME. r=[drug]/[DNA (in base pair)].

Table 1. Increase in Melting Temperature (ΔT_m) of Calf Thymus DNA in the Presence of Quinoline Derivatives[a]

Compounds	ΔT_m/°C		
	$r=0.1$	$r=0.3$	$r=0.5$
2-BQME	ca. 0	1.4	3.2
8-BQME	2.9	5.1	7.1
8-QME	1.4	4.2	5.7
8-AMQ	ca. 0	ca. 0	ca. 0
DMEN	ca. 0	1.5	3.1

a) Measured at 25 °C.

Table 2. C_{50} Values[a] in the Ethidium Displacement Assay Bound to Calf Thymus DNA, Poly[d(AT)]$_2$, and Poly[d(GC)]$_2$[b]

Compound	C_{50}/μM			$\frac{C_{50}(GC)}{C_{50}(AT)}$
	Calf Thymus	Poly[d(AT)]$_2$	Poly[d(GC)]$_2$	
2-BQME	140	105	145	1.4
8-BQME	38	35	57	1.6

a) See text. b) [DNA]=0.5 μM, [ethidium]=1.26 μM.

Fig. 2. Absorbance Change of 2-BQME (2.5×10^{-5} M) in the Presence of an Increasing Amount of Calf Thymus DNA in 1.0 mM Sodium Cacodylate Buffer Containing 4.0 mM NaCl (pH 6.0) at 25 °C

a) Whole spectra, b) magnified spectra of 310—320 nm region.

(0.14 g) for 2 h. After cooling, the solution was filtered, evaporated, and the residue was washed with MeOH to give 8-(bromomethyl)quinoline as white needles (11.4 g, 75%). 2-(Bromomethyl)quinoline[11,12] was obtained in a similar manner (54%).

8-BQME A mixture of ethylenediamine (0.28 g, 4.6 mmol), potassium carbonate (2.3 g, 16 mmol), and anhydrous acetone (20 ml) was stirred for several minutes at room temperature. To the mixture was added dropwise 8-(bromomethyl)quinoline (3.0 g, 14 mmol) in 30 ml of anhydrous acetone. After being refluxed overnight, the reaction mixture was dried under reduced pressure and the residue was extracted with chloroform. The solvent was dried, evaporated, and the resulting residue was dissolved in 2 N HCl (100 ml) and washed with dichloromethane (50 ml×4 times) to remove unreacted 8-(bromomethyl)quinoline. The acidic solution was adjusted with NaOH to pH=14, extracted with dichloromethane, dried, and evaporated to give 8-BQME as a yellow oil. This oil was dissolved in conc.HCl and methanol to give tetrahydrochloride salt (0.052 g, 38%), mp 180—183 °C. ^{1}H-NMR (D$_2$O) δ: 3.88 (s, 4H), 4.94 (s, 4H), 7.34—7.40 (m, 2H), 7.46—7.52 (m, 2H), 7.60 (d, 2H), 7.72 (d, 2H), 8.25—8.30 (m, 2H), 8.55 (d, 2H). *Anal.* Calcd for C$_{22}$H$_{32}$Cl$_4$N$_4$O$_3$ (BQME·4HCl·3H$_2$O): C, 48.72; H, 5.95; N, 10.33. Found: C, 48.84; H, 5.72; N, 9.99.

2-BQME was obtained in a manner similar to that used for 8-BQME (8%), mp 165—168 °C. ^{1}H-NMR (D$_2$O) δ: 3.58 (s, 4H), 4.50 (s, 4H), 7.40 (d, 2H), 7.5—7.62 (m, 4H), 7.7—7.9 (m, 4H), 8.28 (d, 2H). HR-MS (FAB) Calcd for C$_{22}$H$_{23}$N$_4$ (M+H) 343.1923. Found 343.1892.

DNA Denaturation Experiment Absorbance *vs.* temperature melting curves were measured at 260 nm using 5×10^{-5} M (in base pairs) of calf thymus DNA in 1.0 mM sodium cacodylate buffer containing 4.0 mM NaCl (pH 6.0). The heating rate was 3 °C/min. T_m values were determined from the first derivative plots of melting curves.

Spectroscopic Analysis An absorbance change in bisquinolines ([compound]=2.5×10^{-5} M) was monitored in the presence of duplex DNA (2—25 $\times 10^{-5}$ M (in base pairs)) in 1.0 mM sodium cacodylate buffer (pH 6.0) at 25 °C.

Ethidium Displacement Assay C_{50} values (the micromolar drug concentrations necessary to reduce the fluorescence of initially DNA-bound ethidium by 50%) were obtained using 0.5 μM (in base pairs) of DNA (1.0 μM sodium cacodylate buffer containing 4.0 μM NaCl (pH 6.0)) with

1.26 μM of ethidium at 25 °C. The extent of fluorescence quenching due to a non-displacement mechanism was estimated by the similar methods employing 20 μM of DNA and 2 μM of ethidium.

References
1) Kim H. K., Kim J.-M., Kim S. K., Rodger A., Nordén B., *Biochemistry*, **35**, 1187—1194 (1996).
2) Molina A., Vaquiero J. J., Garcia-Navio J. L., Alvarez-Builla J., de Pascual-Teresa B., Gago F., Rodorigo M. M., Ballesteros M., *J. Org. Chem.*, **61**, 5587—5599 (1996).
3) Nasr M., Burckhalter J. H., *J. Heterocyclic Chem.*, **16**, 497—500 (1979).
4) Vannerstrom J. L., Ellis W. Y., Ager, A. L., Jr., Andersen S. L., Gerena L., Milhous W. K., *J. Med. Chem.*, **35**, 2129—2134 (1992).
5) Raynes K., Galatis D., Cowman A. F., Tilley L., Deady L. W., *J. Med. Chem.*, **38**, 204—206 (1995).
6) Alfredson T. V., Maki A. H., Warning A. J., *Biochemistry*, **30**, 9665—9675 (1991).
7) Mikata Y., Yokoyama M., Ogura S., Okura I., Kawasaki M., Maeda M., Yano S., *Bioorg. Med. Chem. Lett.*, **8**, 1243—1248 (1998).
8) Denny W. A., Rewcastle G. W., Bauguley B. C., *J. Med. Chem.*, **33**, 814—819 (1990).
9) Dervan P. B., Becker M. M., *J. Am. Chem. Soc.*, **100**, 1968—1970 (1978).
10) Bu X. H., An D. L., Chen Y. T., Shionoya M., Kimura E., *J. Chem. Soc., Dalton Trans.*, **1995**, 2289—2295.
11) Rukachaisirikul V., Koert U., Hoffmann R. W., *Tetrahedron*, **48**, 4533—4544 (1992).
12) Brown B. R., Hammick D. L., Thewlis B. H., *J. Chem. Soc.*, **1951**, 1145—1148.

Molecular Dynamics Simulations of Bovine Cathepsin B and Its Complex with CA074

Atsushi Yamamoto,[a] Koji Tomoo,*,[a] Hiroo Miyagawa,[b] Yuji Takaoka,[b] Shigeyuki Sumiya,[b] Kunihiro Kitamura,[b] and Toshimasa Ishida*,[a]

Department of Physical Chemistry, Osaka University of Pharmaceutical Sciences,[a] 4-20-1 Nasahara, Takatsuki, Osaka 569-1094, Japan and Research Center, Taisho Pharmaceutical Co., Ltd.,[b] 1-403 Yoshino-cho, Ohmiya, Saitama 330-0031, Japan. Received September 8, 1999; accepted December 10, 1999

To promote our better understanding of the dynamic stability of the bovine cathepsin B structure, which is characterized by an extra disulfide bond at Cys148–Cys252 from the other species, and of the binding stability of CA074 (a cathepsin B-specific inhibitor), molecular dynamics (MD) simulations were performed for the enzyme and its CA074 complex, assuming a system in aqueous solution at 300 K. The MD simulation covering 400 ps indicated that the existence of a Cys148–Cys252 disulfide bond increases the conformational flexibility of the occluding loop, although the conformational stability of the overall structure is little affected. The structural characteristics of the complex elucidated by X-ray analysis were suggested to be also intrinsic and stable in the dynamic state; the hydrogen bonding/electrostatic interactions between the main and side chains of CA074 and the S*n* and S*n'* subsites of the enzyme were maintained throughout the MD simulation. Furthermore, the simulation made clear that the binding of CA074 significantly restricted the conformational flexibility of the substrate binding region, especially the occluding loop, of cathepsin B. Statistical analyses during the simulation suggest that the selectivity of CA074 for cathepsin B stems from the tight P1'–S1' and P2'–S2' interactions, assisted in particular by double hydrogen bonds between the carboxyl two oxygens of the CA074 C-terminus and the imidazole NH groups of His110 and His111 residues.

Key words bovine cathepsin B; CA074; molecular dynamics simulation; conformational fluctuation; substrate specificity; inhibitory mechanism

Careful balance between the degradation and biosynthesis of protein is responsible for the maintenance of various biological processes, whereas imbalance is associated with various pathological phenomena. Lysosomal cysteine proteases are abundant in living cells and play important roles in intracellular proteolysis.[1,2] Among them, cathepsin B (EC 3.4.22.1) is a major component of lysosomal enzymes and its abnormal elevation has been implicated in muscular dystrophy,[3] bone resorption,[4,5] pulmonary emphysema,[6] rheumatoid arthritis,[7] and tumor metastasis.[8,9] Therefore, the development of a low-molecular inhibitor specific for cathepsin B could be expected to be used as a therapeutic drug for these diseases, and in addition, as a tool for physiological clarification of the enzyme.

Previously, we designed a cathepsin B-specific covalent-type inhibitor, CA074 [*N*-(L-3-*trans*-propylcarbamoyloxirane-2-carbonyl)isoleucyl-proline, Fig. 1],[10] based on the crystal structure of papain-E64c (a potent covalent-type inhibitor for wide variety of cysteine proteases) complex[11]; CA074 has been pharmacologically shown to be a potent inhibitor specific for cathepsin B *in vivo*[12] as well as *in vitro*.[13] The X-ray crystal analysis of bovine spleen cathepsin B (BSCB)–CA074 complex[14] made clear the binding modes of the main and side chains of CA074 to the S and S' subsites of the enzyme. It is important, when considering the substrate-specificity of cathepsin B and its inhibitory mechanism by CA074, to further know the dynamic stability of the whole tertiary structure of the enzyme and its binding stability with CA074. Thus, in this article, we deal with the molecular dynamics (MD) simulation of BSCB and its CA074 complex, and compare the results with those observed in the X-ray crystal structure. These data would be useful to develop a noncovalent-type inhibitor specific for cathepsin B.

Also, we investigate in this work the effect of the Cys148–Cys252 disulfide bridge in BSCB for the tertiary structure by the MD simulation, because cathepsin B from other species lacks this bridge.

Experimental

Generation of Complex Structures MD calculations were performed for three systems: BSCB, its reduced form in which the Cys148–Cys252 disulfide bridge was cut (noted as 'BSCB'), and BSCB–CA074 complex, respectively. The atomic coordinate of each system was derived by manual op-
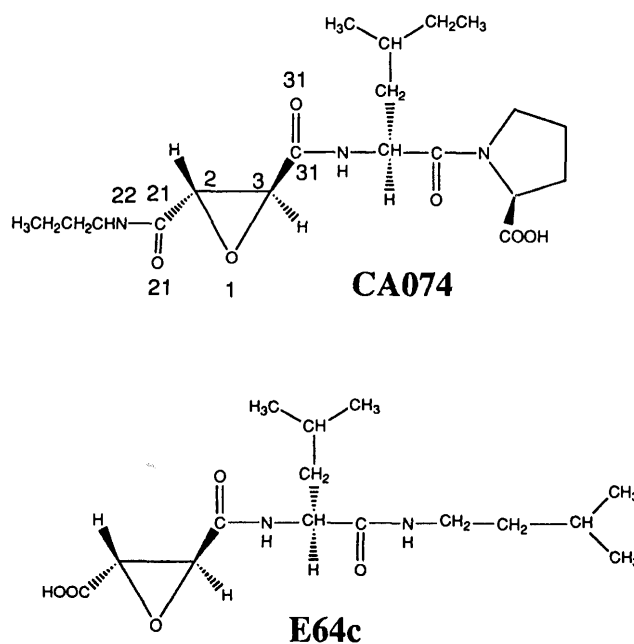

Fig. 1. Chemical Structures of CA074 and E64c

The atomic numbering of CA074 used in this work is given.

* To whom correspondence should be addressed.

eration on a computer graphics program from the atomic coordinates of BSCB-CA074 (PDB code: 1QDQ). The simulation was performed assuming the state of pH 5.0—6.0; the ionization states of respective polar residues were treated by reference to related papers.[15,16] The Pro carboxyl group of CA074 was treated as an anionic state because of the pK_a (=1.95) of proline and the electrostatic interactions with the cationic imidazole NHs of His110 and His111 residues of BSCB (discussed later); the structure of the complex crystallized at pH 3.5 showed an anionic state of the carboxyl group. Initially, to eliminate the bad contacts of hydrogen atoms, each structure was energy-minimized for 1000 steps with non-hydrogen atoms constrained at their initial coordinates. The program AMBER 4.1[17] was used. In order to neutralize the system, sodium ions were placed near each protein surface, where the electrostatic potential was negative. Four sodium ions were placed close to Glu75, Glu122, Asp227, and Glu245 for BSCB and 'BSCB', and five close to Glu53, Glu75, Glu122, Asp227, and Glu245 for the complex. Hereafter, we call these molecules (enzyme, sodium ions, and inhibitor) solute. Then each solute was placed in a rectangular box (size of 68×63×51 Å^3) filled with TIP3P[18] water molecules. The total numbers of atoms were 20179, 20196, and 19938 for the respective systems. For BSCB and CA074, an AMBER all-atom force field[19] was used and the atomic charges of CA074 were calculated using the Gaussian 92 program[20] with the 6-31 G* basis set, employing restrained electrostatic potential fitting.[21]

MD Simulation For the MD simulation, the periodic boundary condition was used, and electrostatic interaction was calculated by the particle mesh Ewald method.[22] To accelerate the calculation, a special-purpose parallel computer for non-bonded force sum, MD-Engine,[23] was used for the real space sum of the Ewald method. Using the Berendsen algorithm[24] with a coupling time of 0.2 ps, temperature and pressure were controlled at 300 K and 1 bar, respectively. The simulations of each system were performed according to the following procedure: a) the width of a time step was 0.5 fs for 500 steps, b) the SHAKE[25] constraints were applied to hydrogen atoms, and the time step was 1 fs for 2500 steps, c) the time step was 2 fs with SHAKE constraints for hydrogen atoms for 500 steps, then d) the time step was 2 fs with SHAKE constraints for hydrogen atoms for 200000 steps. In the procedure of a)—c), the temperature control for the solute and solvent was done separately, and the non-hydrogen atoms of the solute were constrained at their initial coordinates. In the procedure d), the sodium ions close to Glu245 of BSCB, Asp227 and Glu245 of 'BSCB', and all ions of the BSCB-CA074 complex, stayed at the initial position on this simulation time scale. Other ions strayed from the initial positions and moved around near BSCB.

Results and Discussion

Increased Flexibility of Occluding Loop by Extra Disulfide Bridge of BSCB The Cys148-Cys252 disulfide bridge in BSCB is a unique structural feature of bovine cathepsin B, because all cathepsin Bs from chicken,[26] mouse,[27] human,[28] and rat[29] lack this bridge. This extra disulfide bridge of BSCB has been considered to be closely related to its enzymatic activity, based on human and rat cathepsin Bs being about three times less active than bovine cathepsin B against the hydrolysis of N-benzyloxycarbonyl-L-arginyl-β-naphthylamide (Bz-Arg-βNA), a low-molecular-weight substrate analogue.[30] Therefore, it is interesting to investigate the possible relationship between the molecular conformation and this extra disulfide bridge in BSCB. In order to estimate to what extent this disulfide bond contributes to conformational stability, MD simulations were performed for two systems, i.e., BSCB and 'BSCB' (the reduced form of Cys148-Cys252 disulfide bridge). The time profiles of the respective conformational fluctuations are shown in Fig. 2, where the averaged deviations of the occluding loop and all Cα atoms from their respective X-ray structural positions are monitored. The 105—125 sequence (called the occluding loop) constructs the structural feature of cathepsin B which is missing in other lysosomal enzymes, and has been proposed to be important for the peptidyldipeptidase activity of cathepsin B.[31] The mutual orientation of

the occluding loop and the Cys148-Cys252 disulfide bridge in BSCB is shown in Fig. 3.

The aqueous solution systems of BSCB and 'BSCB' both reached to their respective stationary states within the MD simulations of 60 ps, as judged from the ratio of root-mean-square deviation (RMSD) fluctuations against respective potential energies becoming <3% after 60 ps; generally, a value less than 5% has been considered as a criterion to estimate an equilibrium state of the system by the MD simulation. During the MD simulation covering 400 ps, both BSCB and 'BSCB' showed stationary structures similar to the X-ray structure, and meaningful fluctuations were observed for the residues which exhibited relatively large temperature factors in the crystal structure. Nevertheless, it is important to note that the occluding loop in the MD-simulated structures of BSCB shows the considerably large deviation, compared with that of 'BSCB'. Since no notable difference was observed in the whole fluctuation degree of either system, this result indicates that the Cys148-Cys252 disulfide bridge affects the increased flexibility of the occluding loop structure. Since the occluding loop is located at the Sn' subsite of the active site, the increased flexibility of the loop structure may be closely related to the biological function of bovine cathepsin B.[31,32] Since the Cys148-Cys252 disulfide bridge is about 42 Å away from the tip of the occluding loop, direct interaction of the bridge with the loop structure is impossible (Fig. 3). It appears that the increased flexibility of the loop structure is due to the structural behavior of the Ileu105-Cys148 sequence which is located at the surface of the BSCB molecule. The function of the sequence is to cause a large fluctuation of the occluding loop at one end by the disulfide formation at the other end.

Increased Stability of BSCB Active Site Structure by Complex Formation with CA074 To investigate to what extent CA074 affects the conformation of BSCB by its covalent bonding to the Cys29 S$^\gamma$ atom, MD simulations covering 400 ps were performed for an aqueous system of the BSCB-CA074 complex. The time profiles of the conformational RMSD fluctuations for both structures (BSCB alone and complex) are shown in Fig. 4. Characteristically, fluctuations of the occluding loop, as well as the overall structure, observed in the MD simulation of BSCB free form were significantly decreased by the covalent bonding of CA074; the fluctuation of the occluding loop is much more reduced than that of the overall structure. Considering the location of the loop structure is at the active site, it could be said that such an increased stability of the loop structure is important in revealing or inhibiting peptidyldipeptidase activity.

MD-Simulated Binding Mode of CA074 to BSCB Active Site Some interaction pairs, which participate significantly in the complex formation, were made clear by X-ray analysis of the complex.[14] The distance fluctuations of their interaction pairs during the MD simulation are summarized in Table 1. A snapshot of the binding mode of CA074 to the Sn and Sn' (n=1 and 2) subsites of BSCB at 400 ps MD simulation is shown in Fig. 5. Compared with the structure of the enzyme, the inhibitor fluctuated somewhat more largely. However, the double hydrogen bonds between Pro carboxyl O atoms and His110 and His111 imidazole NH were essentially maintained throughout the MD simulation without any breakage, suggesting the tightness of these hydrogen bonds.
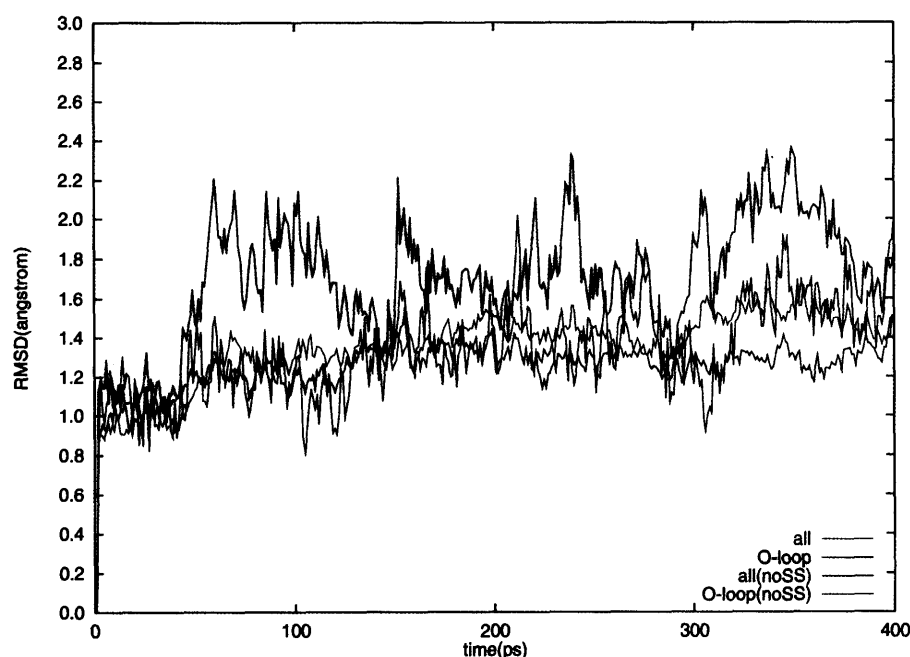
Fig. 2. Time Profiles of RMSD of MD-Simulated $C\alpha$ Atoms of BSCB and 'BSCB' from X-Ray Crystal Structure

The fluctuation of RMSD was monitored for all (blue) and occluding loop (sequence of 105—125) (green, shown as O-loop) $C\alpha$ atoms of BSCB and for all (red) and occluding loop (black) $C\alpha$ atoms of 'BSCB' (shown as noSS).
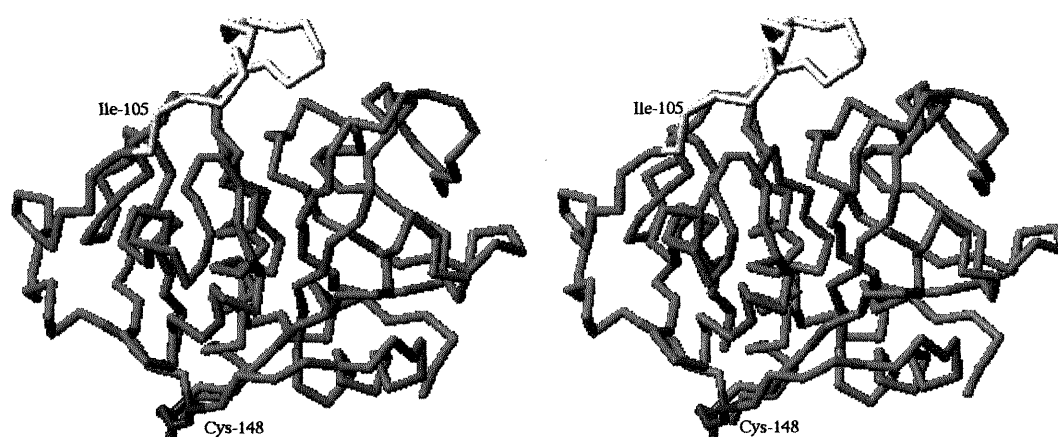
Fig. 3. Stereoscopic View of Spatial Orientations of Occluding Loop (Yellow) and Cys148–Cys252 Disulfide Bridge (Red) in Tertiary Structure of BSCB Backbone (Blue)
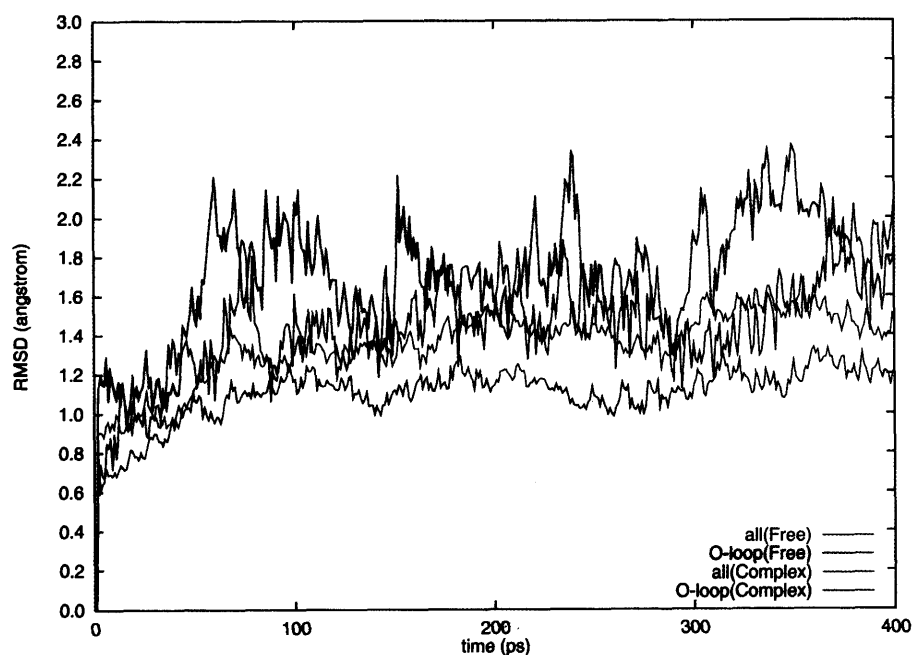
Fig. 4. Time Profiles of RMSD of MD-Simulated $C\alpha$ Atoms of BSCB–CA074 Complex from X-Ray Crystal Structure

The fluctuation of RMSD was monitored for all (blue) and occluding loop (sequence of 105—125) (green) $C\alpha$ atoms of BSCB alone (shown as Free) and for all (red) and occluding loop (black) $C\alpha$ atoms of BSCB–CA074 complex (shown as Complex).

(a)

(b)
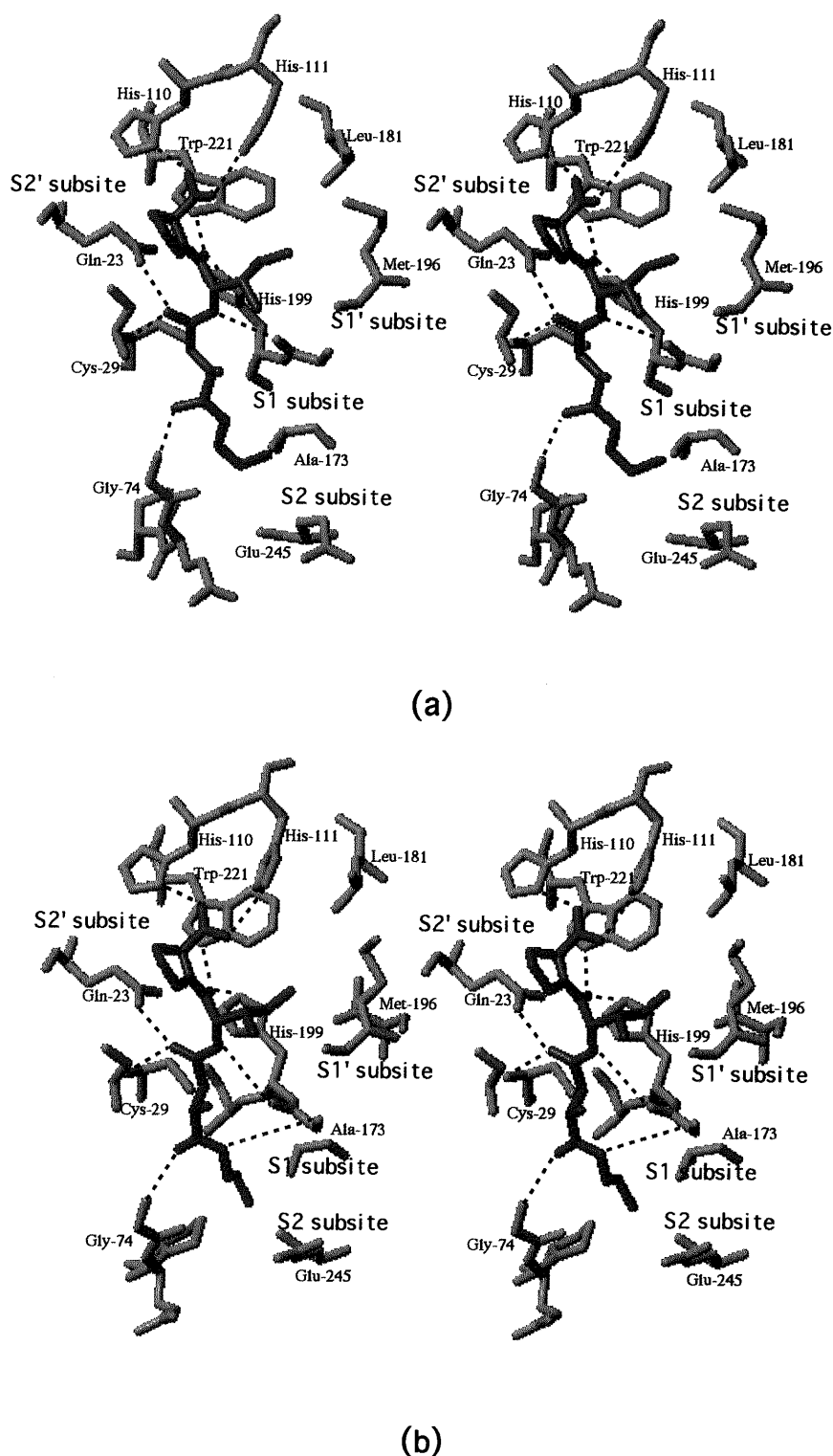
Fig. 5. Stereoscopic Views of Binding Modes of CA074 to BSCB Binding Pocket (a) Snapshot at 400 ps MD Simulation and (b) X-Ray Crystal Structure Interaction pairs less than 4.0 Å are shown by dotted lines.

This is a main reason why the high flexibility of the occluding loop of BSCB is significantly decreased by the complex formation with CA074, thus CA074 exhibits cathepsin B specific inhibitory activity. The same conclusion has been reported by Feng et al.[16] The Ile moiety, the side chain of which is fixed at the S1' subsite (Val176, Leu181, Met196, His199, and Trp221) by hydrophobic interaction, is further stabilized by two (Pro)C=O···HN(Trp221 indole) and

(Ile)C=O···NH (His199 imidazole) hydrogen bonds. At the opposite side of the hydrophobic S1' pocket, the oxyanion hole, which has been thought to stabilize the reaction intermediate, is located, and the oxirane O31 atom formed hydrogen bonds with $N^{\varepsilon 2}H$(Gln23) and NH(Cys29) groups throughout the simulation, thus forming a hydrophilic situation.

On the other hand, the propyl side chain of CA074, al-

Table 1. Averaged Interatomic Distances between the Functional Groups of CA074 and BSCB Active Sites during MD Simulations, together with Values Observed in the X-Ray Crystal Structure

CA074	BSCB	MD[a]	X-ray
O (Pro carboxyl)	NH(His110 imidazole)	2.73 (8)	2.69
O (Pro carboxyl)	NH (His111 imidazole)	2.82 (14)	3.24
O=C (Ile)	NH (Trp221 indole)	3.13 (19)	3.12
O=C (Pro)	NH (His199 imidazole)	2.95 (17)	3.32
NH (Ile)	O=C (Gly198)	3.62 (25)	3.39
O31 (oxirane)	NH (Gln23 side chain)	2.87 (12)	2.82
O31 (oxirane)	NH (Cys29)	3.22 (16)	3.48
O21 (oxirane)	NH (Gly74)	3.53 (46)	3.22
NH (propyl)	N(Gly198)	4.06 (65)	3.39
NH (propyl)	O=C(Gly198)	4.04 (62)	4.44

a) The respective estimated standard deviations are given in parentheses.

Table 2. Variations of CA074 Torsion Angles (°)

Torsion angle	X-Ray	MD(ASD)[a]
$\psi 2$	172	157 (13)
$\phi 2$	-83	-79 (6)
$\omega 2$	158	176 (6)
$\omega 1$	-177	-163 (6)
$\phi 1$	-48	-70 (8)
$\psi 1$	143	146 (7)
$\chi 1$	54	66 (10)
$\chi 2$	158	168 (20)
$\theta 1$	93	104 (8)
$\theta 2$	173	163 (7)
$\theta 3$	80	152 (9)
$\delta 1$	177	-165 (25)
$\delta 2$	91	-163 (57)
$\delta 3$	160	-35 (66)
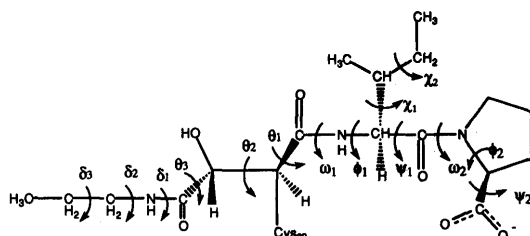
a) MD and ASD represent the mean angle and angular standard deviation during the MD simulation, respectively.

though it was located at the S2 subsite (Pro76, Ala173, Ala200, and Glu245) by hydrophobic interaction, experienced a large conformational fluctuation during the MD simulation, and the O21(oxirane)...NH(Gly74), which is within the range of hydrogen bond in the crystal structure, decreased during the simulation, indicating the relatively wide and flexible space of the S2 subsite.

The above-mentioned binding situation of CA074 to the Sn' and Sn subsites (n=1 and 2) could be also estimated from the torsion angle variation of the inhibitor. The respective mean torsion angles during the simulation are given in Table 2, in which the value of the crystal structure is also given for comparison. The side chain ($\chi 1$ and $\chi 2$) of Ile showed no significant fluctuation during the MD simulation, and this is due to the hydrogen bonds formed by C-terminal carboxyl and carbonyl groups of Pro and Ile residues of CA074 (Table 1), in addition to the hydrophobic interactions of the Ile side chain with the S1' constituting residues, and of the Pro pyrrolidine ring with Gln23 and Trp221. In contrast,

the propylcarbamoyl group ($\theta 3$, $\delta 2$, and $\delta 3$), located at the S1 and S2 subsites, experienced a large conformational change during the simulation because of no specific interactions; the NH(propyl)···O=C(Gly198) electrostatic interaction did not contribute to the stability of this group. These results suggest that the substrate-specificity of cathepsin B is revealed by the binding mode to the S1' and S2' subsites rather than the S1 and S2 subsites; the occluding loop is located so as to block the orientation of the substrate at the Sn' subsite of $n \geq 3$.

In conclusion, the present MD simulations made clear the dynamic structural stability/feature of bovine cathepsin B and its CA074 complex, together with the inhibitory mechanism. These results would be valuable for further designing noncovalent-type inhibitors with high specificity and potent activity.

References
1) Kirschke H., Barrett A. J., "Lysosomes: Their Role in Protein Breakdown," ed. by Glaumann H., Ballard F. J., Academic Press, London, 1987, pp. 193—283.
2) Knop M., Schiffer H. H., Rupp S., Wolf D. H., Curr. Opin. Cell Biol., 9, 990—996 (1993).
3) Katunuma N., Kominami E., Rev. Physiol. Biochem. Pharmacol., 108, 1—20 (1987).
4) Dalaisse J. M., Eeckhout Y., Vaes G., Biochem. Biophys. Res. Commun., 125, 441—447 (1984).
5) Vaes G., Clin. Orthop., 231, 239—271 (1988).
6) Johnson D., Travis J., Biochem. J., 163, 639—641 (1977).
7) Esser R. E., Angelo R. A., Murphey M. D., Watts L. M., Thornburg L. P., Palmer J. T., Talhouk J. W., Smith R. E., Arthritis Rheum., 37, 236—247 (1994).
8) Sloane B. F., Honn K. V., Cancer Metastasis Rev., 3, 249—263 (1984).
9) Sloane B. F., Rozhin J., Robinson D., Honn K. V., Biol. Chem. Hoppe-Seyler, 371 (Suppl.), 193—198 (1990).
10) Sumiya S., Yoneda T., Kitamura K., Murata M., Yokoo C., Tamai M., Yamamoto A., Inoue M., Ishida T., Chem. Pharm. Bull., 40, 299—303 (1992).
11) Yamamoto D., Matsumoto K., Ohishi H., Ishida T., Inoue M., Kitamura K., Mizuno H., J. Biol. Chem., 266, 14771—14777 (1991).
12) Towatari T., Nikawa T., Murata M., Yokoo C., Tamai M., Hanada K., Katunuma N., FEBS Lett., 280, 311—315 (1991).
13) Murata M., Miyashita S., Yokoo C., Tamai M., Hanada K., Hatayama K., Towatari T., Nikawa T., Katunuma N., FEBS Lett., 280, 307—310 (1991).
14) Yamamoto A., Hara T., Tomoo K., Ishida T., Fujii T., Hata Y., Mutara M., Kitamura K., J. Biochem. (Tokyo), 121, 974—977 (1997).
15) Hasnain S., Hirama T., Tam A., Mort J. S., Biol. Chem., 267, 4713—4721 (1992).
16) Feng M. H., Chan S. L., Xiang Y., Huber C. P., Lim C., Protein Engineering, 9, 977—986 (1996).
17) Pearlman D. A., Case D. A., Caldwell J. W., Ross W. S., Cheatham T. E. III, Ferguson D. M., Seibel G. L., Singh U. C., Weiner P. K., Kollman P.A., AMBER 4.1, University of California, San Francisco, 1995.
18) Jorgensen W. L., J. Am. Chem. Soc., 103, 335—340 (1981).
19) Cornell W. D., Cieplak P., Bayly C. I., Gould I. R., Merz K. M., Jr., Ferguson D. M., Spellmeyer D. C., Fox T., Caldwell J. W., Kollman P. A., J. Am. Chem. Soc., 117, 5179—5197 (1995).
20) Frisch M. J., Trucks G. W., Head-Gordon M., Gill P. M. W., Wong M. W., Foresman J. B., Johnson B. G., Schlegel H. B., Robb M. A., Replogle E. S., Gomperts R., Andres J. L., Raghavachari A. K., Binkley J. S., Gonzalez C., Martin R. L., Fox D. J., Defrees D. J., Baker J., Stewart J. J. P., Pople J. A., Gaussian 92, Gaussian Inc, 1992.
21) Bayly C. I., Cieplak P., Cornell W. D., Kollman P. A., J. Phys. Chem., 97, 10269—10280 (1993).
22) Darden T., York D., Pedersen L., J. Chem. Phys., 98, 10089—10092 (1993).
23) Toyoda S., Miyagawa H., Kitamura K., Amisaki T., Hashimoto E., Ikeda H., Kusumi A., Miyakawa N., J. Comput. Chem., 20, 185—199 (1999).

24) Berendsen H. J. C., Postma J. P. M., Van Gunsteren W. F., DiNola A., Haak J. R., *J. Chem. Phys.*, **81**, 3684—3690 (1984).

25) Rychaert J. P., Ciccotti G., Berendsen H. J. C., *J. Comput. Phys.*, **23**, 327—341 (1977).

26) Dong A.-S., Stransky G. I., Whitaker C. H., Jordan S. E., Schlesinger P. H., Edwards J. C., Blair H. C., *Biochim. Biophys. Acta*, **1251**, 69—73 (1995).

27) Chan S. J., Segundo B. S., McCormick M. B., Steiner D. F., *Proc. Natl. Acad. Sci. U.S.A.*, **83**, 7721—7725 (1986).

28) Ritonja A., Popovic T., Turk V., Wiedenmann K., Machleidt W., *FEBS Lett.*, **181**, 169—172 (1985).

29) Takio K., Towatari T., Katunuma N., Teller D. C., Titani K., *Proc. Natl. Acad. Sci. U.S.A.*, **80**, 3666—3670 (1983).

30) Barrett A. J., "Proteinases in Mammalian Cells and Tissues," ed. by Barrett A. J., North-Holland Publishing, Amsterdam, 1977, pp.181—208.

31) Illy C., Quraishi O., Wang J., Purisima E., Vernet T., Mort J. S., *J. Biol. Chem.*, **272**, 1197—1202 (1997).

32) Turk D., Podobnik M., Kuhelj R., Dolinar M., Turk V., *FEBS Lett.*, **384**, 211—214 (1996).

Podophyllotoxin Aza-Analogue, A Novel DNA Topoisomerase II Inhibitor

Akira Iida,[a] Masahiro Kano,[a] Yoshihiro Kubota,[b] Kenji Koga,[c] and Kiyoshi Tomioka*,[a]

Graduate School of Pharmaceutical Sciences, Kyoto University,[a] Sakyo-ku, Kyoto 606–8501, Japan, Faculty of Engineering, Gifu University[b] Gifu 501–9311, Japan, and Graduate School of Pharmaceutical Sciences, The University of Tokyo,[c] Hongo, Bunkyo-ku, Tokyo 113–0033, Japan. Received September 24, 1999; accepted December 27, 1999

The pendant E-ring moiety of the podophyllotoxin aza-analogue 1 that is a potent inhibitor of microtubule assembly was modified in order to acquire inhibitory activity of DNA topoisomerase II. The monophenolic analogue 2 did not exhibit human topoisomerase II inhibition, while the *ortho*-quinone 3 that was obtained by oxidation of 2 inhibited its catalytic activity (decatenation) in a dose-dependent manner and stimulated double strand DNA breaks in supercoiled circular plasmid DNA, resulting in the production of linear DNA. These results showed that the topoisomerase II inhibition of the *ortho*-quinone 3 is due to stabilization of the topoisomerase II–DNA covalent binary complex. On the other hand, the *ortho*-quinone 3 did not inhibit the relaxation process of supercoiled DNA by topoisomerase I at concentrations up to 400 μM, nor was intercalation observed in unwinding measurements of 3. Therefore, the *ortho*-quinone 3 was shown to be a novel nonintercalative topoisomerase II specific inhibitor that stabilizes the cleavable complex. The present results suggest that the 4′-free hydroxyl group on the E-ring and the sugar moiety on the C-ring are not a prerequisite for topoisomerase II inhibition by podophyllotoxin derivatives.

Key words DNA topoisomerase II; etoposide; podophyllotoxin; podophyllotoxin aza-analogue; inhibitor; cleavable complex

DNA topoisomerases, mechanistically divided into two main classes of types I and II, are critical enzymes that control the level of DNA supercoiling by catalyzing the passage of individual DNA strands or double strands through one another.[1] DNA topoisomerases are involved in biological processes of DNA metabolism such as replication, transcription, recombination and chromosome segregation at mitosis. Therefore, compounds that inhibit these enzymes as the primary cellular target are of special interest since those are promising candidates for anticancer drugs.[2]

Etoposide,[3] a DNA topoisomerase II specific inhibitor, is a semisynthetic lignan derived from podophyllotoxin,[4] a microtubule assembly inhibitor isolated from roots of *Podophyllum* sp. (Chart 1). Etoposide inhibits topoisomerase II by trapping the topoisomerase II–DNA covalent binary complex termed the cleavable complex,[5] resulting in cell death. Extensive structure–activity relationship studies on podophyllotoxin derivatives have suggested that the phenolic 4′-hydroxyl group of the pendant E-ring plays a crucial role in the DNA cleavage in which topoisomerase II is implicated.[6]

In our continuing studies toward antitumor compounds,[7] we have already reported the design and synthesis of podophyllotoxin aza-analogues 1 and 2.[8] Both analogues exhibited potent cytotoxicity against KB cells due to the inhibition of microtubule assembly, which resulted in arresting

cells in mitosis. This result allowed us to expect that podophyllotoxin aza-analogues are also potential topoisomerase II inhibitors. The trimethoxy analogue 1 did not show topoisomerase II inhibition, probably due to the lack of the structural requirement described above. However, no inhibitory effect of the monophenolic analogue 2 on the enzyme was observed at all. This unexpected result led to further modification of the E-ring moiety of 2 to the corresponding *ortho*-quinone 3 to exert the potential ability of the podophyllotoxin aza-analogues for topoisomerase II inhibition.[9]

We report herein the inhibitory effect of the *ortho*-quinone 3 on human DNA topoisomerase II. Analogue 3 has been shown to inhibit topoisomerase II by stabilizing the DNA–enzyme cleavable complex nonintercalatively as in the case of etoposide.

Experimental

All melting points were measured with a Buchi 510 melting point apparatus and are uncorrected. IR spectra were recorded on a Jasco IR Report-100 IR spectrometer. NMR spectra were measured with a JEOL GSX-400 spectrometer, and mass spectra were taken on a JEOL JMS-DX300 mass spectrometer. Column chromatography was run with BW-200 silica gel (Fuji Silysia Chemical, Ltd.).

Reagents Purified human placenta topoisomerases I (2 U/μl) and IIα (2 U/μl), kinetoplast DNA (kDNA), etoposide and 4′-(9-acridinylamino)-methanesulfon-*m*-anisidide (*m*-AMSA) were purchased from TopoGen, Inc. (Columbus, Ohio). Supercoiled pUC19 and pBR322 plasmid DNA and

1 R = Me
2 R = H

3

4

podophyllotoxin

etoposide
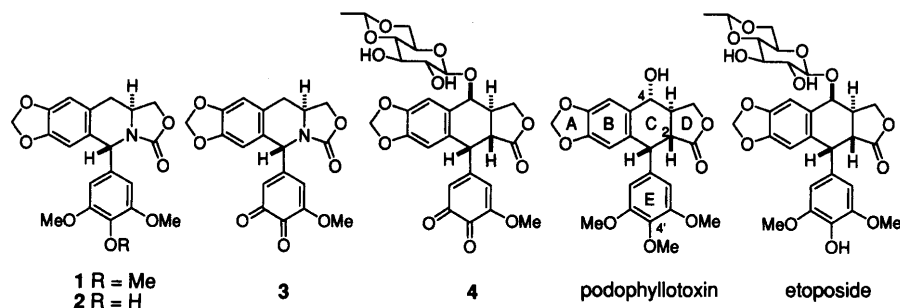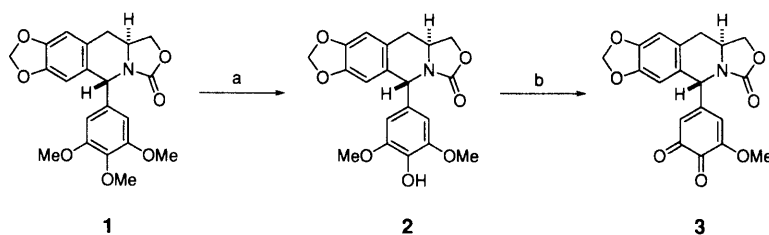
Chart 1

Reagents: a) HBr/Cl(CH₂)₂Cl, 0°C,14h, 80%; b) 6 M HNO₃/CHCl₃, r.t., 30s, 99%.

Chart 2

*Hind*III restriction endonuclease were obtained from Toyobo (Osaka).

Synthesis of *Ortho*-Quinone Analogue (3) To a vigorously stirred solution of the racemate of the monophenolic form **2** (24 mg) in CHCl₃ (1 ml) was added 6 M HNO₃ at room temperature. The reaction mixture was stirred for 30 s, quenched with H₂O (8 ml) and extracted with CHCl₃ (20 ml×3). The organic layer was washed with saturated NaHCO₃ (20 ml) and brine (20 ml×2), dried over Na₂SO₄ and concentrated *in vacuo*. The red oily residue was purified by silica gel column chromatography (CHCl₃/Me₂CO= 6/1), followed by recrystallization from CH₂Cl₂ and benzene to afford **3** (23 mg, 99%) as red powders, mp 185—188 °C (dec.), IR (CHCl₃) cm⁻¹: 1751, 1700, 1667, 1630. ¹H-NMR (CDCl₃) δ: 2.88 (1H, dd, *J*=5.9, 9.8 Hz), 2.90 (1H, d, *J*=9.8 Hz), 3.81 (3H, s), 4.00 (1H, m), 4.21 (1H, dd, *J*=3.3, 8.8 Hz), 4.61 (1H, dd, *J*=8.1, 9.8 Hz), 5.55 (1H, s), 5.66 (1H, d, *J*=1.8 Hz), 5.99 (2H, s), 6.20 (1H, d, *J*=1.8 Hz), 6.53, 6.63 (each 1H, s). ¹³C-NMR (CDCl₃) δ: 33.7 (t), 48.1 (d), 55.9 (d), 56.2 (q), 68.8 (t), 101.6 (t), 107.7 (d), 109.0 (d), 109.6 (d), 121.0 (d), 122.2 (s), 126.0 (s), 147.3 (s), 148.1 (s), 153.7 (s), 155.7 (s), 157.1 (s), 178.9 (s). MS *m/z*: 369 (M⁺). *Anal*. Calcd for C₁₉H₁₅NO₇: C, 61.79; H, 4.09; N, 3.79. Found: C, 62.07; H, 2.28; N, 3.55.

Kinetoplast DNA Decatenation Reaction mixtures contained 50 mM Tris–HCl (pH 8.0), 120 mM KCl, 10 mM MgCl₂, 0.5 mM ATP, 0.5 mM dithiothreitol (DTT), kDNA (200 ng), 2 μl of a drug solution (10% dimethyl sulfoxide [DMSO]) and 1 U of topoisomerase II in a total volume of 20 μl. Samples were incubated at 37 °C for 30 min and terminated with 2 μl of stop buffer (5% sarkosyl, 0.0025% bromophenol blue, 25% glycerol). Reaction products were electrophoresed on a 1% agarose gel in TAE (Tris-acetate-EDTA) running buffer.

Topoisomerase II Mediated DNA Cleavage Reactions (20 μl) containing 30 mM Tris–HCl (pH 7.6), 60 mM NaCl, 8 mM MgCl₂, 3 mM ATP, 15 mM mercaptoethanol, 2 μl of a drug solution (10% DMSO), 8 U of topoisomerase II and 250 ng of pBR322 plasmid DNA were incubated at 37 °C for 30 min. Samples were terminated by the addition of 2 μl of a solution containing 5% sodium dodecyl sulfate (SDS) and 2.5 mg/ml of proteinase K and incubated at 37 °C for 60 min. The samples were electrophoresed through a 1.2% agarose gel in TBE (Tris–borate–EDTA) running buffer containing 0.1% SDS. Both agarose gel and running buffer contained 0.5 μg/ml of ethidium bromide.

Topoisomerase I Mediated DNA Relaxation Reactions were carried out in the same manner as described for the decatenation assay except that reaction mixtures contained 10 mM Tris–HCl (pH 7.9), 1 mM EDTA, 150 mM NaCl, 0.1% bovine serum albumin (BSA), 0.1 mM spermidine, 5% glycerol and pUC19 plasmid DNA (200 ng).

DNA Unwinding Measurements Relaxed closed circular pUC19 DNA (250 ng) that was obtained by incubation with DNA topoisomerase I, followed by phenol extraction and ethanol precipitation, was incubated with DNA topoisomerase I in the standard reaction mixture for the relaxation assay in the presence of increasing amounts of *ortho*-quinone and *m*-AMSA.

Results and Discussion

DNA Topoisomerase II Inhibition by *Ortho*-Quinone 3 The aza-analogue **3** used for measurements of inhibitory activity of DNA topoisomerases was prepared by HNO₃ oxidation of the racemic monophenolic analogue **2** that was derived through treatment of **1** with HBr (Chart 2).

The inhibitory effect of analogue **3** on human DNA topoisomerase II was examined through the conversion of kDNA, a catenated network of DNA rings, to minicircle monomers

(a)

(b)
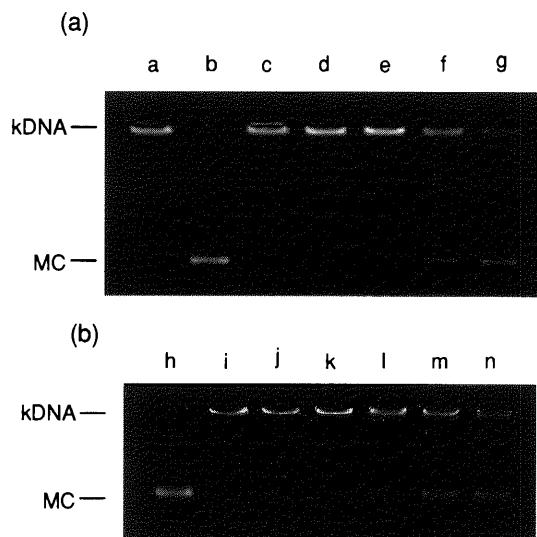
Fig. 1. Effects of *Ortho*-Quinone **3**, *m*-AMSA and Etoposide on the kDNA Decatenation Activity by DNA Topoisomerase II

Decatenation assays were performed in the presence of 1 U of topoisomerase II as described under Experimental. (a) Lane a, kDNA alone (no drug, no enzyme); b, control (no drug); c to g, 100, 50, 25, 12.5 and 6.25 μM of *ortho*-quinone **3**, respectively. (b) Lane h, control; i to k, *m*-AMSA; 1 to n, etoposide. Drug concentrations were 100 μM (lanes i and 1), 50 μM (lanes j and m), 25 μM (lanes k and n). MC: decatenated minicircle DNA.

(decatenation), which is a catalytic process that DNA topoisomerase II mediates. In the presence of 1 U of the enzyme, the *ortho*-quinone **3** inhibited the decatenation process of kDNA in a dose-dependent manner. Figure 1 is a photograph of agarose gels. Aza-analogue **3** completely inhibits the catalytic reaction of topoisomerase II at concentrations above 25 μM (Fig. 1a, lanes c to e), while decatenated minicircle DNA appears with decreasing amounts of **3** (12.5 and 6.25 μM, lane f and g). Its inhibitory activity was compared with those of topoisomerase II inhibitors *m*-AMSA[10] and etoposide (Fig. 1b). Under the same conditions, etoposide is found to require higher amounts for complete inhibition since minicircle DNA appears at all concentrations (lanes 1 to n) though *m*-AMSA shows comparable activity with that of **3** (lanes i to k). It was suggested that the sugar moiety and the partially aromatic polycyclic array in etoposide interact with the enzyme and DNA, respectively, during topoisomerase II processing,[11] and that the 4′-free hydroxyl group in the E-ring is essential for DNA damage in which the enzyme is implicated. In addition, the catechol analogue corresponding to **3**, which was obtained as a minor product in transformation of **1** to **2**, also exhibited topoisomerase II inhibitory activity that was comparable to that of **3** (not shown). Our data suggest at least that the sugar moiety at C-4 is not a prerequisite for

a b c d e f g h

RLXD
SCD
RLX, NC
SC—
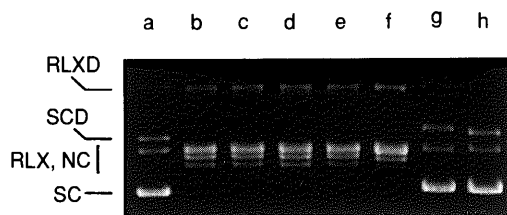
Fig. 2. Topoisomerase I-Mediated DNA Relaxation Reaction in the Presence of *Ortho*-Quinone 3 and *m*-AMSA

Relaxation experiments were carried out in the presence of 1 U of topoisomerase I as described under Experimental. (a) Lane a, supercoiled pUC19 plasmid DNA alone (no drug, no enzyme); b, control (no drug); c to e, 100, 200 and 400 μM of *ortho*-quinone 3; f to h, 25, 50 and 100 μM of *m*-AMSA. SC: supercoiled DNA. RLX: relaxed DNA topoisomers. NC: nicked circle DNA. SCD: supercoiled DNA dimers. RLXD: relaxed DNA dimers. Under our experimental conditions, *m*-AMSA at high concentrations (over 100 μM) appeared to inhibit relaxation of supercoiled DNA by topoisomerase I due to its strong intercalative ability with DNA. However, it was confirmed that unwinding of relaxed DNA by *m*-AMSA occurred at concentrations over 25 μM. Therefore, the SC band at lane g was unambiguously due to unwinding of relaxed DNA.

a b c d e f

NC—
LIN—
SC—
RLX
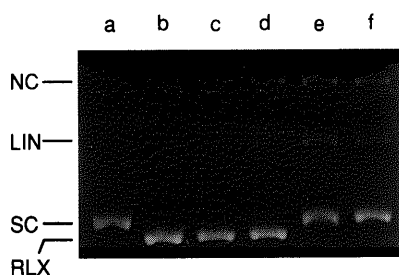
Fig. 3. Effects of *Ortho*-Quinone 3 on Topoisomerase II-Mediated DNA Cleavage Reaction

Cleavage assays were done in the presence of 8 U of topoisomerase II as described under Experimental. (a) Lane a, supercoiled pBR322 plasmid DNA alone (no drug, no enzyme); b, control (no drug); c to f, 1, 10, 50 and 100 μM of *ortho*-quinone 3. LIN: full-length linear DNA.

topoisomerase II inhibition by podophyllotoxin derivatives, and that the catechol and *ortho*-quinone forms for the E-ring are more essential for the activity than the monophenolic form.

The topoisomerase I mediated relaxation processing of supercoiled pUC19 plasmid DNA, however, was not inhibited by the *ortho*-quinone 3 at all at a concentration range up to 400 μM (Fig. 2, lanes c to e). Supercoiled DNA disappears completely to afford a mixture of relaxed DNA topoisomers. When the relaxation reactions were carried out in the presence of *m*-AMSA which is a topoisomerase II specific inhibitor, unwinding of relaxed DNA was observed at 50 μM (Fig. 2, lanes g and h) due to the strong intercalative ability of *m*-AMSA with DNA.[12] These results reveal that the *ortho*-quinone 3 is a nonintercalative DNA topoisomerase II specific inhibitor. Separately from DNA topoisomerase I mediated DNA relaxation experiments, DNA unwinding assays for 3 were done according to the procedures described in the Experimental to obtain a result that this *ortho*-quinone analogue does not intercalate with DNA (not shown).

Topoisomerase II Mediated DNA Cleavage Many natural and (semi)synthetic compounds have been reported as topoisomerase II inhibitors, most of which can be classified as inhibitors that trap a covalent binary complex consisting of DNA and the enzyme (the cleavable complex) resulting in the formation of the putative noncovalent ternary complex. Those compounds are further divided into two classes, intercalative and nonintercalative inhibitors, both of which afford full-length linear DNA due to double stranded DNA cleavage

by treating the ternary complex with a strong protein denaturant and proteinase K. To confirm whether the *ortho*-quinone 3 may stabilize the cleavable complex, DNA cleavage experiments were carried out using supercoiled pBR322 plasmid DNA in the presence of 8 U of topoisomerase II. The agarose gel photograph in Fig. 3 shows effects of the *ortho*-quinone 3 on the DNA processing by topoisomerase II. Formation of full-length linear DNA is enhanced with increasing amounts of 3 and clearly observed at a concentration of 50 μM (lane e). At the same time, nicked DNA that is formed by single stranded DNA breaks accumulates dose-dependently at concentrations up to 50 μM. The levels of formation of both linear and nicked DNA reach steady states between 50 and 100 μM. Another DNA cleavage experiment where the concentration range of 3 was between 10 and 50 μM showed that linear DNA was already present at 25 μM of 3 (not shown). These data indicate that the ortho-quinone 3 interferes with the DNA cleavage/religation equilibrium and stabilizes the covalent binary complex. Therefore, the podophyllotoxin aza-analogue 3 is identified as a nonintercalative DNA topoisomerase II specific inhibitor of which the mode of action is stabilization of the DNA-enzyme cleavable complex.

In this study we succeeded in transformation of microtubule assembly inhibitor 1 to topoisomerase II inhibitor 3 by making slight chemical modifications to the E-ring. This indicates that the E-ring plays a crucial role in affecting biological activities of podophyllotoxin-related lignans. On the other hand, it does not appear that functional groups at C-4 are a prerequisite for activities since the *ortho*-quinone 3 of the aza-analogues inhibits DNA topoisomerase II though it lacks a sugar moiety at C-4. In fact, aza-etoposide, which possesses a sugar moiety at C-4 in addition to the monophenolic E-ring, has been shown to exhibit no DNA topoisomerase II inhibition.[13] Furthermore, Gantchev and Hunting recently reported that the *ortho*-quinone derivative 4 of etoposide traps the cleavable complex more effectively than the parent inhibitor etoposide and suggested that methoxy groups on the E-ring are not a prerequisite for topoisomerase II inhibition.[14] Accordingly, the *ortho*-quinone form for the E-ring of podophyllotoxin-related lignans is most likely to be associated directly with topoisomerase II inhibition though the detailed mechanism of the stabilization of the binary cleavable complex is still unclear.

References and Notes
1) For reviews, see: Wang J. C., *Annu. Rev. Biochem.*, **65**, 635—692 (1996); Wigley D. B., *Annu. Rev. Biophys. Biomol. Struct.*, **24**, 185—208 (1995).
2) Liu L. F., *Annu. Rev. Biochem.*, **58**, 351—375 (1989).
3) Stahëlin H., *Planta Med.*, **22**, 336—347 (1972); Long B. H., Musial S. T., Brattain M. G., *Biochemistry*, **23**, 1183—1188 (1984); Minocha A., Long B. H., *Biochem. Biophys. Res. Commun.*, **122**, 165—170 (1984); Chen G. C., Yang L., Rowe T. C., Halligan B. D., Tewey K. M., Liu. L. F., *J. Biol. Chem.*, **259**, 13560—13566 (1984).
4) Hartwell J. L., Schrecker A. W., *Prog. Chem. Org. Nat. Prod.*, **15**, 83—166 (1958).
5) Corbett A. H., Osheroff N., *Chem. Res. Toxicol.*, **6**, 585—597 (1993); Froelich-Ammon S. J., Osheroff N., *J. Biol. Chem.*, **270**, 21429—21432 (1995); Burden D. A., Kingma P. S., Froelich-Ammon S. J., Bjornsti M.-A., Patchan M. W., Thompson R. B., Osheroff N., *ibid.*, **271**, 29238—29244 (1996).

6) Loike J. D., Horwitz S. B., *Biochemistry*, **15**, 5443—5448 (1976).

7) Iida A., Konishi K., Kubota H., Tomioka K., Tokuda H., Nishino H., *Tetrahedron Lett.*, **37**, 9219—9220 (1996).

8) Tomioka K., Kubota Y., Koga K., *J. Chem. Soc., Chem. Commun.*, **1989**, 1622—1624; Tomioka K., Kubota Y., Koga K., *Tetrahedron Lett.*, **30**, 2953—2954 (1989); Tomioka K., Kubota Y., Koga K., *Tetrahedron*, **49**, 1891—1900 (1993); Kubota Y., Kawasaki H., Tomioka K., Koga K., *ibid.*, **49**, 3081—3090 (1993).

9) Iida A., Kano M., Kubota Y., Koga K., Tomioka K., *Bioorg. Med. Chem. Lett.*, **7**, 2565—2566 (1997).

10) Nelson E. M., Tewey K. M., Liu L. F., *Proc. Natl. Acad. Sci. U.S.A.*,

18, 1361—1365 (1984).

11) Chow K.-C., Macdonald T. L., Ross W. E., *Mol. Pharmacol.*, **34**, 467—473 (1988).

12) Yamashita Y., Kawada S., Nakano H., *Biochem. Pharmacol.*, **39**, 737—744 (1990).

13) Kubota Y., Koga K., Tomioka K., unpublished result. Pearce H. L., Bach N. J., Cramer T. L., Danks M. K., Grindey G. B., Kalterjohn C. J., Rinzel S. M., Beck W. T., *Proc. Am. Can. Res.*, **31**, 441 (1990).

14) Gantchev G. G., Hunting D. J., *Biochem. Biophys. Res. Commun.*, **237**, 24—27 (1997).

490

Chem. Pharm. Bull. **48**(4) 490—495 (2000)

Vol. 48, No. 4

Novel Potassium Channel Opener Prodrugs with a Slow Onset and Prolonged Duration of Action

Haruhiko Horino,* Tetsuya Mimura, Syozo Kobayashi, Masahiro Ohta, Hideo Kubo, Kuniko Ito, Mitsuyoshi Tsumura, and Masayuki Kitagawa

(−)-(3*S*,4*R*,1′*R*,6′*S*)-4-(4-Benzyl-5-oxo-3,4-diazabicyclo[4.1.0]hept-2-en-2-yloxy)-3,4-dihydro-3-hydroxy-2,2-dimethyl-2*H*-1-benzopyran-6-carbonitrile and its derivatives with a modified benzyl group were synthesized with the objective of discovering novel ATP-sensitive potassium channel openers (PCOs) with a slow onset of action and a reduced tendency to induce tachycardia. Among the compounds synthesized, 4-(2-chlorobenzyl) derivative 5bB had potent hypotensive activity in spontaneously hypertensive rats (SHRs). In addition, compound 5bB showed the desired pharmacological profile with a slow onset and long duration of action and induction of only mild tachycardia. Compound 5bB was found to be quantitatively metabolized in rats to give active des-2-chlorobenzyl derivative 6B. These results suggest that the incorporation of an *N*-benzyl group is a useful method for the preparation of prodrugs, the function of which is to delay the onset and prolong the duration of action of the active substance.

Key words diazabicyclo[4.1.0]heptene; potassium channel opener; prodrug; hypotensive activity; 1-benzopyran

The adenosine triphosphate (ATP) sensitive potassium channel is involved in the regulation of smooth muscle tone *via* an efflux of potassium ions from cells. Potassium channel openers (PCOs) such as levcromakalim (**II**), accelerate the efflux of potassium ions and then induce the dilation of smooth muscles of blood vessels.[1] Therefore, PCOs are expected to be useful agents for the treatment of cardiovascular diseases such as hypertension and angina pectoris. In fact, compound **II** showed potent antihypertensive activity in clinical trials. However, adverse reactions (ADRs) such as reflex tachycardia, headache and edema were frequently encountered.[2] These results led to preliminary conclusions that PCOs have no clinical advantage over conventional antihypertensive agents such as calcium channel blockers and angiotensin converting enzyme inhibitors.

It has been suggested that ADRs such as reflex tachycardia and headache might be compensatory reactions in response to the potent hypotensive effect induced immediately following the administration of PCOs, and we therefore expected that a slow onset of hypotensive action would probably decrease these ADRs. Based on this assumption, our investigation targeted PCOs showing a slow onset of action.

We have previously reported the synthesis and activity of a series of PCOs with a 4-[4-alkyl-3,4-diazabicyclo[4.1.0]heptenyloxy]-1-benzopyran pharmacophore (**III**).[3] In that study, we reported structure–activity relationships (SARs) focusing on variations of the 4-substituent of the 3,4-diazabicyclo[4.1.0]heptenyl group: straight-chain alkyl substituents gave compounds which showed potent hypotensive activity, but branched chain substituents such as an isobutyl group resulted in a loss of activity. We have systematically modified the 4-substituent of the 3,4-diazabicyclo[4.1.0]heptenyl group, and found that the incorporation of a 4-benzyl moiety such as compound **IV** produced PCOs with the desired pharmacological profiles. These compounds showed potent activity *in vivo* and, furthermore, they also had the desired profile *i.e.* a slow onset and long-duration of action.

In this paper, we describe the synthesis and biological activity of a series of 3,4-dihydro-2*H*-1-benzopyrans with 4-substituted-3,4-diazabicyclo[4.1.0]heptenyl groups.

Chemistry Chart 2 shows the general method for the synthesis of the 4-benzyl-3,4-diazabicyclo[4.1.0]heptenyl-1-benzopyran derivatives **5**. Condensation of 1,2-cyclopropanedicarboxylic anhydride[4] (**1**) with benzylhydrazines **2a**—**j** and phenethylhydrazine **2k** gave (±)-3-benzyl-3,4-diazabicyclo[4.1.0]heptane-2,5-diones **3a**—**j** and 3-phenethyl congener **3k**, respectively, in 7—34% yields (Table 1). Compounds **3a**—**k** reacted with (3*S*,4*S*)-3,4-epoxy-2*H*-1-benzopyran-6-carbonitrile[5] (**4**) in the presence of pyridine in ethanol at reflux to afford a mixture of two diastereomers **5a**—**kA** (less polar isomer, (3*S*,4*R*,1′*S*,6′*R*)) and **5a**—**kB** (more polar isomer, (3*S*,4*R*,1′*R*,6′*S*)), which were separated by silica gel column chromatography (Table 2).

Oxidative cleavage of the 4-methoxybenzyl group[6] of compounds **5iA** and **5iB** by 2,3-dichloro-5,6-dicyano-1,4-benzoquinone (DDQ) in refluxing 1,2-dichloroethane afforded 4-unsubstituted diazabicyclo[4.1.0]heptenyl derivatives **6A** and **6B**, respectively, in good yield (Chart 3).

Alkylation of diazabicyclo[4.1.0]heptenyl derivative **6B** with 4-cyanobenzyl bromide and 4-pyridylmethyl chloride in the presence of potassium carbonate produced 4-substituted diazabicyclo[4.1.0]heptenyl derivatives **5lB** and **5mB**, respectively, in good yield (Chart 3).

The 3D structures of compounds **5aB** and **6B** were determined by X-ray crystallography and are shown in Fig. 1. Their configurations were determined to be (3*S*,4*R*,1′*R*,6′*S*) from correlation of the relative configurations of **5aB** and **6B** obtained by X-ray crystallographic analysis and the known absolute configuration (3*S*,4*S*) of intermediate **4**.[5]

The NMR *δ* values of the proton at the 4-position (H4) of the benzopyran nucleus of compounds **5** and **6** are listed in Table 2, respectively. In all diazabicyclo[4.1.0]heptenyl derivatives synthesized, the *δ* value of H4 in every isomer B was larger than the value for the corresponding isomer A. The difference between *δ* values of H4 in isomers A and B was in the range 0.04 to 0.26 ppm. Correlations between the configuration, chemical shift and polarity were demonstrated in the series of compounds reported previously.[3] Based on

---

* To whom correspondence should be addressed.

I, cromakalim (3SR,4RS)
II, levcromakalim (3S,4R)

III

IV

Chart 1

1

3a—k

4

, pyridine

5a—kA
(less polar, 3S,4R,1'S,6'R)

+

5a—kB
(more polar, 3S,4R,1'R,6'S)
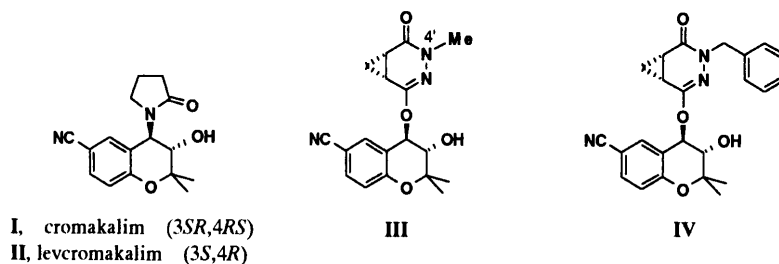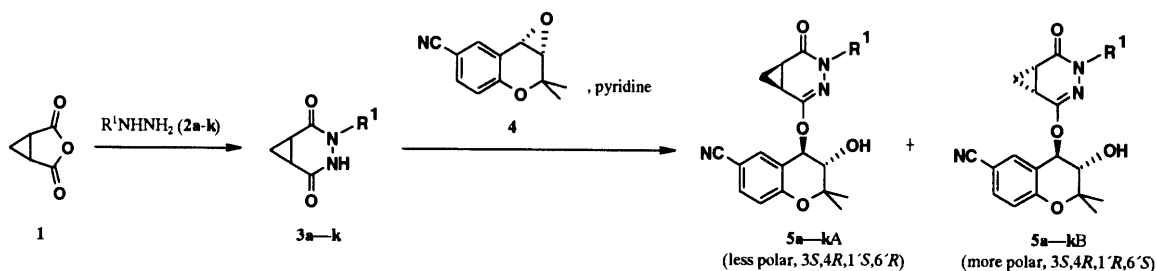
Chart 2

Table 1. 3,4-Diazabicyclo[4.1.0]heptane-2,5-diones (3a—k)

3a—k
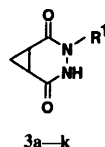
No.	R^1	Reaction solvent[a]	Yield (%)	Recrystallization solvent[a]	mp[b] (°C)	Formula[c]
3a	$CH_2C_6H_5$	E	30	EA	186—188	$C_{12}H_{12}N_2O_2$
3b	$CH_2C_6H_4(2\text{-}Cl)$	A	16	E–H	162—163	$C_{12}H_{11}ClN_2O_2$
3c	$CH_2C_6H_4(3\text{-}Cl)$	A	15	E–H	132—133	$C_{12}H_{11}ClN_2O_2$
3d	$CH_2C_6H_4(4\text{-}Cl)$	E	20	M–IPE	187—188	$C_{12}H_{11}ClN_2O_2$
3e	$CH_2C_6H_3(2,6\text{-}Cl_2)$	E	7	M–IPE	172—174	$C_{12}H_{10}Cl_2N_2O_2$
3f	$CH_2C_6H_3(2,4\text{-}Cl_2)$	A	18	M	199—202	$C_{12}H_{10}Cl_2N_2O_2$
3g	$CH_2C_6H_4(2\text{-}CH_3)$	A	33	M	177—190	$C_{13}H_{14}N_2O_2$
3h	$CH_2C_6H_4(4\text{-}CH_3)$	A	27	M	203—209	$C_{13}H_{14}N_2O_2$
3i	$CH_2C_6H_4(4\text{-}OCH_3)$	A	34	M–H	180—183	$C_{13}H_{14}N_2O_3$
3j	$CH_2C_6H_4(4\text{-}SO_2NH_2)$	A	11	M	250—253	$C_{12}H_{13}N_3O_4S \cdot 0.25H_2O$
3k	$CH_2CH_2C_6H_5$	A	25	E–H	160—162	$C_{13}H_{14}N_2O_2$

a) Solvent: A, acetonitrile; E, ethanol; EA, ethyl acetate; H, hexane; IPE, diisopropyl ether; M, methanol. b) Uncorrected. c) All compounds exhibited satisfactory (±0.4%) elemental analyses for C, H, N.

the observed relationships, all of the compounds **5b**—**mB** were confirmed to have a (3S,4R,1'R,6'S)-configuration, the same as that of **5aB** and **6B**.

Results and Discussion

The *in vivo* antihypertensive activity ($ED_{50\,mmHg}$) of the compounds synthesized in this study was evaluated by oral administration to SHRs. The *in vitro* potassium channel opening activity of selected compounds was evaluated by their effects on K^+ efflux ($EC_{AUC0.2}$) in the rat isolated aorta using $^{86}Rb^+$ as a surrogate marker for K^+ (Table 3).[7]

Most of the compounds tested exhibited potent antihypertensive activity *in vivo*. In particular, 4-benzyl, 4-(2-chlorobenzyl), 4-(4-chlorobenzyl), 4-(2-methylbenzyl), 4-(2,4-dichlorobenzyl), 4-(4-cyanobenzyl), 4-(4-pyridinylmethyl) and 4-phenethyl derivatives (**5a,b,d,f,g,k,l,mB**)

showed high potency. The activities of the remaining compounds were comparable to that of levcromakalim (**II**) or less.

Although 4-benzyl and 4-(2-chlorobenzyl) derivatives **5a,bB** had high potency *in vivo*, they showed no activity in the *in vitro* assay. Similarly, the 4-phenethyl derivative **5kB** was inactive *in vitro*. Generation of an active metabolite seemed to be the most plausible explanation for this anomaly. It is known that an amide *N*-alkyl group, in particular an *N*-benzyl group, is cleaved by cytochrome P-450.[8] Therefore, the common metabolite **6B** may well be produced from compounds such as **5a**—**mB** *via* cleavage of the 4-substituent on the diazabicyclo[4.1.0]heptenyl group. Therefore, we synthesized the suspected metabolite **6B** to confirm our hypothesis. HPLC analysis of serum samples (Fig. 2) showed that compound **5bB** was quantitatively converted into **6B** after oral

Table 2. (3S,4R)-4-(5-Oxo-3,4-diazabicyclo[4.1.0]hept-2-en-2-yloxy)-1-benzopyran Derivatives 5

5a—kA
(less polar, (3S,4R,1'S,6'R))

5a—kB
(more polar, (3S,4R,1'R,6'S))
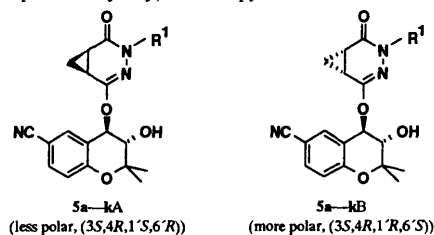
No.	R¹	Yield (%)	Solvent[a]	mp[b] (°C)	Rf value[c]	[α]_D[d]	Formula[e]	δ value[f] (ppm)
5aA	CH₂C₆H₅	35	—	Amorphous	0.64 (B)	−185.7	$C_{24}H_{23}N_3O_4$	5.44
5aB		32	IPE	118—120	0.50 (B)	−212.8	$C_{24}H_{23}N_3O_4$	5.60
5bA	CH₂C₆H₄(2-Cl)	30	E–H	199—201	0.48 (B)	−207.0	$C_{24}H_{22}ClN_3O_4$	5.56
5bB		33	E–H	188—190	0.41 (B)	−266.6	$C_{24}H_{22}ClN_3O_4$	5.60
5cA	CH₂C₆H₄(3-Cl)	25	—	Amorphous	0.64 (A)	−183.6	$C_{24}H_{22}ClN_3O_4$	5.47
5cB		25	E–H	165—167	0.58 (A)	−182.6	$C_{24}H_{22}ClN_3O_4$	5.64
5dA	CH₂C₆H₄(4-Cl)	32	—	Amorphous	0.48 (B)	−165.4	$C_{24}H_{22}ClN_3O_4 \cdot 0.5H_2O$	5.44
5dB		29	E–H	163—164	0.40 (B)	−181.0	$C_{24}H_{22}ClN_3O_4$	5.61
5eA	CH₂C₆H₃(2,6-Cl₂)	26	E	208	0.52 (B)	−211.8	$C_{24}H_{21}Cl_2N_3O_4$	5.57
5eB		34	E	255—256	0.38 (B)	−411.2	$C_{24}H_{21}Cl_2N_3O_4$	5.62
5fA	CH₂C₆H₃(2,4-Cl₂)	38	—	Amorphous	0.53 (B)	−186.8	$C_{24}H_{21}Cl_2N_3O_4 \cdot 0.5H_2O$	5.45
5fB		32	—	Amorphous	0.44 (B)	−233.7	$C_{24}H_{21}Cl_2N_3O_4 \cdot 0.5H_2O$	5.57
5gA	CH₂C₆H₄(2-CH₃)	16	E–H	192—193	0.24 (C)	−208.5	$C_{25}H_{25}N_3O_4$	5.47
5gB		29	—	Amorphous	0.18 (C)	−249.5	$C_{25}H_{25}N_3O_4$	5.53
5hA	CH₂C₆H₄(4-CH₃)	30	—	Amorphous	0.31 (C)	−225.9	$C_{25}H_{25}N_3O_4 \cdot 0.5H_2O$	5.47
5hB		44	—	Amorphous	0.26 (C)	−226.1	$C_{25}H_{25}N_3O_4$	5.65
5iA	CH₂C₆H₄(4-OCH₃)	38	—	Amorphous	0.23 (C)	−195.8	$C_{25}H_{25}N_3O_5 \cdot 0.25H_2O$	5.46
5iB		42	—	Amorphous	0.17 (C)	−205.1	$C_{25}H_{25}N_3O_5 \cdot 0.25H_2O$	5.63
5jA	CH₂C₆H₄(4-SO₂NH₂)	23	—	Amorphous	0.39 (A)	−137.5	$C_{24}H_{24}N_4O_6S \cdot 0.25H_2O$	5.67
5jB		17	—	Amorphous	0.37 (A)	−149.3	$C_{24}H_{24}N_4O_6S \cdot 0.5H_2O$	5.73
5kA	CH₂CH₂C₆H₅	22	—	Amorphous	0.60 (A)	−105.4	$C_{25}H_{25}N_3O_4 \cdot 0.25H_2O$	5.24
5kB		25	—	Amorphous	0.47 (A)	−107.4	$C_{25}H_{25}N_3O_4 \cdot 0.25H_2O$	5.50

a) Recrystallization solvent: E, ethanol; H, hexane; IPE, diisopropyl ether. b) Uncorrected. c) Rf values on silica gel TLC: solvent system: A, chloroform : methanol = 10 : 1 (v/v); B, chloroform : methanol = 20 : 1 (v/v); C, chloroform : methanol = 40 : 1 (v/v). d) c = 1.0 in methanol at 25 °C. e) All compounds exhibited satisfactory (±0.4%) elemental analyses for C, H, N. f) Chemical shifts of the proton at the 4-position of the benzopyran ring observed in CDCl₃.

5iA
(less polar, 3S,4R,1'S,6'R)

6A
(3S,4R,1'S,6'R)

5iB
(more polar, 3S,4R,1'R,6'S)

6B, DY-9708
(3S,4R,1'R,6'S)

5lB
(3S,4R,1'R,6'S)

5mB
(3S,4R,1'R,6'S)

Chart 3

(A) Compound 5aB   (B) Compound 6B
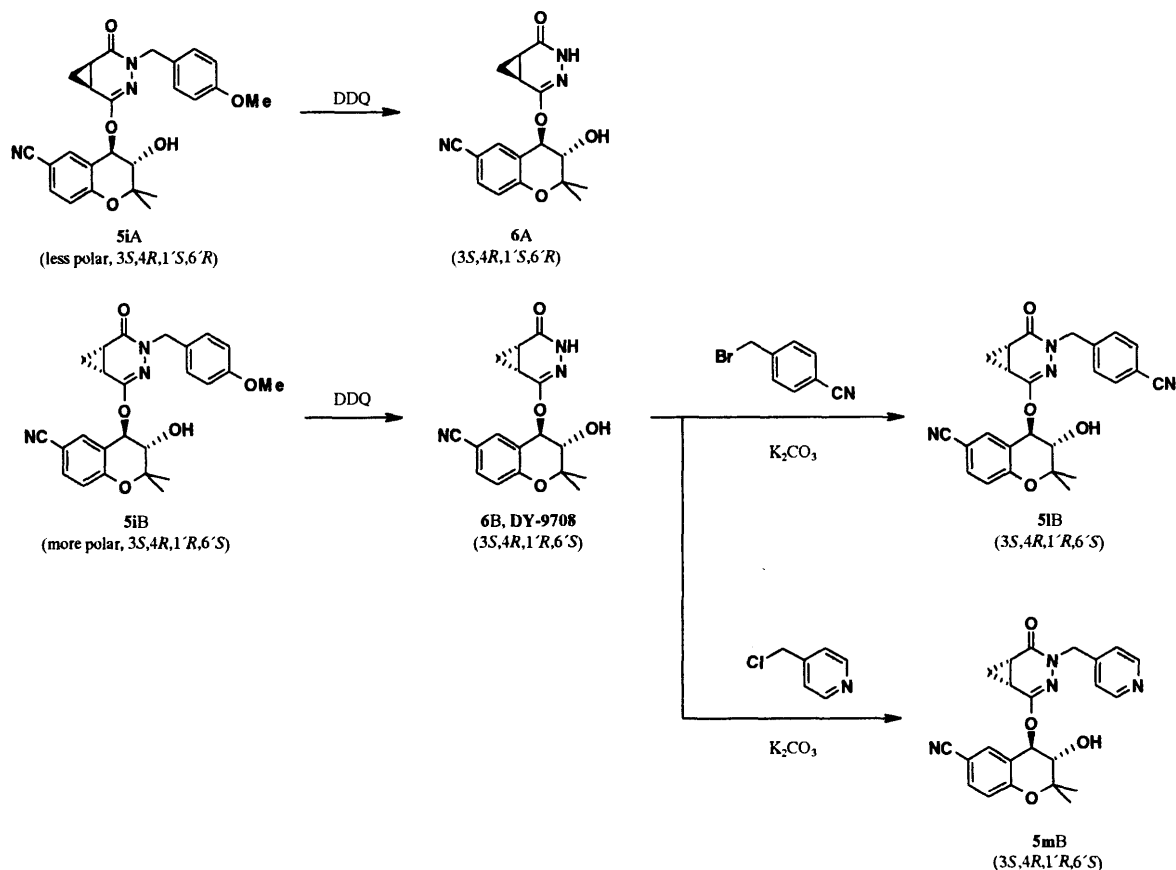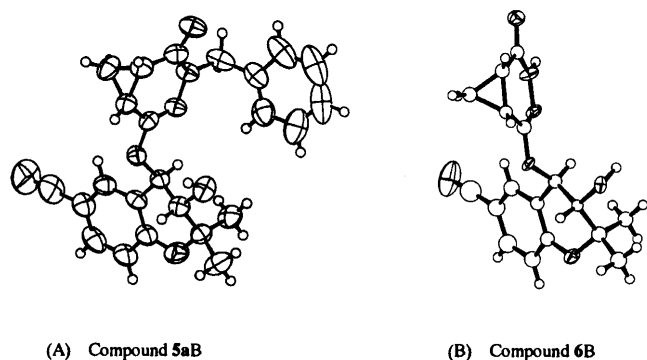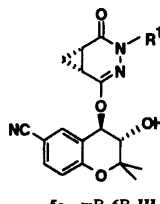
Fig. 1. X-Ray Crystal Structures of Compounds 5aB and 6B

Table 3. Biological Data for 4-(5-Oxo-3,4-diazabicyclo[4.1.0]hept-2-en-2-yloxy)-1-benzopyran Derivatives

5a—mB, 6B, III   II

Compound	R^1	Rb efflux $EC_{AUC0.2}$, $\mu M^{a)}$	Antihypertensive activity $ED_{50\,mmHg}$, mg/kg, $p.o.^{b)}$
5aB	$CH_2C_6H_5$	NA	0.053
5bB	$CH_2C_6H_4(2\text{-}Cl)$	NA	0.031
5cB	$CH_2C_6H_4(3\text{-}Cl)$	NT	0.20
5dB	$CH_2C_6H_4(4\text{-}Cl)$	NT	0.060
5eB	$CH_2C_6H_3(2,6\text{-}Cl_2)$	NT	0.40
5fB	$CH_2C_6H_3(2,4\text{-}Cl_2)$	NT	0.035
5gB	$CH_2C_6H_4(2\text{-}CH_3)$	NT	0.085
5hB	$CH_2C_6H_4(4\text{-}CH_3)$	NT	(>0.3)
5iB	$CH_2C_6H_4(4\text{-}OCH_3)$	NT	1.6
5jB	$CH_2C_6H_4(4\text{-}SO_2NH_2)$	NT	(>0.1)
5kB	$CH_2CH_2C_6H_5$	NA	0.083
5lB	$CH_2C_6H_4(4\text{-}CN)$	NT	0.063
5mB	$CH_2(4\text{-pyridyl})$	NT	0.021
6B	H	0.15	0.0093
II	—	1.6	0.14
III	CH_3	0.18	0.029

a) NT, not tested; NA, not active. b) Blood pressure lowering activity was less than 50 mmHg at the dose shown in parentheses.

dosing. The administration of 0.5 mg/kg of 5bB to rats gave 6B with a t_{max} of 12 h and C_{max} of 0.377 μg/ml.

Since compounds 5a,c—mB are metabolized to the common active metabolite 6B, the *in vivo* SARs in this series of compounds may reflect relative susceptibility to metabolism of the 4-substituent of the 3,4-diazabicyclo[4.1.0]heptenyl group. Thus, 4-benzyl, 4-(2-chlorobenzyl), 4-(4-chlorobenzyl), 4-(2-methylbenzyl), 4-(2,4-dichlorobenzyl), 4-(4-cyanobenzyl), 4-(4-pyridinylmethyl) and 4-phenethyl groups are all probably easily removed by metabolism, since compounds 5a,b,d,f,g,k,l,mB, which have these substituents, show high potency *in vivo*. In contrast, 4-(3-chlorobenzyl), 4-(2,6-dichlorobenzyl), 4-(4-methybenzyl), 4-(4-sulfamoylbenzyl) and 4-(4-methoxybenzyl) groups seem to resist metabolism, as shown by the lower potency of compounds 5c,e,h,i,jB (Table 3).

Figure 3 shows the changes in systolic blood pressure (SBP) and heart rate (HR) after the oral administration of 4-(2-chlorobenzyl) derivative 5bB (0.1 mg/kg), 4-unsubstituted derivative 6B (0.03 mg/kg) and levcromakalim (II, 1 mg/kg) to SHRs. Compound 5bB exhibited a maximal decrease in blood pressure more than 8 h after administration, and the hypotensive effect lasted more than 24 h. Compound 6B also had long-lasting activity, but showed a maximal decrease in blood pressure at 1 h following administration. Compound II also had a rapid onset of action, and the hypotensive effect disappeared within 24 h. Moreover, compound II showed acute elevation of heart rate, while compound 5bB exhibited a gradual and less pronounced increase in heart rate. Thus, 5bB had a desired pharmacological profile with a slow onset, long duration of action, and less acute induced tachycardia.

The above results are consistent with the report that Y-27152 (Va, Chart 4) is a slow-onset and long-acting PCO with reduced tachycardia.[2,9] This compound is also metabolized to an active metabolite, Y-26763 (Vb), through *O*-debenzylation in the liver. Taken together, these results indicate that a slow onset of action can partially overcome some of the adverse effects of first generation PCOs.

In conclusion, we prepared 4-(4-substituted-3,4-diazabicyclo[4.1.0]heptenyl)-2H-1-benzopyrans, and demonstrated that 4-(2-chlorobenzyl) derivative 5bB (DY-9804) is a slow-onset and long-acting PCO which causes only mild tachycardia. Compound 5bB was metabolized to give active des-2-
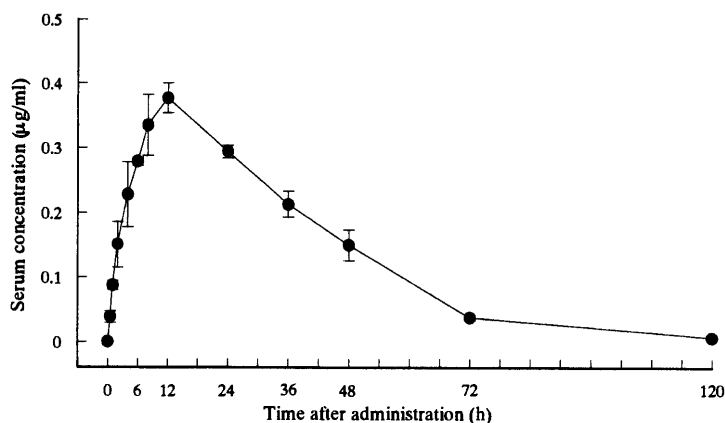
Fig. 2. Serum Concentration of Compound 6B in Wistar Rats after Oral Administration of 5bB

Male Wistar rats (n=3) were treated with compound 5bB (0.6 mg/kg, p.o.). The serum concentration of 6B was determined by HPLC. The data are means±S.E. for 3 rats. Compound 5bB was not detected at any sampling time following dosing.

(A)

(B)
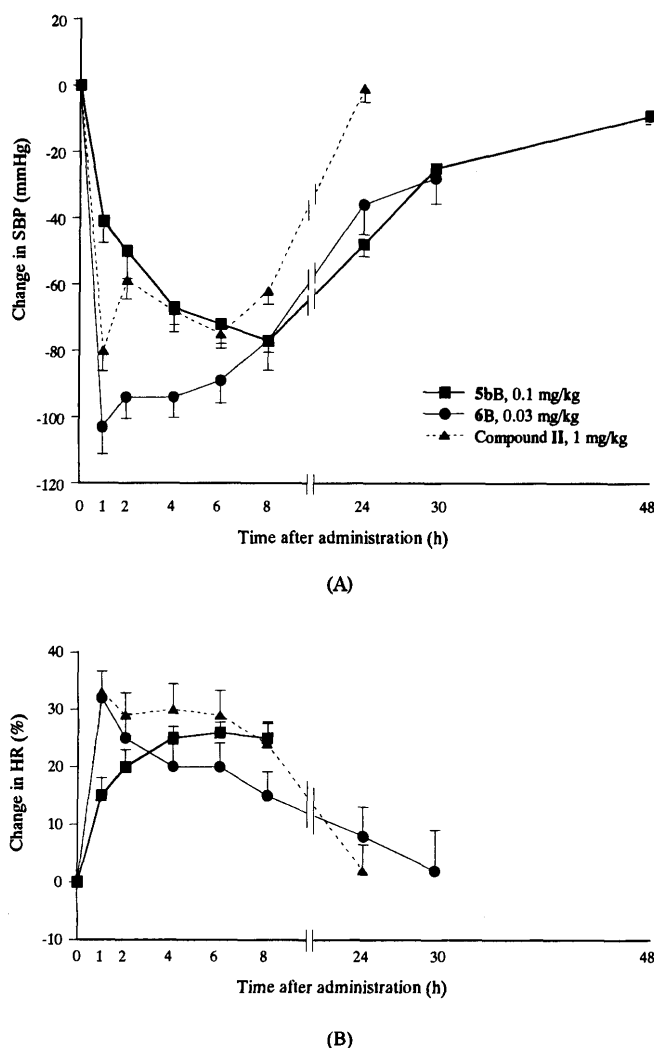
Fig. 3. Hypotensive Activity (A) and Change of Heart Rate (B) of PCOs

Male spontaneously hypertensive rats were treated with compound 5bB (0.1 mg/kg, p.o., ■), 6B (0.03 mg/kg, p.o., ●) and II (levcromakalim, 1 mg/kg, p.o., ▲). The systolic blood pressure (SBP) and the heart rate (HR) were measured by a tail-cuff method, and the changes of SBP and HR are expressed vs. initial. The data are means±S.E. for 5 rats.

Va, Y-27152 (R = Bn)
Vb, Y-26763 (R = H)
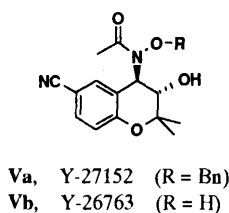
Chart 4

chlorobenzyl derivative 6B (DY-9708). These results suggest that N-benzyl substitution on amides or heterocycles may be a useful method for the preparation of prodrugs which display delayed onset and prolonged duration of action.

Further work is in progress to investigate the metabolism of N-debenzylation by cytochrome P450 in rats, and to determine the extent of metabolic activation in other mammals.

Experimental

Chemistry Melting points were determined on a Büchi 535 melting point apparatus and are uncorrected. Optical rotations were measured on a Horiba SEPA200 digital polarimeter. The ^{1}H-NMR spectra were recorded on a JEOL JNM-EX400 (400 MHz) spectrometer with tetramethylsilane (TMS)

as an internal standard. Signal multiplicities are represented by s (singlet), d (doublet), dd (double doublet), t (triplet), q (quartet), m (multiplet), and br (broad). Chemical shifts are expressed in δ values and the coupling constants in Hz. For column chromatography, silica gel (Kieselgel 60, 70—230 mesh, E. Merck) was used. Mass spectra (MS) were recorded on JEOL JMS-HX110 and JMS-AX505W instruments. Precoated Silica gel 60 F_{254} plates with a layer thickness of 0.25 mm (E. Merck, Darmstadt, Germany) were used for thin-layer chromatography (TLC) to determine Rf values.

Starting Materials 1,2-Cyclopropanedicarboxylic anhydride (1) was prepared according to McCoy's method.[4] Benzylhydrazines (2a—k) were prepared from alkyl halide and hydrazine monohydrate according to the usual procedures.[10] Epoxide 4 was prepared according to the methods previously reported.[5]

(±)-3-Benzyl-3,4-diazabicyclo[4.1.0]heptane-2,5-dione (3a) A solution of benzylhydrazine (2a, 45.8 g, 0.374 mol) in ethanol (50 ml) was added dropwise to a solution of 1 (42.0 g, 0.374 mol) in ethanol (150 ml) with stirring. The reaction mixture was heated under reflux for 15 h. After evaporation of the solvent in vacuo, the resulting residue was purified by silica gel column chromatography with ethyl acetate (EtOAc) as an eluent, followed by recrystallization from EtOAc to give 3a (24.1 g, 30%), mp 186—188 °C. ^{1}H-NMR (CDCl$_3$) δ: 1.14 (1H, m), 1.69 (1H, m), 2.11 (1H, m), 2.28 (1H, m), 4.67 (1H, d, J=15.1 Hz), 4.83 (1H, d, J=15.1 Hz), 7.32 (5H, s). Anal. Calcd for C$_{12}$H$_{12}$N$_2$O$_2$: C, 66.65; H, 5.59; N, 12.95. Found: C, 66.29; H, 5.55; N, 12.75.

Compounds 3b—k were prepared in an analogous manner (see Table 1) from 1 and the appropriate corresponding alkylhydrazines (2b—k).

(−)-(3S,4R,1'S,6'R)-4-(4-Benzyl-5-oxo-3,4-diazabicyclo[4.1.0]hept-2-en-2-yloxy)-3,4-dihydro-3-hydroxy-2,2-dimethyl-2H-1-benzopyran-6-carbonitrile (5aA) and (−)-(3S,4R,1'R,6'S)-4-(4-Benzyl-5-oxo-3,4-diazabicyclo[4.1.0]hept-2-en-2-yloxy)-3,4-dihydro-3-hydroxy-2,2-dimethyl-2H-1-benzopyran-6-carbonitrile (5aB) A mixture of (−)-(3S,4S)-3,4-epoxy-3,4-dihydro-2,2-dimethyl-2H-1-benzopyran-6-carbonitrile (4, 744 mg, 3.7 mmol), 3a (800 mg, 3.7 mmol) and pyridine (0.4 ml, 5.0 mmol) in EtOH (20 ml) was heated under reflux for 16 h. After evaporation of the solvent in vacuo, the resulting residue was purified by silica gel column chromatography with CHCl$_3$:MeOH=50:1 (v/v) as an eluent to give 5aA (less polar) and 5aB (polar). 5aA: Yield 540 mg (35%) as a colorless amorphous solid, $[\alpha]_D^{25} = -185.7°$ (c=1, MeOH). Rf value=0.64 (CHCl$_3$:MeOH=20:1). ^{1}H-NMR (CDCl$_3$) δ: 1.00 (1H, m), 1.24 (3H, s), 1.48 (3H, s), 1.74 (1H, m), 2.28 (1H, m), 2.39 (1H, m), 3.81 (1H, dd, J=2.9, 7.8 Hz), 4.34 (1H, d, J=2.9 Hz, OH), 4.63 (1H, d, J=14.1 Hz), 4.93 (1H, d, J=14.1 Hz), 5.44 (1H, d, J=7.8 Hz), 6.87 (1H, d, J=8.3 Hz), 7.32 (5H, m), 7.48 (1H, dd, J=2.0, 8.3 Hz), 7.53 (1H, d, J=2.0 Hz). Anal. Calcd for C$_{24}$H$_{23}$N$_3$O$_4$: C, 69.05; H, 5.55; N, 10.06. Found: C, 68.89; H, 5.81; N, 9.60. 5aB: Yield 490 mg (32%) as colorless needles (from diisopropyl ether), mp 118—120 °C, $[\alpha]_D^{25} = -212.8°$ (c=1, MeOH). Rf value=0.50 (CHCl$_3$:MeOH=20:1). ^{1}H-NMR (CDCl$_3$) δ: 1.01 (1H, m), 1.25 (3H, s), 1.44 (3H, s), 1.72 (1H, m), 2.17 (1H, m), 2.33 (1H, m), 3.01 (1H, d, J=4.4 Hz, OH), 3.76 (1H, dd, J=4.4, 7.3 Hz), 4.74 (1H, d, J=14.1 Hz), 4.84 (1H, d, J=14.1 Hz), 5.60 (1H, d, J=7.3 Hz), 6.88 (1H, d, J=8.3 Hz), 7.31 (5H, m), 7.48 (1H, dd, J=2.0, 8.3 Hz), 7.53 (1H, d, J=2.0 Hz). Anal. Calcd for C$_{24}$H$_{23}$N$_3$O$_4$: C, 69.05; H, 5.55; N, 10.06. Found: C, 69.42; H, 5.43; N, 10.24. Compounds 5b—kA and 5b—kB were prepared in an analogous manner (see Table 2) from 4 and corresponding (±)-3-alkyl-3,4-diazabicyclo[4.1.0]heptane-2,5-diones (3b—k).

(−)-(3S,4R,1'R,6'S)-4-[4-(4-Cyanobenzyl)-5-oxo-3,4-diazabicyclo[4.1.0]hept-2-en-2-yloxy]-3,4-dihydro-3-hydroxy-2,2-dimethyl-2H-1-benzopyran-6-carbonitrile (5lB) To a solution of 6B (200 mg, 0.61 mmol) in acetone (10 ml) were added 4-cyanobenzyl bromide (130 mg, 0.66 mmol) and potassium carbonate (90 mg, 0.65 mmol). The mixture was heated with stirring under reflux for 40 h. The reaction mixture was diluted with CHCl$_3$ and washed with H$_2$O. The organic layer was dried over Na$_2$SO$_4$ and evaporated in vacuo. The residue was purified by silica gel column chromatography with CHCl$_3$ as an eluent to give 5lB (170 mg, 63%) as colorless crystals, mp 185—187 °C, $[\alpha]_D^{25} = -198.9°$ (c=1, MeOH). Rf value=0.32 (CHCl$_3$:MeOH=20:1, v/v). ^{1}H-NMR (DMSO-d_6) δ: 1.07 (1H, m), 1.22 (3H, s), 1.39 (3H, s), 1.71 (1H, m), 2.27 (2H, m), 3.77 (1H, dd, J=5.4, 6.8 Hz), 4.69 (1H, d, J=15.6 Hz), 4.93 (1H, d, J=15.6 Hz), 5.58 (1H, d, J=6.8 Hz), 5.89 (1H, d, J=5.4 Hz, OH), 6.95 (1H, d, J=8.8 Hz), 7.44 (2H, d, J=8.3 Hz), 7.54 (1H, d, J=2.0 Hz), 7.64 (1H, dd, J=2.0, 8.8 Hz), 7.77 (2H, d, J=8.3 Hz). Anal. Calcd for C$_{25}$H$_{22}$N$_4$O$_4$: C, 67.86; H, 5.01; N, 12.66. Found: C, 67.79; H, 5.18; N, 12.58.

(−)-(3S,4R,1'R,6'S)-3,4-Dihydro-3-hydroxy-2,2-dimethyl-4-[5-oxo-4-(4-pyridylmethyl)-3,4-diazabicyclo[4.1.0]hept-2-en-2-yloxy]-2H-1-benzopyran-6-carbonitrile (5mB) Compound 6B was reacted with 4-

chloromethylpyridine using a similar procedure to that described above to give **5mB** (61%) as a colorless amorphous solid, $[\alpha]_D^{25} = -173.4°$ ($c=1$, MeOH). Rf value=0.64 (CHCl$_3$:MeOH=5:1, v/v). ^{1}H-NMR (CDCl$_3$) δ: 1.07 (1H, m), 1.27 (3H, s), 1.47 (3H, s), 1.78 (1H, m), 2.21 (1H, m), 2.32 (1H, m), 3.52 (1H, br s, OH), 3.84 (1H, d, J=7.3 Hz), 4.74 (1H, d, J= 15.1 Hz), 4.84 (1H, d, J=15.1 Hz), 5.64 (1H, d, J=7.3 Hz), 6.89 (1H, d, J= 8.3 Hz), 7.21 (2H, br s), 7.48 (1H, dd, J=2.0, 8.3 Hz), 7.55 (1H, d, J= 2.0 Hz), 8.56 (2H, br s). *Anal.* Calcd for C$_{23}$H$_{22}$N$_4$O$_4$: C, 66.02; H, 5.30; N, 13.39. Found: C, 65.88; H, 5.46; N, 13.00.

(−)-(3S,4R,1′R,6′S)-3,4-Dihydro-3-hydroxy-2,2-dimethyl-4-(5-oxo-3,4-diazabicyclo[4.1.0]hept-2-en-2-yloxy)-2H-1-benzopyran-6-carbonitrile (6B) A mixture of **5iB** (5.91 g, 13.2 mmol), DDQ (17.7 g, 78 mmol) and H$_2$O (0.9 ml, 50 mmol) in 1,2-dichloroethane (450 ml) was heated under reflux for 8 h. After removal of the insoluble product by filtration, the filtrate was evaporated *in vacuo*. The resulting residue was purified by silica gel column chromatography with CHCl$_3$:MeOH=50:1 (v/v) as eluent, followed by recrystallization from EtOH–H$_2$O (1:2, v/v) to yield **6B** (2.81 g, 65%), mp 199—201 °C, $[\alpha]_D^{25} = -173.8°$ ($c=1$, MeOH). Rf value=0.32 (EtOAc). ^{1}H-NMR (CDCl$_3$) δ: 1.18 (1H, m), 1.33 (3H, s), 1.52 (3H, s), 1.60—2.10 (1H, br s, OH), 1.81 (1H, m), 2.21 (2H, m), 3.92 (1H, d, J=7.3 Hz), 5.71 (1H, d, J=7.3 Hz), 6.91 (1H, d, J=8.3 Hz), 7.50 (1H, dd, J=2.0, 8.3 Hz), 7.59 (1H, d, J=2.0 Hz), 7.71 (1H, s, NH). *Anal.* Calcd for C$_{17}$H$_{17}$N$_3$O$_4$: C, 62.37; H, 5.23; N, 12.83. Found: C, 62.51; H, 5.50; N, 12.48. Compound **6A** was prepared in an analogous manner from the corresponding 4′-methoxybenzyl derivative **5iA**. **6A**: Yield 40%, mp 126—129 °C (from CH$_2$Cl$_2$–hexane), $[\alpha]_D^{25} = -63.7°$ ($c=1$, MeOH). Rf value=0.34 (EtOAc). ^{1}H-NMR (CDCl$_3$) δ: 1.13 (1H, m), 1.31 (3H, s), 1.51 (3H, s), 1.79 (1H, m), 2.30 (2H, m), 3.91 (1H, dd, J=2.9, 7.3 Hz), 4.28 (1H, d, J=2.9 Hz, OH), 5.62 (1H, d, J=7.3 Hz), 6.91 (1H, d, J=8.3 Hz), 7.51 (1H, dd, J=2.0, 8.3 Hz), 7.53 (1H, s, NH), 7.59 (1H, d, J=2.0 Hz). *Anal.* Calcd for C$_{17}$H$_{17}$N$_3$O$_4$: C, 62.37; H, 5.23; N, 12.83. Found: C, 62.02; H, 5.21; N, 12.74.

X-Ray Crystallography of Compound 5aB Crystals of **5aB** were grown from diisopropyl ether as colorless prisms. Diffraction intensities were collected from a crystal which had dimensions of 0.50×0.20×0.15 mm on a Rigaku AFC5R diffractometer with graphite monochromated CuK_α radiation (λ=1.54178 Å) at 23 °C. Crystal data: C$_{24}$H$_{23}$N$_3$O$_4$·0.25C$_6$H$_{14}$O, M.W.=443.01, a=12.142(1) Å, b=8.098(2) Å, c=13.664(1) Å, β= 106.896(9)°, V=1285.5(3) Å^3, space group $P2_1$ (#4), Z=2, Dc= 1.144 g/cm^3, F$_{000}$=469. For structural determination, 1735 observed reflections were used (I>3.00s(I)). The structure was solved by direct methods using SHELXS-86[11] and refined by full-matrix least-squares refinement with anisotropic temperature factors for non-hydrogen atoms. The final R value was 0.052 (R_w=0.066).

X-Ray Crystallography of Compound 6B Crystals of **6B** were grown from ethanol–water as colorless rhomboids. Diffraction intensities were collected from a crystal which had dimensions of 0.30×0.07×0.07 mm on a Rigaku AFC7R diffractometer with graphite monochromated CuK_α radiation (λ=1.54178 Å) at −60 °C. Crystal data: C$_{17}$H$_{17}$N$_3$O$_4$, M.W.=327.34, a=6.422(2) Å, b=10.045(3) Å, c=12.720(1) Å, β=102.27(1)°, V=801.9(2) Å^3, space group $P2_1$ (#4), Z=2, D_c=1.356 g/cm^3, F$_{000}$=344. For structural determination, 713 observed reflections were used (I>3.00s(I)). The structure was solved by direct methods using SHELXS-86[11] and refined by full-matrix least-squares refinement with anisotropic temperature factors for non-hydrogen atoms. The final R value was 0.049 (R_w=0.044).

Potassium Channel Opening Activity The potassium channel opening activity of the test compounds shown in Table 4 was determined according

to Quast's test method.[7] ^{86}Rb was incorporated into a segment of excised aorta from a Wistar rat, and the segment was surface-perfused with a solution containing a test compound for 10 min. The potassium channel opening activity of the test compound was expressed in terms of an effective concentration at which the area under the peak of the ^{86}Rb release rate reached 0.2 (EC$_{AUC0.2}$).

Antihypertensive Activity in SHRs Male SHRs (16- to 20-week-old, body weight, 300—400 g) fed *ad lib.* were dosed orally with test compound suspended in 0.5% (w/v) carboxymethylcellulose aqueous solution. At 1, 2, 4, 6, 8, 24, 30, and 48 h after the administration, the systolic blood pressure and the heart rate were measured by the tail-cuff method.[12] The antihypertensive activity of the test compound was determined as the effective dose for reducing blood pressure by 50 mmHg (ED$_{50\,mmHg}$).

Serum Concentration of Compounds after Oral Administration of 5bB in Rats Unfasted male Wistar rats (9-week-old, body weight, 205—229 g) were dosed orally with compound **5bB** suspended in 0.5% (w/v) carboxymethylcellulose aqueous solution (0.6 mg/5 ml/kg). At 0.5, 1, 2, 4, 6, 8, 12, 24, 36, 48, 72 and 120 h, respectively, after the administration, three rats were killed and their blood samples were taken. Blood samples were centrifuged (3000 rpm, 15 min) to separate plasma. Serum sample (1 ml) and water (6 ml) was added to compound **5fB** (2 μg, as an internal standard), and absorbed in a Sep-pak C$_{18}$ Plus cartridge (360 mg, Waters). After the cartridge was washed with water (10 ml) and eluted using methanol (5 ml), the eluent was concentrated *in vacuo* and the resulting residue was diluted with a mobile phase for HPLC (H$_2$O:MeCN=4:6, 200 μl). Concentrations of compound **5bB** and **6B** were determined by HPLC analysis.

References
1) Ashwood V. A., Buckingham R. E., Cassidy F., Evans J. M., Faruk E. A., Hamilton T. C., Nash D. J., Stemp G., Willcocks K., *J. Med. Chem.*, **29**, 2194—2201 (1986).
2) Nakajima T., *Cardiovasc. Drug. Rev.*, **9**, 372—384 (1991).
3) Horino H., Mimura T., Kagechika K., Ohta M., Kubo H., Kitagawa M., *Chem. Pharm. Bull.*, **46**, 602—609 (1997).
4) McCoy L. L., *J. Am. Chem. Soc.*, **80**, 6568—6572 (1958).
5) Jacobsen E. N., Zhang W., Muci A. R., Ecker J. R., Deng L., *J. Am. Chem. Soc.*, **113**, 7063—7064 (1991).
6) Oikawa Y., Yoshioka T., Yonemitsu O., *Tetrahedron Lett.*, **23**, 885—888 (1982); Oikawa Y., Tanaka T., Hirota K., Yoshioka T., Yonemitsu O., *Tetrahedron Lett.*, **25**, 5393—5396 (1984).
7) Quast U., Baumlin Y., *Naunyn-Schmiedeberg's Arch. Pharmacol.*, **338**, 319—326 (1988).
8) Hall L. R., Hanzlik R. P., *Xenobiotica*, **21**, 1127—1138 (1991).
9) Nakajima T., Shinohara T., Yaoka O., Fukunari A., Shinagawa K., Aoki K., Katoh A., Yamanaka T., Setoguchi M., Tahara T., *J. Pharmacol. Exp. Ther.*, **261**, 730—736 (1992).
10) Biel J. H., Drukker A. E., Mitchell T. F., Sprengeler E. P., Nuhfer P. A., Conway A. C., Horita A., *J. Am. Chem. Soc.*, **81**, 2805—2813 (1959).
11) Sheldrick G. M., "Crystallographic Computing 3," ed. by Sheldrick G. M., Kruger C., Goddard R., Oxford University Press, Oxford, 1985, pp. 175—189.
12) Heptner W., Kellner H.-M., Christ O., Weihrauch D., *Arzneim.-Forsch.*, **19**, 1400—1404 (1969).

496

Chem. Pharm. Bull. **48**(4) 496—504 (2000)

Vol. 48, No. 4

Methyl Quadrangularates A—D and Related Triterpenes from *Combretum quadrangulare*

Arjun Hari BANSKOTA,[a] Yasuhiro TEZUKA,[a] Kim Qui TRAN,[b] Ken TANAKA,[c] Ikuo SAIKI,[a] and Shigetoshi KADOTA*,[a]

Institute of Natural Medicine, Toyama Medical and Pharmaceutical University,[a] 2630 Sugitani, Toyama 930–0194, Japan, National University Ho Chi Minh City,[b] Ho Chi Minh City, Vietnam, and National Research Institute of Police Science,[c] 6 Sanban-cho, Chiyoda-ku, Tokyo 102–0075, Japan. Received October 12, 1999; accepted December 3, 1999

From the MeOH extract of leaves of *Combretum quadrangulare*, fifteen new cycloartane-type triterpenes, methyl quadrangularates A—D (1—4) and N—P (8, 6, 12), methyl 24-epiquadrangularate C (5), quadragularic acid E (9), 23-deoxojessic acid (10), 1-*O*-acetyl-23-deoxojessic acid (11), quadragularols A (7) and B (13) and norquadrangularic acids B (14) and C (15) were isolated together with two known cycloartane-type triterpenes, methyl 23-deoxojessate (16) and 4β,14α-dimethyl-5α-ergosta-9β,19-cyclo-24(31)-en-3β-hydroxy-4α-carboxylic acid (17). Betulinic acid (18), β-sitosterol (19), kamatakenin (20), isokaempferide (21), 5,7,4'-trihydroxy-3,3'-dimethoxyflavone (22) and 5,4'-dihydroxy-3,7,3'-trimethoxyflavone (23) were also obtained from the same extract. The structures of the new compounds were elucidated on the basis of spectral analysis and chemical conversions. All the isolated compounds were tested for their cytotoxicity towards highly liver metastatic murine colon 26-L5 carcinoma cells, and the cycloartane-type triterpenes showed various degrees of cytotoxicity, whereas all the flavonoids possessed strong cytotoxicity with ED$_{50}$ values equal to or less than 6 μM.

Key words *Combretum quadrangulare*; cycloartane-type triterpene; cytotoxicity; flavonoid; murine colon 26-L5

Combretum (*C.*) species (Combretaceae) are used in folk medicine in different parts of Asia and Africa for the treatment of hepatitis, malaria, respiratory infections and even cancer.[1] *C. molle, C. edwardsii* and *C. elaeagnoides* growing in Africa were examined and unique cycloartane-type triterpenes bearing a 1α,3β-dihydroxy group were reported.[2,3] Phenanthrenes, stilbenes and bibenzyls, some of which possess potent cancer cell growth inhibitory activity, were also isolated from *C. caffrum*.[4] *C. quadrangulare* is an evergreen tree that grows in eastern Asia and is known as Tram bau in Vietnam. The seeds, leaves and stem bark of the plant are used in Vietnamese traditional medicine as antipyretic, antidysenteric and anthelminthic agents.[5]

In the course of our study on Vietnamese medicinal plants,[6] we examined constituents of the leaves of *C. quadrangulare* and isolated thirteen novel cycloartane-type triterpenes from the polar fractions.[7] Recently, we have examined the less polar fractions, which had strong cytotoxic activity towards highly liver metastatic murine colon 26-L5 carcinoma cells,[8] and have isolated fifteen new cycloartane-type triterpenes together with two known cycloartanes, methyl 23-deoxojessate (16)[9] and 4β,14α-dimethyl-5α-ergosta-9β,19-cyclo-24(31)-en-3β-hydroxy-4α-carboxylic acid (17).[10] Betulinic acid (18),[11] β-sitosterol (19),[12] kamatakenin (20),[13] isokaempferide (21),[13] 5,7,4'-trihydroxy-3,3'-dimethoxyflavone (22)[14] and 5,4'-dihydroxy-3,7,3'-trimethoxyflavone (23)[15] were also isolated from the less polar fractions. We now report the isolation and structural elucidation of these by the use of a spectroscopic technique and a chemical method.[16]

Methyl quadrangularates A (1) and B (2) were isolated as a colorless amorphous solid and colorless crystals, respectively with a mp of 190 °C. Their ^{1}H- and ^{13}C-NMR spectra were very similar except for a difference in the chemical shifts of an oxygen-substituted quaternary carbon (1, δ 69.5; 2, δ 80.9). Their high-resolution FAB-MS (HR-FAB-MS) data indicated that they have the molecular formula C$_{31}$H$_{48}$O$_6$

and C$_{31}$H$_{48}$O$_7$, respectively. Compound 2 has one oxygen more than 1, suggesting 1 has a hydroxyl and 2 has a hydroperoxyl group. This was confirmed by the fact that the reduction of 2 with triphenylphosphine[17] gave 1. The ^{1}H- and ^{13}C-NMR spectra of 2 were similar to those of mollic acid (24),[2] except for a difference of the signals in the side chain on ring D, where 2 was in ester form. Two olefinic protons at δ 5.78 (dt, $J=16.0$, 6.5 Hz) and 6.05 (d, $J=16.0$ Hz) in the ^{1}H-NMR spectrum of 2 indicated that the position of the olefin should differ from that of 24. Based on detailed analyses of the ^{1}H–^{1}H correlation spectroscopy (COSY) spectrum, together with the ^{1}H–^{13}C and long-range ^{1}H–^{13}C COSY spectra (Fig. 1), the position of the olefin was concluded to be C-23(24) and the aldehyde to be C-21. On the other hand, the location of the hydroperoxyl group was determined to be C-25 based on the long-range correlations between the methyl protons H$_3$-26 and H$_3$-27 and the quaternary carbon at δ 80.9. Thus, the planar structure of methyl quadrangularates A and B was determined to be 1 and 2, respectively.

The stereochemistry of 1 and 2 was elucidated by analyses of coupling constants and nuclear Overhauser effect (NOE) experiments on 2. The lack of diaxial coupling of H-1 (br s) with H-2$_{ax}$ indicated the hydroxyl group at C-1 to be in axial, which was further supported by an NOE enhancement from H-1 to H-19. The H-3 was observed as a double doublet due to diaxial coupling with H-2$_{ax}$ ($J=12.0$ Hz) and axial–equatorial coupling with H-2$_{eq}$ ($J=4.5$ Hz), which suggested the equatorial nature of the hydroxyl group at C-3. Irradiation of the methyl protons at δ 1.60 of 2 caused an NOE increase of H-19 and *vice versa*, indicating that the methyl group at C-4 should be in the β position.

From the data mentioned above, the structure of methyl quadrangularates A and B was concluded as 1 and 2, respectively, which was confirmed by X-ray analysis of 2.[16] After the submission of our communication, Ganzera *et al.* reported a triterpene having the same structure as formula 1.[9] The reported data, however, were the same as those of 2, but
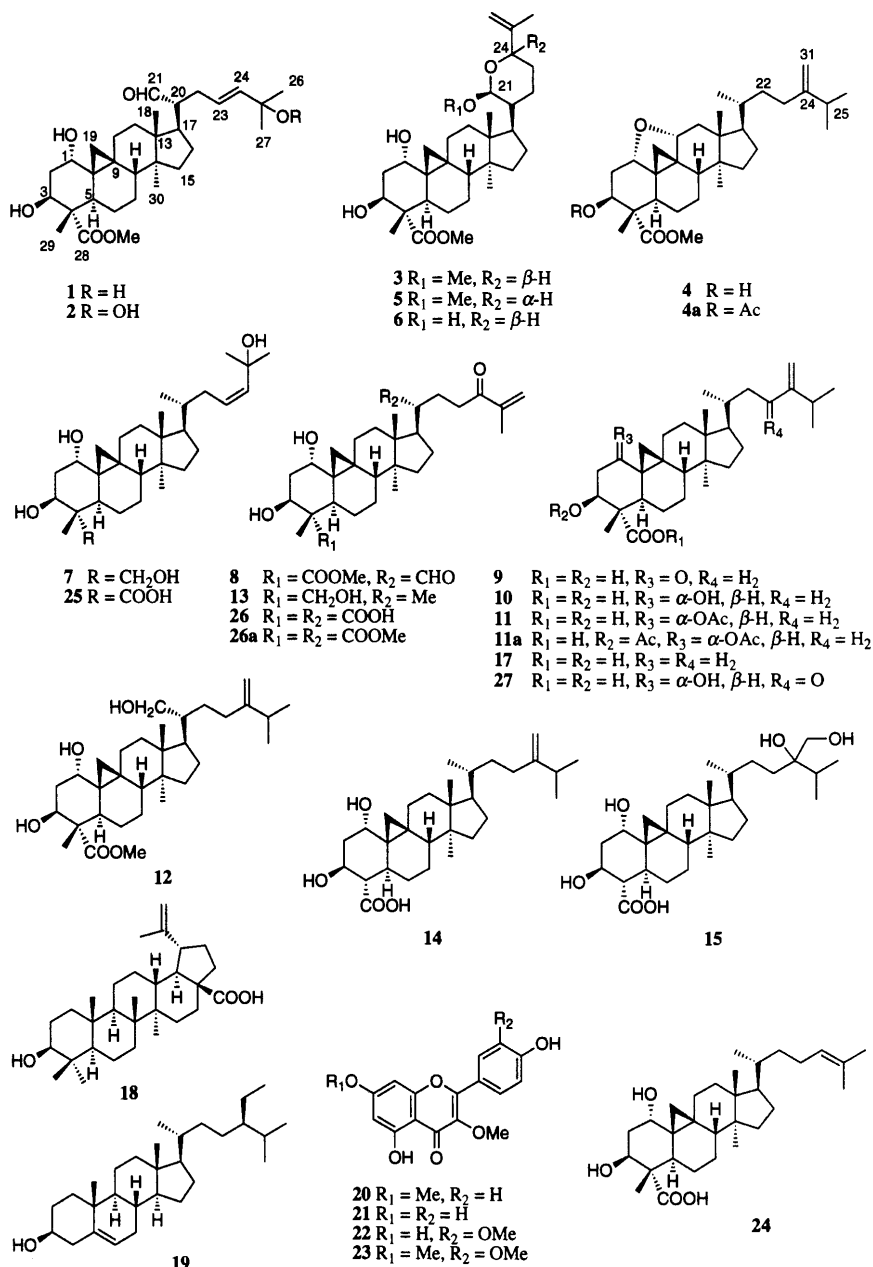
Chart 1

not those of **1**. Thus, the compound reported by Ganzera *et al.* should have the structural formula **2**; *i.e.*, methyl quadrangularate B.

Methyl quadrangularate C (**3**) and its 24-epimer, methyl 24-epiquadrangularate C (**5**), were obtained as an epimeric mixture (1 : 1 from ^{1}H-NMR spectrum), and only the former one succeeded in achieving a pure form as a colorless amorphous solid. The molecular formula of **3** was deduced to be $C_{32}H_{50}O_6$ by HR-FAB-MS. The additional signals of two oxymethines in the ^{1}H- and ^{13}C-NMR spectra of **3** [δ_H 4.90 (br s), δ_C 100.1; δ_H 4.22 (br d, $J=11.0$ Hz), δ_C 71.2] as compared to those of **1** and **2**, suggested the presence of a pyran ring on the ring D side chain.[18] The existence of the pyran ring with a methoxyl and an isopropenyl group was further confirmed by analysis of the ^{1}H–^{1}H COSY and long-range ^{1}H–^{13}C COSY spectra. In addition, analysis of the ^{1}H- and ^{13}C-NMR spectra of the mixture, by the ^{1}H–^{1}H COSY, heteronuclear multiple quantum coherence (HMQC) and het-

eronuclear multiple bond correlation (HMBC) spectra, enabled us to assign the signals of **5**, which showed only small differences with **3** in the chemical shifts of H-24 (**5**, δ 4.26; **3**, δ 4.22), H_2-26 (**5**, δ 5.14, 4.94; **3**, δ 5.18, 4.92) and a methoxyl group (**5**, δ 3.45; **3**, δ 3.35). Methyl quadrangularate O (**6**), with the molecular formula $C_{31}H_{48}O_6$, showed similar ^{1}H- and ^{13}C-NMR spectra to those of **3**, except for the absence of a signal corresponding to the C-21 methoxyl group. The upfield shift of C-21 of **6** (δ 93.0) as compared to **3** (δ 100.1) suggested the presence of a free hydroxyl group at C-21 in **6**.

The stereochemistry of rings A—D of **3**, **5** and **6** was found to be the same as that of **1** based on coupling constants and NOE experiments. The relative stereochemistry of the pyran ring of **3** and **6** was established to be equatorial H-21 (axial OMe) and axial H-24 from the coupling pattern of H-21 (br s) and H-24 (br d, $J=11.0$ Hz). This was further supported by the NOE experiment in which irradiation of

methoxyl protons of **3** caused an NOE increase at H-24, placing them on a 1,3-diaxial arrangement in a chair conformation. Considering a biogenetic pathway (Chart 2), there

2

8   **6**

12
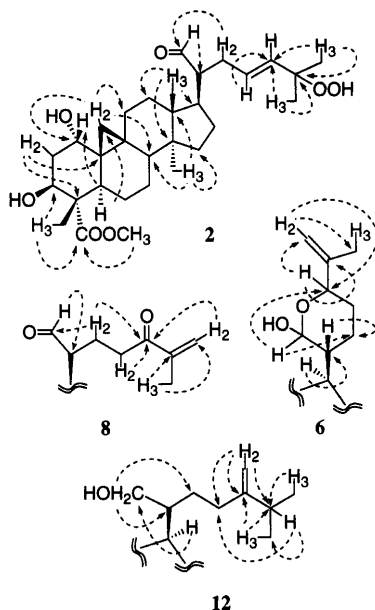
Fig. 1. Significant Correlations Observed in the Long-Range ^{1}H–^{13}C COSY Spectrum of **2** and FG-Pulsed HMBC Spectra of **6**, **8**, and **12**

Compounds **6**, **8** and **12** showed the same significant correlations in rings A—D as **2**.

should be two possible epimeric relations of **5** to **3**; either at C-21 or at C-24. The identical chemical shift and coupling pattern of H-21 of **3** and **5** led us to the conclusion that they should be epimers at C-24. The pyran ring of **5** was considered to be in a boat conformation because of strong 1,3-diaxial repulsion between the methoxyl group at C-21 and the isopropenyl group at C-24. This was further supported by the coupling constant of H-24 (J=11.0 Hz) due to diaxial coupling with H-23$_{ax.}$ in a boat conformation. From these data, the structure of methyl quadrangularate C, methyl 24-epi-quadrangularate C and methyl quadrangularate O were determined to be **3**, **5** and **6**, respectively.

Methyl quadrangularate D (**4**) was isolated as a colorless amorphous solid having the molecular formula $C_{32}H_{50}O_4$. The ^{1}H- and ^{13}C-NMR spectra of **4** showed the presence of three oxymethines (δ_H 4.95, 4.27, 3.93; δ_C 71.7, 80.4, 84.4), an *exo*-olefin (δ_H 4.87, 4.84; δ_C 106.6, t; δ_C 156.6, s), an ester methyl (δ_H 3.67; δ_C 51.7), three secondary methyls and a cyclopropane ring (δ_H 1.37, 0.71). The signal of the *exo*-olefin suggested that **4** might have the same side chain of ring D as 7β-hydroxy-23-deoxojessic acid,[7] which was confirmed by the HMBC spectrum (Fig. 2). The downfield shift of the cyclopropane methylene protons from the usual range suggested the presence of an oxygen substituent at C-11,[19] which was further confirmed by the ^{1}H–^{1}H COSY and HMBC spectra in which H-19 had long-range correlations with both C-1 and C-11. Moreover, a downfield shift of both

Table 1. ^{13}C-NMR Data (100 MHz) of Novel Cycloartane-Type Triterpenes in Pyridine-d_5

	1	1[a]	2	2[a,b]	3	4	4a[c]	5	6	7	8	9	10	11[d]	11a[e]	12	13	14	15
1	72.1	73.3	72.8	73.3	72.4	80.4	79.4	72.3	72.2	72.7	72.1	208.7	72.5	76.5	75.6	72.3	72.7	71.8	71.1
2	38.6	37.6	38.6	37.6	38.7	37.0	37.0	39.3	38.6	38.6	38.7	49.0	38.8	35.0	31.0	38.6	38.7	42.8	42.8
3	70.4	71.3	70.1	71.3	70.5	71.7	74.6	70.5	70.5	69.6	70.4	73.6	70.7	70.3	74.2	70.5	69.6	68.7	68.7
4	55.9	56.3	55.9	56.3	56.1	51.6	50.1	56.0	56.0	45.0	56.0	54.7	55.6	55.1	52.8	56.1	45.0	60.2	60.2
5	37.7	38.5	37.7	38.5	38.0	37.3	37.9	38.0	37.9	34.5	37.8	44.7	37.7	38.9	39.1	38.0	34.5	34.2	34.1
6	23.0	23.9	23.0	23.9	23.3	19.0	19.9	23.4	23.4	21.2	23.1	22.0	23.4	22.8	22.4	23.4	21.2	25.7	25.7
7	25.8	26.4	25.8	26.4	27.2	22.1	22.9	27.4	25.9	28.4	26.9	28.0	28.3	28.2	28.2	27.8	28.3	25.0	25.0
8	47.2	49.7	47.4	49.6	48.2	38.8	38.6	48.2	48.4	48.5	47.5	43.8	48.1	46.3	46.2	48.3	48.5	46.9	47.0
9	20.6	22.0	20.6	22.0	20.8	32.9	33.0	20.7	20.9	20.8	20.7	28.1	20.8	20.8	21.4	20.9	20.8	24.5	24.5
10	30.3	30.4	30.3	30.4	30.2	30.2	37.5	30.2	30.1	30.9	30.3	37.1	30.3	30.0	30.0	29.8	30.5	33.3	33.3
11	25.5	26.4	25.5	26.4	27.2	84.4	84.7	26.1	26.1	26.1	25.6	27.8	26.6	26.4	26.3	26.2	26.1	26.5	26.5
12	31.6	32.4	31.6	32.4	31.6	39.6	39.7	31.6	31.5	33.2	31.7	33.2	33.2	33.0	33.0	32.4	33.3	33.1	33.2
13	45.4	46.3	45.5	46.3	45.9	47.5	47.6	45.2	45.5	45.5	45.5	45.4	45.6	45.2	45.4	45.6	45.5	45.6	45.5
14	48.9	48.3	48.9	48.3	49.1	49.5	49.5	49.5	49.1	49.1	48.9	49.5	49.1	49.2	49.1	49.2	49.1	49.2	49.2
15	35.3	36.5	35.3	36.5	35.9	28.4	28.4	35.7	35.9	36.1	35.4	34.6	35.9	35.5	35.5	35.9	36.0	35.6	35.6
16	26.8	27.8	26.8	27.6	25.8	34.0	33.9	25.9	27.2	26.1	23.4	23.5	25.8	25.1	24.9	25.9	26.1	28.3	28.3
17	47.5	48.4	47.3	48.4	46.9	51.3	51.3	46.8	47.1	52.4	47.4	52.2	52.5	52.5	52.5	46.8	52.6	52.4	52.5
18	19.2	19.7	19.1	19.7	19.1	15.5	15.6	19.1	19.2	18.7	19.2	18.4	18.3	17.9	17.9	19.7	18.4	18.0	17.9
19	29.4	30.9	29.3	30.9	29.9	30.6	30.0	29.8	29.9	30.1	29.4	28.2	29.7	28.0	28.0	30.2	30.0	26.5	26.5
20	55.9	56.9	55.8	56.8	42.8	36.3	36.3	43.8	43.5	36.9	55.8	36.4	36.5	36.4	36.4	43.6	36.2	36.4	37.2
21	205.5	208.0	205.4	208.0	100.1	18.7	18.9	100.5	93.0	18.6	205.7	16.9	18.5	18.5	18.5	61.8	18.5	18.6	19.2
22	32.3	33.0	32.6	33.3	24.7	35.3	35.3	25.2	24.3	39.5	25.9	35.3	35.3	35.2	35.3	29.1	31.4	35.3	29.9
23	122.8	124.2	126.5	127.8	30.8	31.6	31.6	33.2	32.0	124.6	35.1	31.6	31.6	31.7	31.7	31.7	34.9	31.6	31.9
24	142.4	141.7	138.0	138.1	71.2	156.6	156.7	71.7	70.9	141.6	200.1	156.7	156.7	156.7	156.7	157.1	202.2	156.7	75.7
25	69.5	71.0	80.9	82.3	146.8	34.0	34.1	147.0	147.7	69.7	144.5	34.0	34.0	34.0	34.1	34.1	144.8	34.1	33.1
26	30.5	29.9	25.2	25.0	110.4	22.0	22.2	110.4	109.9	30.5	124.8	21.9	22.0	22.1	22.1	22.2	124.6	22.1	17.7
27	30.5	29.8	24.9	24.8	19.0	21.9	22.0	18.6	19.3	30.5	17.8	21.9	21.9	22.0	22.0	22.1	17.8	22.0	17.7
28	176.1	179.1	178.1	179.1	178.1	178.5	177.1	178.1	178.1	68.0	178.1	179.0	179.9	179.5	177.9	178.2	68.0	177.5	177.5
29	9.4	9.1	9.4	9.1	9.5	13.6	13.2	9.5	9.5	10.7	9.5	10.6	9.7	9.6	10.5	9.5	10.7		
30	19.0	19.7	19.1	19.7	19.1	18.8	19.0	19.1	19.1	19.5	19.1	18.5	19.4	19.1	19.1	18.8	19.5	19.2	18.7
31						106.6	106.7					106.6	106.6	106.6	106.7	106.5		106.7	66.1
21-OMe					53.9		54.6												
28-OMe	51.4	52.2	51.0	52.2	51.6	51.7	52.1	51.5	51.1		51.5					51.5			

a) Measured in methanol-d_4. *b*) Identical to the data of reference 9. *c*) Signals of acetyl groups appeared at δ 170.5 and 20.5. *d*) signals of acetyl group were at δ 170.1 and 21.1. *e*) Signals of acetyl groups appeared at δ 170.4, 21.1 and 170.0, 20.0.
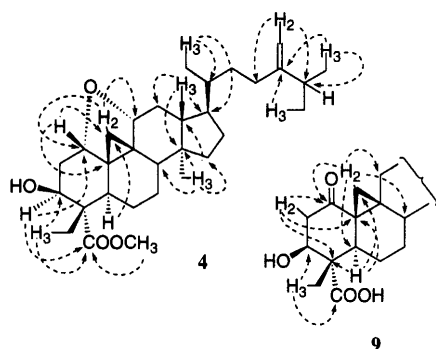
Fig. 2. Significant Correlations Observed in the FG-Pulsed HMBC Spectra of 4 and 9

Compound 9 showed the same significant correlations in rings C and D and side chain on ring D as 4.

carbon signals, C-1 and C-11, of 4 compared with those of 1—3 and cycloartane-type triterpenes bearing a hydroxyl group either at C-1 or C-11,[19] suggested that there may be ether linkage between C-1 and C-11.[20] This was further supported by the fact that on acetylation 4 gave only monoacetate 4a; the possibility that due to steric hindrance the 1-OH group did not take part in acetylation should be ruled out because 23-deoxojessic acid (10) having the same 1-OH group as 4 easily gave a diacetate under the same conditions (see Experimental). From these data, we concluded that there should be an ether linkage between C-1 and C-11, which was further supported by the compositions of 4 and its monoacetate 4a from HR-FAB-MS spectra.

In the NOE experiments, NOEs were observed between H-11 and H3-18, between H-8 and H3-18, between H-19 and H-1, between H-19 and H-11 and between H3-29 and H-1, suggesting that all the protons, H3-29, H3-18, H-19, H-11 and H-1, are in the β position. These NOEs and the coupling constants of H-1 (dd, J=11.0, 6.0 Hz) and H-3 (dd, J=4.5, 2.5 Hz) suggested that the A ring should be in a boat conformation and the hydroxyl group at C-3 in the β-orientation. Accordingly, the structure of methyl quadrangularate D was determined to be 4.

Quadrangularol A (7) was isolated as a colorless amorphous solid having the molecular formula $C_{30}H_{50}O_4$. The IR spectrum of 7 indicated the presence of a hydroxyl group (3400 cm^{-1}). The ^{1}H-NMR spectrum displayed signals corresponding to two olefinic protons (δ 5.94, s, 2H), two oxymethylene protons (δ 4.28, 3.89, both d, J=10.2 Hz), two oxymethine protons (δ 5.08, 3.85), five tertiary methyls (δ 1.54, 1.54, 1.22, 1.06, 0.97), one secondary methyl (δ 0.96) and two highly shielded cyclopropane methylene protons (δ 0.77, 0.52, both d, J=4.5 Hz). Both the ^{1}H- and ^{13}C-NMR data of 7 were similar to those of 1—6, having a 1,3-dihydroxycycloartane skeleton. However, the absence of a signal corresponding to the carboxylic acid group and the presence of signals of an oxymethylene group suggested that 7 should have an oxymethylene group at C-4 instead of the carboxylic acid group, which was further confirmed by the field gradient-pulsed (FG-pulsed) HMBC spectrum (Fig. 3).

The stereochemistry of rings A—D of 7 was determined to be the same as 1 by the rotating frame nuclear Overhauser effect spectroscopy (ROESY) spectrum. The correlation between H3-29 and H-19 in the ROESY spectrum indicated that the methyl group at C-4 should be β. The broad singlet of
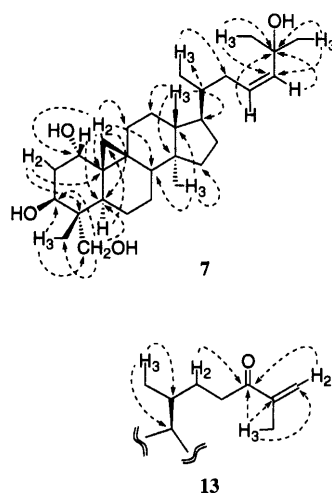
Fig. 3. Significant Correlations Observed in the FG-Pulsed HMBC Spectra of 7 and 13

Compound 13 showed the same significant correlations in rings A—D as 7.

two olefinic protons at δ 5.94 was identical with those of quadrangularic acid J (25, δ 5.94)[7] and (23Z)-3β-acetoxycycloart-23-en-25-ol (δ 5.60)[20] having a cis-23(24) double bond, suggesting the cis configuration of the olefinic group of 7. The cis nature of the double bond was further supported by similar chemical shifts of the olefinic carbons of 7 [δ 124.6 (C-23), 141.6 (C-24), in C_5D_5N] with those of 25 [δ 124.4 (C-23), 141.3 (C-24), in C_5D_5N] and (23Z)-3β-acetoxycycloart-23-en-25-ol [δ 125.6 (C-23), 139.3 (C-24), in $CDCl_3$].[21] Thus, the structure of quadrangularol A was concluded to be 7.

Methyl quadrangularate N (8), $[\alpha]_D^{25}$ +70.8° (c=0.11, MeOH), showed a pseudomolecular ion at m/z 537.3189 corresponding to the molecular formula $C_{31}H_{48}O_4$ in HR-FAB-MS. The ^{1}H-NMR spectrum of 8 was similar to that of quadrangularic acid H (26),[7] but the ^{1}H-NMR spectrum of 8 had one more aldehydic proton at δ 9.59 than that of 26, suggesting the presence of an aldehydic group at C-20 instead of a carboxylic acid group. This was confirmed by the FG-pulsed HMBC spectrum (Fig. 1). Accordingly, the structure of methyl quadrangularate N was concluded to be 8, because oxidation with sodium chlorate,[22] followed by esterification with diazomethane, gave dimethyl quadrangularate H (26a).[7]

Quadrangularic acid E (9), $[\alpha]_D^{25}$ +18.2° (c=0.20, MeOH), had the molecular formula $C_{31}H_{48}O_4$. The ^{1}H-NMR spectrum of 9 demonstrated the presence of only one oxymethine proton at δ 5.20 (t, J=8.0 Hz). Both of the cyclopropane methylene protons of 9 were found to be highly deshielded (δ 1.30 and 1.02) as compared to the other cycloartane-type triterpenes isolated from C. quadrangulare. The disappearance of the oxymethine proton corresponding to H-1 in the ^{1}H-NMR spectrum and the presence of a new ketone signal at δ 208.7 in the ^{13}C-NMR spectrum suggested the presence of a ketone group at C-1. This was further supported by the significant correlation between C-1 and H-3 in the FG-pulsed HMBC spectrum (Fig. 2). The stereochemistry of 9 was also determined by the NOE experiments; NOEs between H-3 and H-5 and between H3-29 and H-19 indicated the OH-3 and H3-29 to be β. Due to the presence of a ketone group at C-1, ring-A has a distorted chair conformation. Finally, the structure of quadrangularic acid E was con-

cluded to be **9**.

23-Deoxojessic acid (**10**) was the major cycloartane-type triterpene isolated from the leaves of *C. quadrangulare*. The molecular formula of **10** was calculated to be $C_{31}H_{50}O_4$ by HR-FAB-MS. The ^{1}H- and ^{13}C-NMR data of **10** were found to be similar to those of jessic acid (**27**),[3] except for a new signal due to a methylene group (δ_H 2.20, 1.98; δ_C 31.6) instead of the signal of a ketone carbonyl carbon. Thus, **10** was presumed to be as 23-deoxojessic acid, which was confirmed by the HMBC spectrum. A monoacetyl derivative of **10**, *i.e.*, 1-*O*-acetyl-23-deoxojessic acid (**11**), was also obtained as a colorless amorphous solid having the molecular formula $C_{33}H_{52}O_5$. The ^{1}H- and ^{13}C-NMR spectra of **11** showed additional signals of an acetyl group (δ_H 2.06; δ_C 170.1, 21.1). The downfield shift of H-1 at δ 5.02 suggested the location of the acetyl group at C-1, which was confirmed by the long-range ^{1}H–^{13}C COSY spectrum. Furthermore, the structure of 1-*O*-acetyl-23-deoxojessic acid was confirmed to be **11** by the fact that acetylation of both **10** and **11** gave the same diacetate **11a**.

Methyl quadrangularate P (**12**) was obtained as a colorless amorphous solid with $[\alpha]_D^{25}$ +163.5° (*c*=0.03, MeOH) and its molecular formula was determined to be $C_{32}H_{52}O_5$ by HR-FAB-MS. The ^{1}H- and ^{13}C-NMR spectra of **12** were found to be almost identical to those of methyl 23-deoxojessate (**16**), except that the ^{1}H-NMR spectrum had additional signals of two oxymethylene protons at δ 4.06 and 3.87 (both dd, *J*=10.7, 3.1 Hz) instead of that of the secondary methyl; also, the ^{13}C-NMR spectrum showed the presence of an oxymethylene carbon instead of a methyl carbon. The long-range correlations between the oxymethylene protons and C-17 and C-22 and between H-17 and the oxymethylene carbon in the FG-pulsed HMBC spectrum (Fig. 1) confirmed the oxymethylene group to be C-21. The stereochemistry of **12** was concluded to be the same as that of **1** by the analysis of NOE difference spectra. Thus, the structure of methyl quadrangularate P was concluded to be **12**.

Quadrangularol B (**13**), having the molecular formula $C_{30}H_{48}O_4$, was isolated as a colorless amorphous solid. The absorption bands at 3400 and 1700 cm^{-1} in the IR spectrum suggested the presence of hydroxyl and carbonyl groups, respectively. The ^{1}H- and ^{13}C-NMR spectra of **13** were almost identical to those of **7** except for some difference in the ring D side chain. The ^{1}H- and ^{13}C-NMR signals of the *exo*-olefin appeared relatively downfield (δ_H 6.02, 5.73; δ_C 124.6, 144.8) instead of those of C-23(24) *cis*-olefin in **7**. Moreover, an additional signal of a ketone carbonyl carbon appeared at δ 202.2 in the ^{13}C-NMR spectrum of **13**. These data suggested the presence of an α,β-unsaturated ketone group as in **8**. The signal of a vinyllic methyl at δ 1.92 in the ^{1}H-NMR spectrum suggested the position of the *exo*-olefin should be at C-25(26) and the ketone group at C-24, which was further confirmed by the FG-pulsed HMBC spectrum (Fig. 3). The stereochemistry of **13** was determined to be the same as **7** by the ROESY spectrum. Thus, the structure of quadrangularol B was concluded to be **13**.

Norquadrangularic acid B (**14**) was isolated as a colorless amorphous solid having $[\alpha]_D^{25}$ +77.7° (*c*=0.15, MeOH). Its HR-FAB-MS showed a quasimolecular ion at *m/z* 495.3410 consistent with the molecular formula $C_{30}H_{48}O_4$. Its IR spectrum suggested the presence of hydroxyl and carbonyl
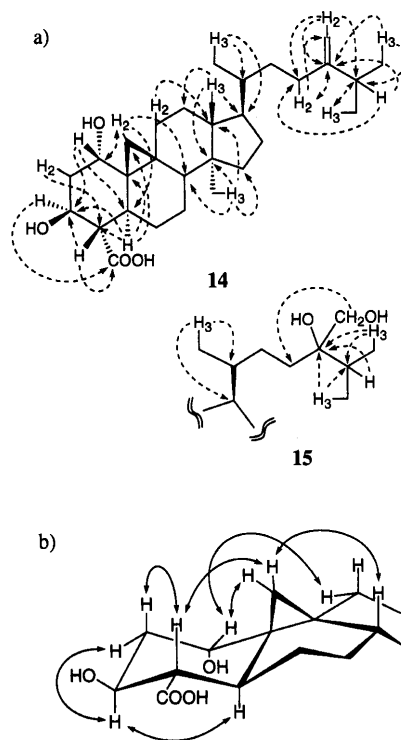
Fig. 4. Significant Correlations Observed in the FG-Pulsed HMBC Spectra of **14** and **15** (a) and ROESY Correlations Observed in the ROESY Spectrum of **14** (b)

Compound **15** showed the same significant correlations in rings A—D as **14**.

groups. The ^{1}H-NMR spectrum displayed signals of two oxymethines (δ 5.28, 3.99), an *exo*-olefin (δ 4.85, 4.87), three secondary methyls (δ 1.07, 1.06, 0.94), two tertiary methyls (δ 1.03, 1.00) and a cyclopropane methylene (δ 0.67, 0.30), which were similar to those of **10**. The additional methine signal at δ 2.85 (t, *J*=11.0 Hz) coupling with both H-3 and H-5, however, suggested that the C-4 of **14** should be a methine, not a quaternary carbon as in **10**. The ^{13}C-NMR spectrum of **14** showed almost identical signals of the rings B—D and the side chain on ring D with those of **10**, but the number of the carbon signals of **14** was thirty, not thirty-one as in **10**. The HR-FAB-MS also showed the molecular formula as one carbon less than **10**. From these data **14** was considered to be a 29-norcycloartane-type triterpene, which was confirmed by the FG-pulsed HMBC spectrum (Fig. 4a). Then, the ROESY spectrum was measured in order to determine the stereochemistry of **14**. Intense correlations were observed between H-3 and H-5, between H-4 and H-19, between H-1 and H-19 and between H-8 and H-19 (Fig. 4b), indicating the β-orientation of H-1, H-4 and H-8 and the α-orientation of H-3 and H-5. Thus, the structure of norquadrangularic acid B was determined to be **14**.

Norquadrangularic acid C (**15**), having the molecular formula $C_{30}H_{50}O_6$, showed absorption bands at 3400 (OH) and 1710 cm^{-1} (CO) in its IR spectrum. The ^{1}H- and ^{13}C-NMR spectra of **15** were almost identical with those of **14** except for differences in the *exo*-olefinic group. The new signals of two oxymethylene protons at δ 4.03 and 3.92 (both d, *J*=10.5 Hz) in **15**, instead of olefinic protons in **14**, suggested the presence of an oxymethylene group at C-24, while the new oxygenated quaternary carbon signal at δ 78.0 was assigned to C-24 from the FG-pulsed HMBC spectrum (Fig.
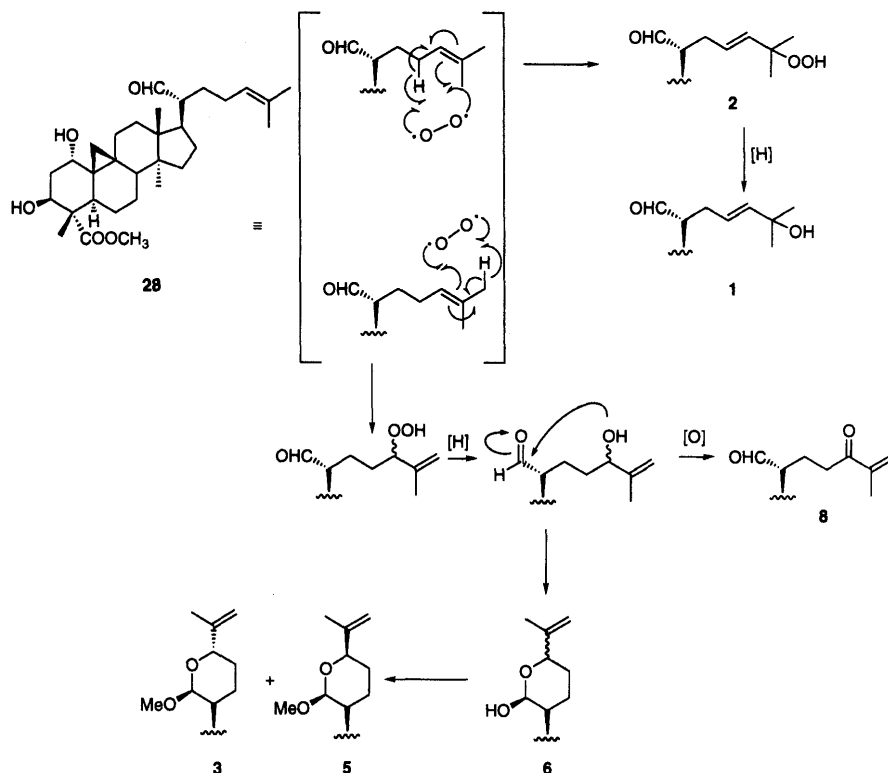
Chart 2. Possible Biogenetic Pathway of 1—3, 5, 6 and 8

4a) based on the correlations with H_3-26, H_3-27 and H-25. The stereochemistry of 15 was determined to be identical with that of 14 by the ROESY spectrum, except for that at C-24, which remains unsolved. Thus, the structure of norquadrangularic acid C was concluded to be 15.

In this paper, we have reported the isolation and structures of fifteen new and two known cycloartane-type triterpenes. Among the isolated cycloartane-type triterpenes 1—3, 5, 6 and 8 differed only in ring D side chain, and thus they would be biosynthesized from a common hypothetical precursor 28 via photooxygenation of an olefin (Chart 2). 23-Deoxojessic acid (10), a major cycloartane-type triterpene in *C. quadrangulare* leaves, may be derived from either 24 or cycloartenol (29) through alkylation at C-24,[23—25] which might produce the rest of the triterpenes (Chart 3).

All the isolated compounds were tested for their cytotoxicity towards highly liver metastatic murine colon 26-L5 carcinoma cells. Cycloartane-type triterpenes showed various degrees of cytotoxicity, and only 2, 3 and 4 had ED_{50} values less than 20 μM. Methyl quadrangularate D (4), having an ether linkage between C-1 to C-11, showed the strongest cytotoxicity with an ED_{50} value of 5.42 μM, while all four flavonoids possessed strong cytotoxicity with ED_{50} values equal to or less than 6 μM (see Experimental).

Experimental

Melting points were determined on a Yanaco micromelting point apparatus and are uncorrected. Optical rotations were recorded on a JASCO DIP-140 digital polarimeter. IR spectra were measured with a Shimadzu IR-408 spectrophotometer in KBr disks. Electron impact-MS (EI-MS) and FAB-MS measurements were performed on a JEOL JMS-700 spectrometer with *m*-nitrobenzylalcohol (NBA) or glycerol as matrices. NMR spectra were taken on a JEOL GX-400 spectrometer or JEOL JNM-GX400 spectrometer with tetramethylsilane (TMS) as the internal standard, and chemical shifts are expressed in δ values. Column chromatography was performed with normal-phase (Fuji Silysia BW-820MH) or reversed-phase silica gel (Nacalai Tesque

Cosmosil 75C_{18}-OPN). TLC and preparative TLC were carried out on precoated Merck Kieselgel 60 F_{254} plates (0.25 and 0.50 mm).

Plant Material Leaves of *C. quadrangulare* Kurz were purchased at the local market at Ho Chi Minh City, Vietnam in 1995. The voucher sample (TMPW 18999) is preserved in the Museum for Materia Medica, Toyama Medical and Pharmaceutical University, Toyama, Japan.

Extraction and Isolation Air dried leaves (2.65 kg) were extracted with MeOH and the MeOH extract (400 g) was chromatographed on a silica gel column and partitioned into eleven fractions.[7]

Fraction 3 (18.0 g) was chromatographed over a silica gel column with an EtOAc–hexane solvent system and thirty-three subfractions were collected. By preparative TLC with MeOH–CHCl₃ (1:19) of subfractions 4, 11 and 22, 19 (10.1 mg), 18 (6.5 mg) and 4 (63.6 mg) were isolated, respectively. Combined subfractions 23—28 afforded a mixture of two flavonoids (1.3 g), and a part of the mixture (100 mg) was separated by preparative TLC with MeOH–CHCl₃ (1:9) to give 20 (36.4 mg) and 23 (50.2 mg).

Fraction 4 (12.0 g) was separated into fourteen subfractions by a Cosmosil 75C_{18}-OPN column with H_2O–MeOH–CH₃CN (1:1:1). Two flavonoids, 21 (19.2 mg) and 22 (23.8 mg), were obtained from subfractions 2 and 5, respectively, as a precipitate. Reversed-phase preparative TLC using H_2O–CH₃CN–MeOH (1:1:1) on subfraction 3 afforded 10 (9.0 mg) and 17 (20.1 mg), and similar treatment on subfraction 10 afforded 16 (10.2 mg).

Fraction 5 (20.0 g) was also applied on a silica gel column and eluted with a MeOH–CHCl₃ solvent system to give five subfractions. Further normal- and reversed-phase silica gel column chromatography and preparative TLC of the subfractions yielded the following compounds: subfraction 1: 2 (13.2 mg), 8 (9.8 mg), 9 (7.2 mg), 11 (14.2 mg), 12 (10.2 mg), 16 (17.1 mg); subfraction 3: 5 (67.1 mg); subfraction 4: 1 (89.2 mg), 2 (117.3 mg), 3 (56.3 mg), a mixture of 3 and 5 (20.5 mg), 6 (32.1 mg), 9 (7.8 mg); subfraction 5: 7 (8.5 mg).

Fraction 6 (22.0 g) was divided into acetone-soluble (19.41 g) and acetone-insoluble (1.74 g) portions. A part of the acetone-insoluble portion (150 mg) was purified by reversed-phase preparative TLC with H_2O–CH₃CN–MeOH (1:1:1) to afford 10 (130.7 mg). The acetone-soluble portion, on the other hand, was further fractionated into five subfractions by a Cosmosil 75C_{18}-OPN column with H_2O–MeOH–CH₃CN (1:1:1). Subfraction 5 on evaporation gave 10 (1.0 g) as a precipitate. Further silica gel column chromatography and preparative TLC on subfraction 4 afforded 10 (82.8 mg) and 14 (34.1 mg).

The combined fractions 7 and 8 were (23.0 g) chromatographed over Cosmosil 75C_{18}-OPN with H_2O–MeOH–CH₃CN (1:1:1) to give twelve sub-

Chart 3. Possible Biogenetic Pathway of 4, 9—12 and 14—17

fractions. Further preparative TLC of subfraction 8 (CHCl₃–CH₃CN–MeOH, 10 : 3 : 1) gave **13** (12.0 mg).

Fraction 9 (20.0 g) was also applied to a Cosmosil 75C₁₈-OPN column with H₂O–MeOH–CH₃CN (1 : 1 : 1), and eight subfractions were collected. Further silica gel column chromatography and preparative TLC of subfraction 3 yielded **15** (48.6 mg).

Methyl Quadrangularate A (**1**): Colorless amorphous solid. ¹H-NMR (pyridine-d_5) δ: 9.61 (1H, d, J=5.5 Hz, H-21), 5.97 (1H, d, J=16.0 Hz, H-24), 5.89 (1H, dt, J=16.0, 6.5 Hz, H-23), 5.35 (1H, dd, J=12.0, 4.5, H-3), 3.82 (1H, br s, H-1), 3.66 (3H, s, 28-OMe), 3.23 (1H, dd, J=12.5, 4.5 Hz, H-5), 2.40 (1H, ddd, J=13.0, 4.5, 3.5 Hz, H-2), 2.34 (2H, dd, J=9.0, 6.5 Hz, H-22), 2.20 (1H, m, H-2), 1.59 (3H, s, H₃-29), 1.49 (3H, s, H₃-26), 1.49 (3H, s, H₃-27), 1.08 (3H, s, H₃-18), 0.98 (3H, s, H₃-30), 0.74 (1H, d, J=4.5 Hz, H-19), 0.44 (1H, d, J=4.5 Hz, H-19). ¹H-NMR (methanol-d_4) δ: 9.44 (1H, d, J=5.5 Hz, H-21), 5.26 (1H, d, J=16.0 Hz, H-24), 5.49 (1H, dt, J=16.0, 6.5 Hz, H-23), 4.49 (1H, dd, J=12.0, 4.5 Hz, H-3), 3.68 (3H, s, 28-OMe), 3.51 (1H, br s, H-1), 2.55 (1H, dd, J=12.5, 4.5 Hz, H-5), 2.32 (3H, m, H-11, H-17, H-20), 2.01 (1H, m, H-16), 1.84 (1H, ddd, J=13.0, 4.5, 3.5 Hz, H-2), 1.76 (1H, ddd, J=13.0, 12.0, 3.5 Hz, H-2), 1.22 (3H, s, H₃-26), 1.21 (3H, s, H₃-27), 1.07 (3H, s, H₃-29), 1.01 (3H, s, H₃-18), 1.01 (3H, s, H₃-30), 0.69 (1H, d, J=4.5 Hz, H-19), 0.46 (1H, d, J=4.5 Hz, H-19). ¹³C-NMR: Table 1. IR (CHCl₃) cm⁻¹: 3450, 1715, 1460, 1380, 1260, 1090, 1050, 1010. HR-EI-MS m/z: 516.3442 [Calcd for C₃₁H₄₈O₆: 516.3443 (M)⁺]. [α]$_D^{25}$ +43.7° (c=0.76, MeOH).

Methyl Quadrangularate B (**2**): Colorless crystals, mp 190 °C. ¹H-NMR

(pyridine-d_5) δ: 9.63 (1H, d, J=5.5 Hz, H-21), 6.05 (1H, d, J=16.0 Hz, H-24), 5.78 (1H, dt, J=16.0, 6.5 Hz, H-23), 5.37 (1H, dd, J=12.0, 4.5 Hz, H-3), 3.85 (1H, br s, H-1), 3.66 (3H, s, 28-OMe), 3.23 (1H, dd, J=12.5, 4.5 Hz, H-5), 2.41 (1H, ddd, J=13.0, 4.5, 3.5 Hz, H-2), 2.34 (2H, dd, J=9.0, 6.5 Hz, H-22), 2.20 (1H, m, H-2), 1.60 (3H, s, H₃-29), 1.53 (3H, s, H₃-26), 1.51 (3H, s, H₃-27), 1.08 (3H, s, H₃-18), 0.98 (3H, s, H₃-30), 0.74 (1H, d, J=4.5 Hz, H-19), 0.44 (1H, d, J=4.5 Hz, H-19). ¹H-NMR (methanol-d_4) δ: 9.45 (1H, d, J=5.5 Hz, H-21), 5.62 (1H, d, J=16.0 Hz, H-24), 5.51 (1H, dt, J=16.0, 6.5 Hz, H-23), 4.49 (1H, dd, J=12.0, 4.5 Hz, H-3), 3.68 (3H, s, 28-OMe), 3.51 (1H, br s, H-1), 2.55 (1H, dd, J=12.5, 4.5 Hz, H-5), 2.32 (3H, m, H-11, H-17, H-20), 2.01 (1H, m, H-16), 1.84 (1H, ddd, J=13.0, 4.5, 3.5 Hz, H-2), 1.76 (1H, ddd, J=13.0, 12.0, 3.5 Hz, H-2), 1.24 (3H, s, H₃-26), 1.23 (3H, s, H₃-27), 1.07 (3H, s, H₃-29), 1.00 (3H, s, H₃-18), 1.00 (3H, s, H₃-30), 0.69 (1H, d, J=4.5 Hz, H-19), 0.46 (1H, d, J=4.5 Hz, H-19). ¹³C-NMR: Table 1. IR (KBr) cm⁻¹: 3500, 1710, 1450, 1380, 1040, 990, 750. HR-FAB-MS m/z: 555.3315 [Calcd for C₃₁H₄₈NaO₇: 555.3312 (M+Na)⁺]. [α]$_D^{25}$ +53.4° (c=0.79, MeOH).

Methyl Quadrangularate C (**3**): Colorless amorphous solid. ¹H-NMR (pyridine-d_5) δ: 5.33 (1H, dd, J=12.0, 4.5 Hz, H-3), 5.18 (1H, br s, H-26), 4.92 (1H, br s, H-26), 4.90 (1H, br s, H-21), 4.22 (1H, br d, J=11.0 Hz, H-24), 3.85 (1H, br s, H-1), 3.65 (3H, s, 28-OMe), 3.35 (3H, s, 21-OMe), 3.23 (1H, dd, J=12.0, 4.5 Hz, H-5), 2.75 (1H, m, H-11), 2.42 (1H, ddd, J=13.0, 4.5, 4.0 Hz, H-2), 2.22 (1H, ddd, J=13.0, 12.0, 3.5 Hz, H-2), 1.85 (3H, s, H₃-27), 1.62 (3H, s, H₃-29), 1.04 (3H, s, H₃-18), 0.99 (3H, s, H₃-30), 0.76 (1H, d, J=4.5 Hz, H-19), 0.52 (1H, d, J=4.5 Hz, H-19). ¹³C-NMR: Table 1.

IR (CHCl₃) cm⁻¹: 3400, 1720, 1450, 1230, 1110, 1030. HR-FAB-MS m/z: 531.3672 [Calcd for $C_{32}H_{51}O_6$: 531.3674 (M+H)⁺]. $[\alpha]_D^{25}$ +37.2° (c=0.33, MeOH).

Methyl Quadrangularate D (4): Colorless amorphous solid. ¹H-NMR (pyridine-d_5) δ: 4.95 (1H, dd, J=5.0, 2.5 Hz, H-3), 4.87 (1H, br s, H-28), 4.84 (1H, br s, H-28), 4.27 (1H, dd, J=11.0, 6.0 Hz, H-1), 3.93 (1H, dd, J=9.5, 6.0 Hz, H-11), 3.67 (3H, s, 28-OMe), 2.62 (1H, dd, J=11.5, 3.0 Hz, H-5), 2.60 (1H, ddd, J=12.5, 6.0, 2.5 Hz, H-2), 2.40 (1H, ddd, J=12.5, 11.0, 5.0 Hz, H-2), 2.30 (1H, dd, J=14.0, 6.0 Hz, H-12), 2.14 (1H, dd, J=10.0, 5.5 Hz, H-8), 1.86 (1H, dd, J=14.0, 9.5 Hz, H-12), 1.55 (3H, s, H₃-29), 1.37 (1H, d, J=4.5 Hz, H-19), 1.06 (3H, s, H₃-30), 1.07 (3H, d, J=7.0 Hz, H₃-26), 1.06 (3H, d, J=7.0 Hz, H₃-27), 0.93 (3H, d, J=6.5 Hz, H₃-21), 0.90 (3H, s, H₃-18), 0.71 (1H, d, J=4.5 Hz, H-19). ¹³C-NMR: Table 1. IR (CHCl₃) cm⁻¹: 3400, 1720, 1460, 1380, 1240. HR-FAB-MS m/z: 499.3814 [Calcd for $C_{32}H_{51}O_4$: 499.3801 (M+H)⁺]. $[\alpha]_D^{25}$ +57.4° (c=0.39, MeOH).

Methyl 24-Epiquadrangularate C (5): ¹H-NMR (pyridine-d_5) δ: 5.36 (1H, dd, J=12.0, 4.5 Hz, H-3), 5.14 (1H, br s, H-26), 4.94 (1H, br s, H-26), 4.90 (1H, br s, H-21), 4.26 (1H, br d, J=11.0 Hz, H-24), 3.81 (1H, br s, H-1), 3.65 (3H, s, 28-OMe), 3.43 (3H, s, 21-OMe), 3.23 (1H, dd, J=12.0, 4.5 Hz, H-5), 2.75 (1H, m, H-11), 2.42 (1H, ddd, J=13.0, 4.5, 3.5 Hz, H-2), 2.22 (1H, ddd, J=13.0, 12.0, 3.5 Hz, H-2), 1.85 (3H, s, H₃-27), 1.62 (3H, s, H₃-29), 1.04 (3H, s, H₃-18), 1.02 (3H, s, H₃-30), 0.76 (1H, d, J=4.5 Hz, H-19), 0.52 (1H, d, J=4.5 Hz, H-19). ¹³C-NMR: Table 1.

Methyl Quadrangularate O (6): Colorless amorphous solid. ¹H-NMR (pyridine-d_5) δ: 5.73 (1H, br s, H-21), 5.34 (1H, dd, J=12.0, 4.5 Hz, H-3), 5.23 (1H, br s, H-26), 4.92 (1H, br s, H-26), 4.80 (1H, br d, J=11.0 Hz, H-24), 3.77 (1H, br s, H-1), 3.64 (3H, s, 28-OMe), 3.22 (1H, dd, J=12.0, 4.5 Hz, H-5), 2.73 (1H, ddd, J=15.3, 10.2, 6.1 Hz, H-11), 2.40 (1H, ddd, J=13.0, 4.5, 3.5 Hz, H-2), 2.29 (2H, m, H-17, H-22), 2.18 (1H, ddd, J=13.0, 12.0, 3.5 Hz, H-2), 1.85 (3H, s, H₃-27), 1.59 (3H, s, H₃-29), 1.10 (3H, s, H₃-18), 1.03 (3H, s, H₃-30), 0.73 (1H, d, J=4.5 Hz, H-19), 0.44 (1H, d, J=4.5 Hz, H-19). ¹³C-NMR: Table 1. IR (KBr) cm⁻¹: 3450, 1710, 1450, 1380, 1250, 1090. HR-FAB-MS m/z: 539.3395 [Calcd for $C_{31}H_{48}NaO_6$: 539.3348 (M+Na)⁺]. $[\alpha]_D^{25}$ +58.7° (c=0.21, MeOH).

Quadrangularol A (7): Colorless amorphous solid. ¹H-NMR (pyridine-d_5) δ: 5.94 (2H, br s, H-23, H-24), 5.08 (1H, dd, J=12.0, 4.5, H-3), 4.28 (1H, d, J=10.2 Hz, H-28), 3.89 (1H, d, J=10.2 Hz, H-28), 3.85 (1H, br s, H-1), 2.94 (1H, dd, J=12.5, 4.5 Hz, H-5), 2.72 (1H, ddd, J=15.0, 8.0, 5.0 Hz, H-11), 2.44 (1H, ddd, J=13.0, 4.5, 3.5 Hz, H-2), 2.28 (1H, ddd, J=13.5, 11.0, 3.5 Hz, H-2), 1.54 (6H, s, H₃-26, H₃-27), 1.22 (3H, s, H₃-29), 1.06 (3H, s, H₃-18), 0.97 (3H, s, H₃-30), 0.96 (3H, d, J=6.5 Hz, H₃-21), 0.77 (1H, d, J=4.5 Hz, H-19), 0.52 (1H, d, J=4.5 Hz, H-19). ¹³C-NMR: Table 1. IR (KBr) cm⁻¹: 3400, 2950, 1470, 1380, 1000. HR-FAB-MS m/z: 497.3557 [Calcd for $C_{30}H_{50}NaO_4$: 497.3607 (M+Na)⁺]. $[\alpha]_D^{25}$ +75.2° (c=0.14, MeOH).

Methyl Quadrangularate N (8): Colorless amorphous solid. ¹H-NMR (pyridine-d_5) δ: 9.59 (1H, d, J=5.6 Hz, H-21), 5.91 (1H, br s, H-26), 5.60 (1H, br s, H-26), 5.33 (1H, dd, J=10.5, 4.5 Hz, H-3), 3.80 (1H, br s, H-1), 3.64 (3H, s, 28-OMe), 3.20 (1H, dd, J=12.0, 4.5 Hz, H-5), 2.75 (1H, m, H-23), 2.62 (2H, m, H-11, H-22), 2.40 (1H, ddd, J=13.0, 4.5, 3.5 Hz, H-2), 2.37 (1H, m, H-20), 2.22 (1H, m, H-17), 2.15 (1H, ddd, J=13.0, 10.5, 3.5 Hz, H-2), 1.86 (3H, s, H₃-27), 1.57 (3H, s, H₃-29), 1.06 (3H, s, H₃-18), 0.98 (3H, s, H₃-30), 0.72 (1H, d, J=4.5 Hz, H-19), 0.82 (1H, d, J=4.5 Hz, H-19). ¹³C-NMR: Table 1. IR (KBr) cm⁻¹: 3400, 1710, 1460, 1250, 1255, 1040. HR-FAB-MS m/z: 537.3189 [Calcd for $C_{31}H_{46}NaO_6$: 537.3192 (M+Na)⁺]. $[\alpha]_D^{25}$ +70.8° (c=0.11, MeOH).

Quadrangularic Acid E (9): Colorless amorphous solid. ¹H-NMR (pyridine-d_5) δ: 5.20 (1H, t, J=8.0 Hz, H-3), 4.87 (1H, br s, H-28), 4.85 (1H, br s, H-28), 3.17 (2H, d, J=8.0 Hz, H-2), 2.90 (1H, dd, J=12.0, 4.0 Hz, H-5), 2.57 (1H, ddd, J=15.0, 8.0, 5.0 Hz, H-11), 1.76 (3H, s, H₃-29), 1.30 (1H, d, J=4.5 Hz, H-19), 1.07 (3H, d, J=6.5 Hz, H₃-26), 1.06 (3H, d, J=6.5 Hz, H₃-27), 1.02 (1H, d, J=4.5 Hz, H-19), 1.01 (3H, s, H₃-30), 0.93 (3H, s, H₃-18), 0.92 (3H, d, J=6.5 Hz, H₃-21). ¹³C-NMR: Table 1. IR (CHCl₃) cm⁻¹: 3400, 1700, 1460, 1370, 1255, 1190. HR-EI-MS m/z: 484.3580 [Calcd for $C_{31}H_{48}O_4$: 484.3575 (M)⁺]. $[\alpha]_D^{25}$ +18.2° (c=0.20, MeOH).

23-Deoxojessic Acid (10): Colorless amorphous solid. ¹H-NMR (pyridine-d_5) δ: 5.57 (1H, dd, J=12.0, 4.5 Hz, H-3), 4.87 (1H, br s, H-28), 4.86 (1H, br s, H-28), 3.92 (1H, br s, H-1), 3.44 (1H, dd, J=12, 4.5 Hz, H-5), 2.76 (1H, ddd, J=14.0, 10.0, 7.0 Hz, H-11), 2.50 (1H, ddd, J=13.5, 4.5, 3.5 Hz, H-2), 2.32 (1H, m, H-2), 2.20 (1H, ddd, J=14.5, 10.0, 3.5 Hz, H-23), 1.98 (1H, ddd, J=14.5, 10.0, 5.0 Hz, H-23), 1.74 (3H, s, H₃-29), 1.07 (3H, d, J=7.0 Hz, H₃-26), 1.06 (3H, d, J=7.0 Hz, H₃-27), 1.06 (3H, s, H₃-18), 1.01 (3H, s, H₃-30), 0.96 (3H, d, J=6.0 Hz, H₃-21), 0.85 (1H, d, J=4.5 Hz, H-19), 0.56 (1H, d, J=4.5 Hz, H-19). ¹³C-NMR: Table 1. IR (CHCl₃) cm⁻¹: 3400, 1700, 1470, 1380, 1260. HR-EI-MS m/z: 486.3663 [Calcd for $C_{31}H_{50}O_4$:

486.3672 (M)⁺]. $[\alpha]_D^{25}$ +75.4° (c=0.24, MeOH).

1-O-Acetyl-23-deoxojessic Acid (11): Colorless amorphous solid. ¹H-NMR (pyridine-d_5) δ: 5.16 (1H, dd, J=12.0, 4.5 Hz, H-3), 5.02 (1H, br s, H-1), 4.87 (1H, br s, H-28), 4.86 (1H, br s, H-28), 3.11 (1H, dd, J=12.0, 4.5 Hz, H-5), 2.55 (1H, ddd, J=13.5, 4.5, 3.5 Hz, H-2), 2.24 (1H, m, H-2), 2.06 (3H, s, 1-OAc), 1.67 (3H, s, H₃-29), 1.07 (3H, d, J=7.0 Hz, H₃-26), 1.06 (3H, d, J=7.0 Hz, H₃-27), 1.01 (3H, s, H₃-30), 0.97 (3H, s, H₃-18), 0.93 (3H, d, J=6.0 Hz, H₃-21), 0.87 (1H, d, J=4.5 Hz, H-19), 0.55 (1H, d, J=4.5 Hz, H-19). ¹³C-NMR: Table 1. IR (CHCl₃) cm⁻¹: 3400, 1700, 1470, 1380, 1250. HR-FAB-MS m/z: 551.3703 [Calcd for $C_{33}H_{52}NaO_5$: 551.3704 (M+Na)⁺]. $[\alpha]_D^{25}$ +55.8° (c=0.11, MeOH).

Methyl Quadrangularate P (12): Colorless amorphous solid. ¹H-NMR (pyridine-d_5) δ: 5.36 (1H, dd, J=12.0, 4.5 Hz, H-3), 4.91 (1H, br s, H-28), 4.87 (1H, br s, H-28), 4.06 (1H, dd, J=10.7, 3.1 Hz, H₂-21), 3.87 (1H, dd, J=10.7, 4.1 Hz, H-21), 3.85 (1H, br s, H-1), 3.65 (3H, s, 28-OMe), 3.24 (1H, dd, J=12.0, 4.5 Hz, H-5), 2.75 (1H, ddd, J=15.0, 8.0, 5.0 Hz, H-11), 2.41 (1H, ddd, J=13.5, 4.5, 3.5 Hz, H-2), 2.33 (1H, m, H-25), 2.24 (1H, m, H-17), 2.17 (1H, ddd, J=13.5, 12.0, 3.5 Hz, H-2), 1.61 (3H, s, H₃-29), 1.13 (3H, s, H₃-18), 1.07 (3H, d, J=7.0 Hz, H₃-26), 1.06 (3H, d, J=7.0 Hz, H₃-27), 1.03 (3H, s, H₃-30), 0.77 (1H, d, J=4.5 Hz, H-19), 0.51 (1H, d, J=4.5 Hz, H-19). ¹³C-NMR: Table 1. IR (KBr) cm⁻¹: 3300, 1700, 1450, 1250. HR-FAB-MS m/z: 539.3731 [Calcd for $C_{32}H_{52}NaO_5$: 539.3712 (M+Na)⁺]. $[\alpha]_D^{25}$ +163.5° (c=0.03, MeOH).

Quadrangularol B (13): Colorless amorphous solid. ¹H-NMR (pyridine-d_5) δ: 6.02 (1H, br s, H-26), 5.73 (1H, br s, H-26), 5.08 (1H, dd, J=12.0, 4.5, H-3), 4.27 (1H, d, J=10.2 Hz, H-28), 3.89 (1H, d, J=10.2 Hz, H-28), 3.84 (1H, br s, H-1), 2.92 (1H, dd, J=12.5, 4.5 Hz, H-5), 2.71 (2H, m, H-11, H-17), 2.42 (1H, ddd, J=13.0, 4.5, 3.5 Hz, H-2), 2.27 (1H, ddd, J=13.5, 11.0, 3.5 Hz, H-2), 1.92 (3H, s, H₃-27), 1.22 (3H, s, H₃-29), 1.08 (3H, s, H₃-18), 0.99 (3H, s, H₃-30), 0.92 (3H, d, J=6.5 Hz, H₃-21), 0.77 (1H, d, J=4.5 Hz, H-19), 0.52 (1H, d, J=4.5 Hz, H-19). ¹³C-NMR: Table 1. IR (KBr) cm⁻¹: 3400, 1680, 1460, 1380, 1050, 1000. HR-FAB-MS m/z: 495.3479 [Calcd for $C_{30}H_{48}NaO_4$: 495.3451 (M+Na)⁺]. $[\alpha]_D^{25}$ +152.9° (c=0.04, MeOH).

Norquadrangularic Acid B (14): Colorless amorphous solid. ¹H-NMR (pyridine-d_5) δ: 5.28 (1H, td, J=11.0, 4.5 Hz, H-3), 4.87 (1H, br s, H-31), 4.85 (1H, br s, H-31), 3.99 (1H, br s, H-1), 3.21 (1H, dd, J=11.5, 4.5 Hz, H-5), 2.86 (1H, t, J=11.0 Hz, H-4), 2.71 (1H, ddd, J=13.5, 4.5, 3.5 Hz, H-2), 2.59 (1H, ddd, J=15.0, 8.0, 5.0 Hz, H-11), 2.28 (1H, m, H-25), 2.20 (1H, m, H-23), 2.16 (1H, ddd, J=13.5, 11.0, 3.5 Hz, H-2), 1.07 (3H, d, J=7.0 Hz, H₃-26), 1.06 (3H, d, J=7.0 Hz, H₃-27), 1.03 (3H, s, H₃-18), 1.00 (3H, s, H₃-30), 0.94 (3H, d, J=7.0 Hz, H₃-21), 0.67 (1H, d, J=4.5 Hz, H-19), 0.30 (1H, d, J=4.5 Hz, H-19). ¹³C-NMR: Table 1. IR (KBr) cm⁻¹: 3400, 1710, 1460, 1030, 880. HR-FAB-MS m/z: 495.3401 [Calcd for $C_{30}H_{48}NaO_4$: 495.3450 (M+Na)⁺]. $[\alpha]_D^{25}$ +77.7° (c=0.15, MeOH).

Norquadrangularic Acid C (15): Colorless amorphous solid. ¹H-NMR (pyridine-d_5) δ: 5.27 (1H, td, J=11.0, 4.5 Hz, H-3), 4.03 (1H, d, J=10.5 Hz, H-31), 3.98 (1H, br s, H-1), 3.92 (1H, d, J=10.5 Hz, H-31), 3.19 (1H, dd, J=11.5, 4.5 Hz, H-5), 2.85 (1H, t, J=11.0 Hz, H-4), 2.70 (1H, ddd, J=13.5, 4.5, 3.5 Hz, H-2), 2.57 (1H, ddd, J=15.0, 8.0, 5.0 Hz, H-11), 2.28 (1H, m, H-25), 2.20 (1H, m, H-23), 2.16 (1H, ddd, J=13.5, 11.0, 3.5 Hz, H-2), 1.21 (3H, d, J=7.0 Hz, H₃-26), 1.19 (3H, d, J=7.0 Hz, H₃-27), 1.10 (3H, s, H₃-18), 0.98 (3H, s, H₃-30), 0.97 (3H, d, J=7.0 Hz, H₃-21), 0.66 (1H, d, J=4.5 Hz, H-19), 0.29 (1H, d, J=4.5 Hz, H-19). ¹³C-NMR: Table 1. IR (KBr) cm⁻¹: 3400, 1710, 1470, 1380. HR-FAB-MS m/z 529.3497 [Calcd for $C_{30}H_{50}NaO_6$: 529.3577 (M+Na)⁺]. $[\alpha]_D^{25}$ +116.9° (c=0.04, MeOH).

Reduction of Methyl Quadrangularate B (2) to Methyl Quadrangularate A (1) To a stirred solution of 2 (5.2 mg) in CH_2Cl_2 (0.5 ml) at 0 °C, a solution of Ph₃P (3.1 mg) in CH_2Cl_2 (0.5 ml) was added. After stirring for 30 min under the same condition, the mixture was directly subjected to preparative TLC (MeOH–CHCl₃, 1 : 9) to yield 1 (4.2 mg, 83%).

Acetylation of 4, 10, and 11 A solution of 4 (8.0 mg) in dry pyridine (0.3 ml) and acetic anhydride (0.3 ml) was stirred overnight at room temperature. After aqueous work-up, the reaction mixture was extracted with CHCl₃ (5 ml×3), and the CHCl₃ extract was washed with water, dried over anhydrous MgSO₄ and evaporated under reduced pressure to yield an acetate 4a (7.6 mg, 87%). By the same procedure, 11 was converted into 11a.

Methyl 3-O-Acetylquadrangularate D (4a): Colorless amorphous solid. ¹H-NMR (pyridine-d_5) δ: 4.93 (1H, dd, J=5.0, 2.5 Hz, H-3), 4.88 (1H, br s, H-28), 4.85 (1H, br s, H-28), 3.98 (1H, dd, J=11.0, 6.0 Hz, H-1), 3.96 (1H, dd, J=9.5, 6.0 Hz, H-11), 3.75 (3H, s, 28-OMe), 2.47 (1H, dd, J=11.5, 3.0 Hz, H-5), 2.34 (1H, m, H-25), 2.32 (1H, m, H-2), 2.28 (2H, m, H-2, H-12), 2.13 (1H, dd, J=10, 5.5 Hz, H-8), 2.04 (3H, s, 3-OAc), 1.82 (1H, dd, J=14.0, 6.0 Hz, H-12), 1.32 (1H, d, J=4.5 Hz, H-19), 1.18 (3H, s, H₃-29), 1.07 (3H, d, J=7.0 Hz, H₃-26), 1.06 (3H, d, J=7.0 Hz, H₃-27), 0.99 (3H, s,

H$_3$-30), 0.93 (3H, d, J=7.0Hz, H$_3$-21), 0.87 (3H, s, H$_3$-18), 0.65 (1H, d, J=4.5Hz, H-19). ^{13}C-NMR: Table 1. HR-EI-MS m/z: 540.3820 [Calcd for C$_{34}$H$_{52}$O$_5$: 540.3815 (M)$^+$].

1-O,3-O-Diacetyl-23-deoxojessic Acid (11a): Colorless amorphous solid. ^{1}H-NMR (pyridine-d_5) δ: 6.23 (1H, dd, J=12.0, 4.5Hz, H-3), 4.99 (1H, brs, H-1), 4.87 (1H, brs, H-28), 4.85 (1H, brs, H-28), 3.11 (1H, dd, J=12.0, 4.5 Hz, H-5), 2.56 (1H, ddd, J=13.5, 4.5, 3.5Hz, H-2), 2.28 (1H, m, H-25), 2.22 (1H, ddd, J=13.5, 12.0, 3.5Hz, H-2), 2.07 (3H, s, 1-OAc), 1.94 (3H, s, 3-OAc), 1.60 (3H, s, H$_3$-29), 1.08 (3H, d, J=7.0Hz, H$_3$-26), 1.07 (3H, d, J=7.0Hz, H$_3$-27), 0.98 (3H, s, H$_3$-30), 0.96 (3H, s, H$_3$-18), 0.93 (3H, d, J=6.0Hz, H$_3$-21), 0.86 (1H, d, J=4.5Hz, H-19), 0.57 (1H, d, J=4.5Hz, H-19). ^{13}C-NMR: Table 1. HR-FAB-MS m/z: 593.3779 [Calcd for C$_{35}$H$_{54}$NaO$_6$: 593.3818 (M+Na)$^+$].

Conversion of Methyl Quadrangularate N (8) to Dimethyl Quadrangularate H (26a) To a stirred solution of **5** (2.1 mg) in a mixture of CH$_3$CN (0.5 ml), aqueous NaH$_2$PO$_4$ (0.1 mg/ml, 0.5 ml) and 30% H$_2$O$_2$ (40 μl), an aqueous solution of NaClO$_2$ (0.4 mg/ml, 125 μl) was added dropwise at 10 °C, and the mixture was stirred for 2 h at 10 °C. After Na$_2$SO$_3$ (1 mg) was added, the mixture was evaporated and dissolved in MeOH and filtered. The filtrate was then treated with excess CH$_2$N$_2$, followed purification with preparative TLC, to give **26a** (0.4 mg, 17%).

Cytotoxic Assay Cellular viability in the presence and absence of experimental agents was determined using the standard 3-(4,5-dimethylthiazol-2-yl)-2,5-dimethyltetrazolium bromide (MTT) assays as described previously.[26] The cytotoxicity of isolated compounds towards murine colon 26-L5 carcinoma cells are as follows. ED$_{50}$ value (μm): **1**, 43.8; **2**, 9.5; **3**, 18.9; **4**, 5.4; **6**, 52.6; **7**, 49.7; **8**, 61.4; **9**, 58.6; **10**, 49.6; **11**, 57.7; **12**, 59.7; **13**, 17.6; **14**, 65.9; **15**, >100; **16**, 65.7; **17**, 62.4; **18**, 55.8; **19**, >100; **20**, 3.0; **21**, 1.8; **22**, 5.2; **23**, 4.5.

References and Notes
1) Pettit G. R., Singh S. B., Boyd M. R., Hamel E., Pettit R. K., Schmidt J. M., Hogan F., *J. Med. Chem.*, **38**, 1666—1672 (1995).
2) Pegel K. H., Rogers C. B., *J. Chem. Soc., Perkin Trans. 1*, **1985**, 1711—1715.
3) Rogers C. B., *Phytochemistry*, **28**, 279—281 (1989); Osborne R., Pegel K. H., *Phytochemistry*, **23**, 635—637 (1984).
4) Pettit G. R., Toki B., Herald D. L., Verdier-Pinard P., Boyd M. R., Hamel E., Pettit R. K., *J. Med. Chem.*, **41**, 1688—1695 (1998).
5) Tran K. (ed.), "Medicinal Plants in Viet Nam," WHO Regional Office for the Western Pacific Manila and Institute of Material Medica Hanoi, Science and Technology Publishing House, Hanoi, 1990, p. 119.
6) Stampoulis P., Tezuka Y., Banskota A. H., Tran K. Q., Saiki I., Kadota S., *Tetrahedron Lett.*, **40**, 4239—4242 (1999); Stampoulis P., Tezuka Y., Banskota A. H., Tran K. Q., Saiki I., Kadota S., *Org. Lett.*, **1**, 1367—1370 (1999).
7) Banskota A. H., Tezuka Y., Tran K. Q., Tanaka K., Saiki I., Kadota S., *J. Nat. Prod.*, **63**, 57—64 (2000).
8) Ohnishi Y., Sakamoto T., Fujii H., Kimura F., Murata J., Tazawa K., Fujimaki M., Sato Y., Kondo M., Une Y., Uchino J., Saiki I., *Tumor Biol.*, **18**, 113—122 (1997).
9) Ganzera M., Ellmerer-Muller E. P., Stuppner H., *Phytochemistry*, **49**, 835—838 (1998).
10) Pascal S., Taton M., Rahier A., *J. Biol. Chem.*, **268**, 11639—11654 (1993).
11) Sholichin M., Yamasaki K., Kasai R., Tanaka O., *Chem. Pharm. Bull.*, **28**, 1006—1008 (1980).
12) Rubinstein I., Goad L. J., Clague A. D. H., Mulheirn L. J., *Phytochemistry*, **15**, 195—200 (1976).
13) Herz W., Fitzhenry B., Anderson G. D., *Phytochemistry*, **12**, 1181—1182 (1973).
14) Voirin B., *Phytochemistry*, **10**, 2107—2145 (1983).
15) Wollenweber E., Karin M., *Z. Naturforsch.*, **39C**, 303—306 (1984).
16) A part of this work was reported as a communication. Banskota A. H., Tezuka Y., Phung L. K., Tran K. Q., Saiki I., Miwa Y., Taga T., Kadota S., *Bioorg. Med. Chem. Lett.*, **8**, 3519—3524 (1998).
17) Kigoshi H., Imamura Y., Mizuta K., Niwa H., Yamada K., *J. Am. Chem. Soc.*, **115**, 3056—3065 (1993).
18) Garlaschelli L., Vidari G., Virtuani M., Vita-Finzi P., Mellerio G., *J. Nat. Prod.*, **58**, 992—1002 (1995).
19) Kadota S., Li J. X., Tanaka K., Namba T., *Tetrahedron*, **51**, 1143—1166 (1995).
20) Silverstein R. M., Webster F. X., "Spectrometric Identification of Organic Compounds," 6th edition, John Wiley and Sons, Inc., New York, 1998, pp. 230—232.
21) Kitajima J., Kimizuka K., Tanaka Y., *Chem. Pharm. Bull.*, **46**, 1408—1411 (1998).
22) Dalcanale E., Montanari F., *J. Org. Chem.*, **51**, 567—569 (1986).
23) Knapp F. F., Nicholas H. J., *Phytochemistry*, **10**, 97—102 (1971).
24) Gold L. J., Hammam A. S. A., Dennis A., Goodwin T. W., *Nature* (London), **210**, 1322—1324 (1966).
25) Castle M., Blondin G., Nes W. R., *J. Am. Chem. Soc.*, **85**, 3306—3308 (1963).
26) Banskota A. H., Tezuka Y., Prasain J. K., Matsushige K., Saiki I., Kadota S., *J. Nat. Prod.*, **61**, 896—900 (1998).

April 2000

Chem. Pharm. Bull. 48(4) 505—508 (2000)

505

Structures of 4-Aryl-coumarin (Neoflavone) Dimers Isolated from *Pistacia chinensis* Bunge and Their Estrogen-like Activity

Satoshi Nishimura,[a] Motohiko Taki,[b] Sachiko Takaishi,[b] Yasuteru Iijima,[b] and Toshiyuki Akiyama*,[a]

Exploratory Chemistry Research Laboratories,[a] and Pharmacology and Molecular Biology Research Laboratories,[b]
Sankyo Co., Ltd., 2–58 Hiromachi 1-Chome, Shinagawa-ku, Tokyo 140–8710, Japan.
Received October 14, 1999; accepted December 18, 1999

Activity-guided fractionation of twigs of *Pistacia chinensis* resulted in the isolation and characterization of two novel ingredients as potent estrogen agonists. On the basis of spectral analysis and comparison with a related compound their structures were elucidated as 3,3″-dimers of 4-aryldihydrocoumarins (3,4-dihydro-4-(4′-hydroxyphenyl)-7-hydroxycoumarin) differing only in the stereochemical disposition of the linkage between the two 4-arylcoumarin moieties. These compounds are the first examples of bis-flavonoids which have been proven to possess estrogen-like activity.

Key words *Pistacia chinensis*; Anacardiaceae; phytoestrogen; neoflavone; dimer; 4-aryldihydrocoumarin

In recent years there has been increasing interest in estrogen replacement therapy, since estrogen is suggested to have beneficial effects for women in preventing heart attacks and other cardiovascular problems, osteoporosis and possibly Alzheimer's disease.[1] Higher plants are known to contain a structurally diverse array of non-steroidal constituents that represent estrogenic activities (phytoestrogens).[2] It is also becoming clear that phytoestrogens exert a variety of beneficial effects in prevention of diseases caused by estrogen deficiency.[3] Previously we reported the isolation and characterization of several phytoestrogens belonging to various structural types which include homoisoflavone,[4] prenylflavone,[5,6] diphenylpropanoid,[7] and iboga alkaloid.[8]

Forest products continue to be a rich source of phytochemical diversity and are, therefore, important sources of new drugs as exemplified by the anticancer agents paclitaxel and camptothecin.[9] Tracts of forest still cover a considerable portion of Japan and a recent environmental profile estimated that approximately 60 percent of the country could be classified as forestland. We have embarked on a program to discover potential therapeutic agents from forest plant species. Plant collections were conducted in forests in Japan as well as several botanical gardens and a total of 221 plants representing 71 families have been collected, extracted and screened.

The MeOH extract of the twigs of *Pistacia chinensis* Bunge was found to have noteworthy inhibitory activity against [³H]estradiol binding to estrogen receptors. *P. chinensis* is a tree belonging to the Anacardiaceae family, and is indigenous to southern China and cultivated in gardens in Japan. *P. chinensis* has not been extensively investigated in the past, and studies of phenolic compounds and terpenes from its leaves[10] are the only publication in recent years. In this paper we wish to report on an activity-guided isolation and the structure determination of two novel dimeric 4-arylcoumarines (neoflavones) in addition to their estrogen-like activity.

Results and Discussion

Approximately 800 g of fresh twigs of *P. chinensis* were chopped into small pieces and an extract was prepared using MeOH. The extract was then partitioned between H_2O and

EtOAc. Activity was concentrated in the organic fraction. This fraction was further separated by silica gel and reversed-phase column chromatography to afford two active ingredients, **1a** and **2**, in good yield.

Compound **1a** was obtained as a colorless, optically active solid ($[\alpha]_D = +237°$). The FAB-MS of **1a** gave a *pseudo*-molecular ion at *m/z* 511 $(M+H)^+$ corresponding to the molecular formula of $C_{30}H_{22}O_8$, which was confirmed by high resolution (HR) FAB-MS [Calcd 511.1393, Found *m/z* 511.1358 $(M+H)^+$]. The UV spectrum showed an absorption maximum at 278 nm and the IR spectrum displayed absorption bands for hydroxyl $(3384\,cm^{-1})$ and lactone $(1752\,cm^{-1})$ groups. The NMR spectra of **1a** indicated a dimeric structure with an asymmetrical coupling of molecules comprised of $C_{15}H_{11}O_4$, since doubling up of signals from the two moieties was clearly observed in its ^1H and ^{13}C resonances (Table 1). The spectral data of **1a** was very similar to those of diphysin $(C_{30}H_{22}O_{10}$, 3-3″-dimer of 3,4-dihydro-4-(4′-hydoxyphenyl)-5,7-dihydroxycoumarin) (3),[11] indicating **1a** to be a 3-3″-dimeric 4-phenyldihydrocoumarin, with two notable differences. A total of 15 carbon signals were observed for **3** in the ^{13}C-NMR spectrum, while 30 signals were clearly distinguished for **1a**. Another major difference was observed in the ^1H resonance in which a pair of AMX coupling systems with signals at δ 6.97 (2H, m (overlapped)), 6.50 (1H, dd, *J*=9.8, 2.4 Hz) and 6.60 (1H, dd, *J*=8.3, 2.4 Hz), and 6.49 (1H, br s) and 6.55 (1H, d, *J*=2.4 Hz) was present. These results suggest that **1a** differs from **3** by lacking hydroxy groups at C-5 and C-5″ positions.

Confirmation of the proposed structure of 4-aryldihydrocoumarin for **1a** was provided by a heteronuclear multiple bond connectivity (HMBC) experiment in which the proton at C-4 (δ 3.97) was found to couple to a carbonyl carbon at C-2 (δ 169.5) in addition to aromatic doublet carbons at C-5 (δ 129.5) and C-2′ (δ 130.6). The connection between the dihydrocoumarin moieties was also supported by long-range correlation of an H-3 proton (δ 2.99) to a C-2″ carbon (δ 168.5). The proof of the relative stereochemistry was given by the coupling constants observed in the ^1H-NMR spectrum of **1a**. The double doublet at δ 2.99 (H-3) had a coupling constant of 5.3 Hz to the signal at δ 3.97 (H-4), supporting a *cis-gauche* relationship, while the coupling constant of 2.2

Table 1. ^{1}H- and ^{13}C-NMR Data for 1a, 1b and 2

Carbon	1a[a]		1b[b]		2[c]	
	δ_C	δ_H (mult. J(Hz))	δ_C	δ_H (mult. J(Hz))	δ_C	δ_H (mult. J(Hz))
2	169.5		166.8		171.1	
3	46.0	2.99 (dd, 10.9, 5.3)	43.8	3.13 (dd, 11.6, 5.2)	44.5	3.09 (d, 3.4)
4	45.3	3.97 (d, 5.3)	44.4	4.14 (d, 5.2)	43.2	4.41 (d, 3.4)
4a	120.2		124.5		119.7	
5	129.5	6.97[d]	128.8	7.11 (d, 8.4)	129.7	7.00 (d, 7.1)
6	113.2	6.50 (dd, 9.8, 2.4)[d]	118.4	6.82 (dd, 8.4, 2.3)	113.1	6.51 (dd, 7.1, 2.4)[d]
7	159.2		150.9		159.4	
8	104.5	6.49 (br s)[d]	111.0	6.89 (d, 2.3)	104.6	6.52 (br s)[d]
8a	152.5		150.7		152.8	
1'	130.3		133.9		130.9	
2', 6'	130.6	7.01 (d, 8.5)	129.7	7.27 (d, 8.6)	129.7	7.12 (d, 8.7)
3', 5'	116.7[d]	6.66[d]	122.2	7.03 (d, 8.6)	117.0	6.72 (d, 8.7)
4'	158.0		150.5		158.3	
2"	168.5		165.6			
3"	49.6	3.20 (dd, 10.9, 2.2)	47.1	3.32 (dd, 11.6, 1.6)		
4"	44.8	4.73 (d, 2.2)	43.7	5.03 (br s)		
4a"	114.8		119.2			
5"	131.8	6.97[d]	130.7	7.16 (d, 8.3)		
6"	113.7	6.60 (dd, 8.3, 2.4)	118.8	6.93 (dd, 8.3, 2.3)		
7"	159.7		151.3			
8"	104.3	6.55 (d, 2.4)	110.6	6.97 (d, 2.3)		
8a"	153.4		151.3			
1‴	133.3		137.5			
2‴, 6‴	129.2	6.82 (d, 8.5)	128.3	7.06 (d, 8.6)		
3‴, 5‴	116.6[d]	6.66[d]	122.3	6.98 (d, 8.6)		
4‴	157.7		150.1			
C̲H₃CO			21.0	2.25		
			3×21.1	2.26		
				2.28		
				2.30		
CH₃C̲O			168.8			
			169.0			
			169.1			
			169.2			

a) In acetone-d_6. b) In CDCl₃. c) In CD₃OD. d) Overlapping.

Hz between H-3" (δ 3.20) and H-4" (δ 4.73) indicated a *syn-periplanar* arrangement. A larger coupling constant (10.9 Hz) suggested a *trans-diaxial* relationship between H-3 and H-3". To establish the relative stereochemistry of the molecule, gradient enhanced nuclear Overhauser effect (NOE) spectroscopy (GOESY)[12] was applied. Although many of the proton signals representing the two "halves" of 1a were nearly overlapping, its acetate 1b gave a well-resolved ^{1}H-NMR spectrum using CDCl₃. It was shown that irradiation of H-3" resulted in NOEs of H-4" and H-4. NOEs were also measured between H-3" and phenolic protons arising from H-2' (H-6') (δ 7.27) in addition to H-2‴ (H-6‴) (δ 7.06), indicating the spatial vicinity of these protons as depicted in Fig. 1. Consequently, 1a is thus represented by the relative stereostructure illustrated in Chart 1.

Compound 2 was also isolated as a colorless, optically active solid ($[\alpha]_D = +267°$) and had a FAB-MS [m/z 511 $(M+H)^+$] similar to that of compound 1a, indicating that it was an isomer of 1a. The presence of only 15 resonances in the ^{13}C-NMR spectrum of 2 indicated that the two components were equivalent. Compounds 1a and 2 showed nearly identical chemical shifts and coupling constants. These results clearly indicated that 2 was a symmetrical 3,3"-dimer of 3,4-dihydro-4-(4'-hydroxyphenyl)-7-dihydroxycoumarin.

Compounds 1a and 2 were then evaluated for their estro-
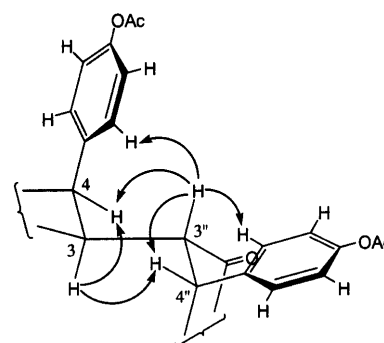
Fig. 1. Important NOE Difference Observed in GOESY NMR Spectrum of 1b

genic activity. The primary *in vitro* assay measured their ability to compete with [^{3}H]estradiol for binding to the bovine uterine estrogen receptor by the method described earlier[4] using genistein as the reference standard for comparison. The apparent IC$_{50}$ value of 1a was 50 nM which was approximately 7 times greater than genistein, while 500 nM was observed for 2. Compound 1a was next tested for its ability to stimulate the growth of estrogen-dependent T47D cells in culture to examine if it functioned as an estrogen receptor agonist or antagonist using the procedures described in our previous paper.[7] Compound 1a stimulated the cell proliferation

1a R=H
1b R=Ac

2
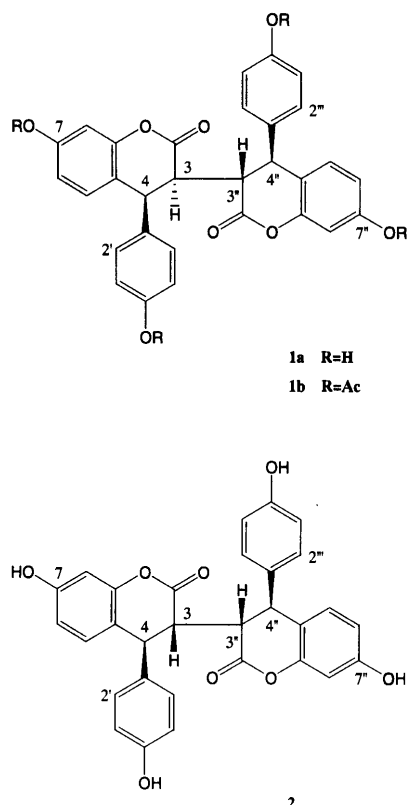
Chart 1
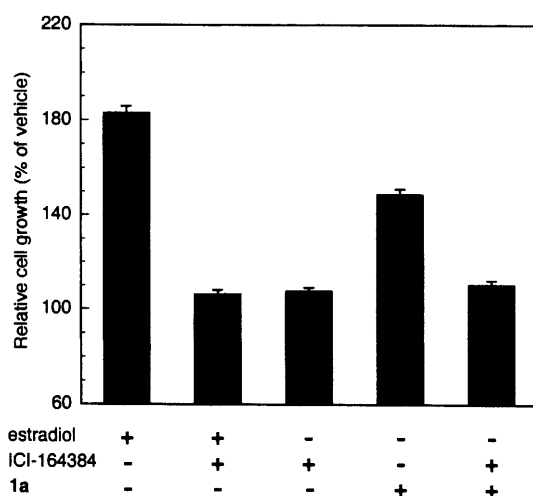
Fig. 2. The Effect of ICI-164384 on the Ability of **1a** to Stimulate the Growth of T47D Cells

Cells were grown in the presence (+) or absence (−) of 100 pM of estradiol, 1 μM of ICI-164384 or 10 μM of **1a**. Columns are mean values, and vertical bars represent standard errors of the mean (*n*=8).

in a concentration dependent manner and induced T47D proliferation to the same extent as estradiol, indicating that the compound was an estrogen agonist. The EC_{50} values (concentration of a compound required to increase the cell number to 50 percent of plateau level) were 800 nM for **1a** and 4 pM for estradiol. It has been shown that estrogen antagonists can inhibit estrogen agonist responses by forming complexes with high affinity to the estrogen receptor. We therefore examined the effect of the pure/complete estrogen antagonist ICI-164384 on the T47D cell proliferation induced by **1a**. As shown in Fig. 2, the stimulatory effect on the cell growth of estradiol and **1a** was clearly blocked by cotreatment with

ICI-164384 in a similar manner. These results indicate that compound **1a** possesses estrogen agonist activity, although exact comparison with other phytoestrogens is somewhat hampered by the fact that the results derive from experiments with different values for the estradiol standard. This compound, however, is the first example of a bis-flavonoid which has been proven to be an estrogen agonist.

Recently the existence of two subtypes of estrogen receptor (ERα, ERβ) was discovered[13] and several phytoestrogens were reported to have higher affinity for ERβ.[14] The results presented here were obtained using bovine uterine extracts which involve mixtures of ERα and ERβ. Additional studies using these respective subtypes are critical to understanding the structure–activity relationship among various types of estrogen receptor ligands. In conclusion, we have now identified a bis-4-arylcoumarine (neoflavone) as a new type of phytoestrogen.

Experimental

Extraction and Isolation Fresh twigs (800 g) of *Pistacia chinensis* collected from Tama Forest Science Garden of the Forestry and Forest Products Research Institute were chopped into small pieces, and an extract was prepared using MeOH at 60 °C for 2 h. The extract was filtered and concentrated to dryness *in vacuo*. The residue was partitioned between EtOAc and H_2O to give a bioactive EtOAc fraction. The fraction (13.4 g) was subjected to column chromatography on silica gel with elution by $CHCl_3$–MeOH (90 : 10) to give three fractions after combination of similar fractions as judged by TLC. A biologically active fraction (2.81 g) was separated by flash chromatography on silica gel with (toluene–EtOAc–MeOH, 60 : 35 : 5). Compounds **1a** and **2** were obtained and each compound was further purified by RP18 silica gel column chromatography (MeOH–H_2O, 60 : 40) to give **1a** (920 mg) and **2** (33 mg).

Compound **1a**: Colorless powder, $[\alpha]_D = +237°$ (c=0.1, MeOH). IR (KBr tablet) cm^{-1}: 3384, 1752. UV λ_{max} (EtOH) nm (ε): 278 (6600). HR-FAB-MS *m/z*: 511.1358 (M+H)$^+$: Calcd for $C_{30}H_{23}O_8$: 511.1363. The analysis of its NMR data including distortionless enhancement by polarization transfer (DEPT), heteronuclear multiple quantum coherence (HMQC), HMBC, and NOE spectra allowed for unambiguous assignment of all proton and carbon signals (Table 1).

Compound **2**: Colorless powder, $[\alpha]_D = +267°$ (c=0.1, MeOH). IR (KBr tablet) cm^{-1}: 1752. UV λ_{max} (EtOH) nm (ε): 278 (7100). FAB-MS: 511 (M+H)$^+$, $C_{30}H_{23}O_8$. The analysis of its NMR data including DEPT, HMQC, HMBC, and NOE spectra allowed for an unambiguous assignment of all proton and carbon signals (Table 1).

Acetylation of 1a Compound **1a** was acetylated by acetic anhydride/pyridine by the usual method to give tetraacetate **1b** as a colorless powder. FAB-MS: 679 (M+H)$^+$, $C_{38}H_{31}O_{12}$. IR (KBr tablet) cm^{-1}: 1766.

Estradiol Receptor Binding Assay The competitive binding assay to measure the affinity for the estrogen receptor follows the method described previously.[4]

Effect on T47D Cell Proliferation Full details of the experimental method used for the cell culture and determination of cell number using the 3-(4,5-dimethyl-2-thiazolyl)-2,5-diphenyl-2*H*-tetrazolium bromide (MTT) method have been published.[7]

References

1) Ettinger B., *Proc. Soc. Exp. Biol. Med.*, **217**, 2—4 (1998).
2) Farnsworth N. R., Bingel A. S., Cordell G. A., Crane F. A., Fong H. H. S., *J. Pharm. Sci.*, **64**, 717—754 (1975).
3) Sheehan D. M., *Proc. Soc. Exp. Biol. Med.*, **217**, 379—385 (1998).
4) Ichikawa K., Kitaoka M., Taki M., Takaishi S., Iijima Y., Boriboon M., Akiyama T., *Planta Med.*, **63**, 540—543 (1997).
5) Kitaoka M., Kadokawa H., Sugano M., Ichikawa K., Taki M., Takaishi

S., Iijima Y., Tsutsumi S., Boriboon M., Akiyama T., *Planta Med.*, **64**, 511—515 (1998).

6) Miyamoto M., Matsushita Y., Kiyokawa A., Fukuda C., Iijima Y., Sugano M., Akiyama T., *Planta Med.*, **64**, 516—519 (1998).

7) Minami E., Taki M., Takaishi S., Iijima Y., Tsutsumi S., Akiyama T., *Chem. Pharm. Bull.*, 389—392 (2000).

8) Masuda K., Akiyama T., Taki M., Takaishi S., Iijima Y., Yamazaki M., Aimi N., Jato J., Waterman P. W., *Planta Med.*, in press.

9) Shu Y.-Z., *J. Nat. Prod.*, **61**, 1053—1071 (1998).

10) De Pooter H. I., Schamp N. M., Aboutabl E. A., El Tohamy S. F., Doss S. L., *Flavour Fragrance J.*, **6**, 229—232 (1991).

11) Stermitz F. R., Mead E. W., Foderaro T. A., Castro O., *Phytochemisrty*, **34**, 287—289 (1993).

12) Stott K., Stonehouse J., Keeler J., Hwang T.-L., Shaka A. J., *J. Am. Chem. Soc.*, **117**, 4199—4200 (1995).

13) Kuiper G. G. J. M., Enmark E., Pelto-Huikko M., Nilsson S., Gustafsson J.-A., *Proc. Natl. Acad. Sci. U.S.A.*, **93**, 5925—5930 (1996).

14) *a*) Kuiper G. G. J. M., Carlsson B., Grandien K., Enmark E., Haggblad J., Nilsson S., Gustafsson J.-A., *Endocrinology*, **138**, 863—870 (1997); *b*) Kuiper G. G. J. M., Lemmen J. G., Carlsson B., Corton J. C., Safe S. H., van der Saag P. T., van der Burg B., Gustafsson J.-A., *ibid.*, **139**, 4252—4263 (1998).

4-Sulfenyl-2-carbamoyl-4-isoxazolin-3-ones: Biological Isostere to 4-Chloro-2-carbamoyl-4-isoxazolin-3-ones

Noriaki Kudo,* Takamitsu Yoneda, Kazuo Sato, Toyokuni Honma, and Soji Sugai

Agroscience Research Laboratories, Sankyo Co., Ltd., 1041 Yasu, Yasu-cho, Shiga 520–2342, Japan.

4-Sulfenyl-2-carbamoyl-4-isoxazolin-3-ones (4) were designed on the basis of biological isosterism and prepared in four steps. Some of these compounds showed sufficient pre-emergent herbicidal activities against various kinds of weeds. Among the synthesized compounds, 2-(N-(4-chlorophenyl)-N-isopropylcarbamoyl)-4-ethylthio-5-methyl-4-isoxazolin-3-one (4cd) exhibited the most promising activity.

The introduction of a sulfur atom into compounds sometimes plays an important role in drugs and agrochemicals. In some aspects the chemical reactivity and property of sulfide resemble those of ether, but in other aspects they are very different.[1] The sulfur atom potentially has the ability to undergo oxidation to the corresponding sulfoxide and sulfone. According to this property a sulfur atom acts distinctively. Metcalf reported that alkylthio-substituents in sulfur-containing cholinesterase inhibitors can be oxidized *in vivo* to the corresponding sulfoxide and sulfone to delay their endometatoxic systemic properties.[2] The introduction of the alkylthio group in place of the chlorine atom sometimes brings about drastic changes in biological properties.[3] The chlorine atom of *s*-triazine herbicide 1, so-called simazine,[4] had herbicidal activity but inflicted serious damage on transplanted rice. On the other hand, simetryne,[5] a compound 2 in which the chlorine atom was replaced with the methylthio group showed improved herbicidal activity and reduced rice injury (Chart 1). In simetryne, the methylthio group plays a biologically isosteric role, equal to that of a chlorine atom. This result indicates that the introduction of the alkylthio group instead of a chlorine atom on heterocyclic rings might increase herbicidal activity and decrease rice injury. The synthesis and herbicidal activities of 2-carbamoyl-4-chloro-4-isoxazolin-3-ones (3) have been reported.[6] These compounds showed effective herbicidal activity against harmful grass weed species such as barnyardgrass (*Echinochloa oryzicola* VASING), but they inflicted undesirable damage on transplanted rice. Thus, the discovery of the bioisosteric transformation[3] prompted us to synthesize 4-alkylthio-4-isoxazolin-3-one derivatives (4), in an effort to enhance the herbicidal activity and reduce undesired damage to rice (Chart 2). In this paper, we report synthesis of 4-alkylthio-2-carbamoyl-4-isoxazolin-3-ones and the herbicidal activity of these compounds in a paddy field.

The easiest way to synthesize the desired 4-alkylthio-2-carbamoyl-4-isoxazolin-3-ones was direct conversion of chlorine atom in 2-carbamoyl-4-chloro-4-isoxazolin-3-ones by alkanethiol. But it seemed that the substitution of chlorine atom attached to sp^2-carbon of α-position of carbonyl group by alkanethiol hardly proceeded. Therefore, to synthesize the target compounds securely, incorporation of alkylthio group prior to forming isoxazoline ring was considered. According to the retro synthetic analysis, it was speculated that 4-alkylthio-2-carbamoyl-4-isoxazolin-3-ones could be selectively synthesized by carbamoylation of 4-alkylthio-3-hy-

droxyisoxazoles (5) at the nitrogen atom, and that 5 could be prepared through the regio-selective condensation of 2-alkylthio-β-ketoesters (6) and hydoxylamine (Chart 2).

A number of synthetic reactions of 2-alkylthio-β-ketoesters have been reported (Chart 3). Kay *et al.* reported that the introduction of methanesulfenyl group into 7 and subsequent reduction with zinc dust gave ethyl 2-methylthioacetoacetate (6a) (Eq. 1).[7] Sasaki *et al.* reported the single step conversion of 2-chloroacetoacetate (7') to 2-arylthioacetoacetate (6p) by treatment with arenethiol and triethylamine (Eq. 2).[8] Held *et al.* described the direct sulfenylation of β-ketoesters using benzenesulfenyl chloride (Eq. 3).[9] However, among the synthetic methods illustrated in Chart 3 (Eqs. 1— 3), only a limited variety of β-ketoesters were available as starting materials, and the yields were low. Moreover, the pursuit of Kay's method did not proceed in good yield nor offer adequate generality for our purposes.[10] Clearly, a more efficient and general synthetic method for 6 was required for the preparation of various kinds of derivatives. From another viewpoint, Malleron *et al.* reported the synthesis of 6r by deprotonation of ethyl 2-phenylthioacetate (10) followed by the
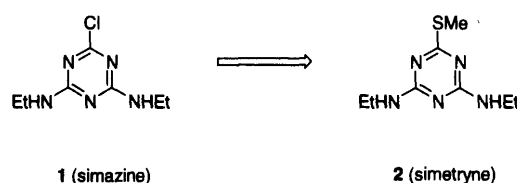
Chart 1
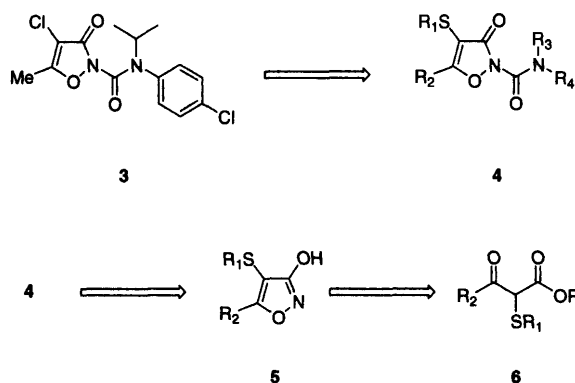
Chart 2

* To whom correspondence should be addressed.
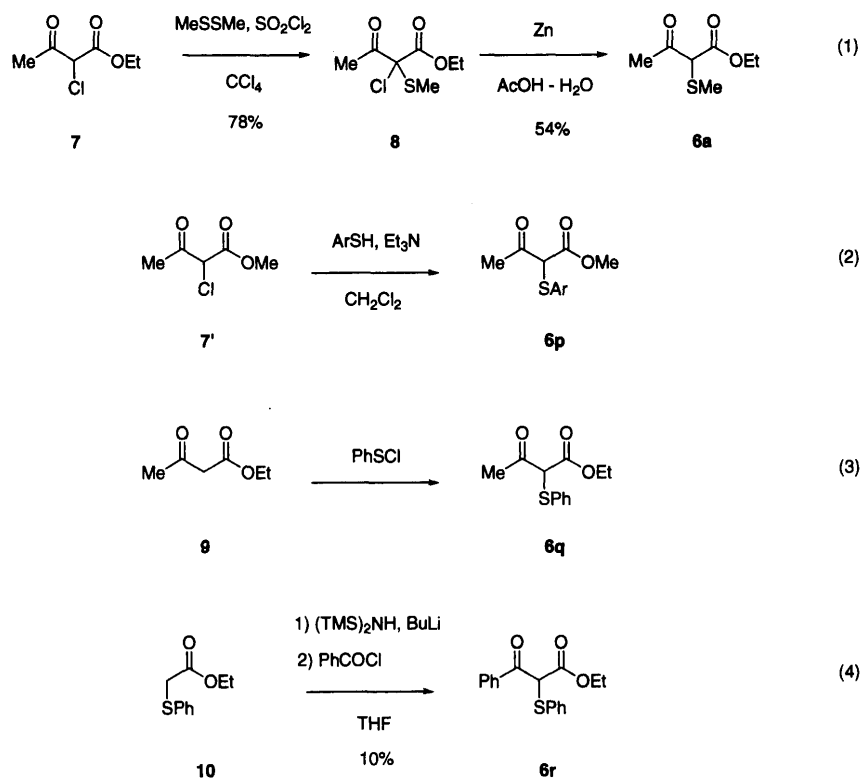
Chart 3
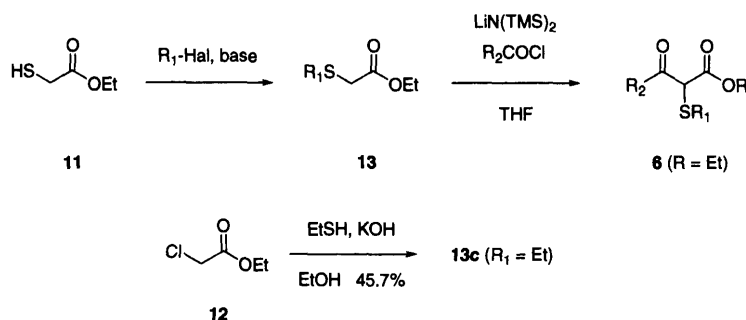
Chart 4

addition of benzoyl chloride.[11] However, the benzoylation in this report was only exemplified and the yield of the product was a mere 10% (Eq. 4).[11] Given the wide range of acylating reagents that can be obtained commercially, and the easy accessibility of the starting materials, 2-alkylthioacetates (13), from thioglycolates (11) or 2-chloroacetates (12), we independently explored a similar preparation reaction of 6. As a result, deprotonation of 2-alkylthioacetates (13) with lithium bis(trimethylsilyl)amide (LiN(TMS)₂)[12] and subsequent treatment with acyl chlorides proved to be the best way to prepare 6. Consequently, a variety of 6 could be prepared in good yields using this method. Details of these results are summarized in Table 1.

A number of synthetic reactions of 3-hydroxyisoxazole from β-ketoesters and hydroxylamine have been reported, but there is always a problem that the cyclization reaction affords a mixture of two regio-isomers. One promising procedure for regioselective preparation of 3-hydoxyisoxazoles was ketalization of β-ketoesters followed by the reaction of hydroxylamine and subsequent acid-hydrolysis.[13] However, when this method was used for the preparation of 4-alkylthio-3-hydoxyisoxazoles, the initial step to ketalize the 2-substituted β-ketoesters generally did not proceed smoothly.[9] In our previous paper we reported that the desired 4-alkylthio-3-hydroxyisoxazoles (5) were produced in good yields by treating 2-alkylthio-β-ketoesters (6) with hydroxylamine in an alkaline solution at a temperature under −10 °C without ketalization, immediately quenching the reaction mixture with concentrated HCl, and quickly heating at 80 °C.[10] Using this method, compounds 5 shown in Table 2 could be obtained without the appearance of regio-isomers. Condensation of difluoromethylthio substituted compound (6l) and hydroxylamine did not proceed under these conditions. Therefore, by simple treatment of the compound 6l with trimethylorthoformate, the ketal 14l was obtained and subsequent addition of hydroxylamine afforded hydroxamic acid, followed by the cyclization with hydrochloric acid to afford the desired 5l in 45.0% yield efficiently (Chart 5).

3-Hydroxyisoxazoles (5) have two positions to be acylated. The reaction of 3-hydroxyisoxazoles with N,N-dialkyl-carbamoyl chloride gave O-carbamoyled product, while the reaction with alkyl isocyanate gave N-carbamoyled product

Table 1
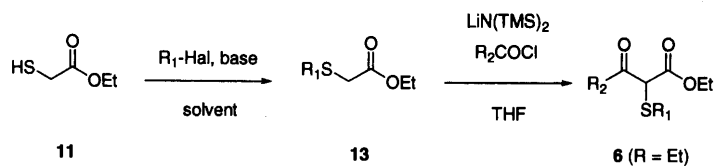
	R₁-Hal	R₁	Base/solvent	13 yield (%)	R₂	6 yield (%)
a	a)	Me			Me	74.2
b		Me			Et	81.2
c	EtI	Et	NaOEt/EtOH	70.4	Me	70.3
d		Et			Et	96.3
e		Et			n-Pr	65.3
f		Et			iso-Pr	64.0
g		Et			tert-Bu	93.4
h	n-PrI	n-Pr	NaOEt/EtOH	59.3	Me	68.6
i	iso-PrI	iso-Pr	NaOEt/EtOH	83.2	Me	76.4
j		iso-Pr			Et	57.2
k	n-BuI	n-Bu	NaH/THF	78.1	Me	61.9
l	CHF₂Cl	CHF₂	NaOEt/EtOH	77.9	Me	48.8
m	MeOCH₂CH₂Cl	MeOCH₂CH₂	NaH/THF	49.6	Me	57.2
n	HC≡CCH₂Br	HC≡CCH₂	NaH/THF	37.8	Me	31.2
o	2,4-Cl₂C₆H₃CH₂Cl	2,4-Cl₂C₆H₃CH₂	NaOEt/EtOH	76.2	Me	36.0

a) Compound 13a (R₁=Me) was commercially available.

Table 2
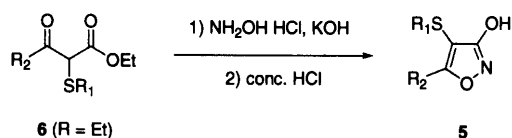
5	R₁	R₂	Yield (%)
a	Me	Me	54.7
c	Et	Me	32.3
d	Et	Et	57.6
e	Et	n-Pr	72.0
f	Et	iso-Pr	32.3
g	Et	tert-Bu	71.0
h	n-Pr	Me	51.3
i	iso-Pr	Me	66.2
j	iso-Pr	Et	51.4
k	n-Bu	Me	35.4
m	MeOCH₂CH₂	Me	41.6
n	HC≡CCH₂	Me	32.6
o	2,4-Cl₂C₆H₃CH₂	Me	22.6
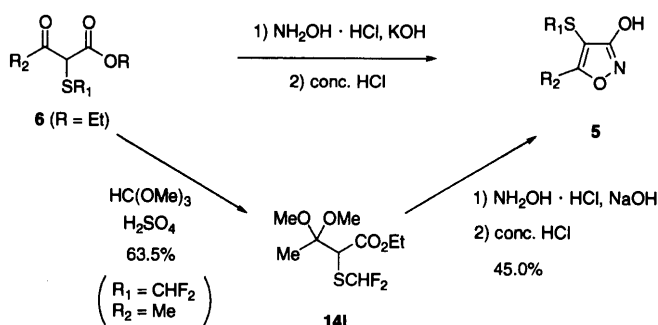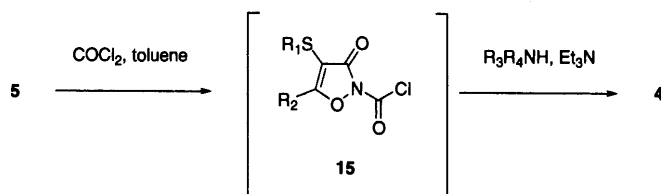
Chart 6

Table 3
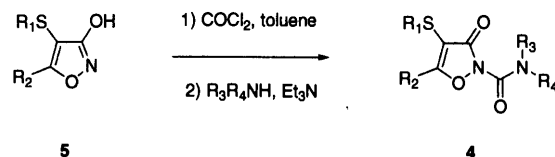
4	R₁	R₂	R₃	R₄	Yield (%)
ad	Me	Me	iso-Pr	4-ClC₆H₄	53.5
ca	Et	Me	Me	4-ClC₆H₄	65.9
cb	Et	Me	Et	4-ClC₆H₄	65.9
cc	Et	Me	n-Pr	4-ClC₆H₄	65.4
cd	Et	Me	iso-Pr	4-ClC₆H₄	58.6
ce	Et	Me	iso-Pr	4-FC₆H₄	63.1
cg	Et	Me	iso-Pr	4-MeC₆H₄	74.7
ch	Et	Me	iso-Pr	2,4-Cl₂C₆H₃	63.2
ci	Et	Me	iso-Pr	4-CNC₆H₄	15.4
cj	Et	Me	iso-Pr	3-NO₂C₆H₄	62.1
ck	Et	Me	iso-Pr	3-CF₃C₆H₄	63.7
dd	Et	Et	iso-Pr	4-ClC₆H₄	60.1
ed	Et	n-Pr	iso-Pr	4-ClC₆H₄	15.1
fd	Et	iso-Pr	iso-Pr	4-ClC₆H₄	62.8
gd	Et	tert-Bu	iso-Pr	4-ClC₆H₄	5.5
hd	n-Pr	Me	iso-Pr	4-ClC₆H₄	63.9
hf	n-Pr	Me	iso-Pr	2,4-F₂C₆H₃	66.7
id	iso-Pr	Me	iso-Pr	4-ClC₆H₄	50.1
jd	iso-Pr	Et	iso-Pr	4-ClC₆H₄	48.1
ld	CF₂H	Me	iso-Pr	4-ClC₆H₄	88.3
md	MeOCH₂CH₂	Me	iso-Pr	4-ClC₆H₄	52.3
nd	HC≡CCH₂	Me	iso-Pr	4-ClC₆H₄	57.2
od	2,4-Cl₂C₆H₄CH₂	Me	iso-Pr	4-ClC₆H₄	62.6

Chart 5

as reported earlier.[14] The latter reaction enabled us to pro-
duce N-carbamoyled compounds selectively, but this reaction
could not be applied to N,N-dialkyl carbamoyled product.
After some attempts were made to synthesize the N,N-dialkyl

Table 4. Spectral Data for Compounds **6**, **5**, and **4**

Compound No.	^{1}H-NMR	IR	MS
6d	4.42—4.01 (3H, m), 2.95—2.37 (4H, m), 1.45—0.98 (9H, m)	2980, 1735, 1705, 1580, 1230, 1025	204 (M$^+$), 158, 148, 102, 57 (base)
6e	4.42—4.02 (2H, m), 2.83—2.36 (4H, m), 1.82—0.81 (9H, m)	2970, 2940, 1710, 1580, 1235, 1220	218 (M$^+$), 148 (base), 120, 102, 71
6f	4.49—4.08 (2H, m), 3.29—2.40 (3H, m), 1.48—1.09 (6H, m), 1.15 (6H, d, J=7.2 Hz)	2980, 2950, 1740, 1710, 1580, 1240, 1150, 1225	218 (M$^+$), 172, 148, 102, 71 (base), 43
6g	4.19 (2H, q, J=7.1 Hz), 1.93—1.50 (2H, m), 1.26 (3H, t, J=7.1Hz), 1.24 (9H, s)	2970, 2930, 1735, 1700, 1240, 1140, 1030	232 (M$^+$), 148, 120, 102, 85, 57 (base), 43
6j	4.26 (2H, q, J=7.4 Hz), 3.21—2.55 (3H, m), 1.47—0.99 (12H, m)	2970, 2860, 1710, 1570, 1230, 1025	218 (M$^+$), 172, 162, 130, 102, 57 (base)
6l	6.55 (1H, t, J=57.0 Hz), 4.27 (2H, q, J=7.1 Hz), 2.36 (3H, s), 1.33 (3H, t, J= 7.1Hz)	3000, 1590, 1240, 1050	212 (M$^+$), 166, 124 (base), 87
6m	4.43—4.07 (2H, m), 3.67—3.32 (2H, m), 3.32 (3H, s), 2.89—2.59 (2H, m), 2.34 (3H, s), 1.47—1.17 (3H, m)	3000, 2940, 1720, 1590, 1245	220 (M$^+$), 178, 174, 146, 144, 59 (base)
6n	4.28 (2H, q, J=7.1 Hz), 3.27 (2H, d, J=2.6Hz), 2.40 (3H, s), 2.17 (1H, t, J= 2.6Hz), 1.37 (3H, t, J=7.1 Hz)	3300, 3000, 2110, 1715, 1590, 1240	200 (M$^+$), 158, 119, 91, 44 (base), 40
6o	7.36—7.02 (3H, m), 4.23 (2H, q, J=7.3 Hz), 3.77 (2H, s), 1.92 (3H, s), 1.34 (3H, t, J=7.3 Hz)	2980, 2930, 1710, 1580, 1240	320 (M$^+$), 159 (base), 87
5d	8.43 (1H, s), 2.95 (2H, q, J=7.0 Hz), 2.87 (2H, q, J=7.0 Hz), 1.45 (3H, t, J=7.0 Hz), 1.39 (3H, t, J=7.0 Hz)	2970, 2925, 1600	172 (M$^+$−1), 158, 102 (base), 57
5e	8.60—8.10 (1H, br s), 2.68 (2H, q, J=7.0 Hz), 2.58 (2H, t, J=7.0 Hz), 1.93—1.40 (2H, m), 1.20 (3H, t, J=7.0 Hz), 0.95 (3H, t, J=7.0 Hz)	2960, 2930, 1600	187 (M$^+$), 149, 102, 71 (base)
5f	8.97 (1H, br s), 3.18 (1H, septet, J=7.0 Hz), 2.88—2.44 (2H, m), 1.32 (2H, d, J=7.0 Hz), 1.22 (3H, t, J=7.8 Hz)	2980, 2940, 1675, 1595	187 (M$^+$), 149, 102, 71 (base)
5g	8.95 (1H, br s), 2.96—2.55 (2H, m), 1.45 (9H, s), 1.24 (3H, t, J=7.2 Hz)	2950, 2920, 1675, 1580	201 (M$^+$), 186, 142, 116, 84, 57 (base)
5j	10.45 (1H, s), 2.99 (1H, septet, J=7.0 Hz), 2.77 (2H, q, J=7.0 Hz), 1.27 (3H, t, J=7.0 Hz), 1.24 (6H, d, J=7.0 Hz)	3000, 2950, 1610	187 (M$^+$), 145, 130, 102, 89, 57 (base)
5l	9.49 (1H, s), 6.70 (1H, t, J=57.2 Hz), 2.47 (3H, s)	2940, 1720, 1610	181 (M$^+$), 158, 149, 71, 40 (base)
5m	8.36 (1H, s), 3.51 (2H, t, J=6.1 Hz), 3.36 (3H, s), 2.80 (2H, t, J=6.1 Hz), 2.37 (3H, s)	3000, 2940, 1610	189 (M$^+$), 163, 129, 73, 59, 44, 40 (base)
5n	8.69 (1H, s), 3.35 (2H, d, J=2.5 Hz), 2.45 (3H, s), 2.16 (1H, t, J=2.5 Hz)	3320, 1610	169 (M$^+$), 152, 126, 40 (base)
5o	9.04 (1H, s), 6.81—7.35 (3H, m), 3.88 (2H, s), 1.92 (3H, s)	2930, 1610	289 (M$^+$), 174, 159 (base), 149, 123
4ad	7.31 (4H, m), 4.65 (1H, septet, J=7.0 Hz), 2.36 (3H, s), 2.22 (3H, s), 1.24 (6H, d, J=7.0 Hz)	1710, 1615	340 (M$^+$), 293, 237, 196 (base), 154
4ca	7.23 (4H, s), 3.41 (3H, s), 2.62 (2H, q, J=7.1 Hz), 2.35 (3H, s), 1.12 (3H, t, J=6.9Hz)	1710, 1615, 1490, 1320, 905	326 (M$^+$), 284, 211, 168, 140 (base), 111, 83
4cb	7.21 (4H, s), 3.78 (2H, q, J=6.9 Hz), 2.58 (2H, q, J=6.9 Hz), 2.30 (3H, s), 1.19 (3H, t, J=6.9 Hz), 1.10 (3H, t, J=6.9 Hz)	1715, 1620, 1490, 1380, 1280, 910	340 (M$^+$), 182 (base), 154, 40
4cc	7.19 (4H, s), 3.70 (2H, t, J=7.6 Hz), 2.59 (2H, q, J=7.6 Hz), 2.30 (3H, s), 1.67 (2H, sextet, J=7.6 Hz), 1.10 (3H, t, J=7.6 Hz), 0.90 (3H, t, J=7.6 Hz)	1700, 1620	354 (M$^+$), 239, 196, 169, 140 (base), 111, 70
4cd	7.19—7.33 (4H, m), 4.63 (1H, septet, J=7.0 Hz), 2.62 (2H, q, J=7.6 Hz), 2.32 (3H, s), 1.22 (6H, d, J=7.0 Hz), 1.13 (3H, t, J=7.6 Hz)	1715, 1620	354 (M$^+$), 196, 169, 154, 42 (base)
4ce	7.34—6.80 (4H, m), 4.59 (1H, septet, J=6.6 Hz), 2.61 (2H, q, J=7.1 Hz), 2.29 (3H, s), 1.20 (6H, d, J=6.6 Hz), 1.01 (3H, t, J=7.1 Hz)	1710, 1620, 1505, 1310, 910	338 (M$^+$), 180, 138, 57, 41 (base)
4cg	7.06 (4H, s), 4.57 (1H, septet, J=6.8 Hz), 2.61 (2H, q, J=7.2 Hz), 2.31 (3H, s), 2.25 (3H, s), 1.20 (6H, d, J=6.8 Hz), 1.11 (3H, t, J=7.2 Hz)	1705, 1615, 1310, 905	334 (M$^+$), 219, 176, 134 (base), 91, 41
4ch	7.53—7.09 (3H, m), 4.62 (1H, septet, J=6.9 Hz), 2.60 (2H, q, J=7.2 Hz), 2.33 (3H, s), 1.17 (6H, d, J=7.2 Hz), 1.11 (3H, t, J=7.2 Hz)	1700, 1610, 1460, 1375	388 (M$^+$), 230, 203, 188, 149 (base), 88, 57, 41
4ci	7.61 (2H, d, J=9.3 Hz), 7.32 (2H, d, J=9.3 Hz), 4.60 (1H, septet, J=6.6 Hz), 2.59 (2H, q, J=7.2 Hz), 2.31 (3H, s), 1.26 (6H, d, J=6.6 Hz), 1.10 (3H, t, J=7.2 Hz)	2230, 1700, 1615, 1460, 1380	345 (M$^+$), 187, 160, 145, 41 (base)
4cj	8.25—8.05 (2H, m), 7.63—7.48 (2H, m), 4.64 (1H, septet, J=6.9 Hz), 2.59 (2H, q, J=7.2 Hz), 2.33 (3H, s), 1.27 (6H, d, J=6.9 Hz), 1.10 (3H, t, J=7.2 Hz)	1680, 1590, 1490, 1430, 1350	365 (M$^+$), 185, 165 (base), 41
4ck	7.45 (4H, s), 4.62 (1H, septet, J=6.6 Hz), 2.53 (2H, q, J=6.9 Hz), 2.29 (3H, s), 1.23 (6H, d, J=6.6 Hz), 1.09 (3H, t, J=6.9 Hz)	1705, 1615, 1320, 1305, 1130, 900	388 (M$^+$), 230, 203, 188, 41 (base)
4dd	7.26 (4H, s), 4.61 (1H, septet, J=7.0 Hz), 2.89—2.45 (4H, m), 1.32—0.99 (6H, m), 1.23 (6H, d, J=7.0 Hz)	1710, 1610	368 (M$^+$), 196 (base), 169, 154, 57

Table 4. (Continued)

Compound No.	^{1}H-NMR	IR	MS
4ed	7.23 (4H, s), 4.61 (1H, septet, J=6.8 Hz), 2.82—2.47 (4H, m), 1.84—1.48 (2H, m), 1.28—0.94 (6H, m), 1.22 (6H, d, J=6.8 Hz)	1710, 1610	382 (M$^+$), 196, 169, 154, 71 (base)
4fd	7.36 (2H, d, J=9.0 Hz), 7.23 (2H, d, J=9.0 Hz), 4.62 (1H, quintet, J=6.9 Hz), 3.23 (1H, quintet, J=6.9 Hz), 2.64 (2H, q, J=7.3 Hz), 1.22 (6H, d, J=7.2 Hz), 1.12 (3H, t, J=7.3 Hz)	1710, 1605, 1490, 1305, 1245, 1095, 1015	382 (M$^+$), 312, 283, 196, 169, 154 (base), 71
4gd	7.22 (4H, s), 4.59 (1H, septet, J=6.6 Hz), 2.49 (2H, q, J=7.3 Hz), 1.33 (9H, s), 1.21 (6H, d, J=6.6 Hz), 1.12 (3H, t, J=7.3 Hz)	1710, 1580, 1310	396 (M$^+$), 196, 169, 149, 57 (base)
4hd	7.20—7.36 (4H, m), 4.65 (1H, septet, J=7.0 Hz), 2.58 (2H, t, J=7.6 Hz), 2.33 (3H, s), 1.47 (2H, qt, J=7.0, 7.6 Hz), 1.23 (6H, d, J=7.0 Hz), 0.94 (3H, t, J=7.0 Hz)	1710, 1615	368 (M$^+$), 294, 239, 196 (base), 169, 154, 144, 131, 111, 87
4hf	7.41—7.50 (1H, m), 6.81—6.92 (2H, m), 4.65 (1H, septet, J=7.0 Hz), 2.56 (2H, t, J=7.0 Hz), 2.34 (3H, s), 1.45 (2H, sextet, J=7.0 Hz), 1.23 (6H, br s), 0.92 (3H, t, J=7.0 Hz)	1710, 1615	370 (M$^+$), 198, 171, 156, 149, 131, 41 (base)
4id	7.20—7.35 (4H, m), 4.65 (1H, septet, J=6.4 Hz), 3.16 (1H, septet, J=6.4 Hz), 2.31 (3H, s), 1.23 (6H, d, J=6.4 Hz), 1.15 (6H, d, J=6.4 Hz)	1710, 1615	368 (M$^+$), 294, 239, 196, 169, 154 (base), 131, 111
4jd	7.11—7.47 (4H, m), 4.60 (1H, septet, J=7.0 Hz), 3.18 (1H, septet, J=7.0 Hz), 2.70 (2H, q, J=7.6 Hz), 1.23 (6H, d, J=7.0 Hz), 1.20 (3H, t, J=7.6 Hz), 1.15 (6H, d, J=7.0 Hz)	1705, 1600	382 (M$^+$), 326, 307, 283, 239, 196, 169, 154 (base), 145, 102, 57
4ld	7.08—7.40 (4H, m), 6.63 (1H, t, J=57.0 Hz), 4.60 (1H, septet, J=7.0 Hz), 2.37 (3H, s), 1.22 (6H, d, J=7.0 Hz)	1720, 1620	376 (M$^+$), 239, 223, 196 (base), 167, 154, 131, 111, 40
4md	7.19 (4H, s), 4.53 (1H, septet, J=7.0 Hz), 3.33 (2H, t, J=6.4 Hz), 3.20 (3H, s), 2.68 (2H, t, J=6.4 Hz), 2.24 (3H, s), 1.23 (6H, d, J=7.0 Hz)	1710, 1620	384 (M$^+$), 352, 293, 239, 196, 154, 111, 59, 41 (base)
4nd	7.00—7.40 (4H, m), 4.59 (1H, septet, J=7.0 Hz), 3.28 (2H, d, J=3.0 Hz), 2.35 (3H, s), 2.10 (1H, t, J=3.0 Hz), 1.20 (6H, d, J=7.0 Hz)	1710, 1620	364 (M$^+$), 294, 239, 196, 154, 111, 41 (base)
4od	7.32—7.39 (3H, m), 7.22—7.27 (2H, m), 7.05 (1H, dd, J=8.1, 2.3 Hz), 6.68 (1H, d, J=8.1 Hz), 4.64 (1H, septet, J=7.0 Hz), 3.82 (2H, s), 1.86 (3H, s), 1.23 (6H, d, J=7.0 Hz)	1710, 1610	484 (M$^+$), 325, 294, 239, 223, 196, 159 (base), 138, 111

Table 5. Physical Data for Compounds 5 and 4

Compound No.	mp (°C)	Formula	Analysis (%)					
			Calcd			Found		
			C	H	N	C	H	N
5f	47—49	$C_8H_{13}NO_2S$	51.31	7.00	7.48	51.06	7.01	7.33
5g	83—88	$C_9H_{15}NO_2S$	53.70	7.51	6.96	53.47	7.44	6.95
5l	73—75	$C_5H_5F_2NO_2S$	33.15	2.78	7.73	33.10	2.80	7.84
4ad	131—134	$C_{15}H_{17}ClN_2O_3S$	52.86	5.03	8.22	52.22	4.87	8.49
4cb	Oil	$C_{15}H_{17}ClN_2O_3S$	52.86	5.03	8.22	52.64	4.96	8.23
4cd	64—65	$C_{16}H_{19}ClN_2O_3S$	54.16	5.40	7.89	54.12	5.36	7.90
4ce	61—62	$C_{16}H_{19}FN_2O_3S$	56.79	5.66	8.28	56.65	5.63	8.35
4ch	95—97	$C_{16}H_{18}Cl_2N_2O_3S$	49.36	4.66	7.20	49.43	4.61	7.22
4cj	111—112	$C_{16}H_{19}N_3O_5S$	52.59	5.24	11.50	52.30	5.17	11.39
4dd	Oil	$C_{17}H_{21}ClN_2O_3S$	55.35	5.74	7.59	55.09	5.69	7.80
4fd	Oil	$C_{18}H_{23}ClN_2O_3S$	56.46	6.06	7.32	56.22	6.02	7.30
4hd	52—54	$C_{17}H_{21}ClN_2O_3S$	55.35	5.74	7.59	55.34	5.67	7.74
4hf	47—48	$C_{17}H_{20}F_2O_3S$	55.12	5.44	7.56	55.22	5.67	7.51
4id	85—87	$C_{17}H_{21}ClN_2O_3S$	55.35	5.74	7.59	55.22	5.67	7.66
4ld	70—72	$C_{15}H_{15}ClF_2N_2O_3S$	47.81	4.01	7.43	47.99	3.95	7.55
4md	92—94	$C_{17}H_{21}ClN_2O_4S$	53.05	5.50	7.28	52.81	5.53	7.22

carbamoyled product, 2-chlorocarbonyl-4-isoxazolin-3-ones (15) generated from 3-hydroxyisoxazoles and phosgene were proved to be satisfactory intermediates. Accordingly, treatment of 3-hydroxyisoxazole derivatives (5) with 4 eq of phosgene in toluene gave 2-chlorocarbonyl-4-isoxazole-3-one derivatives (15), selectively. After evaporating the solvent and excess amount of phosgene, a mixture of aniline derivatives and triethylamine was added to the solution of the crude residue in tetrahydrofuran (THF) to afford the desired 2-carbamoyl-4-isoxazolin-3-ones (4) in good yields. Two strong absorptions observed in the IR spectrum (v_{max} cm^{-1}: 1700—1715 and 1600—1620) strongly suggested the existence of two carbonyl groups in the molecule. Taking this result into consideration, these structures were determined to be N-carbamoyled products rather than O-carbamoyled products. Our results are summarized in Table 3.

Table 6. Herbicidal Activity of Compounds **4**

4	g/a	EO	LP	SJ	EA	CS	EK	OS
ca	25	5	4	4	4	5	5	1
cb	10	5	4	5	4	5	5	2
cc	10	5	5	5	4	5	5	1
cd	25	5	5	5	5	5	5	1
cd	10	5	5	5	5	5	5	0
ce	25	5	5	5	5	5	5	3
cg	10	5	2	5	4	5	5	0
ch	10	5	4	5	4	5	5	0
ci	10	5	4	5	4	5	5	3
cj	10	5	4	5	4	5	5	1
ck	10	5	3	4	2	5	5	0
dd	25	5	4	4	4	5	5	2
dd	10	5	3	3	3	4	5	0
hd	25	5	5	5	5	5	5	2
hd	10	5	3	5	5	5	5	0
hf	10	5	5	5	5	5	5	1
id	25	5	5	5	4	5	5	2
id	10	5	3	5	3	5	5	0
jd	25	5	3	5	3	5	5	0
ld	10	5	3	5	5	5	5	1
md	25	5	3	5	4	5	5	1
md	10	5	2	5	3	5	5	0
nd	25	5	4	5	3	5	5	2
nd	10	5	3	5	3	5	5	0

EO: *Echinochloa oryzicola*, LP: *Lindernia procumbens*, SJ: *Scirpus juncoides*, EA: *Eleocharis acicularis*, CS: *Cyperus serotinus*, EK: *Eleocharis kuroguwai*, OS: transplanted rice.

Biological Results

The comparative herbicidal activity of the synthesized compounds was measured at the whole plant level *via* a greenhouse assay. Table 6 shows the results of herbicidal evaluations of the synthesized compounds. Structures and activity relationships strongly resembled those of 4-chloro-4-isoxazolin-3-one derivatives (**3**).[6] The substitution of a chlorine atom at the 4-position of the 4-isoxazolin-3-one ring with the alkylthio groups maintains herbicidal activity. In this series, an alkylthio group seemed to act as a biological isostere to a chlorine atom. All tested compounds showed good activity against *Echinochloa oryzicola* VASING (EO), *Cyperus serotinus* ROTTB. (CS), and *Eleocharis kuroguwai* OHWI (EK). In general, lower activity was accompanied by a change from methylthio to longer alkylthio substituents at the 4-position (R_1S) of the 4-isoxazolin-3-one ring. Introduction of an alkoxyalkylthio group (**4md**) or alkynylthio group (**4nd**) gave disappointing results. Compared with the more bulky isopropyl group (**4cd**), a small alkyl group such as a methyl (**4ca**) or ethyl group (**4cb**) at the nitrogen atom in the carbamoyl group slightly decreased herbicidal activity and increased injury toward transplanted rice. Electron withdrawing groups such as a nitro (**4cj**) or trifluoromethyl group (**4ck**) on an aryl group (R_4) decreased the activity, and the introduction of a cyano group (**4ci**) increased the unwanted damage to transplanted rice.

In summary, the novel 4-isoxazolin-3-ones (**4**) presented in this paper showed good to excellent herbicidal activity and rice selectivity. In this series, the alkylthio group played a biological isosteric role to a chlorine atom. Among the synthesized compounds, 2-(*N*-(4-chlorophenyl)-*N*-isopropylcarbamoyl)-4-ethylthio-5-methyl-4-isoxazolin-3-one (**4cd**) exhibited the best herbicidal activity against all tested weeds.

While several compounds were investigated more fully in the greenhouse, none of them seemed to show adequate potential to merit detailed field evaluation.

Experimental

Synthesis All melting points (mp) are uncorrected. IR spectra were measured on a Jasco A-102 spectrometer or Perkin-Elmer 1600 spectrometer. ¹H-NMR spectra were recorded at 60 MHz on a Varian 360A spectrometer, at 200 MHz on a Varian Gemini 200 spectrometer, or at 270 MHz on a JOEL GX 270 spectrometer with tetramethylsilane as an internal standard. Mass spectra (MS) and high-resolution mass spectra (HR-MS) were obtained with a JEOL JMS-D300 mass spectrometer and a VG Auto Spec M mass spectrometer.

Ethyl 2-Ethylthioacetate (13c) Sodium ethoxide (12.76 g, 188 mmol) was added to a solution of ethyl thioglycolate (**11**) (15 g, 125 mmol) in ethanol (150 ml) and the resulting mixture was stirred at room temperature for 5 min. Then, ethyl iodide (30 ml, 0.356 mmol) was added and the resulting mixture was refluxed for 1 h. The reaction mixture was concentrated to one-third volume, diluted with water, and extracted with ether (2×). The combined extracts were washed with brine (1×), dried over Na_2SO_4, and evaporated *in vacuo*. The residue was distilled under reduced pressure (bp 85 °C (20 mmHg)) to yield 13.04 g (70.4%) of **13c** as oil.

Compounds **13d**—**13o** were synthesized in the same manner. (Compound **13a** is commercially available.)

Ethyl 2-Ethylthioacetoacetate (6c) A 1.0 M solution of LiN(TMS)₂ in THF (7.08 ml, 7.08 mmol) was gradually added to a solution of ethyl 2-ethylthioacetate (**13c**) (500 mg, 3.37 mmol) in THF (10 ml) at a temperature below −50 °C and after 30 min a solution of acetyl chloride (0.32 g, 4.08 mmol) in THF (5 ml) was added at −50 °C. The resulting mixture was stirred at −50 °C for 50 min, at −20 °C for 1 h, at 0 °C for 40 min, and at room temperature for 30 min. The reaction mixture was quenched by the addition of saturated aqueous solution of NH_4Cl and 1 N hydrochloric acid and then extracted with ether (3×). The combined extracts were washed with brine (1×), dried over Na_2SO_4, and concentrated *in vacuo*. The residue was purified by silica gel chromatography to afford 451 mg of **6c** (70.3%) as oil.

Compounds **6a**, **6b**, **6d**—**6n** were synthesized in the same manner.

Ethyl 2-Ethylthio-3-oxopentanoate (**6d**): Oil, HR-MS Calcd for $C_9H_{16}O_3S$: 204.0820. Found: 204.0821.

Ethyl 2-Ethylthio-3-oxohexanoate (**6e**): Oil, HR-MS Calcd for $C_{10}H_{18}O_3S$: 218.0977. Found: 218.0975.

Ethyl 2-Ethylthio-4-methyl-3-oxopentanoate (**6f**): Oil, HR-MS Calcd for $C_{10}H_{18}O_3S$: 218.0977. Found: 218.0976.

Ethyl 4,4-Dimethyl-2-ethylthio-3-oxopentanoate (**6g**): Oil, HR-MS Calcd for $C_{11}H_{20}O_3S$: 232.1133. Found: 232.1132.

Ethyl 2-Isopropylthio-3-oxopentanoate (**6j**): Oil, HR-MS Calcd for $C_{10}H_{18}O_3S$: 218.0977. Found: 218.0977.

Ethyl 2-Difluoromethylthioacetoacetate (**6l**): Oil, HR-MS Calcd for $C_7H_{10}F_2O_3S$: 212.0319. Found: 212.0317.

Ethyl 2-(2-Methoxyethylthio)acetoacetate (**6m**): Oil, HR-MS Calcd for $C_9H_{16}O_4S$: 220.0769. Found: 220.0770.

Ethyl 2-(2-Propynylthio)acetoacetate (**6n**): Oil, HR-MS Calcd for $C_9H_{12}O_3S$: 200.0507. Found: 200.0508.

Ethyl 2-(2,4-Dichlorobenzylthio)acetoacetate (6o) A 1.0 M solution of LiN(TMS)₂ in THF (62.24 ml, 62.24 mmol) was gradually added to a solution of ethyl 2-(2,4-dichlorobenzylthio)acetate (**13o**) (8.69 g, 31.1 mmol) and acetyl chloride (2.6 g, 31.1 mmol) in THF (200 ml) at a temperature below −50 °C and the resulting mixture was stirred at −50 °C for 1 h. The reaction mixture was quenched by the addition of saturated aqueous solution of NH_4Cl and 1 N hydrochloric acid and then extracted with ether (3×). The combined extracts were washed with brine (1×), dried over Na_2SO_4, and concentrated *in vacuo*. The residue was purified by silica gel chromatography to afford 3.6 g of **6o** (36.0%) as oil. HR-MS Calcd for $C_{13}H_{14}Cl_2O_3S$: 320.0041. Found: 320.0042.

4-Ethylthio-3-hydroxy-5-methylisoxazole (5c) **6c** (2.60 g, 13.7 mmol) was added to a solution of potassium hydroxide (0.90 g, 13.6 mmol) in water (16 ml) and methanol (32 ml) at 0 °C and the mixture was stirred for 30 min. An aqueous solution (16 ml) of potassium hydroxide (2.70 g, 40.9 mmol) and hydroxylamine hydrochloride (2.85 g, 41.0 mmol) was added at −30 °C. After 1.5 h acetone (20 ml) was added to the mixture and the stirring was continued for an additional 10 min. After adding concentrated hydrochloric acid (7 ml) and stirring at 90 °C for 45 min, the mixture was diluted with water and extracted with ether (3×). The combined extracts were washed with brine (1×) and then extracted with 1 N aqueous solution of sodium hy-

droxide (2×). The aqueous extracts were acidified with 6 N hydrochloric acid and extracted with ether (3×), then the combined extracts were washed with brine (1×), dried over Na_2SO_4, and concentrated *in vacuo*. The residue was purified by silica gel chromatography to afford 713 mg of **5c** (32.3%) as amorphous.

Compounds **5a, 5d—5k, 5m—5o** were synthesized in the same manner.

5-Ethyl-4-ethylthio-3-hydroxyisoxazole (5d): Oil, HR-MS Calcd for $C_7H_{11}NO_2S$: 173.0511. Found: 173.0509.

4-Ethylthio-3-hydroxy-5-propylisoxazole (5e): Oil, HR-MS Calcd for $C_8H_{13}NO_2S$: 187.0667. Found: 187.0668.

5-Ethyl-3-hydroxy-4-isopropylthioisoxazole (5j): Oil, HR-MS Calcd for $C_8H_{13}NO_2S$: 187.0667. Found: 187.0666.

3-Hydroxy-4-(2-methoxyethylthio)-5-methylisoxazole (5m): Oil, HR-MS Calcd for $C_7H_{11}NO_3S$: 189.0460. Found: 189.0461.

3-Hydroxy-5-methyl-4-(2-propynylthio)isoxazole (5n): mp 105—110 °C, HR-MS Calcd for $C_7H_7NO_2S$: 169.0198. Found: 169.0199.

4-(2,4-Dichlorobenzylthio)-3-hydroxy-5-methylisoxazole (5o): mp 136—137 °C, HR-MS Calcd for $C_{11}H_9Cl_2NO_2S$: 288.9731. Found: 288.9730.

Ethyl 2-Difluoromethylthio-3,3-dimethoxybutyrate (14l) 95% sulfuric acid (0.2 ml) was added to a mixture of **6l** (16.47 g, 77.6 mmol) and trimethyl orthoformate (10.2 ml, 93.2 mmol) in methanol (20 ml) and the resulting mixture was refluxed for 15 h. After neutralizing the reaction mixture with a solution of potassium hydroxide in methanol and filtering it, the filtrate was concentrated *in vacuo* to give 12.72 g of **14l** (63.5%) as a crude oil, which was subjected to the next reaction without further purification. ^{1}H-NMR (CDCl$_3$) δ: 6.85 (1H, t, $J=56.7$ Hz), 4.20 (2H, q, $J=7.0$ Hz), 4.09 (1H, s), 3.25 (6H, s), 1.50 (3H, s), 1.28 (3H, t, $J=7.0$ Hz); IR ν_{max} cm^{-1} (KBr): 3000, 1730, 1160, 1110, 1040; MS (*m/z*): 243 (M$^+$−15), 227 (base), 213, 132, 99, 89.

5-Difluoromethylthio-3-hydroxy-5-methylisoxazole (5l) Compound **5l** was prepared from **14l** as the compound **5c**.

2-[*N*-(4-Chlorophenyl)-*N*-isopropylcarbamoyl]-4-ethylthio-5-methyl-4-isoxazolin-3-one (4cd) A 2.26 M solution of phosgene in toluene (89 ml, 201 mmol) was added to **5c** (6.25 g, 39 mmol) and the resulting mixture was stirred at room temperature for 3 h. The reaction mixture was concentrated *in vacuo* and diluted again with toluene (50 ml). A solution of *N*-isopropyl-4-chloroaniline (6.97 g, 41 mmol) and triethylamine (6.7 ml, 48.1 mmol) in toluene (30 ml) was added to the solution and the resulting mixture was stirred at room temperature for 35 min. The reaction mixture was diluted with ether, washed with 1 N hydrochloric acid (1×), aqueous solution of NaHCO$_3$ (1×), and brine (1×), dried over Na_2SO_4, and evaporated. The residue was subjected to silica gel column chromatography to give 8.15 g of **4cd** (58.6%) as a light yellow powder.

A series of compounds **4** listed in Table 3 were synthesized by the same method.

2-[*N*-(4-Chlorophenyl)-*N*-methylcarbamoyl]-4-ethylthio-5-methyl-4-isoxazolin-3-one (4ca): Oil, HR-MS Calcd for $C_{14}H_{15}ClN_2O_3S$: 326.0492. Found: 326.0493.

2-[*N*-(4-Chlorophenyl)-*N*-propylcarbamoyl]-4-ethylthio-5-methyl-4-isoxazolin-3-one (4cc): mp 82—83 °C, HR-MS Calcd for $C_{16}H_{19}ClN_2O_3S$: 354.0805. Found: 354.0806.

4-Ethylthio-2-[*N*-isopropyl-*N*-(4-methylphenyl)carbamoyl]-5-methyl-4-isoxazolin-3-one (4cg): mp 60—61 °C, HR-MS Calcd for $C_{17}H_{22}N_2O_3S$: 334.1351. Found: 334.1352.

2-[*N*-(3-Cyanophenyl)-*N*-isopropylcarbamoyl]-4-ethylthio-5-methyl-4-isoxazolin-3-one (4ci): mp 108—109 °C, HR-MS Calcd for $C_{17}H_{19}N_3O_3S$: 345.1147. Found: 345.1147.

4-Ethylthio-2-[*N*-isopropyl-*N*-(3-trifluoromethylphenyl)carbamoyl]-5-methyl-4-isoxazolin-3-one (4ck): Oil, HR-MS Calcd for $C_{17}H_{19}F_3N_2O_3S$: 388.1068. Found: 388.1067.

2-[*N*-(4-Chlorophenyl)-*N*-isopropylcarbamoyl]-4-ethylthio-5-propyl-4-isoxazolin-3-one (4ed): Oil, HR-MS Calcd for $C_{18}H_{23}ClN_2O_3S$: 382.1118. Found: 382.1117.

5-*tert*-Butyl-2-[*N*-(4-chlorophenyl)-*N*-isopropylcarbamoyl]-4-ethylthio-4-

isoxazolin-3-one (4gd): Oil, HR-MS Calcd for $C_{19}H_{25}ClN_2O_3S$: 396.1274. Found: 396.1274.

2-[*N*-(4-Chlorophenyl)-*N*-isopropylcarbamoyl]-5-ethyl-4-isopropylthio-4-isoxazolin-3-one (4jd): mp 74—76 °C, HR-MS Calcd for $C_{18}H_{23}ClN_2O_3S$: 382.1118. Found: 382.1121.

2-[*N*-(4-Chlorophenyl)-*N*-isopropylcarbamoyl]-5-methyl-4-(2-propy-nylthio)-4-isoxazolin-3-one (4nd): mp 52—54 °C, HR-MS Calcd for $C_{17}H_{17}ClN_2O_3S$: 364.0648. Found: 364.0645.

2-[*N*-(4-Chlorophenyl)-*N*-isopropylcarbamoyl]-4-(2,4-dichloroben-zylthio)-5-methyl-4-isoxazolin-3-one (4od): mp 96.5—98.5 °C, HR-MS Calcd for $C_{21}H_{19}Cl_3N_2O_3S$: 484.0182. Found: 484.0183.

Herbicide Tests Plastic pots (surface area = 100 cm^2) were filled with a clay loam soil and kept in a greenhouse. The test plants were five narrowleaf weeds [*Echinochloa oryzicola* VASING., *Scirpus juncoides* ROXB var. *ohwianus* T. KOYAMA, *Eleocharis acicularis* (L.) ROEM. et SCHULT. var. *longiseta* SVEN., *Cyperus serotinus* ROTTB., and *Eleocharis kuroguwai* OHWI] and one broadleaf weed [*Lindernia pyxidaria* L.], and *Sagittaria pygmaea* Miq., and *Oryza sativa* L. A predetermined number of seeds of each weed were placed on top of the soil. An additional 1 cm of soil was placed over the seeds, and then seedlings of *Oryza sativa* L. that had reached the two-leaf stage were transplanted. For the herbicidal test, wettable powders were prepared by mixing the compounds (10%) with Emulgen 810 (surfactant; 0.5%), Demol N (surfactant; 0.5%), Kunilite 210 (diatomaceous earth; 20%), and Dieclite CA (clay; 69%). The wettable powders formulated from the compounds were applied 3 d after the seeds had been sown. Approximately 3 weeks after treatment, the herbicidal activity of each compound was judged by visual observation of the symptoms of the treated plants in comparison with untreated controls. Using the following criteria, the herbicidal potency was scaled from 0 to 5 according to the extent of the injury shown by the plants: 5, >91% growth inhibition; 4, 71—90% growth inhibition; 3, 51—70% growth inhibition; 2, 31—50% growth inhibition; 1, 11—30% growth inhibition; 0, <10% growth inhibition.

References and Notes
1) For reviews, see "Organic Sulfur Chemistry," ed. by Bernardi F., Csizmadia I. G., Mangini A., Elsevier, Amsterdam; "Chemistry of Organosulfur Compounds," ed. by Belen'kii L. I., Ellis Horwood, Chichester.
2) Metcalf R. L., *Agrochemica*, **11**, 105—123 (1967).
3) Sheets T. J., Shaw W. C., *Weeds*, **11**, 15—21 (1963).
4) Pearman W. M., Banks C. K., *J. Am. Chem. Soc.*, **70**, 3726—3728 (1948).
5) Gysin H., *Weeds*, **8**, 541—555 (1960).
6) Tomita K., Murakami T., Honma T., Yamazaki Y., Japan. Kokai 74 62636 (1974) [*Chem. Abstr.*, **82**, 1110z (1975)].
7) Kay I. T., Lovejoy D. J., Glue S., *J. Chem. Soc.* (*C*), **1970**, 445—448.
8) *a*) Sasaki T., Hayakawa K., *Tetrahedron Lett.*, **21**, 1525—1526 (1980); Sasaki T., Hayakawa K., Ban H., *Tetrahedron*, **38**, 85—91 (1982); *b*) Fujisawa T., Itoh T., Sato T., *Tetrahedron Lett.*, **25**, 5083—5086 (1984).
9) Held P., Gross M., Jumar A., *Z. Chem.*, **10**, 187—188 (1970).
10) Sato K., Sugai S., Tomita K., *Agric. Biol. Chem.*, **50**, 1831—1837 (1986).
11) Malleron J. L., Roussel G., Gueremy G., Ponsinet G., Robin J. L., Terlain B., Tissieres J. M., *J. Med. Chem.*, **33**, 2744—2749 (1990).
12) LiN(TMS)$_2$ was purchased from Aldrich Chemical Co., Inc.
13) *a*) Goth H., Gagneux A. R., Eugster C. H., Schmid H., *Helv. Chim. Acta*, **50**, 137—142 (1967); *b*) Jacquier R., Petrus C., Petrus F., Verducci J., *Bull. Soc. Chim. Fr.*, **1970**, 1978—1985.
14) Sampei N., Tomita K., Tsuji H., Yanai T., *Ann. Sankyo Res. Lab.*, **22**, 230—233 (1970).

516

Chem. Pharm. Bull. **48**(4) 516—524 (2000)

Vol. 48, No. 4

Cardenolide and Oxypregnane Glycosides from the Root of *Asclepias incarnata* L.

Tsutomu WARASHINA* and Tadataka NORO

Institute for Environmental Sciences, University of Shizuoka, 52–1 Yada, Shizuoka 422–8526, Japan.
Received October 14, 1999; accepted December 16, 1999

Twenty-nine new oxypregnane glycosides were obtained along with two known cardenolides, frugoside and gofruside, and three known 12-*O*-acylated pregnane glycosides from the roots of *Asclepias incarnata* L.(Asclepiadaceae). By detailed studies of the ¹H- and ¹³C-NMR spectra, the structures were determined to be tri- to penta glycosides of isolineolon, 12-*O*-acetyllineolon, ikemagenin, 12-*O*-benzoylisolineolon, and two new 12-*O*-acylated pregnanes.

Key words *Asclepias incarnata*; Asclepiadaceae; pregnane glycoside; cardenolide glycoside; 2,6-dideoxyhexopyranose; ikemagenin

In previous papers,[1,2] we reported the isolation and structural elucidation of oxypregnane glycosides from the aerial part of *Asclepias incarnata* L. Further studies of the root of this plant have resulted in the isolation of 29 new pregnane glycosides together with two known cardenolide glycosides, frugoside[3,4] and gofruside,[3] and three known 12-*O*-acylated pregnane glycosides (**1**, **6**, **23**).[1,5,6] The sugar sequences of these pregnane glycosides were suggested to be similar to those of compounds acquired from the aerial part of this plant in comparison with the ¹H- and ¹³C-NMR spectral data.[1,2]

The MeOH extract obtained from the dried root of *A. incarnata* L. was suspended in water. The suspension was then extracted with diethyl ether and partitioned into an ether soluble fraction and a water soluble fraction. These fractions were chromatographed on a silica gel column to give a fraction of pregnane glycosides from which 29 new oxypregnane glycosides (**2**—**5**, **7**—**22**, **24**—**32**) were obtained.

In order to acquire the component aglycones and sugars, the fraction containing the pregnane glycosides from silica gel column chromatography was subjected to acid hydrolysis. The obtained aglycones were identified as isolineolon (**35**),[7] 12-*O*-acetyllineolon (**34**),[1] ikemagenin (**36**),[8] 12-*O*-nicotinoyllineolon (**33**)[5] and 12-*O*-benzoylisolineolon (**39**)[9] in view of the ¹H- and ¹³C-NMR spectral data and/or the analysis of HPLC with the authentic samples. In addition, two new acylated pregnanes were obtained (**37**, **38**).

Compound **37** showed a [M+Na]⁺ ion peak at *m/z* 519, which was larger by 2 mass units than that of **36**. In comparing the ¹³C-NMR spectral data of **37** with those of **36**, signals of the cinnamoyl group were observed, but, in addition, two sp^3 carbon signals were seen at δ 45.9 and 25.4 instead of two sp^2 carbon signals at C-5 and C-6. Thus, **37** was considered to be a 5,6-dihydro derivative of ikemagenin. On the basis of ¹H–¹H correlation spectroscopy (COSY) and ¹H-detected heteronuclear multiple quantum coherency (HMQC) spectra, assignments of the proton signals were done as shown in the Experimental. In the nuclear Overhauser effect (NOE) difference experiments, irradiation at the H-3 signal (δ 3.92) showed a NOE on the H-5 signal (δ 1.16), and irradiation at the H-19 signal (δ 1.27) exhibited a NOE on the H-4axial signal (δ 1.71). Based on these findings, the orientation of H-5 was confirmed as α, and finally, **37** was deter-

mined to be 5α,6-dihydroikemagenin.

The ¹H- and ¹³C-NMR spectra of compound **38** was similar to those of sibirigenin.[7,10] The chemical shift of the C-20 signal was consistent with that of sibirigenin, and H-17 signal was observed as a double-doublet signal whose *J* value was 9.5 and 5.5 Hz. This multiplicity and the *J* value of the H-17 signal were the same as those of **35**. Therefore, **38** was considered to be 12-*O*-acylated isolinelon. Moreover, alkaline hydrolysis of **38** afforded tiglic acid (see Experimental). Hence, **38** was concluded to be 12-*O*-tigloylisolineolon.

Table 1. ¹³C-NMR Spectral Data of the Aglycone Moiety

Carbon No.	1	2	3	4	7	8	9
C-1	39.0	39.0	39.2	39.0	38.2	39.0	39.0
-2	29.9	29.9	30.0	29.9	29.6	29.9	29.9
-3	77.7	77.7	77.9	77.7	76.7	77.7ᵃ⁾	77.7
-4	39.3	39.3	39.4	39.4	35.0ᵃ⁾	39.3	39.4
-5	139.5	139.5	139.3	139.5	45.4	139.2	139.2
-6	119.2	119.2	119.7	119.2ᵃ⁾	25.3	119.4	119.3
-7	35.2	35.2	37.3	35.2	34.6ᵃ⁾	35.9	35.8
-8	74.6ᵃ⁾	74.6	74.5	74.6	76.5	74.4	74.4
-9	44.8	44.8	45.6	44.8	47.5	45.1	45.2
-10	37.6	37.5	37.6	37.6	36.7	37.6	37.7
-11	25.0	24.9	28.5	25.0	24.0	24.6	24.8ᵃ⁾
-12	74.3ᵃ⁾	73.3	74.0	73.4	73.9	77.6ᵃ⁾	78.6
-13	56.1	55.7	56.7	55.9	56.3	55.0	55.1
-14	87.5	87.5	86.7	87.5	87.6	86.6	86.6
-15	34.2	34.1	36.2	34.2	33.9	36.7	36.7
-16	22.2	21.8	24.7	22.0	22.4	24.6	24.7ᵃ⁾
-17	60.2	60.5	58.7	60.5	60.5	59.2	59.3
-18	15.9	15.6	11.6	15.8	16.2	12.6	12.7
-19	18.3	18.2	18.5	18.2	13.1	18.4	18.4
-20	209.8	209.6	216.8	209.3	209.4	214.3	214.1
-21	32.4	32.3	32.3	32.2	32.3	31.6	31.6
Ester moiety							
-1'	164.5	167.0	–	165.9	165.9	167.8	166.6
-2'	–	20.8	–	119.3ᵃ⁾	119.4	129.4	133.6ᵇ⁾
-3'	153.8	–	–	144.9	144.8	137.7	129.1
-4'	127.0	–	–	135.1	135.1	12.3	130.0
-5'	137.1	–	–	128.6	128.6	14.3	131.2ᵇ⁾
-6'	ᶜ⁾	–	–	129.3	129.3	–	130.0
-7'	151.1	–	–	130.6	130.5	–	129.1
-8'	–	–	–	129.3	129.3	–	–
-9'	–	–	–	128.6	128.6	–	–

Measured in pyridine-d_5 solution at 35 °C. *a),b)*: Interchangeable in each column. *c)*: Overlapping with the pyridine-d_5 signal.

* To whom correspondence should be addressed.

Table 2. ^{13}C-NMR Spectral Data of the Sugar Moiety

Carbon No.	1	2	4	5	8	10	14	16	20	21	22	24	25	29	32	32'
	Cym	Cym	Cym	Dig	Cym	Cym	Cym	Cym	Cym	Cym	Dig	Dig	Cym	Cym	Cym	Cym
C-1'	96.5	96.5	96.4	96.4	96.4	96.5	96.5	96.5	96.4	96.5	95.9	96.4	96.5	96.4	96.5	96.2
-2'	37.3[a]	37.3[a]	37.3[a]	38.7[a]	37.3	37.3	37.3[a]	37.3[a]	37.4[a]	37.7[a]	37.1	39.0	37.3[a]	37.3[a]	37.8[a]	35.4[a]
-3'	77.9[b]	77.9[b]	78.0[b]	67.6[b]	78.1	78.2[a]	78.0[b]	78.0[b]	78.0[b]	78.1[b]	66.6[a]	67.5	78.1[b]	78.0[b]	77.9	77.2
-4'	83.4[c]	83.4[c]	83.4[c]	83.5[c]	83.5[a]	83.5[b]	83.4[c]	83.4[c]	83.4[c]	83.4[c]	82.8[b]	83.4[a]	83.4[c]	83.4[c]	82.8[b]	82.8[b]
-5'	69.1[d]	69.1[d]	69.1[d]	68.6[d]	69.1	69.1	69.1[d]	69.0	69.1	69.1[d]	68.0	68.6	69.1[d]	69.1[d]	69.0	68.5
-OMe'	58.9	58.9	58.9[e]	–	58.9	58.9	58.9[e]	59.0[d]	58.9	58.9	–	–	58.9	58.9[e]	58.9	58.3
	Cym	Cym	Cym	Dig	Dig	Dig	Cym	Cym	Dig	Cym	Ole	Cym	Cym	Cym	Ole	Ole
C-1"	100.5	100.5	100.4	99.8	100.5	100.5	100.5[f]	100.5	100.5	100.5	100.4[c]	99.7	100.5	100.5	102.0	101.5
-2"	37.3[a]	37.3[a]	37.0[a]	39.1[a]	38.9[b]	38.8[c]	37.0[a]	37.2[a]	38.9	37.3[a]	36.3	36.8	37.1[a]	37.0[a]	37.3[a]	36.4[a]
-3"	78.0[b]	78.1[b]	78.2[b]	67.5[b]	67.5	67.5	78.1[b]	78.0[b]	67.5	77.8[b]	78.8	77.7	77.8[b]	77.8[b]	78.9	78.9
-4"	83.2[c]	83.2[c]	83.1[c]	83.1[c]	83.3[a]	83.2[b]	83.3[c]	83.2[c]	83.2[c]	83.2[c]	82.3	83.3[a]	83.2[c]	83.3[c]	83.3[b]	82.8[b]
-5"	69.0[d]	69.0[d]	69.4[d]	68.6[d]	68.7[c]	68.6	69.0[d]	69.0	68.5	69.0[d]	71.4	69.1	68.9[d]	68.9[d]	71.8	71.2
-OMe"	58.9	58.9	58.8[e]	–	–	–	58.9[e]	58.9[d]	–	58.9	56.8	58.9	58.9	58.8[e]	57.5[c]	56.6[c]
	Ole	Ole	The	Dig	Dig	Dig	Dig	Dig	Cym	Ole	Dig	Ole	Ole	Ole	Dig	Dig
C-1‴	102.2	102.2	106.2	99.8	99.9	99.9	100.6[f]	100.5	99.8	102.0	98.5	101.9	101.9	101.9	98.5	98.5
-2‴	37.0[a]	37.0[a]	75.1	38.6[a]	38.7[b]	38.7[c]	38.9	39.0	37.2[a]	37.4[a]	37.1	37.6	37.6[a]	37.6[a]	39.0	37.1
-3‴	81.4	81.4	87.9	67.5[b]	67.5	67.5	67.5	67.5	77.8[b]	79.1	66.7[a]	79.3	79.2	79.2	67.7	66.7
-4‴	76.3	76.2	75.9	83.1[c]	83.1[a]	83.1[b]	83.2[c]	83.2[c]	83.0[c]	82.7	82.7[b]	83.2[a]	83.1[c]	83.2[c]	83.5	82.5[b]
-5‴	73.0	73.0	72.8	68.7[d]	68.6[c]	68.6	68.6	68.5	69.1	71.7	68.3	72.0[b]	72.1	72.1	68.7	68.2
-OMe‴	57.0	57.0	60.9	–	–	–	–	–	58.9	57.3[e]	–	57.4	57.2	57.3	–	–
	–	–	–	Ole	Ole	Ole	Ole	Ole	Ole	Ole	Ole	The	The	The	Ole	Ole
C-1⁗	–	–	–	101.4	101.6	101.4	101.6	101.4	102.2	100.3	100.3[c]	104.0	104.1	104.0	101.4	100.4
-2⁗	–	–	–	37.2	37.0	37.2	37.0	37.1	36.8	37.2[a]	35.3	75.0	75.3	75.0	37.2	36.0[a]
-3⁗	–	–	–	79.3	81.4	79.3	81.4	79.3	81.4	81.7	80.5	86.4	88.2	86.3	79.4	80.5
-4⁗	–	–	–	83.2[c]	76.2	83.1[b]	76.2	83.2[c]	76.2	76.4	75.3	83.2[a]	76.0	83.2[c]	83.2[b]	75.3
-5⁗	–	–	–	72.1	73.0	72.1	73.0	72.1	73.0	73.0	71.9	72.1[b]	72.9	72.1	72.1	71.8
-OMe⁗	–	–	–	57.3	57.0	57.3	57.1	57.2	57.0	57.1[e]	56.4	60.6	60.9	60.6	57.2[c]	56.4[c]
	–	–	–	Glc	–	Glc	–	Glc	–	–	–	Glc	–	Glc	Glc	–
C-1⁗′	–	–	–	104.4	–	104.5	–	104.5	–	–	–	104.8	–	104.8	104.4	–
-2⁗′	–	–	–	75.7	–	75.7	–	75.7	–	–	–	75.9	–	75.9	75.7	–
-3⁗′	–	–	–	78.7	–	78.7	–	78.7	–	–	–	78.7	–	78.7	78.7	–
-4⁗′	–	–	–	72.1	–	72.1	–	72.1	–	–	–	72.1[b]	–	72.1	72.1	–
-5⁗′	–	–	–	78.2	–	78.1[a]	–	78.2[b]	–	–	–	78.0	–	78.0	78.2	–
-6⁗′	–	–	–	63.2	–	63.2	–	63.2	–	–	–	63.2	–	63.2	63.2	–
-6s	18.7	18.7	18.6×2	18.8	18.6×3	18.8	18.6×3	18.8	18.7	18.8	18.4	18.8	18.8	18.7×2	18.8	18.4
	18.6×2	18.6×2	18.5	18.7	18.5	18.6	18.4	18.6×2	18.6	18.7	18.2×2	18.7×2	18.6	18.6	18.7×2	18.2×2
				18.5×2		18.5×2		18.5×2	18.6	18.6	17.9	18.4	18.5×2	18.5	18.6	17.9
										18.5						

Cym: β-D-cymaropyranosyl, Ole: β-D-oleandropyranosyl, Dig: β-D-digitoxopyranosyl, The: β-D-thevetopyranosyl, Glc: β-D-glucopyranosyl. Measured in pyridine-d_5 solution at 35 °C except for 22 and 32'. 22 and 32' were measured in CDCl$_3$ solution at 35 °C. a—f): Interchangeable in each column.

The acquired sugars were fractionated to cymarose, oleandrose and digitoxose by silica gel column chromatography. The absolute configurations of these monosaccharides were believed to have a D-form based on their optical rotation values.[6,11,12] The absolute configurations of glucose and thevetose were determined to be a D-form based on GC analysis following their reaction with D-cysteine methyl ester hydrochloride (see Experimental).

Compounds 2 and 3 were suggested to have the molecular formulae, $C_{44}H_{70}O_{15}$ and $C_{42}H_{68}O_{14}$, respectively, based on the FAB-MS spectra. According to the consistency between the ^{1}H- and ^{13}C-NMR spectral data of the sugar moieties in 2 and 3, these compounds were considered to have the same sugar sequence. In the ^{1}H- and ^{13}C-NMR spectra of 2, three anomeric proton and carbon signals were observed at δ 5.37, 5.13, 4.77 and δ 96.5, 100.5, 102.2, together with signals due to the aglycone, which was identified as 12-O-acetyllineolon (34)[1] on acid hydrolysis with 0.05 N HCl. In comparison of the ^{13}C-NMR spectral data of 2 with that of 12-O-acetyllineolon,[1] glycosylation shifts were observed at the C-2, -3, and -4 positions [C-2 (-2.1 ppm), C-3 ($+6.1$ ppm), C-4 (-4.0 ppm)].[13] Therefore, 2 was glycosylated at the C-3 position,

and 2 was considered to be 12-O-acetyllineolon 3-O-trioside. Acid hydrolysis of 2 showed the sugar moiety was composed of cymarose and oleandrose, and these sugars were identified as β-D-cymaropyranose and β-D-oleandropyranose as judged from the J values of the anomeric proton signals (J=9.5, 2.0 Hz). Moreover, the ^{1}H- and ^{13}C-NMR spectral data of the sugar moiety in 2 were consistent with those of cynanchoside C_2[14] and 12-O-nicotinoyllineolon 3-O-β-D-oleandropyranosyl-(1→4)-β-D-cymaropyranosyl-(1→4)-β-D-cymaropyranoside (1).[5] Thus, the sugar sequence of 2 was determined to be 3-O-β-D-oleandropyranosyl-(1→4)-β-D-cymaropyranosyl-(1→4)-β-D-cymaropyranoside and the structure of 2 was shown as presented in Chart 1. Because acid hydrolysis of 3 afforded isolineolon as the aglycone moiety, the structure of 3 was determined to be isolineolon 3-O-β-D-oleandropyranosyl-(1→4)-β-D-cymaropyranosyl-(1→4)-β-D-cymaropyranoside.

The following compounds, 4, 5, 7—22 and 24—32, were also glycosylated at the C-3 position of each aglycone based on the observation of glycosylation shifts in the ^{13}C-NMR spectra.

Compound 4 exhibited the molecular formula $C_{51}H_{74}O_{16}$

Table 3. ^{1}H-NMR Spectral Data of the Sugar Moiety

Proton No.	1	2	4	5
	Cym	Cym	Cym	Dig
H-1'	5.28 (dd, 9.5, 2.0)	5.27 (dd, 9.5, 2.0)	5.27 (dd, 9.5, 2.0)	5.46 (dd, 9.5, 2.0)
-3'	4.10 (q, 3.0)	4.09 (q, 3.0)	4.07[a]	4.63 (q, 3.0)
-4'	3.53[a]	3.52 (dd, 9.5, 3.0)	3.49 (dd, 9.5, 3.0)	3.51[a]
-5'	4.23 (dd, 9.5, 6.5)	4.22 (dq, 9.5, 6.5)	4.21 (dq, 9.5, 6.5)	4.29[a]
-6'	1.40 (d, 6.5)	1.39 (d, 6.5)	1.39 (d, 6.5)	1.42 (d, 6.5)
	Cym	Cym	Cym	Dig
H-1"	5.13 (dd, 9.5, 2.0)	5.13 (dd, 9.5, 2.0)	5.12 (dd, 9.5, 2.0)	5.36 (dd, 9.5, 2.0)
-3"	4.07 (q, 3.0)	4.06 (q, 3.0)	4.07[a]	4.62 (q, 3.0)
-4"	3.50[a]	3.50 (dd, 9.5, 3.0)	3.59 (dd, 9.5, 3.0)	3.44 (dd, 9.5, 3.0)
-5"	4.20 (dq, 9.5, 6.5)	4.19 (dq, 9.5, 6.5)	4.21 (dq, 9.5, 6.5)	4.25[a]
-6"	1.42 (d, 6.5)	1.42 (d, 6.5)	1.60 (d, 6.5)	1.33 (d, 6.5)
	Ole	Ole	The	Dig
H-1'"	4.78 (d, 6.5)	4.77 (dd, 9.5, 2.0)	4.76 (d, 8.0)	5.36 (dd, 9.5, 2.0)
-2'"			3.91[a]	
-3'"			3.61[a]	4.58 (q, 3.0)
-4'"			3.61[a]	3.41 (dd, 9.5, 3.0)
-5'"			3.72 (m)	4.27[a]
-6'"	1.58 (d, 6.5)	1.57 (d, 6.5)	1.58 (d, 6.5)	1.35 (d, 6.5)
				Ole
H-1""	—	—	—	4.72 (dd, 9.5, 2.0)
-2""	—	—	—	
-3""	—	—	—	3.63[a]
-4""	—	—	—	3.63[a]
-5""	—	—	—	3.65[a]
-6""	—	—	—	1.64 (d, 6.0)
				Glc
H-1""'	—	—	—	5.09 (d, 8.0)
-2""'	—	—	—	3.98 (t, 8.0)
-3""'	—	—	—	4.20[a,b]
-4""'	—	—	—	4.17 (t, 8.0)[b]
-5""'	—	—	—	3.93 (m)
-6""'	—	—	—	4.52 (dd, 11.5, 2.5)
	—	—	—	4.33 (dd, 11.5, 5.5)
-OMe	3.63 (s)	3.62 (s)	3.89 (s)	3.52 (s)
	3.58 (s)	3.58 (s)	3.62 (s)	
	3.47 (s)	3.47 (s)	3.57 (s)	

Cym: β-D-cymaropyranosyl, Ole: β-D-oleandropyranosyl, Dig: β-D-digitoxopyranosyl, The: β-D-thevetopyranosyl, Glc: β-D-glucopyranosyl. Measured in pyridine-d_5 solution at 35 °C except for 20—22 and 32'. 20—22 and 32' were measured in CDCl$_3$ solution at 35 °C. a) Overlapping with other signals or H$_2$O signal. b) Interchangeable in each column.

on FAB-MS. Acid hydrolysis of 4 suggested that 4 consists of ikemagenin, cymarose and thevetose as the aglycone and sugar moieties. In the ^{13}C- and ^{1}H-NMR spectra of 4, three anomeric carbon and three proton signals were observed at δ 96.4, 100.4, 106.2 and δ 5.27, 5.12, 4.76, two double-doublet signals at δ 5.27 and 5.12 were assigned to the anomeric protons of β-D-cymaropyranose, and the remaining doublet signal at δ 4.76 belonged to the anomeric proton of β-D-thevetopyranose. The sugar sequence of 4 was determined on the basis of difference in NOE experiments. Irradiation at the H-1' signal of β-D-cymaropyranose (δ 5.27) exhibited a NOE to the H-3 signal of the aglycone (δ 3.85). Similarly, NOEs were observed as follows, δ 5.12 (H-1" of β-D-cymaropyranose) and δ 3.49 (H-4' of β-D-cymaropyranose), δ 4.76 (H-1'" of β-D-thevetopyranose) and δ 3.59 (H-4" of β-D-cymaropyranose). Thus, the structure of 4 was established as ikemagenin 3-O-β-D-thevetopyranosyl-(1→4)-β-D-cymaropyranosyl-(1→4)-β-D-cymaropyranoside. This oligosaccharide sugar chain was confirmed in stephanoside E and H from Stephanotis lutchuenis var. japonica.[15]

The molecular formula of compound 5 was $C_{61}H_{90}O_{23}$ based on FAB-MS. Because the ^{1}H- and ^{13}C-NMR spectra of 5 showed five anomeric proton and carbon signals at δ 5.46,

5.36×2, 4.72, 5.09 and δ 96.4, 99.8×2, 101.4, 104.4, along with signals due to ikemagenin, 5 was presumed to be ikemagenin 3-O-pentaoside. The ^{1}H- and ^{13}C-NMR spectral data of the sugar moiety in 5 were identified with those of lineolon 3-O-β-D-glucopyranosyl-(1→4)-β-D-oleandropyranosyl-(1→4)-β-D-digitoxopyranosyl-(1→4)-β-D-digitoxopyranosyl-(1→4)-β-D-digitoxopyranoside,[1] so that the structure of 5 was determined to be ikemagenin 3-O-β-D-glucopyranosyl-(1→4)-β-D-oleandropyranosyl-(1→4)-β-D-digitoxopyranosyl-(1→4)-β-D-digitoxopyranosyl-(1→4)-β-D-digitoxopyranoside.

The molecular formulae of compounds 7—9 were suggested to be $C_{56}H_{84}O_{18}$, $C_{52}H_{82}O_{18}$ and $C_{54}H_{80}O_{18}$, respectively, based on FAB-MS. Based on acid hydrolysis, ^{1}H- and ^{13}C-NMR spectral data, these compounds were supposed to be pregnane 3-O-tetraosides whose aglycones were 5α,6-dihydroikemagenin (37) on 7, 12-O-tigloylisolineolon (38) on 8 and 12-O-benzoylisolineolon (39) on 9, and the sugar moiety contained one β-D-cymaropyranose, two β-D-digitoxopyranose and one β-D-oleandropyranose. Compounds 7—9 possessed the same sugar moieties as ikemagenin 3-O-β-D-oleandropyranosyl-(1→4)-β-D-digitoxopyranosyl-(1→4)-β-D-digitoxopyranosyl-(1→4)-β-D-cymaropyranoside (6)[1] due

Table 3. (continued)

Proton No.	8	10	14	16	20	21
	Cym	Cym	Cym	Cym	Cym	Cym
H-1'	5.28 (dd, 9.5, 2.0)	5.27 (dd, 9.5, 2.0)	5.28 (dd, 9.5, 2.0)	5.27 (dd, 9.5, 2.0)	4.85 (dd, 9.5, 2.0)	4.85 (dd, 9.5, 2.0)
-3'	4.09 (q, 3.0)	4.09 (q, 3.0)	4.08 (q, 3.0)	4.07 (q, 3.0)	3.82 (q, 3.0)	3.81 (q, 3.0)
-4'	3.52 (dd, 9.5, 3.0)	3.52[a)]	3.50 (dd 9.5, 3.0)	3.50[a)]	3.23 (dd, 9.5, 3.0)	3.21 (dd, 9.5, 3.0)
-5'	4.22 (dq, 9.5, 6.5)	4.22[a)]	4.22 (dq, 9.5, 6.5)	4.21 (dq, 9.5, 6.5)	3.85 (dq, 9.5, 6.5)	3.84 (dq, 9.5, 6.5)
-6'	1.38 (d, 6.5)	1.38 (d, 6.5)	1.40 (d, 6.5)	1.39 (d, 6.5)	1.22 (d, 6.5)	1.22 (d, 6.5)
Dig	Dig	Dig	Cym	Cym	Dig	Cym
H-1''	5.32 (dd, 9.5, 2.0)	5.31 (dd, 9.5, 2.0)	5.12 (dd, 9.5, 2.0)	5.12 (dd, 9.5, 2.0)	4.83 (dd, 9.5, 2.0)	4.75 (dd, 9.5, 2.0)
-3''	4.64 (br s)	4.62 (q, 3.0)	4.09 (q, 3.0)	4.07 (q, 3.0)	4.22 (br s)	3.78 (q, 3.0)
-4''	3.48 (br d, 9.5)	3.47 (dd, 9.0, 3.0)	3.48 (dd, 9.5, 3.0)	3.48 (dd, 9.5, 3.0)	3.20 (dd, 9.5, 3.0)	3.21 (dd, 9.5, 3.0)
-5''	4.24 (dq, 9.5, 6.5)	4.24[a)]	4.17 (dq, 9.5, 6.5)	4.16 (dq, 9.5, 6.5)	3.77 (dq, 9.5, 6.5)	3.86 (dq, 9.5, 6.5)
-6''	1.38 (d, 6.5)	1.38 (d, 6.5)	1.33 (d, 6.5)	1.33 (d, 6.5)	1.22 (d, 6.5)	1.22 (d, 6.5)
	Dig	Dig	Dig	Dig	Cym	Ole
H-1'''	5.38 (dd, 9.5, 2.0)	5.37 (dd, 9.5, 2.0)	5.32 (dd, 9.5, 2.0)	5.30 (dd, 9.5, 2.0)	4.82 (dd, 9.5, 2.0)	4.45 (dd, 9.5, 2.0)
-2'''						
-3'''	4.64 (br s)	4.59 (q, 3.0)	4.64 (q, 3.0)	4.59 (q, 3.0)	3.81 (q, 3.0)	
-4'''	3.48 (br d, 9.5)	3.41 (dd, 9.5, 3.0)	3.51 (dd, 9.5, 3.0)	3.43 (dd, 9.5, 3.0)	3.22 (dd, 9.5, 3.0)	3.17 (t, 8.5)
-5'''	4.30 (dq, 9.5, 6.5)	4.28 (dq, 9.5, 6.5)	4.30 (dq, 9.5, 6.5)	4.27 (dq, 9.5, 6.5)	3.91 (dq, 9.5, 6.5)	3.31 (dq, 8.5, 6.0)
-6'''	1.40 (d, 6.5)	1.36 (d, 6.5)	1.46 (d, 6.5)	1.42 (d, 6.5)	1.22 (d, 6.5)	1.30 (d, 6.0)
	Ole	Ole	Ole	Ole	Ole	Ole
H-1''''	4.80[a)]	4.72 (dd, 9.5, 2.0)	4.82[a)]	4.73 (dd, 9.5, 2.0)	4.50 (dd, 9.5, 2.0)	4.72 (dd. 9.5, 2.0)
-2''''						
-3''''	3.44[a)]	3.63[a)]	3.45[a)]	3.63[a)]		
-4''''	3.41[a)]	3.63[a)]	3.42[a)]	3.65[a)]	3.15[a)]	
-5''''	3.58 (dq, 8.5, 6.0)	3.64[a)]	3.60 (dq, 9.0, .6.5)	3.64[a)]	3.29 (dq, 9.0, 6.0)	3.31 (dq, 9.0, 6.0)
-6''''	1.50 (d, 6.0)	1.64 (d, 6.0)	1.51 (d, 6.5)	1.65 (d, 6.0)	1.32 (d, 6.0)	1.35 (d, 6.0)
		Glc		Glc		
H-1'''''	—	5.10 (d, 8.0)	—	5.10 (d, 8.0)	—	—
-2'''''	—	3.99 (t, 8.0)	—	3.99 (t, 8.0)	—	—
-3'''''	—	4.20[a,b)]	—	4.20[a,b)]	—	—
-4'''''	—	4.17 (t, 8.0)[b)]	—	4.17[a,b)]	—	—
-5'''''	—	3.94 (m)	—	3.93 (m)	—	—
-6'''''	—	4.52 (dd, 11.5, 2.5)	—	4.52 (dd, 11.5, 2.5)	—	—
	—	4.33 (dd, 11.5, 5.5)	—	4.33 (dd, 11.5, 5.5)	—	—
-OMes	3.63 (s)	3.62 (s)	3.63 (s)	3.62 (s)×2	3.46 (s)	3.45 (s)
	3.46 (s)	3.53 (s)	3.62 (s)	3.52 (s)	3.45 (s)	3.44 (s)
			3.46 (s)		3.39 (s)	3.40 (s)×2

to good agreement of the ^{1}H- and ^{13}C-NMR spectral data of the oligosaccharide moieties. Thus, the structures of **7—9** were established as shown in Chart 1.

The FAB-MS spectra revealed that the molecular formulae of compounds **10—13** were $C_{62}H_{92}O_{23}$, $C_{62}H_{94}O_{23}$, $C_{58}H_{92}O_{23}$ and $C_{60}H_{90}O_{23}$. ^{1}H- and ^{13}C-NMR spectra and acid hydrolysis suggested that **10—13** possessed **36—39** as each aglycone moiety, and shared the same oligosaccharide sequence which consisted of one β-D-cymaropyranose, two β-D-digitoxopyranose, one β-D-oleandropyranose and one β-D-glucopyranose. As the ^{1}H- and ^{13}C-NMR spectral data of the sugar moieties in **10—13** agreed with those of lineolon 3-O-β-D-glucopyranosyl-(1→4)-β-D-oleandropyranosyl-(1→4)-β-D-digitoxopyranosyl-(1→4)-β-D-digitoxopyranosyl-(1→4)-β-D-cymaropyranoside,[1)] the sugar sequences of **10—13** were determined to be 3-O-β-D-glucopyranosyl-(1→4)-β-D-oleandropyranosyl-(1→4)-β-D-digitoxopyranosyl-(1→4)-β-D-digitoxopyranosyl-(1→4)-β-D-cymaropyranoside. Moreover, enzymatic hydrolysis with cellulase afforded **6—9** from **10—13**, respectively.

Compounds **14—19** had the molecular formulae, $C_{57}H_{84}O_{18}$, $C_{57}H_{86}O_{18}$, $C_{63}H_{94}O_{23}$, $C_{63}H_{96}O_{23}$, $C_{59}H_{94}O_{23}$ and $C_{61}H_{92}O_{23}$ as determined by FAB-MS. By acid hydrolysis, compounds **14—19** produced ikemagenin from **14** and **16**, **37** from **15** and **17**, **38** from **18** and **39** from **19** as the agly-

cone moieties. Cymarose, digitoxose and oleandrose were also yielded from **14—19**, and additionally, **16—19** afforded glucose. The sugar linkages of these compounds were determined by comparing the ^{1}H- and ^{13}C-NMR spectral data of the known compounds in the aerial part of this plant. The NMR spectral data of the sugar moiety in **14, 15** and **16—19** were identified with those of isolineolon 3-O-β-D-oleandropyranosyl-(1→4)-β-D-digitoxopyranosyl-(1→4)-β-D-cymaropyranosyl-(1→4)-β-D-cymaropyranoside[1)] and 15β-hydroxylineolon β-D-glucopyranosyl-(1→4)-β-D-oleandropyranosyl-(1→4)-β-D-digitoxopyranosyl-(1→4)-β-D-cymaropyranosyl-(1→4)-β-D-cymaropyranoside,[1)] respectively. Therefore, the structures of **14—19** were determined as presented in Chart 1. Moreover, the enzymatic hydrolysis of **16** and **17** produced **14** and **15**, respectively, and the ^{1}H-NMR spectral data of the sugar moieties of the derivatives which were produced from **18** and **19** by enzymatic hydrolysis were consistent with those of **14**.

The molecular formula of compound **20** was considered to be $C_{57}H_{84}O_{18}$ on FAB-MS. On the basis of acid hydrolysis and the NMR spectral data, **20** was deduced to be ikemagenin 3-O-tetraoside whose sugar moiety consisted of two β-D-cymaropyranose, one β-D-digitoxopyranose and one β-D-oleandropyranose, the same as that of **14**. However, in the ^{1}H- and ^{13}C-NMR spectral measurement of pyridine-d_5 solu-
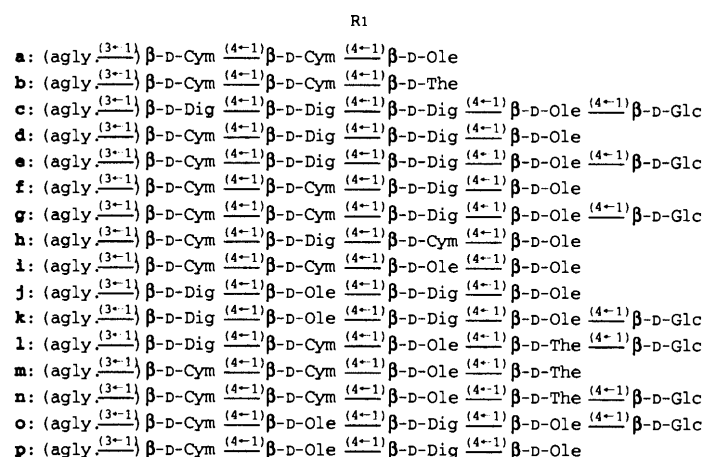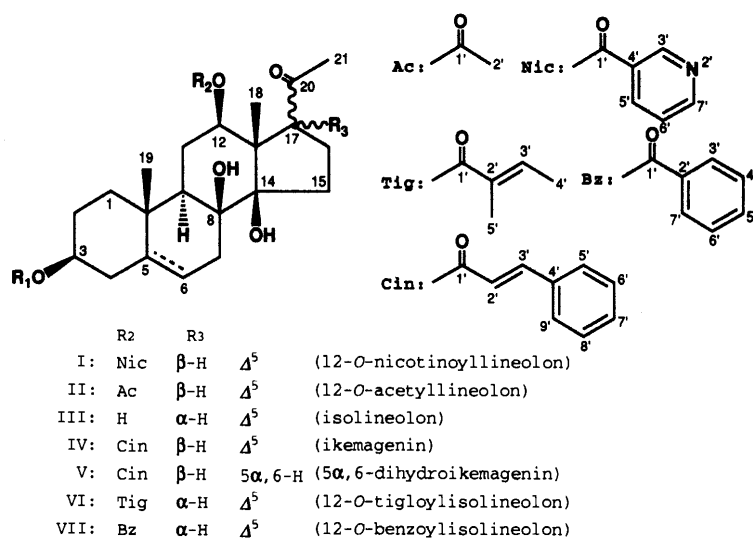
Table 3. (continued)

Proton No.	22	24	25	29	32	32'
	Dig	Dig	Cym	Cym	Cym	Cym
H-1'	4.93 (dd, 9.5, 2.0)	5.47 (dd, 9.5, 2.0)	5.28 (dd, 9.5, 2.0)	5.28 (dd, 9.5, 2.0)	5.28 (dd, 9.5, 2.0)	4.85 (dd, 9.5, 2.5)
-3'	4.22 (br s)	4.62 (q, 3.0)	4.09 (q, 3.0)	4.09 (q, 3.0)	4.05 (q, 3.0)	3.79 (q, 3.0)
-4'	3.20 (dd, 9.5, 3.0)	3.50[a]	3.51[a]	3.51[a]	3.51[a]	3.21 (dd, 9.5, 3.0)
-5'	3.80 (dq, 9.5, 6.5)	4.28 (dq, 9.5, 6.5)	4.22 (dq, 9.5, 6.5)	4.22[a]	4.23 (dq, 9.5, 6.5)	3.87 (dq, 9.5, 6.5)
-6'	1.24 (d, 6.5)	1.43 (d, 6.5)	1.38 (d, 6.5)	1.39 (d, 6.5)	1.44 [a]	1.22 (d, 6.5)
	Ole	Cym	Cym	Cym	Ole	Ole
H-1"	4.50 (dd, 9.5, 2.0)	5.16 (dd, 9.5, 2.0)	5.12 (dd, 9.5, 2.0)	5.12[a]	4.70 (dd, 9.5, 2.0)	4.44 (dd, 9.5, 2.0)
-3"	3.32[a]	4.00[a]	4.02 (q, 3.0)	4.02[a]	3.59[a]	3.35[a]
-4"	3.19 (t, 8.5)	3.39 (dd, 9.5, 3.0)	3.44 (dd, 9.5, 3.0)	3.43 (dd, 9.5, 3.0)	3.54[a]	3.19 (t, 8.5)
-5"	3.32[a]	4.17 (dq, 9.5, 6.5)	4.17 (dq, 9.5, 6.5)	4.16 (dq, 9.5, 6.5)	3.52[a]	3.28 (dq, 8.5, 6.0)
-6"	1.28 (d, 6.5)	1.31 (d, 6.5)	1.39 (d, 6.5)	1.37 (d, 6.5)	1.44[a]	1.28 (d, 6.0)
	Dig	Ole	Ole	Ole	Dig	Dig
H-1‴	5.01 (dd, 9.5, 2.0)	4.66 (br d, 9.5)	4.69 (dd, 9.5, 2.0)	4.68 (dd, 9.5, 2.0)	5.48 (dd, 9.5, 2.0)	5.00 (dd, 9.5, 2.0)
-2‴						
-3‴	4.22 (br s)	3.55[a]	3.58[a]	3.57[a]	4.61 (q, 3.0)	4.23 (q, 3.0)
-4‴	3.21 (dd, 9.5, 3.0)	3.61 (t, 8.0)	3.67 (t, 8.5)	3.59[a]	3.45 (dd, 9.5, 3.0)	3.22 (dd, 9.5, 3.0)
-5‴	3.83 (dq, 9.5, 6.5)	3.55[a]	3.58[a]	3.57[a]	4.29 (dq, 9.5, 6.5)	3.82 (dq, 9.5, 6.5)
-6‴	1.27 (d, 6.5)	1.66 (d, 6.0)	1.70 (d, 6.0)	1.66 (d, 6.5)	1.44[a]	1.27 (d, 6.5)
	Ole	The	The	The	Ole	Ole
H-1⁗	4.55 (dd, 9.5, 2.0)	4.87[a]	4.95 (d, 8.0)	4.87 (d, 8.0)	4.73 (dd, 9.5, 2.0)	4.55 (dd, 9.5, 2.0)
-2⁗		3.89 (t, 8.5)	3.91[a]	3.89[a]		
-3⁗	3.15[a]	3.68 (t, 8.5)	3.60[a]	3.68 (t, 8.5)	3.65[a]	3.16 (m)
-4⁗	3.12 (t, 8.5)	3.86 (t, 8.5)	3.60[a]	3.86 (t, 8.5)	3.65[a]	
-5⁗	3.32[a]	3.74 (dq, 8.5, 6.0)	3.72 (dq, 8.5, 6.0)	3.74 (dq, 8.5, 6.5)	3.65[a]	3.32 (dq, 8.5, 6.0)
-6⁗	1.31 (d, 6.5)	1.75 (d, 6.0)	1.59 (d, 6.0)	1.75 (d, 6.5)	1.65 (d, 6.0)	1.31 (d, 6.0)
		Glc		Glc	Glc	
H-1⁗′	—	5.12 (d, 8.0)	—	5.12 (d, 8.0)	5.10 (d, 8.0)	—
-2⁗′	—	4.01 (t, 8.0)	—	4.02[a]	3.99 (t, 8.0)	—
-3⁗′	—	4.20[a]	—	4.20[a]	4.19[a,b]	—
-4⁗′	—	4.20[a]	—	4.20[a]	4.17[a,b]	—
-5⁗′	—	3.95 (m)	—	3.95 (m)	3.93 (m)	—
-6⁗′	—	4.51 (dd, 11.5, 2.5)	—	4.51 (dd, 11.5, 2.5)	4.52 (dd, 11.5, 2.5)	—
	—	4.33 (dd, 11.5, 5.5)	—	4.34 (dd, 11.5, 5.5)	4.33 (dd, 11.5, 5.5)	—
-OMes	3.41 (s)	3.93 (s)	3.89 (s)	3.93 (s)	3.58 (s)	3.40 (s)×2
	3.40 (s)	3.57 (s)	3.62 (s)	3.62 (s)	3.56 (s)	3.45 (s)
		3.50 (s)	3.58 (s)	3.57 (s)	3.51 (s)	
			3.53 (s)	3.50 (s)		

tion (see Table 2 and Experimental), chemical shifts of the anomeric proton signals were slightly different from those of **14**. Assignments of the proton signals of the sugar moiety are shown in Table 3 based on the ^{1}H–^{1}H COSY spectrum starting from the anomeric proton signals. In the NOE difference experiments with irradiation at the anomeric proton signals, NOEs were observed as follows, δ 4.85 (H-1' of β-D-cymaropyranose) and 3.57 (H-3 of the aglycone), δ 4.83 (H-1" of β-D-digitoxopyranose) and 3.23 (H-4' of β-D-cymaropyranose), δ 4.82 (H-1‴ of β-D-cymaropyranose) and 3.20 (H-4" of β-D-digitoxopyranose), δ 4.50 (H-1⁗ of β-D-oleandropyranose) and 3.22 (H-4‴ of β-D-cymaropyranose). Consequently, **20** was proved to be ikemagenin 3-O-β-D-oleandropyranosyl-(1→4)-β-D-cymaropyranosyl-(1→4)-β-D-digitoxopyranosyl-(1→4)-β-D-cymaropyranoside.

The NMR spectra of compounds **21** and **22** were suggested to be ikemagenin 3-O-tetraosides. Acid hydrolysis afforded cymarose and oleandrose from **21** and digitoxose and oleandrose from **22** as the component sugars. According to identification of the NMR spectral data of each sugar moiety with those of calotroposide E[16] and lineolon 3-O-β-oleandropyranosyl-(1→4)-β-digitoxopyranosyl-(1→4)-β-oleandropyranosyl-(1→4)-β-digitoxopyranoside,[17] the structures of **21** and **22** were shown as presented in Chart 1.

Compounds **24, 29—31** and **25—28** were supposed to be pregnane 3-O-pentaosides and pregnane 3-O-tetraosides, respectively, by observation of anomeric proton and carbon signals in the NMR spectra. Acid hydrolysis of **24—31** yielded **36** from **25** and **29**, **38** from **24, 27** and **30**, **39** from **28** and **31** and **34** from **26**; in addition, monosaccharides were obtained as follows: digitoxose, cymarose, oleandrose, thevetose and glucose from **24**, cymarose, oleandrose, and thevetose from **25—28**, and cymarose, oleandrose, thevetose and glucose from **29—31**. Because the ^{1}H- and ^{13}C-NMR spectral data of the oligosaccharide moieties in these compounds were identified with those of pregnane glycosides from the aerial part of this plant,[2] metaplexigenin 3-O-β-D-glucopyranosyl-(1→4)-β-D-thevetopyranosyl-(1→4)-β-D-oleandropyranosyl-(1→4)-β-D-cymaropyranosyl-(1→4)-β-D-digitoxopyranoside, 15β-hydroxylineolon 3-O-β-D-thevetopyranosyl-(1→4)-β-D-oleandropyranosyl-(1→4)-β-D-cymaropyranosyl-(1→4)-β-D-cymaropyranoside and 15β-hydroxylineolon 3-O-β-D-glucopyranosyl-(1→4)-β-D-thevetopyranosyl-(1→4)-β-D-oleandropyranosyl-(1→4)-β-D-cymaropyranosyl-(1→4)-β-D-cymaropyranoside, the structures of **24—31** were determined to be as shown in Chart 1. Also **25, 27** and **28** were obtained from **29—31** by enzymatic hydrolysis, respectively.

R=H: D-Digitoxopyranose   D-Oleandropyranose   D-Thevetopyranose
R=CH₃: D-Cymaropyranose

	R2	R3		
I:	Nic	β-H	Δ⁵	(12-O-nicotinoyllineolon)
II:	Ac	β-H	Δ⁵	(12-O-acetyllineolon)
III:	H	α-H	Δ⁵	(isolineolon)
IV:	Cin	β-H	Δ⁵	(ikemagenin)
V:	Cin	β-H	5α,6-H	(5α,6-dihydroikemagenin)
VI:	Tig	α-H	Δ⁵	(12-O-tigloylisolineolon)
VII:	Bz	α-H	Δ⁵	(12-O-benzoylisolineolon)

R1

a: (agly.$\frac{(3\leftarrow1)}{}$) β-D-Cym $\frac{(4\leftarrow1)}{}$β-D-Cym $\frac{(4\leftarrow1)}{}$β-D-Ole
b: (agly.$\frac{(3\leftarrow1)}{}$) β-D-Cym $\frac{(4\leftarrow1)}{}$β-D-Cym $\frac{(4\leftarrow1)}{}$β-D-The
c: (agly.$\frac{(3\leftarrow1)}{}$) β-D-Dig $\frac{(4\leftarrow1)}{}$β-D-Dig $\frac{(4\leftarrow1)}{}$β-D-Dig $\frac{(4\leftarrow1)}{}$β-D-Ole $\frac{(4\leftarrow1)}{}$β-D-Glc
d: (agly.$\frac{(3\leftarrow1)}{}$) β-D-Cym $\frac{(4\leftarrow1)}{}$β-D-Dig $\frac{(4\leftarrow1)}{}$β-D-Dig $\frac{(4\leftarrow1)}{}$β-D-Ole
e: (agly.$\frac{(3\leftarrow1)}{}$) β-D-Cym $\frac{(4\leftarrow1)}{}$β-D-Dig $\frac{(4\leftarrow1)}{}$β-D-Dig $\frac{(4\leftarrow1)}{}$β-D-Ole $\frac{(4\leftarrow1)}{}$β-D-Glc
f: (agly.$\frac{(3\leftarrow1)}{}$) β-D-Cym $\frac{(4\leftarrow1)}{}$β-D-Cym $\frac{(4\leftarrow1)}{}$β-D-Dig $\frac{(4\leftarrow1)}{}$β-D-Ole
g: (agly.$\frac{(3\leftarrow1)}{}$) β-D-Cym $\frac{(4\leftarrow1)}{}$β-D-Cym $\frac{(4\leftarrow1)}{}$β-D-Dig $\frac{(4\leftarrow1)}{}$β-D-Ole $\frac{(4\leftarrow1)}{}$β-D-Glc
h: (agly.$\frac{(3\leftarrow1)}{}$) β-D-Cym $\frac{(4\leftarrow1)}{}$β-D-Dig $\frac{(4\leftarrow1)}{}$β-D-Cym $\frac{(4\leftarrow1)}{}$β-D-Ole
i: (agly.$\frac{(3\leftarrow1)}{}$) β-D-Cym $\frac{(4\leftarrow1)}{}$β-D-Cym $\frac{(4\leftarrow1)}{}$β-D-Ole $\frac{(4\leftarrow1)}{}$β-D-Ole
j: (agly.$\frac{(3\leftarrow1)}{}$) β-D-Dig $\frac{(4\leftarrow1)}{}$β-D-Ole $\frac{(4\leftarrow1)}{}$β-D-Dig $\frac{(4\leftarrow1)}{}$β-D-Ole
k: (agly.$\frac{(3\leftarrow1)}{}$) β-D-Dig $\frac{(4\leftarrow1)}{}$β-D-Ole $\frac{(4\leftarrow1)}{}$β-D-Dig $\frac{(4\leftarrow1)}{}$β-D-Ole $\frac{(4\leftarrow1)}{}$β-D-Glc
l: (agly.$\frac{(3\leftarrow1)}{}$) β-D-Dig $\frac{(4\leftarrow1)}{}$β-D-Cym $\frac{(4\leftarrow1)}{}$β-D-Ole $\frac{(4\leftarrow1)}{}$β-D-The $\frac{(4\leftarrow1)}{}$β-D-Glc
m: (agly.$\frac{(3\leftarrow1)}{}$) β-D-Cym $\frac{(4\leftarrow1)}{}$β-D-Cym $\frac{(4\leftarrow1)}{}$β-D-Ole $\frac{(4\leftarrow1)}{}$β-D-The
n: (agly.$\frac{(3\leftarrow1)}{}$) β-D-Cym $\frac{(4\leftarrow1)}{}$β-D-Cym $\frac{(4\leftarrow1)}{}$β-D-Ole $\frac{(4\leftarrow1)}{}$β-D-The $\frac{(4\leftarrow1)}{}$β-D-Glc
o: (agly.$\frac{(3\leftarrow1)}{}$) β-D-Cym $\frac{(4\leftarrow1)}{}$β-D-Ole $\frac{(4\leftarrow1)}{}$β-D-Dig $\frac{(4\leftarrow1)}{}$β-D-Ole $\frac{(4\leftarrow1)}{}$β-D-Glc
p: (agly.$\frac{(3\leftarrow1)}{}$) β-D-Cym $\frac{(4\leftarrow1)}{}$β-D-Ole $\frac{(4\leftarrow1)}{}$β-D-Dig $\frac{(4\leftarrow1)}{}$β-D-Ole

(agly.: aglycone, Dig: digitoxopyranosyl, Cym: cymaropyranosyl, Ole: oleandropyranosyl, The: thevetopyranosyl, Glc: glucopyranosyl)

1:	I -a	11:	V -e	21:	IV -i	31:	VII -n
2:	II -a	12:	VI -e	22:	IV -j	32:	IV -o
3:	III -a	13:	VII -e	23:	IV -k	32':	IV -p
4:	IV -b	14:	IV -f	24:	VI -l	33:	I -H
5:	IV -c	15:	V -f	25:	IV -m	34:	II -H
6:	IV -d	16:	IV -g	26:	II -m	35:	III -H
7:	V -d	17:	V -g	27:	VI -m	36:	IV -H
8:	VI -d	18:	VI -g	28:	VII -m	37:	V -H
9:	VII -d	19:	VII -g	29:	IV -n	38:	VI -H
10:	IV -e	20:	IV -h	30:	VI -n	39:	VII -H

R
CH₂OH (frugoside)
CHO (gofruside)

Chart 1

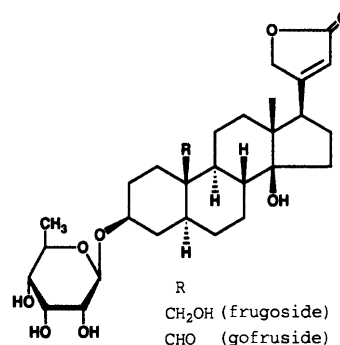R=H: D-Digitoxopyranose   D-Oleandropyranose   D-Thevetopyranose
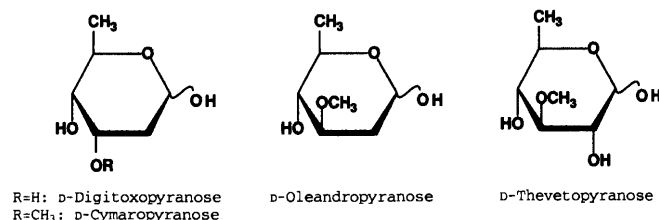R=CH₃: D-Cymaropyranose

Chart 2

Compound 32 was considered to be ikemagenin 3-O-pentaoside whose molecular formula was $C_{63}H_{94}O_{23}$, the same as that of 16 on the basis of acid hydrolysis and FAB-MS. Comparison of the ¹H- and ¹³C-NMR spectra of 32 with those of 16 revealed that the sugar sequence of 32 was composed of one β-D-cymaropyranose, two β-D-oleandropyranose, one β-

D-digitoxopyranose and one β-D-glucopyranose, in which β-D-glucopyranose existed as the terminal sugar. On enzymatic hydrolysis of 32 with cellulase, 32 yielded 32'. The ¹H- and ¹³C-NMR spectra suggested that 32' was ikemagenin 3-O-tetraoside which lost the terminal β-D-glucopyranose in the sugar sequence of 32. The ¹H–¹H COSY experiment of 32' starting from each anomeric proton signal enabled us to assign the proton signals due to each monosaccharide in Table 3. On the NOE difference experiments involving irradiation at each anomeric proton signal, NOEs were observed between δ 4.85 (H-1' of β-D-cymaropyranose) and 3.56 (H-3 of the aglycone), δ 4.44 (H-1" of β-D-oleandropyranose) and 3.21 (H-4' of β-D-cymaropyranose), δ 5.00 (H-1''' of β-D-digitoxopyranose) and 3.19 (H-4" of β-D-oleandropyranose), δ 4.55 (H-1'''' of β-D-oleandropyranose) and 3.22 (H-4''' of β-D-digitoxopyranose). Then, the sugar sequence of 32' was

determined to be 3-O-β-D-oleandropyranosyl-(1→4)-β-D-digitoxopyranosyl-(1→4)-β-D-oleandropyranosyl-(1→4)-β-D-cymaropyranoside. Furthermore, in the NOE difference experiment of **32**, irradiation of the anomeric proton signal of β-D-glucopyranose (δ 5.10) showed a NOE on the H-4'''' signal of β-D-oleandropyranose (δ 3.65). Based on the above evidence, the structure of **32** was elucidated as presented in Chart 1.

Experimental

General Procedure Instrumental analyses were carried out as described previously.[1]

Extraction and Isolation The root of *Asclepias incarnata* L. (870 g) were extracted twice with MeOH under reflux. The extract was concentrated under reduced pressure and the residue was suspended in H_2O. This suspension was extracted with Et_2O. The H_2O layer was passed through a Mitsubishi Diaion HP-20 column, and adsorbed material was eluted with 50% MeOH in water, 70% MeOH in water and MeOH. The Et_2O layer, 70% MeOH eluate and MeOH eluate of the HP-20 column were concentrated, respectively. These residues were then rechromatographed on a silica gel column with a $CHCl_3$–MeOH (98:2—85:15) system and semi-preparative HPLC (Develosil-ODS, PhA, C-8 and YMC-ODS: 45—62.5% MeCN in water and 75—82.5% MeOH in water) to give compounds **1** (4 mg), **2** (8 mg), **3** (5 mg), **4** (4 mg), **5** (11 mg), **6** (24 mg), **7** (7 mg), **8** (3 mg), **9** (3 mg), **10** (28 mg), **11** (4 mg), **12** (9 mg), **13** (9 mg), **14** (23 mg), **15** (5 mg), **16** (206 mg), **17** (10 mg), **18** (13 mg), **19** (10 mg), **20** (3 mg), **21** (7 mg), **22** (5 mg), **23** (16 mg), **24** (4 mg), **25** (22 mg), **26** (6 mg), **27** (6 mg), **28** (11 mg), **29** (16 mg), **30** (15 mg), **31** (10 mg), and **32** (6 mg) in addition to frugoside (83 mg) and gofruside (51 mg). All compounds were obtained as amorphous powders.

Compound **2**: $[\alpha]_D^{25}$ −20.9° (c=0.75, MeOH). FAB-MS m/z: 861 $[M+Na]^+$. ^{13}C- and ^1H-NMR: shown in Tables 1—3.

Compound **3**: $[\alpha]_D^{25}$ +39.7° (c=0.53, MeOH). FAB-MS m/z: 797 $[M+H]^+$, 819 $[M+Na]^+$. ^{13}C-NMR: shown in Table 1. The ^{13}C- and ^1H-NMR spectra of the sugar moiety were in good agreement with those of **2**.

Compound **4**: $[\alpha]_D^{25}$ +19.3° (c=0.29, MeOH). FAB-MS m/z: 965 $[M+Na]^+$. UV λ_{max}^{MeOH} nm (log ε): 217 (4.24), 223 (4.18), 278 (4.42). ^{13}C- and ^1H-NMR: shown in Tables 1—3.

Compound **5**: $[\alpha]_D^{25}$ +7.7° (c=1.13, MeOH). FAB-MS m/z: 1213 $[M+Na]^+$. UV λ_{max}^{MeOH} nm (log ε): 217 (4.13), 222 (4.06), 278 (4.32). ^{13}C- and ^1H-NMR: shown in Tables 2 and 3. The ^{13}C-NMR spectrum of the aglycone moiety was in good agreement with that of **4**.

Compound **7**: $[\alpha]_D^{25}$ +12.7° (c=0.64, MeOH). FAB-MS m/z: 1067 $[M+Na]^+$. UV λ_{max}^{MeOH} nm (log ε): 217 (4.21), 223 (4.15), 278 (4.39). ^{13}C-NMR: shown in Table 1. The ^{13}C- and ^1H-NMR spectra of the sugar moiety were in good agreement with those of **8**.

Compound **8**: $[\alpha]_D^{25}$ +32.9° (c=0.31, MeOH). FAB-MS m/z: 995 $[M+H]^+$, 1017 $[M+Na]^+$. ^{13}C- and ^1H-NMR: shown in Tables 1—3.

Compound **9**: $[\alpha]_D^{25}$ +30.0° (c=0.32, MeOH). FAB-MS m/z: 1039 $[M+Na]^+$. UV λ_{max}^{MeOH} nm (log ε): 230 (4.14), 274 (3.28), 280 (3.23). ^{13}C-NMR: shown in Table 1. The ^{13}C- and ^1H-NMR spectra of the sugar moiety were in good agreement with those of **8**.

Compound **10**: $[\alpha]_D^{25}$ +12.3° (c=1.20, MeOH). FAB-MS m/z: 1227 $[M+Na]^+$. UV λ_{max}^{MeOH} nm (log ε): 216 (4.14), 222 (4.07), 278 (4.32). ^{13}C- and ^1H-NMR: shown in Tables 2 and 3. The ^{13}C-NMR spectrum of the aglycone moiety was in good agreement with that of **4**.

Compound **11**: $[\alpha]_D^{25}$ +13.1° (c=0.42, MeOH). FAB-MS m/z: 1229 $[M+Na]^+$. UV λ_{max}^{MeOH} nm (log ε): 217 (4.25), 278 (4.37). The ^{13}C- and ^1H-NMR spectra of the aglycone moiety and the sugar moiety were in good agreement with those of **7** and **10**.

Compound **12**: $[\alpha]_D^{25}$ +24.1° (c=0.89, MeOH). FAB-MS m/z: 1179 $[M+Na]^+$. The ^{13}C- and ^1H-NMR spectra of the aglycone moiety and the sugar moiety were in good agreement with those of **8** and **10**.

Compound **13**: $[\alpha]_D^{25}$ +24.7° (c=0.88, MeOH). FAB-MS m/z: 1201 $[M+Na]^+$. UV λ_{max}^{MeOH} nm (log ε): 228 (4.10), 274 (3.42). The ^{13}C- and ^1H-NMR spectra of the aglycone moiety and the sugar moiety were in good agreement with those of **9** and **10**.

Compound **14**: $[\alpha]_D^{25}$ +17.1° (c=0.97, MeOH). FAB-MS m/z: 1079 $[M+Na]^+$. UV λ_{max}^{MeOH} nm (log ε): 216 (4.19), 222 (4.12), 278 (4.36). The ^{13}C- and ^1H-NMR: shown in Tables 2 and 3. The ^{13}C-NMR spectrum of the aglycone moiety was in good agreement with that of **4**.

Compound **15**: $[\alpha]_D^{25}$ +15.8° (c=0.49, MeOH). FAB-MS m/z: 1081

$[M+Na]^+$. UV λ_{max}^{MeOH} nm (log ε): 217 (4.18), 222 (4.12), 278 (4.36). The ^{13}C- and ^1H-NMR spectra of the aglycone moiety and the sugar moiety were in good agreement with those of **7** and **14**.

Compound **16**: $[\alpha]_D^{25}$ +15.1° (c=1.26, MeOH). FAB-MS m/z: 1241 $[M+Na]^+$. UV λ_{max}^{MeOH} nm (log ε): 216 (4.17), 222 (4.08), 278 (4.35). ^{13}C- and ^1H-NMR: shown in Tables 2 and 3. The ^{13}C-NMR spectrum of the aglycone moiety was in good agreement with that of **4**.

Compound **17**: $[\alpha]_D^{24}$ +13.3° (c=0.87, MeOH). FAB-MS m/z: 1243 $[M+Na]^+$. UV λ_{max}^{MeOH} nm (log ε): 202 (4.31), 217 (4.23), 222 (4.18), 278 (4.36). The ^{13}C- and ^1H-NMR spectra of the aglycone moiety and the sugar moiety were in good agreement with those of **7** and **16**.

Compound **18**: $[\alpha]_D^{25}$ +26.4° (c=1.33, MeOH). FAB-MS m/z: 1193 $[M+Na]^+$. The ^{13}C- and ^1H-NMR spectra of the aglycone moiety and the sugar moiety were in good agreement with those of **8** and **16**.

Compound **19**: $[\alpha]_D^{25}$ +27.1° (c=0.99, MeOH). FAB-MS m/z: 1215 $[M+Na]^+$. UV λ_{max}^{MeOH} nm (log ε): 229 (4.31), 273 (3.25). The ^{13}C- and ^1H-NMR spectra of the aglycone moiety and the sugar moiety were in good agreement with those of **9** and **16**.

Compound **20**: $[\alpha]_D^{25}$ +17.5° (c=0.28, MeOH). FAB-MS m/z: 1079 $[M+Na]^+$. UV λ_{max}^{MeOH} nm (log ε): 217 (4.21), 223 (4.15), 278 (4.39). ^{13}C- and ^1H-NMR: shown in Tables 2 and 3. ^1H-NMR (pyridine(Py)-d_5 at 35 °C): δ 5.32 (dd, 9.5, 2.0, H-1'' of β-D-digitoxopyranose), 5.28 (dd, 9.5, 2.0, H-1' of β-D-cymaropyranose), 5.16 (dd, 9.5, 2.0, H-1''' of β-D-cymaropyranose), 4.76 (dd, 9.5, 2.0, H-1'''' of β-D-oleandropyranose). The ^{13}C-NMR spectrum of the aglycone moiety was in good agreement with that of **4**.

Compound **21**: $[\alpha]_D^{24}$ +3.6° (c=0.65, MeOH). FAB-MS m/z: 1093 $[M+Na]^+$. UV λ_{max}^{MeOH} nm (log ε): 217 (4.24), 223 (4.17), 278 (4.40). ^{13}C- and ^1H-NMR: shown in Tables 2 and 3. The ^{13}C-NMR spectrum of the aglycone moiety was in good agreement with that of **4**.

Compound **22**: $[\alpha]_D^{25}$ −2.1° (c=0.46, MeOH). FAB-MS m/z: 1065 $[M+Na]^+$. UV λ_{max}^{MeOH} nm (log ε): 202 (4.40), 217 (4.25), 222 (4.18), 277 (4.41). ^{13}C- and ^1H-NMR: shown in Tables 2 and 3. The ^{13}C-NMR spectrum of the aglycone moiety was in good agreement with that of **4**.

Compound **24**: $[\alpha]_D^{25}$ +20.1° (c=0.36, MeOH). FAB-MS m/z: 1209 $[M+Na]^+$. ^{13}C- and ^1H-NMR: shown in Tables 2 and 3. The ^{13}C-NMR spectrum of the aglycone moiety was in good agreement with those of **8**.

Compound **25**: $[\alpha]_D^{25}$ +10.3° (c=1.34, MeOH). FAB-MS m/z: 1109 $[M+Na]^+$. UV λ_{max}^{MeOH} nm (log ε): 216 (4.23), 222 (4.16), 278 (4.40). ^{13}C- and ^1H-NMR: shown in Tables 2 and 3. The ^{13}C-NMR spectrum of the aglycone moiety was in good agreement with that of **4**.

Compound **26**: $[\alpha]_D^{25}$ −17.9° (c=0.64, MeOH). FAB-MS m/z: 1021 $[M+Na]^+$. The ^{13}C- and ^1H-NMR spectra of the aglycone moiety and the sugar moiety were in good agreement with those of **2** and **25**.

Compound **27**: $[\alpha]_D^{25}$ +24.7° (c=0.60, MeOH). FAB-MS m/z: 1061 $[M+Na]^+$. The ^{13}C- and ^1H-NMR spectra of the aglycone moiety and the sugar moiety were in good agreement with those of **8** and **25**.

Compound **28**: $[\alpha]_D^{25}$ +24.2° (c=1.12, MeOH). FAB-MS m/z: 1083 $[M+Na]^+$. UV λ_{max}^{MeOH} nm (log ε): 229 (4.11), 278 (2.99), 280 (2.93). The ^{13}C- and ^1H-NMR spectra of the aglycone moiety and the sugar moiety were in good agreement with those of **9** and **25**.

Compound **29**: $[\alpha]_D^{25}$ +10.7° (c=0.61, MeOH). FAB-MS m/z: 1271 $[M+Na]^+$. UV λ_{max}^{MeOH} nm (log ε): 217 (4.25), 222 (4.19), 278 (4.44). ^{13}C- and ^1H-NMR: shown in Tables 2 and 3. The ^{13}C-NMR spectrum of the aglycone moiety was in good agreement with that of **4**.

Compound **30**: $[\alpha]_D^{25}$ +22.1° (c=1.12, MeOH). FAB-MS m/z: 1223 $[M+Na]^+$. The ^{13}C- and ^1H-NMR spectra of the aglycone moiety and the sugar moiety were in good agreement with those of **8** and **29**.

Compound **31**: $[\alpha]_D^{25}$ +24.0° (c=1.01, MeOH). FAB-MS m/z: 1245 $[M+Na]^+$. UV λ_{max}^{MeOH} nm (log ε): 230 (4.16), 273 (2.93). The ^{13}C- and ^1H-NMR spectra of the aglycone moiety and the sugar moiety were in good agreement with those of **9** and **29**.

Compound **32**: $[\alpha]_D^{25}$ +1.4° (c=0.53, MeOH). FAB-MS m/z: 1241 $[M+Na]^+$. UV λ_{max}^{MeOH} nm (log ε): 217 (4.23), 222 (4.15), 278 (4.38). The ^{13}C- and ^1H-NMR: shown in Tables 2 and 3. The ^{13}C-NMR spectrum of the aglycone moiety was in good agreement with that of **4**.

Acid Hydrolysis of a Mixture of Pregnane Glycosides The fraction of pregnane glycosides eluted from the $CHCl_3$–MeOH (96:4) system on a silica gel column (600 mg) was heated at 60 °C for 5 h with dioxane (8 ml) and 0.2 N H_2SO_4 (2 ml) to obtain the aglycones and sugars. After hydrolysis, this reaction mixture was diluted with H_2O and extracted with EtOAc. The EtOAc layer was concentrated to dryness. Purification of the residue by HPLC (YMC-ODS, 67.5% MeOH in water) afforded two new 12-O-acylated pregnanes (**37** (5 mg) and **38** (2 mg)) along with isolineolon (**35**, 6 mg)[7], 12-O-acetyllineolon (**34**, 7 mg)[1], 12-O-nicotinoyllineolon (**33**, 2

mg),[5] ikemagenin (**36**, 30 mg)[8] and 12-*O*-benzoylisolineolon (**39**, 3 mg).[9]

35: ^{1}H-NMR (Py-d_5 at 35 °C): δ 5.43 (br s, H-6), 3.90 (m, H-3), 3.88 (dd, 9.5, 5.5, H-17), 3.77 (dd, 12.0, 4.5, H-12), 2.29 (s, H-21), 1.67 (dd, 13,5, 2.5, H-9), 1.57 (s, H-18), 1.48 (s, H-19).

37: $[\alpha]_D^{24}$ $-16.5°$ ($c=0.44$, MeOH), FAB-MS *m/z*: 519 [M+Na]$^+$. UV λ_{max}^{MeOH} nm (log ε): 204 (4.25), 217 (4.24), 278 (4.40). ^{13}C-NMR (Py-d_5 at 35 °C): δ 209.5 (C-20), 165.9 (C-1'), 144.8 (C-3'), 135.1 (C-4'), 130.5 (C-7'), 129.3 (C-6', 8'), 128.6 (C-5', 9'), 119.4 (C-2'), 87.6 (C-14), 76.5 (C-8), 74.0 (C-12), 70.8 (C-3), 60.5 (C-17), 56.3 (C-13), 47.6 (C-9), 45.9 (C-5), 38.9 (C-1), 38.4 (C-4), 36.7 (C-10), 35.1 (C-7), 33.9 (C-15), 32.4 (C-21), 32.0 (C-2), 25.4 (C-6), 24.1 (C-11), 22.5 (C-16), 16.2 (C-18), 13.3 (C-19). ^{1}H-NMR (Py-d_5 at 35 °C): δ 7.97 (d, 16.0, H-3'), 6.78 (d, 16.0, H-2'), 5.86 (s, 14-OH), 5.22 (dd, 10.0, 6.0, H-12), 4.30 (s, 8-OH), 3.92 (m, H-3), 3.52 (t, 9.5, H-17), 2.28 (s, H-21), 2.00 (s, H-18), 1.71 (q, 11.5, H-4ax), 1.43 (dd, 12.0, 4.0, H-9), 1.27 (s, H-19), 1.16 (overlapping, H-5).

38: $[\alpha]_D^{24}$ $+40.8°$ ($c=0.20$, MeOH). FAB-MS *m/z*: 447 [M+H]$^+$, 469 [M+Na]$^+$. ^{13}C-NMR (CDCl$_3$ at 35 °C): δ 217.4 (C-20), 167.8 (C-1'), 139.2 (C-5), 137.8 (C-3'), 128.8 (C-2'), 118.8 (C-6), 86.3 (C-14), 75.9 (C-12), 73.9 (C-8), 72.0 (C-3), 57.7 (C-17), 54.2 (C-13), 44.4 (C-9), 42.2 (C-4), 38.9 (C-1), 37.0 (C-10), 37.0, 35.6 (C-7, 15), 33.0 (C-21), 31.2 (C-2), 24.7, 24.0 (C-11, 16), 18.2 (C-19), 14.5 (C-4'), 12.1, 12.0 (C-18, 5'). ^{13}C-NMR (Py-d_5 at 35 °C): δ 214.3 (C-20), 167.8 (C-1'), 140.2 (C-5), 137.7 (C-3'), 129.4 (C-2'), 118.7 (C-6), 86.6 (C-14), 77.7 (C-12), 74.4 (C-8), 71.6 (C-3), 59.2 (C-17), 55.1 (C-13), 45.2 (C-9), 43.4 (C-4), 39.3 (C-1), 37.6 (C-10), 36.7, 35.9 (C-7, 15), 32.1 (C-2), 31.6 (C-21), 24.8, 24.6 (C-11, 16), 18.5 (C-19), 14.3 (C-4'), 12.7 (C-18), 12.3 (C-5'). ^{1}H-NMR (Py-d_5 at 35 °C): δ 7.15 (br q, 7.0, H-3'), 5.53 (s, 14-OH), 5.38 (br s, H-4), 5.09 (dd, 12.0, 4.0, H-12), 4.51 (s, 8-OH), 3.88 (m, H-3), 3.22 (dd, 9.5, 5.5, H-17), 2.25 (s, H-21), 1.99 (br s, H-5'), 1.72 (br d, 7.0, H-4'), 1.56 (s, H-18), 1.42 (s, H-19).

39: $[\alpha]_D^{24}$ $+35.0°$ ($c=0.33$, MeOH). FAB-MS *m/z*: 491 [M+Na]$^+$. UV λ_{max}^{MeOH} nm (log ε): 230 (4.18), 273 (3.06). ^{13}C-NMR (CDCl$_3$ at 35 °C): δ 217.3 (C-20), 166.4 (C-1'), 139.1 (C-5), 133.3, 130.2 (C-5', 2'), 129.6 (C-4', 6'), 128.6 (C-3', 7'), 118.8 (C-6), 86.4 (C-14), 77.2 (C-12), 73.9 (C-8), 72.0 (C-3), 57.8 (C-17), 54.3 (C-13), 44.4 (C-9), 42.1 (C-4), 38.9 (C-1), 37.1 (C-10), 37.1, 35.6 (C-7, 15), 33.0 (C-2), 31.1 (C-21), 24.7, 24.1 (C-11, 16), 18.2 (C-19), 12.2 (C-18). ^{13}C-NMR (Py-d_5 at 35 °C): δ 214.1 (C-20), 166.6 (C-1'), 140.2 (C-5), 133.6, 131.4 (C-5', 2'), 130.0 (C-4', 6'), 129.1 (C-3', 7'), 118.7 (C-6), 86.6 (C-14), 78.6 (C-12), 74.4 (C-8), 71.6 (C-3), 59.3 (C-17), 55.1 (C-13), 45.2 (C-9), 43.4 (C-4), 39.3 (C-1), 37.7 (C-10), 36.7, 35.9 (C-7, 15), 32.1 (C-21), 31.7 (C-2), 24.8, 24.7 (C-11, 16), 18.5 (C-19), 12.7 (C-18). ^{1}H-NMR (Py-d_5 at 35 °C): δ 8.37 (br d, 7.5, H-3', 7'), 7.60 (br t, 7.5, H-5'), 7.53 (br t, 7.5, H-4', 6'), 5.57 (s, 14-OH), 5.39 (br s, H-6), 5.27 (dd, 12.0, 4.0, H-12), 4.59 (s, 8-OH), 3.89 (m, H-3), 3.27 (dd, 9.5, 5.5, H-17), 2.20 (s, H-21), 1.78 (dd, 13.5, 2.5, H-9), 1.66 (s, H-18), 1.44 (s, H-19).

The H$_2$O layer was passed through an Amberlite IRA-60E column and the eluate was concentrated to dryness. The residue was chromatographed on a silica gel with a CHCl$_3$–MeOH–H$_2$O (7:1:1.2 bottom layer) system to obtain cymarose (7 mg), oleandrose (12 mg), and digitoxose (25 mg). As to the absolute configuration of each monosaccharide, all of these monosaccharides were believed to have a D-form based on their optical rotation values. [6,11,12]

D-Cymarose: $[\alpha]_D^{26}$ $+52.1°$ ($c=0.67$, 24 h after dissolution in H$_2$O). (lit: $[\alpha]_D^{21}$ $+51.6°$ ($c=1.02$, H$_2$O)).[11]

D-Oleandrose: $[\alpha]_D^{26}$ $-12.3°$ ($c=1.15$, 24 h after dissolution in H$_2$O). (lit: $[\alpha]_D$ $-11°$ ($c=1.1$, H$_2$O)).[12]

D-Digitoxose: $[\alpha]_D^{26}$ $+43.8°$ ($c=0.71$, 24 h after dissolution in H$_2$O). (lit: $[\alpha]_D^{24}$ $+48.4°$ ($c=0.90$, H$_2$O)).[6]

This H$_2$O layer also produced a disaccharide, thevetopyranosyl-(1→4)-oleandropyranoside (6 mg). Part of this disaccharide (*ca.* 0.5 mg) was hydrolyzed with 0.05 N HCl–dioxane (1:1) at 95 °C for 1.5 h, then the residue was reacted with D-cysteine methyl ester hydrochloride, hexamethyldisilazane and trimethylsilylchloride using the same procedure described in a previous report.[1,2,18,19] After a series of reactions, the precipitate was centrifuged and the supernatant was subjected to GC analysis. GC conditions: column, GL capillary column TC-1 (GL Sciences, Inc., Tokyo, Japan) 0.32 mm×30 m, carrier gas N$_2$, column temperature 195 °C; t_R D-thevetose 15.5 min, L-thevetose 14.0 min. The t_R for D-thevetose was obtained from its enantiomer (L-thevetose+L-cysteine). D-Thevetose was detected from this disaccharide.

Alkaline Hydrolysis of Compounds 37 and 38 Solutions of compounds **37** and **38** (*ca.* 0.3 mg) were hydrolyzed with 2 N NaOH aq. and dioxane (each 40 μl) at 60 °C for 2 h in N$_2$ atmosphere. After alkaline hydrolysis, the reaction mixture was diluted with H$_2$O, then 1 N HCl (*ca.* 100 μl) was added to them. Next, the ester moiety was extracted with di-

ethylether. HPLC analysis suggested that cinnamic acid, tiglic acid and benzoic acid were yielded from **37** and **38**, respectively. Conditions: column, YMC-ODS 4.6 mm×25 cm; flow rate, 1.0 ml/min, 50% MeOH in water+0.05% trifluoroacetic acid (TFA); t_R, cinnamic acid 18.0 min, 40% MeOH in water+0.05% TFA; t_R, tiglic acid 13.4 min.

Acid Hydrolysis of a Mixture of Pregnane Glycosides to Determine the Configuration of Glucose The fraction of pregnane glycosides eluted from the CHCl$_3$–MeOH (9:1) system formed a silica gel column (*ca.* 10 mg) which was heated at 95 °C for 1.5 h with dioxane and 0.05 N HCl (10 drops each). After hydrolysis, the reaction mixture was passed through an Amberlite IRA-60E column, and the eluate was evapolated under reduced pressure. The residue was partitioned with H$_2$O and EtOAc, then the H$_2$O layer was concentrated to dryness. This residue was stirred with D-cysteine methyl ester hydrochloride, hexamethyldisilazane and trimethylsilylchloride in pyridine, as described above. After the reactions, the supernatant was subjected to GC analysis. GC conditions: column, GL capillary column TC-1 (GL Sciences, Inc.) 0.32 mm×30 m, carrier gas N$_2$, column temperature 210 °C; t_R D-glucose 18.8 min, L-glucose 17.8 min. D-Glucose was detected from the mixture of pregnane glycosides.

Acid Hydrolysis of Compounds 2—5, 7—22 and 23—32 Solutions of compounds **2—5**, **7—22** and **23—32** (*ca.* 0.5 mg) in dioxane and 0.05 N HCl (2 drops each) were heated at 95 °C for 1.5 h. The following procedures after hydrolysis for the detection of the aglycone and the monosaccharides of each compound were described in previous papers.[1,2] The acquired aglycone and monosaccharides were analyzed with HPLC and GC, respectively. HPLC conditions: column, YMC-ODS 4.6 mm×25 cm; flow rate, 1.0 ml/min, 47.5% MeOH in water; t_R isolineolon (**35**) 9.4 min, 50% MeOH in water; t_R 12-*O*-acetyllineolon (**34**) 14.0 min, 70% MeOH in water; t_R ikemagenin (**36**) 12.8 min, 5α,6-dihydroikemagenin (**37**) 14.8 min, 12-*O*-tigloylisolineolon (**38**) 14.0 min, 12-*O*-benzoylisolineolon (**39**) 17.0 min; GC conditions: column, Supelco SP-2380™ capillary column 0.25 mm×30 m, carrier gas N$_2$, column temperature 200 °C; t_R cymaritol acetate 7.9 min, oleandritol acetate 8.9 min, digitoxitol acetate 11.5 min, column temperature 215 °C; t_R thevetitol acetate 11.5 min, column temperature 250 °C; t_R glucitol acetate 13.1 min.

Enzymatic Hydrolysis of Compounds 5, 10—13, 16—19, 23 and 29—32 Compounds **5**, **10—13**, **16—19**, **23** and **29—32** (*ca.* 2 mg) were dissolved in H$_2$O (0.7 ml), then cellulase (Sigma Chem. Co.) (*ca.* 20—30 mg) was added. The mixture was stirred at 40 °C for 3 or 4 d. After hydrolysis, the reaction mixture was diluted with H$_2$O and extracted with EtOAc. The EtOAc extract of each compound, except for **18**, **19** and **32**, contained ikemagenin 3-*O*-β-D-oleandropyranosyl-(1→4)-β-D-digitoxopyranosyl-(1→4)-β-D-digitoxopyranosyl-(1→4)-β-D-digitoxopyranoside,[1] **6—9, 14, 15, 22, 25, 27** and **28**, whose structures were confirmed by comparison of their ^{1}H-NMR spectra and HPLC analysis with those of authentic sample. In the ^{1}H-NMR spectra of the products from **18** and **19** by enzymatic hydrolysis, signals due to the sugar moiety were consistent with those of **14**.

References and Notes
1) Warashina T., Noro T., *Phytochemistry*, (accepted, 1999).
2) Warashina T., Noro T., *Chem. Pharm. Bull.*, **48**, 99—107 (2000).
3) Cheng H. T., Nelson C. J., Watson T. R., *J. Chem. Soc. Perkin Trans 1*, **1988**, 1851—1857.
4) Abe F., Mohri Y., Yamauchi T., *Chem. Pharm. Bull.*, **40**, 2917—2920 (1992).
5) Warashina T., Noro T., *Chem. Pharm. Bull.*, **44**, 358—363 (1996).
6) Abe F., Mohri Y., Okabe H., Yamauchi T., *Chem. Pharm. Bull.*, **42**, 1777—1783 (1994).
7) Yamagishi T., Hayashi K., Mitsuhashi H., Inamori M., Matsushita K., *Tetrahedron Lett.*, **1973**, 3531—3534.
8) Yamagishi T., Mitsuhashi H., *Chem. Pharm. Bull.*, **20**, 2070—2071 (1972).
9) Mitsuhashi H., Mizuta Y., *Yakugaku Zasshi*, **89**, 1352—1357 (1969).
10) Yamagishi T., Hayashi K., Mitsuhashi H., Inamori M., Matsushita K., *Tetrahedron Lett.*, **1973**, 3527—3530.
11) Tsukamoto S., Hayashi K., Kaneko K., Mitsuhashi H., *Chem. Pharm. Bull.*, **34**, 3130—3134 (1986).
12) Nakagawa T., Hayashi K., Wada K., Mitsuhashi H., *Tetrahedron*, **39**, 607—612 (1983).
13) Kasai R., Okihara M., Asakawa J., Mizutani K., Tanaka O., *Tetrahedron*, **35**, 1427—1432 (1979).

14) Mitsuhashi T., Hayashi K., *Shouyakugaku Zasshi*, **39**, 1—27 (1985).

15) Yoshikawa K., Okada N., Kann Y., Arihara S., *Chem. Pharm. Bull.*, **44**, 1790—1796 (1996).

16) Shibuya H., Zhang P., Park J. D., Beak N. I., Takeda Y., Yoshikawa M., Kitagawa I., *Chem. Pharm. Bull.*, **40**, 2647—2653 (1992).

17) Warashina T., Noro T., *Phytochemistry*, **39**, 199—204 (1995).

18) Hara S., Okabe H., Mihashi K., *Chem. Pharm. Bull.*, **35**, 501—506 (1987).

19) Zhang D., Miyase T., Kuroyanagi M., Umehara K., Ueno A., *Chem. Pharm. Bull.*, **44**, 173—179 (1996).

April 2000

Chem. Pharm. Bull. **48**(4) 525—528 (2000)

525

Studies on the Reaction of Benzo[X]quinoline N-Oxides (X= f, h, and g) with Methylsulfinyl Carbanion Using the Semi-empirical Molecular Orbital Method. Liberation of the N-Oxide Group

Hisao Matsuzaki,*,[a] Isao Takeuchi,[b] and Yoshiki Hamada[b]

Tohoku Pharmaceutical University,[a] 4-4-1 Komatsushima, Aoba-ku, Sendai 981–8558, Japan and Faculty of Pharmacy, Meijo University,[b] 150 Yagotoyama Tempaku-ku, Nagoya 468–8503, Japan.

The mechanism of the liberation reaction of the N-oxide group has been studied and compared with the methylation reaction using a semi-empirical molecular orbital PM3 method. By comparing the calculated values of Gibbs free energy of activation, we can determine whether a liberation reaction or methylation reaction occurs.

Key words mechanism; transition state; quinoline; MO method; Gibbs free energy

The reaction of quinolines, isoquinolines,[1] and their N-Oxides[2] with methylsulfinyl carbanion (6) has been reported, the products all being methylated compounds. Hamada *et al.* also studied the reaction of 1,X-naphthyridine (X=5, 6, 7, 8),[3] benzo[f]- and benzo[h]quinoline, and their N-oxides[4] with 6. They found that the N-oxides and 6 undergo a new type of reaction which eliminates the N-oxide group from the azaphenanthrene skeleton.[4] On the other hand, the reaction of benzo[g]quinoline with 6 produced only methylated compounds.[5] In the present work, we have theoretically studied the reaction of benzo[f]quinoline 4-oxide (1), benzo[h]quinoline 1-oxide (2), 4-methyl-benzo[h]quinoline 1-oxide (3), 2-methyl-benzo[h]quinoline 1-oxide (4), and benzo[g]quinoline 1-oxide (5) with 6. We show the schemes of these reactions and the experimental yields of phenanthrene (7) for the reactions of 1 and 2, the 4-methylphenanthrene (8), the 2-methylphenanthrene (9), and the 2-methylbenzo[g]quinoline 1-oxide (10) in Chart 1. We have focused our study on explaining whether liberation of the N-oxide group or methylation will occur. We calculated the heat of formation and the Gibbs free energies of formation of the molecules and ions involved in the reaction path at 70 °C. We regarded the energy difference between the transition state (TS) and the initial minimum energy state as the activation energy (Ea) of the reaction. We compared the calculated Ea of the liberation reaction of the N-oxide group with that of the methylation reaction of the N-oxide, and discuss which of these reactions

will actually occur. We also compare the calculated Ea's with the yields of the corresponding products.

Results and Discussion

Hamada *et al.* have carried out the reaction of **2** with deuterated methylsulfinyl carbanion in an NMR sample tube to examine the reaction mechanism, then proposed a mechanism of the liberation of the N-oxide group.[6] As an example,
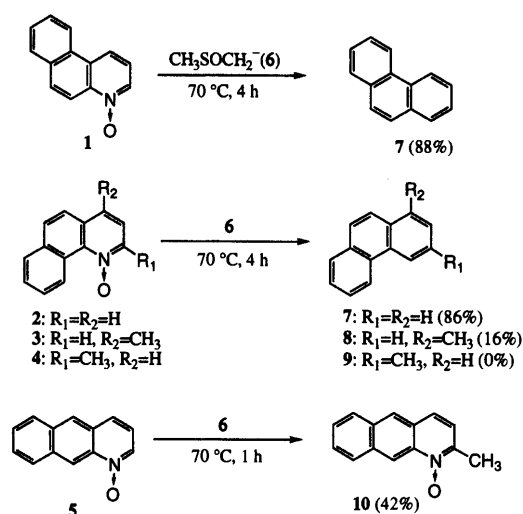
Chart 1

Table 1. Calculated Heat of Formation (ΔH) and Gibbs Free Energies of Formation (ΔG) at 70 °C in Unit of kcal/mol

Reactant		Eq2	Eq3	TS4	TS7	Ea(L)	Ea(M)
1	ΔG	−52.98	−53.05	−3.53	5.54	49.52	58.59
	ΔH	−3.82	−2.23	46.47	53.88	50.29	57.70
2	ΔG	−50.54	−48.97	0.39	3.38	50.93	53.92
	ΔH	−1.77	1.73	50.69	53.77	52.46	55.54
3	ΔG	−62.60	−58.10	−10.57	−6.91	52.03	55.69
	ΔH	−11.81	−3.85	42.72	46.73	54.53	58.54
4	ΔG	−54.77	−60.99	−4.77	—	56.22	—
	ΔH	−5.63	−6.42	45.47	—	51.89	—
5	ΔG	−45.75	−46.96	15.69	8.14	62.65	53.89
	ΔH	2.09	5.35	64.39	58.98	62.30	56.89

The activation energies are also shown. Here, L and M in parentheses denote the liberation of an N-oxide group and the methylation process, respectively.
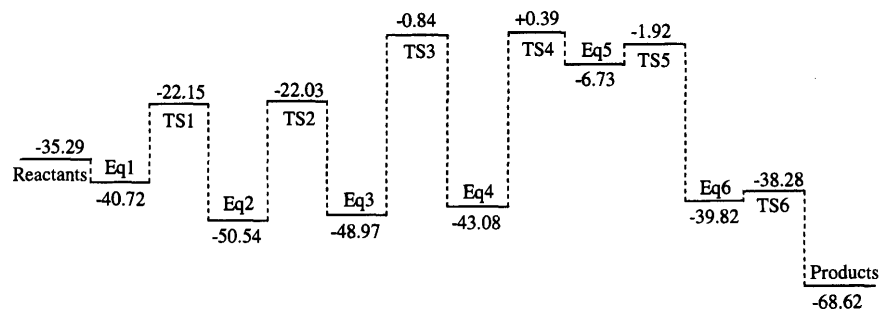
* To whom correspondence should be addressed.

Fig. 1.   Energy Diagram along the Path for the Liberation Reaction of the N-Oxide Group for the Reaction of 2 with 6

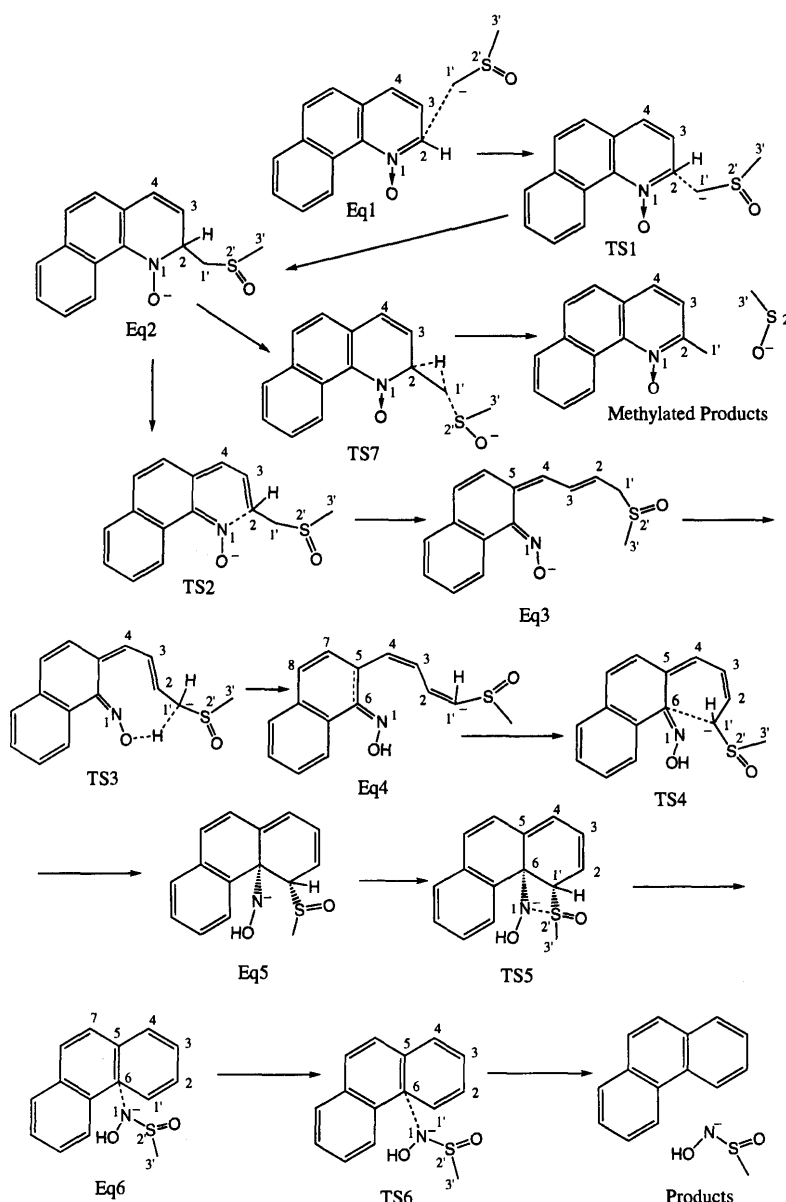Numerical values are the Gibbs free energies of formation in kcal/mol of the optimized states.

Fig. 2.   Schematic View of the Optimized Structures for the Reaction of 2 with 6

The methylated product through TS7 was not experimentally obtained for this reaction. The double bonds and the minus charge in the molecules are drawn based on the calculated values of the bond order and the charge, respectively.[7] The calculated relevant interatomic distances are as follows: $C_2C_{1'}$=4.86 Å (Eq1), $C_2C_{1'}$=2.364 Å (TS1), N_1C_2= 2.031 Å (TS2), OH=1.295 Å (TS3), C_1H=1.491 Å (TS3), $C_6C_{1'}$=2.043 Å (TS4), $N_1S_{2'}$=2.194 Å (TS5), N_1C_6=1.613 Å (Eq6), N_1C_6=1.975 Å (TS6).

we show the reaction path of 2 with 6 in detail following the proposal. We assume that the reaction proceeds through the following steps. When the reactants 2 and 6 are separated an infinite distance, the system has the electric charge -1 and

Gibbs free energy of formation $(\Delta G)=-35.29$ kcal/mol. When 2 and 6 mutually interact by the intermolecular interaction, an equilibrium state (Eq1, $\Delta G=-40.72$ kcal/mol) is realized. Step 1: 6 is added to the 2-position of 1 and an in-

termediate product (Eq2, $\Delta G = -50.54$ kcal/mol) is formed through TS1 ($\Delta G = -22.15$ kcal/mol). We show the heat of formation and Gibbs free energy of formation calculated at 70 °C in Table 1. We also display an energy diagram along the reaction path for the liberation of an N-oxide group in Fig. 1 and the schematic view of the optimized structures in Fig. 2. In experiments, the NMR signal of starting compounds disappeared soon after the beginning of the reaction.[6] Eq2 is the lowest state in energy and the energy of TS1 is low (Fig. 1). Therefore, we consider that the majority of reactants exist in the form of Eq2 and the activation energy must be measured from Eq2.

Step 2: The N_1–C_2 bond of Eq2 is broken, ring opening occurs, and the intermediate state Eq3 ($\Delta G = -48.97$ kcal/ mol) is formed via TS2 ($\Delta G = -22.03$ kcal/mol). Step 3: A hydrogen atom attached to the $C_{1'}$ atom of Eq3 transfers to the oxygen atom in the N-oxide group and Eq4 ($\Delta G = -43.08$ kcal/mol) is formed via TS3 ($\Delta G = -0.84$ kcal/mol). Since the H atom has been removed from the $C_{1'}$ atom, the double bonds at the C_2–C_3 and C_4–C_5 positions in Eq3 move to the $C_{1'}$–C_2 and C_3–C_4 positions in Eq4, respectively.[7] Step 4: After the O–H bond is formed, through TS4 ($\Delta G = +0.39$ kcal/mol), a new C_6–$C_{1'}$ bond and a new 6-membered ring are formed, making Eq5 ($\Delta G = -6.73$ kcal/mol). The 3-dimensional view of TS4 is shown in Fig. 3. TS4 for this ring-closure process is the highest state in energy over the whole process of this liberation reaction of N-oxide. We consider that this reaction proceeds while maintaining equilibrium between Eq2, Eq3, and Eq4 states. Consequently, the Gibbs free energy of activation of this N-oxide liberation process is obtained from the energy difference between TS4 and Eq2 and has a value of 50.93 kcal/mol (Table 1). Step 5: N_1 and $S_{2'}$ atoms of Eq5 approach each other, via TS5 ($\Delta G = -1.92$ kcal/mol), a new N_1–$S_{2'}$ bond is formed, and the $C_{1'}$– $S_{2'}$ bond breaks, making Eq6 ($\Delta G = -39.82$ kcal/mol). The N_1–C_6 bond of Eq6 is weak (the calculated bond-order is 0.751 and the force constant is 1.49 mdyn/Å). The Gibbs free energy of activation required to break this N_1–C_6 bond is only 1.5 kcal/mol, as is seen in the next step. Step 6: Finally, the N_1–C_6 bond of Eq6 is broken and, via TS6 ($\Delta G = -38.28$ kcal/mol), products including 7 ($\Delta G = -68.62$ kcal/mol) are formed (Fig. 2).

At step 2, when the hydrogen atom at the 2-position of Eq2 approaches the $C_{1'}$ atom of the attached carbanion group, the $C_{1'}$–$S_{2'}$ bond becomes longer, and a methyl group will be formed at the 2-position via TS7 ($\Delta G = 3.38$ kcal/ mol). The Gibbs free energy of activation of this methylation process is 53.92 kcal/mol, which is much greater than that of the ring-closure process (50.93 kcal/mol). The calculated heat of formation shows the same tendency (Table 1). This fact coincides with the experimental result that phenanthrene was obtained but no methylated N-oxide was obtained in this reaction (see Table 2).

We can also assume that the reactions of 1, 3, and 4 with 6 proceed in a similar manner. We show the calculated heat of formation and Gibbs free energy of formation in Table 1. For the reaction of 1, Eq3 is the lowest state in Gibbs free energy and the Gibbs free energy of activation for the liberation process is obtained from TS4 and Eq3. Of course, Gibbs free energy of activation for the methylation is obtained from TS7 and Eq2. The circumstances are the same for the reaction of

Table 2. Calculated Gibbs Free Energy of Activation and Experimental Yield of Adduct

Reactant	Ea(L) (kcal/mol)	Ea(M) (kcal/mol)	Yield(L) (%)	Yield(M) (%)	Temperature and time
1	49.52	58.59	88	—	70 °C, 4h
2	50.93	53.92	86	—	70 °C, 4h
3	52.03	55.69	16	—	70 °C, 4h
4	56.22	—	—	—	70 °C, 4h
5	62.65	53.89	—	42	70 °C, 1h

Here, L and M in parentheses indicate the liberation of an N-oxide group and the methylation, respectively.
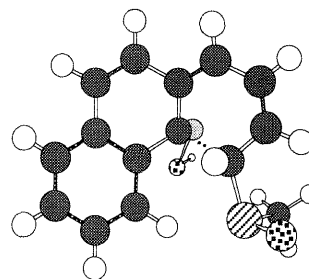

Fig. 3.   3-Dimensional View of TS4 for the Reaction of 2 with 6, Drawn Using CSC Chem3D Routine
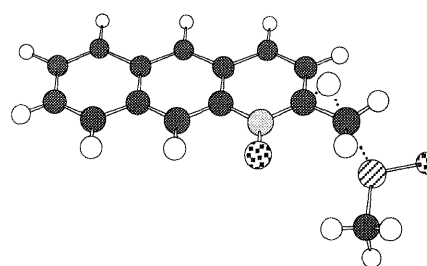

Fig. 4.   3-Dimensional View of TS7 for the Reaction of 5 with 6, Drawn Using CSC Chem3D Routine

The calculated relevant interatomic distances are: $C_2H = 1.588$ Å, $C_1H = 1.429$ Å, and $C_1S_{2'} = 2.168$ Å. The quoted numbers of atoms are identical with those of TS7 in Fig. 2.

4. The calculated Gibbs free energies of activation and the experimental yields of the products are summarized in Table 2. For the reactions of 1 and 3, the calculated Gibbs free energy of activation of the N-oxide liberation process is lower than that of the methylation process in each case. These results are consistent with the fact that 7 and 8 have been obtained, but the methylated compounds have not been obtained experimentally for the reactions of 1 and 3. We suppose that 9 has not been obtained experimentally, since the Gibbs free energy of activation for the reaction of 4 is large. On the other hand, the heat of formation of activation for the reaction of 4 is too small to explain the experiments. For reactants 1, 2, 3, and 4, the Gibbs free energies of activation of the liberation reaction of the N-oxide group correlate well with the experimental yields of the related products.

We have also studied the reaction path of 5 with 6 in a similar way. Here, Eq3 is the lowest state in Gibbs free energy and the Gibbs free energy of activation for the liberation process is obtained from TS4 and Eq3 (Table 1). The Gibbs free energy of activation for the methylation process is obtained from TS7 ($\Delta G = 8.14$ kcal/mol, see Table 1) and Eq2. The 3-dimensional view of TS7 is shown in Fig. 4. As shown

in Tables 1 and 2, the calculated Gibbs free energy of activation for *ortho*-methylation is 53.89 kcal/mol, which is much smaller than that for the liberation reaction of the *N*-oxide group (62.65 kcal/mol). This fact coincides with the experimental result that the *ortho*-methylated compound **10** was obtained, while the anthracene was not obtained experimentally in this reaction. In terms of heat of formation, it seems that the calculated activation energy for the *ortho*-methylation for the reaction of **5** with **6** is too large (Table 1).

To summarize, the reactions of **1**, **2**, and **3** with **6** lead to the liberation of an *N*-oxide group, whereas the reaction of **5** with **6** leads to *ortho*-methylation, on the basis of the reaction path and the calculated Gibbs free energies of activation. The reaction of **4** with **6** cannot occur, since the calculated Gibbs free energies of activation is too large. For reactants **1**, **2**, and **3**, the Gibbs free energies of activation of the liberation reaction of the *N*-oxide group correlate well with the experimental yields of the corresponding products.

Calculation

We calculated the energies of molecules and ions using the semi-empirical molecular orbital PM3 method[8] in the MOPAC 93/97 computational package.[9] All calculations were performed on an IBM RS/6000 model 590 and SGI (Silicon Graphics, Inc.) Indigo2 computers. A graphic interface, MOL-GRAPH,[10] was used for preparing input data for MOPAC 93/97 and for visualizing the resulting structures. The energies of the ground state and transition states were optimized until gradient norms of less than 0.05 kcal/mol/Å were achieved. All structure parameters were optimized. The effect of a solvent was not considered. After optimizing the TS structures, we carried out the vibrational calculation and confirmed that the TS had exactly one imaginary vibrational frequency. We used FORCE and THERMO options and calculated the heat of formation (ΔH) and entropy (S)[11, 12] of the molecules and ions at 70 °C using harmonic oscillator approximation, since the experiments were performed at 70 °C. Then, we calculated the Gibbs free energy of formation (ΔG) by

$$\Delta G = \Delta H - TS$$

Here, T denotes the absolute temperature. Exactly speaking, we must subtract $\Delta H - TS$ for the reference state from above ΔG.[11] When we calculate the Gibbs free energy of activation, these contributions are compensated for. We also performed intrinsic reaction coordinate (IRC) calculations to make sure that the TS connects the initial with the intended final state.

References and Notes

1) Russell G. A., Weiner S. A., *J. Org. Chem.*, **31**, 248—251 (1966).
2) Kobayashi Y., Kumadaki I., Sato H., Yokoo C., Miura T., *Chem. Pharm. Bull.*, **21**, 2066—2067 (1973).
3) *a)* Hamada Y., Takeuchi I., Hirota M., *Chem. Pharm. Bull.*, **19**, 1751—1755 (1971); *b)* Takeuchi I., Hamada Y., *ibid.*, **24**, 1813—1821 (1976).
4) Hamada Y., Takeuchi I., *J. Org. Chem.*, **42**, 4209—4213 (1977).
5) Takeuchi I., Uchida M., Hamada Y., Yuzuri T., Suezawa H., Hirota M., *Heterocycles*, **41**, 2221—2231 (1995).
6) Hamada Y., Morishita Y., Ozawa I., Takeuchi I., Hirota M., *Chem. Pharm. Bull.*, **27**, 1535—1543 (1979).
7) Judging from the calculated values of the bond order, the C_4–C_5, C_5–C_6, and C_5–C_7 bonds in Eq4 have an intermediate nature between the surrounding single and double bonds. We display the C_5–C_6 bond in Eq4 with solid and dotted lines in Fig. 2.
8) Stewart J. J. P., *J. Comput. Chem.*, **10**, 209—220; 221—264 (1989).
9) MOPAC 93 release 2, Stewart J. J. P., Fujitsu Limited, Tokyo, Japan (1994); MOPAC 97, Stewart J. J. P., Fujitsu Limited, Tokyo, Japan (1997).
10) MOL-MOLIS/CRYS version 2.4, Daikin Industries, Ltd., Tokyo, Japan (1995).
11) MOPAC 93.00 Manual, Stewart J. J. P., Fujitsu Limited, Tokyo, Japan (1993).
12) In the MOPAC program package, contributions from the vibrational states which have wave numbers lower than 100 cm^{-1} are excluded. Here, we calibrated the above contributions with the excluded vibrational frequencies.

April 2000

Chem. Pharm. Bull. **48**(4) 529—536 (2000)

529

Improved Synthesis of Paroxetine Hydrochloride Propan-2-ol Solvate through One of Metabolites in Humans, and Characterization of the Solvate Crystals

Kiyoshi Sugi,[a] Nobushige Itaya,*,[a] Tadashi Katsura,[a] Masami Igi,[a] Shigeya Yamazaki,[a] Taro Ishibashi,[a] Teiji Yamaoka,[a] Yoshihiro Kawada,[a] Yayoi Tagami,[a] Michiya Otsuki,[b] and Takao Ohshima[b]

Central Research Laboratories[a] and Quality Assurance Office,[b] Sumika Fine Chemicals Co., Ltd., 1–21, Utajima 3-Chome, Nishiyodogawa-ku, Osaka 555–0021, Japan. Received October 20, 1999; accepted December 20, 1999

Paroxetine, a potent and selective inhibitor of 5-hydroxytryptamine (serotonin) uptake, was prepared through a piperidine derivative, which was reported to be one of the paroxetine metabolites in humans.

Thus, the piperidine derivative was converted to its *N-tert*-butoxycarbonyl (*N*-Boc) derivative, which was then converted to *N*-Boc paroxetine. Paroxetine hydrochloride propan-2-ol (isopropyl alcohol (IPA)) solvate crystals were directly obtained from the *N*-Boc paroxetine by adding hydrogen chloride to the *N*-Boc paroxetine IPA solution. The amount of IPA content in the crystals was reduced by drying with a continuous change of powder X-ray diffraction patterns. Other characterizations of the solvate crystals were also conducted.

Key words paroxetine; paroxetine hydrochloride

Paroxetine is a potent and selective inhibitor of 5-hydroxytryptamine (serotonin) uptake, with a reduced propensity to cause the side-effects usually associated with a tricyclic antidepressant.[1] The metabolic pathway of paroxetine in animals and man was studied using [^{14}C]-labeled paroxetine and one of the metabolites was revealed to be the (3*S*,4*R*)-*trans*-4-(4-fluorophenyl)-3-hydroxymethylpiperidine (6),[2] which seems to be an attractive intermediate for the preparation of paroxetine.

Conventionally, a paroxetine base has been synthesized in several steps, including deprotection of the *N*-alkyl group,[3] whereas recently published journals and a patent report the preparation of enantiomeric paroxetine and paroxetine through an enantiomer of compound 6[4a] and compound 6 itself,[4b,c] respectively. Paroxetine has been used as an active ingredient in anti-depressant drugs in the form of paroxetine hydrochloride (paroxetine HCl) crystals.[3b] Paroxetine HCl was reported to exist in two solid state forms, hemihydrate (form-I) and anhydrate containing bound propan-2-ol (isopropyl alcohol (IPA)) (form-II).[5] The report also describes the following: Form-I is thermodynamically more stable and form-II converts to form-I, if seed crystals of form-I are present, when exposed to humid conditions. There is a higher solubility for form-II at all temperatures, and the effect that such solubility differences between crystal forms have on absorption is therefore relevent.[5] This description implies that form-II is pharmaceutically the more desirable ingredient if form-II can be steadily produced.

Recently, two independent crystal forms (form-I, form-II) of paroxetine HCl were analyzed by X-ray. The form-II crystal was reported to contain IPA molecules in the channel formed by paroxeine molecules and chloride anions, and was reported to be easily decomposed in open air at room temperature because the IPA molecules are easily released through the channels.[6]

In this paper, first, we wish to report the convenient synthesis of *N-tert*-butoxy (*N*-Boc) paroxetine (9) through compound 6 and the direct conversion of compound 9 to paroxetine HCl crystals incorporating IPA (form-II).[4b] Next, we wish to report the particular physical properties of form-II on drying, which are exemplified by a continuous change in analytical data such as IR spectroscopy, thermal analysis profile and powder X-ray diffraction (XRD) patterns. Other physical properties of IPA solvate crystals are also reported.

Preparation of One of the Paroxetine Metabolites (6) Methyl *p*-fluorocinnamate (1) was prepared from *p*-fluorobenzaldehyde and methyl acetate (MeOAc) in the presence of sodium methoxide (NaOMe). Methyl cyanoacetate was successively added to the reaction mixture to afford dimethyl 2-cyano-3-(4-fluorophenyl)glutarate (2) in 79% yield from *p*-fluorobenzaldehyde. Compound 2 was hydrogenated using Raney-cobalt to give (±)-*cis,trans*-4-(4-fluorophenyl)-5-methoxycarbonylpiperidin-2-one (3) as a mixture of crystals in 90% yield, which was then treated with sodium methoxide to give (±)-*trans* isomer (4) crystals. The defluorinated analog of compound 3 is a known compound.[7] The crystals (4) were reduced with lithium aluminum hydride to give (3*SR*,4*RS*)-*trans*-4-(4-fluorophenyl)-3-hydroxymethylpiperidine (5) in 83% yield from compound 3.[3d-i] The racemic amino alcohol (5) was optically resolved using L-*o*-chlorotartranilic acid[8] to give salt crystals of (3*S*,4*R*)-*trans*-4-(4-fluorophenyl)-3-hydroxymethylpiperidine (6). The optically active amino alcohol (6), a paroxetine metabolite, was obtained by decomposition of the salt.

Preparation of Paroxetine HCl IPA Solvate Crystals The *N*-Boc derivative (7) was obtained by adding aqueous sodium hydroxide to a mixture of the L-*o*-chlorotartranilic acid salt of the amino alcohol (6), (Boc)$_2$O, toluene and water. The alcohol moiety of the *N*-Boc derivative (7) was mesylated and reacted with sesamol to give *N*-Boc paroxetine (9). The *N*-Boc paroxetine (9) was dissolved in IPA, and hydrogen chloride was introduced to the solution. In this reaction, Boc deprotection and HCl salt formation were achieved and paroxetine HCl IPA solvate crystals were obtained.[4b] The preparation pathway for proxetine HCl IPA solvate is shown in Chart 1.

Physical Properties of Paroxetine HCl IPA Solvate Crystals Two crystal forms of paroxetine HCl hemihydrate
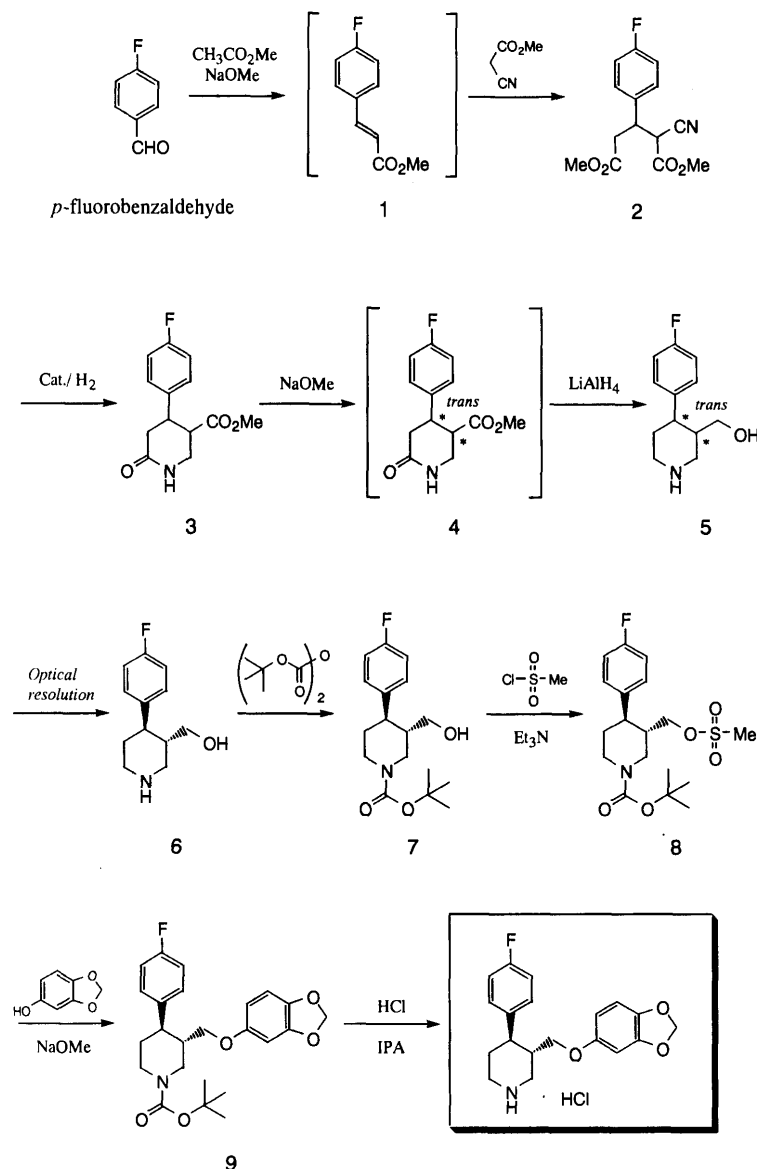

Chart 1.   Synthesis of Paroxetine Hydrochloride Propan-2-ol Solvate

(form-I) and IPA solvate crystals (form-II) were reported to show distinct differences in IR spectra, in XRD patterns, in differential scanning calorimetry (DSC) curves and thermogravimetry (TG) experiments.[5] The form-II crystals used in the above experiments were reported to lose around 3% weight in TG analysis.[5] This means that the form-II crystals used in the experiments had approximately 3% of bound IPA in the crystals.

A patent published afterwards describes that paroxetine HCl IPA solvate crystals initially contain 13.0% of IPA, that the solvate crystals release IPA while being washed with water, and that the amount of IPA content in the crystals is measured to be 0.05% after subsequent drying, claiming that the IPA solvate crystals do not lose bound IPA up to this amount under conventional vacuum oven drying conditions.[9] These foregoing descriptions prompted us to ascertain the properties of paroxetine HCl IPA solvate crystals obtained by our improved preparation process.

Preparation of Form-II Crystals with Various IPA Contents and Their Behavior Related to Atmospheric Moisture: Figure 1 shows photographs of paroxetine HCl IPA solvate crystals

(form-II) obtained by our improved preparation process, as well as conventional hemihydrate crystals (form-I). Form-II crystals are distinctly different from form-I crystals in shape. Form-II crystals initially contained around 14% weight of IPA, *i.e.* IPA molecules are incorporated into paroxetine HCl crystals in a 1-to-1 molar ratio, being consistent with the reported crystallographic analysis.[6]

Table 1 shows the relationship between drying conditions for these two forms of crystals, and the solvate (water, IPA) contents of the dried crystals. Figure 2 depicts the IPA releasing behavior of form-II crystals under various drying conditions. These data also show that these two crystal forms are different and that form-II crystals release IPA depending on the intensities of drying conditions. Figure 3 shows moisture absorption and desorption behavior of dried form-I and form-II crystals. Dried form-I crystals absorbed water rapidly up to around 2.5% weight, and the crystals with 2.5% water did not lose the water easily in a dry atmosphere; meanwhile, dried form-II crystals absorbed water slowly and the crystals with absorbed water released the water easily in a dry atmosphere. From these observations, we assumed that

(a)

(b)
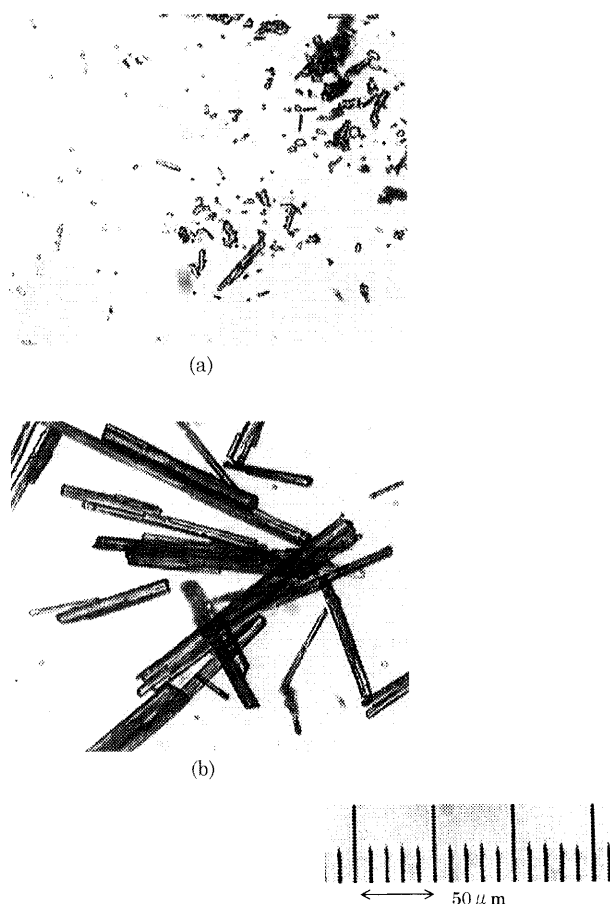
Fig. 1.   Photographs of Paroxetine Hydrochroride

(a) Hemihydrate crystals (form-I), (b) IPA solvate crystals (form-II dried, IPA content 2—3%).

Table 1.   Paroxetine HCl Solvates under Vacuum Drying Conditions

Sample	Solvate	
Form-I	H_2O	2.36%
Form-I-dry (Dry 100 °C, 12 h)	H_2O	0.25%
Form-II-1 (Dry 50 °C, 4 h)	IPA	13.75%
Form-II-2 (Dry 50 °C, 12 h)	IPA	9.17%
Form-II-3 (Dry 75 °C, 14 h)	IPA	5.79%
Form-II-4 (Dry 85 °C, 21 h)	IPA	2.82%
Form-II-5 (Dry 100 °C, 14 h)	IPA	0.48%

form-I crystals recaptured water as bound water in crystals but form-II crystals absorbed water not as bound water.

Thermal Analysis: Figure 4 and 5 show DSC and TG profiles of form-II crystals with various IPA contents, as well as those of form-I crystals, in open pans. Both form-I and dried form-I crystals showed similar DSC profiles, with the endothermic peak of dried form-I crystals being 1.5 °C below that of form-I crystals. DSC profiles of variously dried form-II crystals showed continuous changes in DSC patterns owing to a decrease in IPA content in the crystals, *i.e.* an endothermic peak at around 105 °C gradually diminished and a peak at around 125—131 °C emerged and finally form-II
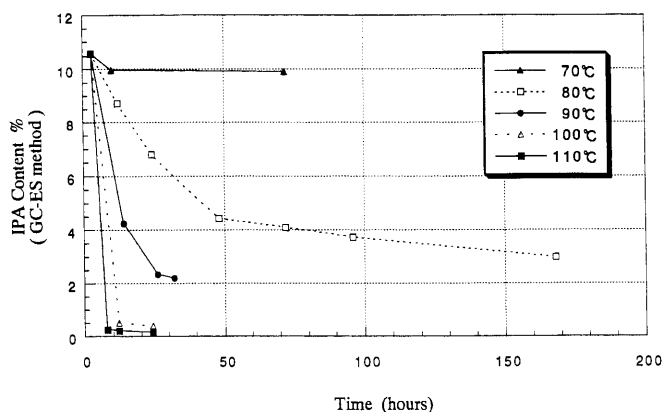
Fig. 2.   IPA Releasing Behavior of Paroxetine HCl Form-II Crystals under Vacuum Drying Conditions
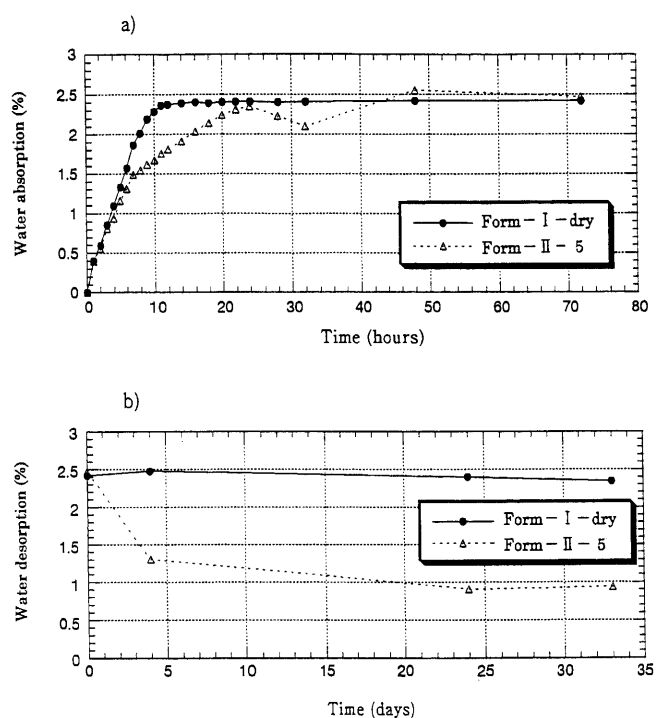
Fig. 3.   Water Absorption and Desorption Curves of Dried Paroxetine HCl Solvates

a) Crystals were left open at ambient condition for 72 h. b) Then, crystals were replaced and dried for 24 d in a desiccator with silica gel in it.

crystals with 0.48% of IPA content showed almost a single peak at 131 °C. TG profiles showed that all form-II crystals lost weight between 50 °C and around 140 °C, indicating that the endothermic peaks at around 105 °C are due to the vaporization of IPA. These observation may be interpreted as follows: Form-II crystals with high IPA contents melt while losing IPA, but form-II crystals with low IPA contents only partly melt while losing IPA, and the remaining micro crystalline parts melt at a higher temperature of 125—131 °C.

IR Spectroscopy: Figure 6 shows OH IR absorption bands of variously dried form-II crystals as well as form-I crystals at between 4000 and 1800 cm^{-1}. Form-I crystals and dried ones showed almost the same IR patterns, and the IR patterns are consistent with that shown in the literature.[5] Meanwhile, form-II crystals showed a continuous change in IR absorption patterns with a decrease in IPA content. Form-II crystals
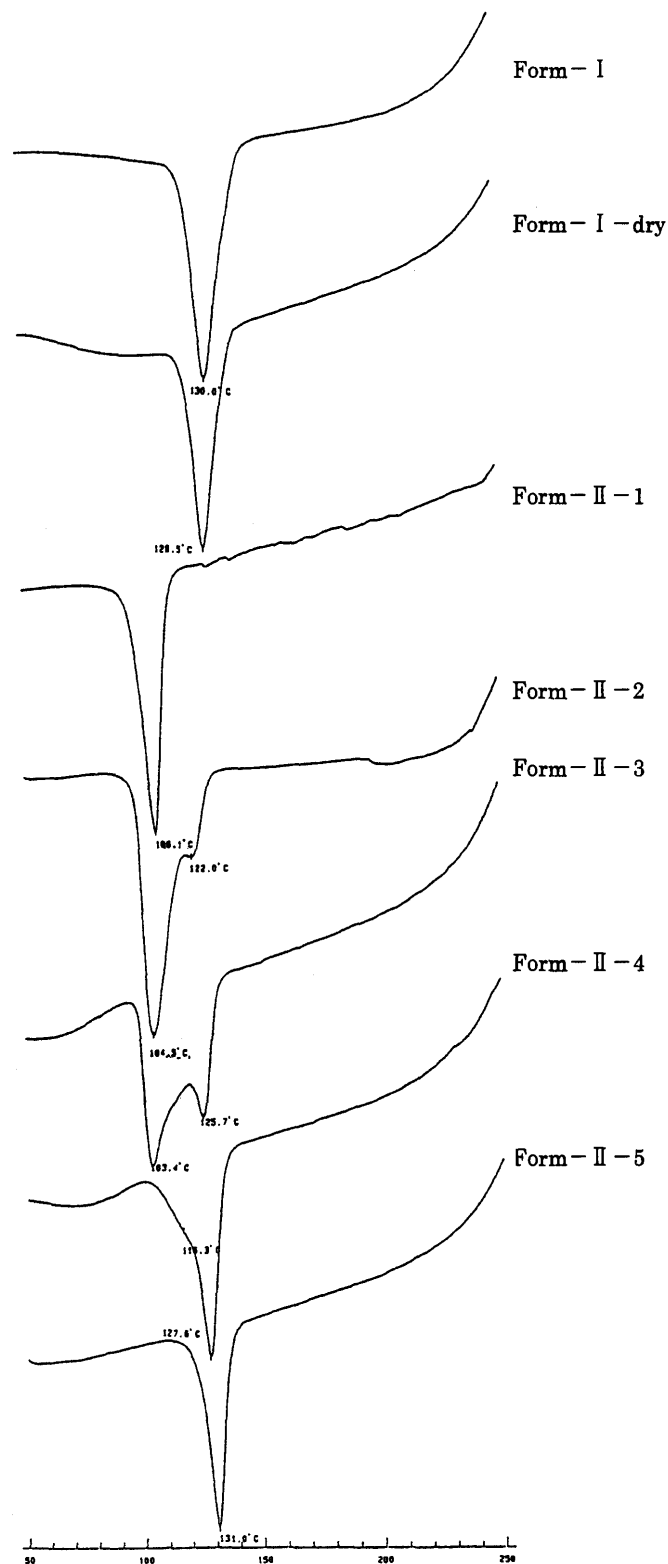
Fig. 4. Effect of Drying on DSC Curves of Paroxetine HCl Solvates

Fig. 5. Effect of Drying on TG Curves of Paroxetine HCl Solvates

with relatively high IPA contents showed relatively strong absorption at around 3400 cm^{-1} compared with an absorption band at around 3632 cm^{-1}, and an absorption intensity at around 3400 cm^{-1} gradually diminished. Finally, the form-II crystals with 0.48% of IPA content showed weak absorption at both 3400 cm^{-1} and 3632 cm^{-1}.

Powder XRD: Figure 7 shows XRD patterns of variously dried form-I and form-II crystals. Both form-I and anhydrous form-I crystals showed almost the same XRD patterns, and

the XRD patterns of these form-I crystals were distinctly different from those of all variously dried form-II crystals. The XRD patterns of variously dried form-II crystals showed continuous changes with a decrease in IPA content in the crystals.

Form-II-1 crystals showed rather sharp XRD peaks which may suggest rather high crystallinity. Form-II-2, -3 and -4 crystals showed similar and rather vague XRD patterns. Form-II-5 crystals showed a rather sharp XRD pattern again. These phenomena may be interpreted as follows: Form-II-1 crystals containing IPA molecules in a 1-to-1 ratio have high crystallinity and the crystallinity is easily diminished with the release of IPA to give form-II-2, -3 and -4 crystals. From
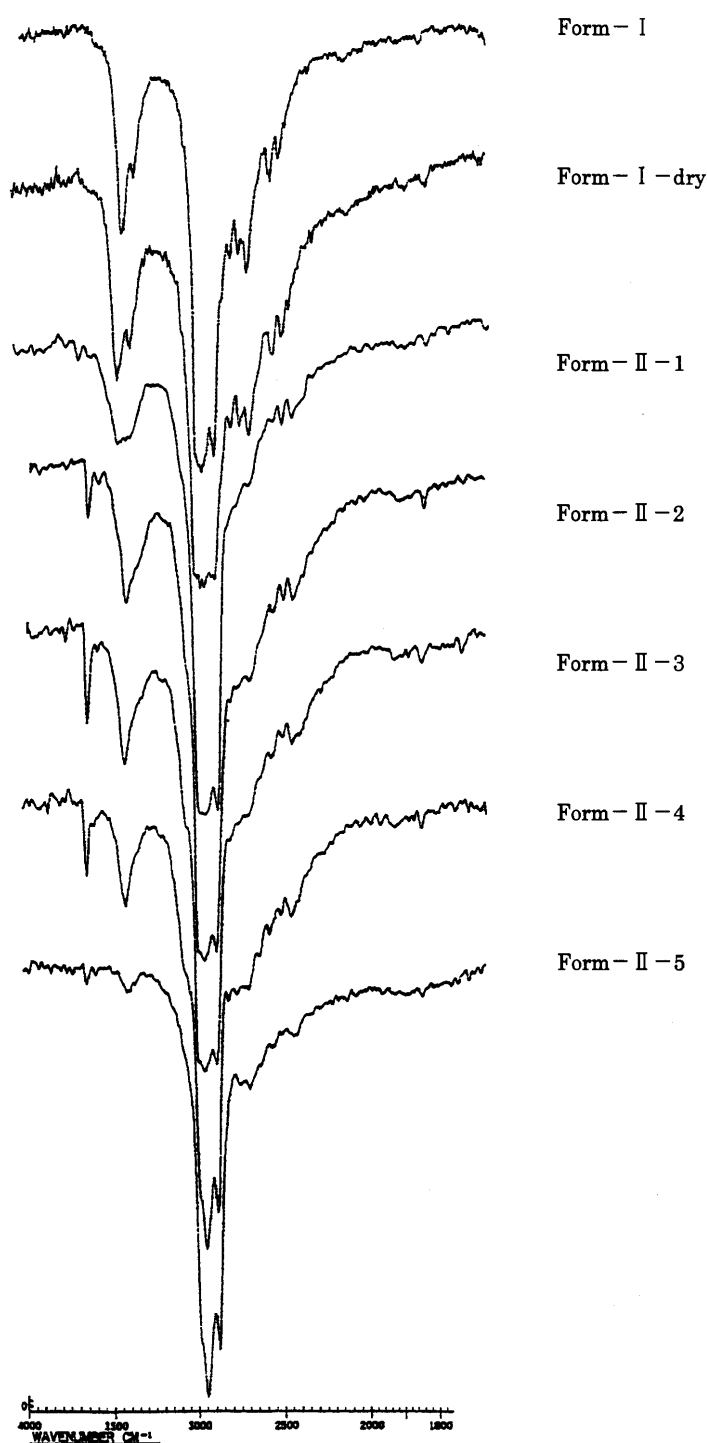
Fig. 6. Effect of Drying on IR Spectra of Paroxetine HCl Solvates

the similarity of all XRD patterns of variously dried form-II crystals, it is presumed that the original lattice of the form-II-1 crystals is not changed drastically by drying, but is partly closely packed together to make newly formed micro crystalline parts and these micro crystalline parts finally become dominant in form-II-5 crystals.

Resolvation and Re-desolvation of Dried Form-II Crystals with IPA: Table 2 shows the IPA contents of the crystals after resolvation and re-desolvation, as well as comparable IPA contents of dried form-II crystals as a reference. Figure 8 shows the XRD patterns of these crystals. These data showed that dried form-II crystals were resolvated with IPA up to about 14% of the weight of IPA content, and were re-desol-

Table 2. Resolvation and Re-desolvation of Dried Paroxetine HCl Form-I Crystals

Resolvated sample	Solvate	Reference dried form-II	Solvate
Form-II-7 (Dry r.t., 1 h)	IPA 14.0%	Form-II-1 (Dry 50 °C, 4 h)	IPA 13.8%
Form-II-8 (Dry 50 °C, 14 h)	IPA 4.37%	Form-II-3 (Dry 75 °C, 14 h)	IPA 5.79%
Form-II-9 (Dry 90 °C, 6 h)	IPA 1.83%	Form-II-4 (Dry 85 °C, 21 h)	IPA 2.82%

Fig. 7. Effect of Drying on XRD Patterns of Paroxetine HCl Solvates

Resolvated and re-desolvated dried form—II crystals
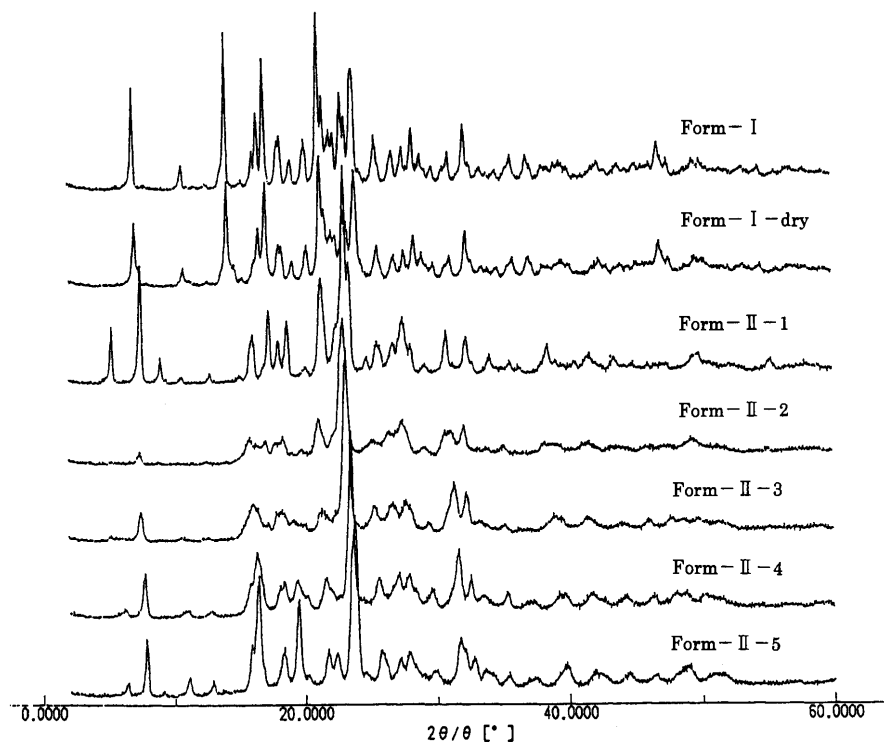
Reference dried form—II crystals
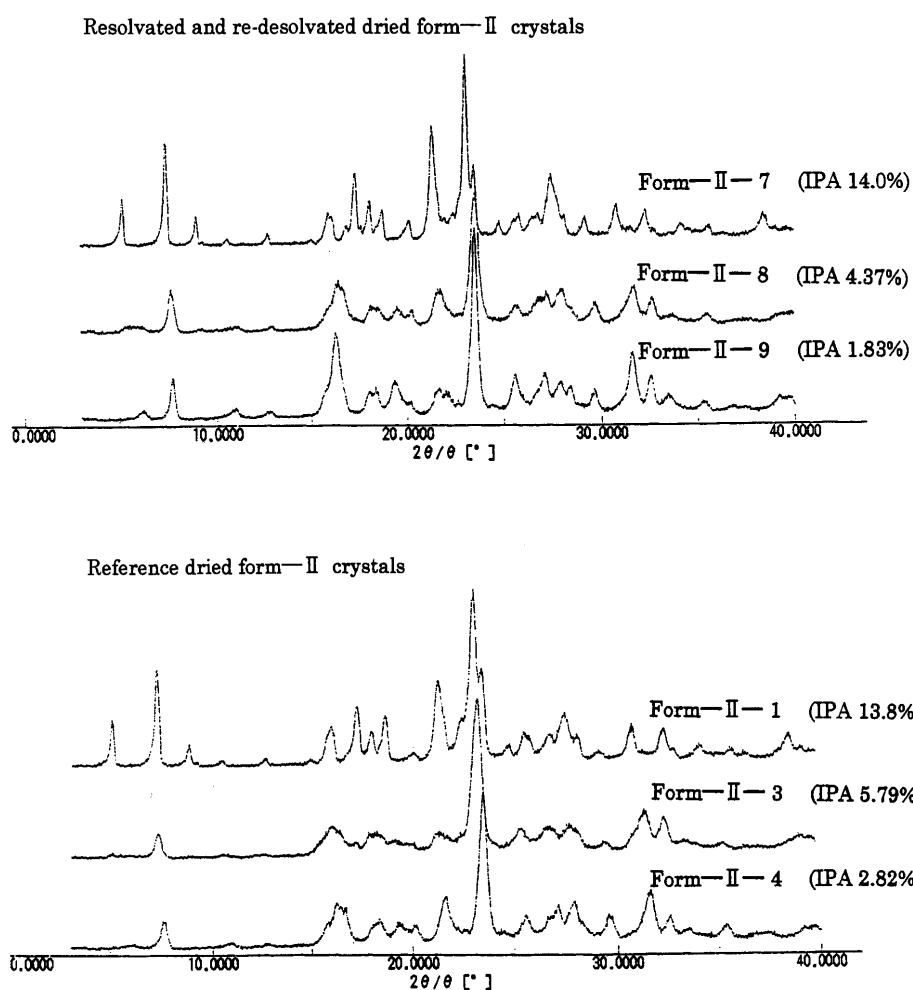
Fig. 8. Effect of Drying on XRD Patterns of Paroxetine HCl Solvates

vated again by drying. The XRD patterns of these crystals were almost the same as those of dried form-II crystals of comparable IPA content. These data show that form-II crystals can contain and release IPA reversibly.

Conclusion

An improved process for the preparation of paroxetine HCl IPA solvate crystals was developed. IPA in the solvate crystals was revealed to be loosely bound and was removed from the crystals by drying to give variously dried form-II crystals with a continuous change in IR spectroscopy, thermal analysis profile and XRD patterns.

Experimental

All melting and boiling points are uncorrected. IR spectra were recorded on a Perkin Elmer FT-IR Spectrum 1000 or on a Hitachi 270-30 IR Spectrophotometer. ^{1}H-NMR spectra were recorded on a JEOL JNM-EX 270 spectrometer, operating at 270 MHz. Chemical shifts were given in δ (ppm) values using tetramethylsilane as an internal standard. Differential scanning calorimeter and thermogravimetric analyzer were Shimadzu DSC-50 and Shimadzu TGA-50, respectively. The operating conditions were: sample weight about 5 mg, open pan, heating rate 10 °C per minute from 30 to 300 °C under nitrogen. Water contents were determined by a Karl-Fischer moisture meter, and IPA contents were determined by the GC method. For powder XRD, a Rigaku Denki Diffractometer (Min Flex) was used. The measurement condition was as follows: target, Cu; filter, Kβ filter; voltage, 30 kV; current, 15 mA; scanning speed, 2.00 degree/min.

Dimethyl 2-Cyano-3-(4-fluorophenyl)glutarate (2) To a mixture of MeOAc (222.2 g) and NaOMe (32.41 g) in toluene (240 ml) was added p-fluorobenzaldehyde (49.64 g, 0.40 mol) at 5—20 °C. After being stirred at 10—20 °C for 2 h, methyl cyanoacetate (47.56 g), 28% NaOMe (77.1 g) and MeOH (120 ml) were successively added to the mixture, and the mixture was warmed to 63—66 °C and kept at that temperature for 3 h. After being cooled to 10—20 °C, the reaction mixture was poured into diluted HCl and pH was adjusted to 8.6 and extracted with toluene. The organic layer was washed with water and evaporated *in vacuo* to remove remaining toluene. To the residue was added methanol (72 ml), and the solvent was evaporated *in vacuo*. To the residue was added methanol (560 ml) and water (240 ml) at 50—65 °C, and the mixture was kept at 40—45 °C for 30 min for crystallization, then gradually cooled to 0—5 °C. Crystals of **2** (88.04 g, yield 78.8% from p-fluorobenzaldehyde) were obtained by filtration and washed with 70% aqueous methanol and dried. The crude crystals were used in the subsequent reaction.

Analytical Sample: mp 81.0—83.8 °C. IR (KBr) cm^{-1}: 2523, 1740, 1605, 1513, 1446, 1341, 1264, 1225, 1177, 1161, 1107, 1062, 1015, 859, 711, 541. ^{1}H-NMR (CDCl$_3$) δ: 1.65 (s, 0.33H), 2.80—3.07 (m, 2H), 3.61 (s, 1H), 3.67 (s, 2H), 3.68 (s, 2H), 3.74 (s, 1H), 3.80—3.94 (m, 1H), 4.21 (d, 0.67H, $J=$ 5.6 Hz), 7.00—7.07 (m, 2H), 7.27—7.33 (m, 2H).

(±)-cis,trans-4-(4-Fluorophenyl)-5-methoxycarbonylpiperidin-2-one (3) One liter autoclave was charged with toluene (100 ml), MeOH (25 ml), Raney-cobalt (2.1 ml) and H$_2$ (16—18 atm), then compound **2** (41.9 g, 0.15 mol) in a mixed solvent of toluene (100 ml) and MeOH (25 ml) was introduced to the autoclave at 90—100 °C and at 13—16 atm of H$_2$ over a period of 3 h. The reaction mixture was kept under a hydrogenating condition for an additional 1 h. The catalyst was removed by filtration and the solvent was partially distilled. The residue was gradually cooled and the crystals were obtained by filtration and washed with toluene to give a mixture of *cis* and *trans* isomers of 4-(4-fluorophenyl)-5-methoxycarbonylpiperidin-2-one (**3**) (33.8 g, yield 89.7%).

(±)-trans-4-(4-Fluorophenyl)-5-methoxycarbonylpiperidin-2-one (4) A mixture of compound **3** (25.13 g, 0.10 mol), 28% NaOMe (1.93 g) and toluene (126 ml) was warmed to 70—80 °C for 30 min, gradually cooled to 0—5 °C, and stirred for 1 h for crystallization and neutralized with HCl in MeOH. The solvent was partially distilled to remove MeOH. Crude crystals of compound **4** in toluene were used in the next reaction.

Analytical Sample: mp 151.0—151.9 °C. IR (KBr) cm^{-1}: 3185, 3052, 1732, 1675, 1604, 1514, 1504, 1443, 1376, 1320, 1222, 1210, 1182, 1172, 843. ^{1}H-NMR (CDCl$_3$) δ: 2.53 (dd, 1H, $J=$ 10.6, 17.8 Hz), 2.72 (dd, 1H, $J=$ 5.9, 17.8 Hz), 2.97 (m, 1H), 3.41 (dt, 1H, $J=$ 5.9, 10.2 Hz), 3.47—3.66 (m, 2H), 3.50 (s, 3H), 6.85 (bs, 1H), 6.99—7.06 (m, 2H), 7.15—7.21 (m, 2H).

(3SR,4RS)-trans-4-(4-Fluorophenyl)-3-hydroxymethylpiperidine (5)

Crude crystals of compound **4** in toluene (from 0.1 mol of **3**) were added to LiAlH$_4$ (7.02 g) in tetrahydrofuran (THF) (126 ml) and warmed to 73—75 °C for 2 h. To 12.8% NaOH (576.7 g) was added the reaction mixture at 25—35 °C and the organic layer was separated, then the lower layer was discarded. The organic layer was filtered to remove insoluble material. The solvent was partially distilled and the residue was gradually cooled to give crystals of compound **5** (17.4 g, yield 83.1%).

Analytical Sample: mp 124.8—125.9 °C. IR (KBr) cm^{-1} : 3276, 3245, 3118, 1602, 1508, 1218, 1159, 1129, 1070, 1046, 1027, 833. ^{1}H-NMR (CDCl$_3$) δ: 1.56—1.86 (m, 3H), 2.36—2.71 (m, 5H), 3.07—3.19 (m, 2H), 3.32—3.39 (m, 2H), 6.94—7.00 (m, 2H), 7.12—7.18 (m, 2H).

(3S,4R)-4-(4-Fluorophenyl)-3-hydroxymethylpiperidine (6) A mixture of compound **5** (20.0 g, 0.096 mol), 26.06 g of L-o-chlorotartranilic acid and Celite (0.4 g) in water was warmed to 83—87 °C and filtered to remove insoluble material, then acetone (50 ml) was added at 45—55 °C and gradually cooled to 30 °C to give 18.25 g of crystals of the L-o-chlorotartranilic acid salt of the compound **6** as a monohydrate (39.2% yield). Pure compound **6** was obtained by decomposition of the salt with aqueous NaOH.

Analytical Sample: The salt; mp 119.4—133.9 °C. IR (KBr) cm^{-1}: 3336, 3120, 1694, 1597, 1525, 1511, 1442, 1303, 1220, 1143, 1083, 834, 755. $[\alpha]_D^{25}=+42.6°$ ($c=0.5$, EtOH(95)). Compound **6** (1 H$_2$O); mp 86.8—91.9 °C. IR (KBr) cm^{-1}: 3413, 3288, 3168, 1602, 1511, 1222, 1163, 1136, 1075, 1026, 915, 834. ^{1}H-NMR ((CD$_3$)$_2$SO) δ: 1.60—1.86 (m, 3H), 2.40—2.69 (m, 4H), 3.03—3.39 (m, 7H), 7.21—7.27 (m, 2H), 7.34—7.40 (m, 2H). $[\alpha]_D^{25}=-38.1°$ ($c=0.5$, EtOH (95)).

Paroxetine HCl IPA Solvate To a mixture of the L-o-chlorotartranilic acid salt of compound **6** (monohydrate, 24.35 g, 0.05 mol), (Boc)$_2$O (11.46 g, 0.315 mol), toluene (61 ml) and water (49 ml), was added dropwise 25% aqueous NaOH (8.4 g) at 25—30 °C, then the mixture was gradually warmed and stirred at 45—55 °C for 2 h. The organic layer was separated and washed with water. The solvent was partially distilled to remove water azeotropically, and the same amount of toluene was added to give a solution of compound **7** in toluene. To the solution was added triethylamine (6.58 g, 0.39 mol), and then methanesulfonyl chloride (6.87 g) was added dropwise at 10—35 °C. The reaction mixture was stirred at 22—25 °C for 75 min and water (56 ml) was added, then the organic layer was separated and washed with aqueous 25% NaOH (8.0 g). The toluene solution of compound **8** thus obtained was added to a mixture of sesamol (7.60 g), 28% NaOMe (10.13 g) and toluene (68 ml) and heated at reflux for 5.5 h. The reflux temperature was raised to 110 °C by the removal of methanol and kept at the temperature for 1.5 h. After cooling, the reaction mixture was washed with aqueous 25% NaOH and with water to give a solution of N-Boc paroxetine (**9**) in toluene. Toluene was removed by distillation, and IPA (19 ml) was added and distilled off. Again, IPA (19 ml) was added to the residue, and to the solution was added 20% HCl IPA solution (13.67 g) at 71—75 °C over a period of 1 h followed by stirring for 2.5 h. The solution was decolorized with active carbon (1.07 g) and filtered. The filtrate was gradually cooled to 3 °C to give crystals of paroxetine HCl IPA solvate. The crystals were dried under a vacuum at 50 °C for 3 h and at 85 °C for 12 h to give crystals of paroxetine HCl containing IPA (2.58%) and water (0.49%) (15.94 g, yield 87.14% from compound **6**).

Analytical Sample: Compound **9**: mp 72.1—74.1 °C. IR (KBr) cm^{-1}: 1688, 1628, 1606, 1506, 1491, 1473, 1404, 1391, 1279, 1243, 1223, 1188, 1164, 1125, 1037, 1020, 937, 838. ^{1}H-NMR (CDCl$_3$) δ: 1.50 (s, 9H), 1.67—1.77 (m, 3H), 2.01 (br s, 1H), 2.68—2.80 (m, 3H), 3.41—3.47 (m, 1H), 3.58—3.61 (m, 1H), 4.32 (br d, 2H, $J=$ 52.8 Hz), 5.88 (s, 2H), 6.13 (dd, 1H, $J=$ 2.3, 8.6 Hz), 6.35 (d, 1H, $J=$ 2.3 Hz), 6.62 (d, 1H, $J=$ 8.6 Hz), 6.94—7.01 (m, 2H), 7.11—7.16 (m, 2H). $[\alpha]_D^{25}=-27.9°$ ($c=0.5$, EtOH(95)).

Typical Sample of Dried Paroxetine HCl Form-II Crystals with around 2.6% Weight of Bound IPA: mp 114.4—119.4 °C. IR (Nujol) cm^{-1}: 3632, 3390, 1603, 1512, 1467, 1378, 1340, 1286, 1220, 1195, 1132, 1090, 1034, 923, 888, 831, 805. ^{1}H-NMR ((CD$_3$)$_2$SO) δ: 1.94 (br d, 1H, $J=$ 12.2 Hz), 2.18 (dd, 1H, $J=$ 22.6, 12.7 Hz), 2.59 (m, 1H), 2.91—3.09 (m, 3H), 3.45—3.68 (m, 4H), 6.01 (s, 2H), 6.27 (dd, 2H, $J=$ 8.6, 2.3 Hz), 6.58 (d, 1H, $J=$ 2.3 Hz), 6.82 (d, 1H, $J=$ 8.6 Hz), 7.24 (t, 2H, $J=$ 8.6 Hz), 7.70—7.35 (m, 2H). [For bound IPA in the crystals: 1.06 (d, 6H/6, $J=$ 6.3 Hz), 3.85 (m, 1H/6), 4.46 (d, 1H/6)]. $[\alpha]_D^{25}=-88.0°$ ($c=0.5$, EtOH(95)).

Desolvation of Form-II Crystals A 100 ml flask was charged with 3.8 g of paroxetine HCl form-II crystals. The flask was connected with a vacuum line (2—3 mmHg) and placed in an oven. The temperature of the oven was gradually raised, then kept at a fixed temperature for a fixed number of hours. The IPA content and water content of the crystals were determined by appropriate analysis methods.

Resolvation and Re-desolvation of Dried Form-II Crystals A 100 ml

flask was charged with 3.8 g of paroxetine HCl form-II crystals and finally dried under a vacuum at 110 °C for 13 h. The flask was cooled to room temperature and 38 ml of IPA was added to the flask. The dried crystals were immersed in IPA and gently stirred for 1 h and filtered. For the re-desolvation experiment, the crystals thus obtained were treated as described in the desolvation experiment above.

References

1) *Drugs Fut.*, **11**, 112—115 (1986).
2) Haddock R. E., Johnson A. M., Langley P. F., Nelson D. R., Pope J. A., Thomas D. R., Woods F. R., *Acta Psychiatr. Scand.*, **80** (supp. 350), 24—26 (1989).
3) *a*) Christensen J. A., Squires R. F., Ger. Offen. DE 2404113 (1974) [*Chem. Abstr.*, **81**, 152011q (1974); *b*) Barnes R. D., Wood-Kaczmar M. W., Richardson J. E., Lynch I. R., Buxton P. C., Curzons A. D., Eur. Pat. Appl. EP 223403 (1987) [*Chem. Abstr.*, **107**, 141102z (1987)]; *c*) Hansen J. B., Treppendahl S., Engelstoft M., Bentzen B., Lehmann S.,

PCT Int. Appl. WO 96 36636 (1996) [*Chem. Abstr.*, **126**, 59872*j* (1997)]; *d*) i; Wang S., Okazoe T., Matsumura Y., Mori N., Nishino J., Ookura K., Eur. Pat. Appl. EP 802185 (1997) [*Chem. Abstr.*, **127**, 358789*b* (1997)]; ii; Wang S., Matsumura Y., Eur. Pat. Appl. EP 810225 (1997) [*Chem. Abstr.*, **128**, 61506*c* (1998)].
4) *a*) Amat M., Hidalgo J., Bosch J., *Tetrahedron: Asymmetry*, **7**, 1591—1594, (1996); *b*) Sugi K., Itaya N., Katsura T., Igi M., Yamazaki S., Ishibashi T., Yamaoka T., Kawada Y., Tagami Y., Eur. Pat. Appl. EP 812827 (1997) [*Chem. Abstr.*, **128**, 75308*b* (1998)]; *c*) Patil V. D., Viswanathan C. L., *Indian Drugs*, **35**, 686—692 (1998) [*Chem. Abstr.*, **130**, 18232*t* (1999)].
5) Buxton P. C., Lynch I. R., Roe J. M., *Int. J. Pharm.*, **42**, 135—143 (1988).
6) Yokota M., Uekusa H., Ohashi Y., *Bull. Chem. Soc. Jpn.*, **72**, 1731—1736 (1999).
7) Koelsch C. F., *J. Am. Chem. Soc.*, **65**, 2459—2460 (1943).
8) Montzka T. A., Pindell T. L., Matiskella J. D., *J. O. Chem.*, **33**, 3393—3395 (1968).
9) Ward N., Jacewicz V. W., Ger. Offen. DE 19603797 (1996) [*Chem. Abstr.*, **125**, 204558*y* (1996)].

Structural and Spectral Characteristics of the Electrogenerated Tetracyanoethylene Dianion

Noriko OKUMURA, Masashi GOTO, and Bunji UNO*

Gifu Pharmaceutical University, Mitahora-higashi, Gifu 502-8585, Japan.

Structural and spectral characteristics of the electrogenerated tetracyanoethylene dianion (TCNE^{2-}) were experimentally and theoretically examined. Spectroelectrochemistry of TCNE gives the spectra of TCNE^{2-} in CH$_3$CN at 220 nm, and in CH$_2$Cl$_2$ at 300 nm. These spectral characteristics are well explained by CIS/6-31G(d) and semiempirical CNDO/S-CI calculations. The bands in CH$_3$CN and in CH$_2$Cl$_2$ are assigned to the degenerate ^{1}E$\leftarrow^1$A$_1$ transition at the D_{2d} structure and the ^{1}B$_{2u}\leftarrow^1$A$_g$ transition at the D_{2h} structure, respectively. The rotation barrier of the C=C bond in TCNE^{2-} is estimated by Hartree–Fock (HF), second-order Møller–Plesset perturbation (MP2) and fourth-order MP (MP4) calculations with 6-31G(d), 6-31+G(d) and 6-311+G(d) basis sets as 42—51 kJ mol^{-1}. The D_{2d} structure is most stable, and the D_{2h} structure represents the transition state of the internal rotation. The calculations reveal that the two-electron addition to the antibonding LUMO of TCNE causes an easy rotation around the C=C bond of TCNE^{2-} characterized by the formal single bond. These results show that TCNE^{2-} preferentially adopts D_{2d} and D_{2h} structures in solvents depending upon the solvent nature by virtue of the easy rotation around the C=C bond.

Key words   tetracyanoethylene dianion; spectroelectrochemistry; structural property; MO calculation; rotational barrier

The chemistry of a two-electron reduced product of organic molecules has received much attention in recent years from both theoreticians and experimentalists, as subjects for studying aromaticity and electronic multiplicity,[1—3] structural and spectral properties,[4—12] reactivity,[13] and intermolecular interaction with cationic species and hydrogen donors.[6—9,14—17] A recent and exciting prospect in the area of organic molecular metamagnetism and ferromagnetism lies in understanding the structure–function relationship of metallocenium salts of strong acceptor anions such as the mono- and dianionic species of tetracyanoethylene (TCNE) and tetracyanoquinodimethane.[10,11,18] The structural characteristics of the organic π-dianions are of fundamental interest in chemistry, and are essential to understanding peculiar properties and characteristic function. Information on the structure of organic π-dianions is, however, quite limited,[4,6—8,10,11] whereas the structural characteristics of the anion radical are well documented. The most investigated dianions are quinones with regard to biological function and electron and proton transfer in the hydrogen-bonding systems.[6—8,14] The π-dianions have been considered to have the same planar π-conjugation system as those of the neutral and monoanionic species. Miller and co-workers have documented for the first time a three-dimensional structure of the dianion, with the aid of X-ray crystallographic analyses of the TCNE^{2-} metallocenium salts.[10,11] The interesting results involving the D_{2d} and skewed structures of TCNE^{2-} are proposed for the [(Me$_2$N)$_2$C=C(NMe$_2$)$_2$]$^{2+}$TCNE^{2-} and {[Co(C$_5$Me$_5$)$_2$]$^+$}$_2$TCNE^{2-} salts.[10,11] There has been, however, no experimental report on the structure in solvents. We are particularly interested in the structure of TCNE^{2-} in solution as it plays an important role in molecular recognition and complex formation based on the π–π interaction of the dianion.[19] Recently, we have reported the experimental and theoretical results of the D_{2d} structure of TCNE^{2-} in solution.[12]

In this study, the structural and spectral properties of TCNE^{2-} in CH$_3$CN and CH$_2$Cl$_2$ are primarily examined by

spectroelectrochemical measurements and MO calculations. The electronic spectra of TCNE^{2-} in solution have not been fully analyzed yet. Discussion has been extended to the structural characteristics of TCNE^{2-} on the basis of *ab initio* MO calculations. The purpose of this paper is to gain deeper insight into the problem of the structure of TCNE^{2-}, showing how the C(CN)$_2$ planes of TCNE^{2-} easily rotate around the C=C bond in such molecular environments as solvents.

Experimental

Chemicals TCNE (Fig. 1) was commercially available from Nacalai Tesque, Inc., and was purified by repeated sublimation under reduced pressure, then once again just before use. CH$_2$Cl$_2$ and CH$_3$CN of spectrograde purity used for electrochemical and spectroelectrochemical measurements were purchased from Nacalai Tesque, Inc., and were dried over molecular sieves (4A for CH$_2$Cl$_2$ and 3A for CH$_3$CN) for more than 2 d, then carefully rectified. Tetrabutylammonium perchlorate (TBAP) was used as a supporting electrolyte for these solvents, being prepared by a dropwise addition of 70% perchloric acid to an aqueous tetrabutylammonium bromide solution, and then recrystallized three times from a mixture of ethyl acetate and pentane. TBAP was sufficiently dried in a high vacuum just before use.

Electrochemical and Spectroelectrochemical Measurements Cyclic voltammetry was performed at 25.0±0.1 °C with a BAS 100B electrochemical workstation, using a three electrode system consisting of a glassy carbon working electrode, a platinum wire counter electrode and a saturated calomel reference electrode (SCE). Other details of the electrochemical measurements were described in a previous paper.[20] Electronic spectra of TCNE$^-$ and TCNE^{2-} were observed with a method involving rapid circulation of the electrolyzed solution *via* a Shimadzu SPD-M10A photodiode array detector.[6] Controlled-potential electrolyses were performed in a bulk electrolysis cell with a Hokuto Denko HA-501 potentiostat in a three-electrode mode consisting of a reticulated vitreous carbon working electrode, an Ag/AgNO$_3$ reference electrode (containing CH$_3$CN solution of 0.1 mol dm^{-3} TBAP and 0.01 mol dm^{-3} AgNO$_3$), and a platinum wire counter electrode.
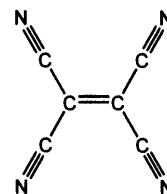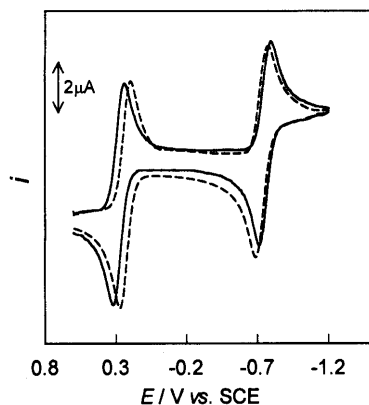

Fig. 1.   Molecular Structure of TCNE

Fig. 2. Cyclic Voltammograms of 4.0×10^{-4} mol dm^{-3} TCNE in CH$_2$Cl$_2$ (Solid Line) and in CH$_3$CN (Dotted Line) Containing 0.1 mol dm^{-3} TBAP

Fig. 3. Spectral Changes of TCNE in CH$_2$Cl$_2$ Containing 0.5 mol dm^{-3} TBAP (a) and in CH$_3$CN Containing 0.1 mol dm^{-3} TBAP (b) with Electrolysis

Concentrations of TCNE are 2.76×10^{-4} mol dm^{-3} (a) and 1.45×10^{-4} mol dm^{-3} (b). Applied potentials are 0.0 V vs. Ag/AgNO$_3$, corresponding to the TCNE$^-$ generation from TCNE.

Fig. 4. Spectral Changes of TCNE in CH$_2$Cl$_2$ Containing 0.5 mol dm^{-3} TBAP (a) and in CH$_3$CN Containing 0.1 mol dm^{-3} TBAP (b) with Electrolysis

Concentrations of TCNE are 2.76×10^{-4} mol dm^{-3} (a) and 1.45×10^{-4} mol dm^{-3} (b). Applied potentials are -1.5 V vs. Ag/AgNO$_3$ (a) and -1.0 V vs. Ag/AgNO$_3$ (b), corresponding to the TCNE^{2-} generation from TCNE$^-$.

The details and procedures of the spectroelectrochemical measurements were described in a previous paper.[6]

MO Calculations Postulating that TCNE^{2-} is a closed-shell singlet species, the geometry for TCNE was gradient optimized at the self-consistent field (SCF) level with the Gaussian98 program.[21,22] The basis sets used here were the 6-31G(d) basis sets that are very common for calculations involving up to medium-sized systems. The 6-31+G(d) basis sets suitable for the anionic species and the triple split valence 6-311+G(d) basis sets were utilized to get results with higher accuracy.[21] The conformational energies were computed in the rotations around the C=C bond at every 10° angle by HF calculations, by MP2 calculations, and by MP4 calculations including singles, doubles, triples and quadruples (SDTQ). The MP2 and MP4 calculations were done at HF geometries optimized with the corresponding basis sets. The geometries of neutral TCNE and the open-shell doublet anion were obtained in the HF and unrestricted HF (UHF) frameworks by gradient techniques at the 6-31G(d) level, respectively. Solvation energy to the dianion was calculated by the Tomasi polarized continuum model (PCM) based on the self-consistent reaction field methods.[21,23,24] The dielectric constants of CH$_2$Cl$_2$ and CH$_3$CN necessary for the calculations were cited as 8.93 and 36.64, respectively.[21]

The configuration interaction calculations (CIS/6-31G(d) calculations) involving combinations of single substitutions out of the ground state calculated by the HF/6-31G(d) and UHF/6-31G(d) methods, and semiempirical CNDO/S-CI calculations were carried out to interpret the experimental absorption spectra. Later calculations were done with parameters taken from the literature of Jaffe's group and others,[25] and two-center repulsion integrals were evaluated using the Nishimoto–Mataga equation.[26] The description of spectra based on the group theory is derived from the molecular coordinates as follows. The main axis (z-axis) was given to the C$_2$-axis perpendicular to the molecular plane for D$_{2h}$ symmetry, and to one of the C$_2$-axes perpendicular to the C=C bond for D$_2$ symmetry. Under these symmetries, the C=C bond was put on the x-axis. For D$_{2d}$ symmetry, the main axis (z-axis) was given to the C$_2$ axis involving the C=C bond.

Results and Discussion

Electrochemistry and Spectroelectrochemistry of TCNE in CH$_2$Cl$_2$ and CH$_3$CN In dry CH$_2$Cl$_2$ and CH$_3$CN, TCNE typically shows two cathodic polarographic waves which correspond to the formation of TCNE$^-$ and TCNE^{2-}, respectively. In these reductions, the first step is reversible and the second is at least quasi-reversible at customary scan rates, as is seen from the cyclic voltammograms shown in Fig. 2. The energetics of these steps have been discussed on the basis of MO theory in previous papers.[20,27] Spectroelectrochemistry of TCNE gives the spectra of TCNE$^-$ and TCNE^{2-} electrogenerated in these solvents, showing clear isosbestic points resulting from the reversible redox equilibrium, as shown in Figs. 3 and 4. The spectral profiles of TCNE$^-$ in CH$_2$Cl$_2$ and in CH$_3$CN closely resemble each other, being in good agreement with the previously published
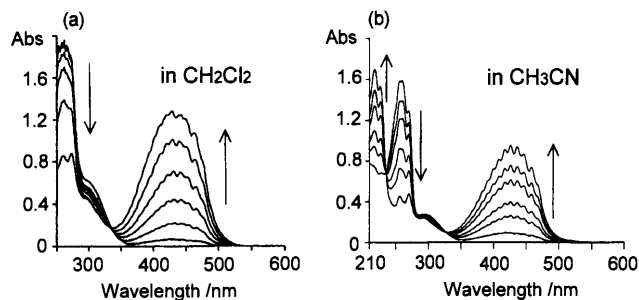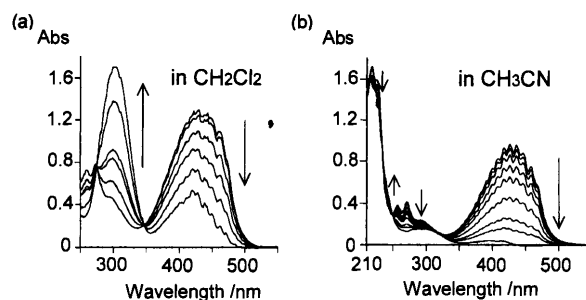
spectra.[10,28,29] On the other hand, the spectrum of TCNE^{2-} in CH$_3$CN looks very different from that in CH$_2$Cl$_2$, as is clearly seen from Fig. 4. The spectrum of TCNE^{2-} in CH$_2$Cl$_2$ shows a clear strong peak near 300 nm, undoubtedly contributed from the π-conjugation in TCNE^{2-}. The spectral profiles for the TCNE$^-$ and TCNE^{2-} generations in CH$_2$Cl$_2$ are similar to those of quinones previously investigated.[6] It seems that the spectrum in CH$_2$Cl$_2$ results from the D$_{2h}$ structure of TCNE^{2-} as well as TCNE and TCNE$^-$. The spectrum of TCNE^{2-} in CH$_3$CN shows no structure attributable to the dianion except for a weak band near 300 nm and the onset of a strong peak near 250 nm in the direction of shorter wavelengths, as illustrated in Fig. 4b. The spectrum is in considerable agreement with the published spectrum of the ([Co(C$_5$Me$_5$)$_2$]$^+$)$_2$TCNE^{2-} salt.[10] The structure of TCNE^{2-} in CH$_3$CN seems to be quite different from that in CH$_2$Cl$_2$.

Spectral and Structural Characteristics of TCNE^{2-} The CIS/6-31G(d) calculation and semiempirical CNDO/S-CI calculations were performed to gain more insight into the relation between the spectra and the structure of TCNE^{2-} as well as TCNE$^-$. Table 1 lists the CIS calculation results and the observed spectral data. Figure 5 shows the calculated MOs concerning the electronic transition of TCNE and the reduced species. The 430 nm band of TCNE$^-$ with a progression of vibrational transitions is assigned to the single $^2B_{3u} \leftarrow$ $^2B_{2g}$ transition. The calculated transition energy, however, did not reproduce the experimental value. This is probably due to a deficiency in the CIS method rather than the red shift of the

Table 1. Spectral Data and CIS/6-31G(d) Calculation Results for the Longest Wavelength Bands of TCNE⁻ and TCNE²⁻

Compounds	Observed		Calculated			
	E/eV (λ/nm)	E/eV (λ/nm)	$f^{c)}$	CI(%)$^{d)}$	Assignment$^{e)}$	
TCNE⁻ (D_{2h})	2.88 (430)$^{a,b)}$	3.40 (365)	0.26	90 (b$_{1u}$→b$_{2g}$)	$^2B_{3u}$←$^2B_{2g}$	
TCNE²⁻ (D_{2h})	4.13 (300)$^{b)}$	6.87 (181)$^{f)}$	0.54	32 (b$_{2g}$→a$_u$), 6 (b$_{1u}$→b$_{3g}$)	$^1B_{2u}$←^1A_g	
TCNE²⁻ (D_{2d})	5.64 (220)$^{a)}$	7.13 (174)$^{g)}$	0.21	23 (e→a$_2$), 11 (e→b$_1$)	^1E←$^1A_1$	
		7.13 (174)$^{g)}$	0.21	23 (e→a$_2$), 11 (e→b$_1$)	^1E←$^1A_1$	

a) Values at the maximum intensity in CH₃CN. b) Values at the maximum intensity in CH₂Cl₂. c) Oscillator strengths. d) For example, (b$_{1u}$→b$_{2g}$) means a singly excited configuration from the b$_{1u}$ π-MO to the b$_{3g}$ π-MO. e) The coordinates were given in the text. f) The value was estimated by CNDO/S-CI calculations as 3.94 eV (316 nm). g) The value was estimated by CNDO/S-CI calculations as 4.19 eV (297 nm).
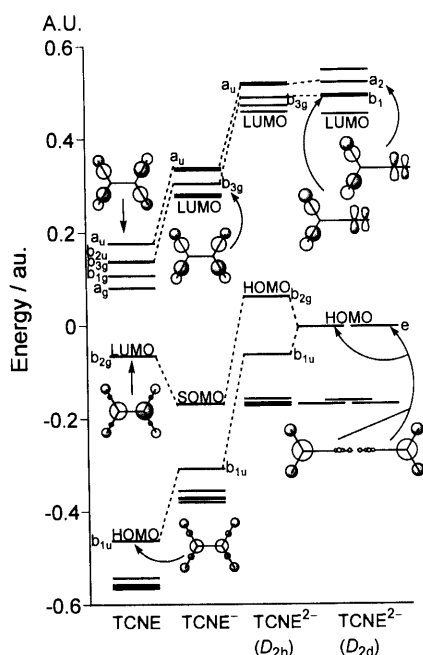
Fig. 5. HF/6-31G(d) and UHF/6-31G(d) SCFMO Energy Levels and the Illustrations of MOs Concerning the Longest Wavelength Band of TCNE, TCNE⁻ and TCNE²⁻

The axes used for the MO calculations are described in the experimental section. Energies in au (1 au=2625.500 kJ mol⁻¹).
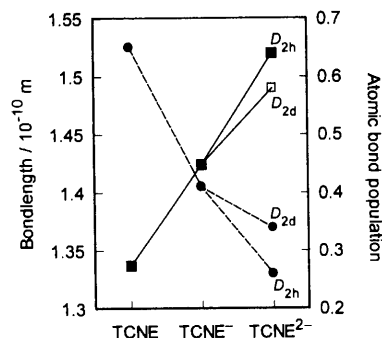

Fig. 6. Distances (Solid Line) and Atomic Bond Population (Dotted Line) of the C=C Bond of TCNE, TCNE⁻ and TCNE²⁻

Fig. 7. Illustration of the LUMO of TCNE
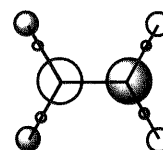
experimental value by solvents. The band of TCNE⁻ appears in the longer wavelength region than those for TCNE and TCNE²⁻, arising from the small energy gap between the filled b$_{1u}$-MO and the singly occupied b$_{2g}$-MO (SOMO) derived from the HOMO and the LUMO of TCNE, respectively. The CIS/6-31G(d) calculation results for TCNE²⁻ are in good agreement with the CNDO/S-CI calculation trends in the spectral characters but not in the transition energies. CNDO/S-CI calculations gave the transition energies for the D_{2h} and D_{2d} structures of TCNE²⁻ at 3.94 eV (316 nm) and 4.19 eV (297 nm), respectively. The CIS method again predicted much larger transition energies than the experimental results. The CIS and CNDO/S-CI calculation results for the D_{2h} structure indicate that the strong band near 300 nm is assigned to the $^1B_{2u}$←^1A_g transition delocalized in a whole molecule of TCNE²⁻, as is seen from Table 1 and Fig. 5. The spectral characteristics are the same as those of the 1,4-benzoquinone dianion adopting the D_{2h} structure.⁶) The observed band near 300 nm in CH₂Cl₂ is reasonably assigned to the π–π* band of TCNE²⁻ adopting the D_{2h} structure. The calculations for the D_{2d} structure of TCNE²⁻ give a single peak

in the UV–Vis region, which is assigned to the overlapping degenerate ^1E←$^1A_1$ transitions localized in the [C(CN)₂]⁻ groups separated by the C=C bond, as shown in Table 1 and Fig. 5. The rotation from the D_{2d} structure of TCNE²⁻ causes the electronic configuration interaction between the degenerate transitions, giving a strong absorption band in the longer wavelength region. Furthermore, the calculations provided clear-cut evidence for a difference in transition energies between the D_{2h} and D_{2d} structures. The red-shift of the TCNE²⁻ band with the rotation is attributed to the destabilization of the HOMO (the b$_{2g}$-HOMO of the D_{2h} structure) derived from the degenerate e-HOMOs in the D_{2d} structure, as illustrated in Fig. 5. These results reasonably indicate that the difference between the structures in CH₂Cl₂ and in CH₃CN finds expression in the spectral change.

Calculated Rotational Barrier around the C=C Bond of TCNE²⁻ The geometric parameters optimized for TCNE²⁻ are in good agreement with the experimental results determined by X-ray crystallographic analyses of the TCNE²⁻ metallocenium salt.¹⁰) Conspicuous trends in the geometric parameters of TCNE and the reduced species include a lengthening of the C=C bond with an increasing negative charge, as shown in Fig. 6, which appeared in the experimental results.¹⁰,²⁸,²⁹) Major changes are brought about on the C=C bond order of TCNE as a result of the two-electron addition to the LUMO (b$_{2g}$) of antibonding nature for

Table 2. Calculated Total Energies of TCNE^{2-} at the Dihedral Angles (θ) between the Two C(CN)$_2$ Planes[a]

θ	6-31G(d)			6-31+G(d)			6-311+G(d)		
	SCF[b]	MP2[c]	MP4[c]	SCF[b]	MP2[c]	MP4[c]	SCF[b]	MP2[c]	MP4[c]
0°	-1168049.806	-1171642.982	-1171886.260	-1168146.462	-1171811.937	-1172058.036	-1168386.849	-1172189.893	-1172447.236
10°	-1168051.348	-1171644.547	-1171887.814	-1168148.173	-1171814.210	-1172060.273	-1168388.552	-1172192.111	-1172449.450
20°	-1168055.779	-1171648.572	-1171891.812	-1168153.037	-1171819.955	-1172065.962	-1168393.396	-1172197.269	-1172454.616
30°	-1168062.544	-1171654.714	-1171897.926	-1168160.233	-1171827.240	-1172073.199	-1168400.549	-1172203.819	-1172461.171
40°	-1168070.814	-1171661.893	-1171905.068	-1168168.653	-1171835.431	-1172081.369	-1168408.900	-1172211.162	-1172468.562
50°	-1168079.593	-1171669.165	-1171912.298	-1168177.195	-1171842.943	-1172088.872	-1168417.345	-1172218.362	-1172475.828
60°	-1168087.833	-1171675.984	-1171919.072	-1168184.933	-1171849.363	-1172095.299	-1168424.961	-1172224.517	-1172482.052
70°	-1168094.546	-1171681.337	-1171924.384	-1168191.105	-1171853.967	-1172099.946	-1168431.007	-1172229.004	-1172486.615
80°	-1168098.928	-1171684.773	-1171927.804	-1168195.098	-1171856.290	-1172102.314	-1168434.897	-1172231.496	-1172489.181
90°	-1168100.449	-1171686.088	-1171929.119	-1168196.483	-1171857.064	-1172103.114	-1168436.240	-1172232.236	-1172489.955
$\Delta E^{d)}$	50.643	43.106	42.859	50.021	45.127	45.078	49.391	42.343	42.719

a) Energies in kJ mol^{-1}. b) Values were obtained by HF full optimization calculations. c) Values were calculated at HF optimized geometries. d) The rotational barriers around the C=C bond.

the π bond (Fig. 7). The C=C bond of TCNE^{2-} becomes a formal single bond at any values of the dihedral angle (θ) of the two C(CN)$_2$ planes, characterized by the long bond distance and the small value of atomic bond population. This allows the C(CN)$_2$ planes of TCNE^{2-} to be easily rotated around the C=C bond.

Table 2 lists the total energies of TCNE^{2-} calculated for the structures of various θ values. All the calculation methods used here give very similar trends in the energy dependence upon θ. The most stable structure is the D_{2d} structure, and the D_{2h} structure represents the transition state of the rotation around the C=C bond. The barrier for the internal rotation in TCNE^{2-} was calculated as listed in Table 2. The post SCF calculations give lower barriers than the HF calculations. The rotational barrier for TCNE^{2-} is much lower than that for TCNE and TCNE$^-$ estimated as 422.718 and 70.637 kJ mol^{-1} (HF/6-31(G)), respectively. Figure 8 shows the calculated electronic energies and nuclear repulsion energies upon the θ values. Changes in the electronic stabilization (conjugation) and steric crowding are completely reverse in the direction of energy change upon θ. The balance between them governs the structures of TCNE and the reduced products. The D_{2h} structures of TCNE and TCNE$^-$ are brought about by electronic stabilization through conjugation between the two C(CN)$_2$ planes sufficient to overcome the nuclear repulsion. The easy rotation around the C=C bond of TCNE is caused by a decrease of the difference in electronic energies between the D_{2h} and D_{2d} structures with an increasing the negative charge. This implies that the charge-transfer from TCNE^{2-} to the solvent or additives significantly affects the stability of the D_{2d} structures. The electron accepting nature of CH$_2$Cl$_2$ with low dipole interaction may contribute to the preferable D_{2h} structure of TCNE^{2-}. In addition, significant change seems to be brought about on the structure of TCNE^{2-} as a result of electrostatic and dipole interactions of solvents and counter ions as well as the charge-transfer interaction.[30] Indeed, the solvation energy of TCNE^{2-} calculated by the PCM method runs up to 600—700 kJ mol^{-1}.[31] The preferential stabilization of D_{2h} TCNE^{2-} over D_{2d} TCNE^{2-} depending on the solvent nature, is a novel and interesting result. The presence of real solvent and counter ion molecules in the MO calculations will allow a better understanding of the phenomenon in future work.
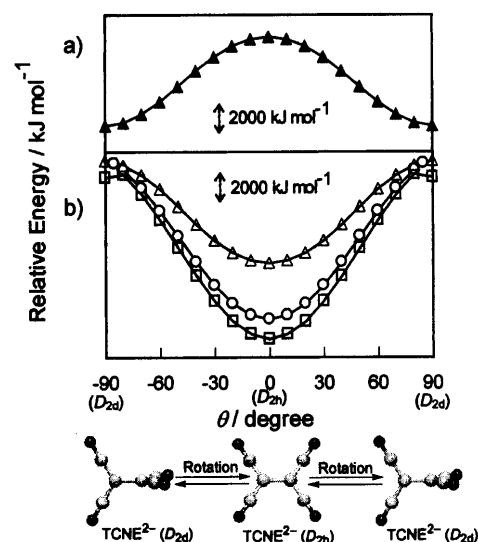

Fig. 8. Change in Nuclear Repulsion (a) and Electronic Energies (b) of TCNE and the Reduced Species upon the Dihedral Angle (θ) of the Two C(CN)$_2$ Planes

The nuclear repulsion was calculated for the optimized HF/6-31G(d) geometries of TCNE^{2-}. The electronic energies were calculated by the HF/6-31G(d) and UHF/6-31G(d) methods. Plots of □, ○ and △ donate the energies for TCNE, TCNE$^-$ and TCNE^{2-}, respectively.

In conclusion, the structure of TCNE^{2-} is characterized by a formal single C=C bond with the low rotational barrier caused by the two-electron addition to the antibonding LUMO of TCNE. The spectral measurements and MO calculations suggest that TCNE^{2-} preferentially adopts the D_{2h} structure in CH$_2$Cl$_2$ and the D_{2d} structure in CH$_3$CN as well as in crystals of the metallocenium salts previously published.[10,11] The nature of solvents and counter ions seems to significantly affect the structure of TCNE^{2-}. The present conclusion is important to extended discussion on molecular recognition and molecular function of the electrogenerated dianions upon the structure.

References and Notes

1) Ebata K., Setaka W., Inoue T., Kabuto C., Kira M., Sakurai H., *J. Am. Chem. Soc.*, **120**, 1335—1336 (1998).

2) Minskey A., Meyer A.Y., Poupko R., Rabinovitz M., *J. Am. Chem. Soc.*, **105**, 2164—2172 (1983).

3) Iyoda M., Sasaki S., Sultana F., Yoshida M., Kuwatani Y., Nagase S., *Tetrahedron Lett.*, **37**, 7987—7990 (1996).

4) Bausch J. W., Gregory P. S., Olah G. A., Prakach G. K. S., Schleyer P. v. R., Segal G. A., *J. Am. Chem. Soc.*, **111**, 3633—3640 (1989).

5) Modler-Spreitzer A., Mannschreck A., Scholz M., Gescheidt G., Spreitzer H., Daub J., *J. Chem. Res. (S)*, **1995**, 180—181.

6) Okumura N., Uno B., *Bull. Chem. Soc. Jpn.*, **72**, 1213—1217 (1999).

7) Uno B., Kawabata A., Kano K., *Chem. Lett.*, **1992**, 1017—1020.

8) Zhao X., Imahori H., Zhan C. G., Sakata Y., Iwata S., Kitagawa T., *J. Phys. Chem. A*, **101**, 622—631 (1997).

9) Oyama M., Takei A., Okazaki S., *J. Chem. Soc., Chem. Commun.*, **1995**, 1909—1910.

10) Dixon D. A., Miller J. S., *J. Am. Chem. Soc.*, **109**, 3656—3664 (1987).

11) James R., Foxman B. M., Guarrera D., Miller J. S., Calabrese J. C., Reis A. H., Jr., *J. Mater. Chem.*, **6**, 1627—1631 (1996).

12) Uno B., Okumura N., *Chem. Lett.*, **1999**, 1167—1168.

13) Wakahara T., Kodama R., Akasaka T., Ando W., *Bull. Chem. Soc. Jpn.*, **70**, 665—670 (1997); Stevenson C. D., Fico R. M., Jr, *J. Org. Chem.*, **60**, 5452—5455 (1995).

14) Gupta N., Linschitz H., *J. Am. Chem. Soc.*, **119**, 6384—6391 (1997).

15) Aquino M. A. S., White C. A., Bensimon C., Greedan J. E., Crutchley R. J., *Can. J. Chem.*, **74**, 2201—2208 (1996).

16) Kurihara M., Saito I., Matsuda Y., *Chem. Lett.*, **1996**, 1109—1110.

17) Sekiguchi A., Matsuo T., Ebata K., Sakurai H., *Chem. Lett.*, **1996**, 1133—1134.

18) Miller J. S., Epstein A. J., *Chem. Commun.*, **1998**, 1319—1325; Miller J. S., Calabrese J. C., Rommelmann H., Chittapeddi S. R., Zhang J. H., Reiff W. M., Epstein A. J., *J. Am. Chem. Soc.*, **109**, 769—781 (1987).

19) Uno B., Okumura N., presented in part at the 195th Meeting of the Electrochemical Society, Inc., Seattle, May, 1999; Uno B., Okumura N., *Chem. Lett.*, **1999**, 983—984.

20) Kubota T., Kano K., Uno B., Konse T., *Bull. Chem. Soc. Jpn.*, **60**, 3865—3877 (1987).

21) Foresman J. B., Frisch A., "Exploring Chemistry with Electronic Structure Methods," 2nd ed., Gaussian, Inc., Pittsburgh, 1993.

22) Frisch M. J., Trucks G. W., Schlegel H. B., Scuseria G. E., Robb M. A., Cheeseman J. R., Zakrzewski V. G., Montgomery J. A., Stratmann R. E., Jr., Burant J. C., Dapprich S., Millam J. M., Daniels A. D., Kudin K. N., Strain M. C., Farkas O., Tomasi J., Barone V., Cossi M., Cammi R., Mennucci B., Pomelli C., Adamo C., Clifford S., Ochterski J., Petersson G. A., Ayala P. Y., Cui Q., Morokuma K., Malick D. K., Rabuck A. D., Raghavachari K., Foresman J. B., Cioslowski J., Ortiz J. V., Baboul A. G., Stefanov B. B., Liu G., Liashenko A., Piskorz P., Komaromi I., Gomperts R., Martin R. L., Fox D. J., Keith T., Al-Laham M. A., Peng C. Y., Nanayakkara A., Gonzalez C., Challacombe M., Gill P. M. W., Johnson B., Chen W., Wong M. W., Andres J. L., Gonzalez C., Head-Gordon M., Replogle E. S., Pople J. A., *Gaussian 98*, Pittsburgh, 1998.

23) Miertus S., Tomasi J., *Chem. Phys.*, **65**, 239—245 (1982); Miertus S., Scrocco E., Tomasi J., *ibid.*, **55**, 117—129 (1981).

24) Foresman J. B., Keith T. A., Wiberg K. B., Snoonian J., Frisch M. J., *J. Phys. Chem.*, **100**, 16098—16104 (1996).

25) Ellis R. L., Kuehnlenz G., Jaffe H. H., *Theor. Chim. Acta*, **26**, 131—140 (1972); Kuehnlenz G., Jaffe H. H., *J. Chem. Phys.*, **58**, 2238—2243 (1973); Tinland B., *Mol. Phys.*, **16**, 413—416 (1969); Lipari N. O., Duke C. B., *J. Chem. Phys.*, **63**, 1768—1774 (1975); Jacques P., Faure J., Chalvet D., Jaffe H. H., *J. Phys. Chem.*, **85**, 473—479 (1981).

26) Mataga N., Nishimoto K., *Z. Physik. Chem.*, **13**, 140—157 (1957).

27) Uno B., Matsuhisa Y., Kano K., Kubota T., *Chem. Pharm. Bull.*, **32**, 1—10 (1984).

28) Hans B., Markus K., *Helv. Chimi. Acta*, **80**, 516—530 (1997).

29) Webster O. W., Mahler W., Benson R. E., *J. Am. Chem. Soc.*, **84**, 3678—3684 (1962).

30) Half-wave reduction potentials are no mirror of the structural change caused by solvent effect because those are given by the free energy change with the redox state change involving structures and solvent effect. Indeed, the second wave in CH_2Cl_2 is almost the same as that in CH_3CN, as shown in Fig. 2.

31) The PCM solvation energies of $TCNE^{2-}$ for the D_{2h} and D_{2d} structures are calculated as -613.1 and $-605.4\,kJ\,mol^{-1}$ for CH_2Cl_2, respectively, and -672.2 and $-663.7\,kJ\,mol^{-1}$ for CH_3CN, respectively. The experimental solvation energy of CH_3CN is estimated for the dianions of benzenoid alternant hydrocarbons as less negative values than $-480\,kJ\,mol^{-1}$, which is well explained by the Born-type equation, as previously published.[20]

542

Chem. Pharm. Bull. **48**(4) 542—546 (2000)

Vol. 48, No. 4

Megastigmane, Benzyl and Phenethyl Alcohol Glycosides, and 4,4'-Dimethoxy-β-truxinic Acid Catalpol Diester from the Leaves of *Premna subscandens* MERR.

Hirokazu Sudo,[a] Toshinori Ide,[a] Hideaki Otsuka,*,[a] Eiji Hirata,[b] Anki Takushi,[c] Takakazu Shinzato,[d] and Yoshio Takeda[e]

Institute of Pharmaceutical Sciences, Hiroshima University School of Medicine,[a] 1-2-3 Kasumi, Minami-ku, Hiroshima 734–8551, Japan, Faculty of Agriculture, University of the Ryukyus,[b] 1 Senbaru, Nishihara-cho, Nakagami-gun, Okinawa 905–0213, Japan, 134 Furugen, Yomitan-son, Nakagami-gun, Okinawa 904–0014, Japan,[c] University Forest, Faculty of Agriculture, University of the Ryukyus,[d] 685 Aza Yona, Kunigami-son, Kunigami-gun, Okinawa 905–1427, Japan, and Faculty of Integrated Arts and Sciences, Tokushima University,[e] Minamijosanjima-cho, Tokushima 770–8502, Japan.

Extensive isolation work on the *n*-BuOH-soluble fraction obtained from the leaves of *Premna subscandens*, collected on Ishigaki island, Okinawa, afforded six compounds. Two were identified as megastigmane glucosides, 7-(3,5-dihydroxy-1,1,5-trimethylcyclohexylidene)-9-methylprop-8-enyl 9-*O*-β-D-glucopyranoside and 3-hydroxy-5,6-epoxy-β-ionol 9-*O*-β-D-glucopyranoside. The structures of the remaining four new compounds were elucidated to be a 2'-*O*-β-D-apiofuranosyl derivative of 3-hydroxy-5,6-epoxy-β-ionol 9-*O*-β-D-glucopyranoside, named premnaionoside, benzyl alcohol β-D-(2'-*O*-β-D-xylopyranosyl)glucopyranoside, phenethyl alcohol β-D-(2'-*O*-β-D-glucopyranosyl)glucopyranoside, and 4,4'-dimethoxy-β-truxinic acid catalpol diester by spectroscopic analyses.

Key words *Premna subscandens*; Verbenaceae; megastigmane glycoside; benzyl alcohol glycoside; phenethyl alcohol glycoside; 4,4'-dimethoxy-β-truxinic acid catalpol ester

In previous papers, we reported the isolation of a number of iridoid glucoside derivatives and phenylethanoids from the leaves of *Premna subscandens*.[1] In continuing work on this plant, together with two known megastigmane glycosides (**1**, **2**), and four new compounds (**3**—**6**) were isolated by means of various chromatographic techniques. The structures of the new compounds were elucidated from spectroscopic evidence and the two known compounds were identified as megastigmane glucosides, 7-(3,5-dihydroxy-1,1,5-trimethyl-cyclohexylidene)-9-methylprop-8-enyl 9-*O*-β-D-glucopyranoside (**1**),[2] and 3-hydroxy-5,6-epoxy-β-ionol 3-*O*-β-D-glucopyranoside (**2**).[3] This paper mainly deals with structural elucidation of the new compounds, although spectroscopic data for the glucoside (**1**) is also included in the text.

Compound **1**, an amorphous powder, was formulated as $C_{19}H_{32}O_8$ on the basis of high-resolution (HR) FAB-MS. The ^1H- and ^{13}C-NMR spectra indicated that **1** is a derivative of grasshopper ketone, except for the missing ketone function on C-9, which should have been reduced to an alcohol function. The planar structure of **1** was identical with that of the megastigmane glucoside isolated from *Lycium halimifolium* as its pentaacetate.[2] Therefore, compound **1** was acetylated and the ^1H-NMR data (CDCl$_3$) for the pentaacetate (**1a**) were superimposable on those reported. Accordingly, the relative orientations of substituents on the six-membered ring must be the same as those in the case of **1**, isolated from *L. halimifolium*, and the absolute stereochemistry of C-9 was tentatively deduced to be *R* from the ^{13}C-NMR chemical shifts of the C-9 and 10 carbon atoms (δ_C 76.0 and 20.7, respectively).[4] However, the absolute stereochemistries at C-3 and C-5, and the axis chirality of the allenic system remain to be determined.

Compound **2** was identified as 3-hydroxy-5,6-epoxy-β-ionol 3-*O*-β-D-glucopyranoside, which has been isolated from flue-cured tobacco,[3] on the basis of NMR data. The ab-
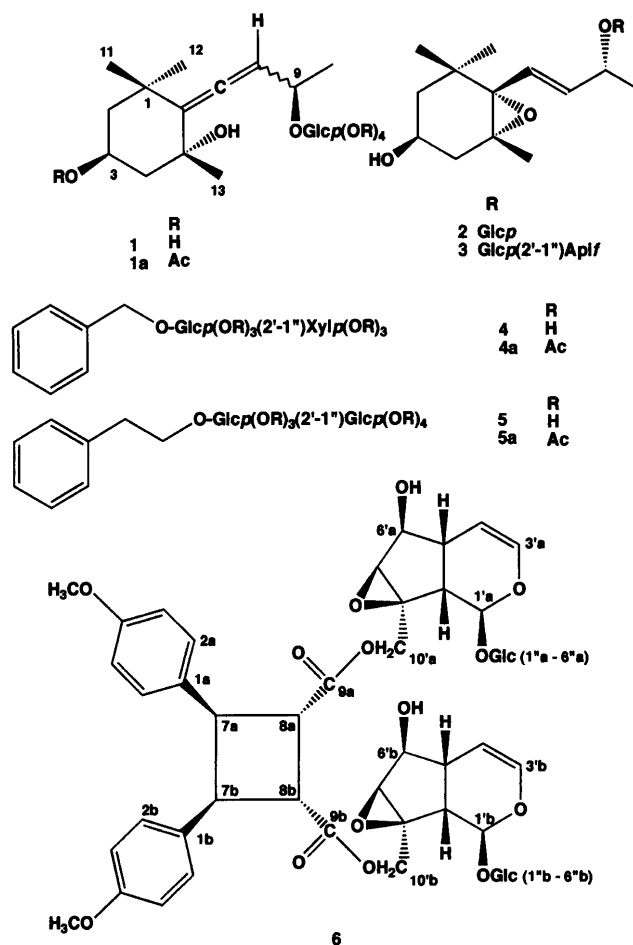

Fig. 1. Structures of Compounds **1**—**6**

Table 1. ^{13}C-NMR Data for Compounds 2 and 3 (100 MHz, CD$_3$OD)

	2	3
1	36.0	36.0
2	48.0	48.0
3	64.6	64.6
4	41.6	41.6
5	68.0	68.1
6	71.2	71.2
7	127.8	127.7
8	137.2	137.1
9	76.9	76.4
10	21.0	20.9
11	30.1	30.2
12	25.2	25.2
13	20.3	20.3
1'	102.7	101.1
2'	75.3	79.3
3'	78.1	78.0
4'	71.4	71.5
5'	77.9	77.8
6'	62.6	62.6
1"		110.9
2"		78.7
3"		80.7
4"		75.4
5"		66.1

Table 2. ^{13}C-NMR Data for Compounds 4 and 5 (100 MHz, CD$_3$OD)

	4	5
1	139.2	139.8
2,6	129.0	129.4
3,5	129.3	130.1
4	128.6	127.3
7	72.1	36.8
8		71.8
1'	102.4	102.5
2'	83.9	81.9
3'	77.9	77.2
4'	71.2	70.9
5'	77.9	77.4
6'	62.8	62.3
1"	106.3	104.1
2"	75.9	75.5
3"	77.4	77.7
4"	71.5	71.1
5"	67.2	77.6
6"		62.2

solute configuration at C-9 was confirmed to be R from the ^{13}C-NMR chemical shifts at C-9 and 10.[4]

Premnaionoside (3) was isolated as an amorphous powder, with the formula $C_{24}H_{40}O_{12}$, as judged by HR-FAB-MS. Spectroscopic data indicated that the structure of 3 is an api-ofuranosyl derivative of 2. Acidic methanolysis gave glucose and apiose, which were identified by GLC analysis. The position of the apiofuranosyl residue was determined to be at the hydroxyl group on C-2 of the glucose moiety by comparison with reported data.[4b] Therefore, the structure of 3 was elucidated to be a 2'-O-β-D-apiofuranosyl derivative of 2.

Compound 4 was obtained as colorless needles, with a formula of $C_{18}H_{26}O_{10}$, on the basis of HR-FAB-MS. The ^{13}C-NMR spectrum showed the presence of monosubstituted-aromatic and primary carbinol carbon signals, along with ones due to substituted hexopyranose and terminal β-xylopyranose moieties. Two anomeric proton signals, observed by ^{1}H-NMR, and GLC analysis revealed the presence of xylose and glucose as sugar units. The xylopyranose linkage was analyzed as its hexaacetate (4a), for which the H-2' signal remained almost intact (δ_H 3.77) by ^{1}H-^{1}H correlation spectroscopy (COSY). Therefore, the structure of 4 was elucidated to be benzyl alcohol β-D-(2'-O-β-D-xylopyranosyl)glucopyranoside.[5]

Compound 5, isolated as colorless needles and with $[\alpha]_D$ $-37.5°$, was similar to compound 4, except for the presence of an additional methylene carbon and β-glucopyranose as the terminal sugar, as deduced by ^{1}H- (see Experimental) and ^{13}C-NMR spectra (Table 1). The inner sugar was also confirmed to be glucose by GLC analysis and the linkage of the sugar moiety was similarly determined from the ^{1}H-^{1}H COSY spectrum of its heptaacetate (5a). Thus, the structure of 5 was concluded to be phenethyl alcohol β-D-(2'-O-β-D-glucopyranosyl)glucopyranoside. This compound has independently been isolated from fruits of Bupleurum falcatum as an amorphous powder with $[\alpha]_D$ $-17.7°$.[6]

Compound 6 was isolated as an amorphous powder. Elemental composition was determined to be $C_{50}H_{60}O_{24}$ by negative-ion HR-FAB-MS. The IR spectrum indicated the presence of ester groups, hydroxyl groups and aromatic rings. Many of the ^{13}C-NMR signals appeared as two close sets, with four neat signals at δ_C 45.9 (d), 46.2 (d), 44.6 (d) and 45.1 (d). Signals assignable to two dihydropyran rings with two hemiacetalic carbons, one set of one primary and one secondary alcohol, one set of tertiary and quarternary carbons with oxygen substituents, and two glucopyranoses were presumably due to the presence of two units of an iridoid glucoside, namely catalpol, in the molecule. The ^{1}H-^{1}H COSY and heteronuclear single quantum correlation spectroscopy (HSQC) spectra showed that four protons on δ_C 45.9, 46.2, 44.6 and 45.1 were coupled in series. Thus, these carbons must form a rare four-membered ring. Compound 6 was then hydrolyzed under methanolic alkaline condition to give a methyl ester of the acid moiety (6a) and catalpol (6b). Spectroscopic analysis revealed that the acid moiety was composed of the four-membered ring and two 4-methoxyphenyl and carbomethoxy units. From these data, the acid moiety was deduced to be truxinic acid (6) or the truxillic acid skeleton. Since the ^{1}H-^{1}H COSY spectrum of 6 showed correlations between H-2a (H-6a) and H-7a, H-7a and H-7b, and H-7b and H-2b (H-6b), truxillic acid was ruled out as a candidate (7) (Fig. 2). Six stereogenic isomers are known for truxinic acid, two meso forms and two sets of enantiomers. Since the methyl ester of the acid moiety of 6, obtained by alkaline hydrolysis, was a symmetrical compound by NMR, and from optical rotation, circular dichroism (CD) and optical rotatory dispersion (ORD) data, it was optically inactive, it was clearly one of the meso forms. Finally, phase-sensitive rotating frame nuclear Overhauser effect (NOE) spectroscopy (ROESY) of 6 showed significant NOE correlations between H-2a (H-6a) and H-7a, 8a and 8b, and between H-2b (H-6b) and H-7b, H-8b and H-8a, leading to the structure of the acid moiety of 6 as shown in Fig. 2. On the basis of the above data, the structure of 6 was determined to be 4,4'-dimethoxy-β-truxinic acid catalpol diester, as shown in Fig. 1.

Truxinic and truxillic acid diesters are relatively rare in na-

ture. Recently, they were found as stachysetin (truxinic acid apigenin glucoside diester) in *Stachys aegyptiaca* (Labiatae),[7] truxillic acid tropane alkaloid diesters in *Erythroxylum moonii* (Erythroxylaceae),[8] incarvillateine and its congeners, truxillic acid N-containing iridoid diesters, in *Incarvillea sinensis* (Bignoniaceae),[9] and sagerinic acid, μ-truxinic acid 3,4-dihydroxyphenyl-1-propanoic acid-8-ol diester in *Salvia officinalis*.[10]
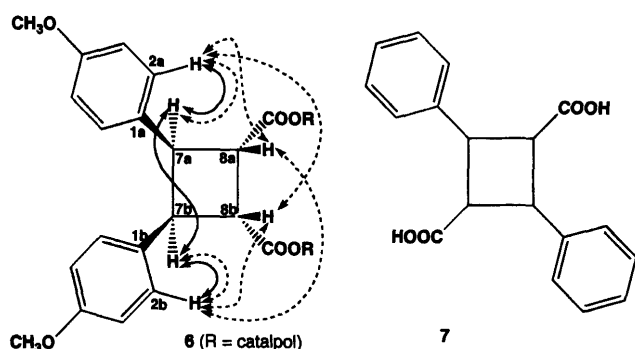

Fig. 2. Skeletons of Truxinic (6) and Truxillic Acids (7)

Solid lines indicate correlations indicated by the ^{1}H–^{1}H COSY spectrum and dotted lines indicate correlations observed in the phase-sensitive ROESY experiment (mixing time, 500 ms).

Experimental

A highly porous synthetic resin (Diaion HP-20) was purchased from Mitsubishi Kagaku (Tokyo). Silica gel column chromatography (CC) and reversed phase [octadecyl silica gel (ODS)] open CC (RPCC) were performed on Silica gel 60 (Merck) and Cosmosil 75C$_{18}$-OPN (Nacalai Tesque, Kyoto) [Φ=50 mm, L=25 cm, linear gradient: MeOH–H$_2$O (1 : 9, 11)→(1 : 1, 11), fractions of 10 g being collected], respectively. Droplet counter-current chromatography (DCCC) (Tokyo Rikakikai, Tokyo) was equipped with 500 glass columns (Φ=2 mm, L=40 cm), and the lower and upper layers of a solvent mixture of CHCl$_3$–MeOH–H$_2$O-n-PrOH (9 : 12 : 8 : 2) were used as the stationary and mobile phases, respectively. Five gram fractions were collected and numbered according to the order of elution of the mobile phase. HPLC was performed on ODS (Inertsil, GL Science, Tokyo; Φ=6 mm, L=250 mm) and the eluate was monitored with UV and refractive index detectors.

All melting points were determined with a Yanagimoto micro-melting point apparatus and are uncorrected. Optical rotations were measured on a Union Giken PM-101 digital polarimeter. IR spectra were measured on a Shimadzu FTIR-4200 spectrophotometer and UV spectra on a Shimadzu UV-160A spectrophotometer. ^{1}H- and ^{13}C-NMR spectra were taken on a JEOL JNM α-400 spectrometer at 400 MHz and 100 MHz, respectively, with tetramethylsilane (TMS) as an internal standard. Negative ion HR-FAB-MS were taken on a JEOL JMS SX-102 spectrometer with PEG-400 or 600 as a matrix. CD and ORD spectra were obtained on a JASCO J-720 spectropolarimeter.

Plant Material The leaves of *Premna subscandens* were collected in Okinawa, Japan, in August 1990, and identified by one of the authors (A.T.). A voucher specimen was deposited in the Herbarium of the Institute of Pharmaceutical Sciences, Hiroshima University School of Medicine (PS-92-Okinawa).

Extraction and Fractionation The air-dried leaves (840 g) of *P. sub-*

Table 3. ^{13}C (100 MHz)- and ^{1}H (400 MHz)-NMR Data for Compounds **6** and **6a** (CD$_3$OD)[a]

		6			6			6a	
		C	H		C	H		C	H
1a	}	132.3	—	1′a	} 95.6	5.01 (d, 10)	1a	} 131.9	—
1b		132.4	—	1′b	95.9	5.03 (d, 10)	1b		
2a		130.1	6.93 (d, 9)	3′a	} 141.9	6.32 (dd, 2, 6)	2a	} 129.8	} 6.99 (d, 9)
2b		130.4	6.96 (d, 9)	3′b		6.35 (dd, 2, 6)	2b		
3a	}	114.4	6.65 (d, 9)	4′a	} 103.9	5.04 (dd, 4, 6)	3a	} 114.0	} 6.69 (d, 9)
3b		114.5	6.67 (d, 9)	4′b	104.1	5.06 (dd, 4, 6)	3b		
4a	}	159.5	—	5′a	} 39.0	2.23 (ddt, 2, 4, 8)	4a	} 158.9	—
4b		159.6	—	5′b		2.25 (ddt, 2, 4, 8)	4b		
5a	}	114.4	6.65 (d, 9)	6′a	} 79.5	=	5a	} 114.0	} 6.69 (d, 9)
5b		114.5	6.67 (d, 9)	6′b		=	5b		
6a		130.1	6.93 (d, 9)	7′a	} 62.8	3.44 (d, 1)	6a	} 129.8	} 6.99 (d, 9)
6b		130.4	6.96 (d, 9)	7′b		3.45 (d, 1)	6b		
				8′a	} 63.3	—	7a	} 45.1	} 4.26 (d, 6)
(Cyclobutane ring)				8′b	63.4	—	7b		
7a		45.9	4.39 (dd, 9, 10)	9′a	} 43.4	2.53 (dd, 8, 10)	8a	} 44.0	} 3.88 (d, 6)
7b		46.2	4.17 (dd, 6, 10)	9′b		2.58 (dd, 8, 10)	8b		
8a		44.6	3.99 (dd, 9, 10)	10′a		4.20 (d, 13)	9a	} 173.7	—
8b		45.1	3.83 (dd, 6, 10)		} 65.2	5.00 (d, 13)	9b		
(Carboxyl carbon)				10′b	} 65.4	4.24 (d, 13)			
9a	}	174.3	—			5.07 (d, 13)	COOCH$_3$	} 52.1	} 3.68 (s)
9b		175.1	—	1″a	} 100.2	4.75 (d, 8)	COOCH$_3$		
				1″b	100.6	4.73 (d, 8)	OCH$_3$	} 55.3	} 3.69 (s)
OCH$_3$	{	55.6	3.65 (s)	2″a	} 74.8	3.25 (dd, 8, 9)	OCH$_3$		
	{	55.6	3.66 (s)	2″b	74.9	=			
				3″a	} 78.64	=			
				3″b	78.62	=			
				4″a	} 71.5	=			
				4″b	71.7	=			
				5″a	} 77.9	=			
				5″b		=			
				6″a	} 63.1	=, =			
				6″b		=, =			

a) Letters and figures in parentheses are multiplicities and coupling constants in Hz.
=: Signals could not be assigned due to overlap of many signals.

sandens were extracted with MeOH (12 l×2). The MeOH extracts were concentrated to 1.5 l, and then 75 ml of H₂O was added to give a 95% aqueous solution, which was washed with 1.5 l of *n*-hexane, and then the MeOH layer was concentrated to give a residue. The residue was suspended in 1.5 l of H₂O, and then extracted with EtOAc (1.5 l) and *n*-BuOH (1.5 l), successively. The *n*-BuOH-soluble fraction (56.3 g) thus obtained was subjected to Diaion HP-20 CC ($\varPhi$=5.5 cm, L=40 cm) with H₂O–MeOH mixtures as eluent [H₂O–MeOH (4 : 1, 31, 20%a: fractions 1—3, and 20%b: fractions 4—7), (3 : 2, 2.5 l, 40%a: fractions 8—11), (2 : 3, 2.5 l, 60%a: fractions 12—13, and 60%b: fractions 14—16), and (1 : 4, 2.5 l, 80%a: fractions 17—18, and 80%b: fractions 19—23), and MeOH (2.5 l), 500 ml fractions being collected]. The residue (1.85 g) of the 20%b eluate was subjected to RPCC. The residue (198 mg) of fractions 44—59 was separated by DCCC, and purification of the residue (24 mg) of fractions 27—31 by preparative HPLC (H₂O–MeOH, 3 : 1) gave 2.0 mg of 1. The residue (144 mg) of fractions 80—92 was separated by DCCC, and purification of the residue (16 mg) of these fractions by HPLC afforded 11 mg of 4 in a crystalline state. The residue of fractions 93—109 was similarly separated by DCCC, and HPLC furnished 15 mg of 2 and 7 mg of 5. Compound 3 (8 mg) was purified from the residue (57 mg) of fractions 110—118 in a similar manner.

A truxinic acid derivative (6) was isolated from the residue (5.14 g) of the 80%a eluate obtained on RPCC by similar chromatographic methods in a yield of 29 mg.

7-(3,5-Dihydroxy-1,1,5-trimethylcyclohexylidene)-9-methylprop-8-enyl 9-*O*-β-D-Glucopyranoside (1): Amorphous powder, UV λ_{max} (MeOH) nm (log ε): 204 (3.67), 324 (3.06). ¹H-NMR (CD₃OD) δ: 1.10 (3H, s H₃-11eq), 1.24 (1H, dd, J=11, 12 Hz, H-2ax), 1.30 (3H, s, H₃-12ax), 1.31 (1H, dd, J=11, 13 Hz, H-4ax), 1.34 (3H, s, H₃-13), 1.85 (1H, ddd, J=2, 4, 12 Hz, H-2eq), 2.14 (1H, ddd, J=2, 4, 13 Hz, H-4eq), 3.16 (1H, dd, J=8, 9 Hz, H-2'), 3.20-3.40 (3H, m, H-3', 4', 5'), 3.67 (1H, dd, J=5, 12 Hz, H-6a), 3.84 (1H, dd, J=2, 12 Hz, H-6'b), 4.17 (1H, tt, J=4, 11 Hz, H-4), 4.39 (1H, d, J=8 Hz, H-1'), 4.41 (1H, quintet, J=6 Hz, H-9), 5.46 (1H, d, J=6 Hz, H-8). ¹³C-NMR (CD₃OD) δ: 20.7 (C-10), 29.6 (C-12ax), 31.6 (C-13), 33.1 (C-11eq), 36.3 (C-1), 50.0 (C-4), 50.6 (C-2), 62.8 (C-1'), 64.8 (C-4'), 71.6 (C-4'), 72.9 (C-5), 75.3 (C-2'), 76.0 (C-9), 78.0 (C-5), 78.3 (C-3), 99.1 (C-8), 103.1 (C-1'), 117.3 (C-6), 200.2 (C-7) (NMR signals were assigned by ¹H–¹H COSY, HSQC and heteronuclear multiple bond correlation spectroscopies). CD (c=1.42×10⁻³ M, MeOH) nm: +1.12 (226), −0.24 (286). ORD (c=1.42×10⁻³ M, MeOH) [α] (nm): +143° (243). HR-FAB-MS (negative-ion mode) m/z: 387.2003 [M−H]⁻ (Calcd for C₁₉H₃₁O₈: 387.2019).

3-Hydroxy-5,6-epoxy-β-ionol 3-*O*-β-D-glucopyranoside (2): Amorphous powder. [α]$_D^{19}$ −35.2° (c=1.08, MeOH). ¹H-NMR (CD₃OD) δ: 0.96 (3H, s, H₃-12ax), 1.12 (3H, s, H₃-11eq), 1.19 (3H, s, H₃-13), 1.21 (1H, dd, J=11, 13 Hz, H-2ax), 1.27 (3H, d, J=7 Hz, H₃-10), 1.55 (1H, ddd, J=2, 3, 13 Hz, H-2eq), 1.60 (1H, dd, J=9, 14 Hz, H-4ax), 2.26 (1H, ddd, J=2, 5, 14 Hz, H-4eq), 3.17 (1H, dd, J=8, 9 Hz, H-2'), 3.21 (1H, ddd, J=2, 5, 10 Hz, H-5'), 3.25—3.35 (2H, m, H-3',4'), 3.67 (1H, dd, J=5, 12 Hz, H-6'a), 3.74 (1H, dddd, J=3, 5, 9, 11 Hz, H-4), 3.81 (1H, dd, J=2, 12 Hz, H-6'b), 4.35 (1H, d, J=8 Hz, H-1'), 4.40 (1H, dquintet, J=1, 7 Hz, H-9), 5.72 (1H, dd, J=7, 16 Hz, H-8), 5.96 (1H, dd, J=1, 16 Hz, H-7). ¹³C-NMR (CD₃OD): Table 1. HR-FAB-MS (negative-ion mode) m/z: 387.2018 [M−H]⁻ (Calcd for C₁₉H₃₁O₈: 387.2019).

Premnaionoside (3): Amorphous powder. [α]$_D^{19}$ −82.6° (c=0.56, MeOH). ¹H-NMR (CD₃OD) δ: 0.96 (3H, s, H₃-12ax), 1.12 (3H, s, H₃-11eq), 1.19 (3H, s, H₃-13), 1.21 (1H, dd, J=11, 13 Hz, H-2ax), 1.27 (3H, d, J=6 Hz, H₃-10), 1.55 (1H, ddd, J=2, 4, 13 Hz, H-2eq), 1.61 (1H, dd, J=9, 14 Hz, H-4ax), 2.26 (1H, ddd, J=2, 5, 14 Hz, H-4eq), 3.19 (1H, ddd, J=2, 5, 10 Hz, H-5'), 3.20—3.35 (3H, m, H-2', 3', 4'), 3.60 (1H, d, J=11 Hz, H-5''a), 3.63 (1H, d, J=11 Hz, H-5''b), 3.66 (1H, dd, J=5, 12 Hz, H-6'a), 3.72 (1H, d, J=11 Hz, H-4''a), 3.74 (1H, dddd, J=3, 5, 9, 11 Hz, H-4), 3.80 (1H, dd, J=2, 12 Hz, H-6'b), 3.94 (1H, d, J=2 Hz, H-2''), 4.05 (1H, d, J=11 Hz, H-4''b), 4.41 (1H, d, J=8 Hz, H-1'), 4.42 (1H, dquintet, J=1, 7 Hz, H-9), 5.38 (1H, d, J=2 Hz, H-1''), 5.71 (1H, dd, J=6, 16 Hz, H-8), 5.98 (1H, dd, J=1, 16 Hz, H-7). ¹³C-NMR (CD₃OD): Table 1. HR-FAB-MS (negative-ion mode) m/z: 519.2441 [M−H]⁻ (Calcd for C₂₄H₃₉O₁₂: 519.2441).

Benzyl alcohol β-D-(2'-*O*-β-D-xylopyranosyl)glucopyranoside (4): Colorless needles, mp 197—198 °C (MeOH). [α]$_D^{19}$ −40.5° (c=0.67, MeOH). UV λ_{max} (MeOH) nm (log ε): 208 (3.75), 258 (2.46). ¹H-NMR (CD₃OD) δ: 3.09 (1H, dd, J=10, 12 Hz, H-5''a), 3.20—3.40 (6H, m, H-3', 4', 5', 2'', 3'', 4''), 3.45 (1H, dd, J=8, 9 Hz, H-2'), 3.68 (1H, dd, J=6, 12 Hz, H-6'a), 3.83 (1H, dd, J=5, 12 Hz, H-5''b), 3.89 (1H, dd, J=2, 12 Hz, H-6'b), 4.50 (1H, d, J=8 Hz, H-1'), 4.51 (1H, d, J=7 Hz, H-1''), 4.65 (1H, d, J=12 Hz, H-7a), 4.94 (1H, d, J=12 Hz, H-7b), 7.26 (2H, t, J=7 Hz, H-3, 5), 7.32 (1H, tt, J=2, 7 Hz, H-4), 7.42 (2H, dd, J=2, 7 Hz, H-2, 6). ¹³C-NMR (CD₃OD): Table 2.

HR-FAB-MS (negative-ion mode) m/z: 401.1431 [M−H]⁻ (Calcd for C₁₈H₂₅O₁₀: 401.1448).

Phenethyl alcohol β-D-(2'-*O*-β-D-glucopyranosyl)glucopyranoside (5): Colorless needles, mp 185—186 °C (MeOH). [α]$_D^{19}$ −37.5° (c=0.40, MeOH). UV λ_{max} (MeOH) nm (log ε): 208 (3.73), 259 (2.45). ¹H-NMR (CD₃OD) δ: 2.95 (2H, td, J=2, 7 Hz, H₂-7), 3.27 (1H, dd, J=8, 9 Hz, H-2''), 3.30—3.45 (6H, m, H-3', 4', 5', 3'', 4'', 5''), 3.52 (1H, dd, J=8, 9 Hz, H-2'), 3.68 (1H, dd, J=5, 12 Hz, H-6'a or 6''a), 3.70 (1H, dd, J=8, 9 Hz, H-6''a or 6'a), 3.84 (1H, dd, J=2, 12 Hz, H-6'b or 6''b), 3.88 (1H, dd, J=2, 12 Hz, H-6''b or 6'b), 4.11 (1H, dd, J=7, 10 Hz, H-8a), 4.13 (1H, dd, J=7, 10 Hz, H-8b), 4.51 (1H, d, J=8 Hz, H-1'), 4.69 (1H, d, J=8 Hz, H-1''), 7.23 (2H, m, H-3, 5). ¹³C-NMR (CD₃OD): Table 2. HR-FAB-MS (negative-ion mode) m/z: 445.1713 [M−H]⁻ (Calcd for C₂₀H₂₉O₁₁: 445.1710).

4,4'-Dimethoxy-β-truxinic acid catalpol diester (6): Amorphous powder. [α]$_D^{22}$ −71.9° (c=1.77, MeOH). IR ν_{max} (KBr) cm⁻¹ 3300, 2875, 1715, 1645, 1605, 1505, 1245, 1075, 1030, 920. UV λ_{max} (MeOH) nm (log ε): 207 (4.30), 230 (4.33), 279 (3.70), 285 (3.67). ¹H- and ¹³C-NMR (CD₃OD): Table 3. HR-FAB-MS (negative-ion mode) m/z: 1043.3400 [M−H]⁻ (Calcd for C₅₀H₅₉O₂₄: 1043.3396).

Acetylation of Compound 1 About 500 μg of 1 was acetylated with 25 μl each of acetic anhydride and pyridine at 20 °C for 14 h. Reagents were removed with a stream of N₂ and then the residue was dried *in vacuo*. Pentaacetate (1a), ¹H-NMR (CDCl₃): essentially the same as the reported data.²⁾ FAB-MS (positive-ion mode) m/z: 621 [M+Na]⁺ (+NaI).

Acetylation of Compounds 4 and 5 to Their Hexaacetate (4a) and Heptaacetate (5a) About 2 mg each of 3 and 4 was acetylated with 50 μl each of acetic anhydride and pyridine at 20 °C for 15 h. The reagents were removed with a stream of N₂ and the residue was dried *in vacuo*. Benzyl alcohol β-D-(2'-*O*-β-D-xylopyranosyl)glucopyranoside hexaacetate (4a), ¹H-NMR (CDCl₃) δ: 2.00, 2.02, 2.03, 2.04, 2.07, 2.08 (each 3H, s, Ac×6), 3.20 (1H, dd, J=8, 12 Hz, H-5''a), 3.66 (1H, ddd, J=2, 5, 10 Hz, H-5'), 3.77 (1H, d, J=8, 9 Hz, H-2'), 4.10 (1H, dd, J=5, 12 Hz, H-5''a), 4.14 (1H, dd, J=2, 12 Hz, H-6'a), 4.25 (1H, dd, J=5, 12 Hz, H-6'b), 4.52 (1H, d, J=8 Hz, H-1'), 4.66 (1H, d, J=12 Hz, H-7a), 4.72 (1H, d, J=6 Hz, H-1''), 4.86 (1H, dd, J=6, 8 Hz, H-2''), 4.91 (1H, td, J=8, 5 Hz, H-4''), 4.93 (1H, d, J=12 Hz, H-7b), 4.98 (1H, t, J=10 Hz, H-4'), 5.07 (1H, t, J=8 Hz, H-3''), 5.17 (1H, t, J=9 Hz, H-3'), 7.26—7.37 (5H, m, H on benzene ring). Electron impact (EI)-MS m/z (rel. int.): 259 (86) [xylose triacetate oxonium ion]⁺, 91 (100) [aglycone tropoloniumion]⁺. Phenethyl alcohol β-D-(2'-*O*-β-D-glucopyranosyl)glucopyranoside heptaacetate (5a), ¹H-NMR (CDCl₃) δ: 1.989, 1.995, 2.00, 2.02, 2.04, 2.05, 2.07 (each 3H, Ac×7), 2.90 (1H, td, J=7, 14 Hz, H-7a), 2.95 (1H, td, J=7, 14 Hz, H-7b), 3.21 (1H, ddd, J=2, 4, 10 Hz, H-5''), 3.65 (1H, ddd, J=2, 5, 10 Hz, H-5'), 3.70 (1H, dd, J=8, 9 Hz, H-2'), 3.74 (1H, td, J=7, 9 Hz, H-8a), 4.01 (1H, dd, J=2, 12 Hz, H-6''a), 4.09 (1H, dd, J=2, 12 Hz, H-6'a), 4.13 (1H, ddd, J=6, 7, 9 Hz, H-8b), 4.15 (1H, dd, J=4, 12 Hz, H-6''b), 4.26 (1H, dd, J=5, 12 Hz, H-6'b), 4.49 (1H, d, J=8 Hz, H-1'), 4.70 (1H, d, J=8 Hz, H-1''), 4.90 (1H, dd, J=8, 9 Hz, H-2''), 4.97 (1H, t, J=9 Hz, H-4'), 5.05 (1H, t, J=8 Hz, H-3''), 5.16 (1H, t, J=9 Hz, H-3'), 7.26—7.38 (5H, m, H on benzene ring). EI-MS m/z (rel. int.): 331 (100) [glucose tetraacetate oxonium ion]⁺, 105 (99) [aglycone methyltropolonium ion]⁺.

GLC Analysis of the Sugar Portions of Compounds 3, 4 and 5 About 2 mg of each sample was treated with 5% HCl in MeOH at 95 °C for 3 h in a sealed tube. The reaction mixture was then neutralized by the addition of Ag₂CO₃. After filtering off the Ag₂CO₃, the solvent was evaporated and the residue dried *in vacuo*. The residue was then silylated with several drops of trimethylsilylimidazole at 60 °C for 15 min. The reaction mixture was partitioned between H₂O and *n*-hexane (2 ml each). The separated *n*-hexane layer was evaporated to dryness and then subjected to GLC analysis with flame ionization detector; Shimadzu CPB-20 capillary column, 0.22 mm×20 m, 0.25 μm film thickness; temperature, 160 °C (isothermal); carrier gas, N₂ at 1.5 kg cm⁻². Standard sugars: apiose, 2. 54, 2.65, 2.79 and 2.96 min; xylose, 5.36 and 5.94 min; glucose, 8.31 and 9.01 min. Compound 3: apiose, 2.53, 2.66, 2.78 and 2.97 min and glucose, 8.35 and 9.04 min. Compound 4: xylose, 5.36 and 5.93 min and glucose, 8.29 and 8.99 min. Compound 5: glucose, 8.34 and 9.03 min.

Alkaline Hydrolysis of 6 to 4,4'-Dimethoxy-β-truxinic Acid Dimethyl Ester (6a) and Catalpol (6b) Compound 6 (17 mg) was treated with 0.1 N methanolic NaOH at 18 °C for 5 h under an N₂ atmosphere. The reaction mixture was neutralized with Amberlite IR-120B (H⁺) and then the solvent was removed. The residue was partitioned with CHCl₃ (1 ml) and H₂O (1 ml). The residue in the organic layer was purified by preparative TLC [Silica gel GF₂₅₄, Merck, 0.25 mm thickness, 10 cm×10 cm, developed with C₆H₆–(CH₃)₂CO (9 : 1) and eluted with CHCl₃–MeOH (9 : 1)] to give 3.8 mg

of 4,4'-dimethoxy-β-truxinic acid dimethyl ester (6a) (64%). The residue in the aqueous layer was purified by silica gel CC [Φ=2.6 cm, L=13 cm, CHCl$_3$ (50 ml) and CHCl$_3$-MeOH (9:1, 100 ml and 7:3, 200 ml), fractions of 12.4 ml being collected] in fractions 30—38, and then by DCCC to give 8.4 mg of catalpol in fractions 15—22 (6b) (68%). 4,4'-Dimethoxy-β-truxinic acid dimethyl ester (6a), amorphous solid, $[\alpha]_D^{21}$ ±0° (c=0.25, MeOH). UV λ_{max} (MeOH) nm (log ε): 207 (4.16), 229 (4.27), 278 (3.57), 285 (3.54). CD (c=7.81×10^{-5} M, MeOH): no significant absorption between 210 and 400 nm. ORD (c=7.81×10^{-5} M, MeOH): no significant absorption between 220 and 600 nm. HR-FAB-MS (negative-ion mode) m/z: 383.1481 [M−H]$^-$ (Calcd for C$_{22}$H$_{23}$O$_6$: 383.1494). Catalpol (6b), amorphous powder, $[\alpha]_D^{22}$ −94.1° (c=0.56, MeOH). ^{13}C-NMR data were essentially the same as reported values.[11]

References and Notes
1) *a*) Sudo H., Takushi A., Ide T., Otsuka H., Hirata E., Takeda Y., *Phytochemistry*, **46**, 1147—1150 (1997); *b*) Sudo H., Ide T., Otsuka H., Hirata E., Takushi A., Takeda Y., *ibid.*, **46**, 1231—1236 (1997); *c*) *Idem*, *ibid.*, **49**, 783—786 (1998).

2) Naf R., Velluz A., Thommen W., *Tetrahedron Lett.*, **31**, 6521—6522 (1990).

3) Kodama H., Fujimori T., Kato K., *Agric. Biol. Chem.*, **45**, 941—944 (1992).

4) *a*) Pabst A., Barron D., Semon E., Schreier P., *Phytochemistry*, **31**, 1649—1652 (1992); *b*) Takeda Y., Zhang H., Matsumoto T., Otsuka H., Ooiso Y., Honda G., Tabata M., Fujita T., Sun H., Sezik E., Yesilada E., *ibid.*, **44**, 117—120 (1997).

5) Kamel M. S., Yamasaki K., Personal communication. This compound has independently been isolated from aerial parts of *Phlomis aurea*.

6) *a*) Sudo H., Otsuka, H., Ide T., Takeda Y., Abstract Papers of the 43rd Annual Meeting of the Japanese Society of Pharmacognosy, p. 192, Tokyo, 1996. *b*) This compound has independently been isolated from fruits of *Bupleurum falcatum*, Ono M., Yoshida A., Ito Y., Nohara T., *Phytochemistry*, **51**, 813—823 (1999).

7) El-Ansari M. A., Nawwar M. A., Saleh N. A. M., *Phyochemistry*, **40**, 1543—1548 (1995).

8) Atta-ur-Rahman, Khattak K. F., Nighat F., Shabbir M., Hemalal K. D., Tillerkerante L. M., *Phytochemistry*, **48**, 377—383 (1998).

9) *a*) Chi Y.-M., Yan W.-M., Li J.-S., *Phytochemistry*, **29**, 2376—2378 (1990); *b*) Chi Y.-M., Hashimoto F., Yan, W.-M., Nohara T., *ibid.*, **46**, 763—769 (1997).

10) Lu Y., Foo L. Y., *Phytochemistry*, **51**, 91—94 (1999).

11) Otsuka H., Kubo N., Yamasaki K., Padolina W. G., *Phytochemistry*, **28**, 513—515 (1989).

Glochidionolactones A—F: Butenolide Glucosides from Leaves of *Glochidion zeylanicum* (GAERTN) A. JUSS

Hideaki OTSUKA,*,a Eiji HIRATA,b Anki TAKUSHI,c Takakazu SHINZATO,d Yoshio TAKEDA,e Masahiko BANDO,f and Masaru KIDOf

Institute of Pharmaceutical Sciences, Hiroshima University Faculty of Medicine,a 1-2-3 Kasumi, Minami-ku, Hiroshima 734-8551, Japan, Faculty of Agriculture, University of Ryukyus,b 1 Senbaru, Nishihara-cho, Nakagami-gun, Okinawa 903-0126, Japan, Okinawa Prefectural Experimental Station of Forestry,c 134 Furugen, Yomitan-son, Nakagami-gun, Okinawa 904-0314, Japan, University Forest, Faculty of Agriculture, University of Ryukyus,d 685 Aza Yona, Kunigami-son, Kunigami-gun, Okinawa 905-1427, Japan, Faculty of Integrated Arts and Sciences, Tokushima University,e 1-1 Minamijosanjima-cho, Tokushima 770-8502, Japan and Second Tokushima Institute of New Drug Research, Otsuka Pharmaceutical Co., Ltd.,f 463-10 Kagasuno, Kawauchi-cho, Tokushima 770-0192, Japan.

From the leaves of *Glochidion zeylanicum*, six new butenolide glucoside, named glochidionolactones A—F, were isolated along with a known related compound, phyllanthurinolactone. The structures of glochidionolactones A—D and F were elucidated mainly by spectroscopic analyses. The absolute stereochemistry of glochidionolactone E was established by X-ray crystallographic analysis.

In the course of chemical investigation of plants in Okinawa, the constituents of the leaves of *Glochidion zeylanicum* (GAERTN) A. JUSS (Euphorbiaceae) were investigated. Using various kinds of chromatographic methods, seven butenolide glucosides (**1**—**7**) were isolated. One was phyllanthurinolactone (**1**), which was isolated by Yamamura and co-workers from *Phyllanthus urinaria* (Euphorbiaceae) as the leaf-closing factor of a nyctianostic plant.[1] The absolute structure of **1** was independently determined to be 4S and 6R through the synthetic work of Mori *et al.*[2] The structures of glochidionolactones A—F (**2**—**7**) were found to be new butenolide glucosides. Glochidionolactones D and F (**5,7**) were found to be the gallic acid esters of glochidionolactones C and E (**4,6**), respectively. This paper deals with the spectroscopic structural elucidation of these compounds and the ab-

solute structure of the aglycone of **6** was determined by X-ray crystallographic analysis.

Phyllanthurinolactone (**1**) and glochidionolactones A—F (**2**—**7**) were purified by various chromatographic techniques (see Experimental).

Phyllanthurinolactone (**1**) was obtained as an amorphous powder, whose elemental composition was determined to be $C_{14}H_{18}O_8$ by negative ion high-resolution FAB-mass spectrometry (HR-FAB-MS). The ${}^1H$- and ${}^{13}C$-NMR spectral data in D_2O were superimposable on those of phyllanthurinolactone, isolated from *Phyllanthus urinaria*.[1]

Glochidionolactone A (**2**), $[\alpha]_D$ *ca.* 0°, was isolated as an amorphous powder. The elemental composition determined by HR-FAB-MS was the same as that of **1**, and other physical data for **2** were similar to those of **1**. The ${}^1H$- and ${}^{13}C$-NMR
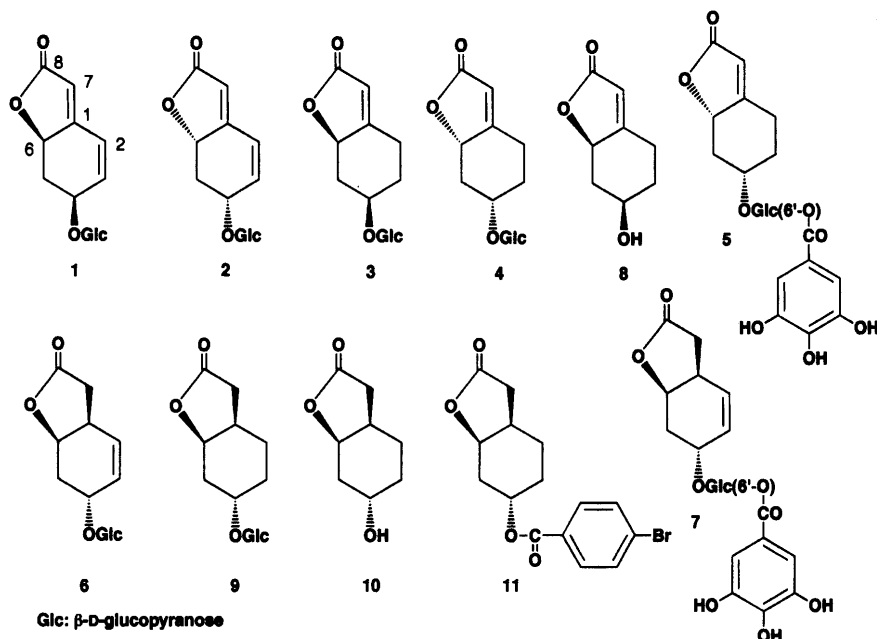

Fig. 1. Structures

* To whom correspondence should be addressed.

Table 1. ^{13}C-NMR Data for Phyllanthurinolactone (1), Glochidionolactones A—F (2—7) and Related Compounds (8—10) (CD$_3$OD and D$_2$O in Parentheses).

	1	2	3	4	8[a]	5	6	9	10	7
1	166.1 (167.1)[b]	166.1 (167.0)[b]	173.9	174.0	174.0	173.9	35.6	35.6	35.6	35.7
2	121.1 (122.3)	121.0 (122.4)	24.8	25.0	25.0	24.8	128.8	26.4	26.9	129.1
3	143.2 (142.3)	144.7 (143.3)	32.8 (−3.0)[c]	34.4 (−1.4)[d]	35.8	34.6	132.5	31.3 (−1.9)[e]	33.2	132.2
4	75.2 (76.0)	74.9 (75.6)	74.8 (+7.4)	74.9 (+7.5)	67.4	75.8	71.0	74.5 (+6.2)	66.3	71.9
5	40.1 (39.3)	38.6 (37.7)	42.0 (−1.3)	40.4 (−2.9)	43.3	40.6	32.1	34.3 (−3.0)	37.3	32.2
6	80.1 (80.9)	80.0 (80.8)	81.7	81.6	81.6	81.5	79.3	82.0	82.5	79.4
7	111.7 (112.0)	111.7 (111.9)	113.4	113.4	113.4	113.3	36.4	37.8	38.4	36.3
8	175.9 (178.5)	175.9 (178.5)	176.0	176.0	176.0	176.0	179.0	179.7	179.7	179.2
1'	104.2 (103.5)	103.6 (102.7)	103.2	103.1		103.7	103.5	103.1		103.8
2'	75.0 (74.6)	75.0 (74.5)	75.1	75.1		75.0	75.2	75.2		75.1
3'	78.1 (77.3)	78.1 (77.2)	78.1	78.1		78.0	78.0	78.0		77.9
4'	71.7 (71.2)	71.7 (71.1)	71.8	71.8		72.2	71.7	71.8		72.0
5'	78.2 (77.6)	78.2 (77.5)	78.1	78.1		75.4	78.2	78.2		75.4
6'	62.9 (62.3)	62.8 (62.2)	62.9	62.9		64.9	62.8	62.9		64.8
1"						139.9				139.9
2",6"						110.2				110.3
3",5"						146.6				146.6
4"						121.6				121.5
7"						168.2				168.3

a) Data taken from ref. 2. b) C-6's of 1 and 2 in D$_2$O were used as the reference peaks (δ_C 62.3 and 62.2, respectively). c) $\Delta\delta_{3-8}$. d) $\Delta\delta_{4-8}$. e) $\Delta\delta_{9-10}$.

data in D$_2$O were essentially the same as those of a synthetic compound, the aglycone of which is the enantiomer of that of 1.[2] This was also supported by the circular dichroism (CD) spectrum in which the opposite Cotton effects to those of the aglycone of 1 were observed.[3] Although this compound is known as a synthetic compound, $[\alpha]_D$ +9.3°, it is now isolated for the first time from a natural source.

Glochidionolactones B (3) and C (4) were obtained as amorphous powders, and had the same elemental composition, which corresponded to C$_{14}$H$_{20}$O$_8$ by HR-FAB-MS. The IR and UV spectra of 4 indicated the presence of an α,β-unsaturated γ-lactone (1736 cm^{-1} and 211 nm, respectively). The ^{13}C-NMR spectra showed that both compounds had the same functionalities in the aglycone part, namely one carbonyl carbon, three methine carbons, two of which are oxygen-bearing, three methylene carbons and one trisubstituted double bond. From the results of two-dimensional NMR spectroscopy, for example ^{1}H–^{1}H correlation spectrometry and heteronuclear single quantum correlation spectroscopy, the structures of 3 and 4 were also butenolide glucosides having a double bond between the 1 and 7 positions. Their ^{1}H-NMR spectra indicated that the relative configurations within the six-membered rings were the same, since the coupling patterns and coupling constants for their protons were indistinguishable. Thus, the aglycones were presumed to be enantiomers of each other. One of the aglycones, which had the 4R and 6R configurations (8) was isolated from Sinomenium acutum, and its configuration was determined by X-ray crystallographic analysis of it p-bromobenzoate.[3] The CD spectrum of 3 revealed a negative Cotton effect at 209 nm, which is similar to the reported data for 8, whereas that of 4 showed a positive one at 210 nm. Since the H-4 protons of both compounds appeared as tt [δ_H 4.06 (J=4, 12 Hz) and 4.05 (J=4, 12 Hz), respectively], the hydroxyl groups had to be in the equatorial orientation. Therefore, β-D-glucosylation-induced shift trends in the ^{13}C-NMR spectra were also applied to confirm the configurations.[4] On going from 8 to 3 and 4, in each case, the methylene carbon signals (C-3 and

C-5) of the so-called pro-S sides shifted upfield more than those of the so called pro-R sides (see Table 1). Finally, the structures of glochidionolactones B and C were elucidated to be 3 and (4R,6R) and 4 (4S,6S) as shown.

Glochidionolactone D (5) was obtained as crystals (mp 160—165°), and its elemental composition was determined to be C$_{21}$H$_{24}$O$_{12}$ by HR-FAB-MS. The ^{1}H- and ^{13}C-NMR spectra indicated that 5 is also a butenolide glucoside with an additional acyl moiety. The structure of the acyl moiety was elucidated to be that of a symmetrically substituted benzoic acid with three hydroxyl substituents, such as gallic acid. The acyl ester was located on the hydroxyl group at the C-6' position of the glucopyranose on the basis of the ^{13}C-NMR data. The absolute stereochemistry of the aglycone portion must be the same as that of 4, since the same β-D-glucosylation-induced upfield shifts were observed at the C-3 and C-5 positions. Therefore, the structure of 5 was elucidated to be glochidionolactone C 6'-O- gallic acid ester, as shown in Fig. 1.

Glochidionolactone E (6) was obtained as an amorphous powder and the spectroscopic evidence indicated that 6 was an analogous compound to 3 and 4, except for the position of a double bond. Since two olefinic protons were observed in the ^{1}H-NMR spectrum, the double bond must be located between C-2 and C-3. Inspection of the phase-sensitive nuclear Overhauser effect spectrum indicated that the two protons at the C-1 and 6 positions were on the same face, however, the absolute configurations could not determined from the β-D-glucosylation-induced shift trends in the ^{13}C-NMR spectrum, since the hydroxyl group at the 4-position was not in the typical equatorial orientation due to the presence of an adjacent double bond [H-4, δ_H 4.41 (m)]. Thus, 6 was catalytically reduced to give dihydroglochidionolactone E (9) and then hydrolyzed with emulsin to give the reduced aglycone (10) and D-glucose. The application of the β-D-glucosylation-induced shift trends in the ^{13}C-NMR chemical shifts of these reduced derivatives may led to the conclusion that C-4 has the S-configuration in 9 and, in turn, the R configuration in 6 (see

Table 2. Determination of Absolute Stereochemistry

h	k	l	Obs (F_O) (+)	(−)	Calcd (F_C) (+)	(−)
1	1	3	18.53<	27.41	20.89<	27.45
1	2	3	89.56<	96.13	85.95<	93.62
1	4	2	25.82>	21.31	42.35>	35.23
1	4	3	21.76<	28.98	20.97<	26.13
1	5	3	48.82>	42.10	49.68>	42.66
2	4	2	36.55>	29.22	35.61>	30.75
2	6	1	42.04>	31.00	47.92>	34.34
2	6	2	17.44<	21.37	14.39<	20.25
2	7	2	43.87>	39.03	43.08>	37.85
2	12	1	40.48<	48.62	39.37<	47.28
2	12	3	24.46<	32.36	23.61<	31.33
2	15	1	46.38<	53.26	42.85<	49.74
3	1	4	28.73>	19.94	29.05>	19.74
3	5	4	50.26>	42.28	51.71>	44.69
3	12	2	68.03>	61.55	68.07>	60.57
3	13	2	32.80<	40.29	35.56<	42.26
4	3	1	79.75<	91.26	79.03<	88.44
4	3	3	86.95<	96.76	80.45<	90.59
4	4	3	33.19>	23.22	30.50>	21.46
4	6	1	38.24>	31.41	38.03>	30.28
4	6	3	35.34>	26.62	32.10>	24.71
4	7	2	15.57<	18.88	12.92<	19.02
4	7	3	27.52<	30.58	26.67<	32.22
4	22	1	32.06>	22.53	35.19>	27.65
5	8	1	41.91<	47.25	41.18<	48.43

Table 1).[4] The quartet proton signal on C-6 suggests that it bisects the two protons at C-5, and the angles between the C-1–H-1 and C-6–H-6 axes must be nearly 60°. This evidence required that the two substituents at C-1 and 6 must oriented towards the same side as the proton at the 4-position. Therefore, the absolute configurations of the 1- and 6-positions were expected to be R and R, respectively in 9 and, in turn, R and S, respectively, in 6. However, there was still the slight ambiguity that when the β-D-glucopyranosylation-shift induced shift trends were applied between 9 and 10, the proton at the 4-position of 9 appeared as triplets of triplet with coupling constants of 4 and 10 Hz (see those of 3 and 4). This implied that the hydroxyl group was in the pseudoequatorial orientation. To confirm the absolute configurations, the reduced aglycone (10) was derivatized to its p-bromobenzoate (11). X-ray crystallographic analysis was performed. The absolute configuration of the stereogenic carbons was determined by Bijvoet's anomalous dispersion method (Table 2)[5] to be 1R, 4S and 6R. The results are consistent with the spectroscopic data discussed above. A perspective drawing is shown in Fig. 2.

Glochidionolactone F (7) was obtained as an amorphous powder and its elemental composition was determined to be $C_{21}H_{24}O_{12}$ by HR-FAB-MS. The spectroscopic data indicated that 7 was the gallic acid ester of 6 and that the position of esterification was the hydroxyl group at C-6′. Therefore, the structure of 7 was elucidated to be glochidionolactone E 6′-O-gallic acid ester, as shown.

It is rare for both enantiomers of compounds with more than two chiral centers to be found in the same batch of plant extract.[6] Formation of both enantiomers in the same plant draws an attention to what kind of enzyme systems are involved in the biosynthetic steps and/or non-enzymatic systems are operated in some steps of the biosynthetic pathway.
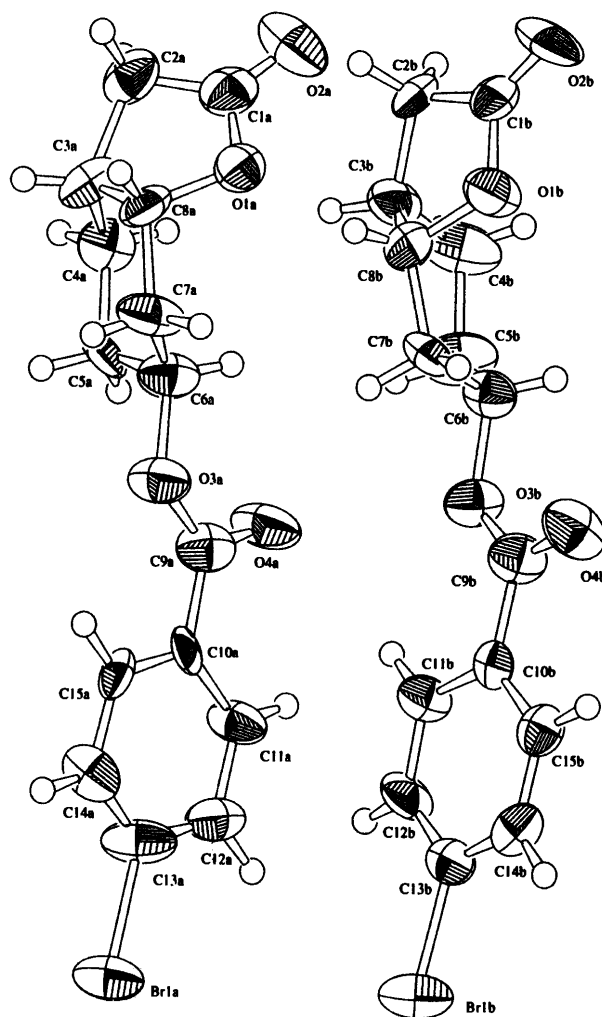
Fig. 2. Computer-Generated Perspective Drawing of 11

There are two independent molecules in the asymmetric unit. Compound has X-ray crystallographic numbering.

Experimental

Highly porous synthetic resin (Diaion HP-20) was purchased from Mitsubishi Kagaku (Tokyo). Silica gel column chromatography (CC) and reversed phase [octadecyl silica gel (ODS)] open CC (RPCC) were performed on silica gel 60 (Merck) and Cosmosil 75C$_{18}$-OPN (Nacalai Tesque, Kyoto) [Φ=50 mm, L=25 cm, linear gradient: MeOH–H$_2$O (1 : 9, 1 1)−>(7 : 3, 1 1), fractions of 10 g being collected], respectively. Droplet counter-current chromatography (DCCC) (Tokyo Rikakikai, Tokyo) was equipped with 500 glass columns (Φ=2 mm, L=40 cm), and the lower and upper layers of a solvent mixture of CHCl$_3$–MeOH–H$_2$O–n-PrOH (9 : 12 : 8 : 2) were used for the stationary and mobile phases, respectively. Five gram fractions were collected and numbered according to their order of elution with the mobile phase. HPLC was performed on ODS (Inertsil, GL Science, Tokyo, Φ=6 mm, L=250 mm) and eluate was monitored by UV and refractive index detectors. Emulsin was purchased from Sigma Chemical Co. (St. Louis, Mo, U.S.A.)

All melting points were determined with a Yanagimoto micro-melting point apparatus and are uncorrected. Optical rotations were measured on a Union Giken PM-101 digital polarimeter. IR spectra were measured on a Shimadzu IR-408 spectrophotometer and UV spectra on a Shimadzu UV-160A spectrophotometer. ^{1}H- and ^{13}C-NMR spectra were taken on a JEOL JNM α-400 spectrometer at 400 MHz and 100 MHz, respectively, with tetramethylsilane (TMS) as an internal standard. Negative-ion HR-FAB-MS were taken on a JEOL JMS SX-102 spectrometer. CD spectra were obtained on a JASCO J-720 spectropolarimeter.

Plant Material The leaves of *Glochidion zeylanicum* (GAERTN) A. JUSS (Euphorbiaceae) were collected in Okinawa, Japan, in August 1990, and a voucher specimen was deposited in the Herbarium of the Institute of Pharmaceutical Sciences, Hiroshima University Faculty of Medicine (90-GZ-

Okinawa-0822).

Extraction and Fractionation The air-dried leaves of *G. zeylanicum* (4.72 kg) were extracted with MeOH three times. The MeOH extract was concentrated to 1.5 l, and then 75 ml of H_2O was added to make a 95% aqueous solution. This solution was washed with 1.5 l of *n*-hexane and then the methanolic layer was concentrated to a viscous gum. The gummy residue was suspended in 1.5 l of H_2O, and then extracted with 1.5 l each of EtOAc and *n*-BuOH, successively, to give 75.7 g and 108 g of EtOAc and *n*-BuOH soluble fractions, respectively. The *n*-BuOH extract (107 g) was subjected to highly porous synthetic resin (Diaion HP-20) CC (Mitsubishi Chemical Co. Ltd., Φ=80 mm, L=55 cm), using H_2O–MeOH (4 : 1, 6 l), (2 : 3, 6 l), (3 : 2, 6 l) and (1 : 4, 6 l), and MeOH (6 l), 2 l fractions being collected. Fractions 2 and 3 were combined (10.6 g) and then subjected to silica gel (150 g) CC eluting with $CHCl_3$ (1 l), $CHCl_3$–MeOH (49 : 1, 2 l), (24 : 1, 2 l), (37 : 3, 2 l), (9 : 1, 2 l), (7 : 1, 2 l), (17 : 3, 2 l), (4 : 1, 2 l) and (31 : 9, 2 l), 500 ml fractions being collected. Combined fractions 15—21 (1.49 g) were then separated by RPCC. The residue (400 mg) of fractions 32—43 was subjected to DCCC and then the residue (271 mg) in fractions 30—37 was subjected to Sephadex LH-20 CC (Φ=20 mm, L=125 cm, MeOH, 5 g fractions being collected) to give two fractions (181 mg in fractions 37—49 and 67 mg in fractions 65—70). Finally, repeated HPLC [H_2O–MeOH (19 : 1)] afforded butenolide glucosides in the following yields: **1** (9 mg), **2** (36 mg), **3** (11 mg), **4** (54 mg), and **6** (34 mg).

The residue (28.7 g) of fractions 4—6, obtained on HP-20 CC, was subjected to silica gel (530 g) CC with a similar solvent system. The residue (1.69 g) of the 20% MeOH in $CHCl_3$ eluent was separated by RPCC (302 mg in fraction 75—88) and then by DCCC (99 mg in fractions 28—34) in a similar manner. HPLC separation [H_2O–MeOH (4 : 1)] of the DCCC fraction gave **5** (50 mg) and **7** (25 mg).

Phyllanthurinolactone (1): Amorphous powder; $[\alpha]_D^{21}$ −40.7° (c=0.59, MeOH), $[\alpha]_D^{19}$ −45.6° (c=0.57, H_2O) ($[\alpha]_D^{25}$ −38.3°²)); ¹H-NMR (CD_3OD): δ 1.68 (1H, td, J=11, 13 Hz, H-5a), 3.02 (1H, ttd, J=1, 5, 11 Hz, H-5b), 3.19 (1H, dd, J=8, 9 Hz, H-2′), 3.28 (1H, t, J=9 Hz, H-4′), 3.37 (1H, t, J=9 Hz, H-3′), 3.67 (1H, dd, J=6, 12 Hz, H-6′a), 3.89 (1H, dd, J=2, 12 Hz, H-6′b), 4.50 (1H, d, J=8 Hz, H-1′), 5.04 (1H, ddd, J=2, 5, 13 Hz, H-6), 5.85 (1H, br s, H-7), 6.50 (1H, br d, J=10 Hz, H-2), 6.67 (1H, dd, J=3, 10 Hz, H-3); ¹³C-NMR (CD_3OD, D_2O): Table 1.¹⁾

Glochidionolactone A (2): Amorphous powder; $[\alpha]_D^{21}$ *ca.* 0° (c=0.60, MeOH); IR ν_{max} (KBr) cm^{-1}: 3407, 2883, 1736, 1638, 1346, 1161, 1074; UV λ_{max} (MeOH) nm (log ε): 255 (4.19); ¹H-NMR (CD_3OD): δ 1.67 (1H, td, J=11, 13 Hz, H-5a), 3.00 (1H, td, J=5, 11 Hz, H-5b), 3.19 (1H, dd, J=8, 9 Hz, H-2′), 3.68 (1H, dd, J=6, 12 Hz, H-6′a), 3.89 (1H, dd, J=2, 12 Hz, H-6′b), 4.48 (1H, d, J=8 Hz, H-1′), 4.78 (1H, m, H-4), 5.08 (1H, ddd, J=2, 5, 13 Hz, H-6), 5.85 (1H, br s, H-7), 6.53 (1H, br d, J=10 Hz, H-2), 6.65 (1H, dd, J=3, 10 Hz, H-3); ¹³C-NMR (CD_3OD, D_2O): Table 1; CD (c=1.15×10⁻⁴ M, MeOH) $\Delta\varepsilon$ (nm): +2.47 (224), 0 (248), −3.05 (265); HR-FAB-MS (negative-ion mode) m/z: 313.0920 [M−H]⁻ (Calcd for $C_{14}H_{17}O_8$: 313.0920).

Glochidionolactone B (3): Amorphous powder; $[\alpha]_D^{21}$ −49.3° (c=0.67, MeOH); UV λ_{max} (MeOH) nm (log ε): 211 (4.06); ¹H-NMR (CD_3OD): δ 1.36 (1H, q, J=12 Hz, H-5a), 1.45 (1H, m, H-3a), 2.27—2.42 (2H, m, H-2a, 3b), 2.82—2.87 (2H, m, H-2b, 5b), 3.15 (1H, dd, J=8, 9 Hz, H-2′), 3.27 (1H, t, J=9 Hz, H-4′), 3.36 (1H, t, J=9 Hz, H-3′), 3.67 (1H, dd, J=6, 12 Hz, H-6′a), 3.89 (1H, dd, J=2, 12 Hz, H-6′b), 4.06 (1H, tt, J=4, 12 Hz, H-4), 4.42 (1H, d, J=8 Hz, H-1′), 4.93 (1H, ddd, J=2, 6, 12 Hz, H-6), 5.80 (1H, s, H-7); ¹³C-NMR (CD_3OD): Table 1; CD (c=1.28×10⁻⁴ M, MeOH) $\Delta\varepsilon$ (nm): −9.19 (209); HR-FAB-MS (negative-ion mode) m/z: 315.1059 [M−H]⁻ (Calcd for $C_{14}H_{19}O_8$: 315.1080).

Glochidionolactone C (4): Amorphous powder; $[\alpha]_D^{21}$ *ca.* 0° (c=0.73, MeOH); IR ν_{max} (KBr) cm^{-1}: 3403, 2926, 1736, 1647, 1443, 1371, 1161, 1047; UV λ_{max} (MeOH) nm (log ε): 211 (4.04); ¹H-NMR (CD_3OD): δ 1.30 (1H, q, J=12 Hz, H-5a), 1.48 (1H, m, H-3a), 2.33—2.48 (2H, m, H-2a, 3b), 2.84—2.92 (2H, m, H-2b, 5b), 3.15 (1H, dd, J=8, 9 Hz, H-2′), 3.27 (1H, t, J=9 Hz, H-4′), 3.36 (1H, t, J=9 Hz, H-3′), 3.66 (1H, dd, J=6, 12 Hz, H-6′a), 3.88 (1H, dd, J=2, 12 Hz, H-6′b), 4.05 (1H, tt, J=4, 12 Hz, H-4), 4.42 (1H, d, J=8 Hz, H-1′), 4.91 (1H, ddd, J=2, 6, 12 Hz, H-6), 5.80 (1H, s, H-7); ¹³C-NMR (CD_3OD): Table 1; CD (c=1.38×10⁻⁴ M, MeOH) $\Delta\varepsilon$ (nm): +5.84 (210); HR-FAB-MS (negative-ion mode) m/z: 315.1075 [M−H]⁻ (Calcd for $C_{14}H_{19}O_8$: 315.1080).

Glochidionolactone D (5): Crystals, mp 160—165 °C (MeOH); $[\alpha]_D^{21}$ +21.1° (c=0.76, MeOH); IR ν_{max} (KBr) cm^{-1}: 3438, 2961, 1732, 1619, 1448, 1346, 1235, 1067, 1032; UV λ_{max} (MeOH) nm (log ε): 213 (4.39), 275 (3.93); ¹H-NMR (CD_3OD): δ 1.24 (1H, q, J=12 Hz, H-5a), 1.37 (1H, dq, J=5, 12 Hz, H-3a), 2.18 (1H, dt, J=2, 12 Hz, H-3b), 2.27 (1H, m, H-2a),

2.70 (1H, ddd, J=2, 5, 12 Hz, H-5b), 2.80 (1H, m, H-2b), 3.18 (1H, t, J=8 Hz, H-2′), 3.59 (1H, ddd, J=2, 6, 9 Hz, H-5′), 3.88 (1H, tt, J=4, 12 Hz, H-4), 4.42 (1H, d, J=8 Hz, H-1′), 4.44 (1H, dd, J=6, 12 Hz, H-6′a), 4.52 (1H, dd, J=2, 12 Hz, H-6′b), 4.80 (1H, dd, J=5, 12 Hz, H-6), 5.74 (1H, s, H-7), 7.08 (2H, s, H-2″, 6″); ¹³C-NMR (CD_3OD): Table 1; CD (c=8.08×10⁻⁵ M, MeOH) $\Delta\varepsilon$ (nm): +8.48 (204), +8.63 (214), +0.945 (272); HR-FAB-MS (negative-ion mode) m/z: 467.1205 [M−H]⁻ (Calcd for $C_{21}H_{23}O_{12}$: 467.1190).

Glochidionolactone E (6): Amorphous powder; $[\alpha]_D^{21}$ +70.8° (c=0.65, MeOH); IR ν_{max} (KBr) cm^{-1}: 3431, 2926, 1736, 1767, 1346, 1161, 1101, 1047, 1033; UV λ_{max} (MeOH): no absorption between 210—360 nm; ¹H-NMR (CD_3OD): δ 1.89 (1H, ddd, J=3, 9, 14 Hz, H-5a), 2.29 (1H, dd, J=3, 14 Hz, H-7a), 2.55 (1H, td, J=5, 14 Hz, H-5b), 2.87 (1H, dd, J=9, 14 Hz, H-7b), 3.06 (H, m, H-1), 3.17 (1H, dd, J=8, 9 Hz, H-2′), 3.6 (1H, dd, J=5, 12 Hz, H-6′a), 3.86 (1H, dd, J=2, 12 Hz, H-6′b), 4.41 (1H, m, H-4), 4.42 (1H, d, J=8 Hz, H-1′), 4.96 (1H, td, J=3, 8 Hz, H-6), 5.59 (1H, dddd, J=1, 2, 3, 10, H-3); ¹³C-NMR (CD_3OD): Table 1; HR-FAB-MS (negative-ion mode) m/z: 315.1105 [M−H]⁻ (Calcd for $C_{14}H_{19}O_8$: 315.1080).

Glochidionolactone F (7): Amorphous powder; $[\alpha]_D^{21}$ +35.1° (c=1.31, MeOH); IR ν_{max} (KBr) cm^{-1}: 3445, 2928, 1765, 1668, 1608, 1379, 1325, 1236, 1062, 1037; UV λ_{max} (MeOH) nm (log ε): 219 (4.25), 276 (3.91); ¹H-NMR (CD_3OD): δ 1.86 (1H, ddd, J=2, 9, 14 Hz, H-5a), 2.27 (1H, dd, J=2, 14 Hz, H-7a), 2.49 (1H, td, J=5, 14 Hz, H-5a), 2.83 (1H, dd, J=9, 14 Hz, H-7b), 3.00 (1H, m, H-1), 3.21 (1H, t, J=8 Hz, H-2′), 3.58 (1H, m, H-5′), 4.42 (1H, dd, J=6, 12 Hz, H-6′a), 4.43 (1H, m, H-4), 4.45 (1H, d, J=8 Hz, H-1′), 4.53 (1H, dd, J=2, 12 Hz, H-6′b), 5.51 (1H, br d, J=10 Hz, H-3), 6.03 (1H, br d, J=10 Hz, H-2), 7.08 (2H, s, H-2″, 6″); ¹³C-NMR (CD_3OD): Table 1; HR-FAB-MS (negative-ion mode) m/z: 467.1222 [M−H]⁻ (Calcd for $C_{21}H_{23}O_{12}$: 467.1190).

Catalytic Hydrogenation of 6 Glochidionolactone E (6) (16 mg) was catalytically reduced with PtO_2 and H_2 for 1.5 h at 20 °C. The catalyst was removed by filtration. The filtrate was concentrated and then the residue was purified by HPLC (H_2O–MeOH, 19 : 1) to give 13 mg of **9** (81%). Dihydroglochidionolactone E (**9**): Colorless needles, mp 120—122 °C (MeOH); $[\alpha]_D^{24}$ +10.8° (c=0.83, MeOH); ¹H-NMR (CD_3OD): δ 1.29 (1H, dddd, J=3, 6, 10, 14 Hz, H-2a), 1.46 (1H, ddt, J=3, 10, 13 Hz, H-3a), 1.76 (1H, ddd, J=4, 10, 14 Hz, H-5a), 1.91 (1H, dtd, J=3, 6, 13 Hz, H-2b), 2.01 (1H, dtdd, J=2, 3, 4, 13 Hz, H-3b), 2.23 (1H, dd, J=2, 17 Hz, H-7a), 2.36—2.48 (2H, m, H-1, 5b), 2.71 (1H, dd, J=7, 17 Hz, H-7b), 3.14 (1H, dd, J=8, 9 Hz, H-2′), 3.36 (1H, t, J=9 Hz, H-4′), 3.66 (1H, dd, J=6, 12 Hz, H-6′a), 3.85 (1H, dd, J=2, 12 Hz, H-6′b), 3.89 (1H, tt, J=4, 10 Hz, H-4), 4.37 (1H, d, J=8 Hz, H-1′), 4.75 (1H, m, H-6, overlapped by HDO signal); ¹³C-NMR (CD_3OD): Table 1; HR-FAB-MS (negative-ion mode) m/z: 317.1221 [M−H]⁻ (Calcd for $C_{14}H_{21}O_8$: 317.1236).

Enzymatic Hydrolysis of 9 Dihydroglochidionolactone E (**9**, 12.5 mg) was treated with emulsin (5 mg) for 2 h at 37 °C in 2 ml of H_2O. The reaction was monitered by TLC. When the starting material had disappeared, the reaction mixture was extracted with $CHCl_3$ (2 ml×2). On evaporation of the organic layer, the aglycone (**10**) was obtained as a liquid. Aglycone (**10**): ¹H-NMR (CD_3OD): δ 1.20—1.35 (2H, m, H-2a, 3a), 1.59 (1H, ddd, J=4, 11, 15 Hz, H-5a), 1.85—1.86 (2H, m, H-2b, 3b), 2.19 (1H, d, J=17 Hz, H-7a), 2.27—2.41 (2H, m, H-1, 5b), 2.74 (1H, dd, J=7, 17 Hz, H-7b), 3.69 (1H, tt, J=4, 11 Hz, H-4), 3.70 (1H, q, J=4 Hz, H-6); ¹³C-NMR (CD_3OD): Table 1; HR-FAB-MS (negative ion mode) m/z: 155.0721 [M−H]⁻ (Calcd for $C_8H_{11}O_3$: 155.0708). The residue of the aqueous layer was subjected to silica gel CC [Φ=20 mm, L=20 cm, $CHCl_3$ (100 ml), $CHCl_3$–MeOH (9 : 1, 100 ml), and $CHCl_3$–MeOH (7 : 3, 300 ml), fractions of 10 ml being collected]. D-Glucose was recovered in fractions 24—29 (5.00 mg). D-Glucose, $[\alpha]_D^{26}$ +33.3° (c=0.33, H_2O), 24 h after being dissolved.

p-Bromobenzoate of 10 (11) The aglycone (**10**), obtained on enzymatic hydrolysis of **9**, was dissolved in 2 ml of $CDCl_3$ at 20 °C, and then to the solution were added 10 mg of *p*-bromobenzoyl chloride and 10 μl of pyridine. The reaction was monitered by TLC, and at 18 and 26 h, the same amount of the reagents were added. After 48 h, 2 ml of H_2O was added and then 1 ml of $CHCl_3$. The organic layer was washed successively with 2 N HCl (2 ml), $NaHCO_3$-saturated H_2O (2 ml) and finally NaCl-saturated H_2O (2 ml×3). After the organic layer had been dried and concentrated, the residue was purified by prep. TLC to afford 7 mg of *p*-bromobenzoate (**11**, 52% from the reduced glucoside) [silica gel, 0.25 mm thickness (10 cm×20 cm), developed with C_6H_6–$(CH_3)_2CO$ (4 : 1) and eluted with $CHCl_3$–MeOH (9 : 1)]. The ester was crystallized from EtOH to give colorless plates. *p*-Bromobenzoate (**11**): mp 155—156 °C; ¹H-NMR ($CDCl_3$): δ 1.44—1.60 (2H, m, H-2a, 3a), 1.91 (1H, ddd, J=4, 10, 14 Hz, H-5a), 1.94 (1H, m, H-2b), 2.10 (1H, m, H-3b), 2.30 (1H, dd, J=2, 17 Hz, H-7a), 2.47 (H, m, H-1), 2.54 (1H,

dddd, J=2, 4, 10, 14 Hz, H-5b), 2.68 (1H, dd, J=7, 17 Hz, H-7b), 4.72 (1H, q, J=4 Hz, H-6), 5.18 (1H, tt, J=4, 10 Hz, H-4), 7.58, 7.87 (each 2H, d, J=9 Hz, p-bromobenzoyl); HR-EI-MS m/z: 338.0155 and 340.0131 $[M]^+$ (Calcd for $C_{15}H_{15}O_4{}^{79}Br$ and $C_{15}H_{15}O_4{}^{81}Br$: 338.0156 and 340.0128, respectively).

X-Ray Crystallographic Analysis of 11 A crystal (0.50 mm×0.50 mm×0.15 mm) was used for analysis. All data were obtained with a Rigaku AFC-5S automated four circle diffractometer with graphite-monochromated Mo$K\alpha$ radiation. Crystal data: $C_{15}H_{15}O_4Br$, M_r=339.2, orthorhombic, space group $P2_12_12_1$, a=10.392 (4) Å, b=32.113 (2) Å, c=8.583 (8) Å, V=2864 (3) Å^3, Z=8, D_x=1.573 g cm^{-3}, $F(000)$=1376, and $\mu(MoK\alpha)$=28.89 cm^{-1}. The intensities were measured in the ω-scan mode for 2θ<50°. Out of 5853 Friedel-pair reflections, 2252 with I>3.00$\sigma(I)$ were used for the structure determination and refinement. The structure was solved by the direct method using the TEXSAN crystallographic software package.[7] All H atoms were calculated at geometrical positions and not refined. The refinement of atomic parameters was carried out by full matrix least squares for all non-H atoms. The final refinement converged with R=0.053 and R_w=0.059 for 361 parameters. The minimum and maximum peaks in the final difference Fourier map were −0.41 and +0.45 eÅ^3. The absolute configuration of the molecule was determined by Bijovet's anomalous-dispersion method[5] based on the observed and calculated structure factors of 25 Friedel pairs (Table 2).

The final atom coordinates, and a list of the tempreture factors and final structure factors have been deposited in the Cambridge Crystallographic Data Centre, University Chemical Laboratory, Lensfield Road, Cambridge CB12 1EW, U.K.

References
1) Ueda M., Shigemori-Suzuki T., Yamamura S., *Tetrahedron Lett.*, **36**, 6267—6270 (1995).
2) Mori K., Audran G., Nakahara Y., Bando M., Kido M., *Tetrahedron Lett.*, **38**, 575—578 (1997).
3) Otsuka H., Ito A., Fujioka N., Kawamata K., Kasai R., Yamasaki K., Satoh T., *Phytochemistry*, **33**, 389—392 (1993).
4) Kasai R., Suzuno M., Asakawa I., Tanaka O., *Tetrahedron Lett.*, 175—178 (1977).
5) Bijovet J. M., Peerdeman A. F., van Bommel A. J., *Nature* (London), **168**, 271—272 (1951).
6) *a*) Inoshiri S., Saiki M., Kohda H., Otsuka H., Yamasaki K., *Phytochemistry*, **27**, 2869—2871 (1988); *b*) Yuasa K., Ide T., Otsuka H., Ogimi C., Hirata E., Takushi A., Takeda Y., *ibid.*, **45**, 611—615 (1997).
7) Molecular Structure Corporation. (1995). TEXSAN. Single Crystal Structure Analysis Software. Version 1.7. MSC, 32000 Research Forest Drive, The Woodlands, TX 77381, U.S.A.

Synthesis of Tricyclic Compounds as Steroid 5α-Reductase Inhibitors

Hitoshi Takami,[1] Hiromi Nonaka, Nobuyuki Kishibayashi, Akio Ishii, Hiroshi Kase,[1] and
Toshiaki Kumazawa*

Pharmaceutical Research Institute, Kyowa Hakko Kogyo Co., Ltd., Nagaizumi, Shizuoka, 411-8731 Japan.

A series of 4-phenoxybutyric acid derivatives attached to a tricyclic skeleton were prepared and evaluated as 5α-reductase inhibitors. Structure activity relationships for these compounds in terms of rat epididymis (type 2) 5α-reductase inhibitory activities reveal that 1) the substitution pattern at the 11-position of dibenz[b,e]oxepin influenced potency, 2) higher lipophilicity of the tricyclic skeleton improved potency, whereas the existence of a basic nitrogen atom in this skeleton was detrimental to potency, and 3) isobutyl substitution at the 8 positon of the azepine skeleton was tolerated. Among the tricyclic compounds studied, 4-[3-[5-benzyl-8-(2-methyl)propyl-10,11-dihydrodibenz[b,f]azepine-2-carboxamido]phenoxy]butyric acid (26) was the most potent inhibitor of rat type 2 5α-reductase at 0.1 μM.

Key words 5α-reductase; benign prostatic hyperplasia; structure–activity relationship; tricyclic compounds; substituent effect

5α-Reductase is an enzyme responsible for the conversion of testosterone (T) into the more potent androgenic metabolite, dihydrotestosterone (DHT). 5α-Reductase inhibitors may be a new type of drug for benign prostatic hyperplasia (BPH)[2] and related disorders associated with elevated levels of DHT such as acne,[3] male pattern baldness,[4] and hirsutism.[5] With the discovery of two 5α-reductase isozymes, the physiological and pharmacological roles of these enzymes in BPH are the subject of current research.[6]

We previously reported indole derivatives, such as 1, exhibiting a potent inhibitory activity for rat prostatic (type 1) 5α-reductase with an IC_{50} value of 9.6 ± 1.0 nM.[7] During the course of structure–activity relationship (SAR) studies of indole derivatives, we discovered that the bulky substituent at the N-1 position of indole was required for potent inhibition of type 1 5α-reductase.[7c] These observations led us to design tricyclic compounds such as carbazoles and azepines, which are bulkier than indoles.

When we started our research program, **2**, (±)-ONO-3805[8] was the only compound reported as a nonsteroidal 5α-reductase inhibitor. Consequently, we designed novel compounds analogous to **2** and considered that the lipophilic part of **2** corresponds to a steroidal skeleton.[7a] The benzyloxyphenyl moiety of **2** can be transformed into dibenz[b,e]oxepin as follows: 1) the three bonds between two benzene rings in conformation **a** are appropriately rotated to conformation **b**, 2) then two benzene rings in **b** are bridged by a C1 unit to afford the dibenz[b,e]oxepin tricyclic system. Thus, we prepared dibenz[b,e]oxepins and evaluated them as 5α-reductase inhibitors.

The starting materials, 6,11-dihydrodibenz[b,e]oxepin-2-carboxylic acids (**3**—**6**) and 5,11-dihydrobenzoxepino[3,4-b]pyridine-7-carboxylic acid (**7**) were available by a known method.[9] Carbazole and azepine carboxylic acids (**8**—**13**) were derived from the corresponding aldehydes.[10] Tricyclic carboxylic acids (**3**—**13**) were converted to butyric acids (**15**—**27**) by condensation with a 2-substituted aniline (**14a, b**)[8] using Mukaiyama's reagent,[11] followed by hydrolysis of ethyl ester (see Chart 1).

The final tricyclic compounds (**15**—**27**) were evaluated for inhibitory activity against rat prostatic (type 1) and epididymis (type 2) 5α-reductases in the manner described pre-

viously.[7] Rat prostatic 5α-reductase showed a broad, neutral-to-basic, pH optimum, whereas the type 2 isozyme obtained from epididymis exhibited an optimal pH of 5.5.[12] Inhibitory activities, expressed as percent inhibition, are summarized in Table 1.

Initially, compounds **16** and **19** were tested for inhibitory effects both on rat prostatic (type 1) and epididymis (type 2) 5α-reductases. Though both compounds showed weak potency for type 1 isozyme, even at 1 μM drug concentration, they exhibited potent activity against type 2 isozyme at 0.1 μM. The 11-hydroxy derivative (**19**) exhibited 73% inhibition at 0.1 μM, which is better than the ketone (**16**). Thus, tricyclic compounds were more responsive to type 2 isozyme and discriminated between subtle structural differences in the same manner as our previous observation: non-steroidal inhibitors, such as indole derivatives and (±)-ONO-3805, more potently inhibited type 2 versus type 1 isozyme.[7b] Consequently, we evaluated the tricyclic compounds for inhibitory activity against type 2 isozyme to investigate structure–activity relationships.

Oxepins with a methylene group at the 11-position showed more potent inhibitory activity than the ketone (**17**, **18** vs. **15**, **16**). Substitution of one of the benzene rings in dibenz[b,e]-oxepin with a pyridine ring apparently led to a loss of inhibitory activity (**21** vs. **20**). C log P values[13] of tricyclic skeletons corresponding to **15**, **17**, **20** and **21**, in which the left part of the molecule was replaced by the acetyl substituent, were calculated as 2.87, 3.98, 2.94 and 1.45, respectively. These results suggest that the higher lipophilicity in dibenz[b,e]oxepin is desirable for potent activity.

It is obvious that the substitution pattern at the 11-position of dibenz[b,e]oxepins influenced potency. Hydroxy and methoxy groups were more potent than ketone (**19**, **20** vs. **15**, **16**). From the result that compound **19** showed more potent activity than **16**, it was concluded that substitution pattern rather than the lipophilicity of this moiety influenced the potency. The configuration of the 11-carbon atom affects the conformation of the dibenz[b,e]oxepin ring system, as we previously reported.[14] Ring inversion occurs easily in the case of the trigonal sp^2 carbon, whereas such a conformational change hardly ever occurs in physiological conditions in tetrahedral sp^3 carbon at the 11 position. ^{1}H-NMR spectra

---

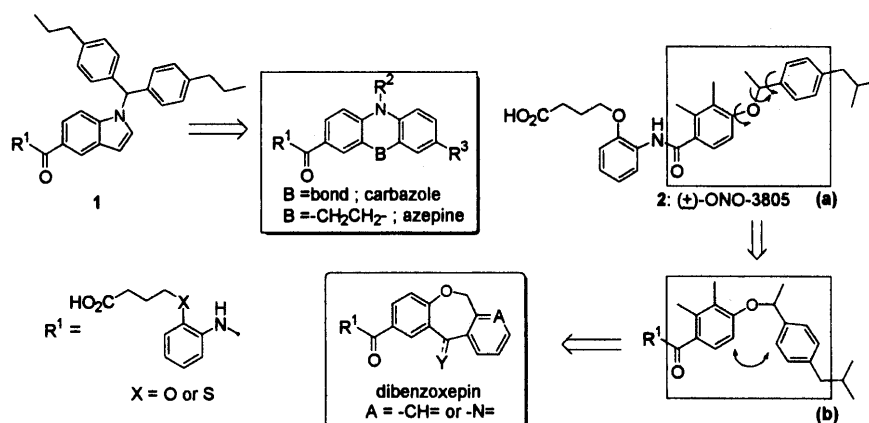* To whom correspondence should be addressed.
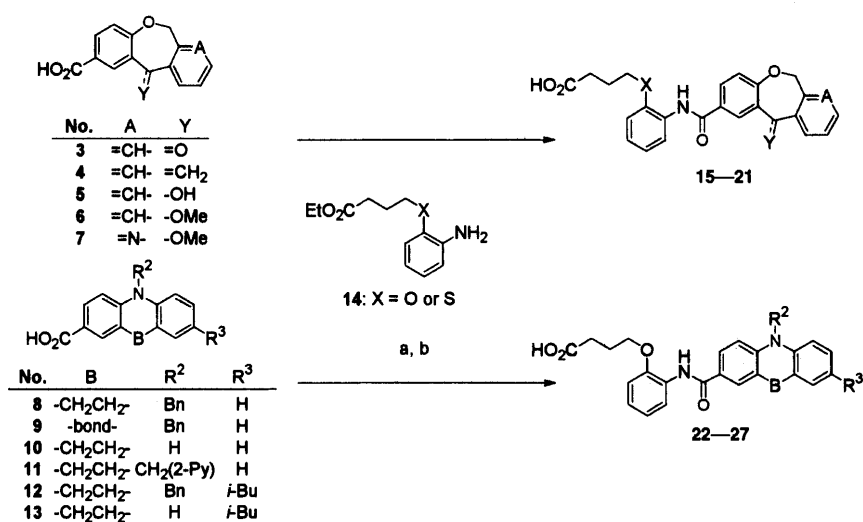
Fig. 1. Design of Tricyclic Compounds

a, **14**, 2-chloro-*N*-methylpyridinium iodide, NBu₃/CH₂Cl₂; b, NaOH/aqueous EtOH

Chart 1

Table 1. 5α-Reductase Inhibitory Activity of Tricyclic Compounds

No.	A	X	Y	B	R²	R³	% inhibition (drug concentration)	
							Type 1 (1 μM)	Type 2 (0.1 μM)
15	–CH=	O	=O	—	—	—	—	28
16	–CH=	S	=O	—	—	—	33	39
17	–CH=	O	=CH₂	—	—	—	—	73
18	–CH=	S	=CH₂	—	—	—	—	63
19	–CH=	S	–H, –OH	—	—	—	45	73
20	–CH=	O	–H, –OMe	—	—	—	—	69
21	–N=	O	–H, –OMe	—	—	—	—	22
22	—	O	—	–CH₂CH₂–	CH₂Ph	H	—	88
23	—	O	—	Bond	CH₂Ph	H	—	72
24	—	O	—	–CH₂CH₂–	H	H	—	75
25	—	O	—	–CH₂CH₂–	CH₂(2-Py)	H	—	42
26	—	O	—	–CH₂CH₂–	CH₂Ph	iso-Bu	—	93
27	—	O	—	–CH₂CH₂–	H	iso-Bu	—	76
1							87[a]	—
2							96[a]	100

a) % inhibition at 0.1 μM.

also indicated these phenomena. The C-6 methylene hydrogen atoms at the linkage of dibenz[b,e]oxepin were observed as a singlet peak for the two protons in the case of ketone at the 11-position (15—18). On the other hand, a doublet in the AB-pattern was observed in compounds possessing hydroxy or methoxy at the 11-position (19, 20). These observations suggest that one of the enantiomers in compound 19, 20 has a higher affinity against type 2 isozyme, and the ring inversion of dibenz[b,e]oxepin might cause decreased potency. Replacement of the ether bond of the phenoxy part by thioether did not show any significant change in potency.

When compared with 22 and 23, dibenzazepine is relatively more potent than carbazole. The substituent (R^2) on the nitrogen of azepine notably influenced inhibitory activity. The N-benzyl azepines (22 and 26) showed potent inhibitory activity. Non-substitution (N-H) retained potency, whereas substitution of the picolyl group caused a drop in potency, even though C log P values of the tricyclic moiety of 24 and 25 were over 4.5. From this result, the existence of a basic nitrogen atom of this moiety appears to be undesirable for potent inhibitory activity. As for the substituent (R^3) at the 8 position of dibenzazepine, the introduction of isobutyl retained potency (26, 27 vs. 22, 24). This result indicates that bulkier substitutents in the tricyclic ring systems are allowed as a lipophilic part of the molecule.

In conclusion, we designed tricyclic compounds, such as dibenzoxepins, carbazole and azepines, and evaluated them as 5α-reductase inhibitors. Several compounds showed potent inhibitory activity for rat type 2 5α-reductase, which were comparable with parent indole derivative 1 and (±)-ONO-3805. These results reveal interesting features of the nonsteroidal 5α-reductase inhibitors and provide a new prototype for novel synthetic candidates.

Experimental

Melting points were determined with a Büchi-510 melting point apparatus and are uncorrected. Infrared spectra (IR) were recorded on a Jasco IR-810 spectrometer. Proton nuclear magnetic resonance spectra (^{1}H-NMR) were recorded on a JEOL JNM GX-270 or EX-270 (270 MHz) spectrometer with Me$_4$Si as an internal standard. Elemental analyses were performed by the analytical department of our laboratories.

5-Benzyl-2-isobutyl-10,11-dihydrodibenz[b,f]azepine To a solution of 1-(5-benzyl-10,11-dihydrodibenz[b,f]azepine-2-carbaldehyde (4.17 g, 13.3 mmol) in tetrahydrofuran (THF) (125 ml), isopropyl magnesium chloride (2 M in THF solution; 13.3 ml, 26.6 mmol) was added at −50 °C. After being stirred at the same temperature for 1 h, 50 ml of water was added and the resulting mixture was extracted with AcOEt. The organic layer was washed with brine, dried and evaporated in vacuo. The oil was dissolved in 200 ml of toluene, then activated MnO$_2$ (11.7 g, 133 mmol) was added. After being stirred under refluxing for 3 h, the reaction mixture was cooled to 25 °C. The mixture was filtered through Celite and the filtrate was evaporated in vacuo. The resulting oil was chromatographed on silica gel and eluted with hexane–AcOEt (5 : 1) to afford ketone (2.5 g, 53%) as a yellow oil. ^{1}H-NMR (CDCl$_3$) δ: 1.14 (6H, d, J=6.7 Hz), 3.24 (4H, s), 3.42—3.47 (1H, m), 5.02 (2H, s), 6.97—7.27 (8H, m), 7.35 (2H, d, J=6.9 Hz), 7.62 (1H, dd, J=2.2 Hz, 8.6 Hz), 7.69 (1H, d, J=2.2 Hz). To a solution of ketone (2.5 g, 7.03 mmol) in 38 ml of trifluoroacetic acid (TFA), Et$_3$SiH (11.4 ml, 70.3 mmol) was added dropwise. After being stirred at the same temperature for 1 h, 50 ml of iced water was added. The reaction mixture was extracted with toluene. The organic layer was washed with saturated aqueous NaHCO$_3$, water and brine successively, dried and evaporated in vacuo. The residue was chromatographed on silica gel and eluted with hexane–AcOEt (10 : 1) to afford an isobutyl substituted compound (2.4 g, 100%) as a yellow oil. ^{1}H-NMR (CDCl$_3$) δ: 0.85 (6H, d, J=6.7 Hz), 1.63—1.82 (1H, m), 2.34 (2H, s), 3.18 (4H, s), 4.88 (2H, s), 6.74—6.82 (3H, m), 6.90—7.20 (8H, m), 2.30 (2H, d, J=7.2 Hz).

5-Benzyl-8-isobutyl-10,11-dihydrodibenz[b,f]azepine-2-carboxylic

Acid (12) To a solution of phosphorous oxychloride (POCl$_3$) (0.18 ml, 2.20 mmol) and 0.5 ml of dichloroethane, N,N-dimethylformamide (DMF) (0.17 ml, 2.20 mmol) was added at 0 °C. After the mixture was stirred at 25 °C for 1 h, a solution of 5-benzyl-2-isobutyl-10,11-dihydrodibenz[b,f]-azepine (0.5 g, 1.46 mmol) in 1.0 ml of dichloroethane was added dropwise over a period of 10 min. After being stirred at 60 °C for 2 h, the reaction mixture was poured into 20 ml of aqueous sodium acetate (2.4 g, 29 mmol). The mixture was stirred at 25 °C for 30 min and extracted with CH$_2$Cl$_2$. The organic layer was washed with brine, dried and evaporated in vacuo. The residue was chromatographed on silica gel and eluted with hexane–AcOEt (3 : 1) to afford 2-aldehyde (0.4 g, 74%) as a pale yellow oil. ^{1}H-NMR (CDCl$_3$) δ: 0.88 (6H, d, J=6.7 Hz), 1.80—1.85 (1H, m), 2.39 (2H, d, J=6.7 Hz), 3.19—3.27 (4H, m), 5.05 (2H, s), 6.91 (1H, dd, J=1.9 Hz, 8.6 Hz), 6.92 (1H, d, J=1.9 Hz), 7.09 (2H, d, J=8.6 Hz), 7.17—7.39 (5H, m), 7.51 (1H, dd, J=1.9 Hz, 8.6 Hz), 7.57 (1H, d, J=1.9 Hz), 9.80 (1H, s). To a solution of 2-aldehyde (0.4 g, 1.08 mmol) in methanol (20 ml), a 2.62 ml of 2 M KOH in methanol and iodine (0.14 g, 0.54 mmol) were added and the resulting mixture was stirred at 0—5 °C for 24 h. Methanol was evaporated in vacuo. The residue was dissolved in 1.01 of water and acidified with 4 M HCl to pH 5. The reaction mixture was extracted with AcOEt. The organic layer was washed with saturated aqueous Na$_2$S$_2$O$_3$ and brine, successively, dried, and evaporated in vacuo. The yellow oil was chromatographed on silica gel and eluted with hexane–AcOEt (3:1) to afford methyl ester (0.43g, 74%), which was obtained as a pale yellow oil. ^{1}H-NMR (CDCl$_3$) δ: 0.90 (6H, d, J=6.8 Hz), 1.80—1.85 (1H, m), 2.41 (2H, d, J=6.8 Hz), 3.09—3.17 (4H, m), 3.86 (3H, s), 5.03 (2H, s), 6.91 (1H, dd, J=2.0 Hz, 8.6 Hz), 6.92 (1H, d, J=2.0 Hz), 7.10 (2H, d, J=8.6 Hz), 7.17—7.39 (5H, m), 7.51 (1H, dd, J=1.9 Hz, 8.6 Hz), 7.57 (1H, d, J=1.9 Hz). The methyl ester was hydrolyzed to afford carboxilic acid (0.33 g, 59%) as amorphous. ^{1}H-NMR (CDCl$_3$) δ: 0.87 (6H, d, J=6.8 Hz), 1.78—1.84 (1H, m), 2.38 (2H, d, J=6.8 Hz), 3.22 (4H, br s), 5.02 (2H, s), 6.87—6.91 (1H, m), 7.01—7.08 (2H, m), 7.16—7.28 (4H, m), 7.35 (2H, d, J=6.9 Hz), 7.72 (1H, dd, J=2.0, 8.6 Hz), 7.72 (1H, d, J=2.0 Hz).

8-Isobutyl-10,11-Dihydro-5H-dibenz[b,f]azepine-2-carboxylic Acid (13) To a solution of 12 (0.52 g, 1.30 mmol), 10 ml of AcOEt and 10 ml of AcOH, Pd–C (5 wt.%, 0.13 g) were added. The reaction mixture was stirred under atmospheric hydrogen at 25 °C for 48 h. After the reaction was completed, the mixture was filtered with Celite, and the filtrate was evaporated in vacuo to afford 13 (0.25 g, 62%) as a yellow amorphous substance. ^{1}H-NMR (CDCl$_3$) δ: 0.90 (6H, d, J=6.8 Hz), 1.80—1.84 (1H, m), 2.84 (2H, d, J=6.8 Hz), 3.07 (4H, s), 6.28 (1H, br s), 6.89 (1H, d, J=7.6 Hz), 7.73 (1H, d, J=7.6 Hz), 7.74 (1H, s).

4-[2-[(6,11-Dihydro-11-oxo-dibenz[b,e]oxepin-2-yl)carboxamido]phenoxy]butyric Acid (15) To a mixture of ethyl 4-(2-aminophenoxy)butyrate (14) (1.23 g, 5.51 mmol), 2-chloro-1-methylpyridinium iodide (1.20 g, 4.72 mmol), and tributylamine (2.3 ml, 9.43 mmol) in 40 ml of CH$_2$Cl$_2$, was added under reflux a suspension of 3 (1.0 g, 3.93 mmol) in 10 ml of CH$_2$Cl$_2$, and the mixture was stirred at reflux for 1 h. After the addition of water, the reaction mixture was extracted with CH$_2$Cl$_2$. The organic layer was washed with 1 M HCl, water, and brine, dried and evaporated in vacuo to afford ethyl 4-[2-(6,11-dihydro-11-oxo-dibenz[b,e]oxepine-2-carboxamido)phenoxy]butyrate (1.41 g, 78%) as a pale yellow oil. ^{1}H-NMR (CDCl$_3$) δ: 1.18 (3H, t, J=7.1 Hz), 2.23—2.33 (2H, m), 2.63 (2H, t, J=6.9 Hz), 4.08 (2H, q, J=7.1 Hz), 4.18 (2H, t, J=6.3 Hz), 5.27 (2H, s), 6.93 (1H, dd, J=2.0, 7.6 Hz), 6.99—7.11 (2H, m), 7.19 (1H, d, J=8.9 Hz), 7.40—7.63 (3H, m), 7.91 (1H, dd, J=1.3, 7.6 Hz), 8.15 (1H, dd, J=2.3, 8.6 Hz), 8.50 (1H, dd, J=2.0, 7.6 Hz), 8.71 (1H, br s), 8.77 (1H, d, J=2.3 Hz). A mixture of the obtained ethyl ester (1.41 g, 2.57 mmol), 0.77 ml of 10 M NaOH, and 42 ml of EtOH was stirred at 50 °C for 1 h. The mixture was evaporated in vacuo and the residue was dissolved in 50 ml of water. The mixture was acidified with 4 M HCl to pH 3 and extracted with AcOEt. The organic layer was washed with brine, dried, and evaporated in vacuo. The pale yellow amorphous substance was recrystallized from isopropylether to give pure 15 (0.86 g, 78%) as colorless crystals, mp 159—160 °C. ^{1}H-NMR (CDCl$_3$+DMSO-d_6) δ: 2.21—2.31 (2H, m), 2.62 (2H, t, J=6.8 Hz), 4.19 (2H, t, J=6.1 Hz), 5.28 (2H, s), 6.94 (1H, dd, J=1.7, 7.8 Hz), 6.97—7.10 (2H, m), 7.19 (1H, d, J=8.6 Hz), 7.42 (1H, d, J=7.8 Hz), 7.48—7.54 (1H, m), 7.58—7.64 (1H, m), 7.91 (1H, d, J=6.3 Hz), 8.12 (1H, dd, J=2.3, 8.6 Hz), 8.47 (1H, dd, J=1.7, 7.8 Hz), 8.74 (1H, s), 8.76 (1H, d, J=2.3 Hz). IR (KBr) cm^{-1}: 3200, 1732, 1605, 1495, 1450, 1301, 1245, 1175, 747. Anal. Calcd for C$_{25}$H$_{21}$NO$_6$: C, 69.60; H, 4.91; N, 3.25. Found: C, 69.56; H, 4.90; N, 3.15.

4-[2-[(6,11-Dihydro-11-oxo-dibenz[b,e]oxepin-2-yl)carboxamido]phenylthio]butyric Acid (16) 16: As a pale yellow crystals, mp 111—112 °C (iso-Pr$_2$O). ^{1}H-NMR (DMSO-d_6) δ: 1.69—1.93 (2H, m), 2.36 (2H, t,

J=7.1 Hz), 2.94 (2H, t, J=7.1 Hz), 5.40 (2H, br s), 7.15—7.32 (3H, m), 7.40—7.70 (5H, m), 7.74 (1H, d, J=8.8 Hz), 8.17 (1H, dd, J=2.2, 8.6 Hz), 8.78 (1H, d, J=2.2 Hz). IR (KBr) cm^{-1}: 3430, 3335, 1732, 1668, 1643, 1519, 1487, 1300, 1254, 1174, 763. Anal. Calcd for $C_{25}H_{21}NO_5S$: C, 67.10; H, 4.73; N, 3.13. Found: C, 67.31; H, 4.60; N, 2.94.

4-[2-[(11-Methylidene-6,11-dihydrodibenz[b,e]oxepin-2-yl)carboxamido]phenoxy]butyric Acid (17) 17: As amorphous. ^{1}H-NMR (DMSO-d_6) δ: 1.90—2.10 (2H, m), 2.45—2.55 (2H, m), 4.00—4.15 (2H, m), 5.23 (2H, s), 5.37 (1H, s), 5.96 (1H, s), 6.85—6.95 (2H, m), 7.00—7.15 (2H, m), 7.35—7.46 (4H, m), 7.85 (2H, d, J=7.3 Hz), 8.12 (1H, s), 9.52 (1H, s). IR (KBr) cm^{-1}: 3440, 1578, 1542, 1494, 1451, 1249, 751. Anal. Calcd for $C_{26}H_{23}NO_5 \cdot 0.5H_2O$: C, 71.22; H, 5.52; N, 3.19. Found: C, 71.10; H, 5.17; N, 3.20.

4-[2-[(11-Methylidene-6,11-dihydrodibenz[b,e]oxepin-2-yl)carboxamido]phenylthio]butyric Acid (18) 18: As pale yellow crystals, mp 116—125 °C (iso-Pr$_2$O). ^{1}H-NMR (CDCl$_3$) δ: 1.68—1.80 (2H, m), 2.28 (2H, t, J=7.1 Hz), 2.70 (2H, t, J=7.1 Hz), 5.16 (2H, s), 5.31 (1H, s), 5.78 (1H, s), 6.84 (1H, d, J=8.6 Hz), 6.97 (1H, t, J=7.6 Hz), 7.26—7.33 (5H, m), 7.55 (1H, dd, J=1.5, 7.6 Hz), 7.71 (1H, dd, J=2.3, 8.6 Hz), 8.11 (1H, d, J=2.3 Hz), 8.57 (1H, dd, J=1.3, 8.2 Hz), 9.33 (1H, s). IR (KBr) cm^{-1}: 3450, 1580, 1525, 1490, 1437, 1303, 1239, 759. Anal. Calcd for $C_{26}H_{23}NO_4S \cdot 0.5H_2O$: C, 68.70; H, 5.32; N, 3.08. Found: C, 68.40; H, 5.54; N, 3.04.

4-[2-[(11-Hydroxy-6,11-dihydrodibenz[b,e]oxepin-2-yl)carboxamido]phenylthio]butyric Acid (19) 19: As pale yellow crystals, mp 152—154 °C (iso-Pr$_2$O). ^{1}H-NMR (DMSO-d_6) δ: 1.67—1.90 (2H, m), 2.34 (2H, t, J=7.1 Hz), 2.91 (2H, t, J=7.1 Hz), 5.31 and 5.79 (2H, AB pattern, J=12.3 Hz), 5.95 (1H, s), 6.86 (1H, d, J=8.6 Hz), 7.15—7.70 (9H, m), 7.80 (1H, dd, J=1.3, 9.2 Hz), 8.12 (1H, d, J=1.3 Hz), 9.66 (1H, s). IR (KBr) cm^{-1}: 3350, 1646, 1579, 1521, 1496, 1436, 1316, 1238, 763. Anal. Calcd for $C_{25}H_{23}NO_5S$: C, 66.80; H, 5.16; N, 3.12. Found: C, 66.75; H, 5.00; N, 2.98.

4-[2-[(6,11-Dihydro-11-methoxydibenz[b,e]oxepin-2-yl)carboxamido]phenoxy]butyric Acid (20) 20: As amorphous. ^{1}H-NMR (CDCl$_3$) δ: 2.12—2.34 (2H, m), 2.58 (2H, t, J=6.4 Hz), 3.31 (3H, s), 4.02—4.09 (1H, m), 4.16—4.24 (1H, m), 4.91 and 6.08 (2H, AB pattern, J=12.4 Hz), 5.22 (1H, s), 6.89 (1H, dd, J=2.0, 7.6 Hz), 6.94 (1H, d, J=8.6 Hz), 6.97—7.08 (2H, m), 7.30—7.38 (4H, m), 7.79 (1H, dd, J=2.3, 8.6 Hz), 7.96 (1H, d, J=2.3 Hz), 8.44 (1H, br s), 8.49 (1H, dd, J=2.3, 7.3 Hz). IR (KBr) cm^{-1}: 3418, 2934, 1728, 1667, 1611, 1537, 1503, 1452, 1240, 1208, 755. Anal. Calcd for $C_{26}H_{25}NO_6 \cdot 0.25H_2O$: C, 69.09; H, 5.69; N, 3.11. Found: C, 69.09; H, 5.59; N, 2.81.

4-[2-[(5,11-Dihydro-5-methoxybenzoxepino[3,4-b]pyridin-2-yl)carboxamido]phenoxy]butyric Acid (21) 21: As white crystals, mp 78—82 °C (iso-Pr$_2$O trituration). ^{1}H-NMR (CDCl$_3$) δ: 2.21—2.30 (2H, m), 2.61 (2H, t, J=6.9 Hz), 3.39 (3H, s), 4.08—4.23 (2H, m), 5.20 and 5.90 (2H, AB pattern, J=13.2 Hz), 5.32 (1H, s), 6.91 (1H, dd, J=2.0, 7.6 Hz), 6.97—7.09 (3H, m), 7.20 (1H, dd, J=5.1, 7.8 Hz), 7.72 (1H, dd, J=1.7, 7.6 Hz), 7.84 (1H, dd, J=2.3, 8.6 Hz). 7.98 (1H, d, J=2.3 Hz), 8.43 (1H, dd, J=1.7, 5.0 Hz), 8.52 (1H, dd, J=2.1, 7.8 Hz), 8.56 (1H, s). IR (KBr) cm^{-1}: 3428, 2934, 1607, 1535, 1500, 1452, 1256, 1228, 745. Anal. Calcd for $C_{25}H_{24}N_2O_6$: C, 66.95; H, 5.39; N, 6.25. Found: C, 66.69; H, 5.54; 6.02.

4-[2-[(5-Benzyl-10,11-dihydrodibenz[b,f]azepin-2-yl)carboxamido]phenoxy]butyric Acid (22) 22: As amorphous. ^{1}H-NMR (CDCl$_3$) δ: 2.14—2.23 (2H, m), 2.56 (2H, t, J=7.1 Hz), 3.27 (4H, s), 4.11 (2H, t, J=6.1 Hz), 5.02 (2H, s), 6.87 (1H, dd, J=2.5,7.1 Hz), 6.93—7.05 (2H, m), 7.10—7.27 (8H, m), 7.35—7.38 (2H, m), 7.53 (1H, dd, J=2.2, 8.4 Hz), 7.64 (1H, d, J=2.2 Hz), 8.04 (1H, s), 8.45 (1H, dd, J=2.3, 7.3 Hz). IR (KBr) cm^{-1}: 3434, 1716, 1608, 1534, 1496, 1452, 1339, 749. Anal. Calcd for $C_{32}H_{30}N_2O_4 \cdot 0.25H_2O$: C, 75.20; H, 6.01; N, 5.48. Found: C, 75.40; H, 6.25; N, 5.35.

4-[2-[(9-Benzylcarbazol-3-yl)carboxamido]phenoxy]butyric Acid (23) 23: As white crystals, mp 110—111 °C (iso-Pr$_2$O trituration). ^{1}H-NMR (CDCl$_3$+DMSO-d_6) δ: 2.15—2.25 (2H, m), 2.54 (2H, t, J=7.1 Hz), 4.15 (2H, t, J=6.1 Hz), 5.53 (2H, s), 6.90 (1H, dd, J=2.6, 6.9 Hz), 6.96—7.03 (2H, m), 7.10—7.13 (2H, m), 7.22—7.31 (4H, m), 7.38—7.47 (3H, m), 7.98 (1H, dd, J=2.0, 8.6 Hz), 8.19 (1H, d, J=7.9 Hz), 8.55 (1H, dd, J=2.5, 7.1 Hz), 8.75 (2H, br s). IR (KBr) cm^{-1}: 3430, 1727, 1599, 1542, 1453, 1330, 756. Anal. Calcd for $C_{30}H_{26}N_2O_4$: C, 75.30; H, 5.48; N, 5.85. Found: C, 75.38; H, 5.59; N, 5.76.

4-[2-[(10,11-Dihydro-5H-dibenz[b,f]azepin-2-yl)carboxamido]phenoxy]butyric Acid (24) 24: As white crystals, mp 162—165 °C (iso-Pr$_2$O trituration). ^{1}H-NMR (CDCl$_3$) δ: 2.17—2.26 (2H, m), 2.55 (2H, t, J=7.1 Hz), 3.09 and 3.13 (4H, AB pattern, J=8.4 Hz), 4.17 (2H, t, J=5.9 Hz), 6.79 (1H, t, J=7.3 Hz), 6.91—7.12 (6H, m), 7.48 (2H, s), 7.59 (1H, t, J=2.3 Hz), 7.62 (1H, s), 7.77 (1H, s), 8.46 (1H, dd, J=1.7, 7.6 Hz), 8.57 (1H, s). IR

(KBr) cm^{-1}: 3366, 1714, 1647, 1522, 1503, 1486, 1449, 1342, 1215, 749. Anal. Calcd for $C_{25}H_{24}N_2O_4 \cdot 0.25H_2O$: C, 71.33; H, 5.87; N, 6.65. Found: C, 71.16; H, 6.12; N, 6.35.

4-[2-[[5-(2-Pyridyl)methyl-10,11-dihydrodibenz[b,f]azepin-2-yl]carboxamido]phenoxy]butyric Acid (25) 25: As amorphous. ^{1}H-NMR (CDCl$_3$) δ: 2.17—2.27 (2H, m), 2.59 (2H, t, J=7.1 Hz), 3.25 (4H, br s), 4.14 (2H, t, J=5.8 Hz), 5.14 (2H, s), 6.89 (1H, d, J=8.9 Hz), 6.98—7.07 (3H, m), 7.12—7.18 (4H, m), 7.34 (1H, d, J=8.3 Hz), 7.52—7.60 (2H, m), 7.69 (1H, d, J=1.7 Hz), 8.45—8.48 (2H, m), 8.52 (1H, s). IR (KBr) cm^{-1}: 3416, 2930, 1602, 1598, 1525, 1508, 1494, 1451, 1250. Anal. Calcd for $C_{31}H_{29}N_3O_4 \cdot 0.5H_2O$: C, 72.08; H, 5.85; N, 8.13. Found: C, 72.24; H, 6.05; N, 8.03.

4-[2-[[5-Benzyl-8-(2-methyl)propyl-10,11-dihydrodibenz[b,f]azepin-2-yl]carboxamido]phenoxy]butyric Acid (26) 26: As amorphous. ^{1}H-NMR (CDCl$_3$) δ: 0.86 (6H, d, J=6.4 Hz), 1.77—1.82 (1H, m), 2.13—2.22 (2H, m), 2.36 (2H, d, J=6.4 Hz), 2.55 (2H, t, J=7.1 Hz), 3.20—3.30 (4H, m), 4.11 (2H, t, J=6.1 Hz), 5.00 (2H, s), 6.85—7.30 (11H, m), 7.36 (2H, d, J=8.3 Hz), 7.51 (1H, d, J=8.6 Hz), 7.64 (1H, s), 8.38 (1H, s), 8.44 (1H, dd, J=2.3, 7.3 Hz). IR (KBr) cm^{-1}: 3435, 2950, 1706, 1601, 1530, 1493, 1452, 1334, 1250, 747. Anal. Calcd for $C_{36}H_{38}N_2O_4 \cdot 0.25H_2O$: C, 76.23; H, 6.84; N, 4.94. Found: C, 76.12; H, 7.10; N, 4.86.

4-[2-[[8-(2-Methyl)propyl-5H-10,11-dihydrodibenz[b,f]azepin-2-yl]carboxamido]phenoxy]-butyric Acid (27) 27: As white crystals, mp 144—145 °C (iso-Pr$_2$O trituration). ^{1}H-NMR (CDCl$_3$) δ: 0.90 (6H, d, J=6.8 Hz), 1.78—1.84 (1H, m), 2.17—2.24 (2H, m), 2.38 (2H, d, J=6.8 Hz), 2.59 (2H, t, J=7.1 Hz), 3.03—3.13 (4H, m), 4.14 (2H, t, J=5.9 Hz), 6.28 (1H, br s), 6.69 (1H, d, J=7.9 Hz), 6.73 (1H, d, J=8.5 Hz), 6.84 (1H, s), 6.86—6.90 (2H, m), 6.97—7.06 (2H, m), 7.57 (1H, dd, J=2.1, 8.5 Hz), 7.63 (1H, d, J=2.1 Hz), 8.44 (1H, s), 8.47—8.50 (1H, m). IR (KBr) cm^{-1}: 3340, 2948, 1601, 1504, 1452, 1348, 1249, 752. Anal. Calcd for $C_{29}H_{32}N_2O_4$: C, 73.71; H, 6.83; N, 5.93. Found: C, 73.39; H, 7.04; N, 5.86.

References and Notes
1) Present address: Kyowa Hakko Kogyo Co., Ltd., 6–1 Ohtemachi, 1-chome Chiyoda-ku, Tokyo 100–8185, Japan.
2) a) Metcalf B. W., Levy M. A., Holt D. A., Trends Pharmacol. Sci., 10, 491 (1989); b) Geller J., Prostate, Suppl., 2, 95 (1989); c) Isaacs J. T., Brendler C. B., Walsh P. C., J. Clin. Invest., 56, 139 (1983).
3) Sansone G. L., Reisner R. M., J. Invest. Dermatol., 56, 366 (1971).
4) Diani A. R., Mulholland M. J., Shull K. L., Kubicek M. F., Johnson G. A., Schostarez H. J., Brunden M. N., Buhl A. E., J. Clin. Endocrinol. Metab., 74, 345 (1992).
5) Brooks J. R., J. Clin. Endocrinol. Metab., 15, 391 (1986).
6) Russel D. W., Wilson J. D., Annu. Rev. Biochem., 63, 25 (1994).
7) a) Kumazawa T., Takami H., Kishibayashi N., Ishii A., Nagahara Y., Hirayama N., Obase H., J. Med. Chem., 38, 2887 (1995); b) Takami H., Koshimura H., Kishibayashi N., Ishii A., Nonaka H., Aoyama S., Kase H., Kumazawa T., J. Med. Chem., 39, 5047 (1996); c) Takami H., Kishibayashi N., Ishii A., Kumazawa T., Bioorg. Med. Chem., 6, 2441 (1998).
8) Nakai H., Terashima H., Arai Y., EP 0291245 (1988) [Chem. Abstr., 110, 212384t, 708 (1989)].
9) a) Yoshioka T., Kitagawa M., Oki M., Kubo S., Tagawa H., Ueno K., J. Med. Chem., 21, 633 (1978); b) Tagawa H., Kubo S., Ishikawa F., Chem. Pharm. Bull., 29, 3515 (1981).
10) a) Sallmann A., Pfister R., Chem. Abstr., 76, 113221k, 893 (1972); b) Ito C., Okahana N., Wu T.-S., Wang M.-L., Lai J.-S., Kuoh C.-S., Furukawa H., Chem. Pharm. Bull., 40, 230 (1992).
11) Bald E., Saigo K., Mukaiyama T., Chem. Lett., 1163 (1975).
12) a) Andersson S., Berman D. M., Jenkins E. P., Russell D. W., Nature (London) 354, 159 (1991); b) Jenkins E. P., Andersson S., Imperato-McGinley J., Wilson J. D., Russell D. W., J. Clin. Invest., 89, 293 (1992).
13) a) Leo A. J., Chem. Rev., 93, 1281 (1993); b) The values were calculated by C log P for Windows Ver. 1.0.0 (BioByte Corp.).
14) Takami H., Ohshima E., Sato H., Kumazawa T., Miki I., Ishii A., Sasaki Y., Ohmori K., Karasawa A., Kubo K., Obase H., Abstracts of Papers, 13rd Medicinal Chemistry Symposium/2nd Annual Meeting of Division of Medicinal Chemistry, Tokyo, November 1992, paper 35.

Cholestane Glycosides from *Solanum abutiloides*. III

Hitoshi Yoshimitsu,*,[a] Makiko Nishida,[a] and Toshihiro Nohara[b]

Faculty of Engineering, Kyushu Kyoritsu University,[a] 1–8 Jiyugaoka Yahata-nishi-ku, Kitakyushu 807–8585, Japan and
Faculty of Pharmaceutical Sciences, Kumamoto University,[b] 5–1 Oe-honmachi, Kumamoto 862–0973, Japan.
Received August 26, 1999; accepted December 9, 1999

Four new cholestane glycosides, named abutilosides D (1), E (2), F (3) and G (4), were isolated from the fresh roots of *Solanum abutiloides*. By chemical and spectroscopic evidence, their structures were elucidated as 26-*O*-β-D-glucopyranosyl 3β,16α,26-trihydroxy-5α-cholestan-22-one 3-*O*-β-D-xylopyranosyl-(1→2)-α-L-rhamnopyranosyl-(1→4)-β-D-glucopyranoside and its desxylosyl compound (1 and 3, respectively), 26-*O*-β-D-glucopyranosyl 3β,16α,26-trihydroxycholest-5-en-22-one 3-*O*-β-D-xylopyranosyl-(1→2)-α-L-rhamnopyranosyl-(1→4)-β-D-glucopyranoside and its desxylosyl compound (2 and 4, respectively). These compounds were regarded as precursors of a dormantinone type compound on a hypothetical pathway of steroid biogenesis.

Key words cholestane glycoside; abutiloside; *Solanum abutiloides*; biogenesis

In the preceding paper,[1] we reported the isolation and structural determination of three cholestane glycosides, named abutilosides A, B and C (5), from the fresh roots of *Solanum abutiloides*. These compounds were important as a key intermediate in the biogenesis of steroidal alkaloids. In a continuing study on glycosidic constituents, we obtained four additional new cholestane glycosides, named abutilosides D (1), E (2), F (3) and G (4). This paper describes their structural characterization.

The methanol extract of the fresh roots of *Solanum abutiloides* was partitioned into an AcOEt–water solvent system. MCI gel CHP-20P column chromatography of the water soluble portion provided the glycosidic constituents, which were purified by using a combination of Sephadex LH-20, silica gel and octadecyl silica gel (ODS) column chromatographies to furnish four abutilosides (1—4).

Abutiloside D (1) was obtained as a white powder, $[\alpha]_D$ −56.6° (MeOH), and showed an ion peak due to $[M-H]^-$ at *m/z* 1035 in the neg. FAB-MS. The ^{1}H-NMR spectrum of 1 displayed two tertiary methyls at δ 0.67 and 0.68, three secondary methyls at δ 0.98 (d, *J*=6.1 Hz), 1.19 (d, *J*=6.7 Hz) and 1.66 (d, *J*=6.7 Hz), and four anomeric protons at δ 4.82 (1H, d, *J*=7.9 Hz), 4.98 (1H, d, *J*=7.3 Hz), 5.23 (1H, d, *J*= 7.9 Hz) and 6.02 (1H, brs). The above ^{1}H-NMR spectrum of 1 was similar to that of abutiloside C (5). In the ^{13}C-NMR spectrum of 1, the signals due to the aglycone moiety, except for C-24, C-25 and C-26 at the side chain, and the sugar moiety were also in good agreement with those of 5. Meanwhile, the neg. FAB-MS of 1 gave a quasi-molecular peak at *m/z* 1035, which was higher by 162 mass units than that of 5. Furthermore, a comparative study of the ^{13}C-NMR spectrum of 1 with that of 5 indicated the presence of an additional glucosyl unit in 1, which was linked to the C-26 hydroxy group of an aglycone moiety. On acid hydrolysis, 1 afforded D-glucose, D-xylose and L-rhamnose, together with several unidentified artificial sapogenoles.[2] The ^{1}H- and ^{13}C-NMR spectrum of 1, which could be assigned with the aid of ^{1}H–^{1}H correlation spectroscopy (COSY), heteronuclear multiple quantum coherence (HMQC), total correlation spectroscopy (TOCSY) and heteronuclear multiple bond correlation spectroscopy (HMBC) techniques, showed signals due to a tetrasaccharide moiety consisting of two glucopyranosyl moieties, one xylopyranosyl moiety and one rhamnopyra-

nosyl moiety. The HMBC experiment showed that the trisaccharide and monosaccharide moieties were linked to the C-3 and C-26 hydroxy groups of the aglycone, respectively. Moreover, the anomeric proton signals at δ 4.82, 4.98, 6.02 and 5.23 showed long-range correlations with the ^{13}C signals at δ 75.1 (C-26 of aglycone), 77.3 (C-3 of aglycone), 77.8 (C-4 of 4-substituted glucose) and 81.9 (C-2 of 2-substituted rhamnose), respectively. From the above evidence, the structure of 1 was concluded to be 26-*O*-β-D-glucopyranosyl 3β,16α,26-trihydroxy-5α-cholestan-22-one 3-*O*-β-D-xylopyranosyl-(1→2)-α-L-rhamnopyranosyl-(1→4)-β-D-glucopyranoside.

Abutiloside E (2) was obtained as a white powder, $[\alpha]_D$ −60.5° (MeOH), and showed an ion peak due to $[M-H]^-$ at *m/z* 1033, which was lower by 2 mass units than that of 1, in the neg. FAB-MS. The ^{1}H-NMR spectrum of 2 displayed two tertiary methyls at δ 0.70 and 0.91, three secondary methyls at δ 0.98 (d, *J*=6.7 Hz), 1.20 (d, *J*=6.7 Hz) and 1.66 (d, *J*=6.1 Hz), an olefinic proton at δ 5.30 (1H, brs) and four anomeric protons at δ 4.81 (1H, d, *J*=7.9 Hz), 4.98 (1H, d, *J*=7.3 Hz), 5.23 (1H, d, *J*=7.9 Hz) and 6.02 (1H, brs). Based on the above ^{1}H-NMR data, the structure of 2 was considered to be analogous to that of 1. In the ^{13}C-NMR spectrum of 2, the chemical shifts of the aglycone moiety, except for the signals owing to the A and B rings, and the sugar moiety showed coincidence with those of 1. This evidence indicated the presence of a double bond in the B ring. In the HMBC experiment, the methyl proton signal at δ 0.91 (H-19) showed long-range correlations with δ 140.9 (C-5 of aglycone). Consequently, the structure of 2 was determined to be 26-*O*-β-D-glucopyranosyl 3β,16α,26-trihydroxycholest-5-en-22-one 3-*O*-β-D-xylopyranosyl-(1→2)-α-L-rhamnopyranosyl-(1→4)-β-D-glucopyranoside.
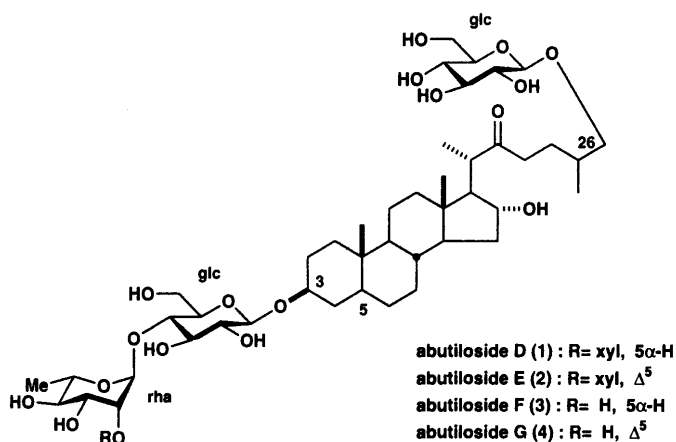
Abutiloside F (3) was obtained as a white powder, $[\alpha]_D$ −51.8° (MeOH), and showed an ion peak due to $[M-H]^-$ at *m/z* 903, which was lower by 132 mass units than that of 1, in the neg. FAB-MS. The ^{1}H-NMR spectrum of 3 displayed two tertiary methyls at δ 0.68 and 0.69, three secondary methyls at δ 0.98 (d, *J*=6.1 Hz), 1.19 (d, *J*=6.7 Hz) and 1.73 (d, *J*= 6.1 Hz), and three anomeric protons at δ 4.82 (1H, d, *J*= 7.9 Hz), 4.98 (1H, d, *J*=7.3 Hz) and 5.90 (1H, brs). In the ^{13}C-NMR spectrum of 3, signals due to the aglycone moiety were in good agreement with those of 1, although the signals

Table 1. ^{1}H-NMR Chemical Shifts for Oligosaccharide Moieties of 1—4 (Pyridine-d_5)

	1	2	3	4
3-O-				
Glc-1	4.98 d (7.3)	4.98 d (7.3)	4.98 d (7.3)	4.98 d (7.3)
Glc-2	3.99 dd (7.3, 9.1)	3.99 dd (8.5, 8.5)	4.01 dd (7.3, 9.1)	4.00 dd (7.3, 9.1)
Glc-3	4.22	4.22 dd (8.5, 8.5	4.17 dd (9.1, 9.1)	4.15 dd (9.1, 9.1)
Glc-4	4.46 dd (9.1, 9.1)	4.46 dd (9.2, 9.2)	4.45 dd (9.1, 9.1)	4.46 dd (9.1, 9.1)
Glc-5	3.92 m	3.87 m	3.90 m	3.87 m
Glc-6	4.25 dd (4.3, 12.0)	4.25	4.23 dd (5.5, 11.8)	4.23 dd (4.3, 11.9)
	4.44 br d (12.0)	4.38 br d (12.0)	4.35 br d (11.6)	4.36 br d (11.6)
Rha-1	6.02 br s	6.02 br s	5.90 br s	5.90 br s
Rha-2	4.69 br d (3.0)	4.68 br d (3.1)	4.71 br s	4.71 br s
Rha-3	4.58 dd (3.0, 9.1)	4.67 dd (3.1, 9.2)	4.58 br d (10.0)	4.58 br d (10.4)
Rha-4	4.27 dd (9.1, 9.1)	4.27	4.37 dd (9.1, 9.1)	4.39 dd (9.1, 9.1)
Rha-5	5.02 m	5.02	5.02 m	5.01 m
Rha-6	1.66 d (6.7)	1.66 d (6.1)	1.73 d (6.1)	1.73 d (6.1)
Xyl-1	5.23 d (7.9)	5.23 d (7.9)		
Xyl-2	4.07 dd (7.9, 8.5)	4.07 dd (7.9, 7.9)		
Xyl-3	4.12 dd (8.5, 8.5)	4.12 dd (8.5, 8.5)		
Xyl-4	4.15	4.14 dd (7.3, 7.3)		
Xyl-5	3.67 dd (10.4, 10.4)	3.66 dd (9.8, 10.6)		
	4.29	4.28		
26-O-				
Glc-1	4.82 d (7.9)	4.81 d (7.9)	4.82 d (7.9)	4.82 d (7.9)
Glc-2	4.02 dd (7.9, 8.5)	4.02 dd (7.9, 8.5)	4.02 dd (7.9, 8.5)	4.01 dd (7.9, 8.5)
Glc-3	4.25	4.25	4.26	4.26
Glc-4	4.25	4.25	4.26	4.26
Glc-5	3.94 m	3.94 m	3.92 m	3.93 m
Glc-6	4.39 br d (11.8)	4.39 dd (5.5, 11.6)	4.33 br d (11.2)	4.34 br d (11.2)
	4.56 br d (11.6)	4.56 dd (3.6, 12.6)	4.56 br d (12.2)	4.56 br d (12.3)

Coupling constants (J in Hz) are given in parentheses.

abutiloside D (1) : R= xyl, 5α-H
abutiloside E (2) : R= xyl, Δ^5
abutiloside F (3) : R= H, 5α-H
abutiloside G (4) : R= H, Δ^5

due to the sugar moiety were not identical. On acid hydrolysis, 3 afforded D-glucose and L-rhamnose, together with several unidentified artificial sapogenoles.[2] The ^{1}H- and ^{13}C-NMR data of the sugar moiety were assigned by ^{1}H–^{1}H COSY and HMQC techniques. In the HMBC experiment, long-range correlations were observed between the anomeric proton [δ 4.82 (d, J=7.9 Hz)] of terminal glucose and the C-26 (δ 75.1) of aglycone, the anomeric proton [δ 4.98 (d, J=7.3 Hz)] of 4-substituted glucose and the C-3 (δ 77.4) of aglycone and the anomeric proton [δ 5.90 (br s)] of terminal rhamnose and the C-4 (δ 78.5) of 4-substituted glucose. Based on the above evidence, the structure of 3 was elucidated as a cholestane glycoside with a terminal xylose absent from 1.

Abutiloside G (4) was obtained as a white powder, [α]$_D$

−81.3° (MeOH), and showed an ion peak due to [M−H]$^-$ at m/z 901, which was lower by 2 mass units than that of 3, in the neg. FAB-MS. In the ^{1}H- and ^{13}C-NMR spectrum of 4, signals due to an aglycone moiety were consistent with those of 2, while signals due to a sugar moiety were almost superimposable on those of 3. From the above evidence, the structure of 4 was concluded to have a double bond at the C-5 of 3. The configuration at C-25 in 1—4 was deduced to be R due to the coexistence of dioscin and solamargine in this plant. However, this presumption was a moot point.

Kaneko *et al.* presented a hypothetical biogenetic pathway of solanidine in *Veratrum*.[3] 1—4 were regarded as precursors of a dormantinone type compound on a hypothetical pathway of steroid biogenesis. Further, 2 and 4 were corresponding 5-ene compounds to 1 and 3. Consequently, the coexistence of a 5-ene type compound was confirmed in the roots of *Solanum abutiloides*.

Experimental

Optical rotations were taken with a JASCO DIP-1000 automatic digital polarimeter. The ^{1}H- and ^{13}C-NMR spectra were measured with a JEOL alpha 500 NMR spectrometer and chemical shifts are given on a δ (ppm) scale with tetramethylsilane (TMS) as an internal standard. The FAB-MS was measured with a JEOL DX-303 HF spectrometer and taken in a 3-nitrobenzyl alcohol matrix. HPLC was carried out using a TSK gel-120T (7.8 mm i.d. ×30 cm) column with a Tosoh CCPM pump and Tosoh RI-8010 differential refractometer as a detector. TLC was performed on precoated Kieselgel 60 F$_{245}$ (Merck), and detection was achieved by spraying them with 10% H$_2$SO$_4$ followed by heating. Column chromatography was carried out on Kieselgel (230—400 mesh, Merck), Sephadex LH-20 (Pharmacia), ODS (PrePAK-500/C$_{18}$, Waters) and MCI gel CHP-20P (Mitsubishi Chemical Ind.)

Extraction and Separation The seeds identified as *Solanum abutiloides* at the National Research Institute of Vegetables, Ministry of Agri-

Table 2. ^{13}C-NMR Data for **1**—**5** (Pyridine-d_5)

	1	2	3	4	5
C- 1	37.1	37.3	37.1	37.4	37.0
C- 2	29.9	30.2	30.0	30.2	29.9
C- 3	77.3	78.2	77.4	78.4	77.3
C- 4	34.8	39.3	34.9	39.3	34.8
C- 5	44.6	140.9	44.6	140.9	44.5
C- 6	28.9	121.8	28.9	121.8	28.9
C- 7	32.2	32.1	32.4	32.1	32.2
C- 8	35.1	31.6	35.1	31.8	35.1
C- 9	54.4	50.3	54.4	50.3	54.4
C-10	35.7	36.9	35.7	36.9	35.7
C-11	21.1	20.9	21.1	20.9	21.0
C-12	40.2	39.9	40.2	39.9	40.1
C-13	44.4	44.1	44.4	44.1	44.4
C-14	53.7	53.9	53.7	53.9	53.7
C-15	37.0	37.0	37.0	37.0	36.9
C-16	75.9	75.9	75.9	75.9	75.9
C-17	63.4	63.3	63.4	63.3	63.4
C-18	13.7	13.4	13.7	13.4	13.7
C-19	12.3	19.4	12.3	19.4	12.3
C-20	49.3	49.3	49.3	49.3	49.3
C-21	16.8	16.8	16.8	16.8	16.8
C-22	214.9	214.8	214.9	214.8	215.0
C-23	39.0	39.0	39.0	39.0	39.1
C-24	28.0	28.0	28.0	28.0	27.9
C-25	33.4	33.4	33.4	33.4	36.1
C-26	75.1	75.1	75.1	75.1	67.3
C-27	17.6	17.6	17.5	17.6	17.3
3-O-					
Glc-1	102.0	102.4	102.8	102.7	102.0
Glc-2	75.6	75.6	75.5	75.5	75.5
Glc-3	76.6	76.6	76.8	76.7	76.6
Glc-4	77.8	77.7	78.5	78.2	77.8
Glc-5	77.4	77.3	77.2	77.2	77.3
Glc-6	61.7	61.7	61.7	61.6	61.7
Rha-1	101.2	101.2	102.1	101.5	101.2
Rha-2	81.9	81.9	72.6	72.6	81.9
Rha-3	72.9	72.9	72.8	72.8	72.8
Rha-4	74.4	74.4	74.0	74.0	74.4
Rha-5	70.0	70.0	70.4	70.4	69.9
Rha-6	18.4	18.4	18.5	18.5	18.4
Xyl-1	107.6	107.6			107.5
Xyl-2	75.2	75.2			75.5
Xyl-3	78.5	78.5			78.4
Xyl-4	71.0	71.0			71.0
Xyl-5	67.4	67.4			67.4
26-O-					
Glc-1	104.9	104.9	104.9	104.9	
Glc-2	75.2	75.2	75.2	75.3	
Glc-3	78.5	78.5	78.5	78.5	
Glc-4	71.7	71.7	71.7	71.7	
Glc-5	78.6	78.6	78.6	78.6	
Glc-6	62.8	62.8	62.8	62.8	

culture, Forestry and Fisheries, Ano, Mie in Japan, were cultivated at the Botanical Garden of Kumamoto University. The harvested roots (2.24 kg) of this plant were extracted with MeOH, and the extract was partitioned in AcOEt and water (1:1, v/v). The water soluble portion (87.6 g) was subjected to MCI gel CHP-20P column chromatography with MeOH–H$_2$O (20→30→40→50→60→70→80→90→100%) to afford ten fractions (fr.1— fr.10). Fraction 3 (1.04 g) was further separated by ODS column chromatography with MeOH–H$_2$O (40→50→60→70%) and silica gel column chromatography with CHCl$_3$–MeOH–H$_2$O (6:4:0.5, v/v), followed by HPLC with MeOH–H$_2$O (3:2), to furnish abutilosides D (**1**) (423 mg) and E (**2**) (27 mg). Fraction 4 (1.67 g) was subjected to ODS column chromatography with MeOH–H$_2$O (40→50→60→70→80%) to afford two fractions (fr.11—

fr.12). Fraction 11 was further separated by Sephadex LH-20 column chromatography with MeOH and silica gel column chromatography with CHCl$_3$–MeOH–H$_2$O (6:4:0.5, v/v), followed by HPLC with MeOH–H$_2$O (3:2), to furnish abutiloside G (**4**) (72 mg). Fraction 12 was further separated by Sephadex LH-20 column chromatography with MeOH and silica gel column chromatography with CHCl$_3$–MeOH–H$_2$O (6:4:0.5, v/v), followed by HPLC with MeOH–H$_2$O (3:2), to furnish abutiloside F (**3**) (229 mg).

Abutiloside D (**1**) A white powder, $[\alpha]_D^{25}$ −56.6° (c=0.80, MeOH). Neg. FAB-MS (m/z): 1035 [M−H]$^-$. ^{1}H-NMR (pyridine-d_5) δ: 0.67 (3H, s, H-19), 0.68 (3H, s, H-18), 0.98 (3H, d, J=6.1 Hz, H-27), 1.19 (3H, d, J= 6.7 Hz, H-21), 3.61 (1H, dd, J=6.7, 8.7 Hz, H-26a), 3.87 (1H, m, H-3), 3.95 (1H, dd, J=6.7, 9.1 Hz, H-26b), 4.24 (1H, H-16). Signals for the saccharide moiety are shown in Table 1. ^{13}C-NMR (pyridine-d_5): Table 2.

Abutiloside E (**2**) A white powder, $[\alpha]_D^{25}$ −60.5° (c=0.35, MeOH). Neg. FAB-MS (m/z): 1033 [M−H]$^-$. ^{1}H-NMR (pyridine-d_5) δ: 0.70 (3H, s, H-18), 0.91 (3H, s, H-19), 0.98 (3H, d, J=6.7 Hz, H-27), 1.20 (3H, d, J= 6.7 Hz, H-21), 3.60 (1H, dd, J=5.9, 9.2 Hz, H-26a), 3.82 (1H, m, H-3), 3.96 (1H, H-26b), 4.23 (1H, H-16), 5.30 (1H, br s, H-6). Signals for the saccharide moiety are shown in Table 1. ^{13}C-NMR (pyridine-d_5): Table 2.

Abutiloside F (**3**) A white powder, $[\alpha]_D^{25}$ −51.8° (c=0.75, MeOH). Neg. FAB-MS (m/z): 903 [M−H]$^-$. ^{1}H-NMR (pyridine-d_5) δ: 0.68 (3H, s, H-19), 0.69 (3H, s, H-18), 0.98 (3H, d, J=6.1 Hz, H-27), 1.19 (3H, d, J= 6.7 Hz, H-21), 3.61 (1H, dd, J=6.1, 9.2 Hz, H-26a), 3.81 (1H, m, H-3), 3.95 (1H, dd, J=6.1, 9.2 Hz, H-26b), 4.24 (1H, H-16). Signals for the saccharide moiety are shown in Table 1. ^{13}C-NMR (pyridine-d_5): Table 2.

Abutiloside G (**4**) A white powder, $[\alpha]_D^{25}$ −81.3° (c=0.75, MeOH). Neg. FAB-MS (m/z): 901 [M−H]$^-$. ^{1}H-NMR (pyridine-d_5) δ: 0.71 (3H, s, H-18), 0.92 (3H, s, H-19), 0.98 (3H, d, J=6.1 Hz, H-27), 1.20 (3H, d, J= 6.1 Hz, H-21), 3.61 (1H, dd, J=6.7, 9.8 Hz, H-26a), 3.74 (1H, m, H-3), 3.95 (1H, dd, J=6.1, 9.8, H-26b), 4.24 (1H, H-16), 5.31 (1H, br s, H-6). Signals for the saccharide moiety are shown in Table 1. ^{13}C-NMR (pyridine-d_5): Table 2.

Sugars Analysis of 1 and 3 A solution of each of **1** and **3** (2 mg) in 2 N HCl–dioxane (1:1, 2 ml) was heated at 100 °C for 1 h. The reaction mixture was diluted with H$_2$O and evaporated to remove dioxane. The solution was neutralized with Amberlite MB-3 and passed through a SEP-PAK C$_{18}$ cartridge to give a sugar fraction. A solution of sugar fraction analyzed by TLC [CH$_3$CN–MeOH–H$_2$O (6:4:1), **1**: rhamnose, Rf 0.54; xylose, Rf 0.40; glucose, Rf 0.29; **3**: rhamnose, Rf 0.54; glucose, Rf 0.29]. A solution of the sugar fraction in 1 ml of H$_2$O was treated with a solution of L-(−)-α-methylbenzylamine (150 μl) and NaBH$_3$CN (8 mg) in 1 ml of EtOH, and the mixture was kept at 40 °C for 3 h. Then, several drops of acetic acid were added and the mixture was concentrated to dryness. The residue dissolved in Ac$_2$O–C$_5$H$_5$N (1:1, 2 ml) was treated with 4-(dimethylamino)pyridine (DMAP) (20 mg), and the whole mixture was left at room temperature overnight. After the removal of excess Ac$_2$O and C$_5$H$_5$N, the residue dissolved in 20% CH$_3$CN was loaded into a SEP-PAK C$_{18}$ cartridge and eluted with 20% CH$_3$CN (total 7 ml) and 100% CH$_3$CN. The fraction eluted with 100% CH$_3$CN was analyzed by normal-phase HPLC. Conditions of HPLC: column, Develosil 60-3, 3 μm (4.6 mm i.d. ×150 mm); solvent, n-hexane–EtOH (19:1); flow rate, 1.20 ml/min; detection, UV (230 nm). t_R (min) of 1-(N-acetyl-L-α-methylbenzylamino)-1-deoxyalditol acetates were as follows. **1**: L-rhamnose 17.2, D-xylose 30.8, D-glucose 30.8 (reference: L-rhamnose 17.0, D-xylose 30.7, D-glucose 30.8). **3**: L-rhamnose 17.2, D-glucose 30.7.

References

1) a) Ohmura H., Nakamura T., Tian R.-H., Yahara S., Yoshimitsu H., Nohara T., *Tetrahedron Lett.*, **36**, 8443—8444 (1995); b) Tian R.-H., Ohmura O., Yoshimitsu H., Nohara T., Matsui M., *Chem. Pharm. Bull.*, **44**, 1119—1121 (1996).

2) Oshima R., Yamauchi Y., Kumanotani J., *Carbohydr. Res.*, **107**, 169—176 (1982).

3) Kaneko K., Tanaka W., Mitsuhashi H., *Phytochemistry*, **15**, 1391—1393 (1976).

Butyrolactones from *Aspergillus terreus*

K. V. Rao, A. K. Sadhukhan, M. Veerender, V. Ravikumar, E. V. S. Mohan, S. D. Dhanvantri,
M. Sitaramkumar, J. Moses Babu, K. Vyas, and G. Om Reddy*

Dr. Reddy's Research Foundation, Bollaram Road, Miyapur, Hyderabad-500 050, India.
Received August 30, 1999; accepted November 30, 1999

In the process development of lovastatin using *Aspergillus terreus* DRCC 152 in solid state fermentation, we have isolated a new butyrolactone-IV (3) along with the previously reported butyrolactone-I (1) and butyrolactone-II (2) produced under submerged conditions. The structure of compound 3 has been characterized as 3-hydroxy-5-{2-(1-hydroxy-1-methylethyl)-2(*R*)-2,3-dihydro-benzo[*b*]furan-5 ylmethyl}-4-(4-hydroxyphenyl)-5-methoxycarbonyl-(5*R*)-2,5-dihydro-2-furanone on the basis of spectroscopic studies. The absolute stereochemistry has been determined by single crystal X-ray diffraction studies. The cytotoxic and antibacterial activities of these compounds were determined.

Key words *Aspergillus terreus*; solid state fermentation; butyrolactone; biological activity

We have successfully developed a novel process for the production of lovastatin[1] using *A. terreus* DRCC 152. In the course of our investigations on the secondary metabolites of *A. terreus* in solid state fermentation, we have isolated a new butyrolactones (3) along with two known butyrolactones, butyrolactone-I (1) and butyrolactone-II (2) from the ethyl acetate extract of solid substrate of *A. terreus*. In the present communication we describe the fermentation, isolation and characterization of these butyrolactones (1, 2 and 3) and their biological activities.

Compounds 1 and 2 were known in the literature (with partial NMR data) as butyrolactone I (1) and II (2), respectively.[2,3] The ¹H- and ¹³C-NMR data of 1 and 2 were unambiguously assigned with the help of 2D-NMR experiments *viz.*, double-quantum filtered-correlation spectroscopy (DQF-COSY), nuclear Overhauser enhancement exchange spectroscopy (NOESY), heteronuclear correlation (HETCOR) and long range HETCOR (LRHETCOR) spectra.

Compound 3 was obtained as colorless crystals and

1 R=

2 R=H

4 R=

3

showed IR absorption bands at 3425 and 1739 cm⁻¹ which indicated the presence of hydroxyl and ester carbonyl groups, respectively. The molecular formula was deduced to be $C_{24}H_{24}O_8$ with 13 unsaturations from MS and ¹³C-NMR spectral data. The twenty-four carbon signals and their multiplicities were determined by distortionless enhancement by polarization transfer (DEPT).

The ¹H-NMR spectrum showed a 4H A_2B_2 system at δ 7.5 (2H, d, *J*=8.6 Hz) and 6.9 (2H, d, *J*=8.6 Hz), indicating the presence of a *para*-disubstituted phenyl group in 3. An AB quartet at δ 6.6 (*J*=9.0 Hz) integrating for two protons and a singlet at δ 6.5 integrating for one proton, suggested the presence of a tri-substituted benzene ring. The presence of a methylene group and a methoxy group was inferred from the signals at δ 3.4 (2H, s) and δ 3.8 (3H, s). ¹H-NMR signal (eventually shown to be that of H-21) at δ 4.5 (1H, t, *J*=7.6 Hz) was coupled (as shown by COSY) to a multiplet at δ 3.0 and to two overlapped methyl singlets at δ 1.1 (a *gem*-dimethyl group). This is characteristic of a furan ring formed from the prenyl residue with the oxygen function on C-17. Heteronuclear couplings between C-18 with the proton of C-20 (Fig. 2) defined the location of this isoprenoid moiety involving the carbon atom C-18. The ¹H-NMR spectrum of 3 displayed a long-range hetero nuclear coupling between a proton at δ 4.5 and the C-24 methyl carbon. On the basis of these results the structure of 3 was determined as 3-hydroxy-5-{2-(1-hydroxy-1-methylethyl)-2,3-dihydro-benzo[*b*]furan-5 ylmethyl}-4-(4-hydroxyphenyl)-5-methoxycarbonyl-2,5-dihydro-2-furanone. The structure was supported by 2D-NMR experiments [DQF-COSY, HETCOR, NOESY (Fig. 1) and LRHETCOR (Fig. 2)].
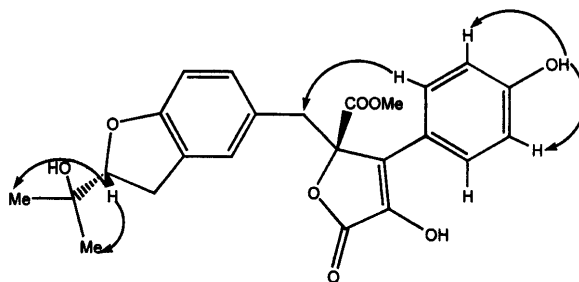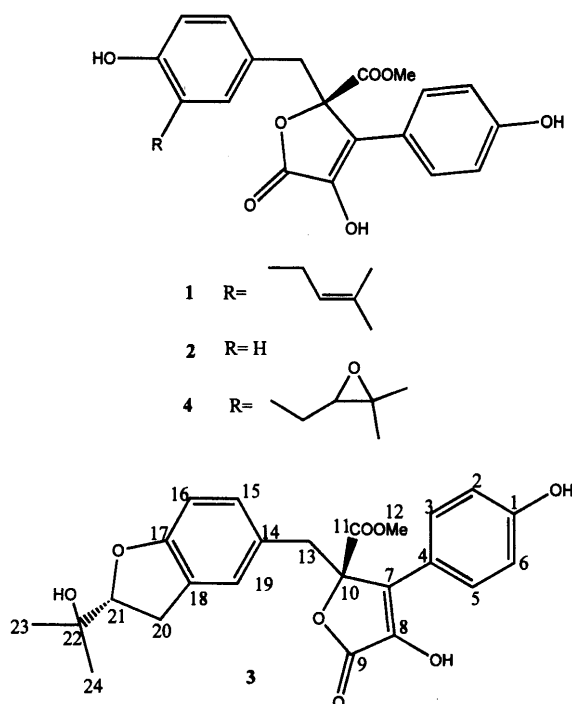

Fig. 1.   NOE Correlations

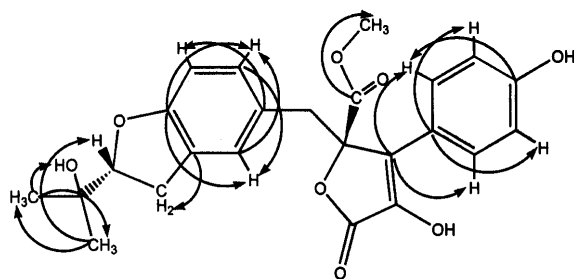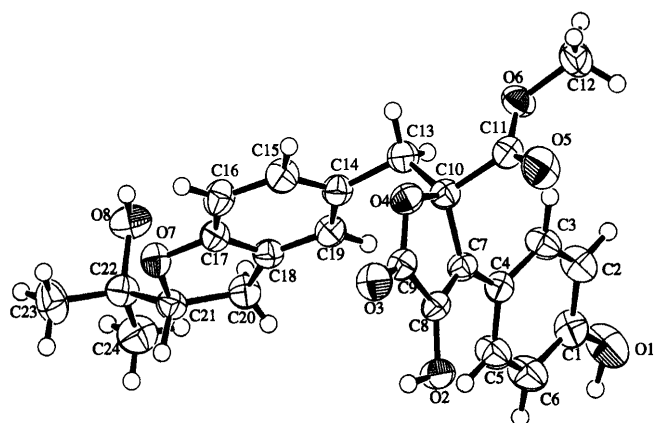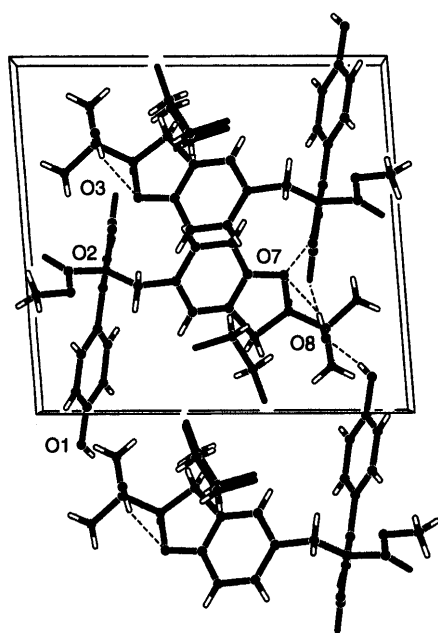* To whom correspondence should be addressed.

Fig. 2. LRHETCOR Correlations

Table 1. The Hydrogen Bond Interactions of **3**

Donor	H	Acceptor	Sym. code of acceptor	D...A	D-H	H...A	D-H...A
O(1)	H(26)	O(8)	54602	2.703(4)	1.00	1.75	158.9
O(2)	H(27)	O(7)	64602	2.912(3)	0.97	2.04	149.0
O(8)	H(28)	O(3)	65602	2.917(4)	1.01	2.01	148.9
O(8)	H(28)	O(7)	1	2.838(3)	1.01	2.33	110.0

Fig. 3

Table 2. Cytotoxic Activities of **1—4** on Human Cancer Cell Lines

Cell line	Percentage growth (10^{-5} M)			
	1	**2**	**3**	**4**
MCF-7/ADR	60.9	100	46.7	83
U251	57.6	100	67.3	91
SW620	96.4	75	76.7	54
H522	100	100	100	38
M14	100	100	77.7	100
SKOV3	100	70.3	53.6	100
DU145	94.6	74	47.4	90
A498	73	62.6	62.6	16

Data are mean±S.D. from three separate experiments.
Cell lines: MCF-7/ADR, human breast cancer; U251, human CNS cancer; SW620, human colon cancer; H522, human lung cancer; M14, human melanoma; SKOV3, human ovarian cancer; DU145, human prostate cancer; A498, human renal cancer.

the lattice (Fig. 4).

Butyrolactone III (**4**), an isomer of **3** was synthesized from **1** and the spectral data was compared. The biological activities of **4** were also determined.

Cytotoxicity of **1—4** was measured *in vitro* using both sensitive and multi-drug resistant (MCF7/ADR) cell lines. As shown in Table 2, all the compounds exhibited mild cytotoxic activity. No detectable antibacterial activity was noticed against Gram (+) and Gram (−) strains at a concentration of 100 μg/disc.

Experimental

General Procedures Melting points (mp) were determined on Buchi micromelting point apparatus without corrections. Optical rotations were determined using JASCO polarimeter. UV spectra were taken in MeOH on a Shimadzu Model 2100S double beam UV-visible spectrophotometer, and FT-IR spectra were on a Perkin Elmer 1650 FT-IR spectrophotometer. Elemental analyses were performed on Perkin Elmer Series II CHN analyser 2400. NMR spectra were recorded on a Varian Gemini 200 NMR spectrometer in dimethyl sulfoxide (DMSO-d_6) using TMS as internal standard. Mass spectra were obtained in the EI mode at 70 eV.

Isolation of butyrolactones (1, 2 and 3) *Aspergillus terreus* DRCC 152, a mutant developed from ATCC 20542, was cultivated on sterilized wheat bran (1 kg) consisting starch (100 g), millet flour (100 g) and ragi flour (100 g) at 27±1 °C for 9 d in stainless steel trays (775 mm×375 mm×50 mm). The moldy bran (1 kg) was extracted with 10 l of EtOAc and the extact was treated with 0.25 M Na$_2$CO$_3$. The aqueous layer was extracted with a mixture of hexane–EtOAc (2:1) at pH 8.0 and 4.0 to obtain respectively fraction I and fraction II. Fraction I (5 g) was subjected to flash chromatography over silica gel using 1,2-dichloroethane–EtOAc (8:2). A total of 50 fractions, each *ca.* 25 ml, were collected. Fractions 9—12, were combined and upon concentration gave the residue (650 mg) and was recrystallized from hexane to give 550 mg of butyrolactone I (**1**). Fractions 23—45 upon removal of solvent followed by recrystallization yielded 600 mg of butyrolactone II (**2**).

Fraction II (7 g) was subjected to flash chromatography over silica gel using 1,2-dichloroethane–EtOAc (8:2). A total of 17 fractions, each *ca.* 25 ml, were collected. Combined fractions 7—12 were evaporated and the residue (600 mg) recrystallized from chloroform–EtOAc (9:1) to give

Fig. 4

The unambiguous confirmation of the structure came from single crystal X-ray analysis. The ORTEP representation of the molecular structure of **3** is shown in Fig. 3. The molecule crystallizes as a dichloroethane solvate. The 1:1 ratio of molecule to solvent (dichloroethane) has been established by elemental analysis. By collecting the X-ray intensity data of Bijvoet pairs and from using the anomalous scattering of the chlorine atoms, the absolute stereochemistry of both chiral centres in butyrolactone IV are determined to be *R*. The hydrogen bond interactions (Table 1) stabilizes the molecule in

Table 3. ^{1}H- and ^{13}C-NMR Data of **3** in DMSO-d_6 (200 MHz)

Atom	3	
	^{1}H	^{13}C
	δ (Hz)	ppm
1	—	157.89
2	6.9 (d, $J=8.6$)	115.79
3	7.5 (d, $J=8.6$)	128.83
4	—	121.00
5	7.5 (d, $J=8.6$)	128.83
6	6.9 (d, $J=8.6$)	115.79
7	—	127.64
8	—	138.13
9	—	167.89
10	—	84.76
11	—	169.69
12	3.8 (s)	53.36
13	3.4 (s)	38.26
14	—	124.42
15	6.6 (d, 9.0)	126.61
16	6.6 (d, 9.0)	107.77
17	—	158.79
18	—	126.85
19	6.5 (s)	129.40
20	3.0 (m)	29.75
21	4.5 (t, $J=7.6$)	89.04
22	—	69.95
23	1.1 (s)	24.84
24	1.1 (s)	25.91
1-OH	10.0 (s)	—
8-OH	—	—
17-OH	—	—
22-OH	4.5 (s)	—

Table 4. Positional Parameters and B (eq) for Butyrolactone IV

Atom	x	y	z	B (eq)
Cl (1)	0.1796(2)	0.6572	0.4192(1)	11.66(7)
Cl (2)	0.0206(1)	0.6585(6)	0.6113(1)	8.72(5)
O (1)	−0.0988(2)	−0.0550(7)	0.0971(2)	5.59(7)
O (2)	0.4354(2)	−0.1988(6)	0.2040(2)	3.64(5)
O (3)	0.6360(2)	−0.0028(6)	0.2464(2)	4.10(5)
O (4)	0.5227(2)	0.2152(6)	0.2306(2)	3.29(4)
O (5)	0.4493(2)	0.2923(7)	0.0343(2)	5.03(6)
O (6)	0.3410(2)	0.4730(6)	0.1065(2)	3.67(4)
O (7)	0.3898(2)	0.1087(6)	0.6892(1)	3.26(4)
O (8)	0.2087(2)	0.2337(6)	0.7898(2)	4.15(5)
C (1)	0.0117(2)	−0.0292(7)	0.1210(2)	3.80(6)
C (2)	0.0554(2)	0.1210(7)	0.0957(3)	3.95(7)
C (3)	0.1662(2)	0.1562(7)	0.1190(2)	3.57(6)
C (4)	0.2372(2)	0.0409(7)	0.1675(2)	2.96(5)
C (5)	0.1930(3)	−0.1106(7)	0.1904(3)	3.88(7)
C (6)	0.0814(3)	−0.1452(7)	0.1691(3)	4.45(8)
C (7)	0.3555(2)	0.0737(6)	0.1909(2)	2.76(5)
C (8)	0.4387(2)	−0.0345(7)	0.2075(2)	2.81(5)
C (9)	0.5437(2)	0.0522(7)	0.2300(2)	2.97(5)
C (10)	0.4046(2)	0.2433(6)	0.2050(2)	2.91(5)
C (11)	0.4015(2)	0.3398(7)	0.1038(2)	3.11(5)
C (12)	0.3325(3)	0.5732(8)	0.0159(2)	4.40(7)
C (13)	0.3594(3)	0.3442(7)	0.2899(2)	3.42(6)
C (14)	0.3730(2)	0.2669(6)	0.3937(2)	3.09(5)
C (15)	0.4713(3)	0.2895(7)	0.4543(2)	3.61(6)
C (16)	0.4834(2)	0.2388(7)	0.5547(2)	3.66(6)
C (17)	0.3926(2)	0.1622(7)	0.5906(2)	2.94(5)
C (18)	0.2956(2)	0.1307(7)	0.5321(2)	2.96(5)
C (19)	0.2852(2)	0.1829(7)	0.4325(2)	3.17(5)
C (20)	0.2141(2)	0.0529(7)	0.5971(2)	3.48(6)
C (21)	0.2863(2)	0.0158(6)	0.6955(2)	3.00(5)
C (22)	0.2364(3)	0.0620(7)	0.7934(2)	3.45(6)
C (23)	0.3175(3)	0.0270(9)	0.8840(2)	5.01(9)
C (24)	0.1276(3)	−0.0284(8)	0.8024(3)	4.70(8)
C (25)	0.2155(5)	0.573(1)	0.5359(5)	7.2(2)
C (26)	0.1222(6)	0.505(1)	0.5848(6)	8.6(2)

125 mg of butyrolactone IV (**3**).

Butyrolactone I (**1**): Colorless crystals (hexane), mp 95 °C (dec). ^{13}C-NMR (DMSO-d_6) δ: 17.5 (C-24), 25.5 (C-23), 27.6 (C-20), 38.1 (C-13), 53.4 (C-12), 84.8 (C-10), 114.1 (C-16), 115.8 (C-2, 6), 121.1 (C-4), 122.4 (C-21), 123.1 (C-14), 126.5 (C-18), 127.5 (C-7), 128.4 (C-15), 128.8 (C-3, 5), 131.0 (C-19), 131.4 (C-22), 138.1 (C-8), 153.8 (C-17), 157.9 (C-1), 167.9 (C-9), 169.8 (C-11).[4]

Butyrolactone II (**2**): Colorless crystals (EtOAc), mp 94—96 °C. ^{13}C-NMR (DMSO-d_6) δ: 38.2 (C-13), 53.5 (C-12), 84.9 (C-10), 114.8 (C-16), 116.0 (C-2, 6), 121.2 (C-4), 123.4 (C-14), 114.8 (C-18), 127.7 (C-7), 129.0 (C-3, 5), 131.3 (C-15), 131.3 (C-19), 138.3 (C-8), 156.4 (C-17), 158.1 (C-1), 168.1 (C-9), 169.9 (C-11).[4]

Butyrolactone IV (**3**): Colorless crystals (CHCl$_3$: EtOAc); mp 110—112 °C; $[\alpha]_D^{27}$ +92° ($c=0.7$, EtOH); UV λ_{max}^{MeOH} nm 309, 227, 204. IR cm^{-1} 3425, 2974, 1739, 1610, 1519, 1385, 1247, 1180, 1036, 839, 583. ^{1}H- and ^{13}C-NMR: Table 3. (Calcd for C$_{24}$H$_{24}$O$_8$·C$_2$H$_4$Cl$_2$, C, 57.9; H, 5.2% Found: C, 58.6; H, 5.1%). MS m/z (%): 440 (M$^+$, 12), 396 (28), 364 (25), 347 (20), 306 (30), 278 (18), 249 (37), 207 (33), 191 (22), 177 (23), 131 (100), 119 (51), 107 (42), 91 (41).

Single Crystal Analysis of Butyrolactone IV (3) Crystal data: C$_{24}$H$_{24}$O$_8$·C$_2$H$_4$Cl$_2$, M.W.=538, monoclinic, $a=12.066(1)$, $b=8.167(1)$, $c=13.299(1)$ Å, $\beta=94.37(1)°$ $V=1306.8(2)$ Å^3, space group $P2_1$(#4), $Z=2$, $D_{calc}=1.37$ g·cm^{-3}. λ(Cu-K$_\alpha$) 1.5418 Å. μ(Cu-K$_\alpha$) 26.45 cm^{-1}. Intensity data were measured on a Rigaku AFC7S diffractometer up to 2θ of 155.3°. A total of 5721 reflections were collected out of which 2888 reflections were unique (R_{int}=0.03) and 2700 were considered observed [$I > 3\sigma(I)$]. Intensity data were corrected for Lorentz, polarization and absorption (psi-scan) effects. The structure was solved by direct methods (SIR92).[5] The structure was refined by full matrix least squares procedures by TEXSAN[6] software. In view of the presence of heavy chlorine atoms in the structure, Bijvoet pairs were collected and the absolute configuration was determined. The hydrogens of the hydroxyl groups were located from a difference Fourier map while the remaining hydrogen atoms were placed at the calculated positions based on the geometry. The agreement indices were R(F)=0.049, R_w(F)=0.075 with anisotropic refinement done on all non-hydrogen atoms. Final atomic coordinates are listed in Table 4.

Synthesis of butyrolactone III (**4**) from **1**: m-Chloroperbenzoic acid (60 mg) was added to a solution of **1** (500 mg) in CHCl$_3$ (25 ml), and the mixture was kept at 4 °C for 24 h. After concentration *in vacuo* the reaction mixture was subjected to flash chromatography on silica gel (230—400 mesh) and eluted with 1,2-dichloroethane–EtOAc (6 : 4) to obtain 400 mg of **4**. Colorless amorphous solid; mp 71—72 °C. $[\alpha]_D^{27}$ +93° ($c=0.6$, EtOH). ^{13}C-NMR (DMSO-d_6) δ: 20.1 (C-24), 25.7 (C-23), 31.0 (C-20), 38.1 (C-13), 53.5 (C-12), 68.67 (C-21), 77.0 (C-22), 84.8 (C-10), 114.1 (C-16), 115.8 (C-2, 6, 16), 119.6 (C-14), 121.1 (C-4), 124.3 (C-18), 127.7 (C-7), 128.8 (C-15), 128.8 (C-3, 5), 131.6 (C-19), 138.2 (C-8), 151.7 (C-17), 157.9 (C-1), 168.0 (C-9), 169.7 (C-11).[4] MS m/z (%): 440 (M$^+$, 12), 396 (100), 364 (56), 294 (34), 265 (16), 237 (17), 191 (37), 177 (10), 131 (30), 119 (51), 107 (18), 91 (22).

Biological Activity Cytotoxic activities of **1**—**4** were tested against a panel of 8 solid tumor cell lines (Table 2), and cell growth was measured by the SRB method.[7] They (**1**—**4**) were also tested for their anti-microbial activity against five Gram-positive (*Staphylococcus aureus* ATCC 6538P, methicillin resistant *S. aureus* ATCC 33591, *Enterococcus faecalis* ATCC 29212 and NCTC 12201, and *Bacillus subtilis* NCIM 2063) and three Gram-negative bacteria (*Pseudomonas aeruginosa* ATCC 27853, and of *Escherichia coli*, DRCC 091). The zone of inhibition if any, was measured by following the guidelines of National Committee for Clinical Laboratory Standards (NCCLS).

References
1) Sadhukhan A. K., Ramana Murthy M. V., Ganesh Reddy D., Rao K.

V., Venkataramana K., Venkateswarlu A., Indian Patent., 96/MDS/786 (1996).

2) Fujii I., Ebizuka Y., Sankawa U., *Chem. Pharm. Bull.*, **30**, 2283—2286 (1982).

3) Kiriyama N., Nitta K., Sakaguchi Y., Taguchi Y., Yamamoto Y., *Chem. Pharm. Bull.*, **25**, 2593—2601 (1977).

4) The ^{13}C-NMR data have not been reported previously.

5) Altomare A., Cascarano M., Giacovazzo C., Guagliardi A., *J. Appl.*

Cryst., **26**, 343 (1993).

6) Molecular Structure Corporation. (1995). TEXSAN. Single Crystal Structure Analysis Software. Version 1.7. MSC, 3200 Research Forest Drive, The Woodlands, TX 77381, U.S.A.

7) Anne M., Dominic S., Philip S., Robert R., Kenneth P., David V., Curtis H., John L., Paul C., Vaigro-Wolff A., Gray-Goodrich M., Campbell H., Joseph M., Boyd M., *J. Natl. Cancer Inst.*, **83**, 757—776 (1991).

Efficient Synthesis of a Key Intermediate of DV-7751 *via* Optical Resolution or Microbial Reduction

Akihiko MIYADERA,* Koji SATOH, and Akihiro IMURA

Chemical Technology Research Laboratories, Daiichi Pharmaceutical Co., Ltd., Edogawa-ku, Tokyo 134–8630, Japan.
Received September 3, 1999; accepted December 3, 1999

Two efficient and practical methods of synthesis of the C-10 substituent of DV-7751 (1), a novel quinolone carboxylic acid, were established. The first method utilizes an optical resolution of racemic 8-amino-6-benzyl-6-azaspiro[3.4]octane (13), while the second employs an enantioselective microbial reduction of 6-benzyl-5,8-dioxo-6-azaspiro[3.4]octane (8b). The enantiomeric excess of (*S*)-8-amino-6-benzyl-6-azaspiro[3.4]octane (11) with each method of synthesis is greater than 96%.

Key words   DV-7751; antibacterial quinolone carboxylic acid; optical resolution; enantioselective microbial reduction

A large number of 4-piridone-3-carboxylic acid derivatives, so-called 4-quinolones, have been synthesized since the discovery of nalidixic acid.[1] Of them, DV-7751 (1), 10-[8(*S*)-amino-6-azaspiro[3.4]octane-6-yl]-9-fluoro-2,3-dihydro-3(*S*)-methyl-7-oxo-7*H*-pyrido[1,2,3-*de*][1.4]benzoxazine-6-carboxylic acid, exhibits marked antibacterial activity against both Gram-negative and Gram-positive bacteria.[2] These characteristics of 1 correlate well with its (*S*)-amino-6-azaspiro[3.4]octane moiety.

To perform a clinical trial of 1, we needed to prepare large quantities of (*S*)-(*tert*-butoxycarbonylamino)-6-azaspiro[3.4]octane (2), which is easily introduced as the C-10 substituent of 1. The reported method[2] utilizing the separation of a 1 : 1 diastereomeric mixture of (*R*)- and (*S*)-8-amino-6-

[(*R*)-1-phenylethyl]-5-oxo-5-azaspiro[3.4]octanes with silica gel column chromatography seemed unsuitable for large-scale manufacturing.

In this paper, we describe, as shown in Chart 2, the practical synthesis of the key chiral compound 2 using optical resolution or microbial reduction.

Results and Discussion

Preparation of 6-Benzyl-5,8-dioxo-6-azaspiro[3.4]octane (8b)   We selected a commercially available diethyl 1,1-cyclobutane dicarboxylate (3) as a starting material. After treatment of compound 3 with an equimolar amount of 10% aqueous KOH, the resulting half-ester 4 was condensed with benzylamine using ethylchloroformate to afford cyclobutyl carboxamide 5. Compound 5 was treated with trimethylsilyl methyllithium to obtain the β-keto carboxamide derivative 6. After bromination of 6, the resulting bromide 7 was cyclized with sodium hydride to afford 8b.

Optical Resolution of 8-Amino-6-benzyl-6-azaspiro[3.4]octane (13)   Compound 8b was derived to oxime 12 by treatment with hydroxylamine, followed by hydrogenation, which yielded amine 13 as a racemate. The optical resolution of 13 was easily performed with D-tartaric acid in ethanol,

Chart 1
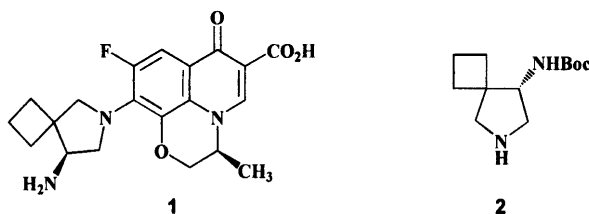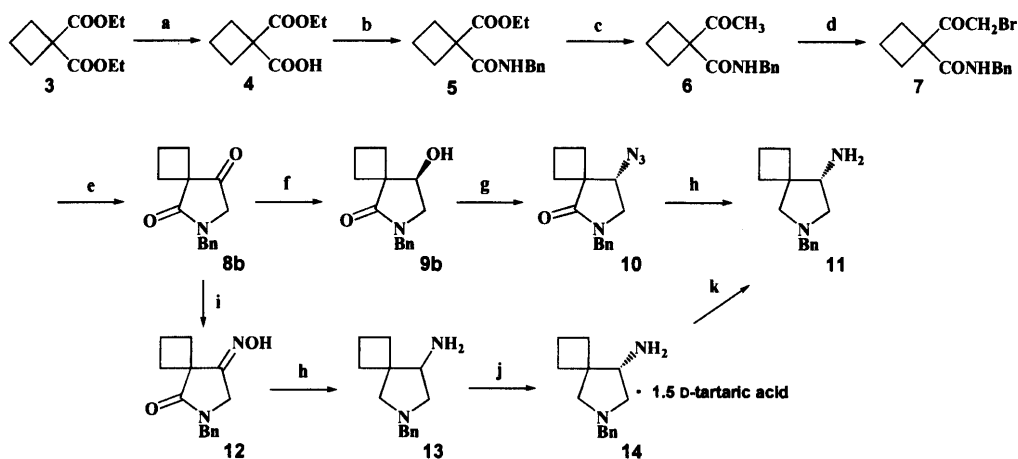

(a) 10% aq.KOH, MeOH; (b) ClCO₂Et, Et₃N, CHCl₃ then benzylamine; (c) TMS-CH₂Li; (d) Br₂, 1,4-dioxane;

(e) NaH, DMF; (f) fungi (JCM 1880), phosphate buffer(pH 6.0); (g) Ph₃P, EtO₂CN₂CO₂Et, DPPA, THF;

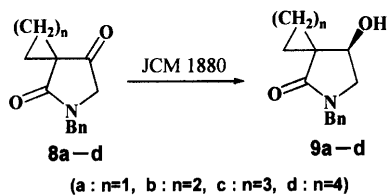(h) LiAlH₄, THF; (i) NH₂OH·HCl, Et₃N, EtOH; (j) D-tartaric acid; (k) 10% aq. NaOH
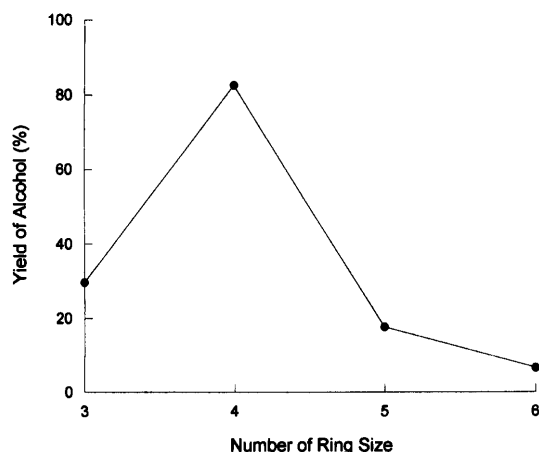
Chart 2

Chart 3

Fig. 1. Relationship between Yield and Ring Size of Substrate

The reaction conditions are described in the Experimental section.

yielding the desired diastereomeric salt, (S)-**13** · 1.5 D-tartaric acid was precipitated as a less soluble salt in 34% yield (>98% de). The resulting salt, **14**, was treated with 10% aqueous NaOH to obtain the requisite (S)-amine **11** (>98% ee). The optical purity of **11** was determined by HPLC analysis using Sumichiral OA-4400 after derivation to the 3,5-dinitrobenzamide. Although we found an alternative approach to **11** via the optical resolution of **13**, we turned our attention to employing the microbial reduction of **8b** to establish a more efficient process.

Synthesis of (S)-8-Amino-6-benzyl-6-azaspiro[3.4]octane (11) via Stereoselective Microbial Reduction In our previous paper, we reported that *Phaeocrepsis* sp. could perform the stereoselective transformation of 5-benzyl-4,7-dioxo-5-azaspiro[2.4]heptane (**8a**).[3] Four substrates with a spiro ring in their structure were examined for the transformation of **8a**—**d** to **9a**—**d** by *Phaeocrepsis* sp. As shown in Fig. 1, compound **8b** was the most reactive among the four substrates examined. The amine **11** was obtained from **9b** in 63% yield and 96% enantiomeric excess via a Mitsunobu reaction[4] using diphenylphosphoryl azide (DPPA), followed by reduction with lithium aluminum hydride. *Phaeocreopsis* sp. JCM 1880 was found to significantly induce stereoselective transformation.

Conclusion

We have demonstrated the efficient syntheses of compound **11**, which can easily be converted to compound **2** in two steps (debenzylation followed by *tert*-butoxycarbonylation), employing optical resolution or asymmetric microbial reduction. We established practical methods of synthesis of the key intermediate for an important quinolone antibacterial agent. The present methods are more suitable than the previously reported method[1] for large-scale production of DV-7751 (**1**).

Experimental

All melting points were measured using a Yanagimoto micromelting point apparatus and are uncorrected. ^{1}H-NMR spectra were measured on a JEOL JNM-EX 270 spectrometer. All signals are expressed in ppm (δ) with tetramethylsilane as an internal standard. Mass spectra (MS) were obtained with JEOL HX110 and JEOL AX505W mass spectrometers. Optical rotations were measured on a JASCO DIP-370 digital polarimeter. Column chromatography was performed on silica gel (Kiesel gel 60, 70—230 mesh, Merck). Unless otherwise noted, all reactions were carried out in anhydrous solvents. The starting material, 1,1-cyclobutane dicarboxylic acid diethy ester, was purchased from Tokyo Kasei Co., Ltd. (Japan).

1,1-Cyclobutanedicarboxylic Acid Monoethyl Ester (4) To a solution of 1,1-cyclobutane dicarboxylic acid diethy ester (**3**, 85 ml, 0.45 mol) in methanol (110 ml) was added 10% aqueous potassium hydroxide (290 ml) at 0 °C over a period of 1 h. The mixture was stirred at room temperature for 14 h. After evaporation of methanol, the residue was washed with CH_2Cl_2 and the aqueous layer was acidified (pH 2) with 10% hydrochloric acid, then extracted with ethyl acetate. The extract was washed with brine, dried over sodium sulfate and concentrated to obtain **4** (77.1 g, 99.5%) as a colorless oil. ^{1}H-NMR ($CDCl_3$) δ: 1.30 (3H, t, J=7.2 Hz, CH_3CH_2O), 1.9—2.2 (2H, m, cyclobutane), 2.5—2.8 (4H, m, cyclobutane), 4.25 (2H, q, J=7.2 Hz, CH_3CH_2O). MS m/z: 172 (M$^+$).

1-Benzylaminocarbonyl-1-ethoxycarbonyl Cyclobutane (5) Ethyl chloroformate (50 ml, 0.50 mol) was added dropwise at 0 °C to a mixture of **4** (77.1 g, 0.45 mol) and triethylamine (78.1 ml, 0.56 mol) in chloroform (420 ml). The mixture was stirred at room temperature for 1 h. After the addition of a solution of benzylamine (49.2 ml, 0.45 mol) in chloroform (140 ml) at 0 °C, the reaction mixture was stirred for 35 min at room temperature. The mixture was washed with 10% aqueous citric acid and brine. The organic layer was dried over sodium sulfate and concentrated to give **5** (113.3 g, 96.3%) as a colorless oil. ^{1}H-NMR ($CDCl_3$) δ: 1.24 (3H, t, J= 7.2 Hz, CH_3CH_2O), 1.7—2.2 (2H, m, cyclobutane), 2.4—2.7 (4H, m, cyclobutane), 4.20 (2H, q, J=7.2 Hz, CH_3CH_2O), 4.44, 4.50 (2H, each s, ArH$_2$CN), 7.30 (5H, br s, aromatic H). MS m/z: 261 (M$^+$).

1-Acetyl-1-benzylaminocarbonyl Cyclobutane (6) A one molar solution of trimethylsilyl methyl lithium in pentane (76.5 ml, 76.5 mmol) was added dropwise to a solution of **5** (5.01 g, 19.2 mmol) in pentane–tetrahydrofuran (THF) (17 : 3, 100 ml) at 0 °C. The reaction mixture was stirred for an additional 45 min at 0 °C. Methanol was added to the solution, then the mixture was stirred at room temperature for 1 h. After water was poured into the mixture, it was extracted with ethyl acetate. The organic layer was washed with brine, dried over sodium sulfate and concentrated to yield a white solid. The solid was washed with pentane to obtain **6** (3.50 g, 78.9%). mp 74—77 °C. ^{1}H-NMR ($CDCl_3$) δ: 1.7—2.2 (2H, m, cyclobutane), 2.1 (3H, s, CH_3CO), 2.4—2.7 (4H, m, cyclobutane), 4.44, 4.50 (2H, each s, ArH$_2$CN), 7.30 (5H, br s, aromatic H). MS m/z: 231 (M$^+$). *Anal.* Calcd for $C_{14}H_{17}NO_2$: C, 72.70; H, 7.41; N, 6.06. Found: C, 72.54; H, 7.51; N, 6.34.

1-Benzylaminocarbonyl-1-bromomethylcarbonyl Cyclobutane (7) Bromine (9.1 g, 57.1 mmol) was added to 1,4-dioxane (24 ml) and the mixture was stirred for 20 min at room temperature. A solution of **6** (12.0 g, 51.9 mmol) in CH_2Cl_2 (120 ml) was added to the mixture, which was stirred for 4 h at room temperature. The reaction mixture was then diluted with CH_2Cl_2, and washed with 5% aqueous sodium thiosulfate, brine and water. The organic layer was dried over sodium sulfate and concentrated to afford **7** (13.2 g, 82.0%) as a yellow oil which was subjected to the next batch without further purification. ^{1}H-NMR ($CDCl_3$) δ: 1.7—2.1 (2H, m, cyclobutane), 2.4—2.8 (4H, m, cyclobutane), 4.12 (2H, s, BrCH$_2$CO), 4.41, 4.50 (2H, each s, ArH$_2$CN), 7.32 (5H, br s, aromatic H). MS m/z: 310 (M$^+$).

6-Benzyl-5,8-dioxo-6-azaspiro[3.4]octane (8b) Sodium hydride in mineral oil (60%, 2.3 g, 57.5 mmol) was added portionwise to a solution of **7** (12.2 g, 39.3 mmol) in dry N,N-dimethylformamide (DMF) (500 ml) at 0 °C. After the mixture was stirred for 75 min at the same temperature, the reaction mixture was poured into ice-water, and extracted with ether. The ether extract was washed with 10% aqueous citric acid and water, then dried over sodium sulfate. After the organic layer was evaporated *in vacuo*, the residue was chromatographed on silica gel using toluene : AcOEt (4 : 1), affording **8b** (6.53 g, 72.4%) as a pale yellow oil. ^{1}H-NMR ($CDCl_3$) δ: 2.0—2.7 (6H, m, cyclobutane), 3.64 (2H, s, NCH$_2$CO), 4.63 (2H, s, ArH$_2$CN), 7.15—7.49 (5H, m, aromatic H). MS m/z: 229 (M$^+$).

7-Benzyl-6,9-dioxo-7-azaspiro[4.4]nonane (8c) The synthesis of **8c** was performed under the same conditions as for **8b**. Compound **8c** (66% from the corresponding cyclopentyl β-keto carboxamide derivative) was obtained as a pale yellow oil. ^{1}H-NMR ($CDCl_3$) δ: 1.6—2.2 (8H, m, cyclopen-

tane), 3.69 (2H, s, NCH$_2$CO), 4.87 (2H, s, ArH$_2$CN), 7.16—7.52 (5H, m, aromatic H). MS m/z: 244 (M$^+$+1).

8-Benzyl-7,10-dioxo-8-azaspiro[5.4]decane (8d) The synthesis of **8d** was performed under the same conditions as for **8b**. Compound **8d** (62% from the corresponding cyclohexyl β-keto carboxamide derivative) was obtained as a pale yellow oil. ^{1}H-NMR (CDCl$_3$) δ: 1.5—2.0 (10H, m, cyclohexane), 3.63 (2H, s, NCH$_2$CO), 4.85 (2H, s, ArH$_2$CN), 7.19—7.46 (5H, m, aromatic H). MS m/z: 258 (M$^+$+1).

(R)-8-Hydroxy-6-benzyl-5-oxo-6-azaspiro[3.4]octane (9b) *Phaeocreopsis* sp. JCM 1880 was grown in a complex medium consisting of 2% (w/v) glucose and 1% (w/v) polypeptone. The medium was adjusted to pH 6.0 with 0.1% K$_2$HPO$_4$ buffer and 0.1% KH$_2$PO$_4$ buffer, placed in a Sakaguchi flask, sterilized (121 °C, 15 min), and inoculated with the preincubated culture. The cultivation was performed for 48 h at 30 °C with shaking. Then, **8b** (800 mg, 3.49 mmol) was added to eight flasks (100 mg×8) and the reaction mixtures were shaken for 14 h at 30 °C. After filtration through Celite, the filtrate was extracted with AcOEt. The organic layer was dried over sodium sulfate and evaporated *in vacuo*. The residue was purified by silica gel column chromatography with toluene: AcOEt=2:1 to afford **9b** (658 mg, 82.3%) as a pale yellow solid, which was 96% ee by HPLC analysis using chiralcel OJ; mobile phase, hexane: isopropanol=10:1; flow rate, 1.0 ml/min; detector, UV (230 nm). Retention time for racemate: 15.1 min [50%, (R)-form], 17.0 min [50%, (S)-form]. Retention time for **8b**: 15.0 min (98%), 16.9 min (2%), 96% ee. mp 107—108 °C. [α]$_D^{25}$ +65.3° (c=0.540, MeOH). ^{1}H-NMR (CDCl$_3$) δ: 1.90—2.41 (6H, m, cyclobutane), 3.02—3.43 (2H, m, NCH$_2$CO), 4.22—4.27 (1H, m, 8-H), 4.46 (2H, s, ArH$_2$CN), 7.18—7.38 (5H, m, aromatic H). MS m/z: 231 (M$^+$+1); *Anal.* Calcd for C$_{14}$H$_{17}$NO$_2$: C, 72.73; H, 7.36; N, 6.06. Found: C, 72.87; H, 7.42; N, 6.02.

Comparison of the Rate of Microbial Reduction Compounds **8a**—**d** (5 mg) were added to the culture (5 ml) of JCM 1880. The resulting suspension was stirred for 8 h at 30 °C. Conversion was observed by HPLC analysis [Inertsil ODS-2 column (GL Science), 4.6×150 mm; eluent, 35% acetonitrile containing 50 mM phosphate buffer (pH 6.0); flow rate, 1.0 ml/min; UV detection, 230 nm].

6-Benzyl-8-hydroxyimino-5-oxo-6-azaspiro[3.4]octane (12) A mixture of **8b** (11.1 g, 48.4 mmol), hydroxylamine hydrochloride (10.1 g, 145.2 mmol) and triethylamine (20.2 ml, 145.2 mmol) in ethanol (440 ml) was stirred for 2 h at room temperature. After the mixture was evaporated *in vacuo*, the residue was dissolved in AcOEt. The organic layer was washed with 10% aqueous citric acid and brine and dried over sodium sulfate. The solvent was removed *in vacuo*, and the residue was chromatographed on silica. Elution with toluene: AcOEt (1:1) yielded **12** (10.3 g, 87.3%) as a white solid, mp 173—178 °C. ^{1}H-NMR (CDCl$_3$) δ: 1.7—2.8 (6H, m, cyclobutane), 3.94 (2H, s, NCH$_2$CN), 4.53 (2H, s, ArH$_2$CN), 7.32 (5H, br s, aromatic H). MS m/z: 244 (M$^+$); *Anal.* Calcd for C$_{14}$H$_{16}$N$_2$O$_2$·1/4H$_2$O: C, 67.58; H, 6.68; N, 11.25. Found: C, 67.38; H, 6.77; N, 11.54.

8-Amino-6-benzyl-6-azaspiro[3.4]octane (13) A one molar solution of lithium aluminum hydride in THF (2 ml, 2 mmol) was added to the solution of **12** (3.0 g, 12.3 mmol) in THF (30 ml) with ice-water cooling. The whole mixture was refluxed for 1 h, then water and 10% aqueous NaOH were carefully added under ice-water cooling. The precipitate was filtered off and the filtrate was concentrated *in vacuo* to afford **13** (2.6 g, 98.2%) as a pale yellow oil.

(S)-8-Amino-6-benzyl-6-azaspiro[3.4]octane·1.5 D-Tartaric Acid (14) The solution of D-tartaric acid (108 mg, 0.72 mmol) in ethanol (1 ml) was added dropwise to a solution of **13** (280 mg, 1.30 mmol) in ethanol (4 ml) at 0 °C. After stirring of the mixture at the same temperature for 30 min, the mixture was refluxed for 30 min and stirred for 30 min at room temperature.

The precipitate was collected and washed with ethanol. The resulting white crystals were filtered to obtain **14** (196 mg, 34.0%), mp 215—221 °C (dec.). [α]$_D^{25}$ −56.3° (c=1.00, water). ^{1}H-NMR (D$_2$O) δ: 1.87—2.32 (6H, m, cyclobutane), 3.56 (1H, dd, J=4.8, 13 Hz, 8-H), 3.69—3.78 (2H, m, CCH$_2$N), 4.0—4.11 (2H, m, NCH$_2$CN), 4.51 (3H, s, CHCO$_2$H), 4.46, 4.55 (each 1H, d, J=13 Hz, ArH$_2$CN), 7.56 (5H, br s, aromatic H). *Anal.* Calcd for C$_{20}$H$_{29}$N$_2$O$_9$: C, 54.41; H, 6.62; N, 6.34. Found: C, 54.23; H, 6.59; N, 6.27.

(S)-8-Amino-6-benzyl-6-azaspiro[3.4]octane (11) i) An ice-cooled solution of **9b** (230 mg, 1.0 mmol), triphenylphosphine (341 mg, 1.3 mmol) and diethylazodicarboxylate (226 mg, 1.3 mmol) in THF (5 ml) was stirred for 30 min, then a solution of DPPA (358 mg, 1.3 mmol) was added over a period of 15 min. Stirring was then continued at room temperature for 24 h. After evaporation of the solvent, Et$_2$O was added to the residue. After removing the precipitate by filtration, the filtrate was concentrated *in vacuo* to obtain crude **10**. The residue was dissolved in THF (5 ml). The mixture was added to an ice-cooled solution of 1 M lithium aluminum hydride in THF (2 ml, 2 mmol), and the entire mixture was refluxed for 1 h. Water and 10% aqueous NaOH were then carefully added under ice cooling. The grainy precipitate was filtered off and the filtrate was concentrated *in vacuo*. The residue was purified by column chromatography with CHCl$_3$: MeOH=10 : 1 to afford **11** (135 mg, 62.5%) as a pale yellow oil. In order to determine the optical purity of **11**, 3,5-dinitrobenzamide was prepared as follows: Triethylamine (9 μl) was added to a solution of **11** (2.0 mg) and 3,5-dinitrobenzoyl chloride (9.2 mg) in THF (3 ml) at room temperature. The reaction mixture was stirred for 1 h, then saturated aqueous NaHCO$_3$ was added, and the resulting mixture was stirred vigorously for 30 min. The mixture was diluted with CHCl$_3$ (3 ml), then dried over sodium sulfate, and filtered through a pad of silica gel to obtain a chloroform solution of the 3,5-dinitrobenzamide usable for chiral HPLC analysis. The conditions for HPLC analysis were as follows: column, Sumichiral OA-4400; mobile phase, hexane: 1,2-dichloroethane: ethanol: trifluoroacetic acid=80:20:5:0.2; flow rate, 1.0 ml/min; detection, UV (254 nm). Retention time for racemate: 19.3 min [50%, (S)-form], 22.1 min [50%, (R)-form]. Retention time for **11**: 19.1 min (98%), 21.8 min (2%), 96% ee. [α]$_D^{25}$ −56.8° (c=1.00, MeOH). ^{1}H-NMR (CDCl$_3$) δ: 1.70—2.40 (9H, m, cyclobutane, −NH$_2$, 8-H), 2.70 (2H, s, CCH$_2$N), 2.84—3.20 (2H, m, NCH$_2$CN), 3.62 (2H, s, ArH$_2$CN), 7.33 (5H, br s, aromatic H). MS m/z: 214 (M$^+$+1).

ii) 10% aqueous sodium hydroxide (20 ml) was added to **14** (1.05 g, 2.40 mmol). The solution was extracted with CHCl$_3$: MeOH (9 : 1). The organic layer was washed with brine, dried and evaporated *in vacuo* to obtain **11** (491 mg, 95.9%) as a pale yellow oil. In order to determine the optical purity of **11**, the 3,5-dinitrobenzamide was prepared in the same fashion. Retention time for racemate: 19.3 min [(S)-form], 22.1 min [(R)-form]. Retention time for **11**: 19.1 min (99%), 21.8 min (1%), 98% ee.

References
1) Lesher G. Y., Froelich E. J., Gruft M. P., Balicy J. M., Brundage R. P., *J. Med. Chem.*, **5**, 1063 (1962).
2) Kawakami K., Atarashi S., Kimura Y., Takemura M., Hayakawa I., *Chem. Pharm. Bull.*, **46**, 1710 (1998).
3) Satoh K., Imura A., Miyadera A., Kanai K., Yukimoto Y., *Chem. Pharm. Bull.*, **46**, 587 (1998).
4) Lal B., Pramanic B. N., Manhas M. S., Bose A. K., *Tetrahedron Lett.*, **1977**, 1977.

Differentiation Inducing Activities of Isocoumarins from Hydrangea Dulcis Folium

Kaoru Umehara,* Misae Matsumoto, Mitsuhiro Nakamura, Toshio Miyase, Masanori Kuroyanagi, and Hiroshi Noguchi

School of Pharmaceutical Sciences, University of Shizuoka, 52-1 Yada, Shizuoka 422-8526, Japan.
Received September 13, 1999; accepted December 20, 1999

In the course of searching for differentiation inducers against leukemic cells from plants, we have recognized the differentiation inducing activities of the methanolic extract of Hydrangea Dulcis Folium. Activity guided separation of the extract was carried out using M1 cells, and seven isocoumarins were isolated as active substances. These isocoumarins showed the activities at the concentration of 100 μM and non-cytotoxic effects even at 300 μM.

Key words   differentiation; Hydrangea Dulcis Folium; M1 cell; phagocytosis

Differentiation inducers are of potential interest for the treatment of human cancers promoting the terminal differentiation of certain human tumor cells. We have reported the differentiation inducing activities of triterpenes, flavones, lignans, and steroids.[1] These compounds differentiated mouse myeloid leukemia (M1) cells into phagocytic cells, and some of them also induced the differentiation of human acute promyelocytic leukemia (HL-60) cells. In the course of searching for differentiation inducers against leukemic cells, the methanolic extract of Hydrangea Dulcis Folium was recognized to have differentiation inducing activities. The active constituents of the extract were identified.

A suspension of the methanolic extract of Hydrangea Dulcis Folium in water was extracted with ethyl acetate. The ethyl acetate layer showing the differentiation inducing activity against M1 cells was subjected to repeated chromatography on silica-gel and high performance liquid chromatography (HPLC) to afford seven active components (1 (3R-phyllodulcin),[2a] 3 (thunberginol C),[2b,c] 4 (thunberginol D),[2b,c] 5 (thunberginol G),[2b,c] 6 (thunberginol A),[2d] 7 (thunberginol B)[2d] and 8 (thunberginol F)[2d]) with non active components (2 (hydrangenol),[2a] 9 (3R-phyllodulcin 3'-glucoside),[2e] 10 (3R-phyllodulcin 8-glucoside)[2a] and 11 ((−)-hydrangenol 4'-glucoside)[2a]) (Chart 1). The absolute configurations at C-3 of phyllodulcin derivatives (1, 9, 10) and hydrangenol glucoside (11) were identified by comparing their circular dichroism (CD) spectra with previously reported values.[2a] The other dihydroisocoumarins (2—5) were known to epimerize at C-3, and they were subjected to bioassay in racemates.[2c]

Differentiation inducing activities of isocoumarins (1—11) were tested using mouse myeloid M1 cell line (Fig. 1). Dihydroisocoumarins (1—5) and isocoumarins (6—8) showed these activities at a concentration of greater than 200 μM against M1 cells. In the case of dihydroisocoumarins, their activities were altered by the number or attached position of hydroxyl groups. Compounds 4 and 5, having an *o*-diphenol group, showed higher activities than 3 and 2, respectively. Compounds 3 and 4, having a 6-hydroxy group in their structures, induced a larger amount of M1 cells into phagocytic cells compared with 2 and 5, respectively. Highly oxygenated isocoumarins seemed to have higher activities.

Dihydroisocoumarin glucosides (9—11) were all inactive in the induction of the differentiation of M1 cells (data not

shown). They showed hardly any antiproliferative activities, and a more than 70% of growth ratio was found in 300 μM of these compound treated groups. Glucosides were good pro-inducers.

Isocoumarins (6—8) were recongnized to have higher activities than dihydroisocoumarins (1—5). Phagocytic activities were observed when M1 cells were treated with 100 μM of isocoumarins (6—8) and the activities were nearly equal to 300 μM treated groups of dihydroisocoumarins (1—5). Compounds 6 and 7 have three hydroxyl groups at the same positions as 5 and 3, respectively. These two isocoumarins induced M1 cells into phagocytic cells at a high ratio. Immunomodulatory activities of thunberginol A (6) and related compounds on lymphocyte proliferation were reported,[3] and isocoumarins (6—8) were shown to have more potent antiallergic activity than dihydoisocoumarins (1, 2).[3] The similarity of the structure requirement for the differentiation activity and the antiallergic activity is interesting.

As 1 showed higher activity than 5 although both have a 8,3',4'-tri O-function, structure–activity relationships of isocoumarins (1, 3, 6) were investigated. Some isocoumarins were methylated, and their differentiation inducing activities against M1 cells were evaluated. Compound 1, which has a 4'-methoxyl group in its structure, exhibited the activity at
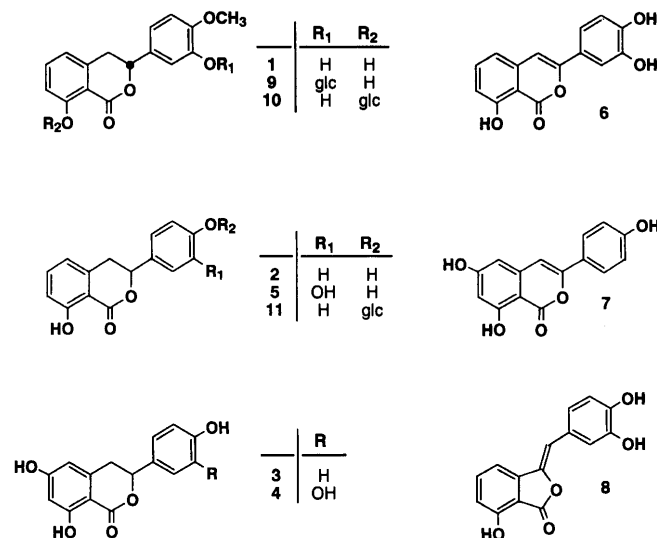

	R_1	R_2
1	H	H
9	glc	H
10	H	glc

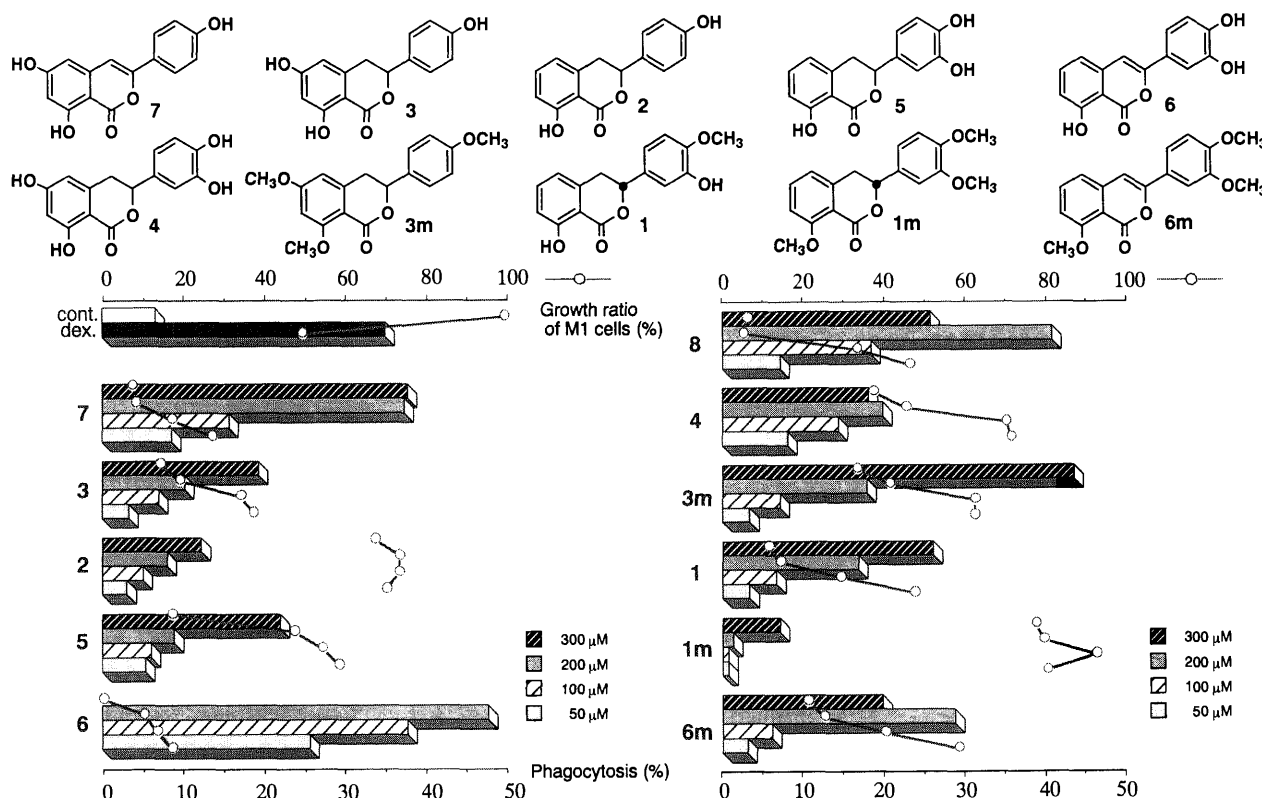|	R_1	R_2
2	H	H
5	OH	H
11	H	glc

	R
3	H
4	OH

Chart 1

Fig. 1.   Cell Growth and Phagocytic Activity f M1 Cells Treated with Isocoumarins

the concentration of 200 μM. But compounds 1m, 3m and 6m, having trimethoxyl groups, were observed to have weak activities compared with their parental compounds. Compound 1m had lost most of the activities, and the importance of the hydroxyl groups was recognized.

Phyllodulcin (1) has differentiation inducing activity against M1 cells and has less cytotoxicity. As it is one of the main components of Hydrangeae Dulcis Folium and present in a high proportion, this crude drug could be valuable as a differentiation inducer source.

Experimental

General Procedure   Mass spectra (MS) were obtained using a JEOL JMS-SX 102 mass spectrometer. ^{1}H- and ^{13}C-NMR spectra were recorded on JEOL JNM-GSX 270, JNM-GSX 500 and JNM-A 400 spectrometers (270.05 and 67.8 MHz, 500.00 and 125.65 MHz, 400.00 and 100.4 MHz, respectively), and chemical shifts were given in δ (ppm) with tetramethylsilane (TMS) as an internal standard. HPLC was carried out on a JASCO model 800 series instrument using D-ODS-7 YMC columns.

Isolation   Commercially available Hydrangea Dulcis Folium (1 kg from Niiya in Shimizu, Shizuoka prefecture) was extracted with hot MeOH under reflux. The extract was concentrated under reduced pressure and then partitioned between ethyl acetate and water. The ethyl acetate layer was passed through a Mitsubishi Diaion CHP-20 column, and absorbed material was eluted with MeOH and ethyl acetate successively. From the MeOH eluate, 1 (3R-phyllodulcin, 21.5 g), 2 (hydrangenol, 8.4 g), 3 (thunberginol C, 70 mg), 4 (thunberginol D, 800 mg), 5 (thunberginol G, 30 mg), 6 (thunberginol A, 1.9 g), 7 (thunberginol B, 10 mg), 8 (thunberginol F, 50 mg), 9 (3R-phyllodulcin 3′-glucoside, 10 mg), 10 (3R-phyllodulcin 8-glucoside, 30 mg) and 11 ((−)-hydrangenol 4′-glucoside, 50 mg) were isolated by subsequent chromatography on silica gel and HPLC.

Methylation of 1   Compound 1 (10 mg) was methylated with diazomethane in the usual manner to give 1m (10 mg). Methylation of 3 and 6 were performed in the same manner. Compounds 1m and 6m were identified by comparison of spectral data with reported values.[2d,e] 3m: Amorphous powder. FAB-MS m/z: 315 [MH]$^+$. ^{1}H-NMR (500 MHz, CDCl$_3$) δ: 7.38 (1H, d, J=8 Hz), 6.92 (1H, d, J=8 Hz), 6.44 (1H, d, J=2 Hz), 6.34 (1H, d, J=2 Hz), 5.35 (1H, dd, J=12, 3 Hz), 3.25 (1H, dd, J=16, 12 Hz), 2.97 (1H,

dd, J=16, 3 Hz), 3.94, 3.87, 3.82 (3H each, s).

Cell Culture   M1 cells were grown in Eagle's mimimum essential medium (MEM) medium containing 100 U/ml penicillin, 100 μg/ml streptomycin, 50 μg/ml kanamycin and 2 mmol/l L-glutamine in 10% heat-inactivated calf serum (CS) over the range of 1×10^5 /ml to 2×10^6 /ml in a 5% CO$_2$ humidified atmosphere at 37 °C.

Materials   Eagle's MEM, Eagle's amino acids and vitamins medium were purchased from Nissui Pharmaceutical Co., Ltd. CS was from Gibco. Antibiotics were from Meiji Seika Kaisha, Ltd. L-Glutamine was from Wako Pure Chemical Industries, Ltd. Dexamethasone was from Nakalai Chemicals, Ltd. and polystyrene latex particles were from The Dow Chemical Company.

Measurement of Phagocytosis   Phagocytic activity was assayed as reported previously.[1]

References

1) a) Umehara K., Takagi R., Kuroyanagi M., Ueno A., Taki T., Chen Y. J., *Chem. Pharm. Bull.*, **40**, 401—405 (1992); b) Sugiyama S., Umehara K., Kuroyanagi M., Ueno A., *ibid.*, **41**, 714—719 (1993); c) Umehara K., Sugawa A., Kuroyanagi M., Ueno A., Taki T., *ibid.*, **41**, 1774—1779 (1993); d) Umehara K., Endoh M., Miyase T., Kuroyanagi M., Ueno A., *ibid.*, **42**, 611—616 (1994); e) Umehara K., Sumii (Shirasu) N., Satoh H., Miyase T., Kuroyanagi M., Ueno A., *ibid.*, **43**, 1565—1568 (1995); f) Umehara K., Nakamura M., Miyase T., Kuroyanagi M., Ueno A., *ibid.*, **44**, 2300—2304 (1996).

2) a) Yoshikawa M., Murakami T., Ueda T., Shimoda H., Yamahara J., Matsuda H., *Heterocycles*, **50**, 411—418 (1994); b) Yoshikawa M., Matsuda H., Shimoda H., Shimada H., Harada E., Naitoh Y., Miki A., Yamahara J., Murakami N., *ibid.*, **44**, 1440—1447 (1996); c) Yoshikawa M., Chatani N., Harada E., Nishido Y., Yamahara J., Murakami N., *Yakugaku Zasshi*, **114**, 176—181 (1994); d) Yoshikawa M., Harada E., Naitoh Y., Inoue K., Matsuda H., Shimoda H., Yamahara J., Murakami N., *Chem. Pharm. Bull.*, **42**, 2225—2230 (1994); e) Hashimoto T., Tori M., Asakawa Y., *Phytochemistry*, **26**, 3323—3330 (1987).

3) Shimoda H., Matsuda H., Yamahara J., Yoshikawa M., *Biol. Pharm. Bull.*, **21**, 809—813 (1998).

Studies on the Constituents of Solanaceous Plants. (46). Steroidal Glycosides from the Fruits of *Solanum anguivi*

Xing-Hua Zhu, Tsuyoshi Ikeda, and Toshihiro Nohara*

Faculty of Pharmaceutical Sciences, Kumamoto University, 5–1, Oe-honmachi, Kumamoto 862–0973, Japan.
Received October 4, 1999; accepted December 9, 1999

Three new glycosides named anguiviosides A—C were isolated from the fruits of *Solanum anguivi* and characterized as follows: 3-*O*-β-chacotrioside (1), 3-*O*-[4-*O*-maloyl-α-L-rhamnopyranosyl(1→2)]-α-L-rhamnopyranosyl(1→4)-β-D-glucopyranoside (2) and 3-*O*-α-L-rhamnopyranosyl(1→2)-[β-D-xylopyranosyl(1→3)]-β-D-glucopyranoide (3), of (25*R*,26*R*)-spirost-5-en-3β,26-diol.

Our extensive search for the bioactive oligoglycosides in solanaceous plants has so far resulted in the isolation of cytotoxitic compounds against several tumour cell lines,[1] antifeeding substances against *Thrips palmi*,[2] and a key intermediate in the biosynthesis of steroidal alkaloids.[3]

Successively, we have planned to search for anti-herpes active compounds among *Solanum* plants, to collect new steroidal specimens, and have investigated the steroidal constituents in the fruits of *Solanum anguivi* to obtain three new steroidal glycosides. This paper deals with their structural elucidation.

The methanolic extract obtained from the fruits of the title plant was subjected to Diaion HP-20, silica gel and Chromatorex ODS to afford three compounds named anguiviosides A—C (1—3, respectively).

Anguivioside A (1), a white powder, showed a quasimolecular ion peak [M+K+H]$^+$ at *m/z* 924 in the positive FAB-MS. The molecular formula was estimated as $C_{45}H_{72}O_{17}$. The ^{1}H-NMR spectrum displayed signals due to two tertiary methyl groups at δ 0.99 and 1.00, four secondary methyl groups at δ 1.15, 1.26, 1.60 and 1.74, and three anomeric protons at δ 4.93, 5.80 and 6.34. The above spectrum suggested 1 to be a steroidal glycoside, therefore, 1 was acid-hydrolyzed to give only D-glucose and L-rhamnose.[4] The ^{13}C-NMR spectrum exhibited 45 carbon signals in total, 18 signals of which were assigned to a β-chacotriosyl moiety. By comparison with the ^{13}C-NMR spectrum of a diosgenin glucoside, glycoside C-2,[5] the remaining 27 carbon signals were assigned to a spirostanol derivative, in which an oxygen-bearing methylene carbon signal ascribable to C-26 disappeared and a new acetal carbon signal appeared at δ 96.1, suggesting the substitution of a hydroxyl group at C-26. Deshielding shifts at C-22 (by +4.1 ppm) and 25 signals (by +5.5 ppm) also indicated the presence of a hydroxyl group at C-26. Other ^{1}H and ^{13}C signals could be assigned as shown in the Experimental and Table 1 based on the ^{1}H-^{1}H chemical shift correlation spectrum (COSY), ^{1}H-^{13}C heteronucler multiple quantum coherence (HMQC) and heteronucler multiple bonds correlation (HMBC) spectra. The proton coupling constant of the H-26 doublet signal at δ 5.18 (*J*=7.3 Hz) indicated diaxial conformation at H-25 and H-26, suggestive of 25*R*,26*R* configurations. Consequently, the structure of 1 was elucidated to be 3-*O*-α-L-rhamnopyranosyl-(1→2)-[α-L-rhamnopyranosyl(1→4)]-β-D-glucopyranosyl

(β-chacotriosyl) (25*R*,26*R*)-spirost-5-en-3β,26-diol.

The glycosides possessing an analogous spirostanol, (25*R*,26*R*)-26-methoxyspirost-5-en-3β-ol,[6] were obtained from the bulbs of *Lilium candidum*, however, the occurrence of the 26-methoxy derivative was regarded as an artifact during the extraction procedure. The genuine sapogenol of 1 could not be obtained owing to rapid decomposition during acid hydrolysis, however, it is worthy of note in terms of hydroxyl groups at C-26 because the presence of the hydroxyl group at C-26 might cause a conversion into a 26-aldehyde form by opening of the F-ring. Therefore, the attachment of the hydroxyl group at C-26 makes this sapogenol unstable and characteristic.

Anguivioside B (2), a white powder, showed a quasimolecular ion peak [M+K+Na+H]$^+$ at *m/z* 1033 in the positive FAB-MS indicating a molecular formula of $C_{48}H_{74}O_{20}$. The ^{1}H-NMR signals exhibited signals due to four methyl groups at δ 1.00 (3H, s, 19-Me), 1.01 (3H, s, 18-Me), 1.16 (3H, d, *J*=6.1 Hz, 27-Me) and 1.27 (3H, d, *J*=6.7 Hz, 21-Me) on the steroidal skeleton, two methyl groups of the 6-deoxyhexosyl moiety at δ 1.57 (3H, d, *J*=6.1 Hz, rha 6-Me) and 1.75 (3H, d, *J*=6.1 Hz, rha' 6-Me), and three anomeric proton signals at δ 4.95 (1H, d, *J*=6.7 Hz), 5.90 (1H, s, rha 1-H), and 6.38 (1H, s, rha' 1-H). The ^{13}C-NMR spectrum displayed a total of 48 carbon signals, 27 signals of which were assigned to the same sapogenol as that of 1, (25*R*,26*R*)-spirost-5-en-3β,26-diol, a malonyl residue at δ 167.8, 43.1 and 170.0 and a chacotriosyl moiety esterified at one of the terminal rhamnosyl residues. The ^{1}H- and ^{13}C-NMR signals could be assigned as shown in the Experimental section based on the ^{1}H-^{1}H, HMQC and HMBC spectra. As to the malonyl ester location, a deshielding signal at δ 5.96 (1H, t-like, *J*=9.8 Hz) was ascribable to H-4 of the rhamnopyranosyl moiety linked to the C-2 hydroxy group of the inner glucopyranosyl moiety by the ^{1}H-^{1}H two dimensional (2D) COSY and HMBC. Therefore, the structure of 2 was elucidated to be 3-*O*-[(4-*O*-malonyl)-α-L-rhamnopyranosyl(1→2)]-[α-L-rhamnopyranosyl (1→4)]-β-D-glucopyranosyl (25*R*,26*R*)-spirost-5-en-3β,26-diol.

Anguivioside C (3), a white powder, showed a quasimolecular ion peak [M+K+H]$^+$ at *m/z* 910 in the positive FAB-MS suggesting its molecular formula to be $C_{44}H_{70}O_{17}$. Acid hydrolysis of 3 gave D-glucose, D-xylose and L-rhamnose. The ^{13}C-NMR signals which originated from the aglycone

---

Table 1. ^{13}C-NMR Spectral Data for Anguiviosides A—C (1—3) and Glycoside C-a

	1	Glycoside C-a	2	3
C-1	37.5	37.7	37.5	37.5
2	30.1	30.5	30.1	30.1
3	78.1	78.4	78.0	77.9
4	38.9	39.6	39.0	38.7
5	140.8	141.3	140.8	140.8
6	121.8	121.7	121.8	121.9
7	32.3	32.5	32.3	32.3
8	31.5	31.9	31.5	31.4
9	50.3	50.6	50.3	50.3
10	37.1	37.3	37.1	37.1
11	21.1	21.3	21.1	21.1
12	40.2	40.1	40.2	40.2
13	41.0	40.7	41.0	41.0
14	56.7	56.9	56.7	56.6
15	32.3	32.4	32.3	32.1
16	81.2	81.2	81.7	81.7
17	62.5	63.2	62.6	62.6
18	19.3	16.5	19.4	19.4
19	16.3	19.5	16.6	16.6
20	41.5	42.2	41.0	41.6
21	14.8	15.1	14.8	14.8
22	113.5	109.4	113.5	113.5
23	32.3	32.1	31.5	32.3
24	30.1	29.5	30.1	30.1
25	36.2	30.7	36.2	36.2
26	96.1	67.1	96.1	96.1
27	17.5	17.4	17.4	17.4
glc				
1	100.2	103.4	100.3	99.9
2	77.8	72.9	78.1	77.4
3	78.6	75.5	77.8	88.2
4	77.8	70.4	77.9	69.5
5	76.8	76.9	77.0	77.7
6	61.3	62.7	61.2	62.3
rha				
1	102.8		102.4	102.4
2	72.4		72.4	72.4
3	72.6		70.2	72.8
4	73.8		76.8	74.0
5	69.5		67.6	69.6
6	18.4		17.9	18.7
rha'				
1	102.0		102.0	
2	72.4		72.5	
3	72.8		72.8	
4	74.0		74.1	
5	70.4		69.5	
6	18.6		18.6	
xyl				
1				105.4
2				74.6
3				78.3
4				70.6
5				67.2
mal				
1				167.8
2				43.1
3				170.0

Anguivioside A (1): R= β-Chacotriosyl

Anguivioside B (2): R=

Anguivioside C (3): R=

were superimposed on those of **2**. On the other hand, signals due to the sugar moiety suggested the presence of a terminal α-L-rhamnopyranosyl moiety, a terminal β-D-xylopyranosyl moiety and a hexopyranosyl moiety, the latter of which correlated to H-1—H-5 and H_2-6 of β-D-glucopyranosyl moiety as shown in the Experimental and Table 1 by ^{1}H–^{1}H COSY
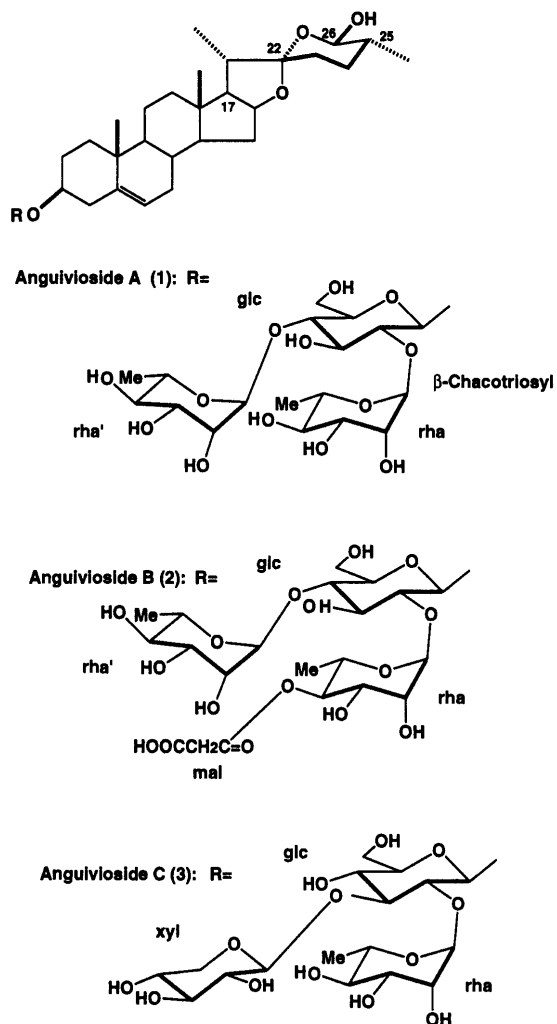
and HMQC. Moreover, the HMBC spectrum revealed connectivities between a xylosyl anomeric proton (overlapped) at around δ 4.97 and the C-3 of a glucosyl moiety at δ 88.2, between a rhamnosyl anomeric proton at δ 6.28 (1H, br s) and the C-2 of a glucosyl moiety at δ 77.4, and a glucosyl anomeric proton at δ 4.97 (overlapped) and the C-3 of a sapogenol moiety at δ 77.9. Carbon signals due to this oligosidic moiety were superimposable on those of a glycoside tentatively named SNF-3 previously obtained from *Solanum nodiflorum*.[7] Therefore, the structure of **3** was represented as 3-O-α-L-rhamnopyranosyl($1\rightarrow$2)-[β-D-xylopyranosyl ($1\rightarrow$3)]-β-D-glucopyranoyl (25R,26R)-spirost-5-en-3β,26-diol.

Experimental

Optical rotations were determined on a JASCO DIP-1000 KUY polarimeter (l=0.5). FAB-MS were obtained with a glycerol matrix in the positive ion mode using a JEOL JMS-DX300 and a JMS-DX 303HF spectrometer. NMR spectra were measured in pyridine-d_5 on a JEOL α-500 spectrometer and chemical shifts were referenced to tetramethylsilane (TMS). GLC was performed on an HP5890A gas chromatograph with a flame ionization detector (FID). Column chromatography was carried out with Silica gel 60 (230—400 mesh, Merck), Sephadex LH-20 (25—100 μm, Pharmacia), MCI gel CHP-20P (75—150 μm, Mitsubishi Chem. Ind.) and Chromatorex ODS (30—50 μm, Fuji Silysia Chem., Ltd.), and TLC was performed on a precoated Silica gel 60F$_{254}$ (Merck) and RP-18 F$_{254S}$ (Merck).

Plant Material The seeds of the title plant were provided from Dr. Masaharu Matsui (National Research Institute of Vegetables, Ornamental Plants and Tea, Ministry of Agriculture, Forestry and Fisheries, Ano, Mie, Japan) and cultivated at the botanical garden of Kumamoto University.

Isolation The fruits (434 g) were extracted with hot MeOH and the re-

sulting extract (22.26 g) was treated with hexane. The hexane insoluble portion (17.3 g) was successively chromatographed on Diaion HP-20 (water and MeOH gradiently increasing MeOH), Sephadex LH-20 (MeOH), silica gel (CHCl$_3$: MeOH : water=7 : 3 : 0.5), Chromatorex ODS (70% and 80% MeOH) and silica gel (CHCl$_3$: MeOH : water=8 : 2 : 0.2 and 7 : 3 : 0.5) to give anguivioside A (**1**, 86 mg), anguivioside B (**2**, 37 mg) and anguivioside C (**3**, 100 mg).

Anguivioside A (**1**) : A white powder, $[\alpha]_D^{26}$ −86.2° (c=0.5, MeOH). Positive FAB-MS m/z : 924 [M+K+H]$^+$. ^{1}H-NMR (pyridine-d_5) δ : 0.99 (3H, s, Me-19), 1.00 (3H, s, Me-18), 1.15 (3H, d, J=5.5 Hz, Me-27), 1.26 (3H, d, J=6.7 Hz, Me-21), 1.60 (3H, d, J=5.5 Hz, rha Me-6), 1.74 (3H, d, J=4.9 Hz, rha' Me-6), 3.63 (1H, m, glc H-5), 3.86 (1H, m, H-3), 4.07 (1H, br d, J=11.6 Hz, glc H-6), 4.18 (overlapped, glc H-2, glc H-3, glc H'-6), 4.34 (overlapped, glc H-4, rha H-4, rha' H-4), 4.51 (1H, br d, J=9.1 Hz, H-16), 4.59 (1H, m, rha H-3), 4.66 (1H, br s, rha H-2), 4.70 (1H, dd, J=3.1, 7.8 Hz, rha' H-3), 4.80 (1H, br s, rha' H-2), 4.93 (overlapped, glc H-1, rha H-5, rha' H-5), 5.20 (1H, d, J=7.3 Hz, H-26), 5.30 (1H, m, H-6), 5.80 (1H, s, rha H-1), 6.34 (1H, s, rha' H-1). ^{13}C-NMR (pyridine-d_5) δ : Table 1.

Anguivioside B (**2**) : A white powder, $[\alpha]_D^{26}$ −62.1° (c=0.2, MeOH). Positive FAB-MS m/z : 1033 [M+Na+K+H]$^+$. ^{1}H-NMR (pyridine-d_5) δ : 1.00 (3H, s, Me-19), 1.01 (3H, s, Me-18), 1.16 (3H, d, J=6.1 Hz, Me-27), 1.27 (3H, d, J=6.7 Hz, Me-21), 1.57 (3H, d, J=6.1 Hz, rha Me-6), 1.75 (3H, d, J=6.1 Hz, rha' Me-6), 3.65 (1H, m, glc H-5), 3.76, 3.80 (each 1H, AB q, J=15.3 Hz), 4.08 (1H, br d, J=12.2 Hz, glc H-6), 4.22 (overlapped, glc H-2, glc H-3, glc H'-6, H-3), 4.35 (1H, dd, rha' H-4, J=9.2, 10.1 Hz), 4.42 (1H, br t, J=9.2 Hz, glc H-4), 4.61 (overlapped, rha H-3, rha' H-3), 4.63 (1H, overlapped, rha H-2), 4.68 (1H, br s, rha H-2), 4.82 (1H, br s, rha' H-2), 4.95 (1H, d, J=6.7 Hz, glc H-1), 4.97 (1H, overlapped, rha' H-5), 5.07 (1H, m, rha H-5), 5.20 (1H, d, J=7.9 Hz, H-26), 5.30 (1H, m, H-6), 5.90 (1H, s, rha H-1), 5.96 (1H, br t, J=9.8 Hz, rha H-4), 6.38 (1H, s, rha' H-1). ^{13}C-NMR (pyridine-d_5) δ : Table 1.

Anguivioside C (**3**) : A white powder, $[\alpha]_D^{26}$ −67.4° (c=0.27, MeOH). Positive FAB-MS m/z : 910 [M+K+H]$^+$. ^{1}H-NMR (pyridine-d_5) δ : 1.01 (6H, s, Me-18, Me-19), 1.15 (3H, d, J=3.1 Hz, Me-27), 1.27 (3H, d, J=6.7 Hz, Me-21), 1.74 (3H, rha Me-6), 3.67 (1H, br t, J=10.7 Hz, xyl H-5), 3.84 (1H, m, glc H-5), 4.00 (2H, overlapped, xyl H-2, glc H-4), 4.10 (1H, br t, J=9.2 Hz, xyl H-3), 4.11 (4H, overlapped, glc H-2, glc H-3, xyl H-4, xyl H-5'), 4.26 (2H, overlapped, glc H-6, rha H-4), 4.45 (1H, br d, J=12.2 Hz, glc H'-6), 4.56 (1H, m, H-16), 4.70 (1H, br t, J=7.9 Hz, rha H-3), 4.86 (1H, br s, rha H-2), 4.91 (1H, m, rha H-5), 4.97 (2H, overlapped, glc H-1, xyl H-1),

5.20 (1H, d, J=7.9 Hz, H-26), 5.31 (1H, m, H-6), 6.28 (1H, br s, rha H-1). ^{13}C-NMR (pyridine-d_5) δ : Table 1.

Analysis of Sugar Components Each of compounds **1**—**3** were hydrolyzed with 2 mol/l HCl in H$_2$O at 80 °C for 4 h . The reaction mixture was neutralized with 2 mol/l NaOH in H$_2$O and extracted with CHCl$_3$. The aqueous layer was concentrated to dryness *in vacuo* to give a residue which was dissolved in dry pyridine, then L-cysteine methyl ester hydrochloride was added to the solution.[7] The reaction mixture was heated at 60 °C for 2 h and concentrated to dryness by blowing N$_2$ gas. To the residue was added trimethylsilylimidazole, and the mixture was heated at 60 °C for 1 h. The reaction mixture was concentrated to dryness by blowing N$_2$ gas. The residue was extracted with a mixture of hexane and H$_2$O, and the organic layer was analyzed by gas liquid chromatography (GLC); column: OV-17 (0.32 mm× 30 m), detector: FID, column temperature: 230 °C, injector temperature: 270 °C, carrier gas: He (2.2 kg/cm^2). Each peak was observed at t_R (min); 17'12" (D-Glc), 11'62" (L-Rha) 9'71" (D-Xyl). The standard monosaccharides were subjected to the same reaction and GLC analysis under the same condition.

References and Notes
1) Nakamura T., Komori C., Lee Y.-Y., Hashimoto F., Yahara S., Nohara T., Ejima A., *Biol. Pharm. Bull.*, **19**, 564—566 (1996).
2) Matsui M., Monma S., Koyama K., *Bull. Natl. Res. Inst. Veg., Ornam. Plants and Tea*, Japan, Ser. A, No. 10, 13—24 (1995).
3) Ohmura E., Nakamura T., Tian R.-H., Yahara S., Yoshimitsu H., Nohara T., *Tetrahedron Lett.*, **36**, 8443—8444(1995).
4) Hara S., Okabe H., Mihashi, K., *Chem. Pharm. Bull.*, **35**, 501—507 (1987).
5) Hirai Y., Konishi T., Sanada S., Ida Y., Shoji J., *Chem. Pharm. Bull.*, **30**, 3476—3484 (1982).
6) Mimaki Y., Satou T., Kuroda M., Sashida Y., Hatakeyama Y., *Chem. Pharm. Bull.*, **46**, 1829—1832 (1998).
7) Ando J., Miyazono A., Zhu X.-H., Ikeda T. and Nohara T., *Chem. Pharm. Bull.*, accepted.

Stereoselective Reactions. XXXII.[1]   Enantioselective Deprotonation of 4-*tert*-Butylcyclohexanone by Fluorine-Containing Chiral Lithium Amides Derived from 1-Phenylethylamine and 1-(1-Naphthyl)ethylamine

Kazumasa Aoki[2a] and Kenji Koga[*,2b]

Graduate School of Pharmaceutical Sciences, University of Tokyo, Hongo, Bunkyo-ku, Tokyo 113–0033, Japan.
Received October 12, 1999; accepted December 18, 1999

Enantioselective deprotonation of 4-*tert*-butylcyclohexanone was examined using 1-phenylethylamine- and 1-(1-naphthyl)ethylamine-derived chiral lithium amides having an alkyl or a fluoroalkyl substituent at the amide nitrogen. The lithium amides having a 2,2,2-trifluoroethyl group on the amide nitrogen are easily accessible in both enantiomeric forms, and were found to induce good enantioselectivity in the present reaction.

Key words   enantioselective deprotonation; 1-phenylethylamine; 1-(1-naphtyl)ethylamine; fluorine-containing alkyl group; chiral lithium amide

Lithium dialkylamides such as lithium diisopropylamide (LDA) are widely used in organic synthesis as strong bases with low nucleophilicity. In recent years, enantioselective deprotonation of prochiral carbonyl compounds by chiral lithium amides as a base and as a chiral auxiliary has received much attention to give the corresponding chiral lithium enolates.[3] We have previously reported enantioselective deprotonation of 4-*tert*-butylcyclohexanone (1) in the presence of excess trimethylsilyl chloride (TMSCl)[4] (internal quench (IQ) method) by a chiral chelated lithium amide ((*R*)-2) having a piperidino group as an internal ligation site for the lithium and 2,2,2-trifluoroethyl group on the amide nitrogen. High enantioselectivity was observed in tetrahydrofuran (THF) and 1,2-dimethoxyethane (DME), or in THF, DME, toluene, and ether in the presence of hexamethylphosphoric triamide (HMPA).[5] Studies on the solution and solid structures[5b] have shown that (*R*)-2 exists as a chelated monomer in THF and DME, as a chelated dimer in toluene and ether, while as a chelated monomer in these solvents in the presence of HMPA. In its monomeric form, it is shown that the piperidino group of (*R*)-2 acts as a ligation site for the lithium to form a five-membered chelated ring, that the 2,2,2,-trifluoromethyl group exists away from the phenyl group on the five-membered chelated ring, and that one of the fluorine atoms exists in close proximity to the lithium due to electrostatic interaction.[5b] Thus, 2,2,2-trifluoroethyl group on the amide nitrogen plays a crucial role in forming a chiral amide nitrogen to induce high enantioselectivity in deprotonation reaction.[5]

In search of easily accessible chiral lithium amides that induce good enantioselectivity in the present kinetic deprotonation reaction, we designed 1-phenylethylamine-derived chiral lithium amides having an alkyl group, a fluorine-containing alkyl group, and a 2-(dimethylamino)ethyl group on

the amide nitrogen, and their ability as chiral bases was examined.

Chiral secondary amines ((*R*)-6c—h) were prepared from commercially available (*R*)-1-phenylethylamine ((*R*)-4a) or (*R*)-1-(1-naphthyl)ethylamine ((*R*)-4b) by acylation to (*R*)-5c—h followed by reduction (Chart 2).[6] C₂-Symmetric chiral amine ((*R*,*R*)-6i) was prepared from (*R*)-2,2,2-trifluoro-1-phenylethylamine ((*R*)-4c)[7] via LiAlH₄ reduction of the corresponding imine ((*R*)-8) with trifluoroacetophenone followed by separation of the diastereomeric mixture ((*R*,*R*)-6i : meso-6i=7 : 3) by column chromatography. Chiral amines (6) were converted to the corresponding chiral lithium amide (7) as usual.

Deprotonation reaction of 1 was carried out using 1.2 eq of 7 in a 50 mM concentration of lithium amide in the presence of 5 eq of TMSCl in the absence and in the presence of HMPA. In the absence of HMPA, a solution of the ketone was added to a solution of lithium amide and TMSCl (referred to as IQ-1). As shown previously,[5b] in cases where the reaction was carried out in the presence of HMPA using chiral lithium amides having a fluoroalkyl group on the amide nitrogen by IQ-1 procedure, chemical yields of the products
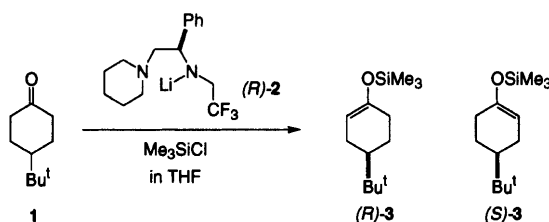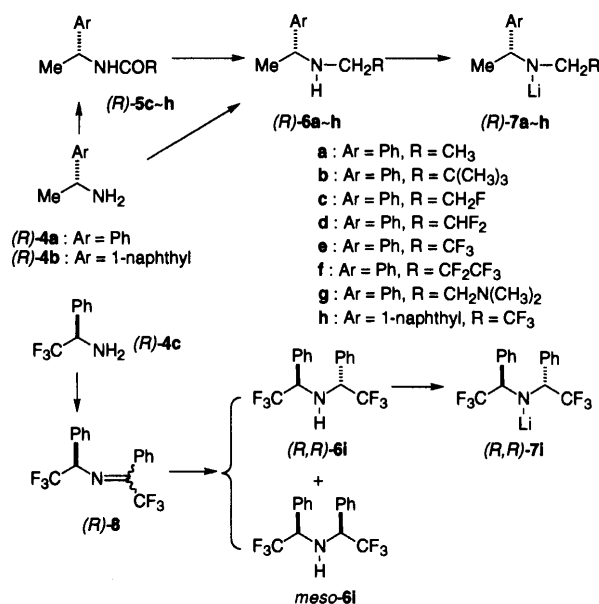

Chart 1

Chart 2

* To whom correspondence should be addressed.

Table 1. Enantioselective Deprotonation of **1** Using **7**[a]

Run	7	Temp. (°C)	Solvent	Additive (eq)	Procedure	Product		
						3	Chem. y. (%)	Ee (%)
1	(R)-**7a**	−78	THF	—	IQ-1	(S)-**3**	55	41
2	(R)-**7b**	−78	THF	—	IQ-1	(S)-**3**	94	32
3	(R)-**7c**	−78	THF	—	IQ-1	(S)-**3**	61	43
4	(R)-**7d**	−78	THF	—	IQ-1	(S)-**3**	66	59
5	(R)-**7e**	−78	THF	—	IQ-1	(S)-**3**	98	89
6	(R)-**7e**	−100	THF	—	IQ-1	(S)-**3**	86	92
7	(S)-**7e**	−100	THF	—	IQ-1	(R)-**3**	83	92
8	(R)-**7e**	−78	Ether	—	IQ-1	(S)-**3**	15	38
9	(R)-**7e**	−78	Ether	HMPA (1.2)	IQ-2	(S)-**3**	82	36
10	(R)-**7e**	−78—−20	Toluene	—	IQ-1	(S)-**3**	6	16
11	(R)-**7e**	−78	Toluene	HMPA (1.2)	IQ-2	(R)-**3**	56	8
12	(R)-**7f**	−78	THF	—	IQ-1	(S)-**3**	92	83
13	(R)-**7g**	−78	THF	—	IQ-1	(S)-**3**	92	18
14	(R)-**7h**	−78	THF	—	IQ-1	(S)-**3**	95	86
15	(R,R)-**7i**	−78—−20	THF	HMPA (1.2)	IQ-2	(R)-**3**	72	16

a) For general procedure, see Experimental.

dropped due to the partial conversion of chiral lithium amides to their corresponding N-silylated amines. Therefore, in such cases, a solution of the ketone and TMSCl was added to a solution of the chiral lithium amide containing HMPA (referred to as IQ-2). The results are summarized in Table 1.

It is shown that the results depend heavily on the substituent on the amide nitrogen. Thus, the amides ((R)-**7a**, **b**) having an alkyl group gave (S)-**3** in low optical yields (runs 1, 2). Among the amides ((R)-**7c**—**e**) having a fluorine-containing alkyl group, chemical and optical yields of (S)-**3** increased as the number of the fluorine atoms increased (runs 3, 4, 5). The amide ((R)-**7e**) having a 2,2,2-trifluoroethyl group gave (S)-**3** in high chemical and optical yields in THF (run 5),[8] while in low chemical and optical yields in ether and toluene (runs 8, 10) under the IQ-1 procedure. Chemical yields of the product were improved in ether and toluene in the presence of HMPA under the IQ-2 procedure, but optical yields were still low (runs 9, 11). By using the amide ((R)-**7f**) having a 2,2,3,3,3-pentafluoropropyl group, enantioselectivity of the reaction slightly goes declined (run 12). The amide ((R)-**7h**), having a 1-naphthyl group instead of a phenyl group on the chiral carbon and a 2,2,2-trifluoroethyl group on the amide nitrogen, also showed good enantioselectivity (run 14), similar to that by (R)-**7e** (run 5). However, the amide ((R,R)-**7i**) gave (S)-**3** in low optical yield (run 15). Based on the assumption that one of the fluorine atoms and the lithium in (R)-**7e** should be forced to come in close proximity due to the electrostatic interaction, as was observed in (R)-**2**,[5,9] (R)-**7g** was designed with the expectation that the dimethylamino group will also orient itself in close proximity to the lithium by coordination to form a five-membered chelated ring. However, it is shown that (R)-**7g** gave (S)-**3** in quite low enantioselectivity (run 13).

In conclusion, 1-phenylethylamine- and 1-(1-naphthyl)ethylamine-derived chiral lithium amides (**7e**, **7h**) having a 2,2,2-trifluoroethyl group on the amide nitrogen are easily accessible in both enantiomeric forms, and are excellent bases for the present enantioselective deprotonation reaction.

Experimental

General All melting and boiling points are uncorrected. IR spectra were

recorded on a Jasco IRA-1 or a Jasco IR Report-100 spectrometer. ^{1}H-NMR spectra were recorded in CDCl$_3$ on a JEOL EX-270 spectrometer. Chemical shifts are given in δ (ppm) using tetramethylsilane as an internal standard. Low resolution mass spectra (MS) were recorded on a JEOL JMS-01 mass spectrometer, and high resolution mass spectra (HR-MS) were recorded on a JEOL DX-300 mass spectrometer under electron impact (EI) conditions. Optical rotations were measured on a JASCO DIP-370 digital polarimeter in the solvent indicated. Enantiomeric excesses of the products (**3**) were calculated based on datum that optically pure (R)-**3** should show $[\alpha]_{365}^{25}$ +237° (benzene).[10] For anhydrous solvents, THF, toluene, and ether were distilled from sodium/benzophenone ketyl, and HMPA was distilled from CaH$_2$. (R)-**6a**[11] and (R)-**6b**[12] were prepared by the reported methods.

(R)-N-Fluoroacetyl-1-phenylethylamine ((R)-5c) A solution of (R)-**4a** (9.00 g, 74.3 mmol), ethyl fluoroacetate (14.1 g, 132 mmol) and NaOMe (96%, 1.25 g, 22.2 mmol) in MeOH (50 ml) was heated under reflux for 4.5 d. The solvent was evaporated to dryness in vacuo, the residue was mixed with saturated aqueous NH$_4$Cl (50 ml), and the whole was extracted with CH$_2$Cl$_2$ (100 ml×3). The combined organic extracts were washed with brine (50 ml), dried (Na$_2$SO$_4$), and evaporated in vacuo to give colorless fine needles. Recrystallization from hexane gave (R)-**5c** (9.70 g, 72%) as colorless fine needles of mp 79—80 °C. $[\alpha]_D^{25}$ +138° (c=0.91, MeOH). IR (KBr) cm^{-1}: 1655, 1545. ^{1}H-NMR: 1.54 (3H, d, J=7 Hz, CH$_3$), 4.74 (1H, dd, J=14, 48 Hz, CH$_2$F), 4.81 (1H, dd, J=14, 48 Hz, CH$_2$F), 5.20 (1H, dq, J=7, 7 Hz, PhCHN), 6.75 (1H, br, NH), 7.25—7.4 (5H, m, C$_6$H$_5$). MS m/z: 182 (M$^+$+1), 181 (M$^+$), 180 (M$^+$−1). Anal. Calcd for C$_{10}$H$_{12}$FNO: C, 66.28; H, 6.67; N, 7.73. Found: C, 66.10; H, 6.70; N, 7.79.

(R)-N-Difluoroacetyl-1-phenylethylamine ((R)-5d) A solution of (R)-**4a** (6.00 g, 49.5 mmol) in MeOH (100 ml) was mixed with ethyl difluoroacetate (8.9 g, 72 mmol) and NaOMe (96%, 0.90 g, 15 mmol), and the whole was stirred at room temperature for 4 d. The reaction mixture was evaporated in vacuo, the residue was mixed with satd aqueous NH$_4$Cl (50 ml), and the whole was extracted with CH$_2$Cl$_2$ (100 ml×3). The combined organic extracts were washed with brine (50 ml), dried (Na$_2$SO$_4$), and concentrated in vacuo to give a colorless solid. Recrystallization from hexane (190 ml) gave (R)-**5d** (8.34 g, 85%) as colorless fine needles of mp 60—61 °C. $[\alpha]_D^{25}$ +147° (c=0.95, MeOH). IR (KBr) cm^{-1}: 1680, 1540. ^{1}H-NMR: 1.53 (3H, d, J=7 Hz, CH$_3$), 5.12 (1H, dq, J=7, 7 Hz, PhCHN), 5.82 (1H, t, J=54 Hz, CHF$_2$), 6.87 (1H, br, NH), 7.2—7.4 (5H, m, C$_6$H$_5$). MS m/z: 200 (M$^+$+1), 199 (M$^+$), 198 (M$^+$−1). Anal. Calcd for C$_{10}$H$_{11}$F$_2$NO: C, 60.30; H, 5.57; N, 7.03. Found: C, 60.56; H, 5.68; N, 7.05.

(R)-N-Trifluoroacetyl-1-phenylethylamine ((R)-5e) Ethyl trifluoroacetate (17.6 g, 124 mmol) was added dropwise to (R)-**4a** (10.0 g, 82.5 mmol) over a period of 5 min at 0 °C. The resulting mixture solidified after stirring at room temperature for 3 min. Benzene (30 ml) was added, and the whole was concentrated to dryness in vacuo. This process was repeated three times. The residue was recrystallized from hexane (450 ml) to give (R)-**5e** (16.0 g, 89%) as colorless needles of mp 93—93.5 °C. $[\alpha]_D^{25}$ +145° (c=0.90, MeOH). IR (KBr) cm^{-1}: 1700, 1545. ^{1}H-NMR: 1.60 (3H, d, J=7 Hz, CH$_3$), 5.15 (1H, dq, J=7, 7 Hz, PhCHN), 6.42 (1H, br, NH), 7.3—

7.4 (5H, m, C_6H_5). MS m/z: 217 (M$^+$), 216 (M$^+$−1). *Anal.* Calcd for $C_{10}H_{10}F_3NO$: C, 55.30; H, 4.64; N, 6.45. Found: C, 55.33; H, 4.63; N, 6.65.

(R)-N-Pentafluoropropionyl-1-phenylethylamine ((R)-5f) By a procedure similar to the preparation of (R)-**5e** described above, addition of methyl pentafluoropropionate (8.8 g, 50 mmol) to (R)-**4a** (5.00 g, 41.3 mmol) followed by recrystallization of the resulting solid from hexane afforded (R)-**5f** (8.40 g, 76%) as colorless needles of mp 101—101.5 °C. $[\alpha]_D^{25}$ +126° (c=0.64, MeOH). IR (KBr) cm^{-1}: 1695, 1540. ^{1}H-NMR: 1.59 (3H, d, J= 7 Hz, CH$_3$), 5.18 (1H, dq, J=7, 7 Hz, PhCHN), 6.56 (1H, br, NH), 7.2—7.4 (5H, m, C_6H_5). MS m/z: 267 (M$^+$), 266 (M$^+$−1), 148 (M$^+$−CF$_2$CF$_3$). *Anal.* Calcd for $C_{11}H_{10}F_5NO$: C, 49.45; H, 3.77; N. 5.24. Found: C, 49.51; H, 3.57; N. 5.52.

(R)-N-Dimethylaminoacetyl-1-phenylethylamine ((R)-5g) Triethylamine (12 ml, 86 mmol) was added dropwise over a period of 20 min to a solution of (R)-**4a** (4.67 g, 41.0 mmol), diethyl phosphorocyanidate (DEPC)[13] (90%, 8.16 g, 45.0 mmol) and N,N-dimethylglycine (86.00 g, 43.0 mmol) in N,N-dimethylformamide (DMF) (120 ml), and the whole was stirred at room temperature for 3 h. The resulting solution was diluted with a mixture of benzene (300 ml) and ethyl acetate (600 ml), and then the whole was washed with 1.5% aqueous NaHCO$_3$ (600 ml×3). The aqueous layer was extracted with a mixture of benzene (100 ml) and ethyl acetate (200 ml). The organic layers were combined and extracted with 2.5% aqueous HCl (500 ml×2, 250 ml). The aqueous extracts were combined, neutralized with solid NaHCO$_3$, and extracted with ether (300 ml×3). The combined organic extracts were washed with brine, dried (Na$_2$SO$_4$), and concentrated *in vacuo* to give (R)-**5g** (5.62 g, 66%) as a pale yellow powder. This sample was used for the next step without further purification. An analytical sample was obtained by recrystallization of a part of this product (210 mg) from hexane (6 ml) as colorless needles (110 mg) of mp 54—55 °C. $[\alpha]_D^{25}$ +102° (c=0.39, MeOH). IR (KBr) cm^{-1}: 1655, 1510. ^{1}H-NMR: 1.50 (3H, d, J=7 Hz, CH$_3$), 2.27 (6H, s, N(CH$_3$)$_2$), 2.95 (2H, m, CH$_2$N), 5.17 (dq, J=7, 8.4 Hz, PhCHN), 7.4 (1H, br, NH), 7.2—7.4 (5H, m, C_6H_5). MS m/z: 206 (M$^+$), 191 (M$^+$−15). *Anal.* Calcd for $C_{12}H_{18}N_2O$: C, 69.87; H, 8.79; N, 13.58. Found: C, 69.60; H, 8.93; N, 13.44.

(R)-N-Trifluoroacetyl-1-(1-naphthyl)ethylamine ((R)-5h) By a procedure similar to the preparation of (R)-**5e** described above, the reaction of (R)-**4b** (11.0 g) with ethyl trifluoroacetate (12.9 g) gave a pale brown powder. Three recrystallizations from ether/hexane gave (R)-**5h** (7.46 g, 46%, 99.8% ee by HPLC analysis using Waters Opti-Pak XC; hexane/iso-PrOH=10/1) as slightly pink needles of mp 112—112.5 °C. $[\alpha]_D^{25}$ +63.0° (c=0.49, MeOH). IR (KBr) cm^{-1}: 1690. ^{1}H-NMR: 1.74 (3H, d, J=7 Hz, CH$_3$), 5.93 (1H, dq, J=7, 7 Hz, ArCHN), 6.6 (1H, br, NH), 7.2—7.7 (4H, m, ArH), 7.8—8.1 (3H, m, ArH). MS m/z: 267 (M$^+$), 252 (M$^+$−15). *Anal.* Calcd for $C_{14}H_{12}F_3NO$: C, 62.92; H, 4.53; N, 5.24. Found: C, 63.02; H, 4.53; N, 5.51.

(R)-N-(2′,2′,2′-Trifluoro-1′-phenethylidene)-2,2,2-trifluoro-1-phenylethylimine ((R)-8) A solution of BuLi in hexane (1.64 N, 18.5 ml, 30.3 mmol) was added to a stirred solution of (R)-**4c**[7] (5.30 g, 30.3 mmol) in THF (200 ml) at −78 °C under argon atmosphere. The resulting solution was stirred for 20 min at −78 °C. After addition of TMSCl (4.03 ml, 31.8 mmol), the reaction mixture was warmed to room temperature, stirred for 45 min, and then cooled to −78 °C. A solution of BuLi in hexane (1.64 N, 18.5 ml, 30.3 mmol) was added, and the resulting mixture was stirred for 30 min. Trifluoroacetophenone (4.54 ml, 33.3 mmol) was added dropwise over a period of 5 min at −78 °C, and the whole was warmed to room temperature and stirred for 2 h. The reaction mixture was quenched with saturated aqueous NH$_4$Cl (200 ml), and the whole was extracted with ether (300 ml×3). The combined organic extracts were washed with brine (50 ml), dried (Na$_2$SO$_4$), and concentrated in vacuo to give a semisolid residue, which was purified by column chromatography (silica gel, hexane/ether= 20/1) to give (R)-**8** as a pale yellow semisolid (8.07 g, 81%), followed by bulb-to-bulb distillation to give a colorless oil of bp$_{0.8}$ 180 °C (bath temperature). $[\alpha]_D^{25}$ −173° (c=0.87, MeOH). *Anal.* Calcd for $C_{16}H_{11}F_6N$: C, 58.01; H, 3.35; N, 4.23. Found: C, 57.74; H, 3.24, N, 4.48.

(R)-N-(2-Fluoroethyl)-1-phenylethylamine ((R)-6c) A solution of (R)-**5c** (6.90 g, 38.1 mmol) in THF (50 ml) was mixed with a solution of borane-THF complex in THF (1.0 M, 115 ml, 115 mmol) at 0 °C, and the resulting mixture was stirred at room temperature for 3 h. After addition of MeOH (30 ml), the solvent was evaporated *in vacuo*. The residue was dissolved in MeOH (30 ml), and was mixed with a solution of HCl in MeOH (38%, 20 ml) at 0 °C. The solvent was evaporated *in vacuo*, and the residue was suspended in benzene, and the benzene was evaporated *in vacuo*. This process was repeated three times to give a colorless solid. Recrystallization from iso-PrOH (150 ml) gave (R)-**6c**·HCl (5.96 g, 77%) as colorless fine needles of mp 219—220 °C (sublimation in the sealed capillary). $[\alpha]_D^{25}$

+14.9° (c=0.95, MeOH). *Anal.* Calcd for $C_{10}H_{15}ClFN$: C, 58.97; H, 7.42; N, 6.88. Found: C, 58.73; H, 7.72; N, 6.96. This salt (3.75 g, 18.4 mmol) was dissolved in 10% aqueous NaOH (30 ml) at 0 °C, and the resulting solution was extracted with hexane (100 ml×3). The combined organic extracts were washed with brine (50 ml), dried (Na$_2$SO$_4$), and concentrated *in vacuo* to give (R)-**6c** (2.98 g, 97% recovery) as a colorless oil, which was subjected to bulb-to-bulb distillation to give a colorless oil of bp$_5$ 170—180 °C (bath temperature). $[\alpha]_D^{25}$ +45.5° (c=0.96, MeOH). ^{1}H-NMR: 1.37 (3H, d, J= 7 Hz, CH$_3$), 1.65 (1H, br, NH), 2.6—2.9 (2H, m, NCH$_2$), 3.81 (1H, q, J= 7 Hz, PhCHN), 4.3—4.7 (2H, m, CH$_2$F), 7.2—7.4 (5H, m, C_6H_5). MS m/z: 168 (M$^+$+1), 167 (M$^+$), 166 (M$^+$−1).

(R)-N-(2,2,-Difluoroethyl)-1-phenylethylamine ((R)-6d) Reduction of (R)-**5d** (8.00 g) by borane-THF and conversion of the product to the corresponding hydrochloride by the procedure similar to that for the preparation of (R)-**6c**·HCl described above gave (R)-**6d**·HCl (7.06 g, 80%) as colorless fine needles of mp 240—241 °C (sublimation in the sealed capillary). $[\alpha]_D^{25}$ +17.8° (c=0.81, MeOH). *Anal.* Calcd for $C_{10}H_{14}ClF_2N$: C, 54.18; H, 6.37; N, 6.32. Found: C, 54.18; H, 6.44; N, 6.53. Conversion of this salt (4.00 g) to the free amine as described above for the preparation of (R)-**6c** gave (R)-**6d** (3.17 g, 95% recovery) as a colorless oil, which was subjected to bulb-to-bulb distillation as a colorless oil of bp$_5$ 170—180 °C (bath temperature). $[\alpha]_D^{25}$ +50.3° (c=1.05, MeOH). ^{1}H-NMR: 1.37 (3H, d, J=7 Hz, CH$_3$), 1.50 (1H, br, NH), 2.7—2.9 (2H, m, NCH$_2$CHF$_2$), 3.82 (1H, q, J=7 Hz, PhCHN), 5.77 (1H, tt, J=57, 4 Hz, CHF$_2$), 7.2—7.4 (5H, m, C_6H_5). MS m/z: 185 (M$^+$), 184 (M$^+$−1).

(R)-N-(2,2,2-Trifluoroethyl)-1-phenylethylamine ((R)-6e) A solution of borane-THF complex in THF (1.0 M, 800 ml, 0.8 mol) was added to a stirred solution of (R)-**5e** (44.0 g, 203 mmol) in THF (250 ml) at 0 °C, and the resulting mixture was refluxed for 10 h. MeOH (200 ml) was added to the reaction mixture, and the whole was concentrated *in vacuo*. The residue was dissolved in MeOH (200 ml), and then a solution of HCl in MeOH (20%, 200 ml) was added at 0 °C. The resulting mixture was heated under reflux for 3 h. After removal of the solvent *in vacuo*, the residue was treated by the procedure similar to that for the preparation of (R)-**6c**·HCl described above to give (R)-**6e**·HCl (46.1 g, 95%) as colorless needles of mp 235—236 °C (sublimation in the sealed capillary). $[\alpha]_D^{25}$ +17.0° (c=1.06, MeOH). *Anal.* Calcd for $C_{10}H_{13}ClF_3N$: C, 50.12; H, 5.05; N, 5.84. Found: C, 49.99; H, 5.30; N, 5.85. This salt (4.00 g) was dissolved in saturated aqueous NaHCO$_3$ (50 ml), and the resulting aqueous mixture was extracted with hexane (100 ml×3). The combined organic extracts were washed with brine (60 ml), dried (Na$_2$SO$_4$), and concentrated *in vacuo* to give (R)-**6e** (3.35 g, 99% recovery) as a colorless oil, which was subjected to bulb-to-bulb distillation as a colorless oil of bp$_5$ 170—180 °C (bath temperature). $[\alpha]_D^{25}$ +54.9° (c=0.98, MeOH). ^{1}H-NMR: 1.37 (3H, d, J=7 Hz, CH3), 1.62 (1H, br, NH), 3.01 (2H, q, J=10 Hz, CH$_2$CF$_3$), 3.91 (1H, q, J=7 Hz, PhCHN), 7.2—7.4 (5H, m, C_6H_5).

(R)-N-(2,2,3,3,3-Pentafluoropropyl)-1-phenylethylamine ((R)-6f) Reduction of (R)-**5f** (8.20 g) by borane-THF and conversion of the product to the corresponding hydrochloride by the procedure similar to that for the preparation of (R)-**6e**·HCl described above gave (R)-**6f**·HCl, which was recrystallized from iso-PrOH (150 ml) as colorless fine needles (6.53 g, 73%). It was not possible to measure mp of this compound in a sealed capillary because of sublimation. *Anal.* Calcd for $C_{11}H_{13}ClF_5N$: C, 45.61; H, 4.52; N, 4.84. Found: C, 45.86; H, 4.48; N, 4.90. By a procedure similar to that described above, this salt (4.00 g) was converted to (R)-**6f** (3.41 g, 98% recovery) as a colorless oil, which was subjected to bulb-to-bulb distillation to give a colorless oil of bp$_5$ 180 °C (bath temperature). $[\alpha]_D^{25}$ +49.7° (c=1.58, MeOH). ^{1}H-NMR: 1.37 (3H, d, J=7 Hz, CH$_3$), 1.52 (1H, br, NH), 3.04 (2H, t, J=15 Hz, NCH$_2$), 3.88 (1H, q, J=7 Hz, PhCHN), 7.2—7.5 (5H, m, C_6H_5). MS m/z: 253 (M$^+$), 252 (M$^+$−1).

(R)-N-(2-(N′,N′-Dimethylamino)ethyl)-1-phenylethylamine ((R)-6g) A solution of (R)-**5g** (5.45 g, 26.4 mmol) in THF (25 ml) was added over a period of 20 min to a stirred suspension of LiAlH$_4$ (6.00 g, 158 mmol) in THF (60 ml), and the whole was stirred under reflux for 7 d. Under stirring, water (6 ml), 15% aqueous NaOH (18 ml), water (6 ml), and K$_2$CO$_3$ were added successively to the reaction mixture, and the whole was filtered. The filtrate and THF washings were combined, and evaporated to dryness *in vacuo* to give a pale yellow oil. A solution of this oil in MeOH (10 ml) was mixed with a solution of oxalic acid (5.28 g, 59 mmol) in MeOH (50 ml). The white powder, which precipitated immediately, was recrystallized from MeOH (2.7 l) to give oxalic acid salt of (R)-**6g** (8.06 g, 82%) as colorless fine needles of mp 208—208.5 °C. To a suspension of the above salt (5.00 g) in CH$_2$Cl$_2$ (50 ml) was added 10% aqueous NaOH (20 ml). After dissolution of the salt, the organic layer was separated, and the aqueous layer was ex-

tracted with CH_2Cl_2 (50 ml×2). The combined organic extracts were washed with brine, dried (Na_2SO_4), and concentrated *in vacuo* to give (*R*)-**6g** (2.53 g, 98% recovery) as a colorless oil, which was subjected to bulb-to-bulb distillation as a colorless oil of $bp_{0.6}$ 170—180 °C (bath temperature). $[\alpha]_D^{25}$ +48.4° (*c*=0.94, MeOH). ^{1}H-NMR: 1.18 (3H, d, *J*=7 Hz, CH_3), 1.8 (1H, br, NH), 2.15 (6H, s, $N(CH_3)_2$), 2.2—2.6 (4H, m, NCH_2CH_2N), 3.73 (1H, q, *J*=7 Hz, PhCHN), 7.1—7.3 (5H, m, C_6H_5). MS *m/z*: 192 (M$^+$). HR-MS *m/z*: Calcd for $C_{12}H_{20}N_2$: 192.1626. Found: 192.1626.

(*R*)-*N*-(2,2,2-Trifluoroethyl)-1-(1-naphthyl)ethylamine ((*R*)-6h) Reduction of (*R*)-**5h** (9.00 g) by borane-THF and conversion of the product to the corresponding hydrochloride by the procedure similar to that for the preparation of (*R*)-**6e**·HCl described above, followed by recrystallization from EtOH gave (*R*)-**6h**·HCl (6.72 g, 69%) as colorless needles of mp *ca.* 210 °C (sublimation in a sealed capillary). $[\alpha]_D^{25}$ −11.7° (*c*=0.45, MeOH) *Anal.* Calcd for $C_{14}H_{15}ClF_3N$: C, 58.04; H, 5.22; N, 4.83. Found: C, 58.18; H, 5.11; N, 5.09. By a procedure similar to that described above, this salt was converted to the free amine ((*R*)-**6h**) as a pale yellow oil in almost quantitative yield, and was subjected to bulb-to-bulb distillation as a colorless oil of $bp_{0.4}$ 175—185 °C (bath temperature). $[\alpha]_D^{25}$ +75.8° (*c*=0.98, MeOH). ^{1}H-NMR: 1.48 (3H, d, *J*=7 Hz, CH_3), 1.70 (1H, br, NH), 3.08 (2H, dq, *J*=3, 10 Hz, CH_2CF_3), 4.75 (1H, q, *J*=7 Hz, ArCHN), 7.1—8.2 (7H, m, ArH). MS *m/z*: 235 (M$^+$), 238 (M$^+$−15).

(*R,R*)-Bis(2,2,2-trifluoro-1-phenylethyl)amine ((*R,R*)-6i) A solution of (*R*)-**8** (6.40 g, 19.3 mmol) in THF (38 ml) was added to a stirred suspension of LiAlH$_4$ (2.2 g, 58.0 mmol) in THF (12 ml) at −20 °C under argon atmosphere. The resulting mixture was stirred at −20 °C for 15 min. Usual workup gave a mixture of crude amine (6.37 g), whose diastereomeric ratio was 7:3 by gas chromatography (SE-30, 150 °C), Purification by column chromatography (silica gel, hexane/benzene=50/1) gave (*R,R*)-**6i** (3.39 g, 53%) as colorless prisms of mp 66.5—67.5 °C. $[\alpha]_D^{25}$ −153° (*c*=1.14, MeOH). ^{1}H-NMR: 2.55 (1H, t, *J*=7 Hz, NH), 3.92 (2H, dq, *J*=7, 7 Hz, PhCHN), 7.2—7.5 (10 H, C_6H_5). MS *m/z*: 333 (M$^+$). *Anal.* Calcd for $C_{16}H_{13}F_6N$: C, 57.66; H, 3.93; N, 4.20. Found: C, 57.68; H, 3.83; N, 4.50. meso-**6i** (0.71 g, 10%) was also isolated as a colorless oil. ^{1}H-NMR: 2.36 (1H, t, *J*=7 Hz, NH), 4.25 (2H, dq, *J*=7, 7 Hz, PhCHN), 7.2—7.4 (10H, m, C_6H_5). MS *m/z*: 333 (M$^+$). *Anal.* Calcd for $C_{16}H_{13}F_6N$: C, 57.66; H, 3.93; N, 4.20. Found: C, 57.36; H, 3.63; N, 4.46.

A Typical Procedure for the Deprotonation Reaction in the Absence of HMPA (IQ-1) (Table 1, Run 6) A solution of BuLi in hexane (1.55 N, 1.55 ml, 2.4 mmol) was added to a stirred solution of (*R*)-**6e** (508 mg, 2.5 mmol) in THF (50 ml) at −78 °C under argon atmosphere. The resulting solution was stirred at −78 °C for 30 min, and then cooled to −100 °C. After addition of TMSCl (1.27 ml, 10 mmol), a solution of **1** (308 mg, 2.0 mmol) in THF (4 ml) was added dropwise during a period of 6 min. After stirring at −100 °C for 50 min, the reaction mixture was quenched by addition of triethylamine (4 ml) and saturated aqueous NaHCO$_3$ (10 ml), and the whole was allowed to warm to room temperature. After addition of water (15 ml), the mixture was extracted with hexane (50 ml×3). The combined organic extracts were washed successively with water (20 ml×2), 0.1 N aqueous citric acid (100 ml×2, 50 ml×3), water (20 ml), saturated aqueous NaHCO$_3$ (20 ml) and brine (40 ml), dried (Na$_2$SO$_4$), and evaporated *in vacuo* to give a yellow oil. Purification by column chromatography (silica gel,

hexane) followed by bulb-to-bulb distillation gave (*S*)-**3** (388 mg, 86%) as a colorless oil of $bp_{0.5}$ 150 °C (bath temperature). $[\alpha]_D^{25}$ −217° (*c*=1.49, benzene), corresponding to be 92% ee.[10]

Rotational Values of 3 Obtained by the Reactions (Table 1) Run 1: $[\alpha]_{365}^{25}$ −97° (*c*=1.59, benzene); run 2: $[\alpha]_{365}^{25}$ −76° (*c*=1.50, benzene); run 3: $[\alpha]_{365}^{25}$ −103° (*c*=1.38, benzene); run 4: $[\alpha]_{365}^{25}$ −141° (*c*=1.42, benzene); run 5: $[\alpha]_{365}^{25}$ −211° (*c*=1.44, benzene); run 7: $[\alpha]_{365}^{25}$ +217° (*c*=1.49, benzene); run 8: $[\alpha]_{365}^{25}$ −89° (*c*=1.29, benzene); run 9: $[\alpha]_{365}^{25}$ −86° (*c*=1.45, benzene); run 10: $[\alpha]_{365}^{25}$ −37° (*c*=0.90, benzene); run 11: $[\alpha]_{365}^{25}$ −18° (*c*=1.70, benzene); run 12: $[\alpha]_{365}^{25}$ −197° (*c*=1.64, benzene); run 13: $[\alpha]_{365}^{25}$ −44° (*c*=1.48, benzene); run 14: $[\alpha]_{365}^{25}$ −203° (*c*=1.58, benzene); run 15: $[\alpha]_{365}^{25}$ +9.3° (*c*=1.00, benzene).

References and Notes

1) Part XXXI: Imai M., Hagihara A., Kawasaki H., Manabe K., Koga K., *Tetrahedron*, **56**, 179—185 (2000).

2) Present addresses: *a*) Medicinal Chemistry Research Lab., Sankyo Co., Ltd., Hiro-machi, Shinagawa-ku, Tokyo 140–8710, Japan; *b*) Research and Education Center for Materials Science, Nara Institute of Science and Technology, Takayama-cho, Ikoma-shi, Nara 630–0101, Japan.

3) For reviews: *a*) Koga K., *Yuki Gosei Kagaku Kyokai Shi*, **48**, 463—475 (1990); *b*) Cox P. J., Simpkins N. S., *Tetrahedron: Asymmetry*, **2**, 1—26 (1991); *c*) Waldmann H., *Nachr. Chem. Tech. Lab.*, **39**, 413—419 (1991); *d*) Koga K., *Pure Appl. Chem.*, **66**, 1487—1492 (1994); *e*) Koga K., Shindo M., *Yuki Gosei Kagaku Kyokai Shi*, **52**, 1021—1032 (1995); *f*) Simpkins N. S., *Pure Appl. Chem.*, **68**, 691—698 (1996); *g*) Idem, "Advanced Asymmetric Synthesis," ed by Stephenson, G. R., Chapman & Hall, London, 1996, Chapter 6.

4) Corey E. J., Gross A. W., *Tetrahedron Lett.*, **25**, 495—498 (1984).

5) *a*) Aoki K., Noguchi H., Tomioka K., Koga K., *Tetrahedron Lett.*, **34**, 5105—5108 (1993); *b*) Aoki K., Tomioka K., Noguchi H., Koga K., *Tetrahedron*, **53**, 13641—13656 (1997).

6) Enantiomers were prepared similarly starting from commercially available (*S*)-**4a** or (*S*)-**4b**.

7) *a*) Wang Y., Mosher H. S., *Tetrahedron Lett.*, **32**, 987—990 (1991); *b*) Pirkle W. H., Hauske J. R., *J. Org. Chem.*, **42**, 2436—2439 (1977).

8) A part of these results has been reported as a communication: Aoki K., Koga K., *Tetrahedron Lett.*, **38**, 2505—2506 (1997).

9) For reviews on F–Li electrostatic interaction: *a*) Yamazaki, T., Kitazume, T., *Yuki Gosei Kagaku Kyokai Shi*, **54**, 665—674 (1996); *b*) Plenio, H., *Chem. Rev.*, **97**, 3363—3384 (1997).

10) Aoki K., Nakajima M., Tomioka K., Koga K., *Chem. Pharm. Bull.*, **41**, 994—996 (1993).

11) Majewski M., Gleave D. M., *J. Org. Chem.*, **57**, 3599—3605 (1992)

12) Brown E., Moudachirou M., *Tetrahedron*, **50**, 10309—10318 (1994).

13) Shioiri T., Yokoyama Y., Kasai Y., Yamada S., *Tetrahedron*, **32**, 2211—2217 (1976).

Two Novel *C*-Glycosides of Aureolic Acid Repress Transcription of the *MDR1* Gene

Motoyuki Tagashira,*,[a] Takanori Kitagawa,[a] Naoko Nozato,[a] Seiji Isonishi,[b] Aikou Okamoto,[b] Kazunori Ochiai,[b] and Yasuyuki Ohtake[a]

Foods and Pharmaceuticals Research and Development Laboratory, Asahi Breweries, Ltd.,[a] 1-1-21, Midori, Moriya-machi, Kitasohma-gun, Ibaraki 302-0106, Japan and Department of Obstetrics and Gynecology, The Jikei University School of Medicine,[b] 3-25-8, Nishi-shinbashi, Minato-ku, Tokyo 105-8461, Japan.

In the search for compounds which repress *MDR1* gene expression, two novel aryl *C*-glycosides were isolated from a broth of *Streptomyces* sp. They had the characteristic structure of a dideoxy-carbohydrate (oliose or olivose) linked directly to chromomycinone, an aglycone of aureolic acids. Further investigation revealed that they were artifacts yielded from an aureolic acid, mithramycin. Acid and methanol were necessary to yield the *C*-glycosides. This reaction would contribute to the design of useful aryl *C*-glycosides.

Key words　multidrug resistance; *C*-glycoside; aureolic acid; mithramycin; *MDR1* gene

Chemotherapeutic research on cancer has advanced, but the problem remains that tumor cells acquire resistance to antitumor drugs.[1] Multidrug resistance (MDR) is one of the most serious problems preventing therapy. In recent years, several studies have revealed the molecular mechanism of MDR P-glycoprotein, a membrane protein encoded by the *MDR1* gene, removes exogenous organic substances such as anticancer drugs from the cells.[2] Hence, it depletes intracellular drug concentrations with low selectivity and causes MDR. In most cases, a high level of *MDR1* expression was observed in MDR tumor cells.[3]

Several drugs such as calcium antagonists (verapamil)[4] and immunosuppressive agents (cyclosporin A, FK506)[5] are reported to inhibit P-glycoprotein function and sensitize the MDR tumor cells. However, their original activities such as calcium antagonism or immunosuppression has prevented their therapeutic application. Their analogues with low-toxicity such as MS-209 and SDZ PSC 833, are still undergoing clinical trials.[6]

We are researching *MDR1* gene expression inhibitors derived from microorganisms. From the broth of the *Streptomyces* species KS12571, two active compounds were isolated. Spectrometric studies elucidated their chemical structures as **1** and **2**. The compounds had quite characteristic chemical structures categorized in aryl *C*-glycosides: C-1″ of dideoxy carbohydrate (oliose or olivose) directly bonded to the C-5 of their aglycone, chromomycinone.[7] High resolution (HR)-FAB-MS data showed that they had the same molecular formula ($C_{27}H_{34}O_{12}$), and the ^{1}H- and ^{13}C-NMR spectrum suggested they contained a chromomycinone moiety in their chemical structures (Table 1). ^{1}H-detected multiple-bond heteronuclear multiple quantum coherence (HMBC) spectrum showed a correlation between the H-1″ of carbohydrate and C-5, C-6 and C-10a of aglycone (Table 2). Nuclear overhauser and exchange spectroscopy (NOESY) data also showed that the H-1″ of the carbohydrate correlated to the H-10 of the aglycone (Fig. 1). This result strongly suggested that the dideoxy carbohydrates directly bonded to their aglycone. From the NOESY spectrum, the carbohydrates of **1** and **2** were suggested to be oliose and olivose respectively (Fig. 1).

Their activity was tested using a *MDR1*-high expressing human small lung tumor cell line, SBC-3/ADM.[8] Figure 2 shows that **1** and **2** (0.1—0.6 mg/ml) inhibited *MDR1* gene expression in a dose-dependent manner. They had little effect on that of β_2-microgroblin (β_2-m), used as a control. This result suggests that these compounds would be candidates for drugs against MDR in cancer chemotherapy.

We tried to investigate the mechanism of biosynthesis of the *C*-glycosides, and further research revealed that the compounds were artifacts yielded from an aureolic acid, mithramycin (**3**).[9] At first, from the broth of KS12571, the peak of mithramycin (Fig. 3a) was fractionated by HPLC with HCl conditions. In the concentration process, the rotary vacuum evaporator N-2NR (Tokyo Rika Kikai Co.) equipped with a digital water bath SB-651 (Tokyo Rika Kikai Co.) was used. The water bath temperature was fixed at 40 °C. We collected the fraction (about 800—1000 ml) containing mithramycin in a 2 l glass flask. When the solvent was concentrated to about 100—150 ml, the fraction was moved into a smaller glass flask (300 ml). At that point, we washed the 2 l flask with MeOH (10—30 ml) and added the wash solvent to the concentrated sample. Then, the solvent was dried by the same evaporator to give a pale yellow-green residue (about 180 mg). Finally, 100 mg of the residue was dissolved in MeOH (10 ml), filtered by a Cosmonice Filter S (pore size, 0.5 μm; Nacalai Tesque Ltd.), and subjected to preparative HPLC again (Fig. 3c). The *C*-glycosides were then isolated (yields from 180 mg of residue: **1**, 8 mg; **2**, 14 mg). Without HCl in HPLC conditions, mithramycin was detected again by HPLC (Fig. 3b, 3d). Besides, without MeOH in the concentration process, mithramycin was degraded, but no *C*-glycosides were obtained. In conclusion, as far as we tested, without HCl or MeOH, **1** and **2** were not isolated from the fraction. We also checked that **1** and **2** could be obtained from authentic mithramycin purchased commercially (Sigma-Aldrich). The mechanism of this reaction has not been elucidated, but the chemical structure of mithramycin would suggest that its 6-*O*-glycoside (carbohydrate A in Chart 1) was converted into a 5-*C*-glycoside when it was hydrolyzed.

In recent years, interest in aryl *C*-glycosides has been growing because of their various biological functions, such

---

* To whom correspondence should be addressed.

Table 1. ¹H- and ¹³C-NMR Data of Isolated Aryl C-Glycosides in CD₃OD

Part	Position	1		2	
		δ_C	δ_H	δ_C	δ_H
Aglycone[a]	1	204.2		204.2	
	2	72.7	4.48 (1H, d, J=11.3 Hz)	72.7	4.48 (1H, d, J=11.2 Hz)
	3	43.9	2.81 (1H, m)	43.9	2.77 (1H, m)
	4	27.8	2.74 (1H, m)	27.8	2.69 (1H, m)
			3.01 (1H, m)		3.02 (1H, m)
	5	109.8		108.6	
	6	159.8		159.4	
	7	110.8		110.8	
	8	156.0		156.0	
	9	164.4		164.6	
	10	111.4	6.96 (1H, s)	111.4	6.93 (1H, s)
	4a	136.6		136.8	
	8a	106.4		106.6	
	9a	107.0		107.1	
	10a	134.9		134.9	
	1'	82.8	4.91 (1H, m)	82.8	4.91 (1H, m)
	2'	212.4		212.3	
	3'	79.1	4.24 (1H, d, J=2.7 Hz)	79.1	4.24 (1H, d, J=2.7 Hz)
	4'	68.3	4.28 (1H, dq, J=2.7, 6.4 Hz)	68.3	4.28 (1H, dq, J=2.7, 6.4 Hz)
	5'	18.7	1.28 (3H, d, J=6.4 Hz)	18.6	1.28 (3H, d, J=6.4 Hz)
	OMe1'	58.6	3.48 (3H, s)	58.6	3.48 (3H, s)
	6'	7.1	2.16 (3H, s)	7.1	2.15 (3H, s)
Carbohydrate	1"	74.7	5.31 (1H, m)	39.0	2.12 (1H, m)
	2"	32.8	2.16 (1H, m)	39.0	2.12 (1H, m)
			1.82 (1H, m)		1.81 (1H, m)
	3"	69.3	3.95 (1H, m)	71.8	3.82 (1H, m)
	4"	70.2	3.68 (1H, m)	77.7	3.15 (1H, dd, J=9.1, 9.3 Hz)
	5"	75.6	3.78 (1H, dq, J=6.4, 1.9 Hz)	77.6	3.59 (1H, dq, J=6.4, 9.1 Hz)
	6"	16.8	1.36 (3H, d, J=6.4 Hz)	17.6	1.45 (3H, d, J=6.4 Hz)

a) NMR data of chromomycinone were previously reported.[7]

Table 2. HMBC Correlation between ¹H and ¹³C of Compound 2

¹H	→	¹³C
2-H		1-C
3-H		2-C
4-Ha		2-C, 3-C, 4a-C, 9a-C, 10-C
4-Hb		3-C, 4a-C
10-H		4-C, 5-C, 8a-C, 9a-C, 10a-C
1'-H		2-C, 3-C, 4-C, 2'-C, OMe1'-C
3'-H		2'-C, 4'-C
4'-H		5'-C
5'-Me		3'-C, 4'-C
OMe1'		1'-C
6'-Me		5-C, 6-C, 7-C, 8-C, 8a-C
1"-H		5-C, 6-C, 10a-C
2"-Ha		3"-C
2"-Hb		1"-C, 3"-C
3"-H		ND
4"-H		3"-C, 5"-C
5"-H		ND
6"-Me		5"-C

ND: Not detected.

Fig. 1. NOE Interactions Observed in the NOESY Spectra of the Carbohydrate Moiety of 1 and 2

Fig. 2. Repression of MDR1 Gene Expression by 1 and 2
Control denotes the results of experiments without drugs.

as antibacterial activity,[10] protection against radiation,[11] inhibition of platelet aggregation,[12] and antitumor activities.[13] Therefore, it is worth investigating 1 and 2 for further activities. C-Glycosides also have some advantages over O-glycosides in terms of chemical stability. In fact, in the present study we showed that 1 and 2 were not degraded under acidic HPLC conditions while mithramycin, an O-glycoside com-
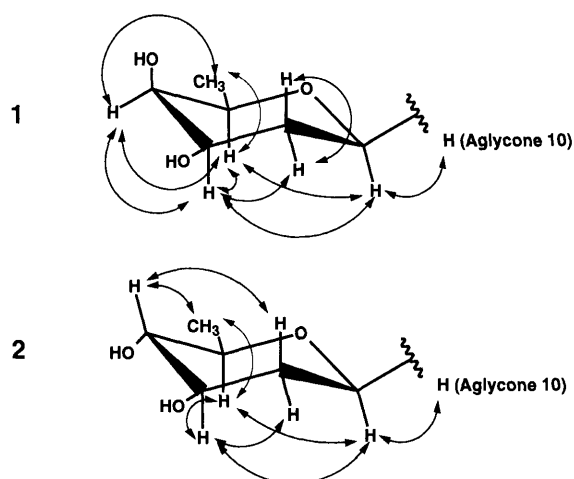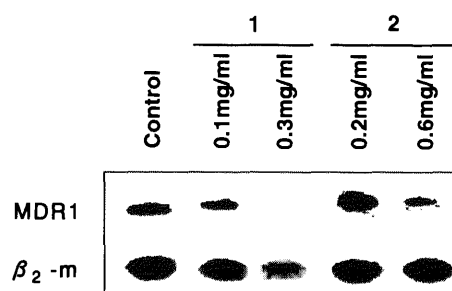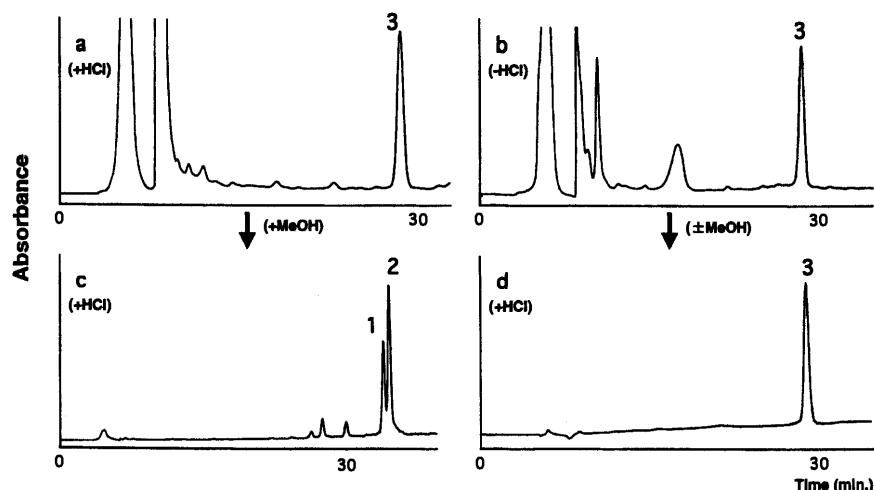
Fig. 3.   HPLC Chromatogram in Isolating 1 and 2

a) Chromatogram of the broth of KS12571 (with HCl conditions); HPLC conditions: system, Shimadzu LC-8A system; column, TSK-Gel ODS-80Ts (55 mm i.d.×30 cm, Tosoh Ltd.); flow rate, 80 ml/min; mobile phase, linear gradient from A to B in 30 min (solvent A, 30% CH_3CN containing 0.1% HCl; B, 45% CH_3CN containing 0.1% HCl); detection, UV 220 nm; sample concentration, 30 mg/ml (MeOH); injection volume, 10 ml.   b) Chromatogram of the broth of KS12571 (without HCl conditions); HPLC conditions: mobile phase, linear gradient from A to B in 35 min (solvent A, 25% CH_3CN; B, 60% CH_3CN); other conditions were as for chromatogram (a).   c) Chromatogram of the fractionated peak 3 in (a); HPLC conditions: column, Shim-pack PREP-ODS (H) column (20 mm i.d.×25 cm, Shimadzu Corp.); flow rate, 10 ml/min; mobile phase, linear gradient from A to B in 40 min (solvent A, 25% CH_3CN containing 0.1% HCl; B, 45% CH_3CN containing 0.1% HCl); other conditions were as for chromatogram (a).   d) Chromatogram of the fractionated peak 3 in (b); HPLC conditions were as for chromatogram (a).
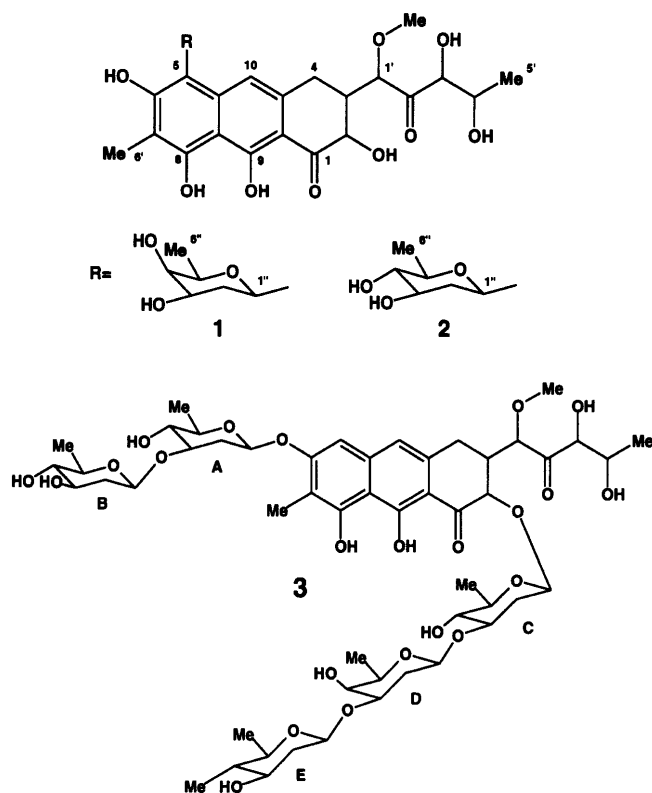

Chart 1

pound, was easily hydrolyzed.

The carbohydrate structure of aureolic acid is thought to be important because it regulates its binding to DNA. Indeed, an NMR study showed that mithramycin and chromomycin, which differ only in carbohydrate structure, had different binding regions for DNA and different anti-tumor activities.[14] Therefore, several attempts have been made to create more useful aureolic acid analogues by the modification of their carbohydrate structures.[15] Further study of this reaction

would contribute to the creation of novel useful aryl C-glycoside analogues, not only of the aureolic acids, but of other aryl bioactive compounds.[16]

Also, we are now investigating the *MDR1* repressing activity of mithramycin and other aureolic acids. The results will be described in another paper.

Experimental

All melting points were determined on a Yanagimoto micromelting point apparatus and are uncorrected. Spectroscopic measurements were done with the following instruments: Hitachi U-2000 spectrometer (UV), Shimadzu FTIR-8700 (IR), JEOL JMS-700 (MS), Bruker DRX-500 (500 MHz-NMR), JASCO DIP-360 (optical rotation).

Bacterial Strain   The *Streptomyces* sp., named KS12571, was isolated from a soil sample collected in Ibaraki Prefecture, Japan by a method previously described.[17] Identification of the species was performed by Japan Food Research Laboratories.

Repression of the MDR1 Gene Expression   SBC-3/ADM tumor cells were cultured for 48 h in RPMI1640 medium (Gibco BRL.) containing 2 μl doxorubicin (Sigma-Aldrich). The medium was replaced with RPMI1640 medium containing 0.1—0.6 mg/ml 1 or 2. The cells were cultured for 48 h and the mRNA was collected and tested. The cultivation was done at 37 °C under a humidified 5% CO_2 atmosphere. SBC-3/ADM tumor cells were kindly provided by Dr. N. Saijo (National Cancer Center-Japan).

RNA Preparation, Reverse Transcription, and cDNA-PCR   Total cellular RNA was isolated using a Trizol kit (Life Technologies, Inc.). Total RNA(3 μg) was used for reverse transcription and cDNA-PCR, using an RNA PCR kit (AMV) Ver.2.1 (Takara). Primers *MDR1*-F (5'-cgc cat tgc acg tgc cct gg) and *MDR1*-R (5'-cct ttc tct ttc atg agt tc) were used to amplify *MDR1*. Primers β_2-m-F (acc ccc act gaa aaa gat ga) and β_2-m-R (atc ttc aaa cct cca tga tg) were used to amplify β_2-m. β_2-m was used as a control to check the integrity of RNA preparations and accuracy of the dilutions, as well as to demonstrate that the effect of mithramycin on *MDR1* expression in SBC-3/ADM tumor cells was not due to nonspecific decreases in transcription. PCR was performed for 15 and 20 cycles on the dilution of cDNA.

Spectroscopic Data   **1**: mp 121—124 °C (dec.). HR-FAB-MS *m/z*: 551.2136 (Calcd for $C_{27}H_{35}O_{12}$ (M+H)$^+$ 551.2128). $[\alpha]_D^{22}$ +91.3° (c=0.1, MeOH). IR (KBr) cm^{-1}: 1629, 1265, 1188, 1094, 1063. UV λ_{max} (MeOH) nm (log ε): 420 (3.92), 326 (3.81), 282 (4.58), 233 (4.40), λ_{min} (MeOH) nm (log ε): 358 (3.56), 318 (3.77), 251 (4.14), 219 (4.31).

2: mp 127—131 °C (dec.). HR-FAB-MS *m/z*: 551.2141 (Calcd for $C_{27}H_{35}O_{12}$ (M+H)$^+$ 551.2128). $[\alpha]_D^{22}$: +92.0° (c=0.1, MeOH). IR (KBr) cm^{-1}: 1628, 1261, 1186, 1070. UV λ_{max} (MeOH) nm (log ε): 419 (3.94),

324 (3.76), 282 (4.59), 233 (4.40), λ_{min} (MeOH) nm (log ε), 353 (3.46), 317 (3.72), 252 (4.13), 219 (4.31).

3: The mithramycin isolated from KS12571 was consistent with the authentic compound purchased from Sigma-Aldrich. mp 180—183 °C (lit. 180—183 °C), $[\alpha]_D^{22}$: $-44.9°$ (c=0.1, MeOH), the authentic: mp 180—183 °C, $[\alpha]_D^{22}$: $-44.3°$ (c=0.1, MeOH).

References

1) Redwood W. R., Colvin M., *Cancer Res.*, **40**, 1144—1149 (1980); Godwin A. K., Meister A., O'Dwyer P. J., Huang C. S., Hamilton T. C., Anderson A. E., *Proc. Natl. Acad. Sci. U.S.A.*, **89**, 3070—3074 (1992).

2) Hamada H., Tsuruo T., *Proc. Natl. Acad. Sci. U.S.A.*, **83**, 7785—7789 (1986); Tsuruo T., *Jpn. J. Cancer Res. (Gann)*, **79**, 285—296 (1988).

3) Fojo A. T., Ueda K., Slamon D. J., Poplack D. G., Gottesman M. M., Pastan I., *Proc. Natl. Acad. Sci. U.S.A.*, **84**, 265—269 (1987).

4) Tsuruo T., Iida H., Tsukagoshi S., Sakurai Y., *Cancer Res.*, **41**, 1967—1972 (1981); *Idem, ibid.*, **42**, 4730—4733 (1982).

5) Slater L. M., Sweet P., Stupecky M., Gupta S., *J. Clin. Invest.*, **77**, 1405—1408 (1986); Saeki T., Ueda K., Tanigawa Y., Hori R., Komano T., *FEBS Lett.*, **324**, 99—102 (1993).

6) Sato W., Fukazawa N., Nakanishi O., Baba M., Suzuki T., Yano O., Naito M., Tsuruo T., *Cancer Chemother. Pharmacol.*, **35**, 271—277 (1995); Mayer U., Wagebar E., Dorobek B., Beijnen J. H., Borst P., Schinkel A. H., *J. Clin. Invest.*, **100**, 2430—2436 (1997); Naito M., Tsuruo T., *Cancer Chemother. Pharmacol.*, **40**, S20—S24 (1997).

7) Yoshimura Y., Koenuma M., Matsumoto K., Tori K., Terui Y., *J. Antibiot.*, **41**, 53—67 (1988); Katahira R., Uosaki Y., Ogawa H., Yamashita Y., Nakano H., Yoshida M., *ibid.*, **51**, 267—274 (1998).

8) Kiura K., Ohnoshi T., Ueoka H., Takigawa N., Tabata M., Segawa Y., Shibayama T., Kimura I., *Anti-Cancer Drug Res.*, **7**, 463—470 (1992).

9) Grundy W. E., Goldstein A. W., Rickher C. J., Hanes M. E., Varren H. B., Sylvester J. C., *Antibiot. Chemother.*, **3**, 1215—1217 (1953); Berlin Y. A., Kiseleva O. A., Kolosov M. N., Shemyakin M. M., Soifer V. S., Vasina I. V., Yartseva I. V., *Nature* (London), **218**, 193—194 (1968).

10) Uchida T., Imoto M., Watanabe Y., Miura K., Dobashi T., Matsuda N., Sawa T., Naganawa H., Hamada M., Takeuchi T., Umezawa H., *J. Antibiot.*, **38**, 1171—1181 (1985); Drautz H., Zahner H., *ibid.*, **39**, 1657—1669 (1986).

11) Devi P. U., Ganasoundari A., Rao B. S. S., Srinivasan K. K., *Radiat. Res.*, **151**, 74—78 (1999).

12) Omura S., Nakagawa A., Fukamachi N., Miura S., Takahashi Y., Komiyama K., Kobayashi B., *J. Antibiot.*, **41**, 812—813 (1988); Kawashima A., Yoshimura Y., Goto J., Nakaike S., Mizutani T., Hanada K., Omura S., *ibid.*, **41**, 1913—1914 (1988).

13) Sehgal S. N., Czerkawshi H., Kudelski A., Pandev K., Saucier R., Vezina C., *J. Antibiot.*, **36**, 355—361 (1983).

14) Keniry M. A., Banville D. L., Simmonds P. M., Shafer R., *J. Mol. Biol.*, **231**, 753—767 (1993).

15) Binkley R. W., Sivik M. R., *J. Carbohydr. Chem.*, **10**, 399—416 (1991); Sebasta D. P., Roush W. R., *J. Org. Chem.*, **57**, 4799—4802 (1992); Vasella A., *Pure Appl. Chem.*, **70**, 425—430 (1998).

16) Matsumoto T., Katsuki M., Jona H., Suzuki K., *J. Am. Chem. Soc.*, **113**, 6982—6992 (1991); Kuribayashi T., Ohkawa N., Satoh S., *Tetrahedron Lett.*, **39**, 4537—4540 (1998); *Idem, ibid.*, **39**, 4540—4541 (1998).

17) Tagashira M., Nozato N., Isonishi S., Okamoto A., Ochiai K., Ohtake Y., *Biosci. Biotech. Biochem.*, **63**, 1953—1958 (1999).

The Controlled Release of a Drug from Biodegradable Chitosan Gel Beads

Kyoko Kofuji,* Tomohiro Ito, Yoshifumi Murata, and Susumu Kawashima

Faculty of Pharmaceutical Sciences, Hokuriku University, Ho-3, Kanagawa-machi, Kanazawa 920–1181, Japan.

Chitosan (CS) forms a gel in solutions with a pH above 12, and the gelation occurs at pH of about 9 in 10% amino acid solutions. In this paper, we investigated the enzymatic degradation and the drug release profile of this novel CS gel beads. The degradability of the CS gel beads was affected by the CS properties, *e.g.* the degree of deacetylation. The release of prednisolone (PS), as a model drug, from the CS gel beads was sustained significantly compared with the gel prepared with NaOH only. However, the release was not able to be sustained by the increment of NaOH concentration in the solution employed for the preparation of CS gel beads. We also investigated the control of drug release from CS gel beads by application of a complex formed between chondroitin sulfate (Cho) and CS. The release of PS from the CS gel beads treated with Cho was prolonged, and the release pattern was not affected by the treatment time. The time to 50% drug release was about 5 min with PS powder, about 200 min in CS gel beads with 10% glycine (Gly) (pH 9.0), and about 330 min in the CS gel beads with 10% Gly (pH 9.0) treated with Cho. Thus CS gel beads appear promising as a vehicle for sustained drug delivery, and the degradation of CS gel beads may be controlled by the degree of deacetylation of CS.

Key words chitosan; chondroitin sulfate; gel; biodegradation; amino acid

The polysaccharide chitosan (CS) is known to be an excellent material for drug preparation. CS is a plentiful natural biopolymer and is also non-toxic, biocompatible and biodegradable.[1—5] These properties are important for materials that are implanted in the body, because such materials must avoid the host's defense system during their long-term contact with living structures.[6] CS has been studied as a unique vehicle for the sustained delivery of drugs; in addition, the preparation of CS microspheres has been examined.[7—9] We have been investigating the preparation of a suitable vehicle, for example micro-gel beads, for intra-articular injection in rheumatoid arthritis to allow sustained intra-articular drug delivery. Lu *et al.*[10] described that CS could act on the epiphyseal cartilage and wound healing of articular cartilage. Therefore, we considered CS might be able to utilize as a wound healing of articular cartilage after accomplishment of a role as a vehicle for drug. In the previous study, we found that CS could form sphere gel at a pH of about 9 in amino acid solutions despite usually CS formed a gel in solutions with a pH above 12.[11] We consider that the phenomenon is coacervation. Preparations made at a lower pH are preferable in terms of their effects on the solubility or stability of the drug contained in the gel beads and on the tissue into which they are injected. Steroids have been applied for intra-articular injection therapy in rheumatoid arthritis. Under such conditions, it is difficult to achieve a sustained intra-articular drug level only on the basis of drug solubility. During *in vivo* degradation, the drug release will be governed by both diffusion and biodegradation of the matrix. Therefore, in this study, we investigated the biodegradability and *in vitro* drug release profiles from this novel CS gel beads. Furthermore, we attempted to control the drug release from the CS beads by modifying the structure of gel matrix.

Experimental

Materials CS with various degrees of deacetylation [70% (7B), 80% (8B)] was purchased from Katokichi Co. Ltd. (Japan). The molecular weights of the CS were 2210000 (7B) and 2140000 (8B).[2] Prednisolone (PS) was purchased from Nacalai Tesque Inc. (Japan). Egg-white lysozyme (activity 0.8 mg/mg) and chondroitin sulfate C sodium salt (Cho) were purchased from Wako Pure Chemical Industries (Japan). The other reagents were obtained from Wako Pure Chemical Industries (Japan) and Nacalai Tesque Inc. (Japan).

Preparation of CS Gel Beads CS gel beads were prepared by the following method. CS (1% w/w) was dissolved in 0.1 M acetate buffer (pH 4.5). Then 1% PS was suspended to the CS solution. One gram of the suspension, theoretically containing 10 mg of drug, was dropped slowly into 20 ml of 10% glycine (Gly) solution using a pipette and left at room temperature for 25 min. Hydrogel beads were formed spontaneously. The dried gel beads were obtained by drying at 37 °C for 24 h on a dish, before being held under vacuum in a desiccator in the presence of P_2O_5. The diameter of dried gel bead with 10% Gly (pH 9.0) was about 3 mm. It consisted of Gly (50.7%), PS (12.3%), CS (12.6%). Gly was determined according to the method of Watanabe and Imai.[12]

Preparation of CS–Cho Gel Beads CS hydrogel beads prepared by the method described above were soaked in 20 ml of 1% Cho solution (1—48 h). The gel beads were removed from the Cho solution and dried at 37 °C for 24 h on a dish, before being held under vacuum in a desiccator in the presence of P_2O_5.

Enzymatic Degradation of CS Gel Beads Lysozyme solution (20 μg/ml in 0.1 M phosphate buffer, pH 7.2, containing 0.2 M sodium chloride) was incubated at 37 °C. The dried gel beads were added to 10 ml of the solution in a 100-ml sample bottle and incubated at 37 °C. The beads were retrieved periodically and dried at 37 °C for 24 h, before being held under vacuum in a desiccator in the presence of P_2O_5. The weight of each dried gel bead preparation was measured. The extent of degradation was expressed as the percentage of residual weight of the gel beads after soaking in the lysozyme solution. In this experiment, CS gel beads was also soaked in 0.1 M phosphate buffer (pH 7.2) without lysozyme for 30 min to remove Gly, and their dry weight was adopted as the weight of CS gel beads that did not degrade at all.

Dissolution Test Release of PS from the various types of CS gel beads into 0.1 M phosphate buffer (pH 7.2) was determined. The dried gel beads corresponding to 1 g of hydrogel were added to 500 ml of the dissolution medium in a JP XIII dissolution test apparatus (paddle method, 100 rpm, 37 °C). A 4-ml aliquot of the solution was removed periodically for analysis and replaced with 4 ml of the dissolution medium (pre-warmed to 37 °C) to maintain a constant volume. The absorbance of each sample was determined on a Hitachi model 200-20 spectrophotometer at 246 nm. All the dissolution tests were performed in triplicate.

Results and Discussion

Enzymatic Degradation of CS Gel Beads In general, mucopolysaccharides are degraded by enzymatic hydrolysis; the degradation of CS has been reported.[1—6] In a previous study, the viscosity of CS solutions became gradually lower
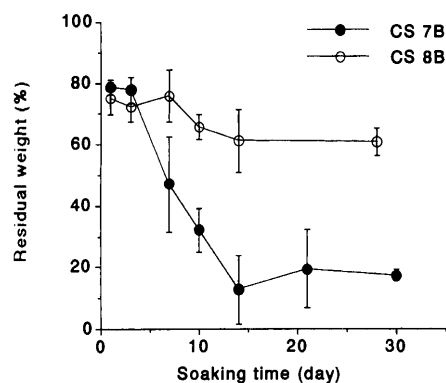
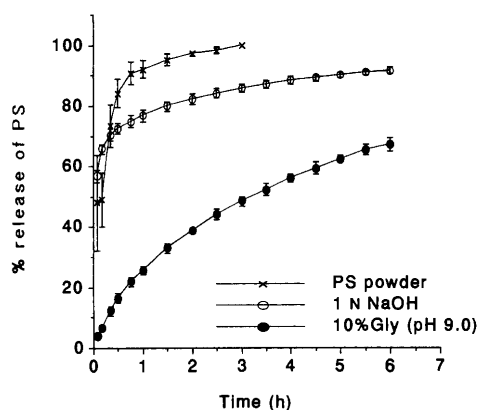Fig. 1. Effect of Deacetylation of CS on the Enzymatic Degradation of CS Gel Beads

Fig. 2. Effect of Amino Acid Addition in the Preparing Solution on the Release of PS from CS (7B) Gel Beads
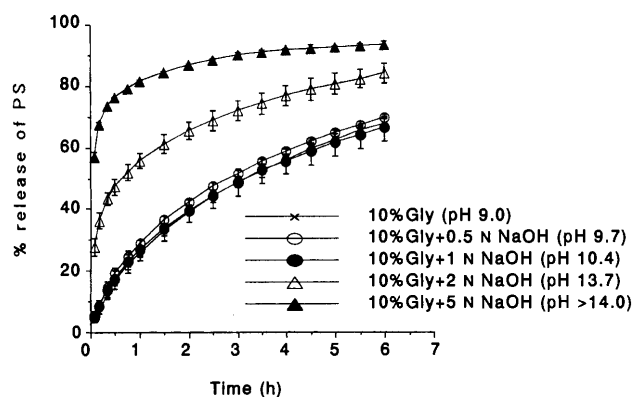

Fig. 3. Effect of NaOH Addition to 10% Gly Solution on the Release of PS from CS (7B) Gel Beads

Fig. 4. Effect of Cho Treatment of CS Gel Beads on the Release of PS

in the presence of lysozyme. The degradation was affected by the CS properties, e.g. the degree of deacetylation, and 100% deacetylated CS was not degraded.[11] The degradation of CS gel beads in 0.1 M phosphate buffer containing lysozyme was investigated. The weight of dried gel beads on CS (7B) began to decrease after 3 d. However, on CS (8B), the loss of weight of the dried gel beads was slight (Fig. 1). Tomihata and Ikada[6] described that the in vitro and in vivo degradations of the CS films, prepared by the solution casting method, occurred less rapidly as their degree of deacetylation became higher, and the films which were more than 73% deacetylated CS showed slower biodegradation. The degradability of the gel may differ with the gel preparation method. However, the degradability of the CS gel beads prepared with 10% amino acid solutions (pH 9.0) was similar to the gel prepared with NaOH only or by the solution casting method. Thus it may be possible to control the degradability of CS gel beads by taking advantage of the differences in degradability of the various species of CS with different degrees of deacetylation.

Retention of PS in CS Gel Beads CS solutions suspending less than 5% PS were able to maintain the spherical shape of the gel beads. The amount of PS retained in the beads decreased according to the increase in the soaking time or the amount of NaOH in 10% Gly solution. PS was retained in the gel beads, which maintained a spherical shape, to about 85—100% of the theoretical total amount.

Profile of PS Release from CS Gel Beads Sustained release of PS from CS gel beads prepared with 10% Gly (pH 9.0) was observed. As shown in Fig. 2, all the PS retained

within the beads was released gradually. However, in the case of the gel beads prepared using 1 N NaOH, the PS release was faster because the beads could not maintain a spherical shape. Also, as shown in Fig. 3, PS was released faster from CS gel beads prepared using the above 2 N NaOH solution, despite the presence of 10% amino acid, because the gel beads could not maintain a spherical shape in the process of removal from the solutions or drying. The PS release pattern was virtually unaffected by increasing the preparation time or changing the species of CS (7B, 8B). Thus, the sustained release was not attributable to the insolubility of the drug, but to its retention in the CS gel matrix.

Profile of PS Release from CS–Cho Gel Beads Changing the gel matrix by utilizing complex formation between CS and other mucopolysaccharides, such as Cho or hyaluronic acid (HA), may be more effective for controlling the release of a drug because the amino group of CS may form an electrostatic complex with the carboxyl group of Cho or HA.[13,14] As shown Fig. 4, the release of PS from the CS–Cho gel beads, which had been soaked for 6 h in 1% Cho solution, was inhibited. We concluded that the complex between CS and Cho was formed the surface of CS gel beads, because the pattern of drug release was not changed by changing the soaking time. The retention of PS in the gel beads decreased as the soaking time increased. However, about 70% of the theoretical total amount of PS was retained in the gel beads, even after the beads had been soaked for 6 h in the Cho solution.

Thus CS gel beads appear promising as a vehicle for sus-

tained drug delivery, and the degradation of CS gel beads may be controlled by the degree of deacetylation of CS. However, *in vivo*, the degradability of CS gel beads will also be affected by enzymes, body constituents and application conditions. Further studies of the effects of these factors should be performed.

References and Notes

1) Sashiwa H., Saimoto H., Shigemasa Y., Ogawa R., Tokura S., *Int. J. Biol. Macromol.*, **12**, 295—296 (1990).
2) Yomota C., Komuro T., Kimura T., *Yakugaku Zasshi*, **110**, 442—448 (1990).
3) Machida Y., Nagai T., Abe M., Sannan T., *Drug Design and Delivery*, **1**, 119—130 (1986).
4) Hirano S., Tsuchida H., Nagao N., *Biomaterials*, **10**, 574—576 (1989).
5) Onishi H., Machida Y., *Biomaterials*, **20**, 175—182 (1999).
6) Tomihata K., Ikada Y., *Biomaterials*, **18**, 567—575 (1997).
7) Oungbho K., Müller B. W., *Int. J. Pharm.*, **156**, 229—237 (1997).
8) Jameela S. R., Jayakrishnan A., *Biomaterials*, **16**, 769—775 (1995).
9) Kawashima Y., Handa T., Kasai A., Takenaka H., Lin S. Y., Ando Y., *J. Pharm. Sci.*, **74**, 264—268 (1985).
10) Lu J. X., Prudhommeaux F., Meunier A., Sedel L., Guillemin G., *Biomaterials*, **20**, 1937—1944 (1999).
11) Kofuji K., Shibata K., Murata Y., Miyamoto E., Kawashima S., *Chem. Pharm. Bull.*, **47**, 1494—1496 (1999).
12) Watanabe Y., Imai K., *J. Chromatogr.*, **239**, 723—732 (1982).
13) Murata Y., Miyamoto E., Kawashima S., *J. Control. Release*, **38**, 101—108 (1996).
14) Denuziere A., Ferrier D., Damour O., Domard A., *Biomaterials*, **19**, 1275—1285 (1998).

Four New Furanone-Coumarins from *Clausena excavata*[1)]

Yuko Takemura,[a] Keiko Nakamura,[a] Tomiko Hirusawa,[a] Motoharu Ju-ichi,[*,a] Chihiro Ito,[b] and Hiroshi Furukawa[b]

Faculty of Pharmaceutical Sciences, Mukogawa Women's University,[a] Nishinomiya, Hyogo 663–8179, Japan and Faculty of Pharmacy, Meijo University,[b] Tempaku, Nagoya 468–8503, Japan.
Received October 27, 1999; accepted December 16, 1999

Four new furanone-coumarins, clauslactones-N (4), -O (5), -P (6) and -Q (7) were isolated from the leaves and twigs of *Clausena excavata* BURM. f. (Rutaceae) collected in Indonesia and their structures were elucidated by spectroscopic analysis.

Key words furanone-coumarin; clauslactone; *Clausena excavata*; Rutaceae

Recently we reported[2)] the isolation and structure elucidation of three new coumarins, named clauslactones-K (1), -L (2) and -M (3), from the twigs and leaves of Indonesian *Clausena excavata* BURM. f. (Rutaceae) which have been used as folk medicine for treatment of dermatopathy in Sumatra. Further investigation resulted in the isolation of four additional new coumarins and we now wish to report the structural elucidation of these compounds.

Clauslactone-N (4) was obtained as a colorless oil, $[\alpha]_D$ +58.6° (CHCl$_3$). The molecular formula was determined as C$_{20}$H$_{22}$O$_7$ by high resolution (HR)-MS which showed a molecular ion at m/z 374.1314. The UV absorption [258 (sh), 318 nm], IR bands (1727, 1609 cm^{-1}) and ^{1}H-NMR signals [δ 7.63, 6.27 (each 1H, d, J=9.2 Hz), 7.15, 6.86 (each 1H, d, J=8.8 Hz) characteristic to H-4, H-3, H-5 and H-6] indicated the existence of a 7, 8-disubstituted coumarin skeleton.[3)] The resonances at δ 4.71 (2H, d, J=6.2 Hz), 5.62 (1H, t, J=6.2 Hz), 1.82 (3H, s), 2.50 (1H, dd, J=14.3, 7.7 Hz) and 2.37 (1H, dd, J=14.3, 7.7 Hz) in the ^{1}H-NMR spectrum and δ 66.0 (t), 123.0 (d), 136.3 (s), 17.2 (q) and 44.9 (t) in the ^{13}C-NMR spectrum were assigned to the signals of the partial structure –O–CH$_2$–CH=C(CH$_3$)–CH$_2$–. The signals due to α-methyl [δ 1.51 (3H, s)], β-methylene [δ 1.79 (1H, dd, J=13.6, 5.5 Hz), 2.44 (1H, dd, J=13.6, 5.5 Hz)], γ-methine

proton [δ 4.79 (1H, m)] on the lactone ring were also observed. To confirm the structure of the side chain, the ^2J and ^3J connectivities were examined by ^{1}H-detected heteronuclear multiple bond connectivity (HMBC) experiments (Fig. 1). The signal of a methyl group at δ_H 1.51 (17-Me) showed cross peaks with the carbon signals at δ_C 42.5 (C-16), 73.7 (C-17) and 177.5 (C-18). The proton signal at δ_H 2.44 (H$_A$-16) showed cross peaks with the carbon signals at δ_C 177.5 (C-18) and 73.7 (C-17). The proton signal at δ_H 1.79 (H$_B$-16) showed cross peaks with the carbon signals at δ_C 44.9 (C-14), 76.2 (C-15) and 24.2 (17-Me). The proton signals at δ_H 2.37 and 2.50 (H-14) showed cross peaks with the carbon signals at δ_C 76.2 (C-15), 42.5 (C-16), 136.3 (C-13), 123.0 (C-12) and 17.2 (13-Me). These connectivities established the structure of the side chain. In the differential nuclear Overhauser effect (NOE) experiments, irradiation of the methylene signal at δ 4.71 showed 12% increments on the signal at δ 6.86 (H-6) suggesting the location of the methoxy group at C-8. When the methyl signal at δ 1.82 was irradiated, 3%, 4% and 7% enhancement were observed for the signals at δ 4.71 (H-11), 4.79 (H-15) and 2.44 (H$_A$-16). Irradiation of the methyl signal at δ 1.51 (17-Me) showed a 5% increment to the signal at δ 1.79 (H$_B$-16). These results supported the E regiochemistry between C-12 and C-13, and the structure around the lactone ring was assigned as shown in structure 4.

Clauslactone-O (5) was isolated as a colorless oil, $[\alpha]_D$ +24.3° (CHCl$_3$), and the molecular formula was determined as C$_{19}$H$_{20}$O$_6$ from HR-MS analysis. The UV, IR absorptions and the signal patterns in the ^{1}H- and ^{13}C-NMR spectrum of
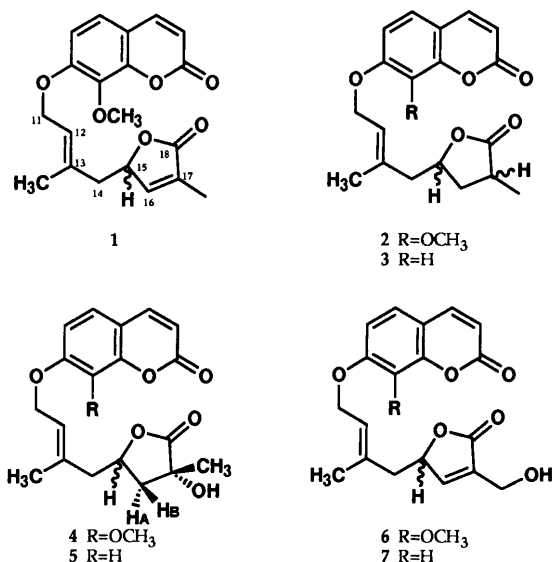
Chart 1. Structures of Coumarins Isolated from *Clausena excavata*

Fig. 1. C–H Long-Range Correlations in the HMBC Spectrum of Clauslactone-N (4)

Fig. 2. C–H Long-Range Correlations in the HMBC Spectrum of Claus-lactone-O (5)

clauslactone-O were similar to those of **4** (see Table 1). The diagnostic difference was the lack of a methoxy signal and the appearance of ABC type signals for aromatic protons [δ 7.38 (1H, d, $J=8.8$ Hz), 6.85 (1H, dd, $J=8.8$, 2.2 Hz), 6.81 (1H, d, $J=2.2$ Hz)] in the ^{1}H-NMR spectrum. The regio-chemistry between C-12 and C-13 was determined as E by differential NOE experiment (see Experimental). Thus, the structure of clauslactone-O was assumed to be **5** and rigorous confirmation of the structure was carried out by HMBC experiments (Fig. 2).

Clauslactone-P (**6**) was obtained as colorless cubes, mp 126—128 °C, $[\alpha]_D$ $-6.8°$ (CHCl$_3$). The molecular formula was determined as C$_{20}$H$_{20}$O$_7$ by HR-MS, which showed a molecular ion at m/z 372.1182. The IR and UV absorptions suggested the presence of a 7,8-dioxygenated coumarin skeleton.[3] The ^{1}H-NMR spectrum of **6** showed characteristic signals at δ 7.61 (1H, d, $J=9.8$ Hz), 6.26 (1H, $J=9.8$ Hz), 7.15 (1H, d, $J=8.6$ Hz) and 6.85 (1H, d, $J=8.6$ Hz) due to H-4, H-3, H-5 and H-6 of coumarin skeleton. The signals at δ 4.71 (2H, d, $J=6.4$ Hz), 5.64 (1H, dt, $J=0.9$, 6.4 Hz), 1.84 (3H, s), 2.50 (1H, dd, $J=5.9$, 14.1 Hz) and 2.45 (1H, dd, $J=7.7$, 14.1 Hz) indicated the presence of the partial structure –O–CH$_2$–CH=C(CH$_3$)–CH$_2$–. The presence of a 2-hydroxymethyl 4-substituted α,β-unsaturated γ-lactone moiety was suggested by the signals at δ 7.25 (1H, dd, $J=3.0$, 1.7 Hz), 5.11 (1H, ddt, $J=1.7$, 1.7, 5.6 Hz), 4.43 (2H, t, $J=1.7$ Hz) in the ^{1}H-NMR spectrum and the signals at δ 172.1 (s), 148.5 (d), 134.0 (s), 80.4 (d), 57.2 (t) in the ^{13}C-NMR spectrum. In the differential NOE experiment (acetone-d_6), irradiation at δ 1.87 (13-Me) gave 4% enhancement at δ 4.79 (H-11), therefore the regiochemistry between C-12 and C-13 was determined as E. From the above data, we assigned the structure **6** to clauslactone-P.

Clauslactone-Q (**7**) was isolated as colorless cubes, mp 168—170 °C, $[\alpha]_D$ $-9.3°$ (CHCl$_3$). The HR-MS showed a molecular ion at m/z 342.1108 consistent with a molecular formula C$_{19}$H$_{18}$O$_6$. The IR and UV absorptions, ^{1}H- and ^{13}C-NMR signal patterns of **7** resembled those of **6** (see Table). The remarkable differences were the lack of a methoxy signal and the appearance of ABC signals at δ 7.62 (1H, d, $J=8.5$ Hz), 7.00 (1H, d, $J=2.6$ Hz) and 6.95 (1H, dd, $J=8.5$, 2.6 Hz) due to aromatic protons on the coumarin skeleton. From these data, the structure of clauslactone-Q was deduced as **7**.

In the previous paper,[2] we described the regiochemistry

around C-12 and C-13 of the side chains of clauslactones -K (1), -L (2) and -M (3) as Z. Upon further examination by differential NOE, irradiation of the 13-methyl signals gave 4% NOE for the 11-methylene signals (see Experimental). This result revealed the E geometry around C-12 and C-13, therefore the structure should be corrected as shown in this paper.

Experimental

Melting points were measured on a Yanagimoto micromelting point hotstage apparatus and are uncorrected. Optical rotations were measured on a JASCO DIP-360 polarimeter. ^{1}H- and ^{13}C-NMR, NOE and HMBC spectra were recorded on an A-400 or A-600 (JEOL) spectrometer. Chemical shifts are shown in δ values (ppm) with tetramethylsilane (TMS) as an internal reference. Electron impact (EI)- and HR-MS were taken with a JMS-HX 110 spectrometer. UV spectra were recorded on a Shimadzu UV 160A in EtOH, IR spectra on a Shimadzu IR-450 in $CHCl_3$. Preparative TLC was done on Kieselgel 60 F_{254} (Merck).

Isolation The eluates[2] of the silica gel column chromatography of the acetone and MeOH extract obtained from dried twigs and leaves (2.5 kg) were subjected to repeated silica gel column and preparative thin-layer chromatography [solvent; acetone–$CHCl_3$ (1 : 9 or 2 : 8); AcOEt–benzene (3 : 7, 1 : 1 or 7 : 3); AcOEt–n-hexane (7 : 3)]. Clauslactone-N (4) (4.4 mg) and -O (5) (1.9 mg) were obtained from the CH_2Cl_2 eluate (56.47 g) and clauslactone-P (6) (3.1 mg) and -Q (7) (7.4 mg) were isolated from the acetone–CH_2Cl_2 eluate (17.82 g).

Clauslactone-N (4): Colorless oil, $[\alpha]_D$ +58.6° (c=0.293, $CHCl_3$). HR-MS Calcd for $C_{20}H_{22}O_7$: 374.1366. Found: 374.1314. EI-MS m/z: 374 [M]$^+$, 192 (base peak), 164. UV λ_{max}: 208, 258 (sh), 318 nm. IR ν_{max} cm^{-1}: 3500, 1768, 1727, 1609. ^{1}H- and ^{13}C-NMR see Table 1. Differential NOE: irradiation at δ 1.82 (13-Me)—3%, 4% and 7% enhancement at δ 4.71 (H-11), 4.79 (H-15) and 2.44 (H$_A$-16); irradiation at δ 4.71—12%, 5% and 5% enhancement at δ 6.86 (H-6), 1.82 (13-Me) and 5.62 (H-12); irradiation at δ 1.51 (17-Me)–5% enhancement at δ 1.79 (H$_B$-16).

Clauslactone-O (5): Colorless oil, $[\alpha]_D$ +24.3° (c=0.0775, $CHCl_3$). HR-MS Calcd for $C_{19}H_{20}O_6$: 344.1259. Found: 344.1266. EI-MS m/z: 344 [M]$^+$, 165, 163, 162 (base peak), 155, 137, 134. UV λ_{max}: 204, 221(sh), 295 (sh), 323 nm. IR ν_{max} cm^{-1}: 3577, 1772, 1730, 1614. ^{1}H- and ^{13}C-NMR see Table 1. Differential NOE: irradiation at δ 1.84 (13-Me)—2%, 4% and 8% enhancement at δ 4.63 (H-11), 4.81 (H-15) and 2.46 (H$_A$-16); irradiation at δ 4.63—3% and 11% enhancement at δ 6.85 (H-6) and 6.81 (H-8).

Clauslactone-P (6): Colorless cubes, mp 126—128 °C, $[\alpha]_D$ −6.8° (c=0.147, $CHCl_3$). HR-MS Calcd for $C_{20}H_{20}O_7$: 372.1209. Found: 372.1182. EI-MS m/z: 372 [M]$^+$, 354, 278, 192 (base peak), 162. UV λ_{max}: 204, 255 (sh), 320 nm. IR ν_{max} cm^{-1}: 1750, 1720, 1600. ^{1}H- and ^{13}C-NMR see Table 1. ^{1}H-NMR (acetone-d_6, δ): 7.87 (1H, d, J=9.5 Hz), 7.42 (1H, br d, J=1.8

Hz), 7.35 (1H, d, J=8.8 Hz), 7.08 (1H, d, J=8.8 Hz), 6.22 (1H, d, J=9.5 Hz), 5.67 (1H, br t, J=6.2 Hz), 5.20 (1H, ddd, J=1.8, 5.5, 7.7 Hz), 4.79 (2H, d, J=6.2 Hz), 4.26 (2H, br s), 3.90 (3H, s), 2.57 (1H, dd, J=5.5, 13.9 Hz), 2.41 (1H, dd, J=7.7, 13.9 Hz), 1.87 (3H, s). Differential NOE: irradiation at δ 1.87 (13-Me)—4% enhancement at δ 4.79 (H-11); irradiation at δ 4.79—3% and 15% enhancement at δ 1.87 and 7.08 (H-6); No enhancement was observed at any proton signal on irradiation of the 8-MeO signal at δ 3.90.

Clauslactone-Q (7): Colorless cubes, mp 168—170 °C, $[\alpha]_D$ −9.3° (c=0.160, $CHCl_3$). HR-MS Calcd for $C_{19}H_{18}O_6$: 342.1103. Found: 342.1108. EI-MS m/z: 342 [M]$^+$, 324, 181, 162 (base peak), 134. UV λ_{max}: 204, 280 (sh), 323 nm. IR ν_{max} cm^{-1}: 3400, 1750, 1720, 1600. ^{1}H- and ^{13}C-NMR see Table 1. Differential NOE: irradiation at δ 1.80 (13-Me)—5% enhancement at δ 4.69 (H-11); irradiation at δ 4.69—12%, 13% and 9% enhancement at δ 1.80, 7.00 (H-8) and 6.95 (H-6).

Differential NOE of Clauslactone-K (1), -L (2) and -M (3) Clauslactone-K (1): irradiation at δ 1.84 (13-Me)—4% and 5% enhancement at δ 2.41 (H-14) and 4.71 (H-11); irradiation at δ 1.91 (17-Me)—2% enhancement at δ 7.00 (H-16); Clauslactone-L (2): irradiation at δ 1.82 (13-Me)—4% enhancement at both δ 4.71 (H-11) and 4.50 (H-15); irradiation at δ 4.71—9% and 3% enhancement δ 6.86 (H-6) and 1.82 (13-Me); Clauslactone-M (3): irradiation at δ 1.83 (13-Me)—each 4% enhancement at δ 4.62 (H-11) and 4.50 (H-15); irradiation at δ 4.62—5%, 11% and 4% enhancement at δ 1.83, 6.81 (H-8) and 6.85 (H-6).

References and Notes

1) This work was presented at the 118th and 119th Annual Meetings of the Pharmaceutical Society of Japan, Kyoto, March, 1998 and Tokushima, March, 1999, Abstracts of Papers, Vol. 2, p.128 (1998) and Vol. 2, p. 155 (1999). Recently, Thuy et al. reported the isolation and structure elucidation of excavatins A—M. Excavatins-E, -G and -I seem to be identical to clauslactones-Q (7), -M (3) and -O (5), respectively. Thuy T. T., Ripperger H., Porzel A., Sung T. V., Adam G., *Phytochemistry*, **52**, 511—516 (1999).

2) Nakamura K., Takemura Y., Ju-ichi M., Ito C., Furukawa H., *Heterocycles*, **48**, 549—553 (1998).

3) Murray R. D. H., Mendez J., Brown S. A., "The Natural Coumarins, Occurrence, Chemistry and Biochemistry," John Wiley & Sons Ltd., New York, 1982, p. 27.

Temperature-Induced Crystallization and Compactibility of Spray Dried Composite Particles Composed of Amorphous Lactose and Various Types of Water-Soluble Polymer

Hirofumi TAKEUCHI, Takehiko YASUJI, Hiromitsu YAMAMOTO, and Yoshiaki KAWASHIMA*

Gifu Pharmaceutical University, 5–6–1 Mitahora-higashi, Gifu 502–8585, Japan.
Received November 8, 1999; accepted December 23, 1999

The purpose of this study was to investigate the temperature-induced crystallization and the compactibility of the composite particles containing amorphous lactose and various types of polymers. The composite particles were prepared by spray-drying an aqueous solution of lactose and various types of gel forming water-soluble polymers at various formulating ratios.

The stabilizing effect of hydroxypropylcellulose (HPC) and polyvinyl pyrrolidone (PVP) on amorphous lactose in the composite particles was smaller than that of sodium alginate in comparing at the same formulating ratios. The difference in the stability of amorphous lactose in the composite particles was attributed to the difference in the glass transition temperature (Tg) of the composite particles caused by the polymers formulated. The tensile strength of compacted spray-dried composite particles containing the polymers was higher than commercial lactose for direct tabletting (DCL21). The tensile strength of the composite particles was increased with an increase in water content in the particles. The difference in compactibility of the composite particles containing the different amount of polymer and water could be explained by the difference in Tg of the particles.

Key words   amorphous lactose; temperature-induced crystallization; tablet tensile strength; glass transition temperature; composite particle; water soluble polymer

Various types of polymers have been investigated to be formulated in the controlled releasing tablet.[1,2] However, polymeric materials are unsuitable for tabletting unless they are agglomerates because of their elastic and poorly flowing properties. In a previous paper,[3] we demonstrated that the spray-dried (SD) composite particles of a polymer with lactose possessed both a good compacting and controlled releasing property when used as a base of matrix tablets.

Lactose is a suitable material for combining with the polymeric materials, because it is widely used in tablet formulations due to its stable physical properties even in hygroscopic conditions. Spray-dried lactose is the first product specially designed for direct tabletting.[4] It has been reported that the compactibility of commercial spray-dried lactose was affected by the amount of amorphous lactose in the particles as well as the primary particle.[5] However, the amorphous lactose in the spray-dried particles is physically and thermally unstable.[6] Several workers have used amorphous lactose as an amorphous model substance. Stubberud *et al.* showed the effect of physically mixing polyvinyl pyrrolidone (PVP) with amorphous lactose on the crystallization of the amorphous lactose.[7] We have also reported that the temperature-induced and moisture-induced crystallization of amorphous lactose in a SD composite particle of lactose and sodium alginate was considerably depressed by the presence of the polymer in the particle.[8] The compaction properties of the composite particles with sodium alginate were found to be dependent on the sodium alginate content in the composite particle.[9]

The purpose of this paper was to investigate the effect of the types of polymers formulated to the composite particles on their thermo- and mechanophysical properties. The composite particles were prepared by spray drying solutions containing lactose and various types of gel-forming water soluble polymers. The temperature-induced crystallization of lactose in the composite particles and the compactibility of the composite particles were evaluated.

Experimental

Materials   Lactose (Pharmatose 450M, hereinafter-called Pharm. 450M) supplied from DMV, Netherlands was used as a base of direct tabletting filler. Sodium alginate (NSPLL), hydroxypropyl-cellulose (HPC-M) and PVP (Kollidon K90) were obtained from Kibun Food Chemifa, Japan, Nihonsouda, Japan and BASF, Germany, respectively. Commercial roller-dried β-lactose anhydrate (DCL21, DMV) was used as a reference of direct tabletting fillers.

Preparation of Spray-Dried Composite Particles   In preparation for SD composite particles, mixtures of lactose (Pharm. 450M) and various types of water-soluble polymers were completely dissolved at various formulating ratios in 3000 ml of distilled water. The aqueous solution was spray-dried using a rotary atomizing spray-dryer (Type L-12, Ohkawara Kakoki, Japan).[3] The resultant SD composite particles were more spherical with smoother surface than the original crystalline lactose (Pharm. 450M) and commercial lactose for direct tabletting (DCL21). Regardless of the types of water-soluble polymer in the SD composite particles, the amorphous state of lactose in the particles was verified by a halo pattern in powder X-ray diffraction analysis (RAD-1C, Rigaku, Japan).

Temperature-Induced Crystallization Studies   Temperature-induced crystallization of amorphous lactose in SD composite particles was measured with a differential scanning calorimeter (DSC 6200, Seiko Instrument Inc., Japan). The powder samples were dried in a vacuum oven at 80 °C (2 weeks) to remove the water from the samples (water content of samples: <0.1%) (10). Each sample (10 mg) was placed in the non-hermetically sealed aluminum sample pans, and scanned at a heating rate of 10 °C/min.

Measurement of Glass Transition Temperature (Tg)   To observe the glass transition of amorphous lactose, DSC analysis was performed at the heating rate of 20 °C/min in aluminum sample pans. To dry the sample and cancel the effect of the thermal history of each formulation before measurement of glass transition temperature (Tg), all amorphous mixtures were heated in the pans to about 150 °C and then cooled down to −50 °C by a liquid nitrogen cooling accessory at 20 °C/min. The Tg was calculated by using the half extrapolated heat capacity method.

Evaluation of Compactibility   The compactibility of SD composite particles was evaluated by means of tensile strength of the compacts. Compaction of SD composite particles was carried out using an Inston-type hydraulic press (Autograph AG 5000D, Shimadzu Co., Japan). The weighed sample (200 mg) was compacted at a compressing velocity of 10 mm/min under the compression pressure (100, 200 and 400 MPa) using a die with an 8.0 mm internal diameter and flat-faced punches. The compacts were diametrically compressed at a velocity of 0.5 mm/min using an Instron-type hydraulic press (Autograph AG 500D, Shimadzu Co., Japan) to measure the

---

* To whom correspondence should be addressed.

tablet crushing strength, which is force required to fracture the compacts. The tablet tensile strength (Ts) required to split the compressed tablets was calculated by the following equation[11]:

$$Ts = \frac{2F}{\pi DT} \tag{1}$$

where F (N) is the crushing force, D (m) and T (m) are the diameter and thickness of the compacts, respectively.

To observe the change in shape of the SD composite particles after tabletting, micrographs of the upper surface of tablets with SD composite particles were taken using a scanning electron microscope (JSM-T330, Nihon Denshi, Japan) at an accelerating voltage of 15 kV. Compacts prepared with 200 mg of particles at a compression pressure of 400 MPa were attached directly on the stage of the scanning electron microscope using a double-sided adhesive tape.

Results and Discussion

Stabilization of Amorphous Lactose in SD Composite Particles As reported in the previous paper,[8] the DSC thermographs of SD composite particles consisting of amorphous lactose and sodium alginate showed no exothermic peak at around 170 °C ascribed to transformation of amorphous to crystalline form of lactose, suggesting thermal stabilization of amorphous lactose in the composite particles with sodium alginate. To clarify the thermally stabilizing effect of the type of polymers on the crystallization of amorphous lactose in SD composite particles, different SD composite particles containing various types of water-soluble polymers such as HPC and PVP were prepared. The DSC analysis showed that the incorporation of the polymers into the SD composite particles led to a decrease in the exothermic peak areas at a temperature of around 170 °C, which represented the transformation of amorphous lactose to crystalline form (Fig. 1). Considering the area of an exothermic peak in DSC curves, the stabilizing effect of HPC and PVP was lower than sodium alginate.

In measuring the Tg of the dried SD composite particles with the polymers (water content: <0.1%), the values increased with increasing polymer content. The SD composite particles containing the sodium alginate showed a higher Tg than those with other polymers, HPC and PVP, at every formulating ratio of polymer (Fig. 2). The lines in Fig. 2 are depicted based on the Gordon Taylor equation[12,13]:

$$Tg_{mix} = \frac{w_1 Tg_1 + Kw_2 Tg_2}{w_1 + Kw_2} \tag{2}$$

where Tg_{mix}, Tg_1 and Tg_2 are the Tg of the mixture, polymer and amorphous lactose, respectively, and w_1 and w_2 are the weight fractions of polymers and lactose, respectively. K is a constant defined by the following equation:

$$K = \frac{\rho_1 Tg_1}{\rho_2 Tg_2} \tag{3}$$

where ρ_1 and ρ_2 are the density of polymer and amorphous material. Considering the Tg of original polymers (sodium alginate: 152±2 °C, HPC: 156±2 °C, and PVP: 176±1 °C), it was expected that the Tg of the composite particles with PVP was higher than that with sodium alginate and HPC. However, the measured Tg values of the composite particles containing sodium alginate were much higher than its theoretical line predicted by the Gordon–Taylor equation (Eq. 2).

Zografi and co-workers have reported a similar specific interaction which affected the Tg values for an amorphous
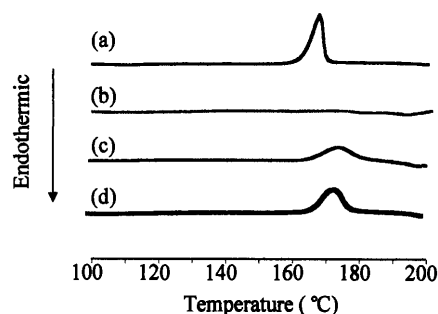

Fig. 1. DSC Thermographs of SD Composite Particles Containing Various Types of Water-Soluble Polymer

(a) None (100% amorphous lactose), (b) sodium alginate (NaAlg), (c) HPC, (d) PVP. Polymer content in SD composite particles: 10%.
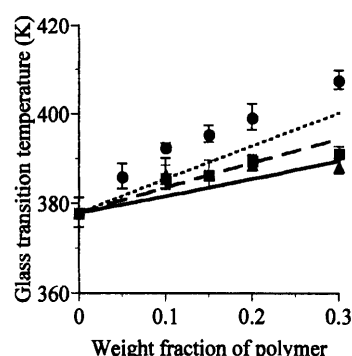

Fig. 2. Glass Transition Temperature (Tg) of SD Composite Particles (SDCP) with Various Types of Water-Soluble Polymer

(●) Sodium alginate, (▲) HPC, (■) PVP. The data are the average values of three runs. The lines show the predicted values from the Gordon Taylor equations; (———): SDCP with sodium alginate, (------): SDCP with HPC and (---) : SDCP with PVP.

mixture of indomethacin and PVP.[13] In this case, hydrogen bonds between the carboxyl group and the carbonyl group may play an important role in those interactions. The smaller change in Tg of the composite particles with HPC and PVP in increasing the polymer contents could explain the lesser thermal stability of the composite particles containing the sodium alginate.

Compactibility of SD Composite Particles The compactibility of SD composite particles was evaluated by comparing the tensile strength of tablets prepared with the composite particles containing the various types of polymers (Table 1). While the compactibility of SD composite particles with sodium alginate was markedly reduced when the sodium alginate content was higher than 20% in SD composite particles, the compactibility of the SD composite particles containing HPC and PVP was comparable to that of the SD amorphous lactose regardless of the polymer content.

To clarify the effect of the polymer type in the SD composite particles on the tablet tensile strength, the microstructure of tablets prepared with the SD composite particles was observed with scanning electron micrographs. The micrographs of the upper surface of the tablets are shown in Fig. 3. When the SD composite particles containing 30% of HPC or PVP were tabletted, a smooth surface of tablet was observed as well as those containing 10% of sodium alginate, suggesting occurrence of the fusion and cohesion of the SD composite particles during compression. These photographic observations clearly explain the difference in tensile strength of

these tablets.

To confirm the factors controlling the fusing and cohering properties of the particles, the effect of the moisture content in SD composite particles containing various formulating ratios of sodium alginate on their tensile strength was evaluated (Table 2). It is well known that the Tg values decrease with increasing the water content of lactose.[14] Irrespective of the sodium alginate content in the particles, the Tg values decreased as expected (Table 2). The tensile strength of tablet with SD composite particles containing 10% of sodium alginate was increased with increasing water content. The micrographs of the upper surface of the tablets with the SD composite particles revealed that the fusing and cohering property of the composite particles decreased with a decrease in water content in the composite particles (Fig. 4). The change in fusing property of the particles during compression can be explained by the change in the Tg of the composite particles (Table 2). However, the tensile strength of tablet prepared with the SD composite particles containing 30% sodium alginate was quite low even at the higher water content, although the particles having 6.3 or 8.8% water content possessed a low enough Tg to be fused. Based on these results, the compaction properties of the composite particles could be attributed to both the glass transition temperature of the composite particles and the bonding characteristics of the original polymers on the surface of composite particles.

Table 1. Tensile Strength of SD Composite Particles with Various Types of Water-Soluble Polymer: Sodium Alginate, HPC and PVP

Sample		Tensile strength (MPa)			
Polymer	Content	(C.P)	10 MPa	200 MPa	400 MPa
NaAlg	10		2.1 (0.1)	3.4 (0.1)	7.3 (0.7)[b]
	20		N.C.[a]	1.1 (0.1)	1.8 (0.3)
	30		N.C	N.C	0.7 (0.1)
HPC	10		1.8 (0.3)	3.1 (0.2)	7.0 (0.4)
	20		2.3 (0.1)	4.2 (0.3)	6.3 (0.5)
	30		2.1 (0.2)	3.5 (0.3)	6.4 (0.5)
PVP	10		2.4 (0.2)	5.5 (0.1)	7.2 (1.2)
	20		3.0 (0.3)	6.4 (0.9)	8.0 (1.0)
	30		2.6 (0.3)	5.2 (0.2)	9.0 (0.6)
100% amorphous lactose				2.4 (0.1)	4.0 (0.2)
7.4 (0.6)					
DCL21			0.7 (0.1)	1.7 (0.0)	3.7 (0.1)

a) N.C.: No compacts were obtained. b) The numbers in parenthesis represent the standard deviation.

Effect of polymer content in SD composite particles on the tensile strength of their tablet. Each data represents the mean±S.D. for four determinations.

Table 2. Effect of Water Content in SD Composite Particles (SDCP) on the Tensile Strength of Their Tablet and Glass Transition Temperature of the Particles

Content in SDCP		Tensile strength (MPa)	Glass transition temp. (K)
NaAlg (%)	Water (%)		
0	0	2.7 (1.0)	378.0 (3.3)[b]
	2.6	5.0 (0.5)	352.6 (2.7)
	3.6	5.2 (0.4)	341.3 (2.9)
	5.2	5.5 (0.6)	323.7 (0.9)
10	0	0.7 (0.1)	392.6 (0.8)
	2.6	2.9 (0.4)	366.1 (3.6)
	4	4.8 (1.1)	357.1 (1.8)
	5.6	6.5 (0.2)	337.6 (5.1)
30	0	N.C.[a]	407.7 (1.9)
	3.6	N.C	363.9 (2.1)
	4.1	N.C	360.8 (0.9)
	6.3	0.3 (0.0)	346.4 (1.6)
	8.8	1.6 (0.1)	340.1 (1.2)

a) N.C.: No compacts were obtained. b) The numbers in parenthesis represent the standard deviation.

Each data represents the mean±S.D. for four or three determinations.
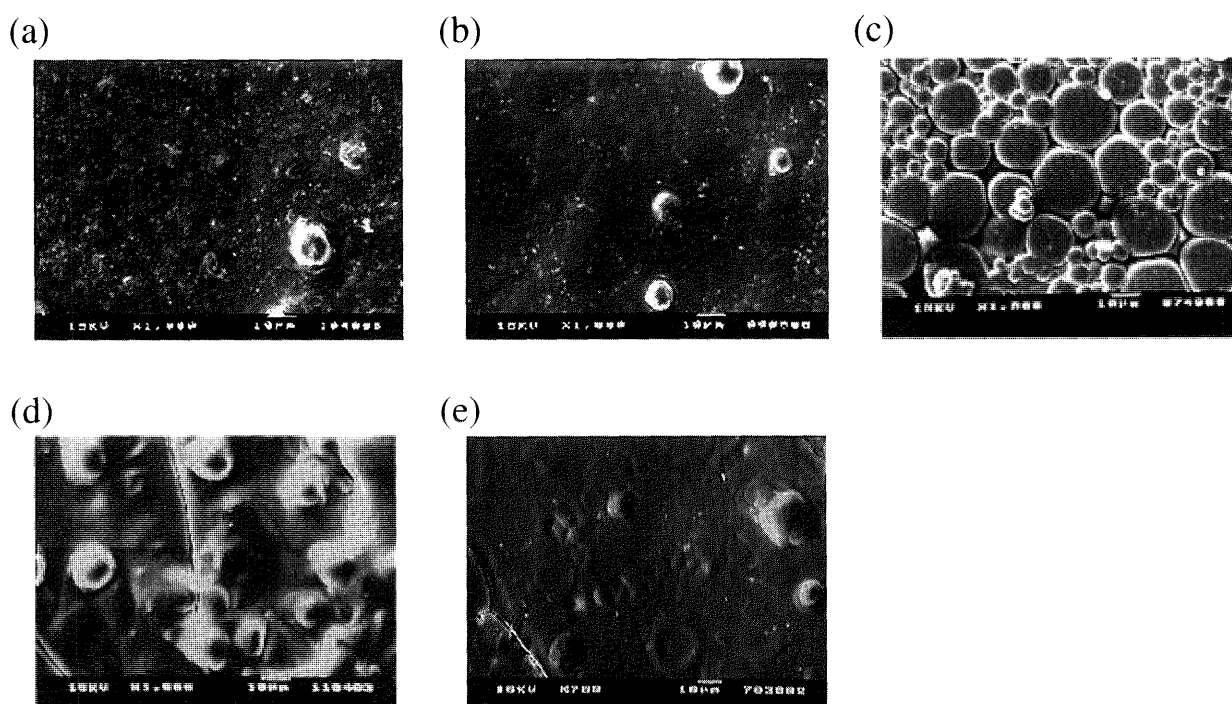

(a)   (b)   (c)

(d)   (e)

Fig. 3. Scanning Electron Micrographs of the Upper Surface of Tablets Compacted at Compression Pressure of 400 MPa

(a) 100% amorphous lactose, (b) SD composite particles (SDCP) with 10% sodium alginate, (c) SDCP with 30% sodium alginate, (d) SDCP with 30% HPC, (e) SDCP with 30% PVP.
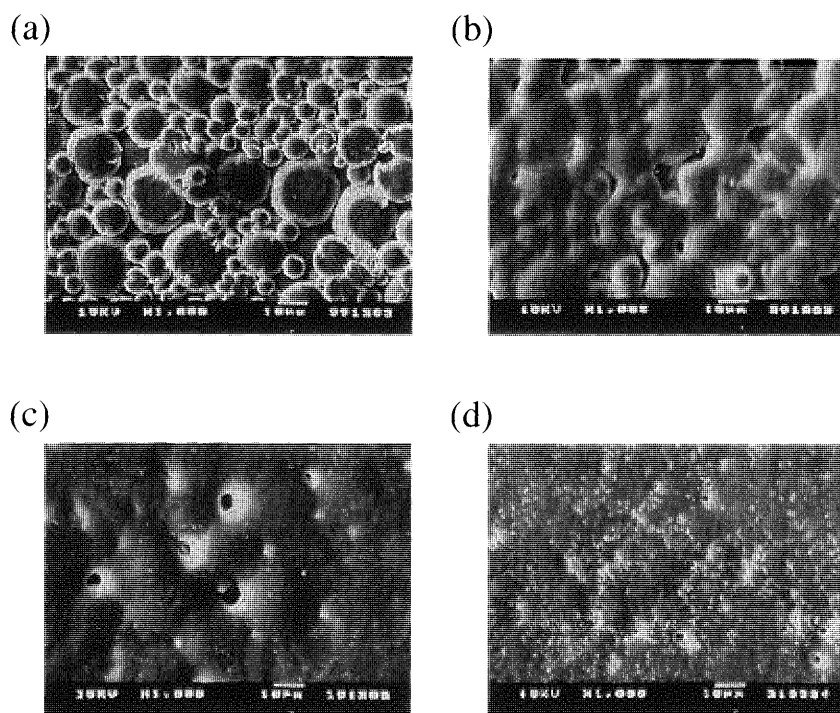
(a)

(b)

(c)

(d)

Fig. 4. Scanning Electron Micrographs of the Upper Surface of Tablets Containing SD Composite Particles Containing 10% Sodium Alginate with Various Water Contents

(a) 0 %, (b) 2.6%, (c) 4.0 %, (d) 5.6 %.

Conclusions

The SD composite particles of lactose and water-soluble polymers (sodium alginate, HPC and PVP) possessed different properties depending on the type of the polymers. The temperature-induced crystallization of amorphous lactose in the particles was most depressed by formulating sodium alginate, which may have a specific interaction with lactose. Tabletting property of the SD composite particles containing HPC or PVP was almost independent of the formulating ratios, while this property was significantly decreased by formulating sodium alginate into the particles.

References

1) Wan L. S. C., Heng P. W. S., Wong L. F., *Int. J. Pharm.*, **116**, 159—168 (1995).

2) Gao P., Skoug J. W., Nixon P. R., Ju T. R., Stemm N. L., Sung K., *J. Pharm. Sci.*, **85**, 732—740 (1996).

3) Takeuchi H., Yasuji T., Hino T., Yamamoto H., Kawashima Y., *Int. J. Pharm.*, **174**, 91—100 (1998).

4) Gunsel W. C., Lachman L., *J. Pharm. Sci.*, **52**, 178—182 (1963).

5) Vromans H., Boluhuis G. K., Lerk C. F., Biggelaar V. D., Bosch H., *Int. J. Pharm.*, **35**, 29—37 (1987).

6) Elamin A. A., Sebhatsu T., Ahlneck C., *Int. J. Pharm.*, **119**, 25—36 (1995).

7) Stubberud L., Forbes, R. T., *Int. J. Pharm.*, **163**, 145—156 (1998).

8) Takeuchi H., Yasuji T., Hino T., Yamamoto H., Kawashima Y., *Pharm. Dev., Tech.*, in press.

9) Takeuchi H., Yasuji T., Hino T., Yamamoto H., Kawashima Y., *Pharm. Res.*, **16**, 1193—1198 (1999).

10) Buckton G., Darcy P., *Int. J. Pharm.*, **123**, 265—271 (1995).

11) Fell J. T., Newton J. M., *J. Pharm. Sci.*, **59**, 688—691 (1970).

12) Gordon M., Taylor J. S., *J. Appl. Chem.*, **2**, 493—500 (1952).

13) Taylor L. S., Zografi G., *Pharm. Res.*, **14**, 1691—1698 (1997).

14) Sebhatu T., Elamin A. A., Ahlneck C., *Pharm. Res.*, **11**, 1233—1238 (1994).

An Efficient Synthesis of the Anti-asthmatic Agent T-440: A Selective N-Alkylation of 2-Pyridone

Masakatsu Sugahara, Yasunori Moritani, Tooru Kuroda,[a] Kazuhiko Kondo,[a] Hideshi Shimadzu, and Tatsuzo Ukita*

Discovery Research Laboratory, Product & Technology Development Laboratory,[a] Tanabe Seiyaku Co., Ltd., 3-16-89 Kashima, Yodogawa, Osaka 532-8505, Japan.   Received November 10, 1999; accepted December 25, 1999

6,7-Diethoxy-1-[1-(2-methoxyethyl)-2-oxo-1,2-dihydropyridin-4-yl]naphthalene-2,3-dimethanol [T-440, (1)] is a potential anti-asthmatic agent based on selective phosphodiesterase 4 inhibition. It was necessary for the further evaluation of 1 to develop an efficient synthetic route for 1, especially the construction of the 1-(2-methoxyethyl)-2-pyridone moiety. We examined an N-selective alkylation of pyridone derivative (2) in basic media. 2-Methoxyethylation of 2 with 2-methoxyethyl iodide utilizing LiH as the base gave predominantly an N-alkyl pyridone derivative (3a) in 82% yield (N/O-alkylation=92/8), which is compatible with an *ab initio* calculation of transition-state structures for the methylation of 2-pyridone. Single crystallization of a crude mixture of 3a and 4a furnished pure 3a, which is a key synthetic intermediate of 1.

Key words   PDE 4 inhibitor; anti-asthmatic agent; alkylation; pyridone; transition state

Cyclic nucleotide phosphodiesterase 4 (PDE 4) is a key enzyme playing an important role in the hydrolysis of purine cyclic nucleotide, cAMP, to form the respective 5′-mononucleotide. Inhibition of PDE 4 activity results in an increase in cellular levels of cAMP, which has been implicated in the relaxation of airway smooth muscle. Recent interest in this area has focused on the search for selective PDE 4 inhibitors as potential anti-asthmatic agents.[1] We reported 6,7-diethoxy-1-[1-(2-methoxyethyl)-2-oxo-1,2-dihydropyridin-4-yl]naphthalene-2,3-dimethanol, T-440 (1, Fig. 1) as a selective and potent PDE 4 inhibitor,[2] and its 1-(2-methoxyethyl)-2-pyridone moiety seems to have a crucial role for PDE 4 inhibitory activity. The regioselective synthesis of the 1-(2-methoxyethyl)-2-pyridone moiety was necessary for the further development of 1.

Additionally, development of a general method for selec-tive N-alkylation of pyridone derivatives would be highly valuable in organic synthesis, since the products would be versatile intermediates for the synthesis of natural products or biologically active compounds.[3] Current synthetic methods of N-alkyl-2-pyridone derivatives include selective N-alkylation by using alkyl halide in the presence of base[4] or alcohol with diethyl azodicarboxylate and Ph_3P,[5] and the quaternization of pyridine followed by oxidation.[6]

In connection with development of an efficient synthetic route for 1, we now report studies on construction of the N-alkyl-2-pyridone moiety of 1, which includes the selective N-alkylation of 2 using alkyl halide and LiH.

Results and Discussion

In the synthesis of 1, we obtained the precursor (3a) of T-440 by the alkylation of pyridone derivative 2 with 2-methoxyethyl iodide in the presence of NaH as a key reaction.[2] Significant amounts of undesired O-alkylated product (4a) were also obtained and the isolation of 3a by silica gel chromatography was necessary for further elaboration. We envisaged that the counter cation (Li, Na, and K) of an ambient anion would play an important role on the N/O selectivity in this reaction.[3c] In order to evaluate our working hypothe-
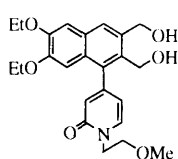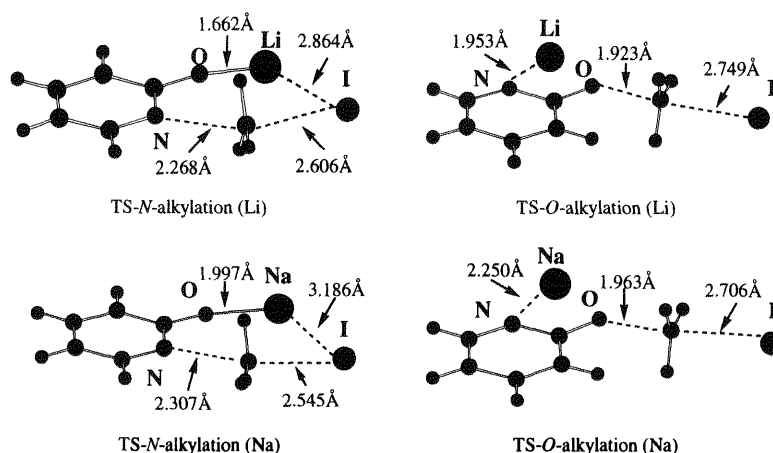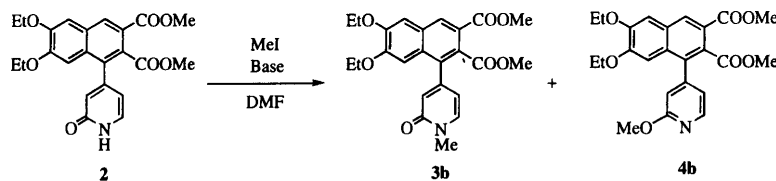

Fig. 1.   Structure of T-440 (1)

Fig. 2.   Transition-State Structures (TS) for N- or O-Methylation of 2-Pyridone with Li or Na Cation

* To whom correspondence should be addressed.   © 2000 Pharmaceutical Society of Japan

Table 1. Methylation of 2 with Methyl Iodide in the Presence of Various Bases

Run	Base	Ratio (3b/4b)[a]	Yield (3b+4b, %)[a]
1	K₂CO₃	97/3	79
2	NaH	98/2	79
3	LiH	>99.9/<0.1	81
4	CsF	93/7	73
5	DBU	96/4	79

a) Ratio (3b/4b) and yield (3b+4b) were determined based on the isolated yield of each product (3b, 4b).

Table 2. Alkylation of 2 with Various Alkyl Halides in the Presence of LiH
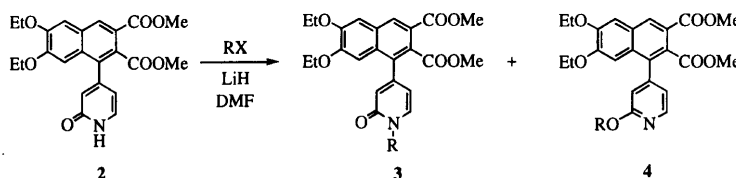
Entry	RX	Ratio (3/4)[a]	Yield (3+4, %)[a]
1	MeOCH₂CH₂I (a)	92/8	84
2	MeI (b)	>99.9/<0.1	81
3	EtI (c)	99/1	85
4	iso-PrI (d)	83/17	28[b]
5	Benzyl bromide (e)	>99.9/<0.1	82
6	Allyl bromide (f)	95/5	80

a) Ratio (3/4) and yield (3+4) were determined based on the isolated yield of each product (3, 4). b) Starting material was recovered in 47%.

sis, we carried out *ab initio* calculations of transition-state structures for the methylation of 2-pyridone as a model study at the HF/3-21G level using GAUSSIAN 94.[7] The energy difference between transition-state structures of *N*-methylation and *O*-methylation using Li metal was 5.45 kcal/mol, whereas for Na metal it was 4.09 kcal/mol (Fig. 2). From these results, *N*-methyl-2-pyridone was estimated to be obtained predominantly by using the Li cation instead of the Na cation.

In order to experimentally confirm the effects of the counter cation on *N/O* selectivity, we tried methylation of 2 with MeI in the presence of K₂CO₃, NaH, LiH, CsF, or 1,8-diazabicyclo[5.4.0]undec-7-ene (DBU) in *N,N*-dimethylformamide (DMF); the ratios were determined on the basis of the isolated yield of each product by silica gel chromatography. The selectivity of *N*-methylation is in fair agreement with the estimation from energy calculation, and LiH gave the best *N*-selectivity among the various bases (Table 1).

Based on these results, we next examined the alkylation of 2 with a variety of alkyl halides, including 2-methoxyethyl iodide, using LiH as the base (Table 2). 2 was treated with alkyl halide and LiH in DMF at 50 °C for 20 h to afford a mixture of 3 and 4 in good to excellent selectivity in high yield, except for isopropyl iodide that gave a lower yield probably because of steric hindrance; the *N/O* ratio was determined on the basis of the isolated yield of each product by silica gel chromatography. Moreover, we found that pure 3a
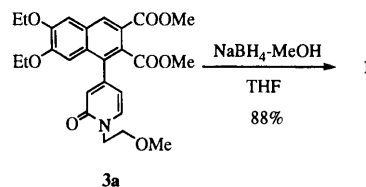
Chart 1. Reduction of 3a to T-440 (1)

could be obtained in 70% yield without difficulty by a single crystallization of the crude mixture (3a/4a=92/8) from AcOEt. Reduction of 3a by treatment with NaBH₄ and MeOH in refluxing tetrahydrofuran (THF)[8] gave T-440 (1) in 88% yield (Chart 1).

In conclusion, we have achieved the selective *N*-alkylation of pyridone derivative 2, which has enabled the large-scale synthesis of the anti-asthmatic agent T-440 (1). In the reaction, we found that the selectivity of *N*-alkylation increases in order of Na and Li metal, which is compatible with the results of *ab initio* calculations in the model study.

Experimental

F254 (E. Merck) glass plates.

General Procedure for the Alkylation of Pyridones (2) Base (1.2 mmol) was added to a solution of **2** (1.0 mmol) in DMF (5 ml), and the mixture was stirred at 50 °C for 2 h under nitrogen atmosphere. Alkyl halide (1.5 mmol) was added, and the mixture was stirred overnight at 50 °C. After being allowed to cool to room temperature, the reaction mixture was poured into a mixture of aqueous NaHCO$_3$ and AcOEt, and extracted with AcOEt. The organic layer was washed with brine, dried over MgSO$_4$, and concentrated under reduced pressure. Purification of the residue by chromatography gave **3** and **4**. All purified compounds were characterized as follows:

6,7-Diethoxy-1-[1-(2-methoxyethyl)-2-oxo-1,2-dihydropyridin-4-yl]naphthalene-2,3-dicarboxylic Acid Dimethyl Ester (3a) mp 101—103 °C. IR (KBr) cm^{-1}: 1724, 1660, 1250, 1126. ^{1}H-NMR (CDCl$_3$) δ: 1.45 (3H, t, $J=7.0$ Hz), 1.55 (3H, t, $J=7.0$ Hz), 3.36 (3H, s), 3.68—3.83 (2H, m), 3.75 (3H, s), 3.93 (3H, s), 3.93—4.12 (2H, m), 4.12—4.31 (4H, m), 6.17 (1H, dd, $J=6.9$, 1.9 Hz), 6.59 (1H, d, $J=1.9$ Hz), 6.91 (1H, s), 7.23 (1H, s), 7.44 (1H, d, $J=6.9$ Hz), 8.42 (1H, s). EIMS m/z: 483 (M$^+$), 425 (base). *Anal.* Calcd for C$_{26}$H$_{29}$NO$_8$: C, 64.59; H, 6.05; N, 2.90. Found: C, 64.30; H, 5.90; N, 2.61.

6,7-Diethoxy-1-[2-(2-methoxyethyl)oxypyridin-4-yl]naphthalene-2,3-dicarboxylic Acid Dimethyl Ester (4a) mp 128—130 °C. IR (KBr) cm^{-1}: 1723, 1251, 1126. ^{1}H-NMR (CDCl$_3$) δ: 1.42 (3H, t, $J=7.0$ Hz), 1.55 (3H, t, $J=7.0$ Hz), 3.46 (3H, s), 3.65 (3H, s), 3.79 (2H, t, $J=5.0$ Hz), 3.82—4.05 (2H, m), 3.93 (3H, s), 4.23 (2H, q, $J=7.0$ Hz), 4.45—4.62 (2H, m), 6.73 (1H, s), 6.83 (1H, dd, $J=1.4$, 0.7 Hz), 6.89 (1H, dd, $J=5.2$, 1.4 Hz), 7.23 (1H, s), 8.23 (1H, dd, $J=5.2$, 0.7 Hz), 8.44 (1H, s). EIMS m/z: 483 (M$^+$), 424 (base). *Anal.* Calcd for C$_{26}$H$_{29}$NO$_8$: C, 64.59; H, 6.05; N, 2.90. Found: C, 64.33; H, 5.81; N, 2.63.

6,7-Diethoxy-1-(1-methyl-2-oxo-1,2-dihydropyridin-4-yl)naphthalene-2,3-dicarboxylic Acid Dimethyl Ester (3b) mp 190—191 °C. IR (KBr) cm^{-1}: 1725, 1662, 1248, 1126. ^{1}H-NMR (CDCl$_3$) δ: 1.47 (3H, t, $J=7.0$ Hz), 1.55 (3H, t, $J=7.0$ Hz), 3.64 (3H, s), 3.77 (3H, s), 3.93 (3H, s), 3.92—4.15 (2H, m), 4.24 (2H, q, $J=7.0$ Hz), 6.20 (1H, dd, $J=6.9$, 1.9 Hz), 6.61 (1H, d, $J=1.9$ Hz), 6.89 (1H, s), 7.23 (1H, s), 7.37 (1H, d, $J=6.9$ Hz), 8.42 (1H, s). EIMS m/z: 438 (M$^+-1$, base). *Anal.* Calcd for C$_{24}$H$_{25}$NO$_7$: C, 65.59; H, 5.73; N, 3.19. Found: C, 65.45; H, 5.45; N, 2.99.

6,7-Diethoxy-1-(2-methyloxypyridin-4-yl)naphthalene-2,3-dicarboxylic Acid Dimethyl Ester (4b) mp 67—69 °C. IR (KBr) cm^{-1}: 1724, 1250, 1126. ^{1}H-NMR (CDCl$_3$) δ: 1.42 (3H, t, $J=7.0$ Hz), 1.55 (3H, t, $J=7.0$ Hz), 3.66 (3H, s), 3.94 (3H, s), 4.01 (3H, s), 3.83—4.08 (2H, m), 4.24 (2H, q, $J=7.0$ Hz), 6.75 (1H, s), 6.77 (1H, d, $J=1.4$ Hz), 6.89 (1H, dd, $J=5.2$, 1.4 Hz), 7.23 (1H, s), 8.27 (1H, d, $J=5.2$ Hz), 8.44 (1H, s). EIMS m/z: 439 (M$^+$, base). *Anal.* Calcd for C$_{24}$H$_{25}$NO$_7$: C, 65.59; H, 5.73; N, 3.19. Found: C, 65.29; H, 5.64; N, 2.94.

6,7-Diethoxy-1-(1-ethyl-2-oxo-1,2-dihydropyridin-4-yl)naphthalene-2,3-dicarboxylic Acid Dimethyl Ester (3c) mp 163—164 °C. IR (KBr) cm^{-1}: 1728, 1661, 1251, 1126. ^{1}H-NMR (CDCl$_3$) δ: 1.45 (3H, t, $J=7.2$ Hz), 1.46 (3H, t, $J=7.0$ Hz), 1.55 (3H, t, $J=7.0$ Hz), 3.76 (3H, s), 3.93 (3H, s), 3.93—4.17 (4H, m), 4.23 (2H, q, $J=7.0$ Hz), 6.21 (1H, dd, $J=6.9$, 1.9 Hz), 6.59 (1H, d, $J=1.9$ Hz), 6.90 (1H, s), 7.23 (1H, s), 7.36 (1H, d, $J=6.9$ Hz), 8.42 (1H, s). EIMS m/z: 452 (M$^+-1$, base). *Anal.* Calcd for C$_{25}$H$_{27}$NO$_7$: C, 66.21; H, 6.00; N, 3.09. Found: C, 65.98; H, 5.85; N, 2.98.

6,7-Diethoxy-1-(2-ethyloxypyridin-4-yl)naphthalene-2,3-dicarboxylic Acid Dimethyl Ester (4c) mp 124—125 °C. IR (KBr) cm^{-1}: 1725, 1251, 1126. ^{1}H-NMR (CDCl$_3$) δ: 1.42 (3H, t, $J=7.0$ Hz), 1.43 (3H, t, $J=7.0$ Hz), 1.55 (3H, t, $J=7.0$ Hz), 3.66 (3H, s), 3.94 (3H, s), 3.95 (2H, q, $J=7.0$ Hz), 4.24 (2H, q, $J=7.0$ Hz), 4.41 (2H, q, $J=7.0$ Hz), 6.70—6.80 (2H, m), 6.87 (1H, dd, $J=5.2$, 1.4 Hz), 7.23 (1H, s), 8.24 (1H, dd, $J=5.2$, 0.6 Hz), 8.44 (1H, s). EIMS m/z: 453 (M$^+$, base). *Anal.* Calcd for C$_{25}$H$_{27}$NO$_7$: C, 66.21; H, 6.00; N, 3.09. Found: C, 66.20; H, 6.00; N, 2.92.

6,7-Diethoxy-1-(1-isopropyl-2-oxo-1,2-dihydropyridin-4-yl)naphthalene-2,3-dicarboxylic Acid Dimethyl Ester (3d) mp 152—153 °C. IR (KBr) cm^{-1}: 1731, 1656, 1256, 1126. ^{1}H-NMR (CDCl$_3$) δ: 1.35—1.50 (9H, m), 1.55 (3H, t, $J=7.0$ Hz), 3.74 (3H, s), 3.93 (3H, s), 3.92—4.11 (2H, m), 4.24 (2H, q, $J=7.0$ Hz), 5.35 (1H, septet, $J=6.8$ Hz), 6.25 (1H, dd, $J=7.0$, 1.9 Hz), 6.59 (1H, d, $J=1.9$ Hz), 6.91 (1H, s), 7.23 (1H, s), 7.42 (1H, d, $J=7.0$ Hz), 8.42 (1H, s). EIMS m/z: 466 (M$^+-1$, base). *Anal.* Calcd for C$_{26}$H$_{29}$NO$_7$: C, 66.80; H, 6.25; N, 3.00. Found: C, 66.78; H, 6.00; N, 2.89.

6,7-Diethoxy-1-(2-isopropyloxypyridin-4-yl)naphthalene-2,3-dicarboxylic Acid Dimethyl Ester (4d) mp 147—148 °C. IR (KBr) cm^{-1}: 1724, 1250, 1125. ^{1}H-NMR (CDCl$_3$) δ: 1.30—1.49 (9H, m), 1.55 (3H, t, $J=7.0$ Hz), 3.65 (3H, s), 3.94 (3H, s), 3.96 (2H, q, $J=7.0$ Hz), 4.24 (2H, q, $J=7.0$ Hz), 5.34 (1H, septet, $J=6.2$ Hz), 6.70 (1H, d, $J=1.4$ Hz), 6.78 (1H, s),

6.84 (1H, dd, $J=5.2$, 1.4 Hz), 7.23 (1H, s), 8.24 (1H, d, $J=5.2$ Hz), 8.43 (1H, s). EIMS m/z: 467 (M$^+$, base). *Anal.* Calcd for C$_{26}$H$_{29}$NO$_7$: C, 66.80; H, 6.25; N, 3.00. Found: C, 66.61; H, 6.11; N, 2.80.

6,7-Diethoxy-1-(1-benzyl-2-oxo-1,2-dihydropyridin-4-yl)naphthalene-2,3-dicarboxylic Acid Dimethyl Ester (3e) mp 160—161 °C. IR (KBr) cm^{-1}: 1719, 1662, 1251, 1126. ^{1}H-NMR (CDCl$_3$) δ: 1.44 (3H, t, $J=7.0$ Hz), 1.55 (3H, t, $J=7.0$ Hz), 3.73 (3H, s), 3.93 (3H, s), 4.02 (2H, qd, $J=7.0$, 2.2 Hz), 4.23 (2H, q, $J=7.0$ Hz), 5.25 (2H, s), 6.18 (1H, dd, $J=6.9$, 1.9 Hz), 6.65 (1H, d, $J=1.9$ Hz), 6.88 (1H, s), 7.22 (1H, s), 7.22—7.45 (6H, m), 8.42 (1H, s). EIMS m/z: 515 (M$^+$, base). *Anal.* Calcd for C$_{30}$H$_{29}$NO$_7$: C, 69.89; H, 5.67; N, 2.72. Found: C, 69.80; H, 5.92; N, 2.56.

6,7-Diethoxy-1-(1-allyl-2-oxo-1,2-dihydropyridin-4-yl)naphthalene-2,3-dicarboxylic Acid Dimethyl Ester (3f) mp 135—136 °C. IR (KBr) cm^{-1}: 1724, 1663, 1251, 1126. ^{1}H-NMR (CDCl$_3$) δ: 1.46 (3H, t, $J=7.0$ Hz), 1.55 (3H, t, $J=7.0$ Hz), 3.76 (3H, s), 3.94 (3H, s), 3.93—4.15 (2H, m), 4.24 (2H, q, $J=7.0$ Hz), 4.67 (2H, dd, $J=5.6$, 1.5 Hz), 5.23 (1H, dd, $J=17.0$, 1.2 Hz), 5.34 (1H, dd, $J=10.2$, 1.2 Hz), 6.06 (1H, ddt, $J=17.0$, 10.2, 5.6 Hz), 6.22 (1H, dd, $J=6.9$, 1.9 Hz), 6.62 (1H, d, $J=1.4$ Hz), 6.90 (1H, s), 7.23 (1H, s), 7.34 (1H, d, $J=6.9$ Hz), 8.43 (1H, s). EIMS m/z: 465 (M$^+$, base). *Anal.* Calcd for C$_{26}$H$_{27}$NO$_7$: C, 67.09; H, 5.85; N, 3.01. Found: C, 67.04; H, 5.91; N, 2.97.

6,7-Diethoxy-1-(2-allyloxypyridin-4-yl)naphthalene-2,3-dicarboxylic Acid Dimethyl Ester (4f) mp 108—110 °C. IR (KBr) cm^{-1}: 1720, 1252, 1126. ^{1}H-NMR (CDCl$_3$) δ: 1.42 (3H, t, $J=7.0$ Hz), 1.55 (3H, t, $J=7.0$ Hz), 3.66 (3H, s), 3.94 (3H, s), 3.95 (2H, q, $J=7.0$ Hz), 4.24 (2H, q, $J=7.0$ Hz), 4.91 (2H, dd, $J=5.4$, 1.5 Hz), 5.27 (1H, dd, $J=10.4$, 1.4 Hz), 5.42 (2H, dd, $J=17.2$, 1.6 Hz), 6.12 (1H, ddt, $J=17.2$, 10.4, 5.4 Hz), 6.75 (1H, s), 6.80 (1H, dd, $J=1.4$, 0.7 Hz), 6.89 (1H, dd, $J=5.2$, 1.4 Hz), 7.23 (1H, s), 8.25 (1H, dd, $J=5.2$, 0.7 Hz), 8.44 (1H, s). EIMS m/z: 465 (M$^+$, base). *Anal.* Calcd for C$_{26}$H$_{27}$NO$_7$: C, 67.09; H, 5.85; N, 3.01. Found: C, 66.91 H, 5.90; N, 2.95.

6,7-Diethoxy-1-[1-(2-methoxyethyl)-2-oxo-1,2-dihydropyridin-4-yl]naphthalene-2,3-dimethanol T-440 (1) To a stirred suspension of **3a** (4.3 g, 8.9 mmol) and NaBH$_4$ (3.4 g, 89.0 mmol) in THF (60 ml) was added MeOH (15 ml) dropwise under reflux over 1 h, and the mixture was stirred under reflux for another 1 h. The reaction mixture was allowed to cool to room temperature and concentrated under reduced pressure. The residue was poured into a mixture of 10% aqueous HCl (75 ml) and CHCl$_3$ (150 ml), and the organic layer was washed with brine, dried over MgSO$_4$, and concentrated under reduced pressure. Crystallization of the residue from AcOEt–hexane gave **1** (3.3 g, 88%), mp 130—131 °C. IR (KBr) cm^{-1}: 3387, 1656. ^{1}H-NMR (CDCl$_3$) δ: 1.41 (3H, t, $J=7.0$ Hz), 1.53 (3H, t, $J=7.0$ Hz), 3.35 (3H, s), 3.72 (2H, t, $J=5.0$ Hz), 3.82—4.03 (2H, m), 4.03—4.35 (4H, m), 4.35—4.70 (2H, m), 4.70—5.00 (2H, m), 6.10 (1H, dd, $J=6.8$, 1.8 Hz), 6.46 (1H, d, $J=1.8$ Hz), 6.65 (1H, s), 7.02 (1H, s), 7.43 (1H, d, $J=6.8$ Hz), 7.62 (1H, s). EIMS m/z: 427 (M$^+$), 351 (base). *Anal.* Calcd for C$_{24}$H$_{29}$NO$_6$: C, 67.43; H, 6.84; N, 3.28. Found: C, 67.01; H, 6.66; N, 2.84.

References and Notes

1) *a*) Torphy T. J., Undem B. J., *Thorax*, **46**, 512—523 (1991); *b*) Reaburn D., Souness J. E., Tomkinson A., Karlsson J.-A., *Prog. Drug. Res.*, **40**, 9—32 (1993); *c*) Christensen S. B., Torphy T., *Annu. Rep. Med. Chem.*, **29**, 185—194 (1994).

2) Iwasaki T., Kondo K., Kuroda T., Moritani Y., Yamagata S., Sugiura M., Kikkawa H., Kaminuma O., Ikezawa K., *J. Med. Chem.*, **39**, 2696—2704 (1996).

3) *a*) Pierce J. B., Ariyan Z. S., Ovenden G. S., *J. Med. Chem.*, **25**, 131—136 (1982); *b*) Schmidhauser J. C., Khouri F. F., *Tetrahedron Lett.*, **34**, 6685—6688 (1993); *c*) Liu H., Ko S-Bo., Josien H., Curran D. P., *ibid.*, **36**, 8917—8920 (1995).

4) Scriven E. F. V., "Comprehensive Heterocyclic Chemistry," Vol. 2, ed. by Katritzky A. R., Rees C. W., Pergamon Press, Oxford, 1984, pp. 165—314.

5) Comins D. L., Jianhua G., *Tetrahedron Lett.*, **35**, 2819—2822 (1994).

6) Prill E. A., McElvain S. M., *Org. Synth. II.*, **1943**, 419—421.

7) Vibrational frequencies calculated for all the studied systems confirmed the nature of the stationary points (energy minimum, all positive frequencies; transition states, one imaginary frequency with largest contributions from internal coordinates involved in the reaction).

8) Soai K., Oyamada H., Takase M., Ookawa A., *Bull. Chem. Soc. Jpn.*, **57**, 1948—1953 (1984).